UNIVERSITY OF SOUTHAMPTON

FACULTY OF NATURAL AND ENVIRONMENTAL SCIENCES

Ocean and Earth Sciences

Phytoplankton communities of subsurface chlorophyll maxima in the summer stratified waters of the Western English Channel

by

Michelle Louise Barnett

Thesis for the degree of Doctor of Philosophy

March 2018

UNIVERSITY OF SOUTHAMPTON

ABSTRACT

FACULTY OF NATURAL AND ENVIRONMENTAL SCIENCES

Ocean and Earth Sciences

Doctor of Philosophy

PHYTOPLANKTON COMMUNITIES OF SUBSURFACE CHLOROPHYLL MAXIMA IN THE SUMMER STRATIFIED WATERS OF THE WESTERN ENGLISH CHANNEL

Michelle Louise Barnett

In the summer stratified temperate shelf waters of the Western English Channel, a subsurface chlorophyll maximum (SCM) is typically observable within the seasonal thermocline. Surveys were conducted in these summer (June/July) stratified waters from 2013 to 2016 investigating SCM phytoplankton communities. A SeaBird CTD with fluorometer and Niskin rosette sampler was routinely used to collect water column profiles and discrete water samples, and an Acoustic Doppler Current Profiler (ADCP) measured current profiles. In 2013 SCM thin layers (SCMTL; < 5 m thick) and broader SCM were studied in detail. SCMTL were detected in 18 of 52 profiles, typically characterised by higher maximum chlorophyll concentrations than broader SCM. Water column structure and physical forcing governed SCM chlorophyll structure, with SCMTL generally associated with a stepped thermocline and greater stratification. Community structure within SCMTL was statistically distinct from that of broader SCM, proposed to result from promotion of phytoplankton better adapted to conditions more specific to SCMTL compared to broader SCM. Findings suggest that with more intense stratification projected for the NW European shelf there may be increased prevalence of SCMTL and associated specialised flora. In 2015, a digital in-line holographic camera (holocam) was deployed, the data from which identified a transition of phytoplankton through the stratified water column, showed how one taxon can be dominant over a small part of the water column, and provided evidence of the SCM as a considerable source of carbon flux. Following methodological developments, *in situ* holography has the potential to be powerful in the assessment of the phytoplankton community on a large spatial and temporal scale, and as a tool for obtaining quantitative carbon flux data. Primary production was also assessed in 2015, using a combination of ^{13}C incubation experiments and Fluorescence Induction and Relaxation (FIRe) measurements. The SCM was estimated to account for, on average, 50 % of total water column primary production and was identified as a key site of new production. Variation in the magnitude of water column production was driven by changes in SCM layer production, which was governed by factors including chlorophyll concentration, irradiance, and the photophysiology and structure of the phytoplankton community, with increases in SCM carbon fixation associated with greater contributions of red fluorescing nano-phytoplankton due to their enhanced light utilisation efficiency. Greater percentages of these nano-phytoplankton generally coincided with stronger stratification, which may have implications for our understanding of the relationship between stratification and primary production. Finally, data from all four years was gathered to study environmental controls of interannual variability in SCM chlorophyll and phytoplankton community structure at one location in the Western Channel. Stability (given by the instantaneous index of stability; IIS) and temperature were found to be key governing factors. Changes in stability were related to interannual variation in SCM maximum chlorophyll, the 50 m:SCM maximum chlorophyll ratio, and proportions of red fluorescing nano-phytoplankton and dinoflagellates within the SCM community. Changes in water temperature were associated with interannual variation in SCM maximum chlorophyll and proportions of small versus large diatoms within the SCM. These findings may have implications, in particular, for the silica cycle, carbon export to depth and the microbial loop. Possible causes and implications of all results, as described above, are discussed in detail within this thesis.

List of contents

List of Tables

List of Figures

UNIVERSITY OF Southampton

Academic Thesis: Declaration Of Authorship

I, **Michelle Louise Barnett**, declare that this thesis entitled '**Phytoplankton communities of subsurface chlorophyll maxima in the summer stratified waters of the Western English Channel'** and the work presented in it are my own and has been generated by me as the result of my own original research.

I confirm that:

1. This work was done wholly or mainly while in candidature for a research degree at this University;
2. Where any part of this thesis has previously been submitted for a degree or any other qualification at this University or any other institution, this has been clearly stated;
3. Where I have consulted the published work of others, this is always clearly attributed;
4. Where I have quoted from the work of others, the source is always given. With the exception of such quotations, this thesis is entirely my own work;
5. I have acknowledged all main sources of help;
6. Where the thesis is based on work done by myself jointly with others, I have made clear exactly what was done by others and what I have contributed myself;
7. None of this work has been published before submission.

Signed: ……

Date: ……

Acknowledgements

I would like to extend my gratitude to a number of people who have supported me during the course of my PhD. First and foremost, thanks must go to my principal supervisor Professor Duncan Purdie, and co-supervisors Professor Alan Kemp and Dr Anna Hickman for their expertise, encouragement and guidance throughout my four years of study. I would also like to specially thank Dr Adrian Martin for his encouragement and advice in panel meetings over the course of my PhD. Others that helped me at NOCS who I would like to thank include Dr Alex Poulton for answering my questions on phytoplankton taxonomy; Professor Mark Moore who helped me to understand principles of the Fluorescence Induction and Relaxation (FIRe) technique and phytoplankton photophysiology, and for collecting phytoplankton samples from the Celtic Sea on the RRS Discovery cruise DY033; crew members of RV Callista, Bill Fletcher, Gary Fisher, Nick Hazeldine, Graham Blythe and Charles Matthews who made my research in the Western English Channel possible; coordinators of the University of Southampton undergraduate oceanography field course to Falmouth, Dr Simon Boxall and Professor Tom Bibby for allowing me to conduct my research during the field course, and to Tom for providing the FIRe instrument and being an additional source of help for my understanding of the principles of the FIRe technique and phytoplankton photophysiology; Matt O'Shaughnessy and Nicola Pratt for their abundant assistance with both lab and field preparations; Kelvin Aylett for his design, construction and maintenance of the 'slurp gun'; Dr Alex Nimmo Smith and the crew of RV Falcon Spirit for the opportunity to conduct research with Alex's holocam; Dr Cynthia Dumousseaud, Dr John Gittins, Dr Alex Forryan, Corinne Pebody and Shir Akbari for helping me with sample/data processing and analysis; and finally to all others of the NOC community that have lent support over the duration of my studies. Additional thanks go to the Graduate School of the National Oceanography Centre Southampton (GSNOCS), University of Southampton by whom this research was funded. Also to the Shelf Sea Biogeochemistry programme, the PSO of RRS Discovery cruise DY026A Professor Richard Sanders, and the officers and crew of RRS Discovery for allowing me the opportunity to conduct research in the Celtic Sea.

Last but not least I would like to say a massive thank you to my family - I couldn't have done it without you! To my mum, a true inspiration, for her wonderful encouragement and constant belief in me. To my sister, for proof reading drafts of this thesis, and for her enduring support and patience. Finally to my dad, who helped pave the way for success in my academic endeavours.

Abbreviations used in text

AACE	AutoAnalyser Control and Evaluation
ADCP	Acoustic Doppler Current Profiler
ALS	Actinic light source
ANOSIM	Analysis of Similarity
ANOVA	Analysis of Variance
C	Carbon
CCA	Canonical Correspondence Analysis
CCD	Charge coupled device
CH_2O	Organic matter
Chl	Chlorophyll
Chl_{50m}:Chl_{SCM}	Ratio of chlorophyll concentration within the top 50 m of the water column to SCM maximum chlorophyll concentration
$Cl^{15}NH_4$	^{15}N labelled ammonium chloride
CO_2	Carbon dioxide
CTD	Conductivity temperature depth
DCCA	Detrending Canonical Correspondence Analysis
DIC	Dissolved inorganic carbon
DIN	Dissolved inorganic nitrogen
DMS	Dimethyl sulphide
DOC	Dissolved organic carbon
DOM	Dissolved organic matter
DON	Dissolved organic nitrogen
DOP	Dissolved organic phosphate
E	Irradiance/light
EA-IRMS	Elemental analysis isotope ratio mass spectrometry
EA-MS	Elemental analysis mass spectrometry
Ek	Light saturation parameter
EPS	Extracellular polymeric substances
ETR	Electron transport rate
FIRe	Fluorescence Induction and Relaxation
FRRF	Fast repetition rate fluorometry
FL	Fluorescence
Fm	Maximal fluorescence yield

Fo	Minimal fluorescence yield
Fq'/Fm'	Quantum yield of electron transport through PSII
Fv	Variable fluorescence
Fv/Fm	Maximum photochemical efficiency
FWS	Forwards scatter
GF/F	Glass fibre filter
GUI	Graphical user interface
H	Hydrogen
H_2O	Water
HAB	Harmful algal bloom
Holocam	Digital in-line holographic camera
HPLC	High performance liquid chromatography
ICES	International Council for the Exploration of the Sea
IIS	Instantaneous index of stability
$K^{15}NO_3$	^{15}N labelled potassium nitrate
Kd	Diffuse attenuation coefficient for downward irradiance
LOCO	Layered Organization in the Coastal Ocean
m/z	Mass to charge ratio
N	Nitrogen
Ni	Nitrate
N_2	Molecular nitrogen
$NaH^{13}CO_3$	^{13}C labelled sodium bicarbonate
NH_4^+	Ammonium
nMDS	Non-metric multi-dimensional scaling
O	Oxygen
O_2	Molecular oxygen
OFL	Orange fluorescence
OPA	Orthophthaldialdehyde
P	Phosphorus/Phosphate
P vs. E	Photosynthesis vs. irradiance
PAR	Photosynthetically active radiation
P_{max}	Maximum photosynthetic rate
PML	Plymouth Marine Laboratory
POC	Particulate organic carbon
POM	Particulate organic matter

PON	Particulate organic nitrogen
PP	Primary production/ primary productive
PRIMER	Plymouth Routines in Multivariate Ecological Research
RDA	Redundancy Analysis
rETR	Relative electron transport rate
$rETR_{max}$	Maximum relative electron transport rate
RF	Response factor
RFL	Red fluorescence
RFU	Raw fluorometer units
Ri	Richardson number
rpm	Revolutions per minute
RT	Retention time
S	Sulphur
SCM	Subsurface chlorophyll maximum
SCMTL	Subsurface chlorophyll maximum thin layer
SEM	Scanning Electron Microscope
Si	Silicon/silicate
SigmaPSII	Maximum photosystem II effective absorption cross section
SIMPER	Similarity Percentage Analysis
SIMPROF	Similarity Profile Analysis
SWS	Sideways scatter
TFWS	Total forwards scatter
TOFL	Total orange fluorescence
TRFL	Total red fluorescence
WCO	Western Channel Observatory
α	Initial slope of P or rETR vs. E curve
α_{ETE}	Electron transport efficiency
α_{LHE}	Light harvesting efficiency
λ_1	Marginal effects
λ_a	Conditional effects

Chapter 1: Introduction

1.1. Phytoplankton

1.1.1. What are phytoplankton?

The word phytoplankton is derived from the Greek words *'phyton'*, meaning plant, and *'planktos'*, meaning drifter. It is a generic name for plants and plant-like organisms that are too small to be individually seen with the naked eye and that inhabit the upper reaches of almost all oceans and freshwater bodies (Thurman, 1997, Ghosal et al., 2000). These organisms span the unicellular, multicellular, pseudocolonial and colonial (Beardall et al., 2009). The term phytoplankton is inclusive of all photosynthesising microscopic algae, bacteria and ciliates that utilise solar energy to form organic matter (CH_2O) by the reduction of inorganic carbon (CO_2) (Eq. 1.1), and therefore are agents of primary production (Falkowski and Raven, 1997). This includes autotrophs that derive nourishment through photosynthesis, and mixotrophs that derive nourishment through both autotrophic and heterotrophic mechanisms (Falkowski and Raven, 1997). Additionally, the term phytoplankton can be used to refer to non-pigmented heterotrophic plant/plant-like microorganisms that derive nourishment from the intake of other microscopic algae or detritus, such as many gymnodinoid and peridinoid dinoflagellates (Falkowski and Raven, 1997, Falkowski et al., 2004, Olenina et al., 2006, Beardall et al., 2009).

$$2H_2O + CO_2 + Light \xrightarrow{\substack{Photosynthetic \\ pigment}} (CH_2O) + H_2O + O_2 \quad (1.1)$$

Phytoplankton are polyphyletic, evolving from over one billion years ago, with tens of thousands of species existing in the modern aquatic ecosystem that span at least eight major phyla (Falkowski et al., 2004), including approximately 5000 marine species formally described by the 1990s (Sournia et al., 1991). High taxonomic diversity equates to high morphological, physiological, ecological and functional diversity within the phytoplankton (Falkowski et al., 2004). One key morphological parameter that is vastly variable across the phytoplankton is size, with a range of over nine orders of magnitude (Fig. 1.1). A variety of key physiological and ecological processes scale with phytoplankton cell size (Finkel et al., 2010), including metabolism (rates of photosynthesis, respiration and growth), which has been documented to scale with volume according to Kleiber's law (Kleiber, 1932) in several studies (Hemmingsen, 1960, Blasco et al., 1982, López-Urrutia et al., 2006); maximum nutrient uptake and uptake affinity, since these processes are a function of surface area, size of the diffusion boundary

layer and enzyme and transporter concentrations (Litchman et al., 2007, Litchman and Klausmeier, 2008, Beardall et al., 2009, Finkel et al., 2010); light absorption, as self-shading of pigment is enhanced with increasing size such that fewer photons per unit of pigment are absorbed in phytoplankton of greater size (Agustí, 1991, Fujiki and Satotu, 2002, Finkel et al., 2004); and sinking rates, since density and the surface area to volume ratio of a cell typically increases with size as described by Stokes' law (Stokes, 1851, Denny, 1993). Consequently, this morphological parameter is one of the most significant, albeit simple, for categorising phytoplankton, and is commonly applied in observational and theoretical studies. Maximum linear dimension is specifically used for size classification of the phytoplankton into the pico-phytoplankton (0.2 – 2 µm), nano-phytoplankton (2 – 20 µm), micro-phytoplankton (20 – 200 µm) and meso-phytoplankton (200 – 20000 µm) (Sieburth et al., 1978).

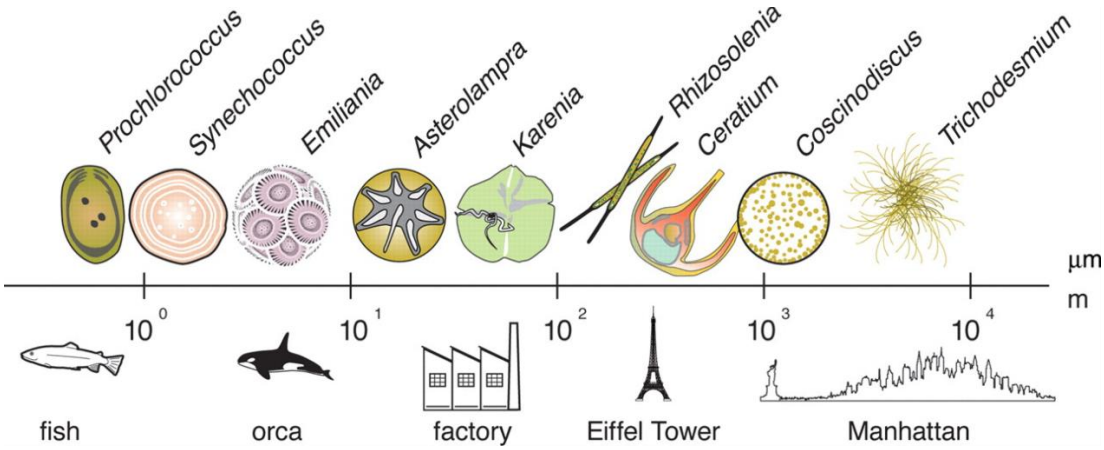

Figure 1.1. Schematic illustrating the vast size range (maximum linear dimension) of phytoplankton by comparison of phytoplankton size relative to macroscopic objects. Taken from Finkel et al. (2010).

There are exceptions to the size relationships described above, with many larger cells having traits that help counterbalance constraints imposed by their size, many of which are taxon specific (Smetacek, 1985, Tang, 1995, Litchman et al., 2007, Finkel et al., 2010, Marañón et al., 2013, López-Sandoval et al., 2014, Marañón, 2015). In fact, many morphological, physiological, ecological and functional phytoplankton traits are taxon specific, such that different taxa may have particular roles in the marine ecosystem, either for biogeochemical processes or to higher trophic levels. Thus, it is important to study phytoplankton using taxonomic classification. The major groups are diatoms (Bacillariophyta) dinoflagellates (Dinoflagellata), flagellates (mainly Haptophtya, Cryptophyta, Chlorophyta, Euglenophyta, Chrysophyceae, Dictyochophyceae), ciliates (Ciliophora) and cyanobacteria (Cyanophyta). A description of each of these major phytoplankton groups follows, with an overview of their key properties provided in Table 1.1.

Diatoms

Diatoms constitute one of the largest and most diverse phytoplankton groups, contributing approximately 40 % of all marine species currently described (Simon et al., 2009), and one of the most important in terms of primary production, accounting for approximately 40 - 45 % of net oceanic primary production (Mann, 1999). As with all photosynthetic microalgae, chlorophyll a is their primary pigment for photosynthesis, which is supplemented by a set of accessory pigments characteristic of diatoms, including fucoxanthin, β-carotene and diadinoxanthin (Round et al., 1990). Diatoms tend to be among the largest of phytoplankton, with some species forming large colonies (Simon et al., 2009), such as *Proboscia spp.*, forming colonies up to 9 mm in length (Sukhanova et al., 2006). Diatoms are traditionally divided into centric forms, which have striae arranged with central symmetry, and pennate forms, which have striae arranged in a line (Simon et al., 2009), all of which are housed within a silica frustule. Thus, diatoms are the only major phytoplankton group that need silicate as a nutrient and as such have a role in regulating the ocean's silicon cycle (Yool and Tyrrell, 2003, Simpson and Sharples, 2012). The frustule has several advantages, including a lesser energy requirement for synthesis compared to an organic cell wall (Raven, 1983), greater mechanical strength, potential provision of protection (Hamm et al., 2003), and it can act to increase surface area enabling a reduced sinking rate/promotion of suspension in the case of frustules with setae or ellipsoidal forms (Smetacek, 1985, Round et al., 1990). The frustule is dense, which in combination with large size and tendency to aggregate as marine snow with the assistance of extracellular polymeric substances (EPS), results in a fast sinking rate that may exceed 100 m per day. Therefore, diatoms are a major contributor to particulate organic matter flux (Billet et al., 1983, Smetacek, 1985, Thornton, 2002), estimated to be responsible for approximately 40 % to upward of 50 % of organic carbon exported to the ocean interior globally (Dugdale and Wilkerson, 1998, Jin et al., 2006). Diatoms exhibit rapid growth rates under favourable conditions, with maximum *in situ* growth rates of 2 – 6 divisions d^{-1} documented (Furnas, 1982, Furnas, 1990). Actively growing diatom cells are typically positively or neutrally buoyant, whilst physiologically stressed cells become negatively buoyant and sink (Richardson and Cullen, 1995). Diatoms are nonmotile, but can regulate their buoyancy, allowing occupancy of regions of the water column where conditions are favourable for growth, e.g. at the pycnocline in stratified waters (Villareal, 1988, Moore and Villareal, 1996b, Woods and Villareal, 2008). Otherwise diatoms rely on vertical turbulent mixing to maintain them within the photic zone. Other physiological adaptations within the diatoms include the ability to maintain relatively high growth rates under low light (Goldman, 1993, Goldman and McGillicuddy, 2003); production of toxins as a potential means of refuge from predation (Trainer et al., 2008,

Durham and Stocker, 2012); low respiratory losses (López-Sandoval et al., 2014); and an increased ability to acquire nutrients relative to requirements by mechanisms including vacuole nutrient storage (Dortch, 1982, Raven, 1987), luxury nutrient uptake (Sunda and Huntsman, 1995) and a reduced volume-specific nutrient requirement (Thingstad et al., 2005), allowing maintenance of growth during periods when nutrients are limited or deplete. The suite of physiological advantages possessed by diatoms likely underlie their high ecological success.

Dinoflagellates and flagellates

Dinoflagellates, like the diatoms, constitute a large and diverse phytoplankton group, contributing approximately 40 % of all marine species described (Simon et al., 2009). Other flagellates on the other hand contribute < 20 % of all marine species, although diversity is still high (Simon et al., 2009). Dinoflagellates and flagellates have a large size range from 1 µm up to several 100 µm, and thus are important components of the pico-, nano-, micro- and meso-phytoplankton. Dinoflagellates are generally at the upper end of this range and flagellates at the lower (Simpson and Sharples, 2012), but flagellates can form colonies so large that they are visible to the naked eye. One such flagellate is *Phaeocystis* (Thornton, 2012), which is a major producer of the cloud formation agent Dimethyl sulphide (DMS) and therefore a key player in climate regulation (Stefels and Van Boekel, 1993, Ayers and Gillett, 2000). Dinoflagellates and flagellates are key contributors of primary production in the global ocean after diatoms (Uitz et al., 2010, Thornton, 2012), with coccolithophores and chlorophytes alone estimated to contribute approximately 20 % of net oceanic primary production (Rousseaux and Gregg, 2014). However, many marine dinoflagellates and flagellates are not autotrophs. Approximately half of dinoflagellate species are heterotrophic, with the other half acquiring nutrition through photosynthesis, although that does not imply autotrophy as many dinoflagellates also employ mixotrophy (Gómez, 2012). Similarly, flagellates are nutritionally diverse and employ autotrophy, mixotrophy or heterotrophy (Sleigh, 2000). Photosynthetic dinoflagellate species contain the major accessory pigments peridinin, diadinoxanthin and dinoxanthin, which give them their typical golden brown colour, and photosynthetic flagellates exhibit an array of pigment compositions (Jeffrey and Vesk, 1997). As the name suggests both dinoflagellates and flagellates have flagella, which are whip-like locomotory appendages. Dinoflagellates possess two flagella and flagellates possess one or more flagella, as many as eight for some prasinophytes (Tomas, 1997). These flagella propel dinoflagellates and flagellates through the water at documented speeds of 50 – 1500 µm s^{-1} (Kamykowski and McCollum, 1986, Levandowsky and Kaneta, 1987, Sommer, 1988) and 75 – 450 µm s^{-1}

(Sommer, 1988) respectively. This swimming ability allows for vertical migration in response to resource cues and is thus a mechanism for achieving and maintaining maximal rates of photosynthesis and growth through exploitation of resource gradients (Eppley et al., 1968, Cullen and Horrigan, 1981, Raven, 2000). For example, in a stratified water column where there are opposing gradients of nutrient concentrations and light availability. However, maximum growth rates of dinoflagellates and flagellates are typically ≤ 2.5 divisions d^{-1} (Furnas, 1990), with dinoflagellate growth rates often being < 1 division d^{-1} (Banse, 1982, Tang, 1995), which may be attributed to their lesser photosynthetic capacity as a result of their lower chlorophyll to carbon ratios (Chan, 1980, Tang, 1996), and high respiratory losses (López-Sandoval et al., 2014). Dinoflagellates are typically divided into the thecate (armoured) and athecate (unarmoured), where thecate forms have thick cellulose plates and athecate forms do not (or are inconspicuous) (Simon et al., 2009). Similarly, flagellates can have organic plates or scales covering the cell (Simon et al., 2009). One particularly prominent and unique example being the coccolithophores, which produce calcified scales known as coccoliths and are key in the global carbon cycle, being responsible for approximately half of all modern calcium carbonate precipitation in the ocean (Milliman, 1993) and approximately 10 % of organic carbon exported to the ocean interior globally (Jin et al., 2006). Plates and scales confer greater mechanical strength, potentially serving as a protection mechanism, possibly enhanced by having projecting spines or protuberances as seen in many dinoflagellates (Tomas, 1997). A supposition supported by observations of avoidance of dinoflagellates with spines as prey items (Verity and Paffenhofer, 1996). Thecate dinoflagellates have been documented to form large, unusually cohesive, rapidly sinking aggregates more rich with particulate organic carbon and nitrogen, and chlorophyll than more common types of marine snow, indicating thecate dinoflagellates could be key contributors of particulate organic matter flux to the seabed (Alldredge et al., 1998). In coastal areas dinoflagellate and flagellate species that produce toxins are common, with approximately 75 - 80 % of toxic (harmful algal bloom - HAB) species being dinoflagellates (Cembella, 2003). Toxicity has been suggested to have the benefit of providing potential means of refuge from grazers (Durham and Stocker, 2012), but for the rest of the ecosystem, toxicity can have a considerable negative impact as it percolates through the food web (Smayda, 1997, Lehane and Lewis, 2000).

Cyanobacteria

Cyanobacteria have existed for around 3.5 billion years, being the first organisms to release oxygen into the atmosphere, and the origin of all other phytoplankton as photosynthesising eukaryotes evolved by incorporating cyanobacteria into their own cells (Graham and Wilcox,

2000). However, the significance of these organisms to the marine ecosystem has only been uncovered in the past 40 years. These photosynthetic bacteria are the smallest of the phytoplankton in the marine ecosystem, belonging to the pico-phytoplankton at approximately 0.2 – 2 μm in size. They are also the only prokaryotic phytoplankton, meaning that they have no nucleus or any other membrane bound organelle (Simpson and Sharples, 2012). There are just four living marine cyanobacteria genera (Sournia et al., 1991), but numerically they are the most dominant phytoplankton in the world's oceans (Simpson and Sharples, 2012). The most abundant and common cyanobacteria genera are *Synechococcus* and *Prochlorococcus* (Simon et al., 2009), whilst the genera *Trichodesmium* and *Crocosphaera* are restricted to tropical regions, but unlike *Synechococcus* and *Prochlorococcus* are nitrogen fixers and thus play a key regulating role in the nitrogen cycle (Zehr et al., 2007). *Synechococcus* is distributed throughout the world's oceans and seas, although rarer in polar latitudes, and *Prochlorococcus* is ubiquitous between the latitudes of 40 °N and 40 °S, with population declines past these latitudinal limits and possible absence at temperatures below 15 °C (Partensky et al., 1999, Zubkov et al., 2000, Calvo-Díaz et al., 2004, Flombaum et al., 2013). *Prochlorococcus* is unique within the phytoplankton, as it is the only species known to possess a distinct divinyl derivative of chlorophyll a as the main pigment compound (Chisholm et al., 1988), and in *Synechococcus*, the green colouration of chlorophyll a is often concealed by carotenoids such as β carotene and water soluble accessory pigments such as phycocyanin and phycoerythrin (Jeffrey and Vesk, 1997). *Synechococcus* and *Prochlorococcus* are major primary producers, estimated to contribute 16.7 % and 8.5 % of net oceanic primary production respectively (Flombaum et al., 2013), and grow rapidly, with growth rates of 3 division d^{-1} (Furnas, 1990) and 1 divisions d^{-1} (Partensky et al., 1999) reported respectively. Potentially the biggest advantage for *Synechococcus* and *Prochlorococcus* is their small size, which allows them to acquire nutrients at submicromolar concentrations and thus thrive in nutrient poor environments. However, as nutrients increase they can be outcompeted by larger phytoplankton, so their biomass tends to negatively correlate with nutrient concentrations and the associated meso-, micro-, and nano-phytoplankton biomass (Agawin et al., 2000). Other adaptations of these cyanobacteria include the possession of light-harvesting apparatus that is uniquely adapted to the spectral quality of light in the ocean (Wood, 1985), and in the case of some isolates of *Synechococcus*, the ability to swim (Waterbury et al., 1985). These isolates can move at speeds of 5 – 25 μm s^{-1} in the absence of any motile apparatus and use this motility to respond to gradients in sources of nitrogen (Waterbury et al., 1985, Willey and Waterbury, 1989); a potential mechanism for exploiting nutrient resources to maintain and maximise growth, such as in a stratified water column.

Ciliates

Ciliates are typically classified as micro- or meso-zooplankton, yet like cyanobacteria and microscopic algae they have a key role in the microbial food web (Simpson and Sharples, 2012), and many photosynthesise (Stoecker et al., 1989). Since these ciliates function similarly to phytoplankton they can be considered part of the phytoplankton and are now often included in routine phytoplankton counts. Photosynthetic ciliates harbour photosynthetic pigments such as chlorophyll and phycoerythrin in isolated plastids or in algal endosymbionts within their cytoplasm (Parsons and Blackbourn, 1968, McManus and Fuhrman, 1986, Laval-Peuto and Rassoulzadegan, 1988). They include the aloricate ciliate *Mesodinium rubrum* (aka *Myrionecta rubra*), the only known obligate photoautotroph, and various mixotrophic aloricate and loricate ciliates of the orders Oligotrichida and Tintinnida (Lindholm, 1985, McManus and Fuhrman, 1986, Stoecker et al., 1987, Laval-Peuto and Rassoulzadegan, 1988, Stoecker et al., 1989). Photosynthetic ciliates are most common in coastal summer waters and can contribute significantly to primary production (Stoecker et al., 1987, Stoecker et al., 1989, Stoecker et al., 1991). In fact, *Mesodinium rubrum* has the highest rate of primary production of any aquatic microorganism on record at 2000 mg C m^{-3} h^{-1} (Smith and Barber, 1979). *Mesodinium rubrum* is also associated with hypoxic and anoxic events, and thus is considered a HAB species (Safran, 2009). Ciliates can exhibit high growth rates under favourable conditions, with maximum growth rates of 0.3 - 2.2 divisions d^{-1} documented (Montagnes, 1996, Pérez et al., 1997, Yih et al., 2004). Ciliates are motile and can undergo vertical migration by beating their cilia in response to environmental cues. It has been suggested this migratory behaviour helps maximise photosynthesis and growth as it allows for efficient exploitation of resources (Stoecker et al., 1989). In a stratified water column motility can allow photosynthetic ciliates to take advantage of nutrients at the base of/below the pycnocline and high light surface waters (Stoecker et al., 1989). Mixotrophic ciliates and *Mesodinium rubrum* have high swimming speeds, with reported speeds of 2 – 3 m h^{-1} (Buskey et al., 1993) and 2 – 7 m h^{-1} (Smith and Barber, 1979) respectively. It has been proposed that in addition to resource exploitation, fast swimming is also a mechanism to resist predation (Pérez et al., 1997). This may particularly be the case for *Mesodinium rubrum*, which can achieve burst swimming speeds of 8 mm s^{-1} (Crawford and Purdie, 1992). Another advantage of pigmented ciliates is that they likely obtain inorganic nutrients when ingesting other cells, allowing for maintenance of growth in nutrient limiting conditions (Stoecker et al., 1989).

Table 1.1. Key properties of each of the major phytoplankton groups, including percentage contribution to the total number of marine phytoplankton species described (Simon et al., 2009), estimated percentage contribution to net oceanic primary production (Mann, 1999, Flombaum et al., 2013, Rousseaux and Gregg, 2014), estimated percentage contribution to organic carbon exported to the ocean interior globally (Dugdale and Wilkerson, 1998, Jin et al., 2006), maximum documented growth rates (Furnas, 1982, Furnas, 1990, Montagnes, 1996, Pérez et al., 1997, Partensky et al., 1999, Yih et al., 2004) and size classification (Simpson and Sharples, 2012). NQ indicates values that have not been specifically quantified.

Phytoplankton group	% of marine species described	% contr. to net 1ry prod.	% contr. to carbon export	Max. growth rates (divisions d^{-1})	Size classification
Diatoms	~ 40	40 – 45	40 – 50+	2 - 6	nano-, micro- and meso-
Dinoflagellates	~ 40	> 20	NQ	≤ 2.5	pico-, nano-, micro- and meso-
Flagellates	~ 20		> 10		
Cyanobacteria			NQ		
• *Prochlorococcus*		8.5		1	pico-
• *Synechococcus*		16.7		3	pico-
Ciliates	NQ	NQ	NQ	0.3 – 2.2	nano-, micro- and meso-

1.1.2. Natural assemblages of marine phytoplankton

Natural assemblages of phytoplankton are taxonomically diverse, typically consisting of multiple species from multiple different taxonomic groups that successfully coexist, with maximum diversity associated with intermediate levels of phytoplankton carbon biomass (Irigoien et al., 2004). The situation whereby a wide range of phytoplankton are supported by a limited range of resources, associated with relatively little competitive exclusion is described by the 'paradox of the plankton' (Hutchinson, 1961), for which a myriad of solutions have been offered over the past five decades as summarised by Wilson (2011). Two key mechanisms that can explain the high diversity of natural phytoplankton assemblages are 'alpha-niche differentiation' and 'environmental fluctuation', both of which are stabilising mechanisms originally classified by Connell (1978), focusing on intraspecific competition relative to interspecific competition (Wilson, 2011). 'Alpha-niche differentiation' is a mechanism whereby exclusion of species by interspecific interference can be prevented. Therefore, co-existence is promoted if different species occupy differing alpha niches. Niche differentiation can include nutrient requirement, most notably silica in the case of diatoms, nutrient source, such as use of nitrate versus ammonium, and light requirement, as seen for high light flora and shade flora

(Titman, 1976, Wilson, 2011). 'Environmental fluctuation' is based upon variation in external factors generating co-existence and can be divided into two key sub-mechanisms: (1) 'relative non-linearity', a dynamic co-existence mechanism driven by endogenous control of resource dynamics that arises when the response of two (or more) species to a shared resource is different, and (2) 'the storage effect', a dynamic co-existence mechanism driven by exogenous control of resource dynamics that arises when temporal differences exist between species in their competitive abilities, species persist through unfavourable conditions and there is positive temporal covariation between phases of low competition and high growth potential (Chesson, 1994, Chesson et al., 2004, Chesson, 2008, Wilson, 2011). The co-existence mechanisms of 'alpha-niche differentiation' and 'environment fluctuation' are both dependent upon environmental variability, thus fluctuations in environmental parameters stand to alter community structure, whilst maintaining diversity. On the other hand, monospecific communities are occasionally observed in the world's oceans and seas, possibly representing climax communities formed due to stability of environmental parameters (Connell, 1978, Connell, 1979).

1.1.3. The importance of marine phytoplankton

Phytoplankton are small in size and biomass, being responsible for less than 1 % of global photosynthetic biomass. However, these microscopic organisms have a key role in the dynamics and functioning of the marine ecosystem, controlling biogeochemical cycles, sustaining aquatic food webs and regulating the global climate (Falkowski et al., 2004). Phytoplankton are ubiquitous in the photic zone and their ability to photosynthesise, incorporating carbon dioxide into organic matter with oxygen as a byproduct, means they are central in carbon and oxygen cycling. Photosynthesis by phytoplankton accounts for approximately half of the oxygen that we breathe (Hoppenrath et al., 2009), more than 45 % of global net primary production (Field et al., 1998) and is one of the largest sinks of atmospheric carbon dioxide (Hoppenrath et al., 2009). Phytoplankton primary production supports life of non-photosynthetic organisms and thus phytoplankton form the foundation of marine food webs, with more than 99 % of all oceanic species relying, directly or indirectly, on phytoplankton for food (Hoppenrath et al., 2009). Phytoplankton also play a key role in the microbial loop (Fig.1.2), which is a return pathway for dissolved organic matter (DOM; inclusive of dissolved organic carbon (DOC) and dissolved organic nutrients (nitrogen (DON), phosphorus (DOP)) released by phytoplankton through a range of processes, including 'sloppy feeding' and cell lysis. DOM is not available to larger heterotrophs, but heterotrophic bacteria can consume DOM, a fraction of which is consumed by microzooplankton. Phytoplankton play

a part in returning DOM to the food web as they utilise the carbon dioxide released by the heterotrophic bacteria via respiration during DOM catabolism. Heterotrophic bacteria can also remineralise organic nutrients (DON and DOP) to inorganic forms (Fig. 1.3), which can then be used by phytoplankton in regenerated primary production (Azam et al., 1983, Buchan et al., 2014).

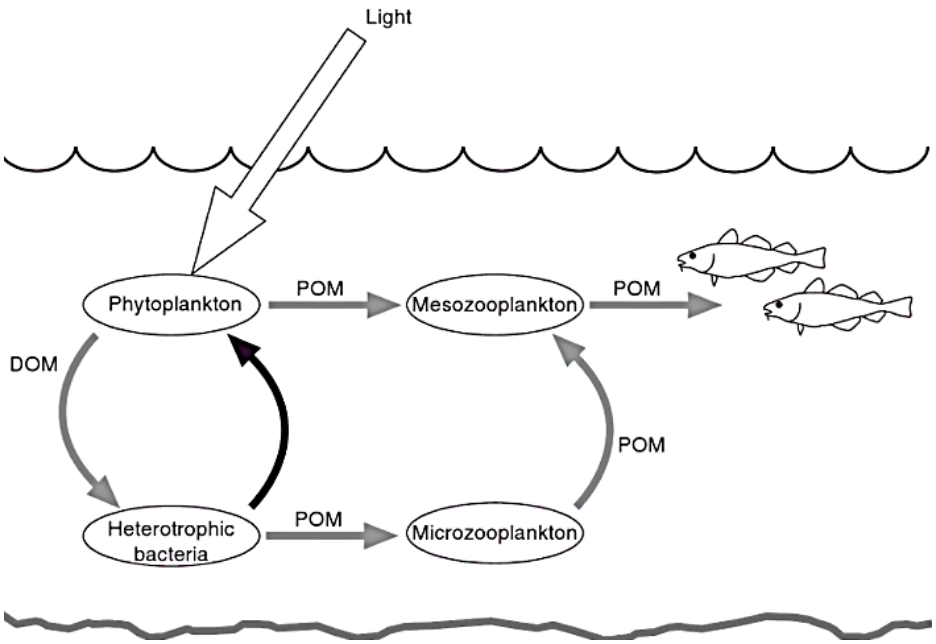

Figure 1.2. Schematic summary of the microbial loop. Arrows indicate the pathways of organic matter (particulate - POM and dissolved - DOM), and the black arrow specifically indicates the return of POM back to phytoplankton. Taken from Simpson and Sharples (2012).

Not all DOC released into the water column is transferred back to the food web via the microbial loop. Instead a fraction of DOC is processed by the microbial carbon pump (Jiao et al., 2010), which acts simultaneously alongside the biological pump (Honjo et al., 2008, Marañón, 2009, Passow and Carlson, 2012) to sequester phytoplankton derived carbon in the ocean (Fig. 1.3). The biological pump and microbial carbon pump, while serving a common purpose, are conceptually different. The biological pump involves transport of fixed organic carbon to the deep ocean via gravitational sinking (Honjo et al., 2008, Passow and Carlson, 2012), with some 20 % of phytoplankton global net primary production exported to the ocean's interior (Laws et al., 2000). Whereas, the microbial carbon pump does not involve physical transportation of organic carbon, instead it involves transformation of labile DOC to recalcitrant DOC by heterotrophic bacteria (Jiao et al., 2010). Since the biological and microbial carbon pumps are mechanisms that can significantly influence the marine ecosystem's capacity to store atmospheric carbon dioxide, these mechanisms and the phytoplankton that drive them have a key role in climate regulation (Falkowski et al., 1998, Falkowski, 2012). This

is especially seen in modern times, as the oceans are estimated to have taken up approximately 40 % of anthropogenic carbon dioxide since the start of the industrial revolution, thus in part buffering the effects of its increasing levels, partially ameliorating climate warming (Reid et al., 2009). Phytoplankton have a further role in climate regulation through their generation of DMS, which promotes cloud formation and thus enhanced albedo, and may also help offset anthropogenically driven climate warming (Ayers and Gillett, 2000).

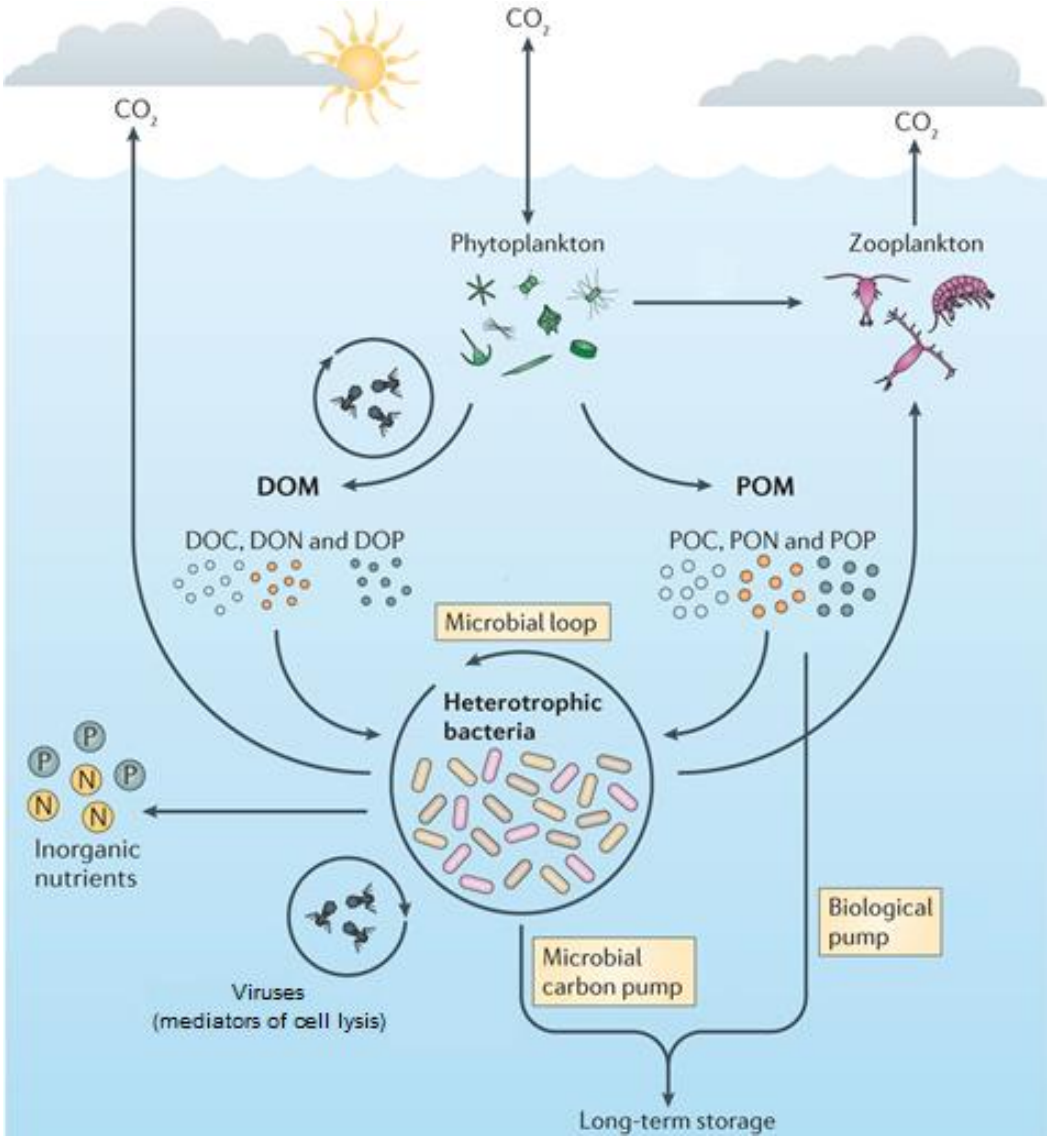

Figure 1.3. Schematic of the cycling of organic matter in the ocean, including the microbial loop and carbon pump, and the biological pump. Taken from Buchan et al. (2014).

In addition to regulating the climate, phytoplankton are key indicators of climate (Falkowski and Oliver, 2007). Phytoplankton are sensitive to modifications within their environment, with environmental parameters such as temperature, nutrient concentrations and turbulence affecting phytoplankton physiology at an individual level (Beaugrand et al., 2000, Beaugrand,

2005, Paerl et al., 2007, Simpson and Sharples, 2012). As their growth is rapid, phytoplankton populations respond quickly to any such changes and since they form the foundation of marine food webs, any impact of environmental change on phytoplankton populations can cascade through the food web, potentially having an effect on an entire ecosystem (Beaugrand, 2005, Paerl et al., 2007). Therefore, phytoplankton can be studied as relevant indicators of biogeochemical and ecological change, and by association climate change (Beaugrand, 2005, Falkowski and Oliver, 2007, Paerl et al., 2007). Phytoplankton are particularly ideal subjects of study as they have relatively simple life history characteristics (Litchman et al., 2007, Litchman and Klausmeier, 2008), are biogeographically organised over large spatial scales, exhibiting distinctive distribution patterns across the global oceans (Follows et al., 2007, Cermeño et al., 2010), and can be assessed *in situ* and in the laboratory.

1.2. Subsurface chlorophyll maxima of the stratified shelf seas

1.2.1. What is a subsurface chlorophyll maximum?

In stratified shelf seas (seas that overlie continental shelf, the submerged portion of a continent, located between the surface continents and the deep oceans; Simpson and Sharples, 2012) a mid-water accumulation of phytoplankton is often located in close association with the pycnocline, such that a local subsurface maximum in chlorophyll concentration (SCM) can be detected. Shelf sea stratification can be driven by temperature, salinity or both, and varies regionally, with many of the shelf waters in the tropics and subtropics being permanently stratified, whilst in temperate and high latitude waters stratification is seasonal (Cullen, 1982, Longhurst, 1998, Holm-Hansen and Hewes, 2004, Huisman et al., 2006, Martin et al., 2010, Howard et al., 2013). The focus of research presented in this thesis is the seasonal SCM associated with thermal stratification in shallow tidal temperate shelf waters.

In a stratified water column the pycnocline acts as a barrier to free/unhindered vertical transport of properties between the photic surface layer and the darker, nutrient replete deeper water. Consequently, the surface layer becomes nutrient deplete, divided from deeper nutrient rich waters by the nitracline (Sharples et al., 2001, Williams et al., 2013b), and as such, two opposing resource gradients exist in stratified waters. Since the pycnocline presents an interface at which both light availability and nutrient concentration are sufficient to support phytoplankton growth, explicably the SCM is generally located within/close to the pycnocline (Pingree et al., 1978, Holligan et al., 1984a, Sharples et al., 2001, Huisman et al., 2006).

However, the SCM has been documented to be more tightly coupled with the nitracline than the pycnocline on occasion (Cullen and Eppley, 1981). SCM chlorophyll concentrations observed in stratified shelf sea waters can be relatively low, < 1 μg l^{-1} (Martin et al., 2010, Hickman et al., 2012), but SCM with much greater peak chlorophyll concentrations have often been reported. For example, Martin et al. (2010) observed SCM with chlorophyll concentrations of up to 4.52 and 16.65 μg l^{-1} in addition to low chlorophyll SCM in the Canadian Arctic; Rines et al. (2010) reported SCM chlorophyll concentrations of 12 – 40 μg l^{-1} in Monterey Bay, California; Sharples et al. (2001) reported concentrations of 14 - 80 μg l^{-1} in the southern Celtic Sea/ Western Channel; and Sullivan et al. (2010a) even reported concentrations of 100 μg l^{-1} in Monterey Bay, California. In some cases, however, higher chlorophyll concentrations have been related to a lower carbon:chlorophyll ratio as this ratio varies with photophysiological status (Steele, 1964, Cullen, 1982, Fennel and Boss, 2003, Cullen, 2015). However, while in the open ocean the chlorophyll peak can be attributed entirely to higher chlorophyll content of cells, i.e. is not a biomass maximum (Veldhuis and Kraay, 2004), in shelf seas the maximum in chlorophyll concentration does typically represent the phytoplankton biomass maximum (Holligan et al., 1984b, Sharples et al., 2001, Simpson and Sharples, 2012). Consequently, the shelf sea SCM has a much more significant role in augmenting annual oceanic primary production compared to the open ocean SCM (Simpson and Sharples, 2012).

While the existence of a SCM within a stratified water column may be initially explained by the vertically opposing gradients of light and nutrients (Cullen, 1982, Cullen, 2015), mechanisms that control SCM development and maintenance are still under debate (Durham and Stocker, 2012, Cullen, 2015). Both physical and biological processes have been proposed, all of which are not exclusive and could have joint governing roles over SCM. These mechanisms include, although are not limited to, *in situ* growth, where net growth is specifically possible in waters above the compensation depth given sufficient nutrient concentrations (Sharples and Tett, 1994, Sharples et al., 2001, Birch et al., 2008); active accumulation of phytoplankton by convergent swimming and buoyancy regulation guided by environmental cues that direct cells towards desirable conditions, i.e. a depth where light and nutrients are available (Cullen and Eppley, 1981, Macintyre et al., 1997, Ralston et al., 2007, Stacey et al., 2007); passive sinking of cells to the density interface where cells can reach neutral buoyancy and so are maintained within the pycnocline (Steele and Yentsch, 1960, Alldredge et al., 2002), or cells accumulate due to a reduction in sinking velocity associated with changes in the intensity of turbulent mixing (Ruiz et al., 2004, Macías et al., 2013); reduced/differential zooplankton grazing due to

the presence of toxic or unpalatable phytoplankton (Bjørnsen and Nielsen, 1991, Turner and Tester, 1997, Kononen et al., 1998, Webster et al., 2016); and convergence of phytoplankton by mechanisms associated with vertical shear, namely straining and gyrotactic trapping (Dekshenieks et al., 2001, Stacey et al., 2007, Birch et al., 2008, Durham et al., 2009). All of the above were discussed to some extent by Durham and Stocker (2012) and Cullen (2015), and are represented in Figure 1.4.

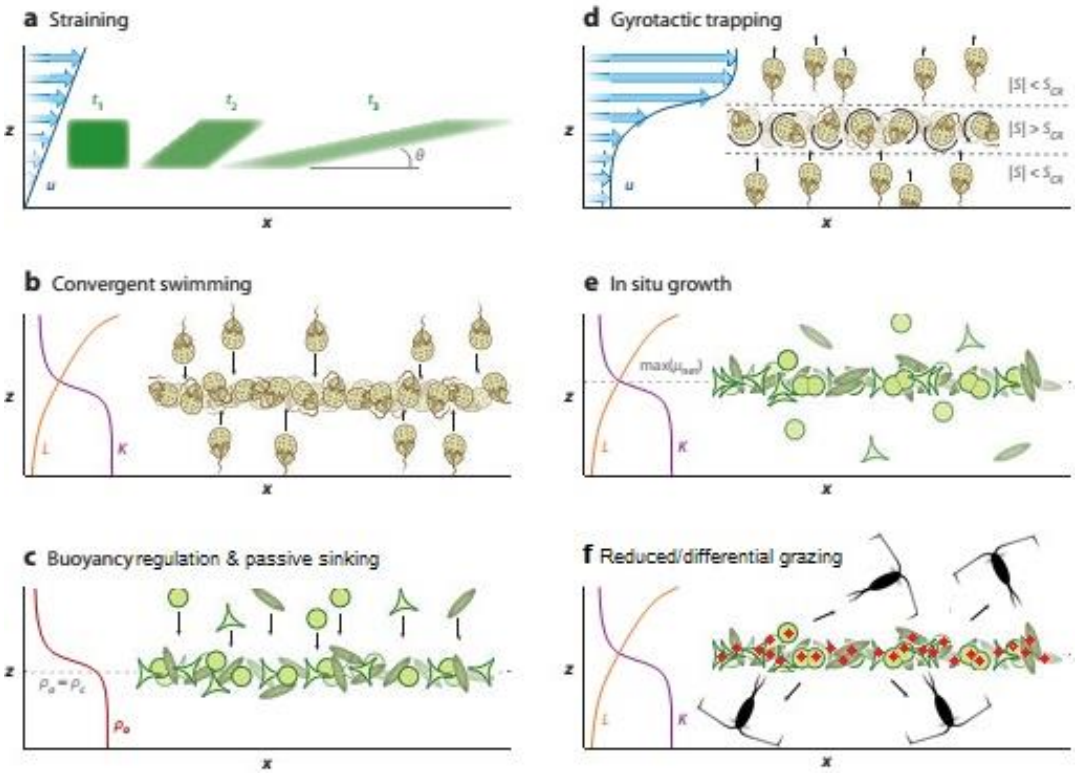

Figure 1.4. Mechanisms of SCM development and maintenance in a stratified water column, where z represents depth and x represents distance. **(a)** Straining, a mechanism of convergence due to vertical shear. Straining transforms initial time (t_1) horizontal phytoplankton heterogeneity into a thinner phytoplankton maximum (t_3) by progressively tilting (t_2) a phytoplankton patch as a result of vertical shear of the horizontal current (u) causing differential advection of the phytoplankton patch. **(b)** Active accumulation by convergent swimming driven by environmental cues, e.g. light (L) and nutrient availability (K). **(c)** Active accumulation by buoyancy regulation to reach optimal growth conditions as provided within the pycnocline, and passive sinking of cells to the depth of neural buoyancy (dotted line, where density of the surrounding water (ρ_o) = density of the cell (ρ_c)). **(d)** Gyrotactic trapping, another mechanism of convergence due to vertical shear. As motile cells migrate into a region where the magnitude of the shear rate (|S|), exceeds a threshold S_{CR}, they can be trapped at that depth due to high vertical shear. **(e)** Enhanced *in situ* growth can occur in association with the pycnocline as the light (L) and nutrient (K) environment is suitable for growth. Net growth (μ_{net}) (maximum μnet is represented by the dotted line) is specifically achieved in waters above the compensation depth given sufficient nutrients. **(f)** Reduced/ differential grazing, whereby grazers, such as copepods, avoid an SCM due to the

presence of toxic or unpalatable species (represented by red on the schematic), allowing an SCM to increase its chlorophyll concentration. Taken (with some adaptation) from Durham and Stocker (2012).

SCM began to be recognised when Lorenzen (1966) developed and introduced a method for the continuous measurement of *in vivo* chlorophyll. Over fifty years later, these features are routinely observed and appreciated to be ubiquitous in the stratified waters of the shelf seas (Cullen, 1982, Cullen, 2015). More recent technologies, including AUVs, autonomous profilers, towed undulators and airborne lidar systems have clearly demonstrated the contiguous and persistent nature of SCM, revealing horizontal length scales of several, even hundreds to thousands of kilometres and durations of several weeks (Churnside and Donaghay, 2009, Wang and Goodman, 2009, Martin et al., 2010, Sullivan et al., 2010a, Hickman et al., 2012, Zhang et al., 2012).

SCM in the stratified waters of the shelf sea ecosystem vary widely in thickness, in the order of 10s of meters (Cullen, 1982, Sharples et al., 2001, Martin et al., 2010, Rines et al., 2010, Hickman et al., 2012, Fishwick, 2017), but often occur as thin layers (SCMTL; subsurface chlorophyll maximum thin layers) (Durham and Stocker, 2012), with studies quantifying the occurrence of thin layers in stratified shelf waters reporting them to be present 21 - 87 % of the time (Dekshenieks et al., 2001, Sullivan et al., 2010a). As the name suggests SCMTL are limited in their vertical extent, but can span several kilometres and persist anywhere from a few hours to a few weeks (Bjørnsen and Nielsen, 1991, Cowles et al., 1998, Dekshenieks et al., 2001, Cheriton et al., 2009, Durham and Stocker, 2012). Beam (sound and light) attenuation/ absorption and chlorophyll-fluorescence profiling have provided means to regularly observe these thin features in a range of shelf environments (Bjørnsen and Nielsen, 1991, Dekshenieks et al., 2001, Sharples et al., 2001, McManus et al., 2003, Cheriton et al., 2009, Rines et al., 2010, Sullivan et al., 2010a, Donaghay and Ryan, 2012, Durham and Stocker, 2012, McManus et al., 2012, Churnside and Marchbanks, 2015, Ríos et al., 2016). Yet they remain greatly under-sampled by traditional techniques, such as CTD with Niskin carousel samplers, particularly relative to broader SCM.

As summarised in Sullivan et al. (2010b) and Durham and Stocker (2012) many independent sets of criteria have been proposed to identify SCMTL that are specific to the various environments and methodologies used in different SCMTL studies, ranging from chlorophyll-fluorescence profiling in the tropical stratified waters offshore of Oahu, Hawaii (McManus et al., 2012), to spectral absorption profiling in the temperate stratified waters of East Sound,

Washington (Dekshenieks et al., 2001). Nevertheless, all of these different sets of criteria have been identified to share three common requirements (Sullivan et al., 2010b, Durham and Stocker, 2012): (1) thin layer structure must persist in time and space; (2) the intensity of the thin layer must meet a minimum signal strength; and (3) the thickness of the thin layer must be below a certain maximum, and there must be a clearly-defined method for determining vertical thickness. These shared criteria for identification of a SCMTL set a framework for developing criteria to identify SCMTL in future studies, which is necessary for consistent comparison of SCMTL observed by different investigators in diverse locations and using various instrumentation. Therefore, in this thesis to distinguish a SCMTL from a broader SCM the criteria adhered to followed the above framework, and were specifically based upon those presented by Dekshenieks et al. (2001). These were as follows:-

1. Vertical thickness of the thin layer must not exceed 5 m, where thickness is measured at half maximum intensity of the chlorophyll signal, i.e. at half layer intensity (Fig. 1.5).
2. The peak chlorophyll concentration must be at least 3 times greater than the background intensity values, where background values are those taken from the bottom mixed layer (Fig. 1.5). To determine if a chlorophyll peak adhered to this requirement, the ratio of peak chlorophyll concentration to background chlorophyll concentration was determined.
3. The thin layer must exist as a persistent feature, occurring in at least two CTD casts.

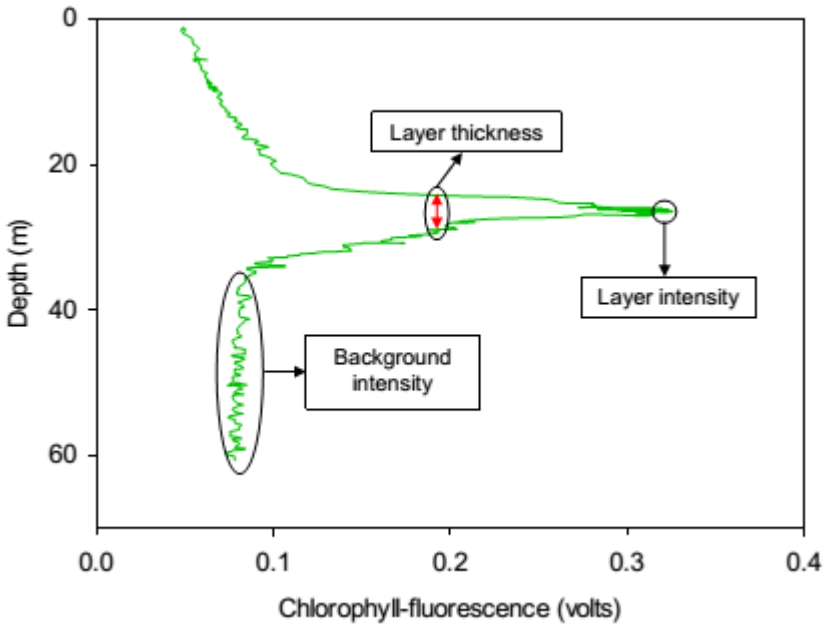

Figure 1.5. Terminology used in criteria to define a SCMTL: background intensity, layer intensity and layer thickness.

1.2.2. The importance of studying SCM in the stratified shelf seas

The shelf seas account for approximately 9 % of the area of the global ocean (Fig. 1.6) and less than 0.5 % of the volume, since they are typically < 200 m depth (Simpson and Sharples, 2012). Yet, they are estimated to be responsible for 15 – 30 % of annual oceanic primary production (Muller-Karger et al., 2005), being 2.5 times more productive than the open ocean on average (Simpson and Sharples, 2012). This productivity supports significant fisheries and particulate carbon export, with more than 90 % of global fish catches coming from the shelf seas and adjacent upwelling areas of the continental slope (Pauly et al., 2002), and greater than 40 % of global annual carbon export occurring in shelf seas (Muller-Karger et al., 2005, Jahnke, 2010). One fundamental difference between the shelf seas and the open ocean, and a key reason why the shelf is so productive, is water column depth. The open oceans are on average 3.8 km deep, as opposed to the < 200 m for the shelf. A shallow water column means deep water and the seabed are in much closer proximity to the photic zone, thus recycled organic material always has the potential to be returned to this zone given sufficient turbulent mixing (Simpson and Sharples, 2012). A shallow water column also enhances longer-term POC export and therefore the shallow depth of the shelf seas also has a direct role in their high particulate carbon export potential relative to the open ocean (Simpson and Sharples, 2012). In the case of SCM, these are generally more productive on the shelf compared to the open ocean because, as noted in section 1.2.1., shelf SCM typically represent a biomass maximum and are not just a result of changes in the chlorophyll content of phytoplankton cells as typically seen in the open ocean. This difference may be principally attributed to pycnocline depth, and tidal mixing or internal wave mixing caused by tidal flows over an uneven seabed in shelf seas. Specifically, in shelf seas the presence of the opposing deepening and shallowing forces of wind mixing and tidal mixing respectively (as opposed to just wind mixing in the case of the open ocean) tends to result in a shallower pycnocline allowing the SCM to receive more light; and tidal/internal wave mixing on the shelf promotes relatively high nitrate fluxes into the SCM, in the order of 1 – 10 mmol m^{-2} d^{-1} compared to only 0.1 mmol m^{-2} d^{-1} (Lewis et al., 1986, Planas et al., 1999) in the open ocean gyres where a strong source of turbulence at the pycnocline is lacking (Simpson and Sharples, 2012). Overall, given the significance of the shelf seas for global biogeochemical cycling, trophic dynamics and their socio-economic importance for the supply of living marine resources, particularly relative to the open ocean, it is necessary to gain an improved understanding of shelf sea phytoplankton, especially in the case of high biomass communities, such as that presented by the SCM.

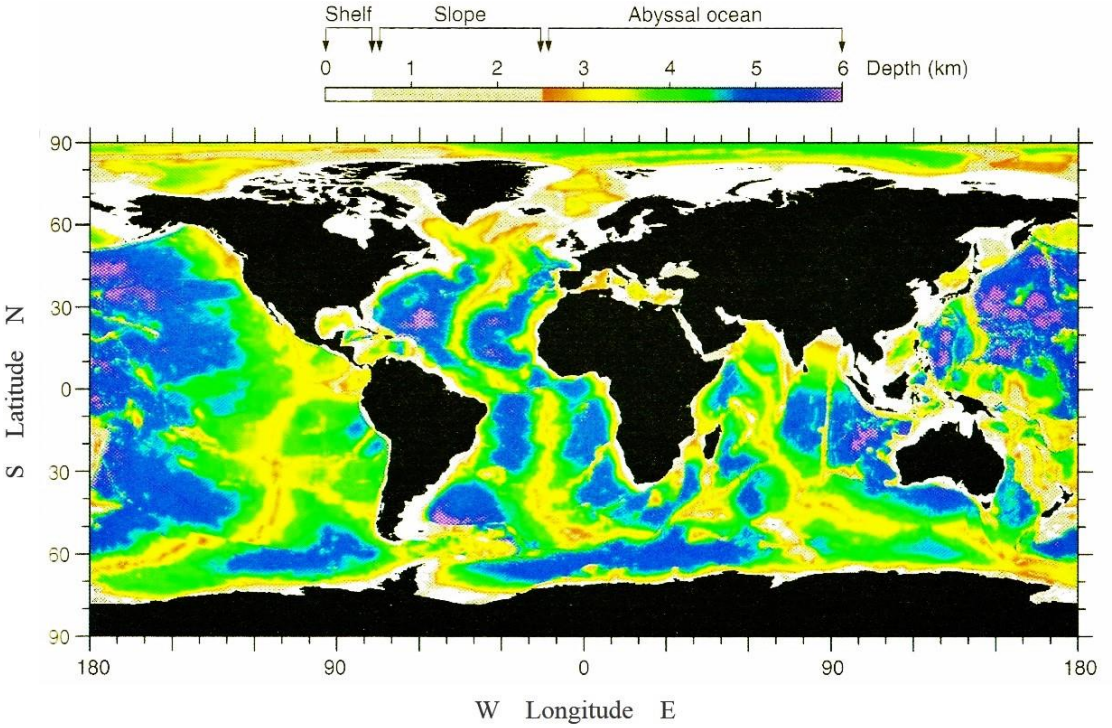

Figure 1.6. Global ocean depths based on GEBCO bathymetry, split by shelf, slope and abyssal ocean, revealing the limited coverage of the shelf seas. Taken from Simpson and Sharples (2012).

In a shelf sea stratified water column the contribution of chlorophyll (and biomass) made by the SCM is very significant relative to the rest of the water column. SCM have been observed to contain chlorophyll concentrations greater than half an order of magnitude, even up to two orders of magnitude greater than that found in the surface layer (Steele, 1964, Holligan and Harbour, 1977, Holligan et al., 1984a, Sharples et al., 2001, Martin et al., 2010, Rines et al., 2010, Sullivan et al., 2010a). Such accumulations of phytoplankton can only be maintained when carbon fixation exceeds losses by passive sinking of cells, turbulent mixing of cells out of the SCM, active motion of cells, and mortality by grazing or lysis (Sharples et al., 2001, Cullen, 2015). The high phytoplankton concentrations often reported for SCM reflect a high potential for primary production and by association, export production and trophic interaction.

Studies of primary production within stratified waters of the shelf seas have demonstrated that the SCM is generally the primary production maximum (Cullen and Eppley, 1981, Holligan et al., 1984c, Estrada et al., 1993, Richardson et al., 2000, Hickman et al., 2012, Kwak et al., 2014), with varying estimates of primary production documented for the stratified water column. For example, Hickman (2012) reported estimates of water column primary production ranging 113 – 490 mg C m^{-2} d^{-1}, whilst Barnes (2015b) reported estimates ranging 295 - 997 mg C m^{-2} d^{-1}, and Kwak et al. (2014) reported estimates of 257 - 758 mg C m^{-2} d^{-1}. A significant

proportion of this primary production has been identified to be fuelled by nitrate, i.e. is new production (Holligan et al., 1984c, Richardson et al., 2000, Sharples et al., 2001, Hickman et al., 2012), thus the pycnocline can be considered the main region of new production within the stratified shelf seas (Sharples et al., 2001). Such a significant 'pulse' of production as presented by the SCM within a water column with otherwise relatively low biological activity, has the potential to promote substantial carbon flux to the seabed, as supported by modern- and palaeo-oceanographic evidence (Sancetta, 1994, Kemp et al., 2000, Sharples et al., 2001, Alldredge et al., 2002, Kemp and Villareal, 2013). Furthermore, as phytoplankton production is a vital source of nourishment within the food web, SCM have the potential to play a key role in the sustenance of higher trophic levels, which is supported by observations of predator accumulation at the SCM (Lasker, 1975, Menden-Deuer, 2008, Benoit-Bird et al., 2010, Greer et al., 2013) and correlation between SCM primary production and exploitable living resource yields (Estrada, 1996). A number of HAB species have been observed in SCM, especially SCMTL (Bjørnsen and Nielsen, 1991, Dekshenieks et al., 2001, Alldredge et al., 2002, Rines et al., 2002, Rines et al., 2010, Sullivan et al., 2010a), which can deter grazing and have a detrimental effect on higher trophic levels (Bjørnsen and Nielsen, 1991, Alldredge et al., 2002, Bhat et al., 2006), but also can still provide a good food resource for some planktivorous fish and zooplankton (McManus et al., 2008, Rines et al., 2010). Consequently, the presence of HAB phytoplankton in SCM comes with an alternative set of implications for food web dynamics.

In seasonally stratified temperate and high latitude shelf seas the formation of the SCM is a key part of the seasonal cycle. Typically, the water column is vertically homogeneous in winter with little phytoplankton activity due to convective overturning and weak solar input. In spring increased solar heating promotes stabilisation of the water column allowing phytoplankton to utilise increased light levels and the nutrient replete conditions, triggering the spring bloom. As continued solar heating promotes development and maintenance of stratification, and the spring bloom depletes surface nutrients, a SCM forms as phytoplankton flourish at the pycnocline depth where the nutrient and light supply are sufficient to support growth throughout summer. In autumn, stratification finally breaks down and a surface bloom may ensue due to the 'release' of deep layer nutrients to surface waters. Ultimately water column conditions return to that of winter months (Pingree, 1975, Simpson and Sharples, 2012). SCM that form as part of this seasonal cycle may be of greater significance for the global marine ecosystem than SCM that exist in perennially stratified waters for two key reasons: (1) phytoplankton biomass within seasonal SCM is typically much higher than in permanent SCM (McManus et al., 2012); and (2) the breakdown of stratification at the end of summer in

seasonally stratified shelf seas triggers mass sedimentation of the high phytoplankton biomass constituting the seasonal SCM. This phenomenon, termed the 'fall dump', represents sedimentation of a long-lived episode of considerable primary production and has the potential to generate substantial export production, with significant implications for carbon draw down (Kemp et al., 2000, Kemp and Villareal, 2013).

It is clear that the SCM represents a biogeochemical and trophic hotspot within stratified waters, particularly in regions influenced by seasonal stratification, and is thus of significance for biogeochemical cycling and trophic dynamics. Moreover, shelf seas are potentially highly vulnerable to climate change (Holt et al., 2016) and since their contribution to global primary production, export production and fisheries is so great relative to their contribution to total global ocean area, any impact of climate change on the shelf sea ecosystem may have disproportionate effects on global production and trophic dynamics. Consequently, understanding of these subsurface features is critical for predictions of how the shelf sea ecosystem, and by association the global marine ecosystem will respond to future climate change. Remote sensing cannot be used to monitor SCM as their depth renders them invisible to satellites and as such currently pose a significant challenge for global biogeochemical modelling (Uitz et al., 2006). Instead SCM need to be sampled *in situ*, and while there are many *in situ* studies, the majority only investigate SCM using chlorophyll-fluorescence or beam absorption/attenuation profiling and ignore further biological investigation of the community. This is especially the case for SCMTL, which although known to support substantial biomass, often 50 – 75 % of total water column phytoplankton biomass (Cowles et al., 1998, Holliday et al., 1998, Sullivan et al., 2010b, Ríos et al., 2016), are much less well described compared to broader SCM. Only over the past twenty years has there been an upsurgence of focused studies on thin layers (Durham and Stocker, 2012), recently culminating in the intensive multi-investigator Layered Organization in the Coastal Ocean (LOCO) project conducted in Monterey Bay, California (Sullivan et al., 2010b). A multitude of these studies have been conducted along the west coast of the USA, regularly in Monterey Bay where bottom water turbulence is weak (turbulent diffusivities rarely exceed 10^{-6} m^2 s^{-1} (Steinbuck et al., 2009)) due to small tides. Also, many thin layer studies have often shared common objectives, namely, to quantify thin layer attributes such as depth and maximum chlorophyll concentration (Cowles et al., 1998, Dekshenieks et al., 2001, Rines et al., 2002, McManus et al., 2003, Ryan et al., 2008, Cheriton et al., 2009, Benoit-Bird et al., 2010, Prairie et al., 2010, Sullivan et al., 2010a, McManus et al., 2012, Churnside and Marchbanks, 2015, Ríos et al., 2016), to investigate the spatial and temporal scales of thin layers (Cowles et al., 1998, Dekshenieks et al., 2001, McManus et al.,

2003, Benoit-Bird et al., 2009, Cheriton et al., 2009, Churnside and Donaghay, 2009, Benoit-Bird et al., 2010, Sullivan et al., 2010a, McManus et al., 2012, Ríos et al., 2016), and to assess the relationship between thin layers and the physical environment (Dekshenieks et al., 2001, Rines et al., 2002, McManus et al., 2003, Ryan et al., 2008, Benoit-Bird et al., 2009, Cheriton et al., 2009, Wang and Goodman, 2009, Prairie et al., 2010, Sullivan et al., 2010a, McManus et al., 2012, Churnside and Marchbanks, 2015, Ríos et al., 2016). However, any consideration of phytoplankton community composition within SCMTL investigated in these studies is rare. Therefore, a fundamental understanding of environmental conditions, especially in relation to a relatively weak internal tide, necessary or favourable for the formation and persistence of SCMTL has been developed, and there is an appreciation for the concentrated, recurrent, persistent and contiguous nature of these thin structures. However, a thorough awareness of the significance of thin phytoplankton layers in the global shelf sea ecosystem, and their biogeochemical and ecological implications, especially relative to broader SCM, has not yet been gained. Studies that do investigate phytoplankton within SCM, whether it be SCMTL or broader SCM, most often do not present a detailed quantitative assessment of phytoplankton community structure, which may be attributed to the tedious and time consuming nature of phytoplankton sizing and enumeration by microscopy. Since natural assemblages are typically diverse and the various phytoplankton taxa may have distinct functional roles due to their taxon-specific traits, different SCM communities may present distinct biogeochemical and ecological functionality. Therefore, studying SCM taxonomic community structure and dynamics is key for enhancing our understanding of the influence of SCM communities in biogeochemical cycling, trophic dynamics and climate regulation within the shelf seas.

1.3. Factors affecting SCM phytoplankton in a stratified shelf sea

Environmental factors that can regulate phytoplankton growth and biomass within a SCM in a stratified shelf sea are mainly: (1) strength of stratification, (2) turbulent mixing, (3) irradiance levels, (4) nutrient concentrations, (5) water temperature, (6) salinity, and (7) biological agents.

1.3.1. Stratification and turbulent mixing

Stratification develops when the input of heat and/or fresher water produces more buoyancy than can be dissipated by turbulent mixing and is a prerequisite for the formation of SCM as it presents an interface where both light and nutrients can support growth (Pingree, 1975, Pingree et al., 1978, Holligan et al., 1984a, Sharples et al., 2001, Huisman et al., 2006). The

extent of phytoplankton growth and biomass accumulation within an SCM is governed by the strength of stratification and turbulent mixing. The pycnocline acts to greatly reduce the capacity for vertical transfer of properties, including phytoplankton (Sharples et al., 2001). Therefore, stronger stratification can act to maintain phytoplankton cells within the SCM. However, stratification also reduces transfer of nutrients from deep waters (Sharples et al., 2001), thus very strong stratification could severely depress or inhibit growth within the SCM. Therefore, it follows that an SCM will only develop given that there is some 'background' mixing associated with the pycnocline (Sharples and Tett, 1994).

Turbulent mixing at the pycnocline can be driven by winds, which generate motion of the surface layer over the pycnocline; tides, which generate turbulence from friction between the tidal current and the seabed; and internal waves, which introduce velocity shear across the pycnocline (Simpson and Sharples, 2012). All of these turbulence generating mechanisms can provide the source of energy required to drive a supply of nutrients from the nutrient replete bottom layer across the pycnocline, referred to as the diapycnal nutrient flux. This flux can support substantial new production and phytoplankton growth within the SCM (Sharples and Tett, 1994, Sharples et al., 2001, Rippeth, 2005, Rippeth et al., 2009, Simpson and Sharples, 2012, Williams et al., 2013a, Williams et al., 2013b). For instance, Sharples et al. (2001) estimated a nutrient flux capable of supporting rates of new production as high as 256 mg C m^{-2} d^{-1} within an SCM located in the southern Celtic Sea/ Western Channel. On the other hand, turbulent mixing can act to reduce the phytoplankton biomass within an SCM since mixing will act to erode a chlorophyll peak (Donaghay and Osborn, 1997, Sharples et al., 2001). Yet, vertical turbulent mixing can return sinking phytoplankton, particularly diatoms, back to the pycnocline and the conditions supporting their growth (Simpson and Sharples, 2012). Nevertheless, for an SCM to persist and for its biomass to increase over time phytoplankton growth within the SCM must exceed cell losses caused by mixing, amongst other cell loss mechanisms (Sharples et al., 2001).

Turbulent mixing can also alter the light environment at the SCM, which too can influence phytoplankton growth due to a requirement for light in photosynthesis. Strong winds have the potential to deepen the surface mixed layer and consequently the depth of the pycnocline, reducing the light levels to which SCM phytoplankton are exposed (Simpson and Sharples, 2012). Conversely, strong tides, namely spring tides, can act to move the depth of the pycnocline shallower, such that light levels experienced by the SCM phytoplankton increase.

This period of pycnocline shoaling only persists until tidal flow and current shear decrease on the run up to neap tides (Pedersen, 1994, Sharples, 2008).

1.3.2. Light and nutrients

SCM reflect a compromise of phytoplankton growth exposed to the opposing gradients of nutrients and light in a stratified water column (Cullen, 1982, Huisman et al., 2006). Light is essential for photosynthesis, and it is the products of the photosynthetic reactions, in combination with nutrients, that are vital for the synthesis of many essential cellular components, including amino acids, lipids and nucleic acids (Falkowski and Raven, 1997).

Phytoplankton use light in photosynthesis as the source of energy for the reducing reaction where carbon dioxide is converted to organic matter, with photosynthetic rate tending to increase almost linearly with light intensity until it saturates. Irradiance useful for photosynthesis has a wavelength of 400 – 700 nm and is referred to as photosynthetically active/available radiation (PAR) (Falkowski and Raven, 1997). As light is attenuated by water as well as by absorbing and scattering particles suspended within the water (Kirk, 1994), at the depth of the SCM light levels are typically no higher than 10 % of that at the surface (Holligan et al., 1984a, Simpson and Sharples, 2012). Growth of phytoplankton within the SCM requires the SCM to be located above the compensation depth (Sharples and Tett, 1994, Sharples et al., 2001, Birch et al., 2008), where the compensation depth is defined as the depth at which light is at such a level that photosynthesis just balances the requirements of cellular respiration and grazing (Sverdrup, 1953). Several species identified within SCM are described as shade flora, which are characterised by low light saturated photosynthesis and are inhibited at light levels typical of the surface layer (Ryther and Menzel, 1959, Sournia, 1982b). However, phytoplankton within the SCM tend to have increased photosynthetic pigment within their light harvesting antennae to maximise their light absorption potential (Falkowski and Owens, 1980, Perry et al., 1981, Dubinsky et al., 1986), which is associated with self-shading within the thylakoid membranes. A reduction in light capture efficiency known as the package effect thus ensues (Morel and Bricaud, 1981, Dubinsky et al., 1986, Berner et al., 1989), increasing the energetic cost of photosynthesis and possibly diverting energy that could otherwise be used for growth (Raven, 1986, Falkowski and Raven, 1997). Phytoplankton growth may also be affected by the spectral composition of light within the SCM as different taxa have specific pigment compositions and absorption spectra (Hickman et al., 2009).

Key nutrients required by phytoplankton are the macronutrients nitrogen (assimilated mostly in the form of nitrate, but also as nitrite, ammonium and urea), phosphorus (phosphate), and for diatoms and silicoflagellates silicon (silicate), along with many other additional elements, such as zinc, iron and manganese (Falkowski and Raven, 1997). The minimum nutrient requirement for phytoplankton maintains basal cellular function. Beyond this minimum phytoplankton growth increases asymptotically with increasing nutrient supply and when nutrients are not limiting growth reaches a maximum (Klausmeier et al., 2008). However, nutrients associated with an SCM can often be low, and since nutrient uptake is a function of nutrient concentration, and uptake relative to cellular nutrient concentration defines growth, phytoplankton growth can often be limited (Herbert et al., 1956, Dugdale and Goering, 1967, Falkowski and Raven, 1997). The average (varies with taxonomic composition and growth conditions) proportion of the major elements in marine phytoplankton is 106C: 16N: 1P: 15Si, which is known as the Redfield ratio, first described by Redfield (1958) and modified to include silicate by Brzezinski (1985) (Falkowski and Raven, 1997, Falkowski, 2000). Deviation of the elemental composition of seawater from the optimal elemental composition of phytoplankton can be used to infer nutrient limitation of growth (Healey, 1978). Nitrate is typically the limiting nutrient to phytoplankton growth in the shelf seas (Simpson and Sharples, 2012).

1.3.3. Temperature and salinity

In addition to driving stratification, both temperature and salinity can affect phytoplankton growth since individual species have specific optimal temperature and salinity requirements, whereby their maximum growth rate can be achieved given other resources are not limiting (Collier et al., 1972, Eppley, 1972, Marañón et al., 2018). Temperature is of particular importance because it is a fundamental controlling factor of phytoplankton metabolic processes. Growth, respiration, photosynthesis, resource attainment, motility and sinking all depend on temperature (Eppley, 1972, Raven and Geider, 1988, Moisan et al., 2002). Also, it is a prime environmental axis that governs phytoplankton distribution (Litchman and Klausmeier, 2008).

1.3.4. Biological agents

Biological agents, principally zooplankton and viruses, can also be important in regulating phytoplankton biomass. Microzooplankton are considered to be the most significant grazers of phytoplankton biomass, consuming 60 - 75 % of daily primary production (Landry and Calbet, 2004), followed by mesozooplankton, consuming 10 - 40 % of daily primary production (Calbet,

2001). Although, the degree to which phytoplankton populations are affected by zooplankton grazing is dependent upon the life history of the major grazers and the growth conditions of the phytoplankton (Heinrich, 1962). Viruses are highly abundant in the oceans, with approximate concentrations of 10^8 ml^{-1} in waters of the continental shelf (Suttle, 2005), and are a major potential source of mortality for phytoplankton, specifically by causing cell lysis (Sorensen, 2009).

1.4. The Western English Channel

1.4.1. Setting and relevance

The English Channel is a temperate water body on the NW European shelf separating the north coast of France from the south coast of England. Covering approximately 77000 km^2 and with an average depth range of 45 – 120 m it is the smallest of the shallow seas on the continental shelf of Europe (Pingree, 1980, Dauvin, 2012). The Channel is a transition area between the boreal Baltic and North Sea continental systems, and the temperate Atlantic Oceanic system (Southward et al., 2005b, Dauvin, 2012). The hydrography across the English Channel is heavily influenced by ambient weather conditions and by the double tide (Pingree, 1980). Distinct hydrographical differences exist between the western and eastern reaches of the Channel, such that it is divided into two systems, namely the Western English Channel and Eastern English Channel (Fig. 1.7a) (Cabioch, 1968, Pingree, 1980, Dauvin, 2012). A key difference between the two systems is the presence of a seasonal thermocline in the Western Channel, but absence in the East due to stronger tidal streams (1.0 – 2.5 m s^{-1}) and shallower water (Pingree, 1980, Dauvin, 2012). Within the Western Channel surface tidal streams generally do not exceed 1 m s^{-1} (Pingree, 1975, Pingree, 1980), enabling development of a summer thermocline when solar heating is sufficient to produce more buoyancy than can be dissipated (Pingree, 1975).

The transition zone between the two systems is a tidal mixing front, which manifests at the surface as a rapid change in temperature between the relatively warm surface water of the stratified regions and the cool mixed waters (Simpson and Sharples, 2012), observable in satellite imagery (Fig. 1.7b). The front is specifically where forces of turbulent mixing and solar heating are in balance, and the thermocline outcrops at the surface (Simpson and Hunter, 1974, Pingree, 1980, Simpson and Sharples, 2012). The front dividing the Western and Eastern English Channel is known as the Western English Channel front (Simpson and Sharples, 2012) (Fig 1.7b). Since the thermocline is an interface at which light and nutrient concentrations are favourable for phytoplankton growth (Holligan and Harbour, 1977, Pingree et al., 1978,

Sharples et al., 2001), study of the Western English Channel in summer is of particular importance when understanding biogeochemical cycling across the shelf.

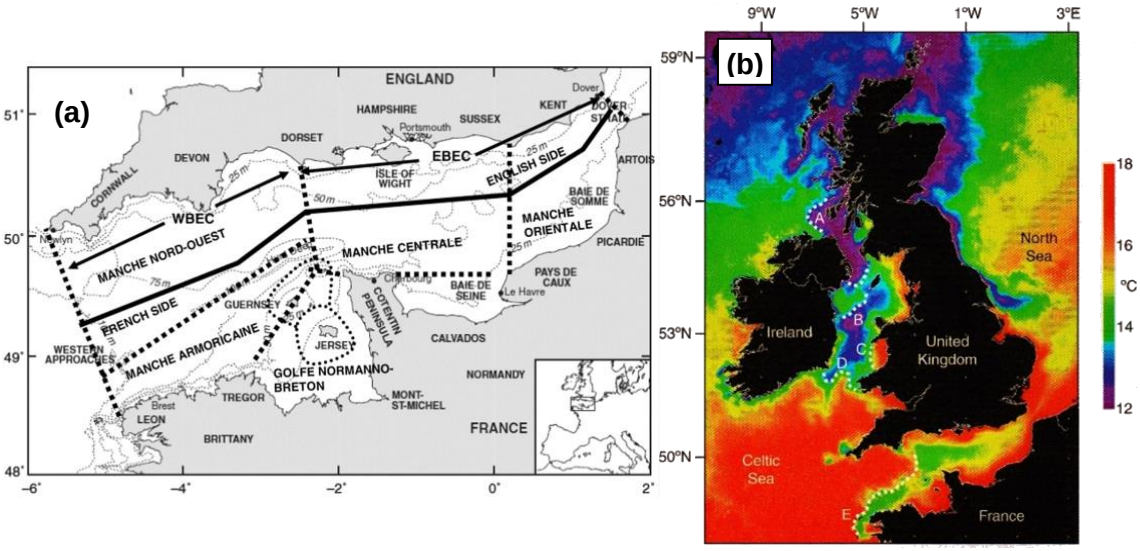

Figure 1.7. (a) A map of the English Channel taken from Cabioch (1968) and Dauvin (2012) indicating the division between the Western (WBEC – Western Basin of the English Channel) and Eastern English Channel (EBEC – Eastern Basin of the English Channel), defined based on physical and biological components of each basin. The English/French divide is given by the bold solid line, and dashed lines divide key regions of the Channel. Depth contours are also given. **(b)** I-R composite (9^{th} – 15^{th} July 2006) image of sea surface temperature courtesy of NEODAAS, Plymouth Marine Laboratory (PML), UK. All main fronts to the west of the UK are marked (A-E) with white dashed lines; the Western English Channel (and Ushant) front is E. Taken from Simpson and Sharples (2012).

The thermocline in the Western English Channel typically forms at 20 – 30 m depth and at 1 – 10 % of surface PAR, with a temperature difference of 2 – 3 °C, beginning in late April/May and persisting throughout the summer, until being completely eroded in October (Pingree, 1975, Holligan and Harbour, 1977, Pingree, 1980, Smyth et al., 2010). The thermocline does not develop close to shore because in shallower waters the influence of tidal generated turbulence is greater, so waters remain mixed. Moving away from shore, as the influence of tidal generated turbulence lessens, stratification is able to prevail (Pingree, 1975, Pingree, 1980). The position of the front dividing the mixed waters inshore and the stratified waters further offshore advances and retreats as a result of spring-neap adjustment, a transitional mixed-stratified zone thus exists (Pingree, 1975, Pingree and Griffiths, 1978, Sharples, 2008).

Although the Western English Channel is shallower than many shelf water bodies, it may be considered representative of other shelf seas with similar hydrography. This includes seas on

the NW European shelf, such as the Celtic Sea, Bay of Biscay and northern North Sea (Pingree, 1980, Lavin et al., 2006, Rodhe et al., 2006, Hickman et al., 2012), and possibly shelf seas further afield, such as the Bering Sea (Sukhanova et al., 2006). Phytoplankton taxa typical of the Western Channel are also characteristic of the aforementioned shelf seas (Holligan and Harbour, 1977, Holligan et al., 1980, Reid et al., 1990, Pemberton et al., 2004, Weston et al., 2005, Sukhanova et al., 2006, Widdicombe et al., 2010) and several other shelf water bodies (Gribble et al., 2007, Rines et al., 2010, Trainer et al., 2012), such that understanding of key SCM phytoplankton derived from study in the Western Channel may be relevant to these other shelf seas. Moreover, a substantial portion of the world's oceans feature a seasonal or permanent subsurface thermocline with associated chlorophyll maximum (Cullen, 2015). Therefore, comprehension of the biogeochemical and ecological role of SCM gained from studies in the Western Channel may be usefully applied to SCM across the global ocean.

1.4.2. Climate change

In the Western English Channel surface temperature increases of approximately 0.6 °C per decade over the past 20 years have been reported (Fig. 1.8), leading to temperatures around 0.8 °C higher than the long term average (Smyth et al., 2010). This rise is consistent across the NW European shelf (MCCIP, 2008). Ocean warming is increasing stratification (Bindoff et al., 2007), which is projected to develop further in the future (Capotondi, 2010, Capotondi et al., 2012), with more persistent and intense summer stratification specifically predicted for NW European shelf seas (Lowe et al., 2009, Sharples et al., 2013, Tinker et al., 2016).

Since formation of SCM in the Western English Channel and the surrounding NW European shelf seas is dependent upon the development of stratification (Holligan and Harbour, 1977, Pingree et al., 1978, Pingree, 1980, Holligan et al., 1984b, Sharples et al., 2001, Hickman et al., 2012), it is fair to assume that ocean warming could impact upon these subsurface features. As different phytoplankton may have specific roles in biogeochemical cycling and/or to higher trophic levels, monitoring and understanding SCM phytoplankton is thus also imperative for our prediction of how the shelf sea ecosystem will respond to future climate change. Currently, phytoplankton community response to changes in climate has only been tested by biogeochemical models, which predict smaller phytoplankton will be favoured, causing decreases in primary production and associated export production (Steinacher et al., 2010). However, these predictions are based on highly simplified models that cannot replicate the phytoplankton community or the physics within the marine ecosystem, and have already been challenged by practical evidence from studies in stratified waters of the modern ocean and

palaeo-sediment trap records (Kemp et al., 2006, Kemp and Villareal, 2013), reinforcing a need for enhanced understanding of SCM phytoplankton, their physiology and ecology.

The Western English Channel has been identified to be ideal for detecting ecosystem responses to climate change as it is not influenced by confounding localised and regional factors, such as eutrophication (Smyth et al., 2010). In addition, as the Channel is a transition area, with boreal and temperate flora present (Southward et al., 2005b, Dauvin, 2012), monitoring of the region can allow changes in taxonomic composition to be identified early, providing a warning for changes in the community further afield (Smyth et al., 2010).

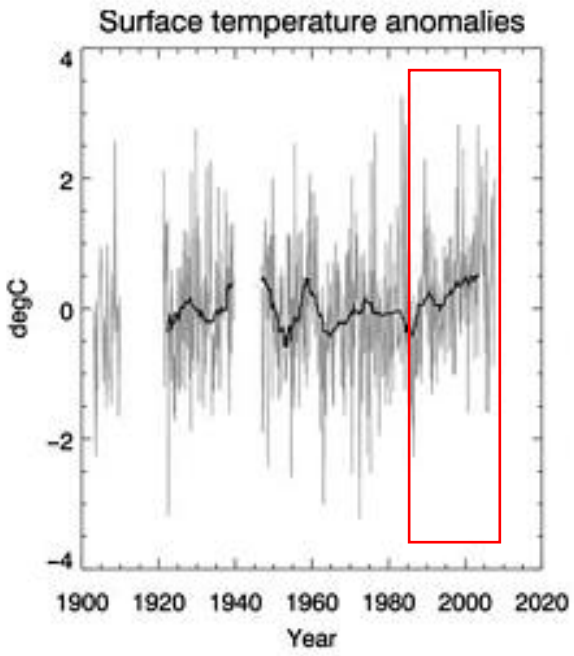

Figure 1.8. Temperature anomalies for surface waters (2 m) at station E1 in the Western English Channel from the beginning of the 20th century to the present. The current period of warming (outlined in red) captured in the sea surface temperature satellite record began in the mid-1980s, with temperature increases of 0.6 °C per decade over the last 20 years resulting in temperatures approximately 0.8 °C above the long term average (Smyth et al., 2010).

1.4.3. Previous studies

Routine monitoring of the Western English Channel began in 1888, with measurements made at a number of major long term sampling stations, namely the ICES (International Council for the Exploration of the Sea) E and L stations (E1, L4, L5, L6) off the Plymouth coast (Southward et al., 2005b). Presently, the Western Channel Observatory (WCO), established in 2005,

maintains these long term observations, principally at stations L4 (50° 15.00 N, 4° 13.02 W; depth 50 m) and E1 (50° 02.00 N, 4° 22.00 W; depth 75 m) (Harris, 2010, Smyth et al., 2015).

The L4 station has been sampled since the latter part of the nineteenth century and represents coastal waters, while sampling at the E1 station began in 1903 and is more representative of open shelf waters. Both of these stations become thermally stratified throughout the summer period (Southward et al., 2005b, Harris, 2010, Smyth et al., 2010, Smyth et al., 2015). Weekly and fortnightly profiling at station L4 and E1 respectively has revealed that SCM are a recurrent feature of summer stratification, at typical depths of 20 – 30 m (Fishwick, 2017). Sampling at other locations within the Western Channel has also revealed the SCM to be a common and persistent seasonal feature. Since 2006, SCM, often of high intensity and meeting the criteria of SCMTL, have been observed during the annual summer (June/July) monitoring of the area offshore of Falmouth by the University of Southampton undergraduate Oceanography field course. In addition, over the years there have been isolated studies within the Western Channel that too have documented SCM associated with the summer stratification (Sharples et al., 2001).

Recent studies have demonstrated or at least suggested the biogeochemical significance of SCM on the NW European shelf. Kitidis et al. (2012) identified the Western English Channel to be a sink for carbon dioxide and suggested it to be due to undersaturation of carbon dioxide at the sea surface because of production and export from the SCM. Practical and theoretical studies of the seasonally stratifying regions of the Celtic Sea and North Sea have reported the SCM to be responsible for about half (possibly more) of the total annual primary production in their respective regions of investigation (Richardson et al., 2000, Hickman et al., 2012, van Leeuwen et al., 2013). Furthermore, Sharples et al. (2001) identified substantial turbulent carbon flux from a SCM in the Western Channel (edge of the southern Celtic Sea) and estimated it to represent a removal of 10 – 40 % of total annual production, illustrating a significant potential for carbon export to the seafloor. This result is consistent with the observation of ancient deposits of known SCM dwelling phytoplankton within seafloor sediments of stratifying water bodies (Kemp and Villareal, 2013).

In spite of chlorophyll-fluorescence profiles consistently indicating the SCM to be a persistent feature of the seasonal stratification in the Western English Channel, and an abundance of evidence to attest to their potential biogeochemical significance, SCM have been little-studied in the Western Channel compared to those in the Celtic Sea and North Sea. Instead, surface

(10 m) sampling and sampling of pre-determined depths has formed the basis of a majority of Western English Channel studies (Llewellyn et al., 2005, Kamenir et al., 2010, Widdicombe et al., 2010, Kitidis et al., 2012, Downes-Tettmar et al., 2013, Barnes et al., 2015b, Tarran and Bruun, 2015). As such, detailed investigations of SCM phytoplankton community structure in the Channel are rare (and rather isolated), which is also the case across the NW European shelf despite the more extensive SCM sampling that has occurred in the North and Celtic Seas. A common observation documented in existing reports of SCM phytoplankton is the presence of a monospecific/near monospecific assemblage (Holligan and Harbour, 1977, Holligan et al., 1984b, Sharples et al., 2001). Yet a range of different taxa have been documented as dominant within SCM of the Western English Channel and other NW European shelf seas, from < 2 µm cyanobacteria (Hickman et al., 2009, Sharples et al., 2009) and < 10 µm naked flagellates (Holligan et al., 1984b), to 10 – 15 µm coccolithophores (Sharples et al., 2001) and > 50 µm rhizosolenid diatoms (Holligan and Harbour, 1977, Weston et al., 2005). To improve our understanding of SCM phytoplankton and their ecological and biogeochemical role within the shelf sea ecosystem, detailed quantitative taxonomic analysis of SCM community structure in relation to the surrounding environment is needed, along with investigation into the physiology and ecology of key taxa.

1.5. Thesis aim and research questions

The overall aim of this thesis is to investigate subsurface chlorophyll maxima in the summer stratified waters of the Western English Channel, specifically their phytoplankton community structure, the primary production and photophysiology of these communities, and environmental parameters influencing the chlorophyll and community structure of SCM.

The following specific questions are addressed in this thesis:-

- What are the key phytoplankton taxa found within SCM of the Western English Channel?
- Is the phytoplankton community structure within SCMTL distinct from that of broader SCM?
- What environmental factors control the development and structure of SCM?
- What environmental factors control community structure within an SCM?
- How does community structure of the SCM vary from the rest of the water column?

- How important is the primary production contribution of the SCM and how does resource availability and the phytoplankton community influence SCM primary production?
- How does SCM phytoplankton community structure change in time and space?

1.6. Thesis structure and objectives

Chapter 1: Introduction

This section provides an overview of phytoplankton, their importance, and the SCM they form within stratified shelf seas. Environmental factors influencing phytoplankton growth and biomass accumulation within SCM, and the importance of studying these features is also addressed. Finally, the study area is introduced, and the main aim, research questions and objectives of the research are set out.

Chapter 2: Methods

This section provides a detailed description of sampling strategy and procedures, and sample/data processing and analysis techniques applied.

Chapter 3: Phytoplankton community structure within shelf sea subsurface chlorophyll maximum thin layers

This section addresses physical forcing factors influencing the development and structure of SCM, and describes the community structure of SCMTL and broader SCM in the Western English Channel during the summer of 2013, with the objectives:-

- To present the first detailed study of SCMTL and broader SCM on the NW European shelf.
- To assess temporal and spatial variation in phytoplankton community structure within SCM.
- To assess the similarities/differences in community structure between SCMTL and broader SCM, and between the SCM, and surface and bottom waters.
- To evaluate controls on the occurrence of SCMTL compared to broader SCM, and relate their development to water column structure and physical conditions.

Chapter 4: Vertical transition of phytoplankton community structure in a stratified water column measured using *in situ* holography

This section addresses high depth resolution taxonomic study of phytoplankton community structure throughout a stratified water column, with the objectives:-

- To present the first high depth resolution taxonomic study of phytoplankton community structure within an SCM and throughout the surrounding water column using *in situ* holographic imagery.
- To investigate phytoplankton community structure across the Western English Channel in order to put the holography results in context of the wider shelf.
- To evaluate the feasibility of using holographic imaging for assessing phytoplankton community structure on a temporally and spatially larger scale in future.

Chapter 5: SCM primary production and the influence of resource availability and the phytoplankton community in the summer stratified waters of the Western English Channel

This section addresses water column and SCM primary production within the stratified waters of the Western English Channel during the summer of 2015, the importance of SCM primary production and factors influencing this production, with the objectives:-

- To present estimates of total water column primary production using FIRe and ^{13}C incubation data.
- To investigate the contribution of the SCM to total water column primary production.
- To evaluate the significance of the SCM for new production within the water column.
- To investigate the influence of chlorophyll concentration, nutrient availability, irradiance levels, phytoplankton photophysiological state and phytoplankton community structure on the magnitude of SCM primary production.

Chapter 6: Environmental controls on the interannual variability in chlorophyll and phytoplankton community structure within subsurface chlorophyll maxima in the Western English Channel during summers of 2013 to 2016

This section addresses environmental parameters influencing the interannual variability in SCM chlorophyll and phytoplankton community structure at a single location in the Western English Channel during the summers of 2013 to 2016, with the objectives:-

- To assess interannual variation in SCM chlorophyll structure from 2013 to 2016, and relate to physical forcing factors.

- To assess interannual variation in phytoplankton (pico-, nano-, micro- and meso-) community structure within SCM from 2013 to 2016, and relate to environmental parameters.

Chapter 7: Summary, conclusions and future work

This section summarises the main findings and conclusions to be drawn from the research. Suggestions for further study are also given.

Chapter 2: Methods

Data was collected during four summer field surveys in the stratified waters of the Western English Channel (offshore of Falmouth), conducted on an annual basis from 2013 - 2016. Dates as follows:-

2013: 24th June – 4th July
2014: 14th June – 3rd July
2015: 19th June – 2nd July
2016: 17th June - 30th June

All field surveys were conducted simultaneously with the University of Southampton 3rd year undergraduate field course on board the University vessel RV Callista, a 19.75 m catamaran purpose built for research.

2.1. Sampling procedure

During all four field surveys, sampling strategy included repeat sampling of individual stations and sampling along inshore – offshore transects. Repeat stations were chosen based on past data revealing their location to be far enough away from the tidal mixing front (that separated shallower mixed inshore waters from deeper stratified waters further offshore) to be permanently stratified in June/July, but also within a reasonable travel distance to enable regular sampling. A more detailed description of sampling strategy is presented in the methods of each of the following four data chapters (chapters 3 – 6). Sampling consisted of *in situ* profiling and collection of discrete water samples analysed for a range of chemical and biological parameters as shown in Table 2.1. Water samples were collected on the up-cast of the CTD deployment using 5 L Niskin bottles mounted on a SBE32 sampling carousel. In 2013 additional water samples were collected using a custom made horizontal sampler consisting of three 50 ml syringes spaced approximately 20 cm apart, acting as a multiple 'slurp gun' (Fig. 2.1). This slurp gun was also mounted on the CTD rosette frame, with the 2nd (middle) syringe in alignment with the fluorometer.

Table 2.1. List of measurements/samples collected during each of the four field surveys conducted between 2013 and 2016. All measurements/samples denoted in this table were processed/analysed, but not all are represented in data chapters 3 – 6. Asterisks represent when additional samples were collected: In 2015, in addition to analysis for the usual suite of nutrients, ammonium was also measured, and in 2015 size-fractionated and PAR stepping mode FIRe measurements were collected.

Measurement/sample	2013	2014	2015	2016
CTD	✓	✓	✓	✓
ADCP	✓	✓	✓	✓
Holocam			✓	
Niskin bottle water sampling	✓	✓	✓	✓
Slurp gun water sampling	✓			
Chlorophyll a	✓	✓	✓	✓
HPLC pigments		✓	✓	✓
Nutrients		✓	✓ *	✓
POC/N		✓	✓	✓
Phytoplankton - microscopy	✓	✓	✓	✓
Phytoplankton – flow cytometry		✓	✓	✓
FIRe measurements	✓	✓	✓ *	✓
Primary production			✓	

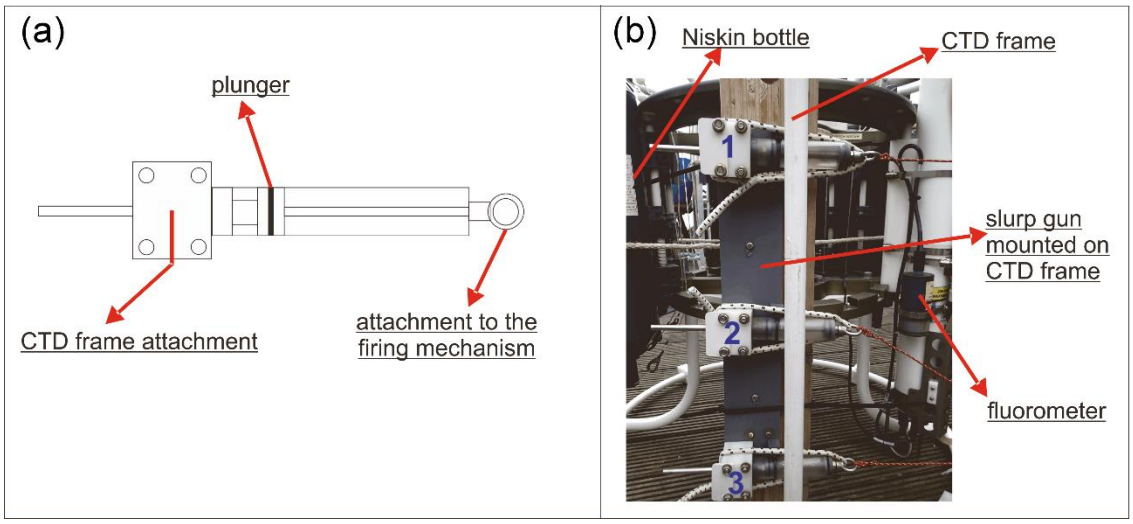

Figure 2.1. (a) Schematic of a slurp gun syringe and **(b)** photograph of the slurp gun on the CTD frame. The slurp gun consisted of 3 x 50ml horizontal, simultaneously firing syringes positioned vertically (position ID numbers in dark blue), approximately 20 cm apart, and mounted on the CTD frame such that the middle syringe was aligned with the fluorometer.

2.2. *In situ* profiling

2.2.1. CTD measurements

A SeaBird SBE19plus V2 conductivity, temperature, depth (CTD) probe mounted with a Wet Labs ECO FLNTU fluorometer-turbidity sensor, LI-COR Biospherical PAR sensor and Wet Labs C-Star transmissometer was used to collect vertical water column profiles of temperature, salinity, chlorophyll – fluorescence, turbidity, irradiance, and light transmittance. The configuration of the CTD package allowed for slow descent/ascent rates without slowing sensor responses, thus improving dynamic accuracy and allowing small scale structure to be resolved. The CTD system was typically deployed at a descent/ascent rate of 0.01 - 0.1 m s^{-1} (rate slowed on approach to the SCM), with a data acquisition rate of 2 Hz, which provided vertical resolution of 0.5 – 5 cm, thus allowing very thin SCM to be resolved.

Processing of the CTD data was performed using SBE Data Processing software following recommendations of the manufacturer (Janzen, 2012). The specific data processing module sequence employed was as follows:-

1. Data Conversion: To convert raw data in HEX files to engineering voltages and values using dedicated configuration files.
2. Align CTD: To correct for response time mismatches and pumped sensors transit delays.
3. Filter: To match conductivity and temperature response times, and filter digital noise in pressure.
4. Cell Thermal Mass: To correct for the thermal lag experienced by the conductivity cell when travelling through a temperature gradient.
5. Derive: To derive dependent variables, namely salinity.
6. Split: To separate up-cast from down-cast data.

For each field survey the fluorometer was calibrated using values of chlorophyll a determined for discrete water samples collected by the Niskin bottles mounted on the CTD rosette frame (section 2.3.1.). CTD chlorophyll-fluorescence profiles were converted to profiles of chlorophyll a concentration using the linear equation derived from the linear regression analysis performed between chlorophyll a concentrations and fluorescence (Fig. 2.2).

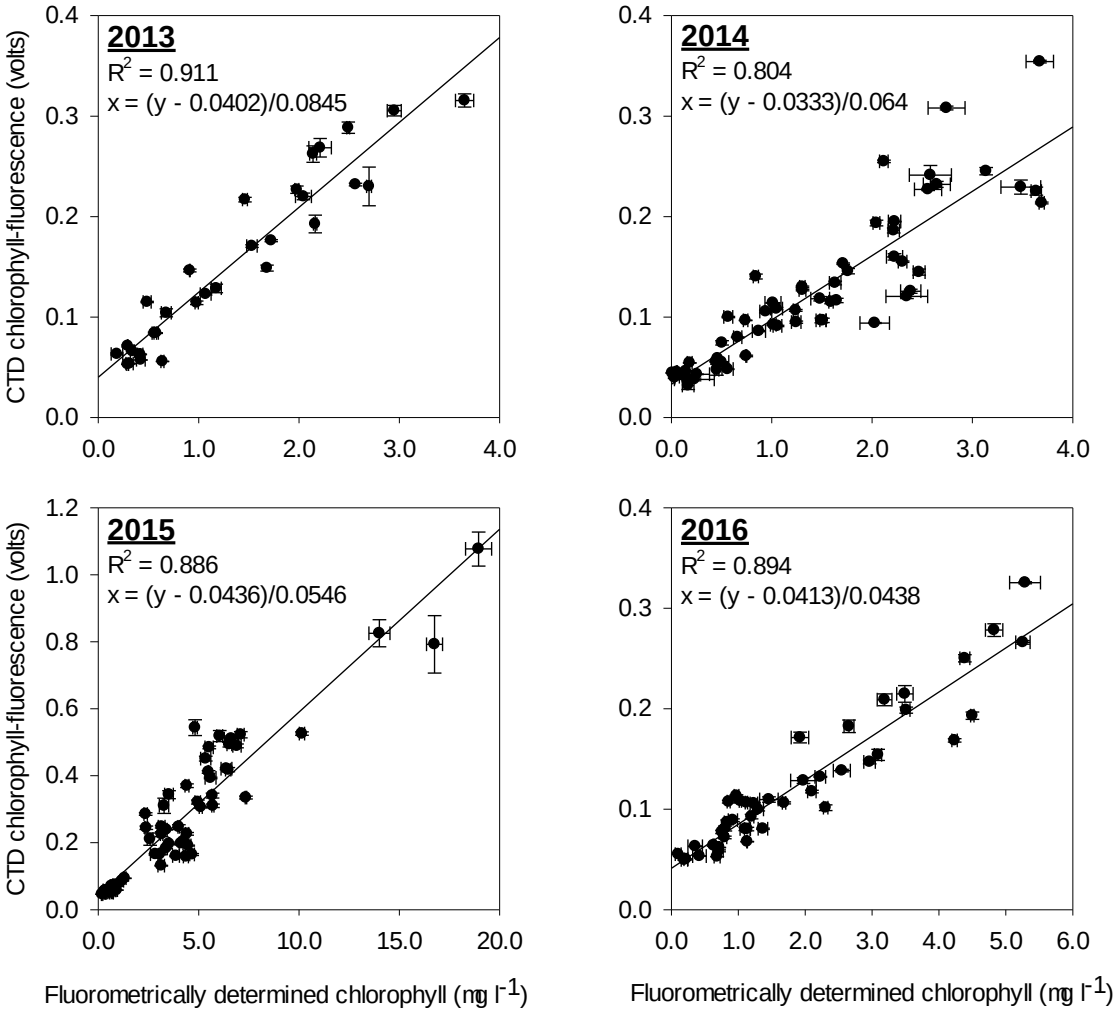

Figure 2.2. Relationship between chlorophyll a concentration of discrete samples and fluorescence values from the CTD fluorometer for 2013-16 (goodness of fit indicated by R^2). Error bars indicate standard error. The linear equations displayed were applied to obtain calibrated CTD chlorophyll a.

Buoyancy frequency

Using CTD data profiles of density and pressure, buoyancy frequency (N^2 rad^2 s^{-2}) could also be determined using the SBE Data Processing's Buoyancy module. 0.25 m depth binned data was applied in the Fofonoff adiabatic levelling method (Bray and Fofonoff, 1981), following equation 2.1:

$$N^2(rad^2\, s^{-2}) = -1.0e^{-4}\, rho\_bar^2\, g^2\, \frac{\delta v}{\delta p} \quad (2.1)$$

Where rho_bar is density (Kg m^{-3}), g is gravitational acceleration (9.81 m s^{-2}), v is 1/density and p is pressure (db).

2.2.2. ADCP measurements

A hull mounted Teledyne RDI Workhorse Mariner 600 kHz Acoustic Doppler Current Profiler (ADCP) with a maximum profiling range of 80 m (Fisher, 2018) and ping rate of 2 Hz (Jones et al., 2014) measured current velocities through the water column, and this data was recorded with Teledyne WinRiver II software. The ADCP measures 3D velocity components (U, V, Z) by applying the acoustic principle of 'Doppler shift'. The ADCP transmits pulses of acoustic energy (pings) and the frequency of the reflected acoustic pulses is Doppler shifted relative to current velocity. Measurements of 3D velocity were made for 0.5 m bins throughout the water column and each velocity profile ensemble was composed of ten pings. GPS was used as the velocity reference for all measurements. ADCP limitations are described by Teledyne RD instruments (2011) and include inability to collect measurements near the sea bed and surface, and reduction of profiling range in rough waters.

Raw ADCP data was processed using Teledyne WinRiver II software. The data was smoothed by averaging every 10 ensembles and then converted to Earth referenced current velocity and direction data.

Richardson number

CTD density measurements and values of velocity shear determined from ADCP current velocity data were used to determine the Richardson number at 1 m intervals through the water column using equation 2.2:

$$Ri = \frac{-g}{\rho}\frac{\delta\rho\delta z}{\delta U^2} = \frac{N^2}{S^2} \quad (2.2)$$

Where N is buoyancy frequency (rad^2 s^{-2}), S is velocity shear (m s^{-1}), g is gravitational acceleration (9.81 m s^{-2}), ρ is the *in situ* density (Kg m^{-3}), z is depth (m) and U is horizontal velocity (m s^{-1}).

Shear tends to generate turbulence, while buoyancy tends to supress it and therefore the Richardson number is an indicator of dynamic stability. A Richardson number of 0.25, as classically reported by Miles (1961), is typically accepted as the general threshold between a stable and unstable regime, although it is recognised that the critical Richardson number may lie anywhere between 0.2 and 1 (Galperin et al., 2007).

Shear can vary greatly over a semi-diurnal tidal cycle in a shallow stratified tidal sea to the extent that temperate shelf sea thermoclines have been demonstrated to be of marginal stability (Rippeth, 2005, Rippeth et al., 2005, Burchard and Rippeth, 2009). Therefore, to establish a careful understanding of the dynamic stability regime associated with a SCM and its influence on that SCM, the Richardson number should ideally be measured over a semi-diurnal tidal cycle. However, it was not logistically possible to calculate Richardson numbers over the course of a tidal cycle during the summer surveys conducted to collect data for this thesis. Instead, dynamic stability could only be measured over the duration of the CTD profiling process (~ 15 minutes), the caveats of which are discussed in section 6.3.1.

2.2.3. Holocam measurements

In a two ship operation on the 19th June 2015, holocam measurements of a stratified water column (50° 06.07 N, 004° 24.65 W) were collected. Holocam profiling was conducted by Dr Alex Nimmo Smith and his crew aboard Plymouth University's RV Falcon Spirit, while discrete sampling of the water column was conducted on board the RV Callista.

The digital in-line holographic camera system, updated from that described in Graham and Nimmo Smith (2010), hereafter referred to as a holocam, was mounted on a frame alongside a AML CTD Plus V2 probe with chlorophyll-fluorescence sensor (Fig. 2.3), which was slowly lowered through the water column, with a sampling frequency of 15 Hz. The holocam used had a vertical configuration, similar to that described by Graham et al. (2012) as a system 2, which is adapted for vertical profiling, keeping water column disruption to a minimum. The holocam system was composed of a laser (658 nm, 60 mW) and charge coupled device (CCD) camera, separated by low-profile housing extensions and 90° mirrors spaced 82 mm apart to distance the sample volume (between mirrors) from the CCD camera and laser as illustrated in Figure 2.3. To capture a hologram the laser illuminated the sample volume and the CCD camera captured interference patterns as particles diffracted the laser beam (Graham and Nimmo Smith, 2010) in a series of slices in 3 dimensional space. Together, these slices formed a hologram, which had a size of 1536 x 1024 pixels, where pixel size was 4.65 µm and so hologram volume was 2.78 ml. During the holocam deployment 3323 holograms were digitally recorded from the surface to a depth of 50 m.

On return to the laboratory the imagery captured by the CCD camera was cleaned up by subtraction of the static background based on a moving average of +/- 10 images surrounding the image being processed. This process was completed by Dr Alex Nimmo Smith of Plymouth

University. Images were then reconstructed computationally by applying the deconvolution technique, following methods developed by Graham and Nimmo Smith (2010). The 3D stack presented by each hologram was analysed using 'HOLO_Detail', a Sequoia Scientific MATLAB GUI (graphical user interface). First the stack was cleaned by 1.1 % to remove background pixels and then all particles were counted as they came into focus when moving though the stack at 0.5 mm depth intervals (e.g. Fig. 2.4). Particles identified and counted included phytoplankton, marine aggregates and zooplankton. Holograms analysed were at 0.3 m depth intervals, increased to 0.2 m intervals for the SCM (between 25 – 30 m).

Holography has many advantages as documented by Graham and Nimmo Smith (2010) and Graham et al. (2012). These include high depth resolution sampling, impossible to achieve with classical discrete sampling with Niskin bottles, and observation of particles *in situ*, overcoming the limitation of much more intrusive discrete sampling techniques where fragile phytoplankton, phytoplankton chains and other marine particles tend to be disturbed. However, holography does present some limitations, principally the pixel size of holograms limits phytoplankton identification, with phytoplankton below ~30 - 50 µm being difficult or impossible to observe or identify.

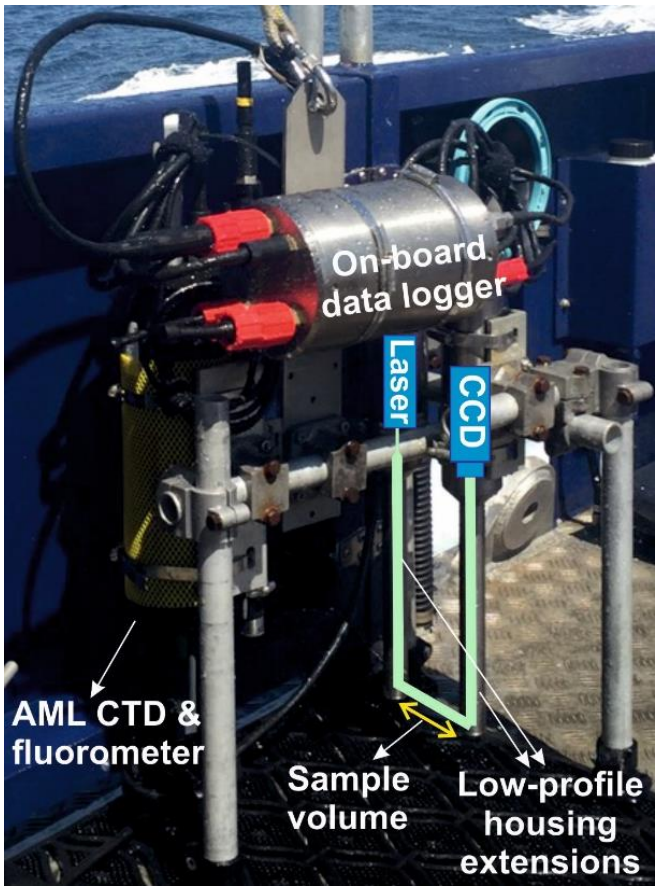

Figure 2.3. Holocam mounted with the AML CTD Plus V2 probe.

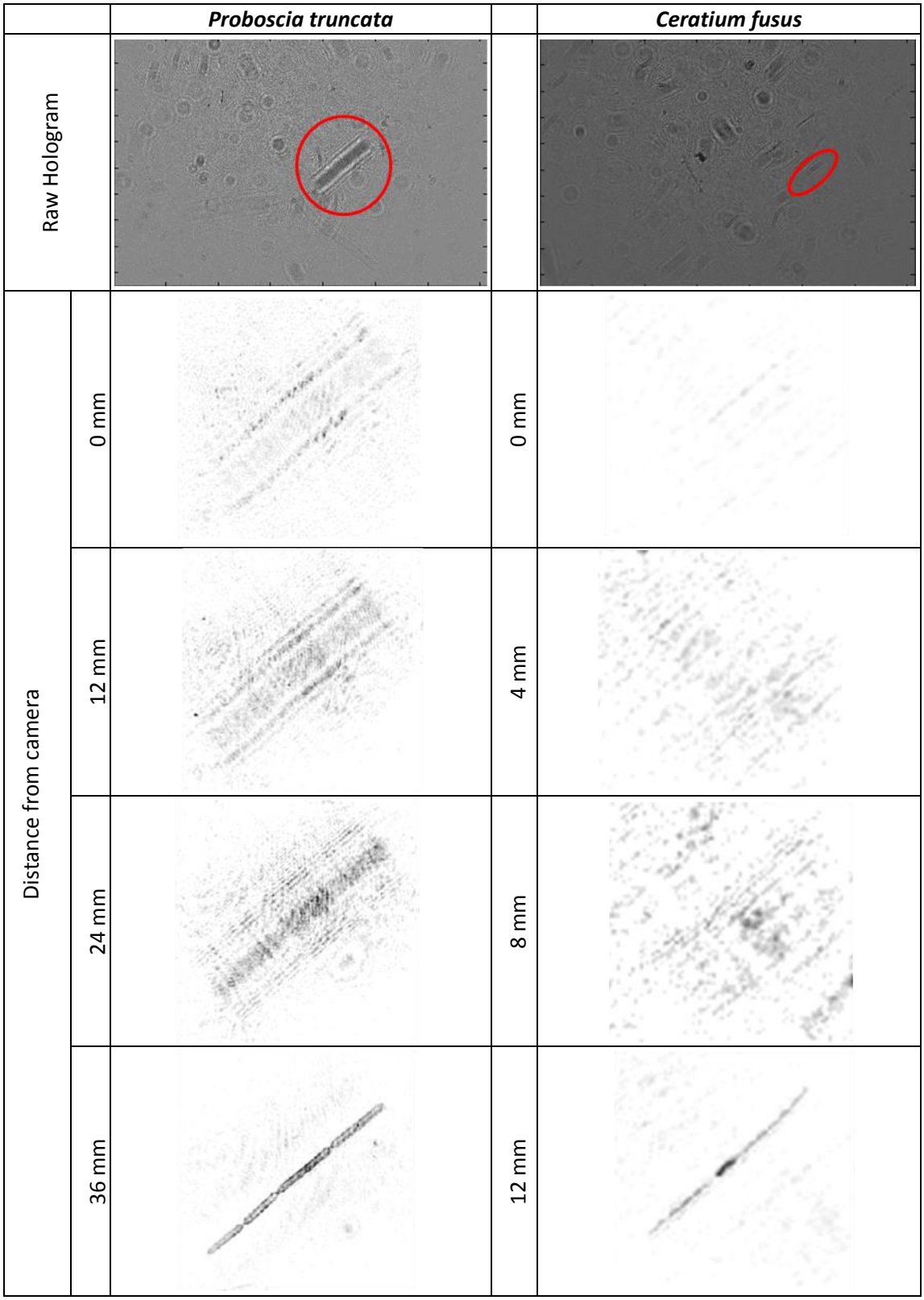

Figure 2.4. Examples of particles (chain of 4 *Proboscia truncata* and *Ceratium fusus*) brought into focus moving through the sample volume/away from the camera. Raw hologram dimensions 7.14 x 4.76 mm.

2.3. Discrete sampling

Water samples were analysed for a range of biological and chemical parameters when and where possible. These included chlorophyll a and other phytoplankton pigments, nutrient concentrations, particulate load, phytoplankton identification and enumeration, Fluorescence Induction and Relaxation (FIRe) parameters and rates of primary production. Due to the limited volumetric capacity of the slurp gun, water samples collected by the slurp gun were only analysed for phytoplankton identification and enumeration, and for FIRe parameters.

2.3.1. Chlorophyll a concentration

Chlorophyll a concentrations (referred to as chlorophyll concentrations in data chapters 3 – 6) were determined following the methods of Welschmeyer (1994). Three 50 ml subsamples were passed through 25 mm Whatman GF/F filters immediately after collection, and then kept frozen (-20 °C) in darkness prior to analysis. Size-fractionated chlorophyll samples were also collected in 2013 by filtering water sample through a Whatman track-etched polycarbonate membrane with a pore size of 10 µm before being passed through a GF/F filter. Analysis was conducted as soon as possible on return to the lab to avoid errors associated with pigment degradation at -20 °C (Graff and Rynearson, 2011). For analysis (under subdued light) each frozen filter was added to 7 ml of 90 % acetone (analytical reagent grade) in plastic centrifuge tubes. Samples were sonicated for 30 seconds using a Vibra Cell sonicator to allow extraction, and centrifuged at 4000 rpm for 10 minutes in a Baird and Tatlock Bench Mark IV centrifuge to settle out filter particulates. The supernatant was decanted into a fluorometer cuvette and placed into a Turner Designs 10AU fluorometer (acetone blank correction was applied before running sample batches). The fluorometer was used to excite the extracted sample with blue light (436 nm) and the subsequent red fluorescence emission (680 nm) was recorded. The fluorometer provided a reading of chlorophyll a concentration in acetone (µg l^{-1}), which was used to calculate chlorophyll a concentration of the seawater sample using equation 2.3:

$$Chlorophyll\ a\ concentration\ (\mu g\ l^{-1}) = C \times (\frac{v}{V}) \quad (2.3)$$

Where C is the concentration of chlorophyll a in acetone (µg l^{-1}), v is the volume of acetone (ml), i.e. 7 ml, and V is the volume of seawater filtered (ml), i.e. 50 ml.

The fluorometer was calibrated before analysis using a chlorophyll a standard solution (Sigma-Aldrich) made up with 90% acetone (analytical reagent grade). The chlorophyll a concentration

of the standard solution was predetermined using a Cecil CE1010 spectrophotometer and the trichromatic equation derived by Jeffrey and Humphrey (1975) (equation 2.4):

$$Chlorophyll\ a\ (mg\ l^{-1}) = (11.85 \times E_{664}) - (1.54 \times E_{647}) - (0.08 \times E_{630}) \quad (2.4)$$

Where E_{664} is the absorbance value at 664 nm corrected for absorbance at 750 nm, E_{647} is the absorbance value at 647 nm corrected for absorbance at 750 nm, and E_{630} is the absorbance value at 630 nm corrected for absorbance at 750 nm.

The main source of error associated with determining chlorophyll a fluorometrically following the methods of Welschmeyer (1994) arises as a result of other fluorescent pigments with similar absorption spectra to chlorophyll a. These pigments include chlorophyll-b, chlorophyll-c and their associated phaeopigments. Their presence in water samples can cause overestimation of chlorophyll a concentration (Gibbs, 1979).

2.3.2. HPLC pigments

High performance liquid chromatography (HPLC) was used for separating, identifying and quantifying photosynthetic pigments in water samples. Samples for HPLC analysis were collected by filtering 0.7 – 2.0 L of water sample onto 25 mm Whatman GF/F filters. Filters were stored in darkness at -80 °C until analysis. Prior to analysis solvent A was freshly prepared, which was a 70:30 mix of methanol (HPLC grade) and 1 M ammonium acetate buffer solution. The 1 M ammonium acetate buffer solution was prepared by dissolving 77.08 g (molecular weight) of HPLC grade ammonium acetate crystals in 1 L of Milli-Q water.

For analysis (under subdued light) each frozen filter was added to 5-7 ml of 90 % acetone (HPLC grade) in plastic centrifuge tubes. Samples were sonicated for 30 seconds using a Vibra Cell sonicator to allow extraction, and centrifuged at 4000 rpm for 10 minutes in a Baird and Tatlock Bench Mark IV centrifuge to settle out filter particulates. Samples were then filtered through a 0.2 µm Teflon syringe filter into HPLC sample vials (1 ml filtered in total per sample: 0.25 ml to flush filter with sample and 0.75 ml into vial) and placed in the autosampler cooling rack (4 °C) of the Thermo Finnigan SpectraSYSTEM HPLC system ready for analysis. Vials of 'pigmix' (a pure pigment mixture of known concentrations; Table 2.2) and chlorophyll a standard (Sigma-Aldrich and DHI) were also set up in the cooling tray (0.75 ml per vial), where two chlorophyll a standard vials and a single 'pigmix' vial were placed to run at the beginning and end of the sequence, while chlorophyll a standards were also placed every 5-6 samples in

the sequence. Before commencing analysis, a preview run was performed to check the baseline; a successful preview run showed the baseline to drift no more than 1 mA, with noise < 0.01 mA. The HPLC instrument performed pigment analysis as described by Barlow et al. (1997) and Gibb et al. (2001).

The HPLC system comprised of the mobile phase (solvent A: 70:30 HPLC grade methanol and 1 M ammonium acetate buffer solution, Solvent B: 100 % HPLC grade methanol, Solvent C: 1M ammonium acetate and HPLC grade methanol flush), a SpectraSYSTEM SCM1000 solvent degasser, a SpectraSYSTEM P2000 solvent pump, a SpectraSYSTEM AS3000 autosampler, a Thermo Fisher Scientific Hypersil HPLC column, a SpectraSYSTEM UV6000LP UV detector, a SpectraSYSTEM FL3000 fluorescence detector and SN4000 system controller. 500 µl of pigment extract sample was mixed with 500 µl of 1 M ammonium acetate and 100 µl of the mixture injected into the HPLC column where the different pigments were separated. Detector output was recorded as a series of peaks, each one representing a different pigment, where peak area was directly proportional to pigment concentration. This data output was analysed using Thermo Fisher Scientific ChromQuest software. The different peaks were identified by comparing their retention times and spectral properties with those of the known 'pigmix' and chlorophyll a standards. Pigment concentrations (ng l^{-1}) were calculated using equation 2.5:

$$Pigment\ concentration\ (ng\ l^{-1}) = \frac{peak\ area \times extraction\ volume \times 1000}{pigment\ RF \times volume\ injected \times volume\ filtered \times 0.5} \qquad (2.5)$$

Where peak area (mA x min) was measured at a wavelength of 440 nm, extraction volume is the volume of 90 % acetone used for extraction (ml), pigment RF is the response factor of each pigment, the volume injected in the HPLC column was consistently 100 µl, volume filtered is the volume of water sample passed through the filter (L), and 0.5 is the buffer dilution factor.

Pigment response factors were obtained, along with retention times (RT), during calibration of the HPLC column by Dr John Gittins of the University of Southampton and Tom Jackson of the University of Oxford following methods of Mantoura and Repeta (1997). Concentrations of each pigment needed for calibration of the HPLC column were measured using a Cecil CE1010 spectrophotometer and the trichromatic method (Strickland and Parsons, 1972, Jeffrey and Humphrey, 1975). A list of pigments identified and quantified in HPLC samples, including their RF and RT values, is given in Table 2.2.

Table 2.2. List of phytoplankton pigments identified and quantified in HPLC samples, and their response factors and retention times as determined by Dr John Gittins of the University of Southampton and Tom Jackson of the University of Oxford during calibration of the HPLC column. All these pigments were present in the 'pigmix' solution.

Phytoplankton pigment	RF	RT (min)
Chlorophyll c3	43104	2.20
Chlorophyll c2	76143	3.08
Peridinin	33533	3.73
19 Butanoyloxyfucoxanthin	53754	4.56
Fucoxanthin	51458	4.86
19 Hexanoyloxyfucoxanthin	54441	5.53
Violoxanthin	83669	5.70
Prasinoxanthin	50301	5.77
Diadinoxanthin	72869	6.92
Alloxanthin	77930	7.74
Zeaxanthin	78736	9.34
Lutein	80161	9.88
Gyroxanthin	84027	13.66
Chlorophyll b	15544	18.14
Divinyl chlorophyll a	25507	22.95
Chlorophyll a	22120	23.87
β carotene	63772	27.15

2.3.3. Nutrient concentrations

Measurements of dissolved nutrients, including nitrate, nitrite, ammonium, phosphate and silicate were obtained using a single water sample. Water samples were passed through 25 mm Whatman GF/F filters, to remove particles that could influence nutrient concentration (Kremling and Brügmann, 1999), and placed in 15 ml sterile polypropylene tubes that were immediately frozen at -20 °C until later analysis (Dore et al., 1996).

Upon return to the laboratory, samples were transferred to a refrigerator for a period of 24 hours prior to analysis to thaw the samples and to allow for depolymerisation of dissolved silicate. Samples were also mixed regularly throughout the thawing process to aid depolymerisation of dissolved silicate. Samples were then analysed for total nitrate (nitrate +

nitrite), nitrite, phosphate and silicate by Dr Cynthia Dumousseaud of the University of Southampton using a SEAL Analytical QuAAtro segmented flow AutoAnalyser with AutoAnalyser Control and Evaluation (AACE) software, and standard colorimetric techniques described by Grasshoff (1976) and Kirkwood (1996). These techniques are based on the reaction of the different nutrients with specific reagents to produce coloured compounds, the colour intensity of which is proportional to nutrient concentration.

To measure total nitrate (nitrate + nitrite), the sample was passed through a copper-cadmium reduction column where nitrate was reduced to nitrite. Nitrite concentration was then determined by diazotising with sulphanilamide and coupled with N-1-napthylethylenediamine to form a coloured azo dye measured at 520 nm. Nitrite concentrations were determined separately by omitting the cadmium reduction phase of the technique, and this allowed nitrate concentrations to be obtained by subtraction of nitrite values from total nitrate values (Zhang et al., 1997). To measure phosphate, the sample was mixed with an acidified molybdate reagent, producing phosphomolybdate acid as a result of reaction with phosphate ions. The phosphomolybdate acid was then reduced by ascorbic acid to form an intensely blue-coloured compound, measured at 880 nm (Zimmermann and Keefe, 1997).To measure silicate, sample was mixed with molybdate in acidic solution, which produced molybdosilicic acid as a result of reaction with silicate. The molybdosilicic acid was then reduced by ascorbic acid to form molybdenum blue, measured at 820 nm (Zhang and Berberian, 1997).

Calibration curves were produced for each nutrient for each sample batch by preparing and running standards of known concentration (e.g. total nitrate: 0, 0.2, 3, 6, 9, 12 µmol l^{-1}; nitrite: 0, 0.1, 0.5, 1, 1.5, 2 µmol l^{-1}; phosphate: 0, 0.1, 0.5, 1, 1.5, 2 µmol l^{-1}; silicate: 0, 0.1, 2.5, 5, 7.5, 10 µmol l^{-1}) in the AutoAnalyser (each standard run in duplicate). Linear regression analyses of calibration curves generated linear equations for calculation of nutrient concentration using peak height values from the chart recorder of the AutoAnalyser. Detection limits for total nitrate, nitrite, phosphate and silicate were 0.03 µmol l^{-l} (NIOZ, 2016), 0.01 µmol l^{-l} (NIOZ, 2015c), 0.01 µmol l^{-l} (NIOZ, 2015a) and 0.02 µmol l^{-l} (NIOZ, 2015b) respectively (Stinchcombe, 2017).

Nutrient samples collected in conjunction with ^{13}C and ^{15}N incubations were also analysed for ammonium concentrations following the ammonium fluorometric method described by Holmes et al. (1999). This method is based on the reaction of ammonium with orthophthaldialdehyde (OPA) to produce a highly fluorescent compound, the fluorescence

intensity of which is proportional to ammonium concentration. 0.5 ml of mixed reagent consisting of sodium sulphite solution (0.8 g sodium sulphite in 100 ml of Milli-Q water), sodium tetraborate solution (40 g sodium tetraborate in 1 L of Milli-Q water) and OPA solution (2 g OPA in 50 ml of high grade ethanol) was added to 2 ml of water sample and left to react for 3 – 6 hours in the dark. Samples were then decanted into a fluorometer cuvette and placed into a Turner Designs Triology laboratory fluorometer, the ammonium detection limit of which was 0.1 µmol l^{-1}. The fluorometer was used to excite the extracted sample with 360 nm ultra violet light and the subsequent 420 nm violet emission was recorded. The fluorometer provided a reading in raw fluorometer units (RFU) and these values were used to calculate ammonium concentration using equation 2.6:

$$Ammonium\ concentration\ (nmol\ l^{-1}) = \frac{RFU - 469777}{1089.6} \quad (2.6)$$

Equation 2.6 was determined from linear regression analysis of a calibration curve produced by running standards of known ammonium concentration (0, 100, 200, 1000, 2000 nmol l^{-1}) on the fluorometer (each standard was run in triplicate) (Fig. 2.5).

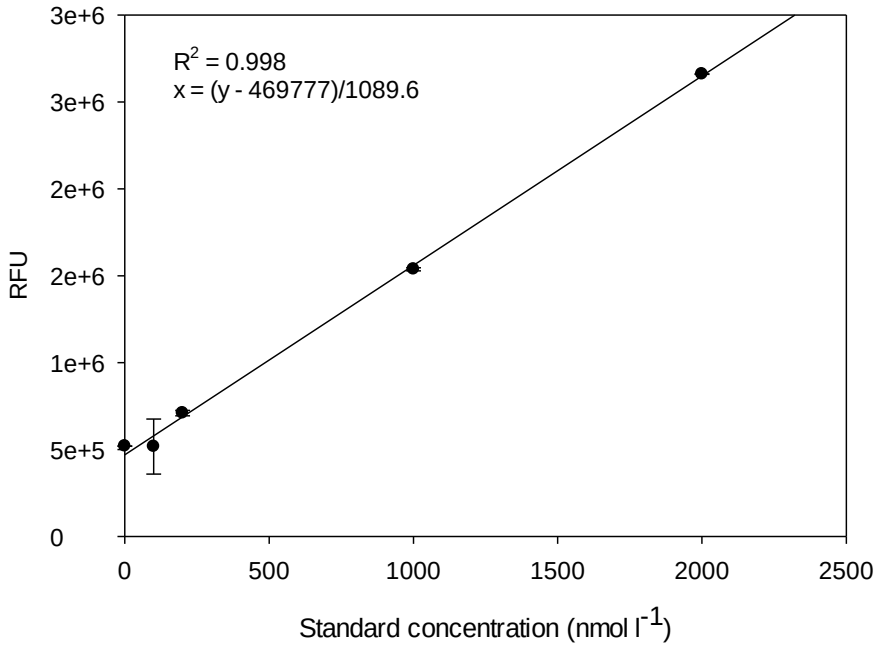

Figure 2.5. Relationship between standard concentration and RFU (goodness of indicated by R^2). Error bars indicate the standard error of the RFU measurements. The linear equation displayed was used to determine ammonium concentrations of water samples based on their RFU readings.

A limitation of this method of measuring ammonium arises due to samples being preserved via filtration and freezing for analysis at a later date, as opposed to being immediately measured in the field. Preservation of ammonium at the *in situ* concentration is difficult, and in the case of very low concentrations adequate preservation may be impossible (Holmes et al., 1999).

2.3.4. POC/N

Samples for analysis of particulate organic carbon (POC) and nitrogen (PON) concentration were collected following methods of Poulton et al. (2006) by filtration of 0.35 - 1.2 L of water sample onto pre-combusted (450 °C, 6 hrs) 25 mm Whatman GF/F filters under low vacuum (< 200 mg Hg). Filters were stored in petri slides and frozen (-20 °C) until analysis (precautions were taken whenever handling filters to ensure no external particulates were introduced). Before analysis filters were dried at 40 °C for a minimum of 12 hours, acid-fumed for 24 hours using 35 % hydrochloric acid to remove inorganic carbon, and then dried again. Filters were halved, packed into 11 x 8 mm tin capsules and pelleted ready to be analysed using elemental analysis mass spectrometry (EA-MS) by a carbon, hydrogen, nitrogen, sulphur - oxygen (CHNS-O) elemental analyser (Carlo-Erba Instruments CHNS-O EA1108). Principles of this analysis are described by Zimmermann et al. (1997) and Collos (2002).

For every 10 samples one standard and one blank was also prepared. Standards used in this analysis were prepared by weighing out 1 mg ± 0.1 mg of 44.7 % carbon/6.60 % nitrogen chitin standard into a 11 x 8 mm tin capsule, packed with half of a pre-combusted GF/F filter and pelleted. Blanks were prepared by packing pre-combusted GF/F filter halves into tin capsules and pelleting. All tin capsule pellets containing samples, blanks or standards were then loaded into the auto-sampler tray of the CHNS-O instrument for analysis.

From the auto-sampler tin capsule pellets were sequentially dropped into a furnace held at 1030 ^{o}C where they flash combusted in the presence of pure oxygen, raising the temperature to 1800 °C. The gases produced on combustion were then swept along in a helium stream over a combustion catalyst (Cr_2O_3) and other suitable reagents, e.g. silver wool to assure complete oxidation and removal of undesirable by-products, such as sulphur and halides. The mixture of combustion gases was then passed over copper to reduce the nitrogen oxides to elemental nitrogen and to remove excess oxygen. Finally, a magnesium perchlorate chemical trap was used to remove water before the gas mixture was directed to the chromatographic column, where the individual components were separated and eluted (as carbon dioxide and nitrogen in C and N analysis) with the help of a thermal conductivity detector. The thermal conductivity

detector's signal fed to the automatic workstation EAGER 200, where the detector output was recorded as a series of peaks representing the elements of interest, i.e. C and N, where peak area (mV x sec) was directly proportional to element concentration.

The data output from the CHNS-O elemental analyser was used to calculate carbon and nitrogen concentrations (µg l^{-1}) using equation 2.7 (Zimmermann et al., 1997):

$$Carbon\ or\ Nitrogen\ concentration\ (\mu g\ l^{-1}) = \frac{corrected\ carbon\ or\ nitrogen\ in\ \ sample}{volume\ filtered \div 2} \quad (2.7)$$

Where volume filtered was divided by 2 since only half filters were pelleted for analysis, and corrected carbon or nitrogen (C or N) in the sample (µg) was calculated using equation 2.8:

$$Corrected\ C\ or\ N\ in\ sample\ (\mu g) = \frac{(std.1\ C\ or\ N\ peak\ area \times C\ or\ N\ in\ sample)}{(std.1\ C\ or\ N\ peak\ area + std.2\ C\ or\ N\ peak\ area) \div 2} \quad (2.8)$$

Where peak area units are mV x sec, standard 1 (std.1) was run before samples and standard 2 (std.2) after samples, and C or N in sample was calculated using equation 2.9:

$$C\ or\ N\ in\ sample\ (\mu g) = \frac{(std.C\ or\ N\ conc. \times std.1\ weight) \times sample\ C\ or\ N\ peak\ area}{std.1\ C\ or\ N\ peak\ area} \times 1000 \quad (2.9)$$

2.3.5. Phytoplankton identification and enumeration

Water samples were collected for phytoplankton analysis by (1) inverted light microscopy and (2) CytoBuoy CytoSense flow cytometry.

2.3.5.1. Inverted light microscopy

25 – 100 ml of water sample was decanted into a darkened glass bottle and fixed with 0.25 – 1 ml of Lugol's iodine (final concentration of 1 % iodine), for inverted light microscope analysis of phytoplankton. The darkened bottles were kept at ambient temperature prior to analysis.

Phytoplankton cells were counted based on the method described by Utermöhl (1958). A preserved water sample was gently inverted and 10 ml decanted into a sedimentation chamber to settle for 24 hours prior to counting. Phytoplankton cells were then identified and

counted using a Brunel SP951 inverted trinocular light microscope, where a single counting unit was an individual cell, whether part of a colony/chain or solitary. Numerically abundant taxa (> 50 cells per ml) were counted along a single middle transect under 100x or 250x magnification depending on cell size. Cryptophytes and unidentified small naked dinoflagellates were also counted along a single middle transect at 250x magnification (Strategy A; Fig. 2.6). All other cells ≥ 10 µm were counted at 100x magnification during examination of the entire chamber base plate (Strategy B; Fig. 2.6). Phytoplankton were identified to species where possible, but when this level of identification could not be achieved phytoplankton were generally identified to genus or grouped, e.g. pennate diatoms, small naked dinoflagellates, and classified into size categories where appropriate, e.g. small pennate: 20 – 40 µm length, medium pennate: 40 – 65 µm length, large pennate: 65 – 110 µm length, extra-large pennate: 110 – 175 µm length; small *Pleurosigma*: ~50 µm length, medium *Pleurosigma*: 80 – 170 µm length, large *Pleurosigma*: 170 - 200 µm length, extra-large *Pleurosigma*: > 200 µm length. Further details of the phytoplankton identification and enumeration strategy employed is presented in the methods of the data chapters (chapters 3 - 6). Methodological issues and limitations associated with this phytoplankton analysis are well documented (Uehlinger, 1964, Rott, 1981, Leakey et al., 1994), and include irregular or patchy sedimentation, subsampling discrepancies and sample degradation during storage (e.g. reduction in cell size and abundance).

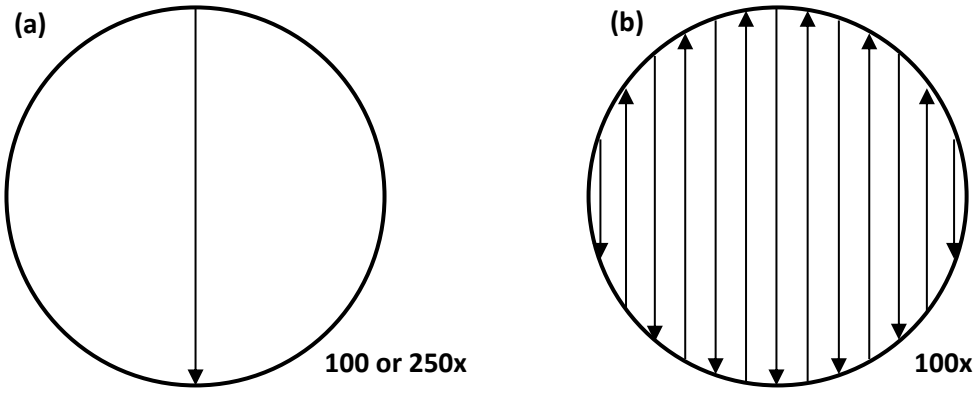

Figure 2.6. Strategies of counting cells settled in a sedimentation chamber (circle represents the bottom of the chamber). **(a)** single central transect (either at 100x or 250x magnification); **(b)** entire sedimentation chamber (at 100x magnification).

The following equations (2.10 and 2.11) were applied to determine cell numbers per millilitre:

Counting strategy A: $Cells\ ml^{-1} = \frac{Total\ cells\ counted}{Sample\ volume}$ (2.10)

Counting strategy B: $Cells\ ml^{-1} = \frac{\left(Total\ cells\ counted \times \left(\frac{CA}{TA}\right)\right)}{Sample\ volume}$ (2.11)

Where CA is sedimentation chamber area (mm^2) and TA is transected area (mm^2), which were calculated using equations 2.12 and 2.13 respectively:

$$CA = \pi(CR)^2 \quad (2.12)$$

$$TA = (CD \times FD) \quad (2.13)$$

Where CR is the sedimentation chamber radius (12 mm), CD is the chamber diameter (24 mm), and FD is the field of view diameter at the magnification used (1.85 mm at 100x magnification and 0.73 mm at 250x magnification).

Phytoplankton biovolume and carbon estimations

Use of carbon biomass data instead of abundance data provides a more accurate representation of phytoplankton community structure when the community consists of many different taxa of a variety of sizes (Paasche, 1960). Therefore, carbon biomass data was estimated for all phytoplankton identified, including for separate size categories and where appropriate for different years (Table 2.3).

Microscopic digital images of phytoplankton were taken using a fixed aperture Canon EOS 1000D digital SLR camera. These images were analysed in open source software Image J for dimensions (length/height/width/diameter in µm) needed to determine biovolume (μm^3). Biovolumes were generally determined for 30 - 50 cells per taxon/taxon size category to avoid bias (only less in cases of rarely occurring taxa) using the geometric shapes and formulae documented by Olenina et al. (2006). Cell biovolumes were converted to cell carbon biomass using carbon – biovolume relationships of Menden-Deuer and Lessard (2000), following equations 2.14 – 2.23. Sources of error associated with cell carbon biomass estimation are discussed by Menden-Deuer and Lessard (2000) and Olenina et al. (2006), including the use of

basic geometric shapes that are very simplified forms of actual cell shape and determination of 'hidden' dimensions.

Diatoms and silicoflagellates: $Pg\ C\ cell^{-1} = 0.288 \times biovolume^{0.811}$ (2.14)

Dinoflagellates: $Pg\ C\ cell^{-1} = 0.760 \times biovolume^{0.819}$ (2.15)

Loricate ciliates: $Pg\ C\ cell^{-1} = 0.679 \times biovolume^{0.841}$ (2.16)

Aloricate ciliates: $Pg\ C\ cell^{-1} = 0.230 \times biovolume^{0.984}$ (2.17)

Chlorophytes: $Pg\ C\ cell^{-1} = 0.094 \times biovolume^{1.088}$ (2.18)

Chrysophytes: $Pg\ C\ cell^{-1} = 0.020 \times biovolume^{1.218}$ (2.19)

Prasinophytes: $Pg\ C\ cell^{-1} = 0.285 \times biovolume^{0.886}$ (2.20)

Prymnesiophytes: $Pg\ C\ cell^{-1} = 0.228 \times biovolume^{0.899}$ (2.21)

Other/unidentified flagellates > 3000 µm^3: $Pg\ C\ cell^{-1} = 0.216 \times biovolume^{0.939}$ (2.22)

Other/unidentified flagellates < 3000 µm^3: $Pg\ C\ cell^{-1} = 0.261 \times biovolume^{0.860}$ (2.23)

Total carbon biomass of each taxon was calculated by multiplying cell carbon by cell abundance.

Table 2.3. Average cell biovolume (µm^3) and carbon content (Pg C cell^{-1}) of different phytoplankton taxa identified from summer field surveys in the Western English Channel between 2013 and 2016.

Phytoplankton	Cell biovolume (µm^3)	Carbon content (Pg C cell^{-1})
Diatoms		
Asterionellopsis glacialis	348.86	33.23
Bacillaria paxillifer	2177.52	146.72
S centric diatom (20-30 µm dia.)	7199.26	386.95
M centric diatom (30-50 µm dia.)	38072.82	1493.73
L centric diatom (60-150 µm dia.)	109857.02	3527.80
XL centric diatom (> 150 µm dia.)	660779.79	15116.75
Cerataulina pelagica	21623.53	944.10
2013 *Chaetoceros spp.*	650.54	55.08
2014 *Chaetoceros spp.*	748.94	61.74
2015 *Chaetoceros spp.*	653.26	55.26
2016 *Chaetoceros spp.*	300.53	29.44
Corethron criophylum	34453.99	1377.51
Cylindrotheca closterium	287.07	28.37

Dactyliosolen fragillissimus	2662.68	172.71
Delphineis surirella	175.00	18.99
Detonula confervacea	3533.00	217.24
Detonula pumila	28218.74	1171.60
Diploneis spp.	2818.28	180.85
Ditylum brightwelli	45575.49	1728.32
Entomoneis spp.	5070.29	291.19
Eucampia zoodiacus	7995.34	420.46
Guinardia delicatula	9209.88	472.50
Guinardia flaccida	277922.74	7488.85
2014 *Guinardia striata*	9437.87	481.96
2015-6 *Guinardia striata*	60553.50	2176.24
Helicotheca tamesis	6007.88	334.15
Lauderia annulata	6057.07	336.36
Leptocylindrus danicus	1299.90	96.55
Leptocylindrus minimus	178.04	19.26
Licmophora sp.	24523.98	1045.56
Lithodesmium undulatum	4142.62	247.17
Meuniera membranacea	21586.63	942.79
Odontella regia/mobiliensis	96230.07	3168.53
Odontella sinensis	707729.86	15982.14
Paralia sulcata	2052.97	139.87
2013-2015 S pennate diatom (20-40 µm length)	563.66	49.03
2016 S pennate diatom (20-40 µm length)	1167.43	88.49
2013-15 M pennate diatom (40-65 µm length)	3162.71	198.58
2016 M pennate diatom (40-65 µm length)	1749.68	122.87
L pennate diatom (65-110 µm length)	16182.54	746.33
2013-15 XL pennate diatom (110-175 µm length)	45731.02	1733.10
2016 XL pennate diatom (110-175 µm length)	5218.99	298.10
S *Pleurosigma spp.* (~50 µm)	1450.65	105.54
M *Pleurosigma spp.* (80-170 µm)	14548.80	684.61
L *Pleurosigma spp.* (170-200 µm)	33872.00	1358.61
XL *Pleurosigma spp.* (> 200 µm)	53466.30	1967.28
Podosira stelligera/glacialis	77673.87	2663.21
Proboscia alata	9579.54	487.82
Proboscia truncata	525936.62	12562.31
2013 S *Pseudo-nitzschia spp.* (< 2.5 µm dia.)	324.42	31.33
2014-5 S *Pseudo-nitzschia spp.* (< 2.5 µm dia.)	255.63	25.82

2016 S *Pseudo-nitzschia spp.* (< 2.5 µm dia.)	274.90	27.39
2014-5 L *Pseudo-nitzschia spp.* (> 2.5 µm dia.)	1909.04	131.87
2016 L *Pseudo-nitzschia spp.* (> 2.5 µm dia.)	1989.97	136.38
2013-15 S *Rhizosolenia spp.* (≤ 10 µm dia.)	5992.79	333.46
2016 S *Rhizosolenia spp.* (≤ 10 µm dia.)	16673.96	764.66
M *Rhizosolenia spp.* (10-20 µm dia.)	29744.24	1222.71
2013-15 L *Rhizosolenia spp.* (> 20 µm dia.)	225629.13	6324.06
2016 L *Rhizosolenia spp.* (> 20 µm dia.)	386276.68	9780.64
Skeletonema costatum	41.85	5.95
Stephanopyxis turris	127714.18	3986.14
Striatella unipunctata	48227.55	1809.44
Thalassionema nitzchioides	612.97	52.48
2015 XS *Thalassiosira spp.* (< 10 µm height)	486.77	43.53
S *Thalassiosira spp.* (10-25 µm height)	2569.81	167.03
M *Thalassiosira spp.* (25-45 µm height)	11820.39	578.49
L *Thalassiosira spp.* (> 45 µm height)	15343.20	714.78
Dinoflagellates		
2013-15 10-30 µm armoured dinoflagellates	2795.15	505.15
2016 10-30 µm armoured dinoflagellates	4977.82	810.38
2013-15 10-20 µm naked dinoflagellates	245.15	68.83
2016 10-20 µm naked dinoflagellates	306.77	82.70
2013-15 20-25 µm naked dinoflagellates	1157.47	245.37
2016 20-25 µm naked dinoflagellates	1875.99	364.41
Alexandrium ostenfeldii	35848.98	4082.54
Amphidinium carterae	5154.58	833.87
Amylax triacantha	4937.28	804.97
Ceratium furca	56714.78	5944.16
Ceratium fusus	15036.11	2003.95
Ceratium lineatum	15162.35	2017.72
Ceratium macroceros	50001.09	5361.39
Ceratium tripos	157559.06	13725.23
Ceratoperidinium falcatum	49753.06	5339.60
2013-15 *Dinophysis acuminata*	12459.10	1717.98
2016 *Dinophysis acuminata*	10231.24	1461.99
Dinophysis acuta	70002.55	7062.56
Dinophysis caudata	64688.23	6620.33
Dinophysis norvegica	8365.36	1239.73
Dinophysis tripos	78165.74	7730.26

Diplopsalis lenticula	14919.97	1991.27
Dissodinium sp.	52610.90	5589.52
2013-15 *Gonyaulax spinifera*	6942.31	1064.16
2016 *Gonyaulax spinifera*	8332.65	1235.76
Gyrodinium spp.	15195.32	2021.31
Heterocapsa spp.	625.79	148.28
Karenia mikimotoi	6971.88	1067.87
Katodinium glaucum	1674.49	332.03
Micracanthodinium sp.	302963.86	23446.21
Nematodinium torpedo	5416.92	868.47
2013-14, 16 *Noctiluca scintillans*	4597188.63	217467.72
2015 *Noctiluca scintillans*	34583933.27	1135407.38
Oblea rotundata	4605.66	760.41
Phalacroma rotundatum	20432.19	2576.09
2013-14 *Polykrikos schwartzii/kofoidii*	162797.26	14097.84
2015-16 *Polykrikos schwartzii/kofoidii*	201192.57	16767.63
Pronoctiluca sp.	1912.27	370.17
2013-15 *Prorocentrum micans*	8814.06	1293.94
2016 *Prorocentrum micans*	10701.83	1516.84
Prorocentrum minimum	982.12	214.49
Prorocentrum triestinum	2181.18	412.29
2013-15 S *Protoperidinium spp.* (10-30 µm dia.)	3929.82	667.74
2016 S *Protoperidinium spp.* (10-30 µm dia.)	4479.64	743.33
2013-15 M *Protoperidinium spp.* (30-65 µm dia.)	28108.46	3345.12
2016 M *Protoperidinium spp.* (30-65 µm dia.)	19709.46	2501.22
2013-15 L *Protoperidinium* (65-120 µm dia.)	212451.12	17532.29
2016 L *Protoperidinium spp.* (65-120 µm dia.)	102697.60	9666.77
Scrippsiella trochoidea	3167.00	559.49
Torodinium robustum/teredo	1656.56	329.11
unidentified gymnoid athecate dinoflagellate	15069.13	2007.56
Flagellates		
Chlamydomonas spp.	16117.41	3560.72
Chrysochromulina spp.	2325.22	242.35
Chrysophaerella longispina	13042.00	2082.04
2013 cryptophytes	22.11	3.74
2014-16 cryptophytes	26.62	4.39
Cymbomonas tetramitiformis	649.58	88.51
Dictyocha fibula/speculum	44321.64	1689.65

Eutreptiella spp.	754.00	77.90
Leptocylindrus mediterraneus - Solenicola setigera	10426.72	1282.45
Pleurasiga spp.	43359.00	4888.97
2013 *Pseudopedinella/pyramimonas spp.*	872.33	77.22
2016 *Pseudopedinella/pyramimonas spp.*	947.85	123.71
Schroederia setigera	900.17	154.28
Solenicola setigera	1870.14	170.14
2014 *Trachelomonas volvocinopsis*	928.90	93.21
2016 *Trachelomonas volvocinopsis*	1513.96	141.87
unidentified chlorophytes (> 20 µm)	1450.26	259.21
unidentified spherical flagellate (10-20 µm dia.)	521.28	56.71
Non-flagellated chlorophyceae		
Oocystaceae sp.	1977.87	363.30
Tetraedron spp.	18618.58	4165.83
Ciliates		
S aloricate ciliates (< 20µm)	1539.57	314.34
2013-15 M aloricate ciliates (20-40 µm)	6547.66	1306.26
2016 M spherical aloricate ciliates (20-40 µm dia.)	9277.76	1840.62
2016 M 'pear-shaped' aloricate ciliates (20-40 µm length)	4571.20	917.21
2013-15 L aloricate ciliates (> 40 µm)	30558.11	5947.91
2016 L spherical aloricate ciliates (> 40 µm dia.)	67908.31	13050.05
2016 L 'pear-shaped' aloricate ciliates (> 40 µm length)	52410.54	10113.65
Tiarina fusus	25104.70	4901.84
S bowl shaped tintinnids (20-50 µm length)	11706.68	1792.89
L bowl shaped tintinnids (> 60 µm length)	223799.78	21440.35
S tapering tintinnids (40-60 µm)	11027.67	1705.02
L tapering tintinnids (> 60 µm)	37284.85	4749.62

A linear regression analysis was performed to assess the relationship between carbon derived from POC analysis (see 2.3.4.) and carbon estimates derived from cells counts (Fig. 2.7).

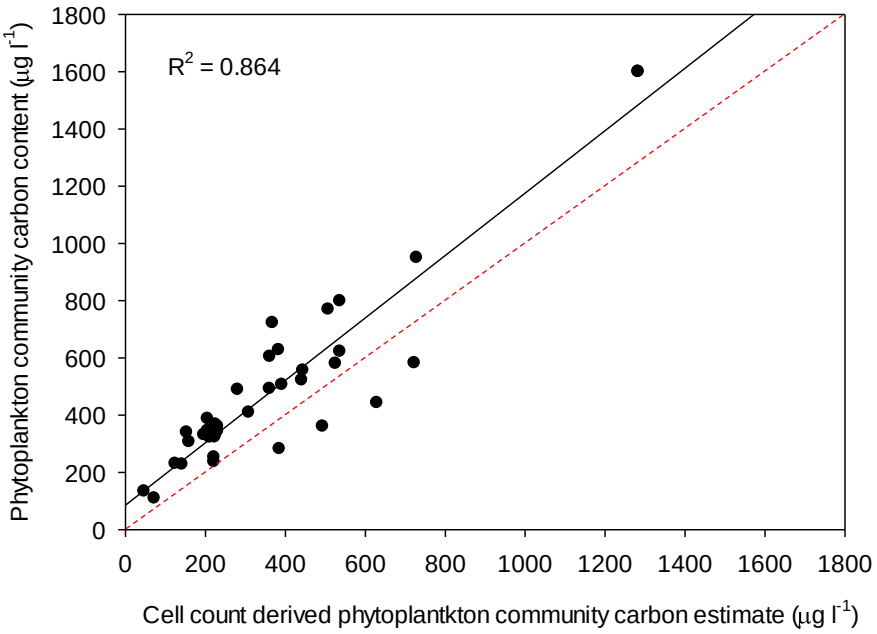

Figure 2.7. Relationship between carbon estimates derived from cell counts and carbon derived from POC analysis (goodness of fit indicated by R^2). 1:1 line is also presented (dashed red line).

Regression analysis showed very good agreement between cell count derived carbon estimates and carbon concentrations derived from POC analysis (R^2 = 0.864). Therefore, confidence could be had in the estimates of phytoplankton carbon biomass derived from cell counts. Carbon concentrations derived using cell counts were typically lower than those derived by POC analysis (33 of 37 data points fell above 1:1 line; Fig. 2.7). This observed difference may have arisen for a number of reasons, including cell counts did not include most phytoplankton < 10 µm; POC samples were collected on Whatman GF/F filters with a porosity of 0.7 µm, thus retaining not only phytoplankton, but any particle above this threshold, such as heterotrophic bacteria, zooplankton and detritus; and Lugol's iodine fixation can reduce cell volume (Montagnes et al., 1994).

2.3.5.2. CytoSense flow cytometry

Samples for flow cytometric analysis were collected following Marie et al. (2005). 10 ml of water sample was decanted into a sterile polypropylene tube and fixed with 50 µl of Sigma-Aldrich 50 % glutaraldehyde solution to achieve a final concentration of 0.25 %. Glutaraldehyde was used as it preserves chlorophyll-fluorescence. Samples were stored in a - 80 °C freezer prior to analysis.

Samples were analysed on a CytoBuoy CytoSense flow cytometer (Fig. 2.8), which is a fixed beam scanning flow cytometer, with a 20 mW 488 nm excitation laser. Prior to analysis the CytoSense was primed with appropriate (of similar refractive index to sample) sheath fluid (0.2 µm sterile filtered seawater + 0.1 % Proclin 950 biocide). CytoUSB v5.7.5.7 software was then loaded, diagnostic checks performed (Table 2.4) and the sample inlet tube rinsed with sheath fluid by running the sample pump at 10 µl s^{-1} for 1 minute.

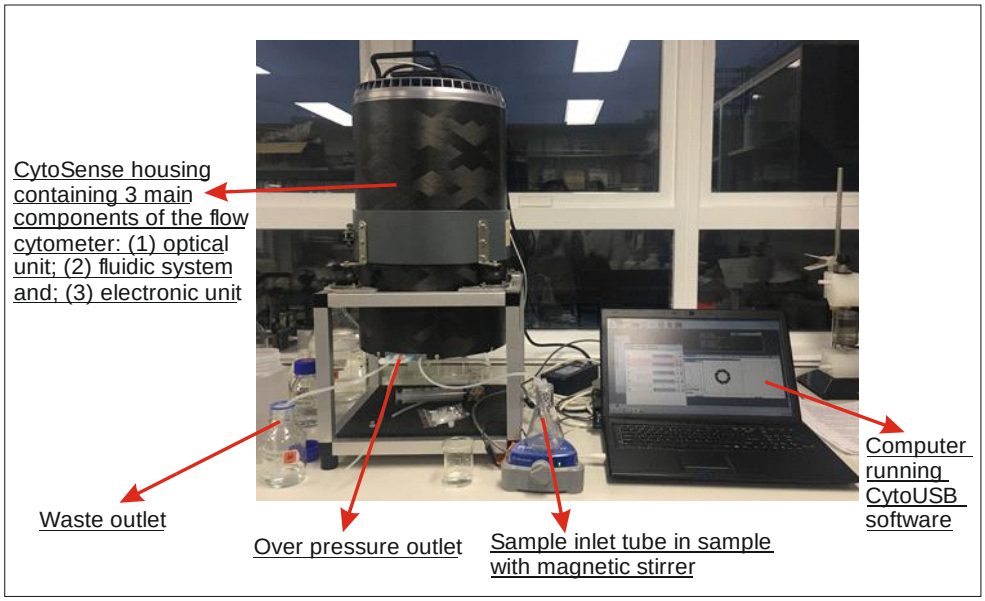

Figure 2.8. CytoSense in operation (photograph courtesy of Amani Alshatti (2016)).

Table 2.4. Diagnostic parameters examined during diagnostic checks (CytoBuoy, 2014).

Diagnostic Parameter	Safe range
Internal battery	10 – 13.6 V
Wall power voltage	13 – 13.6 V
Recharge current	0 – 700 mA
System and sheath temperature	1 – 50 °C
Differential pressure	-300 – 0 mB
Absolute pressure	0.2 – 600 mB

Each sample was homogenised via gentle inversion and a small magnetic stirrer (minimal rpm) was added to prevent sedimentation of heavier cells during the data acquisition period. Each sample was run twice using two different protocols; run 1 with optimal acquisition settings for meso- micro- and nano-phytoplankton, and run 2 with optimal acquisition settings for pico-phytoplankton (and heterotrophic bacteria) (Table 2.5). For run 1 a red fluorescence trigger

level was chosen to exclude dead cells and debris, and for run 2 a sideways scatter (SWS) trigger channel was originally chosen to prevent exclusion of heterotrophic bacteria. However, heterotrophic bacteria data was not considered in later analysis, and therefore particles with a total red fluorescence (TRFL) signal below 10 mV were gated and removed from the raw data during processing. Gating and removal of particles with a TRFL < 10 mV ensured exclusion of non-phytoplankton pico-particles/debris/electronic noise. A high pump speed was chosen for run 1 as this captures more 'rare events' such as larger cells, i.e. nano-, micro- and meso-phytoplankton, but in combination with a high trigger level is at the expense of small cells. Therefore, a low pump speed was chosen for run 2 to ensure small cells were included in the data collected. Image in flow was disabled for run 2 as the camera could not capture cells < 5 µm.

Table 2.5. CytoSense acquisition settings for run 1 and 2 performed on each sample.

	Run 1	**Run 2**
Replicates	3	2 (insufficient sample for 3)
Trigger channel	Red fluorescence (RFL)	Sideways scatter (SWS)
Trigger level	30 mV	25 mV
Pump speed	10 µl s^{-1}	0.1 µl s^{-1}
Stop conditions	150 seconds or 10,000 cells	10,000 cells
Image in flow	Enabled	Disabled

To run a sample the sample inlet tube was placed into the sample and flushed through the machine at high speed for approximately 1 minute (flush time was calibrated to tube length). Flow rate was then reduced to the acquisition rate specified and data acquisition by the CytoUSB software began. Replicate analyses were performed for all samples and between each replicate run the instrument was flushed. For every 100 ml of sample run through the CytoSense an injection of 400 µl Proclin 950 biocide was performed by attaching a Proclin syringe to the sample inlet tube, running the sample pump for 40 seconds at a rate of 10 µl s^{-1} and then running the sheath pump for 5 minutes to let the biocide permeate the system.

To calibrate cell size estimates generated by the CytoSense a set of Thermo Fisher Scientific nonfluorescent polystyrene microspheres with different diameters (1, 2, 6, 10, 15 µm) were analysed for total forwards scatter (TFWS) (Table 2.6). Each microsphere solution was vortexed to break up microsphere aggregates and then 10 µl of each solution was pipetted into 2 ml of

sheath fluid. A magnetic stirrer was added to the microsphere solution mixture to prevent settling and then the solution run in the CytoSense for 1 minute using a pump speed of 1 µl s^{-1} and a SWS trigger of 40 mV. Bead data was processed using CytoClus v3.7.15.3 software by Nicola Pratt of the University of Southampton. Each bead cluster was identified and gated (Fig. 2.9) allowing average values of TFWS to be generated for each cluster (Table 2.6). A square root transformation of the data was performed and used to generate a size calibration curve (Fig. 2.10). TFWS data could then be converted to length (µm) using the linear equation derived from the regression analysis performed between TFWS and bead length (Fig. 2.10).

Table 2.6. Calibration standards with their known lengths and TFWS recorded by the CytoSense.

Calibration standard	Actual length (µm) ± SD	TFWS (mV) ± SD
Bead	1 ± 0	980 ± 50
Bead	2 ± 0	2523 ± 1161
Bead	6 ± 0	10241 ± 419
Bead	10 ± 0	20472 ± 4191
Bead	15 ± 0	49784 ± 1196

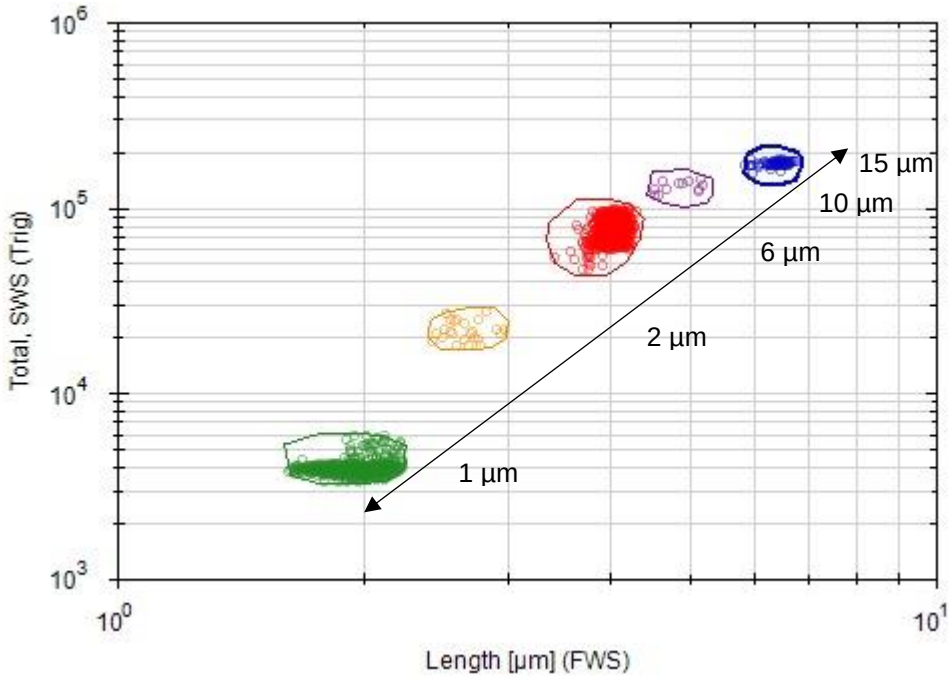

Figure 2.9. Cytogram of the particle properties SWS (mV) and FWS (mV) used to identify and gate each bead cluster. Where the 1 µm bead cluster is in green, the 2 µm bead cluster is in orange, the 6 µm bead cluster is in red, the 10 µm bead cluster is in purple, and the 15 µm bead cluster is in blue.

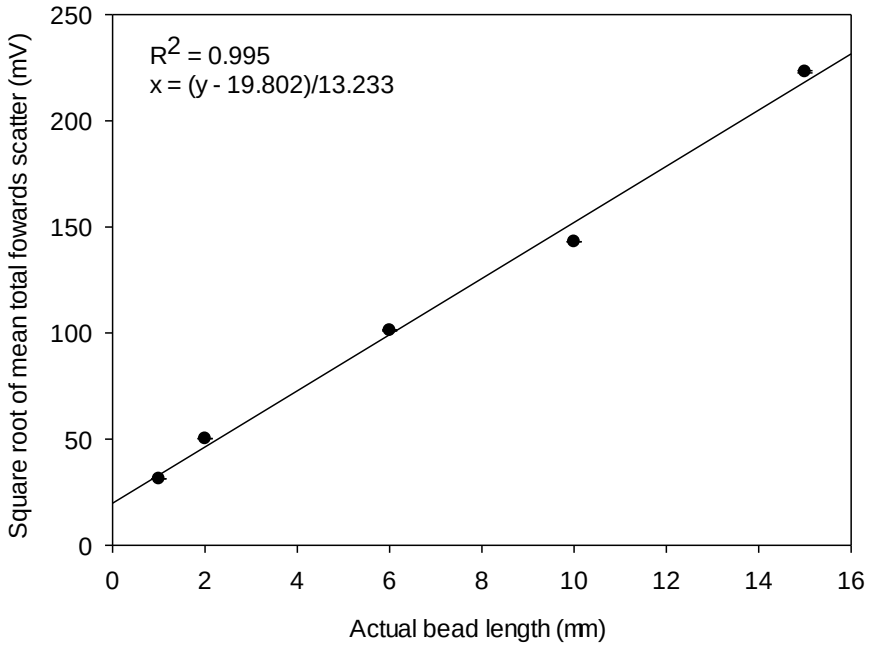

Figure 2.10. Relationship between TFWS (square root transformed) and bead length (goodness of fit indicated by R^2). Error bars indicate standard error of the square root transformed TFWS measurements (all ≤ ± 0.5 mV). The linear equation displayed was applied to obtain calibrated particle sizes.

CytoSense sample data was processed using CytoClus v4.3.1.1 software. First, instrument noise was gated and removed and then the entire population of cells was gated to produce data on community TRFL, where TRFL is a proxy for chlorophyll concentration (Thyssen et al., 2015). TRFL data generated for all gated phytoplankton clusters allowed the contribution of each cluster to total chlorophyll to be determined. Heterotrophic bacteria were gated and removed from all run 2 data files (as described above) before generating community TRFL data.

Phytoplankton clusters within the bulk population were identified based on the fluorescence and scatter properties of each cell. For each sample a cytogram of total orange fluorescence (TOFL) vs. TRFL (e.g. Fig. 2.11 A) was generated to identify cells containing phycoerythrin secondary photopigments (Jeffrey and Vesk, 1997), and a cytogram of TFWS vs. TRFL (e.g. Fig. 2.11 B) was generated to determine cell size, where cell length was approximated from TFWS calibrated against external reference microspheres (Fig. 2.9-10; Table 2.6). This allowed clusters of orange fluorescing pico-phytoplankton, red fluorescing pico-phytoplankton, orange fluorescing nano-phytoplankton, red fluorescing nano-phytoplankton, and micro- and meso-phytoplankton to be resolved (Fig. 2.11 C; Table 2.7). Batch processing was then performed to produce a numerical data output of the measured parameters for cells within each cluster, including TRFL, cell concentration and percentage contribution to total population TRFL.

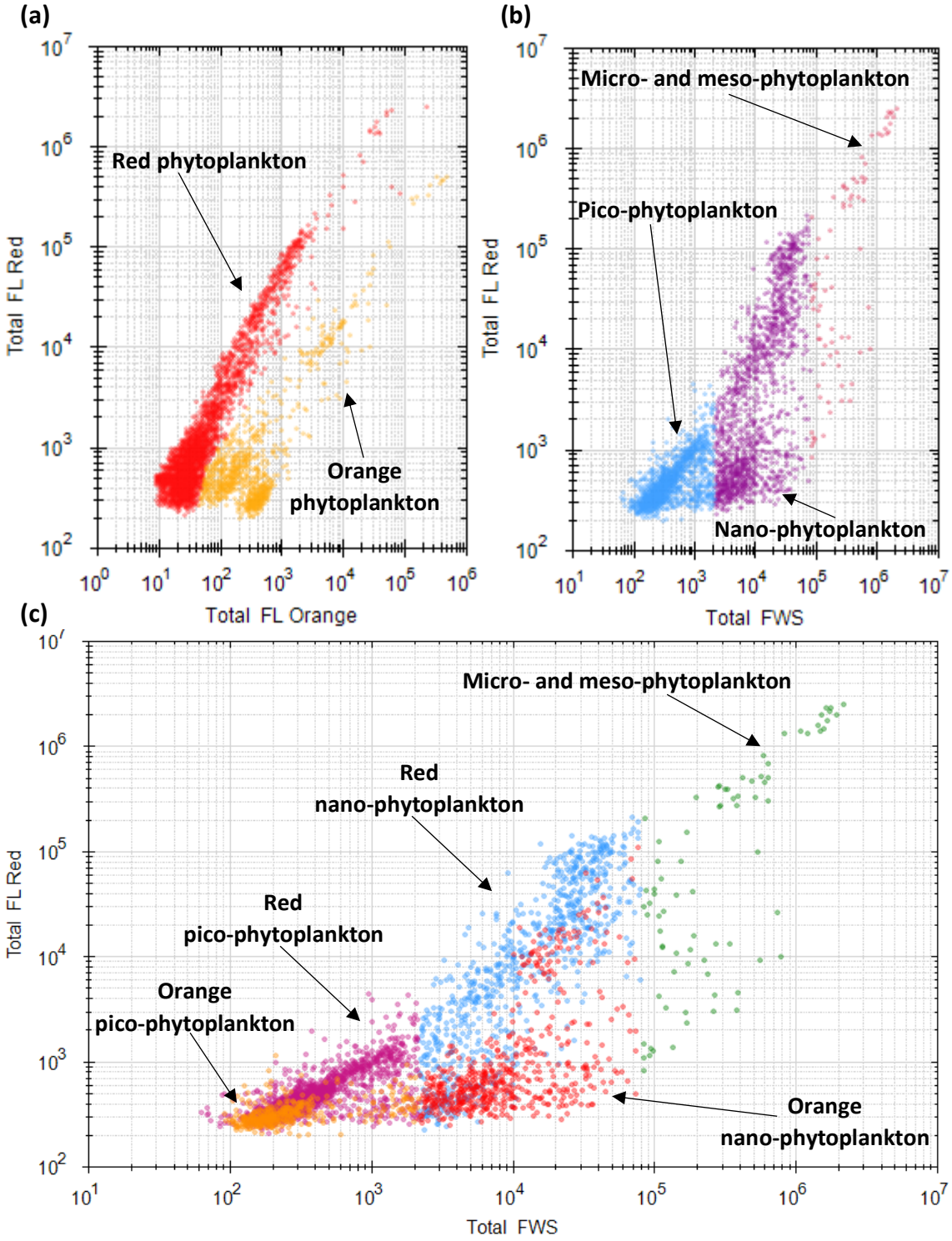

Figure 2.11. Cytograms from CytoClus of a sample analysed with the CytoSense. **(a)** Cytogram of total orange fluorescence (mV) vs. total red fluorescence (mV) allowing identification of orange (orange dots) and red (red dots) fluorescing phytoplankton. **(b)** Cytogram of total forwards scatter (mV) vs. total red fluorescence (mV) allowing identification of pico- (blue dots), nano- (purple dots), and micro- + meso- (crimson dots) phytoplankton. **(c)** Intersections of clusters identified in cytograms (a) and (b) combined to identify orange fluorescing pico-phytoplankton (orange dots), red fluorescing pico-phytoplankton (pink dots), red fluorescing nano-phytoplankton (blue dots), orange fluorescing nano-phytoplankton (red dots), and micro- + meso-phytoplankton (green dots).

Table 2.7. Description of phytoplankton types identified by CytoSense flow cytometric analysis of water samples from the Western English Channel in June/July of 2014 to 2016. RFL represents red fluorescence (> 670 nm) and OFL represents orange fluorescence (590 – 620 nm). The size classification of phytoplankton is as given by Sieburth et al. (1978).

Size	ID	Fluorescence	Description
< 2 µm < 2141 TFWS	Orange pico-phytoplankton/ Pico-prokaryotes	RFL and OFL	→ Cyanophytes, e.g. *Synechococcus*
	Red pico-phytoplankton/ Pico-eukaryotes	RFL	→ Flagellates, such as Prymnesiophytes and Chlorophytes
2 – 20 µm 2141 - 80919 TFWS	Orange nano-phytoplankton	RFL and OFL	→ Cryptophytes → Rhodophytes
	Red nano-phytoplankton	RFL	→ Diatoms → Dinoflagellates → Flagellates, such as Chlorophytes and Prymnesiophytes (including *Phaeocystis* and coccolithophores)
> 20 µm > 80919 TFWS	Micro- and meso-phytoplankton	High RFL	→ Diatoms → Dinoflagellates → Flagellates → Silicoflagellates → Photosynthetic ciliates, e.g. *Mesodinium rubrum*

CytoSense flow cytometry holds a significant advantage over the more conventional light microscopy analysis of phytoplankton as it allows for quantification of the entire nano- and pico-phytoplankton population, which cannot be achieved with light microscopy (Peperzak et al., 2000). Since recent evidence suggests that the nano- and pico-phytoplankton populations within coastal waters are a significant contributor of primary productivity (Tarran and Bruun, 2015), it is important these phytoplankton are considered too when studying phytoplankton community structure and its relationship to biogeochemical cycling and higher trophic levels.

CytoSense flow cytometry also has advantages over other types of commercial flow cytometry as detailed by CytoBuoy (2014). Most notably the CytoSense analyses particles over a much

larger size range (~0.2 - 2000 µm) in comparison to other flow cytometers, thus possessing the ability to analyse cells across the entire phytoplankton size range. In addition, the CytoSense records scatter (forward and side) and fluorescence profiles (e.g. Fig. 2.12), presenting the opportunity for taxonomic identification of cells. However, absence of a sufficient scan profile library prevented thorough taxonomic identification of particles via particle profile analysis.

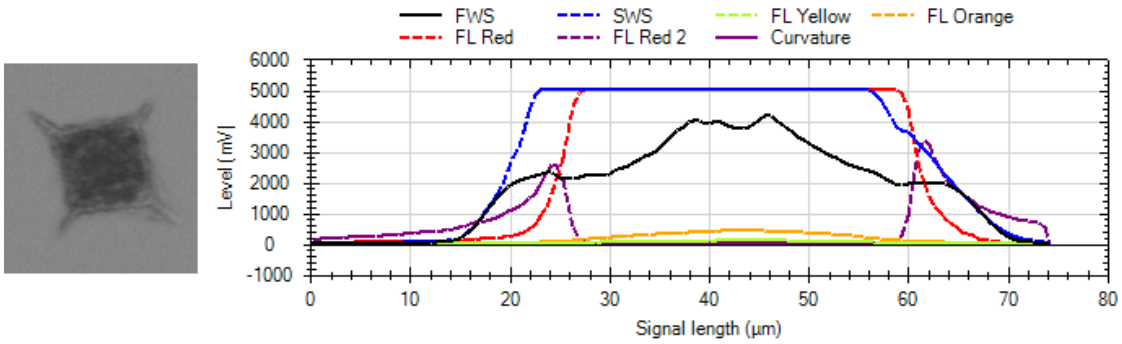

Figure 2.12. *Dictyocha fibula* cell captured by the CytoSense camera and its corresponding scan profile. Where FWS is forward scatter, SWS is sideways scatter, FL yellow is yellow fluorescence, FL orange is orange fluorescence and FL red is red fluorescence.

Sources of error associated with this CytoSense flow cytometric analysis of the phytoplankton community arise principally due to preservation and storage of samples for later analysis as documented by Owen (2014). Issues associated with preservation with glutaraldehyde and storage for later analysis include sample degradation, e.g. reduction in cell abundance and red fluorescence (Hall, 1991, Sato et al., 2006, Katano et al., 2009), and shifts in cell size (Menden-Deuer et al., 2001, Owen, 2014).

2.3.6. Fluorescence Induction and Relaxation (FIRe)

The FIRe technique is an extension of fast repetition rate fluorometry (FRRF), whereby induction and subsequent relaxation of chlorophyll fluorescence yield is detected and measured following active stimulation by a sequence of excitation flashlets, providing information on the photophysiological characteristics of the phytoplankton community (Bibby et al., 2008). The Satlantic FIRe instrument was used to obtain measurements of photophysiological parameters detailed in Table 2.8 and Figure 2.13, following the protocol described by Bibby et al. (2008). Approximately 5 ml of water sample was decanted into a cuvette, following at least 25 minutes of being dark adapted (sample placed in dark cupboard), and placed into the FIRe instrument. 30 unique iterations from the same sample were averaged, the sample delay was set at 1000 ms and gain was set at 50-70 % of the sensor's

saturation. The blank was deduced twice daily (beginning and end) by running a water sample in the FIRe instrument that had been filtered through a Whatman GF/F filter.

Table 2.8. List of photophysiological parameters measured by the FIRe instrument or derived from measurements taken by the FIRe instrument as described by Kromkamp and Forster (2003).

Parameter	Definition	Measured/Derived
Fm	Maximal fluorescence yield, a measure of total chlorophyll.	Measured
Fo	Dark adapted minimal fluorescence yield.	Measured
Fv	Variable fluorescence (Fv = Fm – Fo).	Measured
SigmaPSII ($Å^2$ $quanta^{-1}$)	The maximum PSII effective absorption cross section, a measure of the size of the light-harvesting antenna system associated with the photochemical reaction centre PSII.	Measured
Fv/Fm	The maximum photochemical efficiency, which represents the amount of energy PSII absorbs to that which is emitted, thus is a measure of photosynthetic efficiency. Among other parameters, Fv/Fm is related to light and nutrient availability (Kolber et al., 1988), with maximal values of 0.65-0.7 (Koblížek et al., 2001).	Derived

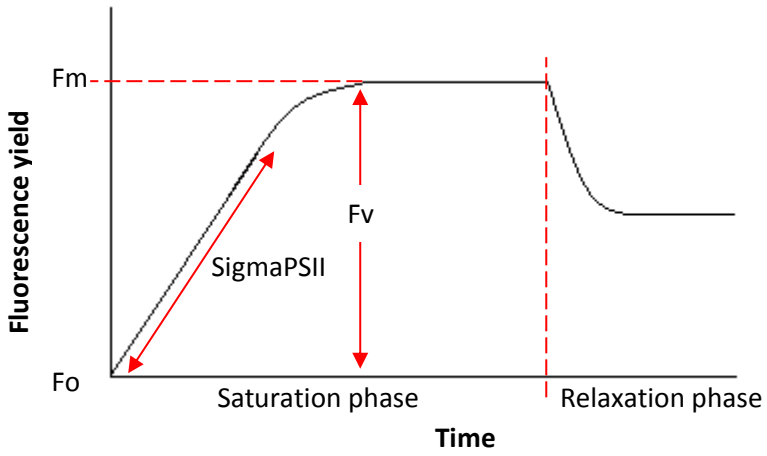

Figure 2.13. FIRe measurement protocol. Photophysiological parameters generated are indicated (Table 2.8 for parameter definitions).

Size fractionated water samples were also run in the FIRe system. 50 ml of water sample was first passed through a 50 µm pore size mesh circle (25 mm diameter) and then passed through a series of 25 mm Whatman track-etched polycarbonate membranes of varying pore sizes (20 → 10 → 5 µm). Particles collected on each mesh/membrane circle were resuspended with filtered seawater and measured in the FIRe instrument immediately. The final filtrate (with particles < 5 µm) was measured last. Thus, photophysiological parameters were measured for the following size fractions: > 50 µm, 20 – 50 µm, 10 – 20 µm, 5 – 10 µm and < 5 µm.

Raw FIRe data was processed in MATLAB R2013a using script generated by Professor Mark Moore of the University of Southampton that fitted the variable fluorescence data to the model of Kolber et al. (1988). This script was modified to include correction for gains of 0, 200, 400, 600, 800, 1000, 1200 and 2400. The parameter of Fv/Fm could then be calculated using equation 2.24, which includes blank correction:

$$\frac{Fv}{Fm} = \frac{(Fm_{sample} - Fm_{blank}) - (Fo_{sample} - Fo_{blank})}{(Fm_{sample} - Fm_{blank})} \quad (2.24)$$

Chlorophyll determination using FIRe measurements of Fm

The small syringe volume of the slurp gun precluded chlorophyll determination by the standard method described in section 2.3.1. Instead FIRe generated Fm values were used to determine chlorophyll concentration. Fm measurements were collected for slurp gun samples and for corresponding Niskin water bottle samples on 30 occasions, so the relationship between Fm and chlorophyll concentration could be investigated (Fig. 2.14). Fm measurements were well correlated with chlorophyll a concentrations determined by the standard method (R^2 = 0.870), and the equation of this linear relationship (x = (y – 3.9274)/10.576) was used to convert Fm values to chlorophyll a concentrations.

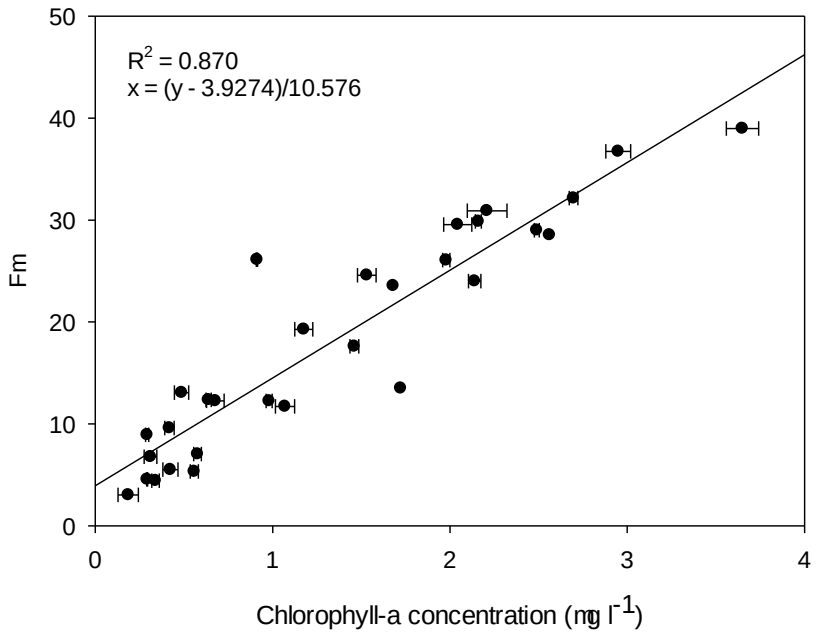

Figure 2.14. Relationship between chlorophyll a concentration and Fm (goodness of fit indicated by R^2). Error bars indicate standard error of the chlorophyll concentration values. The linear equation displayed was used to derive chlorophyll a concentrations from Fm values measured for slurp gun samples.

FIRe determined rETR as a function of irradiance

In conjunction with ^{13}C and ^{15}N incubations, relative electron transport rates (rETR) as a function of irradiance were determined (as described in section 2.3.7.2.) from FIRe measurements acquired using the actinic light source (ALS) and PAR stepping acquisition mode. rETR is a measure of photosynthetic activity (Genty et al., 1989, Kromkamp et al., 1998) that when determined as a function of irradiance over a light range can be used to generate a light response curve of photosynthetic activity, much like a photosynthesis vs. irradiance (P vs. E) curve. PAR stepping was set up with 20 PAR increments between 0 – 1000 µmol m^{-2} s^{-1} and a PAR on interval of 90 seconds between data acquisition events (each PAR step with its associated iterations is one data acquisition event). This data was used to generate rETR vs. irradiance curves, the method and use of which is described in section 2.3.7.2.

2.3.7. Measurements of primary production

Primary production within the stratified waters of the Western English Channel was investigated by running $NaH^{13}CO_3$ + $K^{15}NO_3$ and $Cl^{15}NH_4$ uptake incubation experiments, and taking FIRe measurements using the PAR stepping acquisition mode.

2.3.7.1. ^{13}C and ^{15}N incubations

To determine rates of primary production and the contribution of new and regenerated production to total production, dual ^{13}C (Hama et al., 1983) and ^{15}N (Dugdale and Goering, 1967) incubations were set up as first described by Slawyk et al. (1977).

Samples for use in the incubation experiments were collected from two depths, one from the SCM and one from the surface layer (~10 m: deep enough to avoid issues associated with nonphotochemical quenching processes that occur under excess irradiance (Falkowski and Raven, 1997)). These samples were decanted directly from the Niskin bottle into a blacked-out carboy. Each water sample was divided into two separate 1 L acid washed and Milli-Q rinsed polycarbonate bottles. To one bottle 0.2 ml of 99 atom % ^{15}N 0.5 mmol l^{-1} $K^{15}NO_3$ solution (51.0 mg dissolved in 1 L Milli-Q) and 0.2 ml of 98 atom % ^{13}C 0.5 mol l^{-1} $NaH^{13}CO_3$ solution (0.475 g dissolved in 10 ml pH adjusted Milli-Q (pH 9.5)) was added. To the other bottle 0.2 ml of 99 atom % ^{15}N 0.5 mmol l^{-1} $Cl^{15}NH_4$ solution (27.3 mg dissolved in 1 L Milli-Q) was added. After tracer additions (within 30 minutes of sample collection) the samples were gently mixed and transferred into a Gallenkamp illuminated cooled incubator for 4 hours at simulated *in situ* water temperature (15 – 20 °C), and light levels of 15 and 33 µmol m^{-2} s^{-1} for SCM and surface

samples respectively. Incubations were terminated by simultaneous filtration of samples onto pre-combusted (450 °C, 6 hrs) 25 mm Whatman GF/F filters under low vacuum (< 150 mg Hg) in darkness. Filters were rinsed with pre-filtered seawater from the respective sampling site to remove excess tracer and then stored in petri slides at -20 °C until analysis.

The incubation time chosen was important as too short or too long an incubation can affect nutrient uptake kinetics. It is often the case that uptake rates are not constant over time (Collos, 1983, Lomas et al., 1996) and therefore a short incubation time could result in significant over- or under-estimates of uptake rates. On the other hand, too long an incubation could lead to substrate (C or N) depletion and in the case of ammonium, dilution of $^{15}NH_4^+$ by regenerated NH_4^+ can occur (Fisher et al., 1981). Consequently, a long incubation time could result in significant under-estimation of uptake rates. Dugdale and Wilkerson (1986) reported incubation periods of 2 – 6 hours to be optimal for overcoming issues associated with isotope dilution and inconstant uptake rates. In line with this recommendation and taking into consideration time restraints, a 4 hour incubation period was chosen. This incubation period is similar to that used in many other marine uptake experiments (Slawyk et al., 1977, Hama et al., 1983, Hickman et al., 2012, Seeyave et al., 2013, Fragoso et al., 2017). A relatively short incubation period had the additional benefit of overcoming or minimising many bottle effects that could have influenced C and N uptake rates. These effects include contamination (Dugdale and Wilkerson, 1986, Cullen, 2001), enhanced algal cell damage and mortality (Gieskes et al., 1979), 'unnatural' changes in population structure (Cullen, 2001), and the absence of turbulence experienced *in situ*, which influences nutrients, light, excretion products and CO_2 inside the incubation bottle (De Vooys, 1979). Further bottle effects and other sources of error/limitations associated with incubation experiments are largely discussed by De Vooys (1979), Dugdale and Wilkerson (1986) and Cullen (2001).

The nitrogen tracer to be added during the incubation experiments ideally needed to be ≤ 10 % of that of the ambient N-nutrient concentration, as greater enrichment could promote increased uptake rates (Dugdale and Goering, 1967). On board nutrient analysis was not possible and therefore the concentration of the nitrogen tracer to be added was predetermined by investigation of ambient nutrient concentrations in the Western English Channel in June/July of three previous years (2012-2014) using data collected by the WCO (Woodward, 2015).

Light levels in the surface mixed layer (~10 m) and SCM (at peak intensity) in the Western English Channel during a previous field survey (2013) were also investigated prior to commencement of the incubation experiments. This allowed light intensity ranges at which the samples should be incubated to be determined (10 m: 83.50 – 340.00 µmol m^{-2} s^{-1}; SCM: 9.63 – 64.90 µmol m^{-2} s^{-1}). As it was also important to mimic the *in situ* spectral light environment, following recommendations of Poulton (2004), the polycarbonate sample bottles were wrapped with a single layer of spectrally-correct LEE-Filters colour filter to try to achieve simulation of the light environment representative of 10 m and SCM depth. Mist Blue filter was used to cover surface sample bottles and Marine Blue filter was used to cover SCM sample bottles (Fig. 2.15). Light levels within the wrapped polycarbonate bottles when placed in the incubator were measured with a Biospherical Instruments QSL-2101 4π PAR Scalar Irradiance sensor. A light level of 15 µmol m^{-2} s^{-1} was measured within the marine blue filter wrapped bottles, a light intensity within the range of SCM light levels determined from analysis of 2013 data. A light level of 33 µmol m^{-2} s^{-1} was measured within the mist blue filter wrapped bottles, which was below the range of 10 m light levels determined from analysis of 2013 data. Nevertheless, surface incubations were still operated at this light level as a higher light level could not be achieved with the incubator available for the field survey.

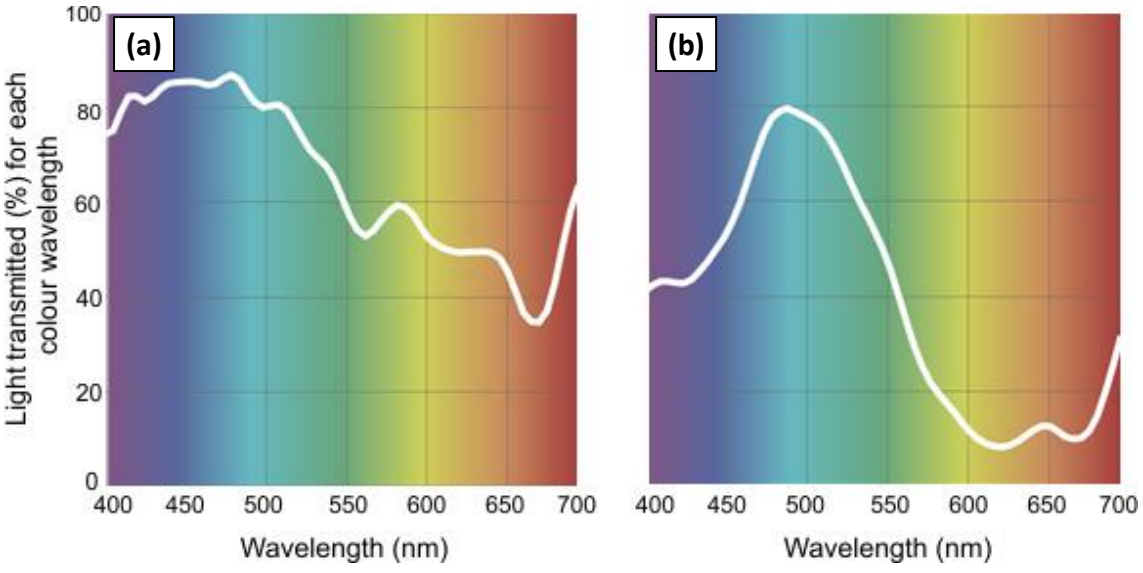

Figure 2.15. Transmission spectra of **(a)** LEE-Filters mist blue colour filter (LEE-Filters, no date-a) and **(b)** LEE-Filters marine blue colour filter (LEE-Filters, no date-b).

On return to the laboratory, samples were dried in a 40 °C oven for 24 hours. Filters were then halved, packed into 8 x 5 mm tin capsules and pelleted ready to be analysed. Three blanks

were also set up by pelleting pre-combusted GF/F filter halves. Analysis was conducted by Iso-Analytical (Crewe, UK) using elemental analysis isotope ratio mass spectrometry (EA-IRMS). Principles of this analysis are described by Fiedler and Proksch (1975).

Prior to running the samples four reference samples and triplicate control check samples were also set up for analysis. The reference material used was wheat flour ($\delta^{13}C_{V\text{-}PDB}$ = -26.43 ‰, $\delta^{15}N_{AIR}$ = 2.55 ‰). Control check samples used in the analysis of samples spiked with $K^{15}NO_3$ and $NaH^{13}CO_3$ included a mixture of ammonium sulphate ($\delta^{15}N_{AIR}$ = -4.71 ‰) and beet sugar ($\delta^{13}C_{V\text{-}PDB}$ = -26.03 ‰), and a mixture of ^{15}N enriched ammonium sulphate ($\delta^{15}N_{AIR}$ = 4692.65 ‰) and ^{13}C enriched glucose ($\delta^{13}C_{V\text{-}PDB}$ = 535.4 ‰). Control check samples used in the analysis of samples spiked with $Cl^{15}NH_4$ included ammonium sulphate ($\delta^{15}N_{AIR}$ = -4.71 ‰) and ^{15}N enriched ammonium sulphate ($\delta^{15}N_{AIR}$ = 4692.65 ‰). Samples were loaded into the auto-sampler of a Europa Scientific elemental analyser (20-20 IRMS) for analysis.

From the auto-sampler tin capsule pellets were sequentially dropped into a furnace held at 1000 °C, where they flash combusted in the presence of oxygen raising the temperature to 1700 °C. The gases produced on combustion were swept in a helium stream over a combustion catalyst (Cr_2O_3), copper oxide wires (to oxidise hydrocarbons), and silver wool to remove sulphur and halides. Resultant gases were carried into a copper reduction stage, held at 600 °C, where nitrogen oxides were converted to elemental nitrogen and any oxygen was removed. Water was removed next when remaining gases passed through a magnesium perchlorate chemical trap. If C was not being analysed then it was also removed using a carbosorb trap, and N was resolved using a packed column gas chromatograph held at 100 °C. If C and N were analysed together they were separated using a packed column gas chromatograph held at 65 °C. The resultant nitrogen peak entered the ion source of the Europa Scientific 20-20 IRMS, where it was ionized and accelerated. Nitrogen gas species of different mass were separated according to their mass to charge ratio (m/z) in a magnetic field. They were then simultaneously measured using a Faraday cup collector array to measure the isotopomers of N_2 at m/z 28, 29, and 30. When both C and N were being analysed the carbon dioxide peak next entered the ion source, being separated in the magnetic field and isotopomers of CO_2 at m/z 44, 45, and 46 measured in the Faraday cup collector array.

The data output from the isotope ratio mass spectrometry analysis included carbon and nitrogen filter content, in units of µg 500 ml^{-1} (since only half filters were packed into tin capsules for analysis), and ^{13}C and ^{15}N atom percent values. ^{13}C atom percent represents the

ratio of ^{13}C atoms to the total number of carbon atoms (^{13}C + ^{12}C) in the sample, i.e. ^{13}C enrichment, and ^{15}N atom percent represents the ratio of ^{15}N atoms to the total number of nitrogen atoms (^{15}N + ^{14}N) in the sample, i.e. ^{15}N enrichment (Fiedler and Proksch, 1975). This data output was used to calculate uptake rates of carbon, nitrate and ammonium (µmol l^{-1} hr^{-1}) using equations 2.25 and 2.26 (Dugdale and Wilkerson, 1986). Following Dugdale and Wilkerson (1986), Legendre and Gosselin (1996) and Marra (2002) all rates determined are considered to be representative of net uptake, although in reality rates captured were somewhere between net and gross uptake.

$$C\ uptake\ rate\ (\rho\ in\ \mu mol\ C\ l^{-1}\ hr^{-1}) = C\ concentration \times V \quad (2.25)$$

$$N\ uptake\ rate\ (\rho\ in\ \mu mol\ N\ l^{-1}\ hr^{-1}) = N\ concentration \times V \quad (2.26)$$

Where C and N concentration (µmol l^{-1}) were determined using equation 2.27:

$$C\ or\ N\ concentration\ (\mu mol\ l^{-1}) = \frac{(C\ or\ N\ filter\ content \div volume\ filtered) \times 1000}{C\ or\ N\ atomic\ weight} \quad (2.27)$$

and V (hr^{-1}) is the transport rate of ^{13}C or ^{15}N from a dissolved inorganic carbon or nitrogen pool (DIC atom % or DIN atom %) into the particulate carbon or nitrogen pool (PC atom % or PN atom %) after time t (4 hours), expressed as equation 2.28:

$$V\ (hr^{-1}) = \frac{PC\ or\ PN\ atom\%}{DIC\ or\ DIN\ atom\% \times t} \quad (2.28)$$

Where PC and PN atom %, and DIC and DIN atom % were calculated using equations 2.29 and 2.30 respectively:

$$PC\ or\ PN\ atom\% = C\ or\ N\ atom\% - {}^{13}C or\ {}^{15}N\ na\ atom\% \quad (2.29)$$

$$DIC\ or\ DIN\ atom\% = \frac{(DIC\ or\ DIN\ conc. \times na\ atom\%) + (tracer\ conc. \times tracer\ atom\%)}{(DIC\ or\ DIN\ conc. + tracer\ conc.) - na\ atom\%} \quad (2.30)$$

Where DIC or DIN concentration refers to the ambient DIC or DIN (nitrate or ammonium) concentration. DIC concentration was not directly measured, instead it was estimated to be 2114 µmol l^{-1}, based on DIC concentrations measured in the Western English Channel in

June/July from 2008-2014 (range of 2036 – 2176 µmol l^{-1}) (Begley, 2016). Total nitrate and ammonium concentrations were measured as described in 2.3.3. However, ammonium concentrations were consistently below the detection limit of 0.1 µmol l^{-1}. Consequently, ammonium concentrations were assumed to be 0.1 µmol l^{-1} for all samples, based on ammonium concentrations measured in the stratified waters (at 0, 10 and 20 m) of the Western English Channel from 2007-2014 (Woodward, 2015). The use of an assumed ambient ammonium concentration may have caused under or overestimation of ammonium uptake rates and thus f-ratios. Specifically, ambient ammonium concentrations below the assumed value of 0.1 µmol l^{-1} would mean f-ratios were underestimated and vice versa. However, it is likely any under or overestimation of f-ratios was fairly minimal (no more than approximately ± 0.17) based on previous ammonium concentrations (typically between 0 – 0.3 µmol l^{-1} at 0, 10 and 20 m depth) in the stratified waters of the Western English Channel (Woodward, 2015). Natural abundance atom % (na atom %) is 1.092 for ^{13}C and 0.3663 for ^{15}N (Bury et al., 1995), tracer concentration after addition to water sample was 100 µmol l^{-1} for ^{13}C and 0.1 µmol l^{-1} for ^{15}N, and tracer atom % was 98 for ^{13}C and 99 for ^{15}N.

Primary production rates determined from a single point in the water column are more typically expressed as weight of carbon per unit volume per unit time following equation 2.31:

$$Primary\ production\ (mg\ C\ m^{-3}hr^{-1}) = ((C\ uptake \times 12.01) \times 0.001) \times 1000 \qquad (2.31)$$

To determine the contribution of new (supported by external sources of N) and regenerated (supported by recycling of N) production to total primary production the f-ratio was determined using equation 2.32 (Dugdale and Goering, 1967):

$$f\ ratio = \frac{Nitrate\ uptake}{(Nitrate\ uptake + Ammonium\ uptake)} \qquad (2.32)$$

2.3.7.2. Depth integrated primary production

Primary production at each quarter of a meter through the water column was estimated using data obtained from ^{13}C incubations and FIRe measurements of rETR, both obtained for discrete samples collected from two depths, surface (10 m) and the SCM. rETR values were determined under a range of irradiances, allowing construction of a light response curve (discussed below). From the light response curve, values of $rETR_{max}$ (maximum relative rate of electron transport) and for the initial slope (α) could be derived. On a rETR light response curve, the value for the

initial slope represents electron transport efficiency, hereafter referred to as α_{ETE}, whereas on a photosynthesis light response curve it represents light harvesting efficiency, hereafter referred to as α_{LHE}. The photophysiological parameters of rETR and α_{ETE} were converted to P_{max} (maximum photosynthetic rate) and α_{LHE} using conversion equations derived by modelling the relationship between rETR (measured by the FIRe) and carbon fixation (measured by ^{13}C incubations) as detailed below. P_{max} and α_{LHE} were then normalised to chlorophyll (P^*_{max} and α_{LHE}*) and profiles of these parameters were determined by linear interpolation through the water column (Hickman et al., 2012). The linear interpolation technique used was based on that of Hickman et al. (2012) except that values were linearly interpolated between sample depths. Values of these two parameters obtained from measurements on the surface discrete sample were assumed representative between 0 m and the depth of the surface sample, and values obtained from measurements on the SCM discrete sample were assumed representative from the depth of the SCM sample to the base of the thermocline. Primary production (PP) at each quarter of a meter (z) could then be estimated using equation 2.33 (Hickman et al., 2012), and water column integrated primary production values were obtained by summing the primary production values estimated at each quarter of a meter through the water column.

$$PP(z) = Chl_{CTD}\,(z) \times P^*{}_{max}(z) \times tanh\left(\frac{E(z) \times \alpha_{LHE}{}^*(z)}{P^*{}_{max}(z)}\right) \quad (2.33)$$

Where Chl_{CTD} is chlorophyll concentration (mg m^{-3}) provided by the CTD mounted fluorometer profile, P^*_{max} is the maximum photosynthetic rate per unit chlorophyll (mg C mg chl^{-1} hr^{-1}), tanh is the hyperbolic tangent function, α_{LHE}* is light harvesting efficiency per unit chlorophyll (mg C mg chl^{-1} hr^{-1} (µmol m^{-2} s^{-1})$^{-1}$), and E is the *in situ* irradiance (µmol m^{-2} s^{-1}) provided by the CTD mounted PAR sensor profile.

When data from the CTD and mounted sensors (fluorometer and PAR sensor) was not recorded up to 0 m (most often profiles were recorded up to 0.5 - 1.5 m only) chlorophyll concentrations were assumed constant between the last value recorded and 0 m. Missing irradiance data was estimated using the light attenuation coefficient (Kd), which was determined using the available irradiance data of the profile, following equation 2.34:

$$Kd\ (m^{-1}) = -\frac{Ln\left(\frac{E_z}{E_0}\right)}{\Delta z} \quad (2.34)$$

Where E_z and E_0 are the final and initial recorded irradiance values (µmol m^{-2} s^{-1}) of the water column profile respectively, and Δz is the change in depth (m) between E_z and E_0. Determination of Kd also allowed primary production to be estimated through the water column at any chosen surface (0 m) irradiance (detailed methods are supplied in the methods section of chapter 5).

Sources of error associated with similar methods of modelling water column primary production are well discussed in the literature (Morel et al., 1996, Arbones et al., 2000, Tilstone et al., 2003, Hickman et al., 2012). The most significant sources of error using the technique described above are considered to be as follows. Photoinhibition in the surface waters was not considered, which may possibly have caused overestimation of primary production near the surface. In contrast, primary production below the SCM/base of the thermocline was assumed negligible, potentially leading to underestimates of water column primary production, as demonstrated by Weston et al. (2005) who estimated primary production below the thermocline of a summer stratified water column in the North Sea to be approximately 7 % of total water column primary production. Also, linear interpolation of the photophysiological parameters P_{max} and α_{LHE} may not be truly representative of the vertical gradients of these parameters *in situ*, especially given that samples were only taken from two depths. However, any linear interpolation method is not without error associated with assumptions regarding phytoplankton physiology variability with depth, and therefore linear interpolation between sample depths is considered acceptable for estimations of water column primary production (Tilstone et al., 2003, Hickman et al., 2012). Finally, the *in situ* light spectrum and phytoplankton light absorption throughout the water column could not be measured, and therefore these factors could not be corrected for. It was considered that a generic spectral correction be applied, however this method has the potential to introduce considerable further error, conceivably in excess of 10 % (Arbones et al., 2000, Moore, 2017) and therefore was rejected.

Determination of $rETR_{max}$ and α_{ETE} values

In parallel with ^{13}C primary production incubations using surface (10 m) and SCM discrete water samples, rETR as a function of irradiance was determined from FIRe measurements acquired using the ALS and PAR stepping acquisition mode (described in section 2.3.6). Measurements of rETR and carbon fixation were made simultaneously on the same water sample to minimise error introduced when relating rETRs to rates of carbon fixation in order to derive P_{max} and α_{LHE} values from $rETR_{max}$ and α_{ETE} values. Using the same water sample avoids

error that would otherwise arise due to differences in sample handling and treatment, and variation in phytoplankton community structure between separate samples (Suggett et al., 2010, Lawrenz et al., 2013). Due to the relatively fast nature of obtaining FIRe measurements using the ALS and PAR stepping acquisition mode, values of rETR as a function of irradiance were also determined for water samples collected from a number of stratified sites where primary production incubations could not be conducted.

Values of rETR were calculated using equation 2.35 (Baker, 2008, Cosgrove and Borowitzka, 2010, Suggett et al., 2010, Silsbe and Kromkamp, 2012, Wangpraseurt et al., 2014). rETR was calculated as opposed to true ETR as the chlorophyll specific absorption coefficient of PSII required for determination of true ETR could not be obtained. As such rETR was not assigned the units µmol e^{-1} s^{-1} m^{-2}, instead rETR units are stated as arbitrary (a.u.) (Suggett et al., 2010).

$$rETR\ (a.u.) = E \times (Fq'/Fm') \quad (2.35)$$

Where E is actinic light intensity (µmol m^{-2} s^{-1}), and Fq'/Fm' is the quantum yield (efficiency) of electron transport through PSII (dimensionless), which was determined using equation 2.36 (Genty et al., 1989):

$$Fq'/Fm' = (Fm' - F')/Fm' \quad (2.36)$$

Where Fm' is the maximum fluorescence yield under actinic light and F' is the steady state fluorescence yield under actinic light (all units are dimensionless (fluorescence ratios) or in instrument-specific values (fluorescence yields) as given in (Kromkamp and Forster, 2003)).

rETR is a measure of photosynthetic activity (Genty et al., 1989, Kromkamp et al., 1998) that when determined as a function of irradiance over a light range can be used to generate a light response curve of photosynthetic activity, much like a photosynthesis vs. irradiance (P vs. E) curve. rETR vs. irradiance curves were generated by fitting E-dependent rETR data to the Jassby and Platt (1976) PE model (Eq. 2.37) using the open source statistical program R v.3.2.3 and the 'phytotools' package (Silsbe and Malkin, 2015).

$$rETR\ (a.u.) = \alpha_{ETE} \times ek \times tanh\frac{E}{Ek} \quad (2.37)$$

Where α_{ETE} is given by the light limited initial slope of the curve (dimensionless), tanh is the hyperbolic tangent function, Ek is the light saturation parameter (µmol m^{-2} s^{-1}) calculated as the light intensity at which the initial slope of the curve (α) intercepts the horizontal asymptote ($rETR_{max}$), and E is the actinic light level (µmol m^{-2} s^{-1}).

The PE model was run with rETR data determined using actinic light levels up to 600 µmol m^{-2} s^{-1} only because above 600 µmol m^{-2} s^{-1} actinic light levels were super saturating causing overestimations of Fq'/Fm' (Moore, 2016). An example of a rETR vs. irradiance curve generated by running the Jassby and Platt (1976) PE model is given in Figure 2.16. The parameters of α_{ETE} and Ek were provided by the model output (Fig. 2.16), and from these parameters $rETR_{max}$ (Fig. 2.16) values were derived by applying equation 2.38:

$$rETR_{max} = \alpha_{ETE} \times Ek \quad (2.38)$$

rETR data for one SCM sample did not fit the Jassby and Platt (1976) PE model, preventing confidence in the data output of the model. For this reason data from this rETR vs. irradiance curve was omitted from the regression analysis detailed below.

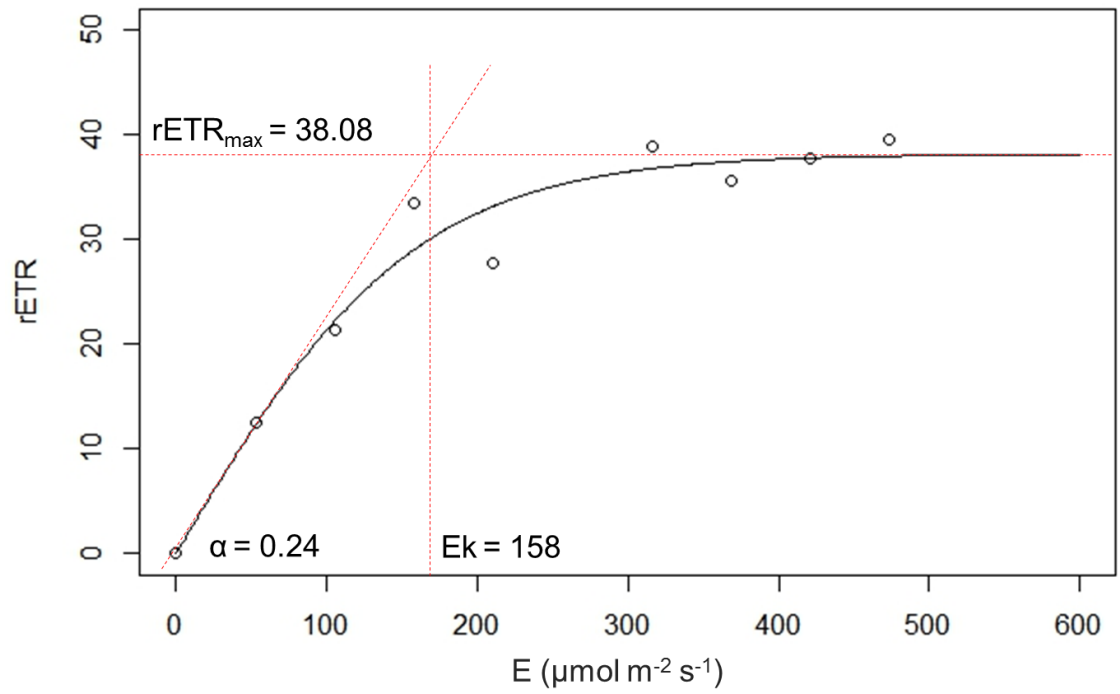

Figure 2.16. rETR vs. E curve generated by fitting E-dependent rETR data to the Jassby and Platt (1976) PE model. The light saturation parameter (Ek) is estimated as the point at which the initial slope (α) crosses maximum rETR ($rETR_{max}$).

Conversion of $rETR_{max}$ and α_{ETE} to P_{max} and α_{LHE}

Using methods similar to that described by Migné et al. (2007) values of $rETR_{max}$ and α_{ETE} were converted to P_{max} and α_{LHE}. The relationship between carbon fixation and rETR values determined at the same light intensity were modelled (Fig. 2.17), specifically 15 µmol m^{-2} s^{-1} for SCM samples and 33 µmol m^{-2} s^{-1} for surface samples. rETR values at these light intensities were determined using equation 2.37. The relationship was modelled separately for surface waters and the SCM to account for factors of variation between surface and SCM samples that would impact any relationship between rETR and carbon fixation, such as phytoplankton community structure, temperature and nutrient availability (Lawrenz et al., 2013). Carbon fixation measurements were significantly correlated with rETR values for the SCM (R^2 = 0.764; p = 0.01) and surface waters (R^2 = 0.500; p = 0.05), and the linear equations derived from the regression analyses (Fig. 2.17) were used to generate conversion equations for $rETR_{max}$ to P_{max} (SCM: Eq. 2.39; surface: Eq. 2.40). Subsequently, values of α_{ETE} could be converted to α_{LHE} (Eq. 2.41). These conversion equations were also applied to rETR and α_{ETE} data obtained for water samples collected at sites where primary production incubations were not conducted.

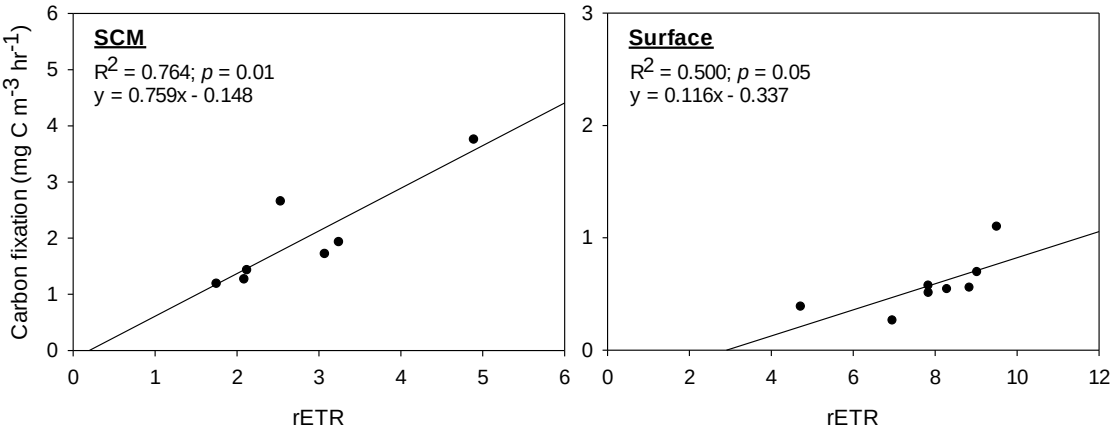

Figure 2.17. Relationship between rETR and carbon fixation (goodness of fit indicated by R^2 and significance indicated by p) for the SCM and surface waters. The linear equations displayed were used to convert $rETR_{max}$ values to P_{max} values.

$$SCM: P_{max}(\text{mg C m}^{-3}\ \text{hr}^{-1}) = (0.759 \times rETR_{max}) - 0.148 \quad (2.39)$$

$$Surface: P_{max}(\text{mg C m}^{-3}\ \text{hr}^{-1}) = (0.116 \times rETR_{max}) - 0.337 \quad (2.40)$$

$$\alpha_{LHE}\ (\text{mg C m}^{-3}\ \text{hr}^{-1}[\text{µmol m}^{-2}\ \text{s}^{-1}]^{-1}) = \frac{P_{max}}{Ek} \quad (2.41)$$

It should be noted that there are many processes that act to decouple rates of electron transport from carbon fixation, including the Mehler reaction, photorespiration,

chlororespiration and nutrient assimilation (Holmes et al., 1989, Badger et al., 2000, Suggett et al., 2009a, Suggett et al., 2010). These processes vary with community taxonomy (Suggett et al., 2009b) and environmental conditions (Lawrenz et al., 2013). This can result in considerable scatter/non-linearity in the relationship between electron transport and carbon fixation (Migné et al., 2007, Kromkamp et al., 2008, Robinson et al., 2009, Suggett et al., 2009a), which could help to explain why the SCM and surface water regression models only explained 76 % and 50 % of the variation in the data respectively. Nonetheless, the relationship between rETR and carbon fixation was significant for the SCM and surface waters separately, indicating that the decision to model the rETR-carbon fixation relationship individually for surface waters and the SCM was key for preserving the link between these parameters.

2.4. Meteorological measurements

Wind speed and direction were logged at two second intervals by the RV Callista's AIRMAR PB150 weather station in 2015 and 2016. This data was not available for 2013 and 2014 and therefore wind measurements collected by the AIRMAR sensor on the WCO L4 autonomous buoy were used (PML, 2017). This buoy is situated at 50° 15.000 N, 004° 13.000 W and has an hourly data logging rate. Daily rainfall measurements were collected by the PML meteorological station Omni Instruments 6" tipping bucket raingauge (RG200) (Smyth, 2017), located on the roof of the PML building and logging data at 5 minute intervals. Daily solar insolation measurements were taken from NASA's CERES FLASHFlux project (NASA, 2018).

2.5. Statistical analyses

Univariate and multivariate statistical methods were performed using SigmaPlot 12.5/13, PRIMER (Plymouth Routines in Multivariate Ecological Research) v6 and CANOCO 4.5 software. Univariate analyses employed included linear regression analysis, which was model-II where appropriate, to allow errors on y-axis and x-axis variables, and one way ANOVA (Analysis of Variance) with post hoc Dunn's pairwise multiple comparison analysis. Multivariate analyses implemented included SIMPROF (Similarity Profile Analysis), SIMPER (Similarity Percentage Analysis), ANOSIM (Analysis of Similarity), and RDA (Redundancy Analysis) with a priori DCCA (Detrending Canonical Correspondence Analysis) and Monte Carlo permutation tests. Details on the application of the different statistical techniques performed are supplied within the methods sections of the data chapters to follow (chapters 3 – 6).

Chapter 3: Phytoplankton community structure within shelf sea subsurface chlorophyll maximum thin layers

This chapter is being prepared for submission for publication in Continental Shelf Research. Michelle Barnett processed CTD and ADCP data, collected and analysed all samples, and wrote the first draft of the manuscript, with edits provided by Professor Alan Kemp, Dr. Anna Hickman and Professor Duncan Purdie.

3.1. Abstract

The Western English Channel is a seasonally stratified temperate coastal sea where a subsurface chlorophyll maximum (SCM) is typically detectable within the seasonal thermocline. The SCM often develops as a thin layer (< 5 m) that may contain elevated concentrations of phytoplankton (subsurface chlorophyll maximum thin layer; SCMTL). During summer 2013 a study was conducted offshore of Falmouth, UK, to assess temporal and spatial variability in SCM thickness in relation to water column structure and physical conditions and to evaluate any associated changes in phytoplankton community structure. SCMTL were observed in 18 of 52 vertical profiles, typically characterised by higher chlorophyll concentrations than broader SCM. SCMTL were generally associated with a 'stepped' thermocline, likely representing the presence of one or more shallow mixed layers forming above/within the seasonal thermocline, and related to increased stratification compared to broader SCM. *Pseudo-nitzschia* was almost exclusively the dominant diatom taxon in SCM, yet distinct differences in community structure existed between SCMTL and broader SCM. The distinction was largely due to a greater biomass of *Proboscia alata* and other rhizosolenid diatoms and the dinoflagellates *Ceratium lineatum* and *Gyrodinium spp.* in SCMTL, and a smaller population of the diatom *Chaetoceros spp.* and dinoflagellate *Diplopsalis lenticula*. This observed difference is proposed to have resulted from promotion of phytoplankton better adapted to environmental conditions more specific to SCMTL compared to broader SCM. With more intense and prolonged stratification projected for the NW European shelf, there may be increased prevalence of SCMTL and the associated larger-sized specialised flora, with implications for increased carbon export. This study adds to a growing body of evidence of the importance of SCMTL in coastal and shelf seas, and highlights the requirement for improved understanding of physical forcing, and the ecology and physiology of key taxa, particularly as predicted changes in stratification could alter the role of SCM phytoplankton in a future influenced by climate change.

3.2. Introduction

Subsurface chlorophyll maxima (SCM) are commonly identified in the seasonally stratified waters of temperate and high latitude coastal and shelf seas (Cullen, 1982, Holligan et al., 1984a, Martin et al., 2010, Cullen, 2015). The introduction of continuous *in vivo* fluorometry fifty years ago (Lorenzen, 1966) allowed these structures to be recognised and increasing deployment of AUVs, towed undulators and autonomous profilers over the past two decades has demonstrated their ubiquity in shelf seas (Wang and Goodman, 2009, Martin et al., 2010, Sullivan et al., 2010a). SCM are commonly observed within the seasonal thermocline that represents an interface at which both light availability and nutrient concentration are sufficient to support phytoplankton growth in a stratified water column (Holligan and Harbour, 1977, Pingree et al., 1978, Holligan et al., 1984a, Sharples et al., 2001, Hickman et al., 2012).

SCM vary widely in thickness, but in coastal and shelf seas they often occur as thin layers (SCMTL: < 5 m thick following the definition of Dekshenieks et al. (2001)) (Durham and Stocker, 2012), with studies quantifying the occurrence of thin layers in stratified shelf waters reporting them to be present between 21 - 87 % of the time (Dekshenieks et al., 2001, Benoit-Bird et al., 2009, Steinbuck et al., 2010, Sullivan et al., 2010a). These thin features can have a horizontal extent of up to several kilometres and duration from a few hours to a few weeks (Bjørnsen and Nielsen, 1991, Dekshenieks et al., 2001, Cheriton et al., 2009, Durham and Stocker, 2012). Whilst methods for continuous measurement of chlorophyll in the subsurface have allowed for the consistent detection of SCMTL in a variety of coastal environments (Bjørnsen and Nielsen, 1991, Dekshenieks et al., 2001, Rines et al., 2010, Churnside and Marchbanks, 2015, Ríos et al., 2016), they remain greatly under-sampled by conventional techniques, such as CTD rosette systems, so that their taxonomic composition is less well described.

Current trends of increasing ocean stratification due to warming (Bindoff et al., 2007) and localised freshening (Lyman et al., 2010) are predicted to develop further in future projections (Capotondi et al., 2012). Biogeochemical models predict a decrease in primary production and export of particulate organic carbon with increasing stratification (Steinacher et al., 2010), but these predictions are based on highly simplified models that cannot replicate the phytoplankton community or the physics within the marine ecosystem. In fact, these model predictions have already been challenged by observational studies conducted in stratified regions of the modern ocean and by palaeoceanographic evidence (Kemp et al., 2006, Kemp and Villareal, 2013). SCM development is promoted in stratified waters, so it is important to improve our understanding of

SCM ecology in the shelf seas, in particular because these regions of the marine environment are highly significant for global biogeochemical cycling and trophic dynamics (Muller-Karger et al., 2005, Jahnke, 2010, Simpson and Sharples, 2012). Moreover, shelf seas are of great socio-economic importance, due to their support of an extensive proportion of global fish catches (Pauly et al., 2002). This study focuses on a region of the NW European continental shelf, where more intense and persistent seasonal stratification has specifically been projected (Lowe et al., 2009, Sharples et al., 2013, Tinker et al., 2016).

Recent studies in the North Sea and the Celtic Sea have attested to the biogeochemical importance of the SCM in the NW European shelf seas. The SCM has been identified to contribute approximately half (Hickman et al., 2012) and potentially more (Richardson et al., 2000) of total annual primary production in the seasonally stratifying regions of the Celtic Sea and North Sea respectively. Modelling of subsurface production in seasonally stratified waters of the North Sea has suggested possible highs of 45 – 55 % of annual net primary production occurring within the SCM (van Leeuwen et al., 2013). The SCM is also an important site of 'new' (nitrate-fuelled) production during summer (Richardson et al., 2000, Hickman et al., 2012, Williams et al., 2013b) and is associated with a high potential for carbon export from the euphotic zone (Sharples et al., 2001). In fact phytoplankton taxa known to occupy SCM have been identified in extensive ancient phytoplankton deposits, providing evidence that SCM have been responsible for significant carbon export to depth (Kemp and Villareal, 2013).

There have been few detailed studies of SCM phytoplankton communities in the NW European shelf seas. Some SCM appear to be abundant in small cells (< 20 µm), such as <10 µm naked flagellates (Holligan et al., 1984b) and cyanobacteria (Hickman et al., 2009, Sharples et al., 2009), but on other occasions high abundances of much larger cells (> 50 µm), such as rhizosolenid diatoms have been reported (Holligan and Harbour, 1977, Weston et al., 2005). The occurrence of rhizosolenid diatoms, in particular, may be significant, since they are known to contribute massive flux to the sea floor (Sancetta et al., 1991, Kemp et al., 2000). It is therefore important to establish an understanding of phytoplankton community structure within SCMTL and broader SCM, as different taxa may have particular roles for biogeochemical processes, such as carbon transfer to depth, or to higher trophic levels and, consequently, for our predictions of how shelf sea ecosystems will respond to future climate change.

The Western English Channel has been routinely surveyed for over a century and time series measurements have been made at a number of locations, most notably stations L4 and E1 (Fig.

3.1) via the Western English Channel Observatory (WCO) (Harris, 2010, Smyth et al., 2015). Weekly water samples from a depth of 10 m from L4 have formed the basis for several studies of phytoplankton community dynamics (Widdicombe et al., 2010, Smyth et al., 2015). However, there has been little sampling of the SCM, although water column profiles of chlorophyll-fluorescence collected by the WCO from both L4 and E1 show that SCM are a recurrent feature of the summer stratification (at typical depths of 20 – 30 m), and studies of CO_2 fluxes have implicated the SCM in CO_2 uptake (Kitidis et al., 2012). Further afield, isolated studies have identified intense SCMTL in the southern Celtic Sea/ Western Channel (Sharples et al., 2001). Repeated surveys of the area off Falmouth during the annual (June/July) University of Southampton undergraduate oceanography field course have also demonstrated a seasonally recurrent SCM, including SCMTL (not shown).

Motivated by these recent observations of a widespread SCM (SCMTL and broader SCM) in the Western English Channel, the aim of this paper is to present the first detailed study of SCMTL and broader SCM in the region. Temporal and spatial variation in phytoplankton community structure with regard to similarities/differences in community structure between SCMTL and broader SCM, and comparison to that of surface and bottom waters is assessed. Variability in vertical chlorophyll structure is also investigated to evaluate controls on the occurrence of SCMTL compared to broader SCM, and relate their development to water column structure and physical conditions.

3.3. Methods

3.3.1. Sampling

The study was conducted offshore of Falmouth, UK (Fig. 3.1) during the summer of 2013, between the 24th June and 4th July, in seasonally stratified waters, with characteristic high sea surface temperatures (12.5 – 15 °C; data not shown). The study area ranged from being in very close proximity to the tidal mixing front to over 30 km offshore, thus representative of a range of conditions. Note that the term tidal mixing front is used in reference to the frontal boundary that separated shallower mixed inshore waters from deeper stratified waters further offshore, as described by Holligan and Harbour (1977). Sampling strategy combined repeat sampling of individual stations, as well as a series of inshore – offshore transects (Fig. 3.1). Transects were completed in approximately 1.5 - 4 hours, with the exception of the 25th June transect completed in approximately 6 hours. Repeat stations were chosen based on past data revealing their location to be far enough away from the tidal mixing front to be permanently stratified in June/July, but also within a reasonable travel distance to enable regular sampling. These repeat stations were

sampled on a daily basis (weather permitting) and in one instance an hourly basis. A SeaBird SBE19plus V2 conductivity, temperature, depth (CTD) probe mounted with a Wet Labs ECO FLNTU fluorometer (sensitivity: 0.025 µg chl/l; fluorescence excitation/emission wavelengths: 470/695 nm) was used to collect vertical water column profiles of temperature, salinity and chlorophyll-fluorescence at 52 stratified sites in the Western English Channel (Fig. 3.1). The configuration of the CTD package allowed for slow descent/ascent rates without slowing sensor responses, thus improving dynamic accuracy and allowing small scale structure to be resolved. Specifically, the CTD system was typically deployed at a descent/ascent rate of 0.01 - 0.1 m s^{-1} (rate slowed on approach to SCM), with a data acquisition rate of 2 Hz, which provided vertical resolution of 0.5 – 5 cm, thus allowing very thin SCM to be resolved. The CTD casting protocol was designed for very high resolution profiling, which in combination with a generally calm sea state allowed SCMTL as thin as 0.04 m to be resolved (Fig. A1.1) (thickness was measured at half maximum intensity of the chlorophyll peak – see 3.3.5 below). In addition, CTD upcasts and downcasts were consistently similar, indicating no significant disruption of SCM chlorophyll structure by the CTD. Niskin bottles used to sample this small vertical extent of the water column were 50.8 cm tall and the approximate midpoint of these bottles was aligned with the fluorometer, so confidence could be had, with the CTD casting strategy, that the bottle samples included material from the narrow peaks.

Current velocity was measured with a hull mounted RDI Workhorse 600 kHz ADCP and wind speed measurements were taken from the WCO L4 autonomous buoy situated at 50° 15.000 N, 004° 13.000 W (PML 2013), approximately 40 km from the sampling area. Vertical profiles of buoyancy frequency, a measure of stratification, were computed from CTD data using SBE data processing software, where the buoyancy frequency was calculated using the Fofonoff adiabatic levelling method (Bray and Fofonoff, 1981).

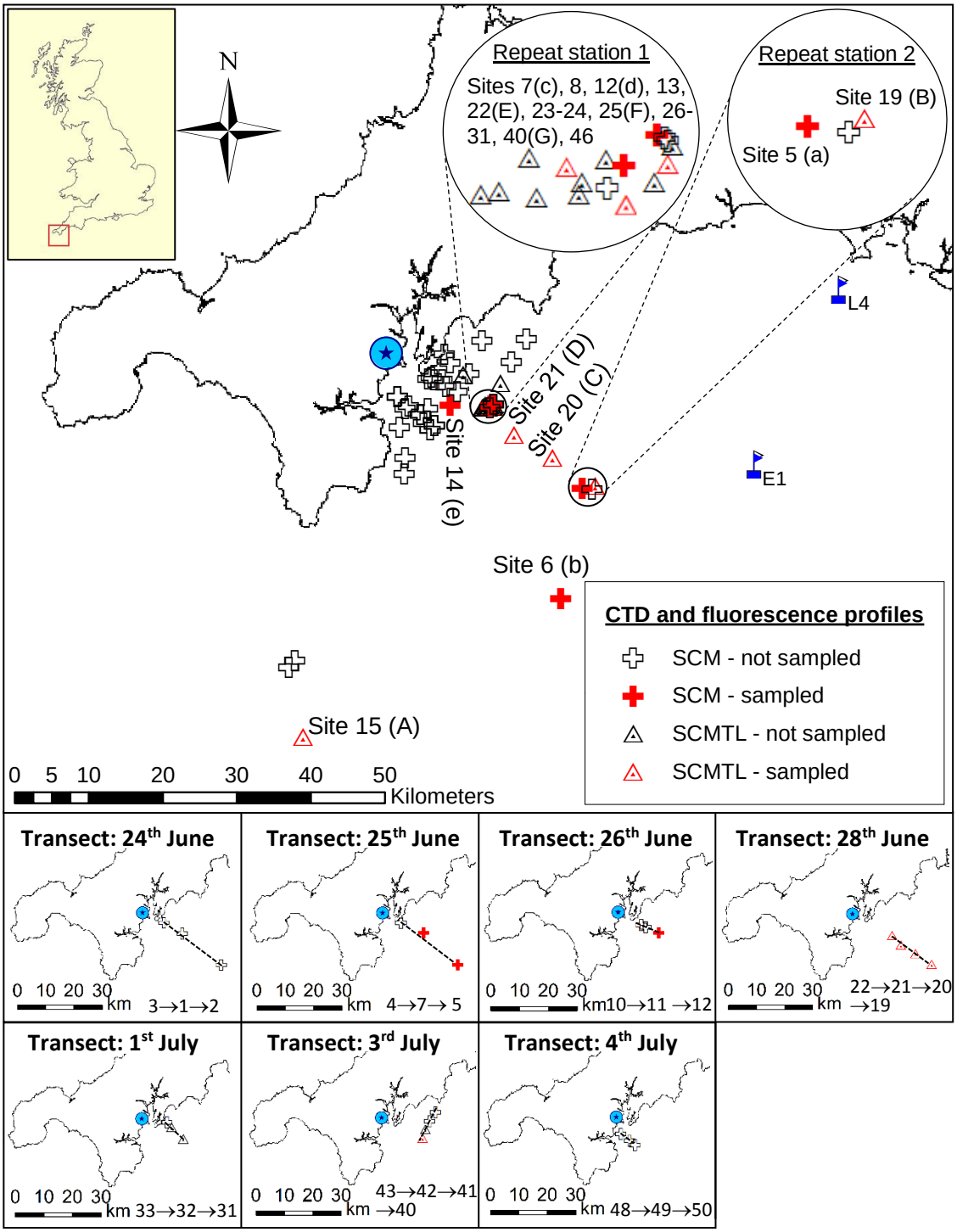

Figure 3.1. Study area in the Western English Channel where sampling occurred from the 24th June to the 4th July 2013. The blue encircled star indicates the location of Falmouth and WCO stations L4 and E1 are marked with blue flags. Crosses indicate where broader SCM were detected and triangles where SCMTL were detected. Red symbols indicate sites where discrete samples analysed for phytoplankton were collected and white symbols represent sites where only a CTD profile and ADCP data was collected. Repeat sampling stations 1 and 2 are circled and all sites that were sampled for phytoplankton analysis are labelled with their site number and sample ID (Table A1.1). Site numbers (1 to 52) were allocated in chronological order to the 52 stratified sites profiled during the study, and sample IDs were allocated to

sites where discrete samples were collected for phytoplankton analysis. An upper case sample ID indicates sampling of a SCMTL and a lower case ID indicates sampling of a broader SCM. Transects travelled during the survey are shown in the miniature transect maps, where a dashed line indicates a transect travelled and site numbers included in each transect are given in order of distance from shore.

Water samples were collected from the SCM at 12 sites (Fig. A1.1) typically using a CTD Niskin rosette system (6 x 5 L Niskin bottles), but in one case using a custom made horizontal sampler consisting of three 50 ml syringes spaced approximately 20 cm apart, acting as a multiple 'slurp gun' (analysis performed on water sample from the middle syringe). The slurp gun was similar in design to the gradient sampler of Bjørnsen and Nielsen (1991), and was mounted on the CTD rosette frame. Water samples were also collected from the surface and bottom waters at 4 of the 12 sites (Fig. A1.1) using the CTD Niskin rosette system. Water samples were analysed for chlorophyll concentration, the Fluorescence Induction and Relaxation (FIRe) parameter of Fv/Fm, a measure of photosynthetic efficiency (Kolber et al., 1988), and for phytoplankton identification, enumeration and biomass determination.

3.3.2. Determination of chlorophyll concentration

Samples for chlorophyll analysis were collected by filtering 50 ml of water sample through 25 mm Whatman GF/F filters immediately after collection. These filters were then stored in a -20 °C freezer until analysis, which was conducted as soon as possible on return to the lab to avoid error associated with pigment degradation at -20 °C (Graff and Rynearson, 2011). Chlorophyll was extracted in 90 % acetone via sonication and then chlorophyll concentration was determined using a Turner Designs 10AU fluorometer based on the method of Welschmeyer (1994). The fluorometer excited the extracted sample with blue light (436 nm) and recorded the subsequent red fluorescence emission (680 nm). Chlorophyll values measured on the water samples were used to calibrate the fluorometer mounted on the CTD. Determining chlorophyll concentrations also allowed identification of where water samples were collected within the SCM, confirming all samples were collected from/very near to the depth of maximal chlorophyll, i.e. relative sampling depth within SCM was consistent (Fig. A1.1 and Table A1.1). Thus, confidence could be had that any difference in community structure observed within SCM of different sampling casts was not a function of the relative depth of sampling within the SCM.

To assess the relative contributions of < 10 µm and > 10 µm phytoplankton to total chlorophyll, water samples were passed through Whatman track-etched polycarbonate membrane with a pore size of 10 µm before being passed through a GF/F filter for chlorophyll analysis.

3.3.3. FIRe measurements

Measurements of Fv/Fm were collected for SCM, bottom water and surface samples by decanting 5 ml (which was first dark adapted by storing in the dark for at least 25 minutes) into a cuvette that was analysed in the Satlantic bench top FIRe instrument. The FIRe protocol is given in Bibby et al. (2008); 30 unique iterations from the same sample were averaged, the sample delay was set at 1000 msec and the gain set at between 50 – 70 % of the sensor's saturation. Raw FIRe data was processed to generate the parameters of Fm and Fo (maximum and minimal fluorescence yield) based on the biophysical model of Kolber et al. (1988) using MATLAB R2013a. The parameter of Fv/Fm was calculated using equation 3.1, which includes blank correction, for which filtered seawater was analysed at the start and end of each day:

$$\frac{Fv}{Fm} = \frac{(Fm_{sample} - Fm_{blank}) - (Fo_{sample} - Fo_{blank})}{(Fm_{sample} - Fm_{blank})} \quad (3.1)$$

3.3.4. Phytoplankton identification, enumeration and biomass determination

Samples for phytoplankton analysis were collected by decanting 50 ml of water sample into a darkened glass bottle and preserving in Lugol's iodine to a final concentration of 1 %. Phytoplankton samples were analysed based on the methods of Utermöhl (1958) with 10 ml of preserved sample settled in a sedimentation chamber for 24 hours and cells then identified and counted using a Brunel SP951 inverted trinocular light microscope (individual cells were counted in all cases, whether they be part of a colony/chain or solitary). Numerically dominant taxa (> 50 cells per ml) were counted along a single middle transect under 100x or 250x magnification depending on cell size. Cryptophytes (> 8 µm) and unidentified small naked dinoflagellates (10 – 20 µm and 20 – 25 µm) were also counted along a single middle transect at 250x magnification. All other cells ≥ 10 µm were counted at 100x magnification during examination of the entire chamber base plate. A complete list of phytoplankton taxa identified by microscopy is presented in Table A1.2. It was not possible to identify most nano-phytoplankton < 10 µm or any pico-phytoplankton, so the chlorophyll concentration of the < 10 µm and > 10µm phytoplankton fraction of all samples analysed for phytoplankton were determined.

Cells were identified to a species level where possible, but when species could not be differentiated accurately with optical microscopy, cells were identified to the genus level, e.g. *Chaetoceros spp.* (thought to be mostly *Chaetoceros brevis* and *Chaetoceros debilis)*, *Pseudo-nitzschia spp.* and *Rhizosolenia spp.*. Any remaining unidentified diatoms were grouped as pennate or centric according to size (small: 20 – 40 µm length, medium: 40 – 65 µm length, large:

65 – 110 µm length; and small: 20 – 30 µm diameter, medium: 30 – 50 µm diameter, large: 60 – 150 µm diameter respectively). Unidentified dinoflagellates and ciliates were also grouped according to size and with reference to cell wall structure where appropriate (e.g. 10 – 20 µm and 20 – 25 µm naked dinoflagellates, 10 – 30 µm armoured dinoflagellates, and small (< 20 µm), medium (20 – 40 µm) and large (> 40 µm) aloricate ciliates. Some genera were classified into size categories, including *Pleurosigma* (small, medium and large: ~50 µm, 80 – 170 µm and 170 - 200 µm length), *Thalassiosira* (small, medium and large: 10 - 25 µm, 25 – 45 µm and > 45 µm height), *Protoperidinium* (small, medium and large: 10 - 30 µm, 30 – 65 µm and 65 - 120 µm diameter) and *Rhizosolenia* (small, medium and large: ≤ 10 µm, 10 – 20 µm and > 20 µm diameter). In the case of *Rhizosolenia*, small diameter cells appeared to be mainly *Rhizosolenia setigera*, and medium and large diameter cells appeared to be a mix of *Rhizosolenia imbricata* and *Rhizosolenia styliformis*. However, as Scanning Electron Microscope (SEM) analysis was not used for counting, it was not possible to differentiate *Rhizosolenia* species so cells were instead differentiated by size. Note that the term rhizosolenids is used more generally in the text to encompass genera within the family Rhizosoleniaceae, including *Rhizosolenia*, *Proboscia*, *Guinardia* and *Dactyliosolen*.

Cell biovolume was calculated for each taxon/taxon size category using geometric shapes and formulae of Olenina et al. (2006). Dimensions of at least 30 cells per taxon or taxon size category (only less for rare taxa) were measured with the open source software 'ImageJ'. Cell biovolume was converted to cell carbon biomass using the carbon - biovolume relationships of Menden-Deuer and Lessard (2000).

3.3.5. Definition of subsurface chlorophyll maximum thin layers and chlorophyll intensity ratio

To distinguish a SCMTL from a broader SCM three specific criteria were used, which were based upon three requirements developed by Dekshenieks et al. (2001) and subsequently adopted by other reviews (Durham and Stocker, 2012). These were: (1) The vertical thickness of the thin layer is less than 5 m, where thickness was measured at half maximum intensity of the chlorophyll signal; (2) The peak chlorophyll concentration is at least three times greater than the background intensity values, where background values were defined as values taken from the bottom mixed layer; and (3) The thin layer is present as a persistent feature, existing in at least two repeated CTD casts. To determine if a SCM adhered to the second requirement the ratio of peak chlorophyll concentration to background chlorophyll concentration was determined and is referred to hereafter as the chlorophyll intensity ratio.

3.3.6. Statistical analysis

Two multiple linear regression analyses were performed using SigmaPlot 12.5 software to identify predictors of the SCM characteristics thickness and chlorophyll intensity ratio from a database of environmental data that included the physical forcing parameters of buoyancy frequency, current velocity and wind speed. Phytoplankton community structure was investigated using PRIMER v6 software (Clarke and Warwick, 2001, Clarke and Gorley, 2006). Statistical analysis was conducted on phytoplankton carbon biomass data as biomass provides a more accurate representation of community structure than abundance when the community consists of taxa spanning a range of different sizes, and because biomass is a more biogeochemically relevant property (Paasche, 1960). Phytoplankton biomass data was standardised by dividing biomass values by the total biomass for a given sample, then normalised by performing a square root transformation to moderate the influence of dominant taxa (e.g. *Pseudo-nitzschia*) on similarity between samples. To explore similarity of community structure among SCMTL and broader SCM a cluster analysis with SIMPROF (Similarity Profile Analysis; significance level at 0.05) was performed, using the Bray-Curtis index as the measure of similarity. SCM that were most similar and significantly different from other SCM were grouped into clusters, and a SIMPER (Similarity Percentage Analysis) was performed to investigate similarities within clusters and dissimilarities between clusters. A second SIMPER analysis was conducted to further investigate the community structure dissimilarity apparent between SCMTL and broader SCM, whereby all SCMTL samples > 68 % similar were grouped to compare to broader SCM samples that were > 68 % similar. A post hoc analysis of similarity (one-way ANOSIM) was applied to determine the level of separation between SCMTL and broader SCM samples (given by global R value, where values close to 0 indicate no separation and values close to 1 indicate high separation), and a non-metric multi-dimensional scaling (nMDS) plot was used to visually display the separation between samples. Samples with greater community resemblances were spatially closer than ones that were less similar. The stress level of the nMDS plot is a measurement of how accurate a representation the ordination is, where a value below 0.2 is considered to indicate a good fit (Zuur et al., 2007).

3.4. Results

3.4.1. Distribution and characteristics of SCMTL and broader SCM

A total of 52 profiles were collected between 24th June and 4th July, with 18 profiles constituting SCMTL meeting the criteria outlined above (Fig. 3.1 and A1.1; details provided in Table A1.1). Broader SCM ranged in thickness from the 5 m threshold to over 20 m, while SCMTL ranged down to less than 10 cm, with most SCMTL being less than 3 m (12 of 18 SCMTL observed) (Fig. 3.2 and

A1.1). Maximum chlorophyll concentrations ranged from 1.1 – 4.5 µg L^{-1} for SCMTL and 0.9 – 3.6 µg L^{-1} for broader SCM (Fig. A1.1; details in Table A1.1), while chlorophyll intensity ratios ranged from 4.9 to 10.7 for SCMTL and were generally between 1.3 and 10.5 for broader SCM. Despite similar ranges, 72 % of SCMTL intensity ratios were > 8, whereas 70 % of intensity ratios for broader SCM were < 8 (Fig. 3.2). The depth of maximal chlorophyll for all SCMTL and broader SCM was shallower than 35 m, with the majority of broader SCM (30 of 34) being 10 – 25 m deep and the majority of SCMTL (12 of 18) being 20 – 25 m deep (Fig. 3.3). SCM depth generally varied according to water column depth, with shallower SCM occurring in shallower water columns and vice versa (Fig. A1.1; details in Table A1.1).

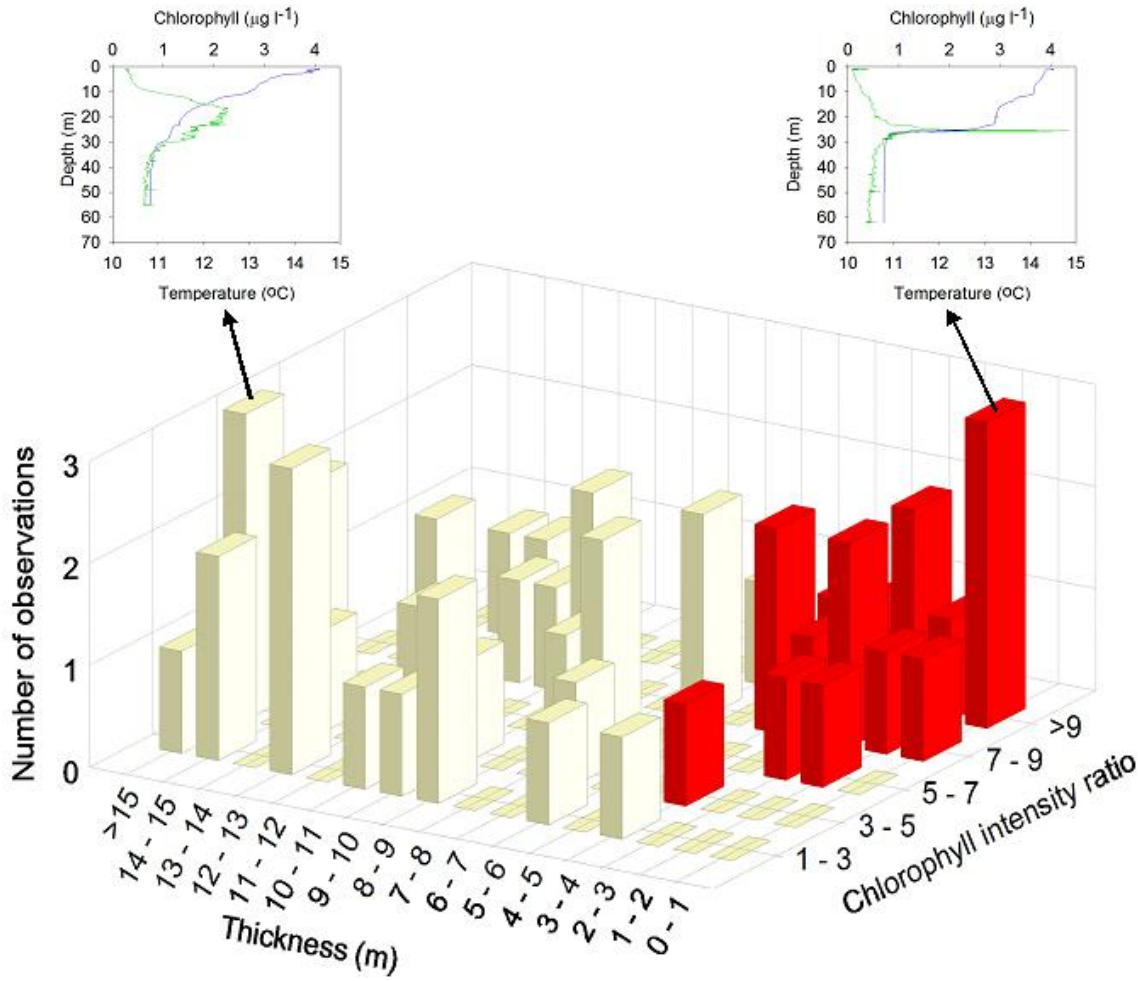

Figure 3.2. Chlorophyll intensity ratio and thickness of chlorophyll maxima at all 52 stratified sites profiled in the Western English Channel. Red bars represent SCMTL and yellow bars represent all other/broader SCM. Depth profiles featured are example 'end members':- an intense and thin SCMTL, and a less intense, broad SCM.

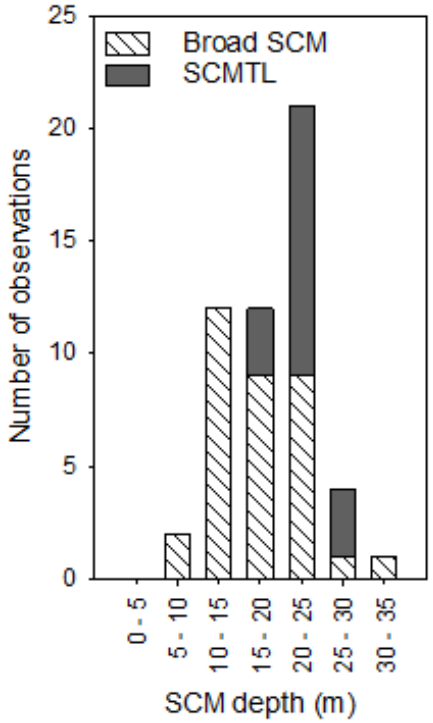

Figure 3.3. Depth of chlorophyll peak (at maximal intensity) at all stratified sites profiled during study of the Western English Channel. The hatched section of the stacked bars represents broad SCM and the block grey section represents SCMTL.

3.4.2. SCM relation to water column structure and physical forcing

3.4.2.1. Association with the thermocline

All SCMTL and broader SCM were closely associated with the base of the thermocline (Figs. 3.4, 3.5, 3.6 and A1.1) (also the pycnocline since density variability was dominated by temperature; data not shown). The thermocline took on three main forms as depicted in Fig. 3.4, which will be referred to as (1) Gradual (one thermocline present, exhibiting a temperature change of < 1 °C over 3 m); (2) Simple steep (one thermocline present, exhibiting a temperature change of > 1 °C over 3 m); and (3) Stepped (two thermoclines present separating three layers of mixed water, where the lower thermocline typically exhibited a temperature change of > 1 °C over 3 m). The difference in temperature between the surface and bottom waters at each site (an indication of the level of stratification) ranged from 0.73 °C to 4.00 °C (Fig. A1.1; details in Table A1.1). SCMTL were most commonly associated with a stepped thermocline (14 of 18 SCMTL observed), and larger differences in temperature (14 of 18 SCMTL profiles had a surface to bottom temperature difference of > 3 °C). Whereas broader SCM were mostly associated with a gradual thermocline (22 of 34 broader SCM observed) spanning smaller differences in temperature (30 of 34 broader SCM profiles had a surface to bottom temperature difference of < 3 °C). A gradual thermocline was often observed at sites furthest inshore, i.e. in closest proximity to the tidal front.

Additionally, chlorophyll peaks with higher chlorophyll concentrations, whether they were SCMTL or broader SCM, were associated with a greater surface to bottom temperature difference (Figs. 3.5, 3.6 and A1.1; details in Table A1.1).

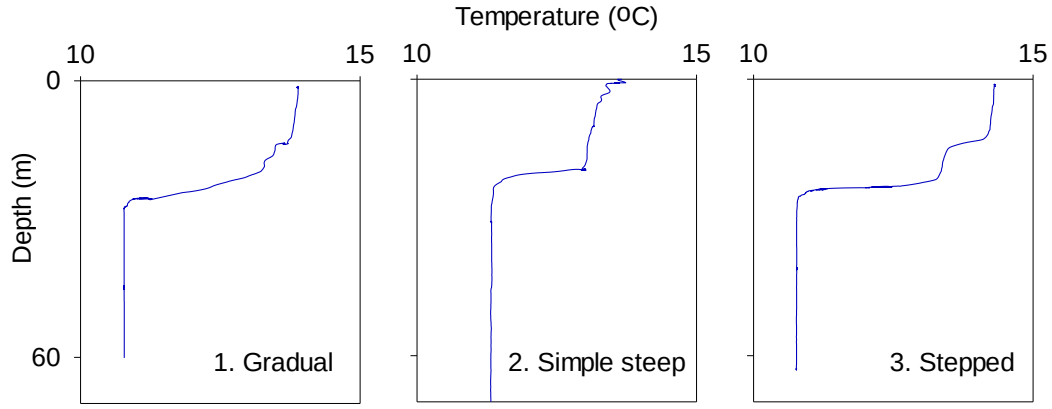

Figure 3.4. Example profiles illustrating the types of thermocline observed: 1. Gradual (site 22 profiled on the 28th June); 2. Simple steep (site 6 profiled on the 25th June); 3. Stepped (site 25 profiled on the 29th June).

3.4.2.2. Repeat stations

At repeat station 1 (Fig. 3.1; sampled frequently from 24th June to 4th July) thermocline form was quite changeable from day to day over the survey period, being a gradual, simple steep and stepped thermocline, with apparent progression in that order (Fig. 3.5). Thermocline depth (at base of thermocline) ranged from approximately 15 m to 27 m and the difference in temperature between the surface and bottom waters ranged from 2.57 – 4.00 °C (Fig. 3.5; Table A1.1). By contrast, an hourly time series over 8 hours at repeat station 1 on 29th June (site 23 – 30) showed the thermocline to remain stepped, at a depth of approximately 24 m, with a surface to bottom water temperature difference ranging only 3.52 – 4.00 °C (Fig. 3.5; Table A1.1). At repeat station 2 (Fig. 3.1) thermocline structure was also variable, taking on a steep and stepped form, ranging in depth from approximately 20 m to 30 m, with a surface to bottom temperature difference ranging between 2.22 – 3.25 °C (Fig. 3.6; Table A1.1). At both repeat stations the characteristics of the chlorophyll peak changed along with the characteristics of the thermocline, with sharper SCM associated with a stepped thermocline and a greater surface to bottom temperature difference.

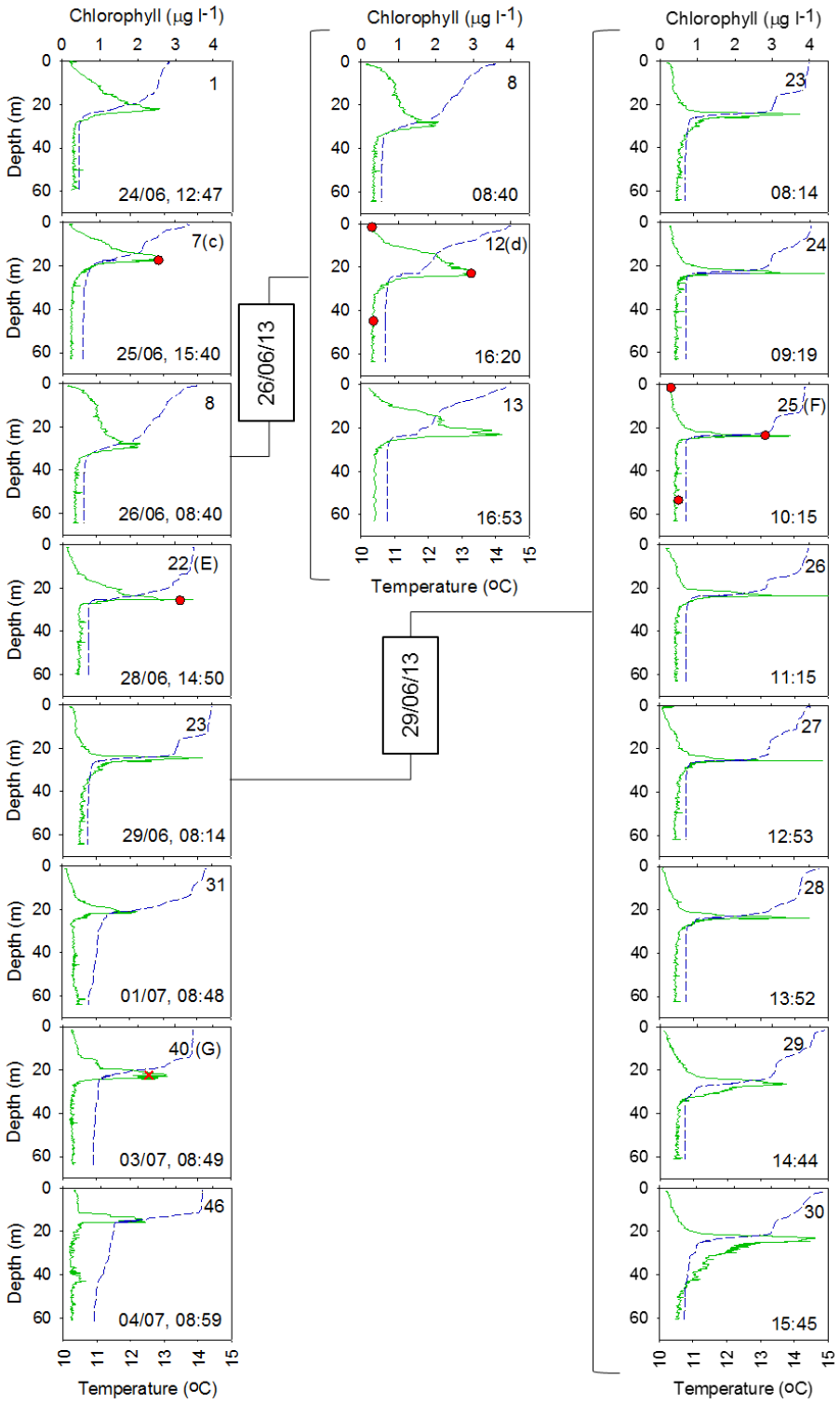

Figure 3.5. Temperature and chlorophyll profiles collected at repeat station 1 (profile dates and times given). Profiles in column one show water column temperature and chlorophyll structure from day to day during the survey, profiles in column two were all collected on the 26th June and profiles in column three were all collected on the 29th June at hourly intervals. Site numbers given in the top right hand corner of each plot, with sample IDs included in brackets, where an upper case ID indicates a SCMTL and a lower case ID indicates a broader SCM. The green line represents chlorophyll concentration determined from CTD chlorophyll-fluorescence, the blue dashed line represents temperature, red circles where Niskin water samples were collected and the red X where a slurp gun sample was collected.

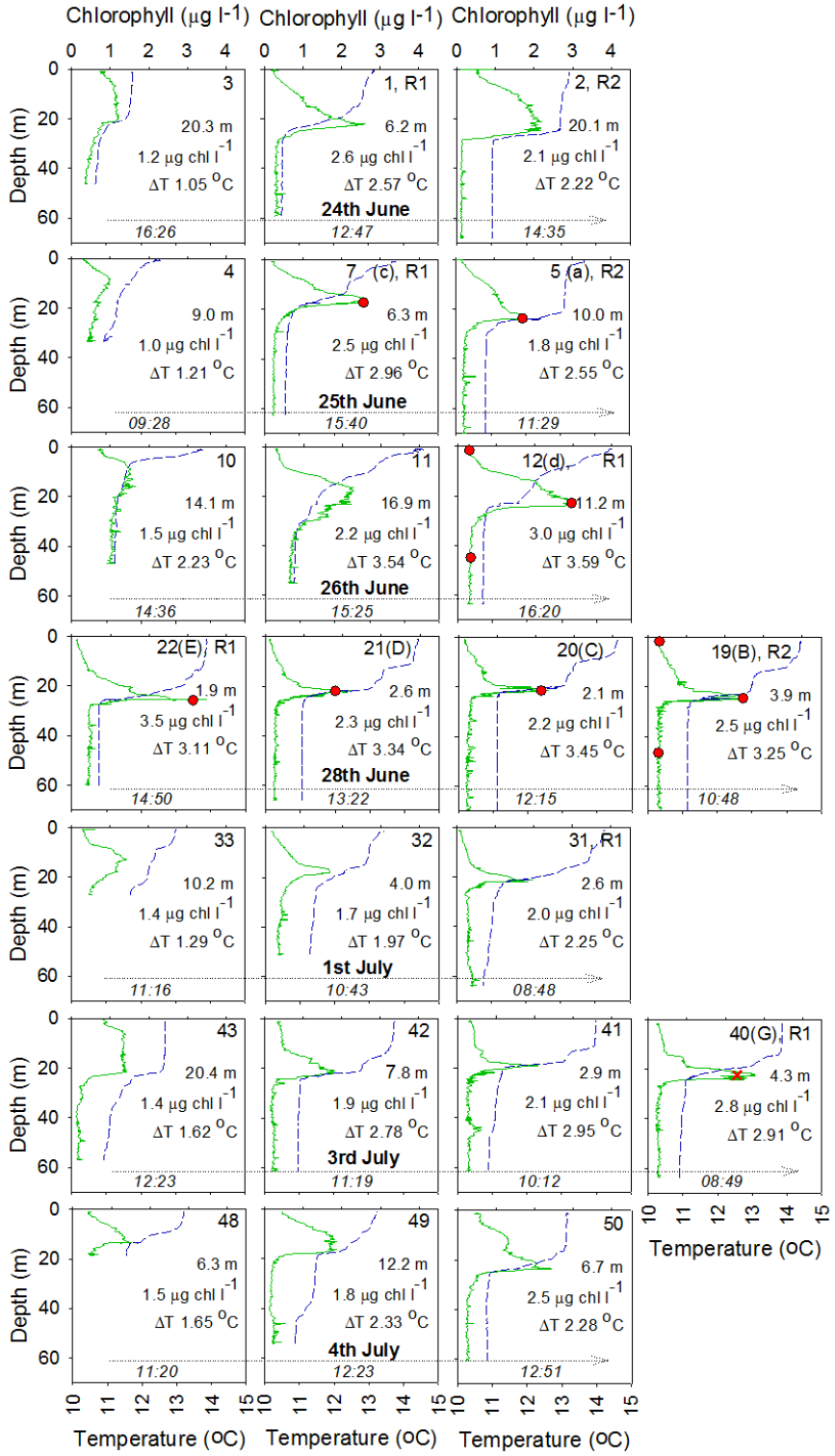

Figure 3.6. Temperature and chlorophyll profiles of stratified sites profiled along seven transects travelled during the survey period as indicated in Fig. 3.1. Site numbers given in the top right hand corner of each plot, with sample IDs in brackets, and profiles at repeat station 1 (R1) and repeat station 2 (R2) are indicated. Upper case sample IDs indicate SCMTL and lower case IDs indicate broader SCM. SCM thickness, SCM maximum chlorophyll and surface to bottom temperature difference (ΔT) for each profile is also given. Plots for each transect are shown in order of location from shore, moving offshore as arrows indicate. Therefore, these profiles represent a range of conditions, from near frontal to well

established stratification. Dates and profiling times for each site are given. The green line represents chlorophyll concentration determined from CTD chlorophyll-fluorescence, the blue dashed line represents temperature, red circles where Niskin water bottle samples were collected and the red X where a slurp gun sample was collected.

3.4.2.3. Inshore – offshore transects

The depth and strength of the thermocline varied moving inshore to offshore. Along each transect travelled it was generally the case that the thermocline deepened as the water column depth increased, and the furthest inshore sites consistently had the lowest surface to bottom temperature differences (Fig. 3.6; Table A1.1). Chlorophyll structure varied along transects also, where chlorophyll peaks of the furthest inshore sites had the lowest chlorophyll concentrations and greater peak chlorophyll concentrations were generally associated with larger surface to bottom temperature differences (Fig. 3.6).

3.4.2.4. SCM relation to strength of stratification (buoyancy frequency)

All 52 profiles exhibited a buoyancy frequency maximum located within the thermocline, which ranged from 0.0001 to 0.0042 $rad^2\ s^{-2}$. The magnitude of buoyancy frequency and SCM chlorophyll intensity ratio were positively correlated (Fig. 3.7a) and a negative correlation was evident between maximum buoyancy frequency and SCM thickness (Fig. 3.7b). Multiple linear regression analysis (Table 3.1) demonstrated buoyancy frequency to be a significant predictor of chlorophyll intensity ratio ($p < 0.001$) and thickness ($p < 0.001$). Maximum buoyancy frequency values for profiles that exhibited a SCMTL were always above 0.001 $rad^2\ s^{-2}$ and reached up to 0.0042 $rad^2\ s^{-2}$, indicating SCMTL occurred when stratification was strongest (as previously recognised through analysis of surface to bottom water temperature difference, a basic metric for stratification strength).

3.4.2.5. SCM relation to current velocity

Water column averaged current velocity averaged over the duration of the CTD profiling process (~ 15 minutes) ranged from 0.06 to 0.73 m s^{-1}, with no relationship with chlorophyll intensity ratio (Fig. 3.7c and Table 3.1) or thickness (Fig. 3.7d and Table 3.1), suggesting current velocity was not a key influencing factor in the development of SCMTL. However, current velocity data acquired at repeat station 1 over the hourly time series on the 29th June did reveal SCMTL to be thinnest (0.04 – 2.2 m) during lower current velocities (0.16 – 0.31 m s^{-1}), and broadest (4.5 m) during maximum current velocities of the time series (0.38 – 0.43 m s^{-1}) (Table A1.1). Additionally all SCMTL observed at repeat station 1 occurred approaching and during the first three days of neap tides

(Table A1.1). These observations indicate low current velocities were not a requirement for SCMTL, but do suggest some influence of current velocity over SCM structure.

3.4.2.6. SCM relation to wind speed

Wind speeds were obtained 30 – 90 mins before the start of each CTD profile (Dekshenieks et al., 2001) and ranged from 1.54 – 13.88 m s^{-1}. Wind speed was not a significant predictor of chlorophyll intensity ratio (Fig. 3.7e and Table 3.1) or thickness (Fig. 3.7f and Table 3.1). However, all SCMTL occurred when wind speed was less than 8 m s^{-1}, suggesting lower wind speeds may have been more favourable for the development of SCMTL.

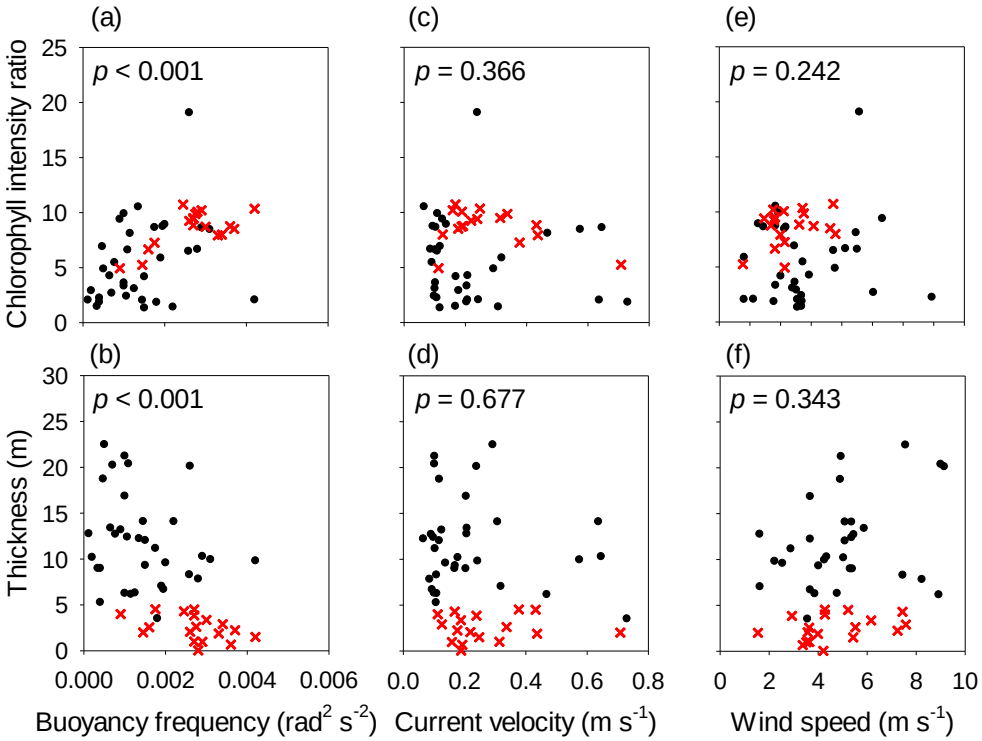

Figure 3.7. Relationship of SCM chlorophyll intensity ratio and thickness with buoyancy frequency (a) & (b), current velocity (c) & (d), and wind speed (e) & (f). Red crosses represent SCMTL, black circles represent other/broader SCM. *p* values determined by multiple regression analysis are given identifying significant predictors of intensity ratio and thickness (further details of multiple linear regression analyses given in Table 3.1). For panels (a), (b), (e) and (f) n = 52, and for panels (c) and (d) n = 50 (Table A1.1 for details of missing values).

Table 3.1. Significant physical forcing predictors of the SCM characteristics chlorophyll intensity ratio and thickness, as determined by multiple linear regression.

	Coeff.	*T*	*P*
Chl intensity ratio			
$R^2 = 0.29$			
Buoyancy Frequency	1746	4.26	< 0.001
Thickness			
$R^2 = 0.30$			
Buoyancy Frequency	-2719	-4.01	< 0.001

3.4.3. Phytoplankton community structure and photophysiology

3.4.3.1. Overall water column community structure

Overall phytoplankton carbon biomass estimates are given in Table A1.2, and key taxa and groups are shown in figures 3.8 and 3.9. At the four stratified sites where surface, SCM and deep waters were sampled, the phytoplankton community structure was broadly similar throughout the water column (Fig. 3.8; sites 12, 14, 19, 25; sample IDs d, e, B, F). The community was a mixed assemblage, primarily of diatoms and dinoflagellates, with > 70 % of the biomass contributed by just seven phytoplankton taxa. These taxa were the diatoms *Pseudo-nitzschia spp.* and *Chaetoceros spp.*, with *Proboscia alata/Rhizosolenia spp.* locally important, and the dinoflagellates *Ceratium lineatum*, *Protoperidinium spp.*, *Diplopsalis lenticula* and small (10 – 25 µm) naked dinoflagellates (genus/species not identified) (Fig. 3.8). Within the diatoms, *Pseudo-nitzschia spp.* were generally dominant except in the furthest offshore sites where rhizosolenids dominated. Within the rhizosolenid diatoms, *Proboscia alata* (3 – 8 µm diameter) was dominant, with significant amounts also (mainly in the offshore sites) of *Rhizosolenia spp.*, most likely *R. styliformis* and *R. imbricata*. Size-fractionated chlorophyll measurements confirmed that the > 10 µm phytoplankton contributed most of the chlorophyll in all samples: specifically, between 64 – 80 % in SCM samples (65 – 79 % for broader SCM and 64 – 80 % for SCMTL), 62 – 79 % in bottom water samples, and 52 – 72 % in surface samples.

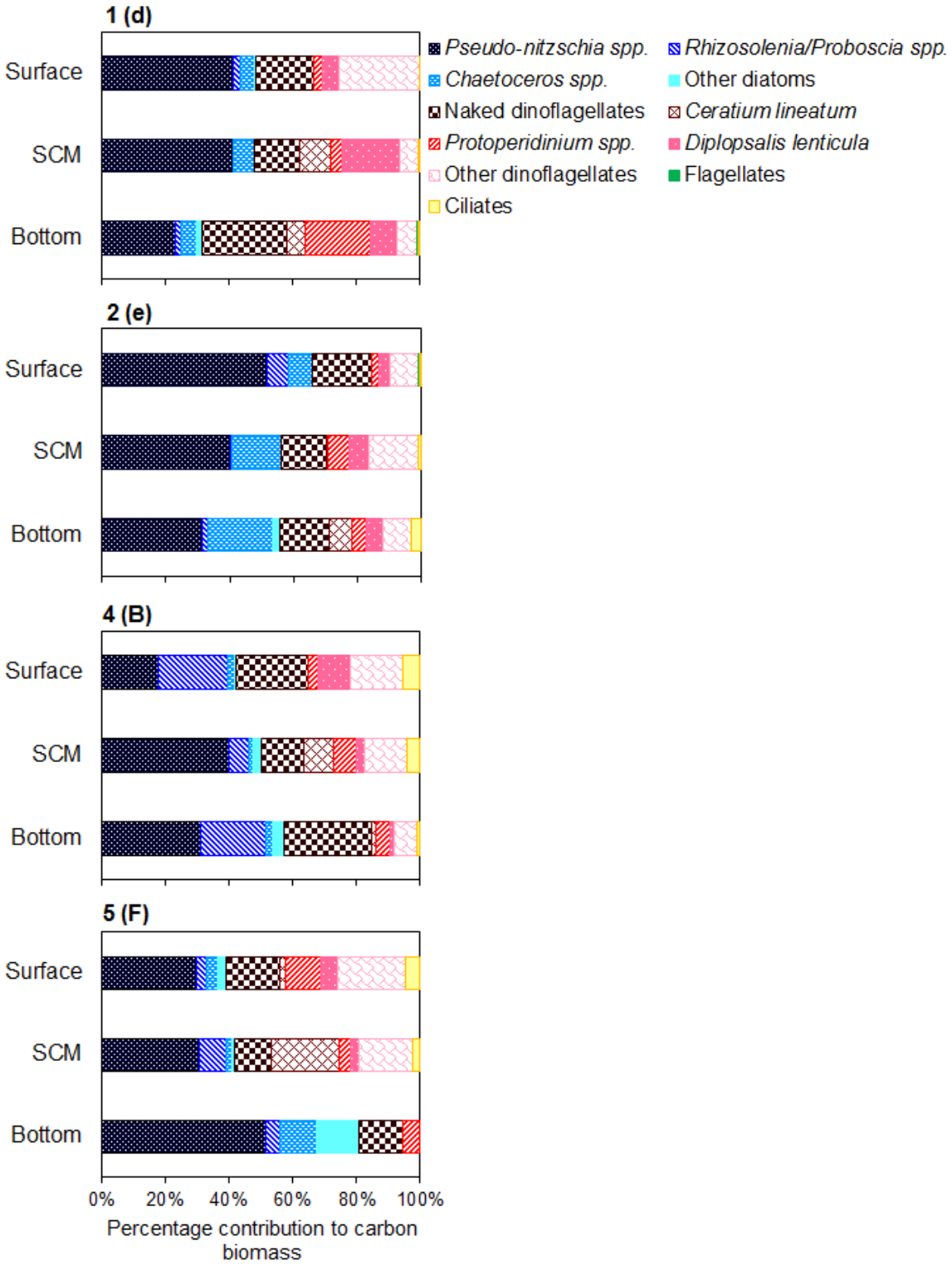

Figure 3.8. Phytoplankton community structure within the surface, SCM and bottom waters at four stratified sites (letters in brackets are sample IDs; Table A1.1): Percentage contribution of diatoms, dinoflagellates, flagellates and ciliates to carbon biomass identified by microscopy, where diatom taxa are indicated by blue colouration and dinoflagellate taxa by red colouration (NB naked dinoflagellates refer to small (10 - 25µm) naked dinoflagellates that were not identified to genus/species).

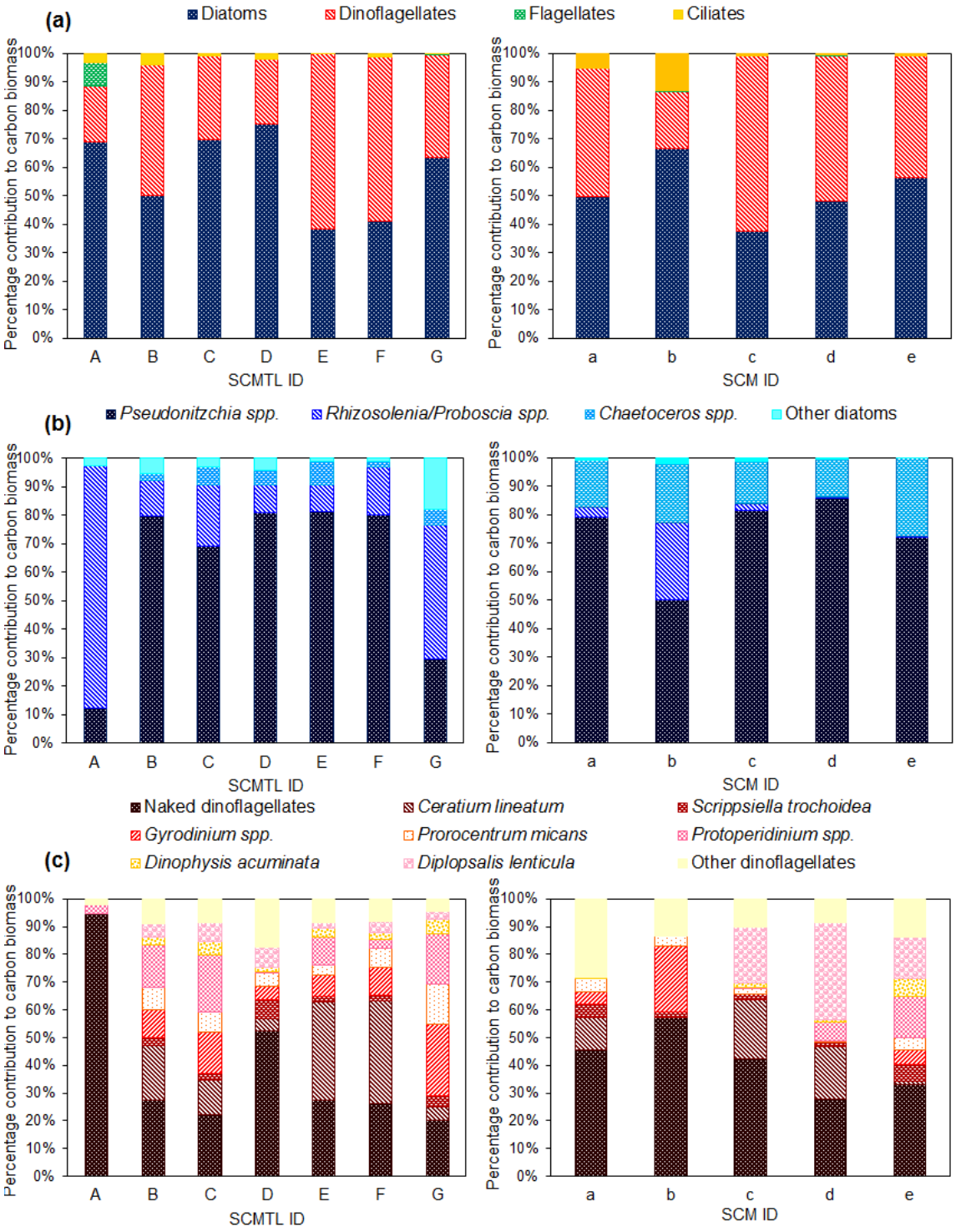

Figure 3.9. Phytoplankton community structure within SCMTL and broader SCM: Percentage contribution of (a) the diatoms, dinoflagellates, flagellates and ciliates to total carbon biomass identified by microscopy; (b) diatom taxa to total diatom carbon biomass; (c) dinoflagellate taxa to total dinoflagellate carbon biomass (NB naked dinoflagellates refer to small (10 – 25 µm) naked dinoflagellates that were not identified to genus/species).

3.4.3.2. Overall water column phytoplankton community health

To establish that the phytoplankton community sampled within the SCM, surface waters and bottom waters was photosynthetically active Fv/Fm values were assessed for all samples that were analysed for phytoplankton (Table A1.3). All Fv/Fm values were ≥ 0.28 indicating that the phytoplankton community at all three depths sampled in the water column had photosynthetic functionality (Genty et al., 1989, Suggett et al., 2009b, Murchie and Lawson, 2013). More specifically, Fv/Fm increased from surface waters (mean and standard deviation of 0.34 ± 0.04; samples taken from 1.5 – 2 m depth) to the SCM (0.45 ± 0.03 for all SCM) and bottom waters (0.44 ± 0.06), indicating that the photosynthetic energy conversion efficiency was greater in the SCM and bottom waters than in the surface.

3.4.3.3. SCMTL community structure

The community within SCMTL was predominantly diatoms and dinoflagellates, which contributed 23 – 75 % and 20 – 76 % of carbon biomass respectively (Fig. 3.9a). Ciliates (Fig. A1.2 o1 - o5) and flagellates (mainly cryptophytes; Fig. A1.2 n) combined contributed less than 4 % of biomass, with the exception of SCMTL A (furthest offshore) where they contributed 11.6 % (Fig. 3.9a).

The diatom population was generally dominated by *Pseudo-nitzschia spp.* (Fig. A1.2 b1 - b3), typically contributing over 68 % of diatom biomass (Fig. 3.9b). The exceptions were SCMTL A and G, where *Proboscia alata/Rhizosolenia spp.* (Fig. A1.2 a1 - a2) dominated, contributing 85.2 % and 47.0 % respectively, with *Pseudo-nitzschia spp.* only contributing 12.2 % and 29.4 % respectively. In SCMTL B – F *Proboscia alata/Rhizosolenia spp.* contributed 9 - 22 % of diatom biomass. Other rhizosolenids, namely *Guinardia flaccida* and *G. delicatula*, were, barring one instance, found only in SCMTL samples, but in low abundance (< 2.5 % of diatom biomass), with the exception of SCMTL G where *G. flaccida* contributed 16.8 % to diatom biomass. *Chaetoceros spp.* (Fig. A1.2 c1 - c4) was also a noteworthy contributor, responsible for up to 8.4 % of diatom biomass (Fig. 3.9b).

A mix of autotrophs, heterotrophs and mixotrophs made notable contributions to dinoflagellate biomass within SCMTL (Fig. 3.9c). Small (10 – 25 µm) naked dinoflagellates (genus/species not identified) (Fig. A1.2 j1 - j3) contributed 20.3 – 94.7 %, making the highest biomass contribution of the dinoflagellate population within SCMTL A – D. *Ceratium lineatum* (Fig. A1.2 d) and *Gyrodinium spp.* (Fig. A1.2 m) generally contributed substantially also, typically 4.5 – 37.0 % and 4.6 – 25.6 % respectively. *Ceratium lineatum* was the most dominant taxon in SCMTL E – F and *Gyrodinium spp.* in SCMTL G. Other key contributors of dinoflagellate biomass were *Protoperidinium spp.* (up

to 20.8 %), *Prorocentrum micans* (up to 14.5 %), *Diplopsalis lenticula* (up to 7.6 %), *Scrippsiella trochoidea* (up to 7.0 %) and *Dinophysis acuminata* (up to 5.3 %) (Fig. 3.9c; Fig A1.2).

3.4.3.4. Comparison of community structure between SCMTL and broader SCM

The community within broader SCM was also a mixed assemblage primarily of diatoms and dinoflagellates, contributing 37.4 - 66.6 % and 19.8 – 61.7 % respectively. Flagellate and ciliate biomass contribution was low, between 0.06 – 0.44 % and 0.7 – 13.2 % respectively (Fig. 3.9a).

The overall diatom assemblage in broader SCM was similar to that of SCMTL with *Pseudo-nitzschia spp.* dominant, contributing 50.1 – 85.6 % of diatom biomass, but with different relative contributions of *Chaetoceros spp.* and *Proboscia alata/Rhizosolenia spp.*. The key difference was that rhizosolenids were a substantial component of SCMTL (9.4 – 89.3 %) but had a minimal presence in broader SCM (0.4 – 3.7 %) (except for broader SCM b, furthest offshore, where rhizosolenids contributed 28.7 %). By contrast *Chaetoceros spp*. contributed more in broader SCM (13.3 – 27.5 %), with minimal presence in SCMTL (0 - 8.4 %) (Fig. 3.9b). The diatom *Guinardia spp.* was almost exclusively found in SCMTL.

The dinoflagellate composition of broader SCM was also broadly similar to that of SCMTL (Fig. 3.9c), but with some key differences. Small (10 – 25 µm) naked dinoflagellates made a considerable contribution to dinoflagellate biomass, between 27.7 – 57.3 %, commonly making the largest biomass contribution of the dinoflagellate community (broader SCM a – c, e). *Ceratium lineatum*, *Scrippsiella trochoidea*, *Prorocentrum micans*, *Dinophysis acuminata*, *Protoperidinium spp.*, *Gyrodinium spp.* and *Diplopsalis lenticula* remained important contributors of carbon biomass, but the contribution of some of these dinoflagellates was quite different in broader SCM compared with SCMTL. Most notably, when present *Diplopsalis lenticula* made a contribution of 14.9 – 35.2 % to dinoflagellate biomass in broader SCM compared with only 2.2 - 7.6 % in SCMTL, and *Ceratium lineatum* generally contributed more in SCMTL, responsible for 4.5 – 37 % of dinoflagellate biomass, compared with 1.3 – 21.4 % in broader SCM (Fig. 3.9c).

3.4.3.5. Statistical analyses of SCMTL and broader SCM community structure

Cluster analysis combined with SIMPROF analysis of phytoplankton carbon biomass from SCMTL and broader SCM distinguished six significant clusters of samples ($p < 0.05$; Fig. 3.10). A SIMPER analysis identified the taxa responsible for the similarity within clusters (full results in Table A1.4). Samples from SCMTL A and J, and broader SCM b were all individually distinct and therefore placed in their own clusters. Cluster 1 only included the sample from SCMTL A, sampled at the

most south westerly and furthest offshore site, approximately 40 – 50 km distant from all other sites sampled for phytoplankton. Cluster 4 only included the sample from SCMTL G, sampled at repeat station 1 on 3rd July. Cluster 6 only included the sample from broader SCM b, sampled at the second most southern site of the study, approximately 30 km from repeat station 1. Cluster 2 included samples from SCMTL B, E and F located at or within 15 km of repeat station 1, and had an average similarity of 82.0 %, with the largest contributions to group similarity made by *Pseudo-nitzschia spp.* (18.1 %), *Ceratium lineatum* (11.7 %) and 10 - 20 µm naked dinoflagellates (10.4 %). Cluster 3 included samples from SCMTL C and D, part of the 28th June transect, both located within 10 km of repeat station 1, and had an average similarity of 73.5 %, almost half of which was contributed by *Pseudo-nitzschia spp.* (27.2 %), *Proboscia alata* (10.5 %) and 10 - 20 µm naked dinoflagellates (10.4 %). Cluster 5 included the samples from broader SCM a, c-e located at or within 15 km of repeat station 1, and had an average similarity of 72.2 %, a majority contributed by only P*seudo-nitzschia spp.*, (22.5 %) 10 - 20 µm naked dinoflagellates (13.3 %) and *Chaetoceros spp.* (9.5 %).

Phytoplankton community structure of cluster 1 and 6 was most dissimilar from the other clusters, between 62.5 - 70.6 % and 41.5 – 45.8 % respectively, and 50.8 % dissimilar from each other. Dissimilarity between cluster groups 2 through 5 was 29.1 – 43.2 % (Table A1.4). The SIMPER analysis also identified the taxa responsible for the dissimilarity between clusters (shown in Table A1.4). The top three contributors to dissimilarity were: large *Rhizosolenia spp.*, *Ceratium lineatum* and medium *Rhizosolenia spp.* (28.4 %) between clusters 1 and 2; *Pseudo-nitzschia spp*., large and medium *Rhizosolenia spp.* (30.5 %) between clusters 1 and 3; large and medium *Rhizosolenia spp.*, and *Guinardia flaccida* (28.0 %) between clusters 1 and 4; *Ceratium lineatum*, *Pseudo-nitzschia spp*. and large *Protoperidinium spp.* (26.0 %) between clusters 2 and 3; *Proboscia alata*, *Guinardia flaccida* and *Ceratium lineatum* (40.2 %) between clusters 2 and 4; *Diplopsalis lenticula*, *Ceratium lineatum* and *Chaetoceros spp.* (24.1 %) between clusters 2 and 5; *Guinardia flaccida*, *Pseudo-nitzschia spp.* and *Proboscia alata* (34.9 %) between clusters 3 and 4; *Proboscia alata*, *Diplopsalis lenticula* and 20 – 25 µm naked dinoflagellates (20.1 %) between clusters 3 and 5; and *Proboscia alata*, *Diplopsalis lenticula* and *Ceratium lineatum* (28.5 %) between clusters 5 and 6.

From the cluster analysis with SIMPROF phytoplankton community structure dissimilarity between SCMTL in clusters 2, 3, 4 and broader SCM in cluster 5 was apparent at a similarity level of 68 %. An ANOSIM analysis comparing groups containing samples that were > 68 % similar (group 1: SCMTL A; group 2: SCMTL B – G; group 3: broader SCM a, c – e; group 4:

broader SCM b) identified groups to be well separated, with a global R of 0.77, and confirmed a significant difference in phytoplankton community structure between SCMTL in group 2 and broader SCM in group 3 (p = 0.001). An nMDS plot provided a 2D spatial representation of the separation between SCMTL and broader SCM based on phytoplankton biomass values (Fig. 3.11). A stress level of 0.01 indicated the ordination to be an accurate representation of similarity among samples. SIMPER analysis identified the largest contributors to dissimilarity between these SCMTL and broader SCM to be *Proboscia alata* (8.7 %), *Diplopsalis lenticula* (7.6 %), *Ceratium lineatum* (6.3 %), *Gyrodinium* (5.2 %) and *Chaetoceros* (5.0 %) (Table 3.2; full list in Table A1.4).

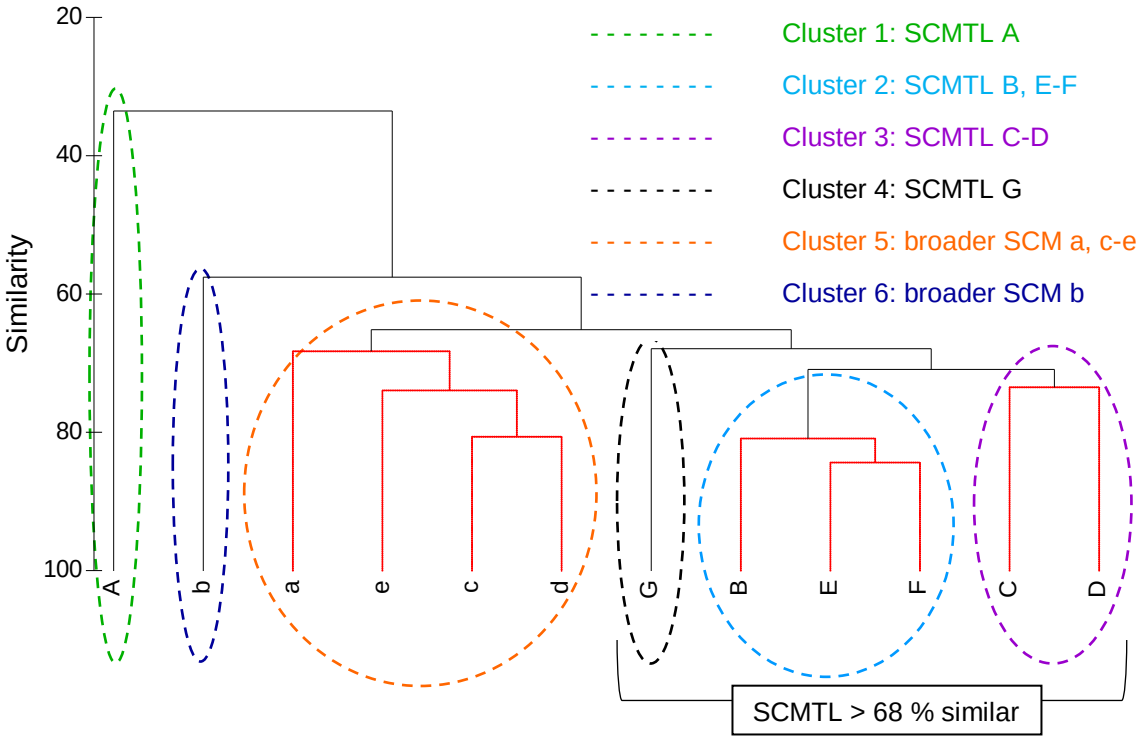

Figure 3.10. Cluster analysis of phytoplankton community structure within SCMTL and broader SCM sampled during the study, based on carbon biomass values. Red branches indicate no significant difference (p > 0.05) in community structure between linked SCMTL/broader SCM as determined by SIMPROF analysis. SCMTL that were > 68 % similar are indicated.

3.4.3.6. Temporal changes in community structure at repeat station 1

At repeat station 1, an initially broad SCM observed between the 24th to the 26th June transitioned to a SCMTL thereafter, and an associated temporal variation in community structure was identified (Figs. 3.5, 3.9 and 3.10; Table A1.4). From the 28th to the 29th June (SCMTL E – F within cluster 2) the community was not statistically different, but by the 3rd of July (SCMTL G) a significant shift in community structure had occurred. This was largely owing

to a further increase in the *Proboscia alata* population (accounted for 14.1 % of the dissimilarity) and the development of a notable population of the large rhizosolenid diatom *Guinardia flaccida* (accountable for 13.3 % of the dissimilarity).

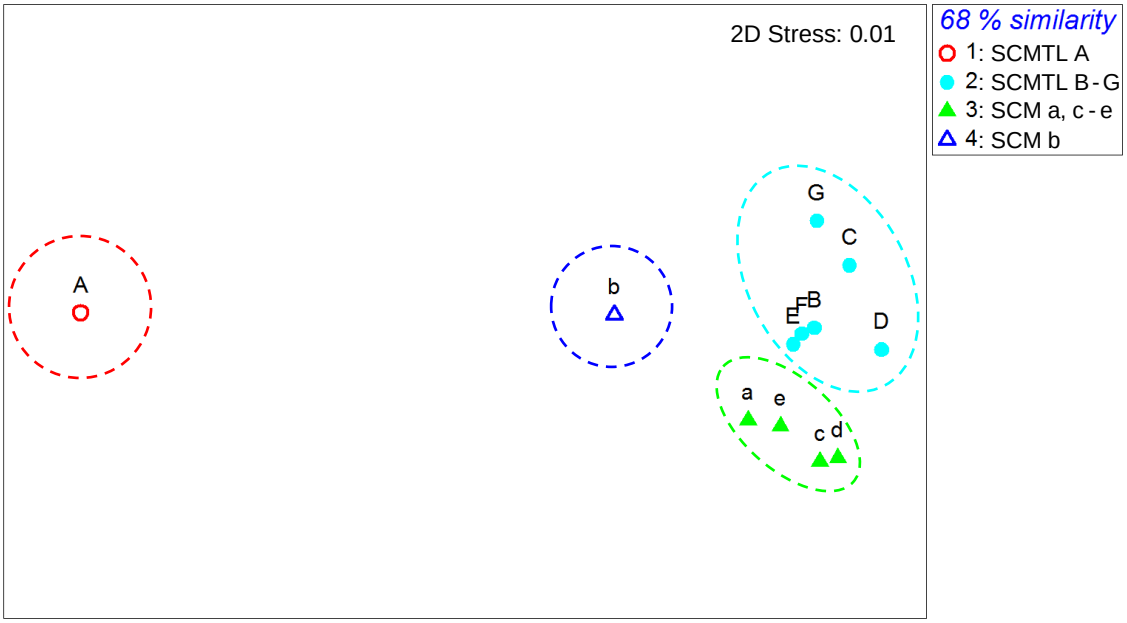

Figure 3.11. nMDS plot representing the similarity in phytoplankton community structure of SCMTL and broader SCM samples at a 68 % similarity level based on carbon biomass values. Circular data points represent SCMTL and triangular data points represent broader SCM.

Table 3.2. The top five greatest contributors to the significant dissimilarity in phytoplankton community structure between SCMTL (cluster 2, 3 and 4) and broader SCM (cluster 5), as determined by a SIMPER analysis. Average percentage dissimilarity between SCMTL and broader SCM samples, and percentage contribution of these taxa to this dissimilarity is given. + or – symbols indicate if the taxon contributed more or less in SCMTL compared to broader SCM. Average cell volumes of the different taxa are also indicated. The full table of results provided by SIMPER analysis is given in Table A1.4.

Phytoplankton taxa (avg. cell volume, μm^3)	Dissimilarity (%) SCMTL vs broader SCM	
Proboscia alata (9600)	8.73	+
Ceratium lineatum (15200)	6.25	+
Gyrodinium spp. (15195)	5.24	+
Chaetoceros spp. (650)	5.03	–
Diplopsalis lenticula (14900)	7.55	–
Cumulative contribution (%)	32.80	
Average dissimilarity (%)	34.87	

3.5. Discussion

Over the past twenty years there has been an upsurgence of studies that have specifically focused on thin layers (Durham and Stocker, 2012), recently culminating in the intensive multi-investigator Layered Organization in the Coastal Ocean (LOCO) project conducted in Monterey Bay, California (Sullivan et al., 2010b). The study presented here complements and builds upon this existing body of work on SCMTL as it shares attributes of previous studies, in particular, quantifying thin layer characteristics, evaluating the occurrence of these features and assessing the influence of the physical environment on their vertical chlorophyll structure, but on a region of the continental shelf where SCMTL have received little attention. Analogous with findings of previous thin layer studies, SCMTL were a relatively common feature of the summer stratification in the Western English Channel during the summer survey in 2013. Specifically, SCMTL were present in water column profiles approximately a third of the time, whilst previous studies that have quantified daytime SCMTL occurrence in stratified shelf waters, from the Gulf of Aqaba in the Red Sea to East Sound and Monterey Bay on the west coast of the USA, have reported them to be present anywhere between 21 - 87 % of the time (Dekshenieks et al., 2001, Benoit-Bird et al., 2009, Steinbuck et al., 2010, Sullivan et al., 2010a). Furthermore, SCMTL observed in this study had maximum chlorophyll concentrations much greater than background chlorophyll concentrations, specifically more than 4.5 times greater than background concentrations, and were located within the water column in correspondence with the pycnocline, both of which are findings frequently documented in the SCMTL literature (Dekshenieks et al., 2001, Rines et al., 2002, Ryan et al., 2008, Rines et al., 2010, Sullivan et al., 2010a, Durham and Stocker, 2012, Churnside and Marchbanks, 2015, Cullen, 2015, Ríos et al., 2016).

In addition to complementing previous SCMTL works, the study presented here is novel because it is the first known in detail investigation of SCMTL in comparison with broader SCM. Moreover, this study does not just focus on the physics or the biology of these features, as is common in other studies, instead it simultaneously examines the vertical chlorophyll structure of both SCMTL and broader SCM, relating this to water column structure and physical conditions, and quantitatively assesses phytoplankton community structure within SCMTL and broader SCM in taxonomic detail.

3.5.1. Distribution and characteristics of SCMTL and broader SCM

During summer (24th June – 4th July) 2013, the stratified waters of the Western English Channel were consistently characterised by a relatively shallow SCM within the seasonal thermocline, exhibiting a range of thicknesses (0.1 to > 20 m) and maximum chlorophyll concentrations/ chlorophyll intensity ratios (0.9 – 4.5 µg L^{-1}/1.3 – 19.1) (Figs. 3.5, 3.6, A1.1; Table A1.1). SCMTL (< 5 m thick) were observed in 18 of 52 profiles, 12 of which were detected at repeat station 1 routinely from 28th June to the 4th July. These observations of SCMTL are consistent with findings of past summer surveys of the area off Falmouth (data not shown) and other coastal studies (Bjørnsen and Nielsen, 1991, Dekshenieks et al., 2001, Rines et al., 2010, Sullivan et al., 2010a, McManus et al., 2012) that suggest SCMTL are recurring and persistent features of stratification in the coastal ocean. SCMTL were generally characterised by higher peak chlorophyll concentrations and consequently higher chlorophyll intensity ratios than broader SCM (Fig. 3.2). As SCMTL are defined by a predetermined thickness they are already arbitrarily separated by vertical scale from the more commonly sampled broader SCM, but this general trend of SCMTL having higher chlorophyll intensity ratios than broader SCM presents a further possible factor of separation. The association of high chlorophyll concentration, substantial biomass of large celled phytoplankton and relatively high Fv/Fm values (photosynthetic efficiency) (Fig. 3.9 and Table A1.3) suggests that SCMTL are hot-spots of biological activity and potentially of great importance in the shelf sea ecosystem in an ecological and biogeochemical context.

3.5.2. SCM relation to water column structure and physical forcing

All SCM occurred within the thermocline (Figs. 3.5, 3.6, A1.1), consistent with previous findings in the Western English Channel (Pingree et al., 1978, Holligan et al., 1984b, Sharples et al., 2001), as well as further afield (Cullen and Eppley, 1981, Cullen, 1982, Dekshenieks et al., 2001, Rines et al., 2002, Sullivan et al., 2005, Ryan et al., 2010, Hickman et al., 2012, Cullen, 2015). The temperature structure appeared to have a governing influence over the nature of the SCM. SCMTL were generally associated with a stepped thermocline (14 of 18 instances), located at the sharp lower step, and with greater surface to bottom temperature differences. By contrast, broader SCM were most associated with a gradual thermocline (22 of 34 instances) that sometimes extended to the surface, and smaller temperature differences (Figs. 3.4, 3.5, 3.6, A1.1; Table A1.1). Stepped thermoclines (Fig. 3.4-3) may form when a sustained episode of strong winds is succeeded by a prolonged calm period, followed by a renewed windy period that mixes the uppermost warm waters and produces the new surface mixed layer and associated (upper) thermocline (Beer, 1983). Alternatively, stepped thermoclines may form in response to internal waves that propagate

along the thermocline density interface, and induce shear and mixing (Orlanski and Bryan, 1969, Dale et al., 2006). The lower (main/seasonal) thermocline represents a layer of sustained stratification that has been stable for a significant time interval and, when temporarily protected from wind mixing by the presence of the shallower thermocline above, may promote the development of the SCMTL. Lateral intrusions in the thermocline have been described (Pedersen, 1994, Richardson et al., 2000, Richardson et al., 2003, Steinbuck et al., 2010), which can also result in a stepped thermocline. However, there was no additional evidence within the dataset of this study to support a lateral intrusion. For example, aside from temperature, there was no change in water column properties, such as salinity, at the interval of the stepped region of the thermocline. The broader SCM were generally associated with more gradual or gentler temperature gradients (Fig. 3.4-1), indicative of weaker stratification with dispersal of phytoplankton over a broader depth range (Donaghay and Osborn, 1997). This relationship between thermal and chlorophyll structure is particularly evident at repeat station 1, where daily sampling demonstrated how SCM structure evolved as thermocline structure transitioned over time (Fig. 3.5).

Profiling along inshore-offshore transects (Fig. 3.6) revealed that the broadest SCM of the transects generally formed near to the tidal mixing front and at the sites furthest offshore from the tidal mixing front, associated with smaller surface to bottom temperature differences. By contrast, the thinnest SCM were associated with greater surface to bottom temperature differences. In the vicinity of the tidal mixing front, waters were shallower and therefore there would be a greater influence of tidally generated turbulence on stratification (Pingree, 1975), thus accounting for the weakest stratification observed, and by association, the broader and least intense SCM. The temperature profiles suggest that the tidal mixing front approached repeat station 1 during spring tides, and retracted again during neaps due to spring-neap adjustment (Pedersen, 1994, Sharples, 2008). The strongest stratification and most likely conditions for SCMTL formation close to repeat station 1 thus occurred on approach to and during neap tides. The outermost sites of the survey area were less influenced by the front and perhaps relatively more strongly affected by ambient weather conditions, particularly the prevailing southwesterly winds (Pingree, 1980, PML, 2013). Increased wind driven turbulence could account for the slightly weaker stratification and broader SCM at these sites.

Investigation into the relationship of buoyancy frequency to SCM chlorophyll intensity ratio and thickness identified all SCM to be associated with a vertical buoyancy frequency maximum (Fig. 3.7a-b), where turbulent mixing would be reduced relative to the surface and bottom mixed layers (Fernando, 1991, Simpson and Sharples, 2012). SCMTL were specifically associated with

stronger stratification (Fig. 3.7a-b), providing further evidence that strong stratification is necessary for the formation of SCMTL. These findings are consistent with several studies that have used turbulence probes to show that chlorophyll maxima do not form in regions of the water column where turbulent mixing is high, but rather SCM occur at depths between turbulent energy dissipation maxima (Sharples et al., 2001, Alldredge et al., 2002, Wang and Goodman, 2009, Macías et al., 2013). The vertical extent of turbulence minima within the water column could therefore have played a role in governing the thickness of SCM, with SCMTL developing when the region of minimal turbulent energy dissipation became particularly focused.

Other possible mechanisms by which turbulence may control SCM and SCMTL include (1) chlorophyll dispersal by turbulent vertical diffusion (Donaghay and Osborn, 1997, Cowles et al., 1998); (2) increased phytoplankton sedimentation velocity promoted by intensification of turbulence (Ruiz et al., 2004), causing accumulation of cells in low turbulence regions below a turbulence maximum (Macías et al., 2013); and (3) enhanced nutrient supply from the bottom mixed layer into the thermocline driven by turbulence, promoting chlorophyll synthesis (Sharples and Tett, 1994, Sharples et al., 2001, Rippeth, 2005, Rippeth et al., 2009, Simpson and Sharples, 2012, Williams et al., 2013a, Williams et al., 2013b).

In shelf seas two main sources of turbulence are wind and tides (Pingree, 1975). To gauge the relative influence of these sources of turbulence on the SCM, the relationships between current velocity and wind speed to SCM chlorophyll intensity ratio and thickness were investigated (Fig. 3.7c-f). No relationship between wind speed and SCM thickness or chlorophyll intensity ratio was found. However, all SCMTL occurred when wind speeds were less than 8 m s^{-1}, perhaps suggesting that SCMTL form and persist when winds were weaker, potentially preventing any significant erosion of the main thermocline and dispersion of the chlorophyll peak. This finding is in agreement with that of McManus et al. (2012), who reported the most persistent SCMTL during periods of strong stratification and light winds. No relationship was identified between current velocity and SCM thickness or chlorophyll intensity ratio either, although it is acknowledged that this lack of a relationship may have resulted due to the short time scale of the current velocity measurements, since currents are highly variable and complex over a semi-diurnal tidal cycle (Rippeth, 2005). Nevertheless, the time series data at repeat station 1 did demonstrate some influence of current velocity on SCMTL structure and formation. During the hourly time series on the 29th June there was a general trend of increasing SCMTL thickness with increasing current velocity (Table A1.1). A similar relationship was also observed in the southern Celtic Sea/ Western Channel by Sharples et al. (2001), who documented a thin layer to persist over current velocities

of approximately 0.2 – 0.6 m s^{-1}, but increase in thickness from approximately < 1 to 4 m as velocity increased. Additionally, all SCMTL observed at repeat station 1 occurred when approaching and during neap tides (Table A1.1) when tidal currents would be weakening/weakest, and thus turbulent erosion of stratification and dispersion of the chlorophyll peak would be reduced (Sharples et al., 2001).

Internal waves have been documented to modulate the thickness of SCM also (Steinbuck et al., 2010), but data available were not suitable for the assessment of effects of possible internal waves on SCM characteristics.

3.5.3. Phytoplankton community structure and photophysiology

The phytoplankton community within surface waters, the SCM and deep waters for four stratified sites was consistently photosynthetically active based on values of Fv/Fm (Table A1.3), which is a robust indicator of the maximum quantum efficiency of photosynthesis (Kolber et al., 1988, Genty et al., 1989, Suggett et al., 2009b, Murchie and Lawson, 2013). The phytoplankton community at the different depths within the water column was also broadly similar in structure, with > 70 % of biomass consistently contributed by the diatoms *Pseudo-nitzschia spp.*, *Chaetoceros spp.* and rhizosolenids (locally), and the dinoflagellates *Ceratium lineatum*, *Protoperidinium spp., Diplopsalis lenticula* and small (10 – 25 µm) naked dinoflagellates (genus/species not identified) (Fig. 3.8). Thus the SCM phytoplankton population was similar to elsewhere in the water column, and could have been seeded from surface phytoplankton that sank to the thermocline at the onset of stratification. Maintenance of these phytoplankton within the thermocline may have been facilitated by alterations in cell buoyancy associated with the local environmental conditions (Steele and Yentsch, 1960, Alldredge et al., 2002) and/or modulation of cell sinking velocity associated with the transition in turbulent energy levels between surface waters and the thermocline (Ruiz et al., 2004, Macías et al., 2013). Evidence was also found to indicate phytoplankton were actively growing at the SCM. Higher Fv/Fm measurements for SCM phytoplankton compared to the surface phytoplankton (Table A1.3) suggest that phytoplankton within the SCM were not senescent cells settling and accumulating, but rather cells of relatively high photosynthetic health. The SCM was thus likely a region of enhanced productivity and growth. This finding is consistent with many observational and theoretical studies that have demonstrated phytoplankton can thrive within a chlorophyll maximum (Revelante and Gilmartin, 1973, Sharples and Tett, 1994, Parslow et al., 2001, Weston et al., 2005, Sullivan et al., 2010a, Hickman et al., 2012, Gong et al., 2015), through being photophysiologically well adapted to the low light SCM environment (Moore et al., 2006, Hickman et al., 2009).

Phytoplankton growth within the SCM was likely sustained/promoted by vertical flux of nutrients from bottom waters (Sharples and Tett, 1994, Sharples et al., 2001, Rippeth, 2005, Rippeth et al., 2009, Simpson and Sharples, 2012, Williams et al., 2013a, Williams et al., 2013b). In addition, phytoplankton motility and buoyancy regulation may have played an important role in maintenance of the SCM. Dinoflagellates capable of vertical migration were key in the SCM community, thus convergent swimming may have contributed to SCM development and intensification (Durham and Stocker, 2012, Cullen, 2015). Diatoms were also prevalent in the SCM and, although non-motile, are capable of regulating their buoyancy, with near-neutral buoyancy evident in many taxa (Waite et al., 1997, Erga et al., 2015), and positive buoyancy observed in rhizosolenids (Moore and Villareal, 1996a) and in some coastal taxa life stages (Waite and Harrison, 1992). Within the thermocline dinoflagellate motility can act to compensate for some of their more modest physiological disadvantages compared to diatoms (Ross and Sharples, 2007), as it provides the potential means to respond to resource gradients and avoid entrainment into bottom waters, assuming swimming capabilities can overcome turbulence. Based on typical turbulent diffusivities of 10^{-4} – 10^{-6} m^2 s^{-1} previously measured in the thermocline of seasonally stratified NW European shelf seas (Sharples et al., 2001, Palmer et al., 2008, Rippeth et al., 2009) and typical dinoflagellate swimming speeds of 50 – 1500 μm s^{-1} (Kamykowski and McCollum, 1986, Levandowsky and Kaneta, 1987, Sommer, 1988, Ross and Sharples, 2007), dinoflagellate swimming within the thermocline was viable (Péclet number as defined in Ross and Sharples (2008) consistently > 1 using a length scale of 10 m). Therefore, as suggested by Ross and Sharples (2007), motility may explain the observed co-existence of dinoflagellates and diatoms within the SCM.

In detail there were some significant differences between the communities of the SCMTL as compared with those of the surface, deep and broader SCM. For example, the rhizosolenid diatom *Guinardia spp.* was not identified in surface or bottom water samples, and in fact typically only occurred within SCMTL. These differences are discussed in more detail below. Spatial variation in overall phytoplankton community structure was limited, but indicated some changes offshore. Most notably, the two most southerly sites sampled, site 15 (SCMTL A) and site 6 (broader SCM b), were 60 – 70 % and 40 – 50 % dissimilar to other SCMTL and broader SCM, with a reduction in *Pseudo-nitzschia* and an increase in rhizosolenids being the principal differences. Although limited to two sites, this may suggest transition from a coastal flora to that of the more open shelf.

3.5.4. The ubiquity of *Pseudo-nitzschia*

Pseudo-nitzschia spp. was generally the most dominant diatom taxon in SCMTL and broader SCM sampled during the study (typically >70 % of diatom biomass; Fig. 3.9b), the main exception being the furthest offshore site (A). This cosmopolitan genus is commonly reported in SCM in many different coastal locations (Rines et al., 2002, Gribble et al., 2007, Velo-Suárez et al., 2008, Gomi et al., 2010, Sullivan et al., 2010a), and is recorded annually in the Western English Channel (Holligan and Harbour, 1977, Widdicombe et al., 2010, Downes-Tettmar et al., 2013). *Pseudo-nitzschia* species local to the Western English Channel include *Pseudo-nitzschia pungens and Pseudo-nitzschia delicatissima*, both of which can produce the neurotoxin domoic acid (Mos, 2001), a potential means of refuge from predation (Durham and Stocker, 2012). This capability to deter grazing along with other adaptations of the genus, including high division rates (e.g. 1.20 div d^{-1} (Pan et al., 1993)) and phenotypic plasticity (Marchetti et al., 2006) may explain the observed dominance of *Pseudo-nitzschia*. In fact, *Pseudo-nitzschia* is observed globally as a ubiquitously dominant component of phytoplankton assemblages (Trainer et al., 2012).

3.5.5. Differences in community structure between broader SCM and SCMTL

The phytoplankton community structure within SCMTL (group 2/cluster 2, 3 and 4) was statistically distinct from that identified for broader SCM (group 3/cluster 5) (Figs. 3.9, 3.10, 3.11; Table 3.2 and A1.4). Within the dinoflagellates, the principal difference was the relative importance of *Ceratium lineatum* and *Gyrodinium spp.* in the SCMTL and of *Diplopsalis lenticula* within the broader SCM (accounting for 19 % of dissimilarity; Table 3.2). *Ceratium lineatum* is primarily photosynthetic, although mixotrophy through phagotrophy of ciliates has been documented in other species from the same genus (Smalley et al., 2003). Species within this genus are strong swimmers, with swimming speeds of up to 280 µm s^{-1} documented (Nielsen, 1991, Baek et al., 2009). *Ceratium lineatum* is also a relatively large dinoflagellate, armoured with an elongate spine and horns, and is avoided as prey by small copepods (Verity and Paffenhofer, 1996). *Gyrodinium spp*. and *Diplopsalis lenticula*, on the other hand, are heterotrophic with a preference for spherical prey typically autotrophic dinoflagellates/flagellates (Hansen, 1992), and diatom prey (Naustvoll, 1998) respectively. *Gyrodinium spp.* have been found to require relatively high prey concentrations in order to grow (1000 – 4000 cells ml^{-1}) (Hansen, 1992), whilst *Diplopsalis lenticula* growth has been recorded in prey concentrations of just 30 cells ml^{-1} (Naustvoll, 1998). *Gyrodinium spp.*, similar to *Ceratium spp.*, are strong swimmers, with speeds in excess of 200 µm s^{-1} documented (Kamykowski et al., 1992), but peridinoid dinoflagellates like *Diplopsalis lenticula* have slower swimming speeds, typically in the range of approximately 60

– 150 µm s^{-1} (Levandowsky and Kaneta, 1987, Kamykowski et al., 1989, Kamykowski et al., 1992). *Protoperidinium spp.*, another heterotrophic dinoflagellate and documented to have a high grazing potential (Gribble et al., 2007), with a predilection for medium to large phytoplankton (Buskey, 1997, Menden-Deuer et al., 2005, Gribble et al., 2007), was also a more persistent minor component of the SCMTL.

The most significant differences in the diatom floras of the SCMTL were the increased abundance of *Proboscia alata*, and reduced significance of *Chaetoceros spp.* (accounted for 13.8 % of dissimilarity; Table 3.2). Temporally, repeat station (R1) surveys indicated further increases of *Proboscia alata* biomass with persistence of the SCMTL. Of the rhizosolenids, *Proboscia alata* was the most significant contributor, but there were important contributions also by *Rhizosolenia spp.* (mainly *R. imbricata* and *R. styliformis*), particularly in more offshore sites (A, B, C). On one occasion at repeat station 1 (G) *Guinardia flaccida* also contributed substantially. Elsewhere *Guinardia spp.* were typically only found in the SCMTL, albeit as a minor component.

Ecologically, both *Proboscia alata* and *Rhizosolenia styliformis* are known to be characteristic of the 'Fall Dump' diatom taxa that are adapted to grow and accumulate significant biomass in summer stratified conditions (Kemp et al., 2000). *Proboscia alata* has previously been recorded as a dominant component of SCM in the North Sea (Weston et al., 2005) and Celtic Sea (Gribble et al., 2007). Furthermore, intense annually recurrent summer blooms of *Proboscia alata* similarly associated with the thermocline at depths of 20 – 30 m are documented in a possibly analogous hydrographic setting with similar water depths on the Bering Sea shelf (Sukhanova et al., 2006). Typically, rhizosolenid mechanisms for growth at depth in stratified waters include the ability to grow in low light conditions (Goldman and McGillicuddy, 2003) and/or buoyancy regulation (Moore and Villareal, 1996a, Woods and Villareal, 2008).

These principle differences in SCMTL and broader SCM flora identified (summarised in Table 3.2) could reflect two key scenarios: (1) promotion of different phytoplankton within SCMTL compared to broader SCM (species succession) relating to environmental conditions associated with SCMTL (as described above); or (2) local lateral advection introducing 'external' phytoplankton to the SCM community. In the study area, possible mechanisms for lateral advection relate to frontal dynamics. For example, instabilities associated with the along-front jet can lead to entrainment of water from the mixed side of the front into the thermocline, potentially providing a lateral supply of nutrients and phytoplankton (Pingree, 1978, Pingree et al., 1978, Pingree et al., 1979, Mork, 1981). However, such a mechanism is unlikely to be the main driver of the distinction in

community structure observed because SCMTL typically occurred at locations further offshore and away from the front. On the other hand, phytoplankton within SCMTL were photosynthetically active and appeared to be thriving under the conditions more specific to SCMTL. This suggests that they may have adaptations to offset potential limiting factors of growth/biomass proliferation within an SCMTL that include enhanced self-shading (Shigesada and Okubo, 1981, Carter et al., 1987) and/or increased grazing pressure associated with the more concentrated nature of SCMTL.

3.5.6. Adaptations of the SCMTL taxa

All three phytoplankton taxa (*Proboscia alata*, *Ceratium lineatum* and *Gyrodinium spp.*) that made a significantly increased contribution to the community within SCMTL compared to broader SCM were large, with relatively high aspect ratios. If photosynthetic cells were horizontally orientated within SCMTL, as has recently been observed (Nayak et al., 2016), they could have enhanced their light absorption quite considerably (McFarland et al., 2016) and by association potentially their growth. Large size also makes ingestion difficult for many predators (Smetacek, 2001, Hamm and Smetacek, 2007), and large colonies, such as those formed by *Proboscia alata* (Sukhanova et al., 2006), can reduce encounter rates and cause avoidance by small grazers (Beardall et al., 2009). *Ceratium lineatum* is known to be avoided by calanoid copepods (Verity and Paffenhofer, 1996) and localised episodes of anoxia have been attributed to *Ceratium* species when in high biomass (Trainer et al., 2010), a potential mechanism for limiting predation pressure when concentrated within a SCMTL. A further attribute of *Proboscia alata* and *Ceratium lineatum* is that they both have adaptations suited to environments with intermittent nutrient supply. Established diatom traits including the vacuole that enables nutrient storage (Dortch, 1982, Raven, 1987, Raven, 1997, Marchetti et al., 2009) and luxury uptake of nutrients (Sunda and Huntsman, 1995), could further enable *Proboscia alata* to exploit the episodic nitrate supply from the bottom layer to the thermocline characteristic of shelf seas (Sharples et al., 2001, Williams et al., 2013a, Williams et al., 2013b). *Proboscia alata* nutrient acquisition could also be enhanced in its colonial form compared to single cells (Beardall et al., 2009). *Ceratium lineatum* is a mixotroph and although its ecology is not reported in detail, the close relative *Ceratium furca* may undertake luxury nutrient uptake and is also known to feed through phagotrophy only in nutrient limited conditions (Baek et al., 2008a), both strategies that would allow populations to subsist, pending nutrient input. *Gyrodinium spp.* are heterotrophic, but interestingly their growth requires high prey densities (Hansen, 1992), such as may be comparable with densities within SCMTL. Therefore, the higher abundance of *Gyrodinium spp.* within SCMTL could have been a result of enhanced

growth and accumulation by convergent swimming. Finally, based on documented swimming speeds as detailed in section 3.5.3., both *Ceratium lineatum* and *Gyrodinium spp*. may have superior swimming capabilities relative to *Diplopalis lenticula*, which could have allowed the former phytoplankton to respond more rapidly to desirable environmental cues.

3.5.7. SCM phytoplankton in a changing climate

Future climate projections show increased intensity and duration of stratification in UK shelf seas (Lowe et al., 2009, Holt et al., 2010, Sharples et al., 2013, Tinker et al., 2016). Increased stratification intensity will reduce the diapycnal nutrient flux (Sharples et al., 2013) and hence nutrient concentrations of open ocean waters transported onto the shelf (Holt et al., 2012), which could likely effect phytoplankton growth and primary production. Similarly, increased temperature could also affect growth and primary production among other metabolic processes (Eppley, 1972, Raven and Geider, 1988, Moisan et al., 2002). Freshening, and changes in wind intensity and circulation have also been predicted to occur across the shelf (Lowe et al., 2009, Holt et al., 2010, Holt et al., 2016, Tinker et al., 2016, Davy et al., 2017), all of which could also influence SCM phytoplankton communities. The effects of climate change on the shelf seas are therefore subject to complex interactions and feedbacks among changing factors (Lowe et al., 2009, Tinker et al., 2016). Nevertheless, given the significance of these regions for global biogeochemical cycling, trophic dynamics and their socio-economic importance for the supply of living marine resources (Pauly et al., 2002, Muller-Karger et al., 2005, Jahnke, 2010, Simpson and Sharples, 2012) it is important to gain some understanding of the role phytoplankton within the SCM may have in the future. Results of this study suggest that increased stratification could lead to increased incidence of SCMTL and the associated larger celled diatoms and dinoflagellates (Table 3.2). Such changes could alter trophic interactions, and potentially contribute to enhanced carbon flow to higher trophic levels and increased carbon transfer to the sediment since the rhizosolenid diatoms, in particular, are known to be efficient exporters of carbon in stratified regions (Sancetta et al. 1991; Kemp et al. 2006; Kemp and Villareal 2013).

3.6. Conclusion

Subsurface chlorophyll maximum thin layers (SCMTL) were identified in 18 of the 52 water column profiles collected over an 11 day period in 2013 in the Western English Channel, adding to a growing body of evidence for the recurring and persistent nature of these features in coastal and shelf seas. SCMTL thickness ranged down to 10 cm and they typically had higher peak chlorophyll concentrations and consequently higher chlorophyll intensity ratios than broader

SCM, suggesting that SCMTL are distinctive, both by vertical scale and their chlorophyll concentration.

Water column structure and physical forcing had an apparent governing influence on the chlorophyll structure of SCM. SCM were closely associated with the thermocline, with SCMTL most associated with the sharp lower step of a strong stepped thermocline, whereas broader (> 5 m) SCM were most associated with a weaker, gradual thermocline. As thermocline structure changed over time, so did the characteristics of the chlorophyll maximum. An association between SCMTL and stronger stratification (greater buoyancy frequencies), suggests this factor to be a prerequisite for the development and persistence of SCMTL.

This study also presents the first detailed investigation of the comparative phytoplankton community structure within SCMTL, broader SCM and the surrounding water column in the NW European shelf seas. Where the whole water column was sampled, the phytoplankton community was broadly similar with depth. Key taxa included the diatoms *Pseudo-nitzschia spp.*, *Chaetoceros spp.* and locally *Proboscia alata/Rhizosolenia spp.*, and the dinoflagellates *Ceratium lineatum, Gyrodinium spp., Protoperidinium spp., Scrippsiella trochoidea*, *Prorocentrum micans*, *Diplopsalis lenticula*, *Dinophysis acuminata* and unidentified small (10 – 25 µm) naked dinoflagellates. However, there were some key differences in community structure within SCMTL compared to broader SCM.

Phytoplankton community structure within SCMTL was identified to be distinct from that of broader SCM, largely due to a greater population of *Proboscia alata*, other rhizosolenid diatoms, *Ceratium lineatum* and *Gyrodinium spp.*, and a smaller population of *Chaetoceros spp.* and *Diplopsalis lenticula*. It is suggested that the occurrence of distinct taxa within SCMTL compared to broader SCM relates to environmental conditions associated with the thin layers. *Proboscia alata*, *Ceratium lineatum* and *Gyrodinium spp*. all have traits that may make them better adapted to conditions potentially more specific to SCMTL. These results suggest that a potential increase in the prevalence of SCMTL in the future may promote higher abundances of these larger-sized specialised SCMTL flora. This may impact on trophic dynamics and the resulting biogeochemical implications may be significant, since larger cells may increase the potential for carbon export, and rhizosolenid diatoms, in particular, are known to enhance carbon transfer to the sediment. An improved understanding of the SCMTL phytoplankton will therefore be necessary if we are to effectively assess the impacts of climate warming on biogeochemical cycling in the coastal and shelf environment. This will require further investigation

of the physical forcing factors, and the physiology and ecology of the key phytoplankton taxa associated with SCMTL.

Chapter 4: Vertical transition of phytoplankton community structure in a stratified water column measured using *in situ* holography

This chapter is being prepared for submission for publication in Nature Communications. Michelle Barnett processed CTD, holocam and FIRe data, collected and analysed all samples, and wrote the first draft of the manuscript, with edits provided by Professor Alan Kemp, Dr. Alex Nimmo Smith and Professor Duncan Purdie. Dr. Alex Nimmo Smith also organised deployment of the digital in-line holographic camera system and performed pre-processing of the raw holocam data.

4.1. Abstract

Study of marine phytoplankton communities has been long standing, but traditional sampling techniques typically involve sampling at a single or few discrete depths. In seasonally stratified shelf seas, where a subsurface chlorophyll maximum (SCM) is commonly detectable within the seasonal pycnocline, these low depth resolution techniques have often led to the description of a broad three-community structure within the water column. In this study, courtesy of *in situ* holography, it is shown that water column phytoplankton community structure is much more complex. Holographic profiling in the summer stratified Western English Channel showed a transition in phytoplankton community structure through the water column, with different taxa becoming dominant over small depth ranges. This research also demonstrates the potential of *in situ* holography for assessment of the phytoplankton community on a large spatial and temporal scale, and as a viable tool for obtaining quantitative carbon flux data.

4.2. Introduction

Phytoplankton are ubiquitous in the photic zone throughout the world's oceans, and are central to ecological dynamics, such as trophic energy flow, and biogeochemical processes, including carbon transfer and primary production (Lalli and Parsons, 1997). These marine microorganisms are diverse, possessing an array of taxon-specific properties. Thus, different phytoplankton may have particular roles in ecological and biogeochemical dynamics (Kiørboe et al., 1990, Kemp and Villareal, 2013, López-Sandoval et al., 2014). Furthermore, natural assemblages are diverse, consisting of multiple taxa that successfully coexist supported by a limited range of resources (Hutchinson, 1961). The diversity of phytoplankton and their communities indicates different populations likely present distinct ecological and biogeochemical functionality. Therefore, comprehension of their distribution and community structure is key for enhancing our understanding of biogeochemical and ecological dynamics, and for assessing how the marine ecosystem will respond to environmental variation, like that presented by climate change.

Study of phytoplankton communities has been long standing, with traditional sampling techniques involving sampling of the community at a single or few, often predetermined, discrete depths, such as by CTD rosette samplers and other bottle samplers, underway samplers and towed filtration samplers. However, these approaches assume microscale variations in the community are absent. Many studies exercising these approaches were governed by the influential paper 'The Paradox of the Plankton' (Hutchinson, 1961), which in addition to recognising natural assemblages were diverse despite a limited range of resources, also had the viewpoint that microstructure did not exist due to the "relatively isotropic or unstructured" nature of the marine environment. More recently, a variety of instruments have been developed to sample the water column at finer scales than that offered by traditional sampling systems, including multiple syringe samplers, peristaltic pumping devices and compact rosette samplers, the use of which has demonstrated microscale structure in the phytoplankton community does exist (Bjørnsen and Nielsen, 1991, Donaghay et al., 1992, Rines et al., 2010, Crump et al., 2011). A relatively new technique offering the ability to determine community structure at high vertical resolution and throughout the water column in a non-intrusive manner, is holography. Holographic imaging systems use optical scattering, specifically interference patterns of particles as they diffract a laser beam, to determine particle characteristics, including size and shape, within a known sample volume. Thus, this technology allows for phytoplankton identification and enumeration (Graham and Nimmo Smith, 2010, Graham et al., 2012). Holography is proven to offer solution to limitations of focal plane photography in imaging small particles, such as the size reduction of the

field of view and depth of field in order to achieve good resolution of small particles (Graham and Nimmo Smith, 2010). Consequently, holography is increasingly becoming the method of choice for imaging and measuring marine particles, with multiple holographic camera systems being deployed in the marine environment for this purpose (Malkiel et al., 1999, Sun et al., 2007, Graham and Nimmo Smith, 2010, Graham et al., 2012, Talapatra et al., 2013). However, studies assessing phytoplankton are rare, and those that do exist typically focus on analysing colonial diatoms, e.g. *Chaetoceros* and *Ditylum*, and very large dinoflagellates, e.g. *Noctiluca* (Katz et al., 1999, Malkiel et al., 1999, Talapatra et al., 2013, McFarland et al., 2016, Nayak et al., 2016). Therefore, the number of different holographic interference patterns/shapes attributed to phytoplankton is relatively low. Moreover, phytoplankton community structure has never been described in any taxonomic detail over an entire water column using holography.

Areas of the global ocean of particular significance in phytoplankton terms are the continental shelf seas. The shelf seas account for approximately 9 % of the area of the global ocean, yet are estimated to be responsible for up to 30 % of annual oceanic primary production, which sustains aquatic food webs, and supports significant particulate carbon export (Pauly et al., 2002, Muller-Karger et al., 2005, Jahnke, 2010). Due to the ecological and biogeochemical importance of the shelf seas there is a particular need to investigate phytoplankton community structure and distribution within them. A key part of the seasonal cycle in temperate and boreal shelf seas is the formation of a subsurface chlorophyll maximum (SCM) when stratification develops. This subsurface feature is a dense accumulation of phytoplankton often associated with the seasonal pycnocline (Holligan and Harbour, 1977, Cullen, 1982, Holligan et al., 1984a, Sharples et al., 2001, Cullen, 2015) that represents a biogeochemical hotspot. Recent studies have presented evidence of a high potential for carbon export to depth (Kemp et al., 2006, Kemp and Villareal, 2013), and approximately half (potentially more) of total annual primary production being contributed by the SCM within the stratifying shelf sea environment (Richardson et al., 2000, Hickman et al., 2012, van Leeuwen et al., 2013), attesting to the importance of understanding key phytoplankton that occupy these subsurface features. This study focuses on the Western English Channel of the NW European shelf, where weekly and fortnightly CTD and chlorophyll-fluorescence profiling at Western Channel Observatory (WCO) sampling stations L4 and E1 respectively has identified a SCM to be a recurrent feature of its summer stratified waters (Smyth et al., 2015, Fishwick, 2017). Phytoplankton community structure is routinely sampled at these stations, but generally limited to a single depth, typically 10 m (Widdicombe et al., 2010, Tarran and Bruun, 2015). Consequently, phytoplankton of SCM and the surrounding water column have not often been

sampled, and in cases where it has (Holligan and Harbour, 1977, Holligan et al., 1984b), sample depth resolution is low (3-6 samples over the entire water column).

Here a survey of 40 sites over 14 days investigating phytoplankton community structure within the SCM and surrounding water column within the Western English Channel is reported on, during which a single deployment of a digital in-line holographic camera (holocam) was conducted. The first high depth resolution taxonomic study of phytoplankton community structure in an SCM and throughout the surrounding water column is presented, possible by analysis of *in situ* holographic imagery, and the photophysiological state of that community is investigated. The holocam results are put into context of the wider shelf, and the feasibility of application of holographic imaging for assessing phytoplankton community structure on a temporally and spatially larger scale in future is discussed.

4.3. Methods

4.3.1. Sampling procedure

The study was conducted in the summer stratified waters of the Western English Channel between the 19th June and 2nd July 2015 (Fig. 4.1 and Fig. A2.1). A single deployment of a digital in-line holographic camera system updated from that described in Graham and Nimmo Smith (2010), hereafter referred to as a holocam, was performed on 19th June. A corresponding *in situ* vertical profile of temperature and chlorophyll-fluorescence was collected by conducting a simultaneous deployment of a SeaBird SBE19plus V2 conductivity, temperature, depth (CTD) probe mounted with a Wet Labs ECO FLNTU fluorometer (sensitivity: 0.025 µg chl/l; fluorescence excitation/emission wavelengths: 470/695 nm). The configuration of the CTD package allowed for slow descent/ascent rates without slowing sensor responses, thus improving dynamic accuracy and allowing small scale structure to be resolved. The CTD system was deployed at a descent/ascent rate of 0.01 - 0.1 m s^{-1} (rate slowed on approach to SCM), with a data acquisition rate of 2 Hz, which provided vertical resolution of 0.5 – 5 cm. Discrete water samples were collected from the surface, SCM (at maximum chlorophyll; see 4.3.3 below) and deep waters (hereafter, the terms deep and bottom are used interchangeably) using a Niskin rosette system (6 x 5 L Niskin bottles) mounted with the CTD package, and analysed for chlorophyll concentration, phytoplankton photophysiology, and phytoplankton community size and taxonomic structure. The water sample from the SCM was also analysed for particulate organic carbon (POC). For the remainder of the field survey the CTD Niskin rosette system was used to collect vertical water column profiles and discrete water samples (from the SCM, and from surface and deep waters

where possible) from a further 39 stratified sites in the Western English Channel (Fig. 4.1 and Fig. A2.1). 14 of these sites were in the same general location (repeat station 1) and the remainder of sites were located further afield, often sampled as part of a transect, either inshore - offshore or adjacent to the shore (Figs. 4.1, A2.1 and A2.2). Water samples were routinely analysed for chlorophyll for the purpose of calibrating the fluorometer mounted with the CTD, the Fluorescence Induction and Relaxation (FIRe) parameter of Fv/Fm, and for phytoplankton community structure in order to assess the applicability of a single holographic profile for the wider Western Channel over the survey period.

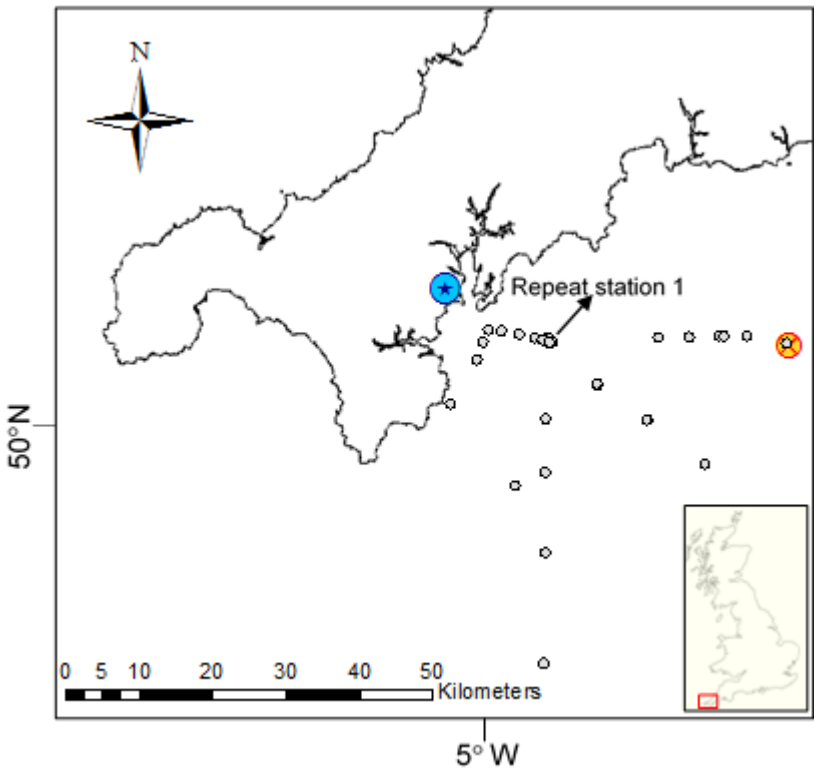

Figure 4.1. Study area in the Western English Channel where sampling occurred between the 19th June and the 2nd July 2015. The encircled blue star indicates the location of Falmouth. Circles indicate the stratified sites profiled and sampled, and the red/orange encircled cross indicates where the holocam was deployed on the 19th June. The location of repeat station 1 is also indicated.

4.3.2. Holocam deployment and data processing

The holocam was mounted on a profiling frame alongside an AML CTD Plus V2 probe with chlorophyll-fluorescence sensor (Fig. 4.2), which was lowered slowly through the water column, with a sampling frequency of 15 Hz. The holocam was adapted for vertical profiling with a vertical configuration that minimised water column disruption, similar to that described in Graham et al. (2012). It was composed of a laser (658 nm, 60 mW) and charge coupled device (CCD) digital

camera, separated by low-profile extension tubes and 90° mirrors (82 mm apart) to distance the sample volume (between mirrors) from the CCD camera and laser, as illustrated in Fig. 4.2. The laser illuminated the sample volume and the CCD camera captured interference patterns as particles diffracted the laser beam (Graham and Nimmo Smith, 2010) in a series of slices in 3 dimensional space. Together these slices formed a hologram, with a size of 1536 x 1024 pixels, where pixel size was 4.65 µm and so hologram volume was 2.78 ml. During the holocam deployment 3323 holograms were digitally recorded from the surface to 50 m depth.

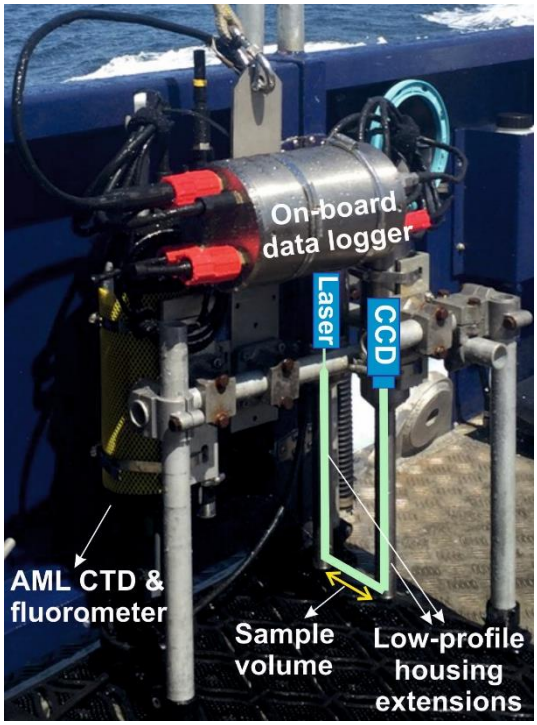

Figure 4.2. Photograph of the holocam system components mounted on a profiling frame with the AML CTD Plus V2 probe and fluorometer. The sample volume is indicated by the yellow arrow between low-profile housing extensions containing the laser and CCD digital camera. Raw data was collected by the on-board data logger.

On return to the laboratory the static background was subtracted from the imagery captured by the CCD camera, which was then reconstructed computationally following methodology developed by Graham and Nimmo Smith (2010). A hologram 3D stack was analysed using 'HOLO_Detail', a Sequoia Scientific MATLAB GUI. The stack was first cleaned by 1.1 % to remove background pixels, and then all particles, specifically phytoplankton and aggregates, were counted as they came into focus when moving through the 3D stack at 0.5 mm depth intervals. Due to the 4.65 µm pixel size of the holograms, pico- and nano- phytoplankton, and any particle below this threshold were impossible to observe/identify. The smallest

phytoplankton that could be unambiguously identified to a taxonomic level were 30 – 50 µm. Therefore, this method was only suitable for investigation of larger phytoplankton (illustrated in Fig. A2.3). Holograms analysed were at 0.3 m depth intervals, increased to 0.2 m intervals for the SCM (between 25 – 30 m). Particle counts were averaged over each meter, allowing presentation of phytoplankton community structure and aggregate abundances throughout the water column at a depth resolution of 1 m. Note that rod diatoms (Fig. A2.3), which were likely rhizosolenids e.g. *Proboscia alata*, were counted as single cells, but it is possible that the holocam interference patterns may have represented a chain of rod diatoms. Similarly, curled-chained diatoms (Fig. A2.3), which were likely a mix of *Chaetoceros* and *Leptocylindrus*, were also counted as single units/cells, because individual cells within the chain were not clear in the holograms.

4.3.3. Determination of chlorophyll concentration

Samples for chlorophyll analysis were collected by filtering 50 ml of water sample through 25 mm Whatman GF/F filters (in triplicate) immediately after collection. These filters were stored in a -20 °C freezer until analysis, which was conducted as soon as possible on return to the lab to avoid error associated with pigment degradation at -20 °C (Graff and Rynearson, 2011). Chlorophyll was extracted in 90 % acetone via sonication and then chlorophyll concentration was fluorometrically determined using a Turner Designs 10AU fluorometer based on the method of Welschmeyer (1994), whereby the fluorometer excited the extracted sample with blue light (436 nm) and the subsequent red fluorescence emission (680 nm) was recorded. Measured values of chlorophyll were used to calibrate the fluorometer mounted with the SeaBird CTD and to derive the carbon to chlorophyll ratio for the SCM at site 1. Determining chlorophyll concentrations also allowed identification of where water samples were collected within the SCM, confirming all samples were collected from/very near to the depth of maximal chlorophyll, i.e. relative sampling depth within SCM was consistent.

4.3.4. Determination of POC

POC was estimated following the methods of Poulton et al. (2006). 0.7 L of water sample was filtered onto a 25 mm pre-combusted (450 °C, 6 hrs) Whatman GF/F filter under low vacuum (< 200 mg Hg) and stored at -20 °C until analysis. Prior to analysis the filter was dried in a 40 °C oven for a minimum of 12 hours, acid-fumed using 35 % hydrochloric acid for 24 hours to remove inorganic carbon and then dried again. The sample was then analysed using a carbon, hydrogen, nitrogen, sulphur-oxygen (CHNS-O) elemental analyser (Carlo-Erba Instruments EA1108)

(Zimmermann et al., 1997, Collos, 2002). This POC concentration was used to derive the carbon to chlorophyll ratio for the SCM at site 1.

4.3.5. Assessment of phytoplankton photophysiology

An Satlantic bench top FIRe instrument was used to obtain measurements of Fv/Fm for unfractionated and fractionated (> 50 µm, 20 – 50 µm, 10 – 20 µm, 5 – 10 µm and < 5 µm) samples. Fv/Fm is a measure of photosynthetic efficiency related to, among other parameters, light and nutrient availability (Kolber et al., 1988), with maximum values of 0.65 - 0.7 (Koblížek et al., 2001). To obtain fractionated samples, 50 ml of water sample was passed through a 25 mm 50 µm pore size mesh circle and then passed through a series of 25 mm Whatman track-etched polycarbonate membranes of varying pore sizes (20 → 10 → 5 µm). Particles collected on each mesh/membrane circle were resuspended in filtered seawater and measured in the FIRe instrument immediately. The final filtrate (containing particles < 5 µm) was last measured. To run a sample, 5 ml (first dark adapted by storing in the dark for at least 25 minutes) was decanted into a cuvette and analysed in the FIRe instrument following the protocol described by Bibby et al. (2008). 30 unique iterations from the same sample were averaged, the sample delay was set at 1000 ms and gain was set at 50 - 70 % of the sensor's saturation. Raw FIRe data was processed to generate the parameters Fo (dark adapted minimal fluorescence yield) and Fm (maximal fluorescence yield) by fitting the variable fluorescence to the model of Kolber et al. (1988) using MATLAB R2013a. Fm and Fo values were used to calculate Fv/Fm using equation 4.1, which includes blank correction, where the blank was deduced by FIRe analysis of filtered seawater.

$$\frac{\mathrm{Fv}}{\mathrm{Fm}} = \frac{(\mathrm{Fm_{sample}} - \mathrm{Fm_{blank}}) - (\mathrm{Fo_{sample}} - \mathrm{Fo_{blank}})}{(\mathrm{Fm_{sample}} - \mathrm{Fm_{blank}})} \quad (4.1)$$

To assess if the dominant phytoplankton (*Ceratium fusus*) was responsible for the majority of chlorophyll in the SCM at site 1, and therefore growing by means of autotrophy rather than heterotrophy, the chlorophyll content of the SCM *Ceratium fusus* population was estimated and compared with the discrete SCM chlorophyll concentration measured. The carbon content of the SCM *Ceratium fusus* population was estimated using cell biovolume and the microscope cell count (as discussed below in section 4.3.6), and converted to chlorophyll concentration using a carbon : chlorophyll ratio of 84. This ratio was determined using chlorophyll and POC concentrations measured for the SCM at site 1 using methods described above.

4.3.6. Microscope phytoplankton analysis and biomass determination

Samples for phytoplankton analysis by light microscopy were collected by decanting 50 ml of water sample into a darkened glass bottle and immediately preserving with Lugol's iodine to a final concentration of 1 %. These Lugol's iodine preserved samples were later counted by settling 10 ml in a sedimentation chamber for 24 hours and examining using a Brunel SP951 inverted trinocular light microscope (Utermöhl, 1958). Where a single counting unit was an individual cell, whether solitary or part of a chain. Numerically dominant taxa (> 50 cells per ml) were counted on one transect of the chamber at 100x or 250x magnification depending on cell size. Cryptophytes (> 8 µm) and unidentified small naked dinoflagellates (10 – 20 µm and 20 – 25 µm) were also counted along a single transect at 250x magnification. All other cells ≥ 10 µm were counted at 100x magnification upon examination of the entire chamber base plate. Since most nano-phytoplankton < 10 µm and all pico-phytoplankton could not be identified with optical microscopy CytoSense flow cytometry was used to analyse the contribution of these phytoplankton. A complete list of identified phytoplankton taxa is presented in Table A2.1.

Diatoms, dinoflagellates and flagellates were identified to species or at least genus wherever possible, and ciliates were grouped according to size and with reference to cell wall structure (loricate or aloricate). Where there was substantial size variation within a diatom or dinoflagellate genus, cells were also classified into size categories. These included *Pleurosigma* (small: ~50 µm length, medium: 80 – 170 µm length, large: 170 - 200 µm length), *Thalassiosira* (xsmall: < 10 µm height, small: 10 - 25 µm height, medium: 25 – 45 µm height, large: > 45 µm height), *Protoperidinium* (small: 10 - 30 µm diameter, medium: 30 – 65 µm diameter, large: 65 - 120 µm diameter) and *Rhizosolenia* (small: ≤ 10 µm diameter, medium: 10 – 20 µm diameter, large: > 20 µm diameter). Any remaining diatoms whose species or genus could not be differentiated accurately with optical microscopy were grouped as pennate or centric according to size (small: 20 – 40 µm length, medium: 40 – 65 µm length, large: 65 – 110 µm length, xlarge: 110 – 175 µm length, and small: 20 – 30 µm diameter, medium: 30 – 50 µm diameter, large: 60 – 150 µm diameter, xlarge > 150 µm diameter respectively). Similarly, any remaining unidentified dinoflagellates were also grouped according to size and with reference to cell wall structure (naked or armoured) where necessary (e.g. 10 – 20 µm naked dinoflagellates, 20 – 25 µm naked dinoflagellates, 10 – 30 µm armoured dinoflagellates).

Cell biovolume was calculated based on the geometric shapes and formulae assigned for each taxon by Olenina et al. (2006). Dimensions of at least 30 cells per taxon or taxon size category (only less in cases of rarely occurring taxa) were measured with the open source software

'ImageJ'. Cell carbon was estimated using the carbon – biovolume relationships of Menden-Deuer and Lessard (2000).

4.3.7. CytoSense flow cytometric phytoplankton analysis

Samples for phytoplankton analysis by flow cytometry were collected by fixing 10 ml of water sample with glutaraldehyde (0.25 % final concentration) and freezing at -80 °C (Marie et al., 2005). Samples were analysed with a CytoBuoy CytoSense flow cytometer and CytoUSB v5.7.5.7 data acquisition software, using two different sets of data acquisition settings; one optimal for larger phytoplankton (meso- and micro phytoplankton: > 20 µm, and nano-phytoplankton: 2 – 20 µm), and the other optimal for small phytoplankton (pico-phytoplankton: < 2 µm). Meso-, micro- and nano-phytoplankton data was collected using a red fluorescence (RFL) trigger (30 mV) at a flow rate of 10 µl s^{-1} for 150 seconds or 10000 cells. Pico-phytoplankton data was acquired using a sideways scatter (SWS) trigger (25 mV) at a flow rate of 0.1 µl s^{-1} for 10000 cells, and pico-particles with a RFL signal < 10 mV were manually removed from the dataset to ensure exclusion of non-phytoplankton pico-particles/debris/electronic noise. Cell size derived from forwards scatter (FWS) was calibrated using a set of Thermo Fisher Scientific nonfluorescent polystyrene microspheres with a range of diameters (1, 2, 6, 10, 15 µm).

During data acquisition the CytoSense instrument recorded particle pulse shapes of FWS enabling description of phytoplankton community size structure using CytoClus v4.3.1.1 data processing software. For each sample a cytogram of total FWS (TFWS) and total RFL (TRFL) was generated to identify cell size. Thus clusters of pico-phytoplankton, nano-phytoplankton, and micro- and meso-phytoplankton could be resolved. As TRFL was calculated for each cell, the TRFL of the entire phytoplankton population and of each phytoplankton cluster could be determined, and was used as a proxy for chlorophyll concentration, which in turn is a proxy for biomass.

4.3.8. Statistical analysis

Phytoplankton community structure was investigated using PRIMER v6 software (Clarke and Warwick, 2001, Clarke and Gorley, 2006). Statistical analysis was conducted on phytoplankton carbon biomass data since biomass is a more biogeochemically relevant property (Paasche, 1960), as it provides a more accurate representation of community structure than abundance when the community consists of taxa of a variety of different sizes. Biomass data was first standardised by dividing biomass values by the total biomass estimated for a given sample, and then normalised by performing a square root transformation to allow each taxon to influence similarity between

samples and not just the dominant taxa (e.g. *Ceratium fusus*). Bray-Curtis similarity was calculated within each pair of samples and a cluster analysis subsequently performed to explore similarity of community structure among samples. Samples were grouped by sampling depth, i.e. surface, SCM and deep, and a non-metric multi-dimensional scale (nMDS) plot was generated to visually display similarity between samples, where a stress level below 0.2 is considered to indicate the ordination to be an accurate representation of the similarity relationship (Zuur et al., 2007). An ANOSIM (Analysis of Similarity) was applied to determine if the three sample clusters (surface, SCM and deep) were statistically distinct from each other in terms of their phytoplankton community structure, and to determine the level of separation between each cluster (given by the global R value, where values close to 0 indicate no separation and values close to 1 indicate high separation). A SIMPER (Similarity Percentage Analysis) was performed to investigate community similarities within clusters and dissimilarities between clusters, and to identify contributions of each taxon to overall similarity within each cluster and dissimilarity between clusters.

4.4. Results

4.4.1. Water column structure

Site 1 (Fig. 4.1) had a depth of approximately 70 m and exhibited an SCM associated with the base of the main thermocline at 27 m depth, with a maximum chlorophyll concentration of 28.0 µg l^{-1} and a thickness (measured at half maximum chlorophyll intensity) of < 10 cm (Fig. 4.3; data in Table A2.2). In surface and bottom waters, chlorophyll concentrations generally did not exceed 1 µg l^{-1}. The thermocline was stepped, where the lower (main) thermocline was located between 25 – 28 m, and the upper thermocline was located between 15 – 18 m. Samples were collected using a CTD Niskin rosette system from the surface (14 m), SCM and deep waters (42 m) for analysis of phytoplankton community structure (in terms of biomass) and photophysiology, including photosynthetic efficiency (Fv/Fm). The holocam was also deployed at this site to analyse phytoplankton community structure (in terms of abundance).

4.4.2. Discrete sampling: Phytoplankton community structure and photophysiology

Within the SCM at site 1 the phytoplankton community was photosynthetically active (Fv/Fm of 0.52; Table 4.1) and predominantly composed of larger cells, with micro- and meso-phytoplankton (> 20 µm) contributing 96 % of community chlorophyll, as determined by CytoSense flow cytometry (Table A2.3). Specifically, the community was overwhelmingly dominated by *Ceratium fusus*, to the extent the community was almost monospecific, with 85 % of carbon biomass identified using light microscopy attributed to *C. fusus* (Fig. 4.3). *C. fusus* was

also estimated to contribute approximately 69 % of total chlorophyll (Table 4.1), where the chlorophyll concentration of the *C. fusus* population was determined by estimating its carbon content using the microscope cell count and biovolume estimate, and converting this to chlorophyll based on a carbon to chlorophyll ratio of 84 calculated using particulate organic carbon (POC) and chlorophyll data collected for the SCM at site 1. This chlorophyll estimate suggests *C. fusus* was growing by autotrophic rather than heterotrophic means, which is supported by an Fv/Fm of 0.43 for the > 50 µm phytoplankton fraction within the SCM (almost exclusively *C. fusus*). The Fv/Fm of the > 50 µm fraction was also the highest, suggesting that this fraction, i.e. *C. fusus* was the most photosynthetically efficient phytoplankton (Table 4.1). All other SCM phytoplankton identified each contributed no more than 3 % to community carbon biomass estimates derived via light microscopy, with the diatom (mostly *Proboscia truncata*), remaining dinoflagellate, flagellate (mainly *Dictyocha spp.*) and ciliate (aloricate and loricate) communities contributing 3.3 %, 7.1 %, 2.2 % and 2.5 % respectively (Fig. 4.3; details in Table A2.1). All phytoplankton smaller than 50 µm had significantly lower photosynthetic efficiency than the > 50 µm fraction, with Fv/Fm values of 0.30, 0.26, 0.13 and 0.10 measured for the 20 – 50 µm, 10 – 20 µm, < 5 µm and 5 – 10 µm fractions respectively (Table 4.1).

In bottom waters the phytoplankton community still had photosynthetic functionality (Fv/Fm of 0.45; Table 4.1) and was mostly micro- and meso-phytoplankton, and nano-phytoplankton (55 and 33 % of community chlorophyll respectively; Table A2.3). Diatoms (37.2 %) and dinoflagellates (45.0 %) dominated biomass identified with microscopy. Ciliates, predominantly aloricate, and flagellates, mainly *Chrysophaerella longispina* and *Dictyocha spp.*, also had relatively substantial biomass, contributing 8.4 % and 9.4 % respectively. Within the diatoms, *Proboscia truncata* (19.6 % of microscope community biomass) and *Chaetoceros spp.* (12.6 % of microscope community biomass) were most dominant, and within the dinoflagellates, *C. fusus* (15.4 %), small naked dinoflagellates (17.2 %) and *Ceratium lineatum* (3.6 %) made the largest contributions of biomass (Fig. 4.3; details in Table A2.1). In bottom waters photosynthetic efficiency of the different size fractions followed the same pattern as in the SCM (Table 4.1), with an overall decrease in Fv/Fm (from 0.44) with decreasing size, but with the 5 – 10 µm fraction being the least photosynthetically efficient (Fv/Fm of 0.07).

In the surface the community had an Fv/Fm of 0.48 (Table 4.1), and was a mix of micro- and meso-phytoplankton (36 % of community chlorophyll), nano-phytoplankton (43 % of community chlorophyll) and pico-phytoplankton (21 % of community chlorophyll) (Table A2.3). The fraction of the community ≥ 10 µm (as identified by light microscopy) was dominated by dinoflagellates (43.2

%) and ciliates (36.6 %). Diatoms, largely *P. truncata*, *P. alata*, and *Chaetoceros spp.*, and flagellates, mostly *Dictyocha spp.* and *Chyrsochromulina spp.*, contributed 16.9 % and 2.9 % respectively. Within the dinoflagellates small naked dinoflagellates (15.6 %) and *Gyrodinium* + *Ceratoperidinium spp.* (6.8 %) made the largest contributions to carbon biomass, and within the ciliates aloricate cells (34.4 %) were dominant (Fig. 4.3; details in Table A2.1). These phytoplankton had relatively low photosynthetic efficiency (Fv/Fm ≤ 0.16 for all fractions between 5 - > 50 µm). Only < 5 µm phytoplankton (not identified by microscopy) were relatively efficient photosynthesisers, with an Fv/Fm of 0.41 (Table 4.1).

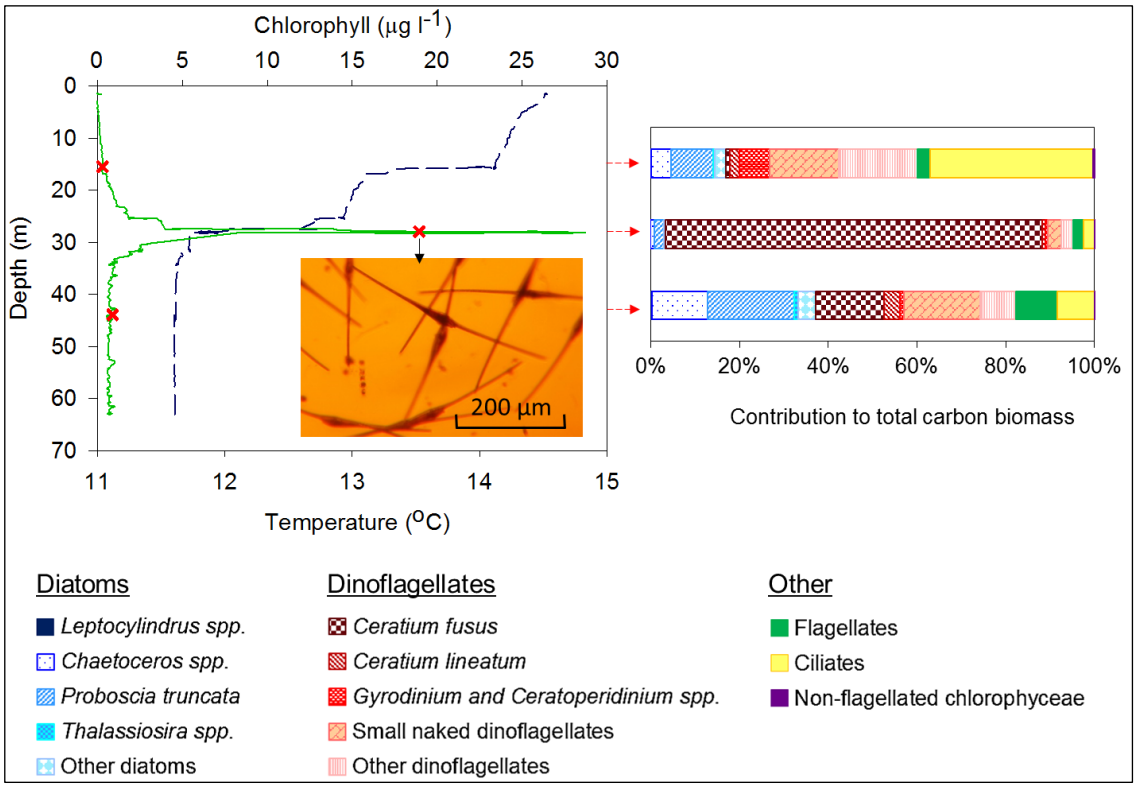

Figure 4.3. Temperature and chlorophyll profile, and phytoplankton (biomass) community structure determined by microscopy at site 1 where the holocam was deployed. The green line represents chlorophyll concentration determined from CTD chlorophyll-fluorescence, the blue dashed line represents temperature and the red Xs (and corresponding red arrows) where water samples were collected for phytoplankton analysis. An image captured down the microscope of the community within the SCM clearly shows the dinoflagellate *Ceratium fusus* to be dominant.

Table 4.1. Photophysiology of the phytoplankton community at site 1. Fv/Fm values for five size fractions of the phytoplankton community (> 50 µm, 20 – 50 µm, 10 – 20 µm, 5 – 10 µm and < 5 µm) and for the unfractionated community from within the surface, SCM and bottom waters, and estimation of the chlorophyll content of the population of the dominant phytoplankton within the SCM, *Ceratium fusus*, as an indication of its trophic state.

Size fraction (µm)	Fv/Fm			Dominant size fraction and species in SCM	Est. chlorophyll of the *Ceratium fusus* population (µg l^{-1})	Percentage of total chlorophyll
	Bottom waters (42 m)	SCM (27 m)	Surface waters (14 m)			
> 50	0.44	0.43	0.07	✓ *Ceratium fusus*	13.04	68.8
20 – 50	0.42	0.30	0.16			
10 – 20	0.23	0.26	0.11			
5 – 10	0.07	0.10	0.02			
< 5	0.19	0.13	0.41			
Unfractionated	0.45	0.52	0.48			

4.4.3. Holographic profiling: Phytoplankton

The holocam mounted alongside an AML CTD Plus V2 probe with chlorophyll-fluorescence sensor digitally recorded 3323 holograms from the surface to 50 m. Holograms at 0.3 m intervals, and 0.2 m intervals within the SCM, were analysed for phytoplankton and aggregates (Fig. A2.3), and counts were averaged over each meter, allowing phytoplankton community structure (in terms of abundance) to be studied at a resolution of 1 m throughout the water column. At depths where discrete samples were collected, holocam data largely reflected phytoplankton data collected by microscope analysis of discrete samples (Fig. 4.4 and Fig. 4.4). Within the SCM *C. fusus* was dominant (81 % of cells identified). In deep waters *C. fusus* was still dominant (approximately 22 % of cells identified) alongside the diatom *P. truncata* (approximately 20 % of cells identified). Finally, in the surface, ciliates made their most significant contribution to the community (approximately 40 % of cells identified), with *P. truncata* and *Gyrodinium + Ceratoperidinium spp.* also making a significant contribution (both approximately 10 % of cells identified), but the *C. fusus* population was quite insignificant (approximately only 3 % of cells identified). However, while discrete samples showed there to be a broad three-community structure within the water column, the holocam showed the situation was more complex, with a transition in community structure through the water column, particularly in the photic zone (Fig. 4.4 and Fig. A2.4), suggesting different taxa to occupy specific niches.

Rod shaped diatoms, most likely rhizosolenids like *Proboscia alata* (Fig. A2.3), were present throughout the water column in concentrations ranging 0.3 – 4.0 ml^{-1}, although were more significant contributors to the phytoplankton community within the surface mixed layer (above 15 m were on average 30 % of phytoplankton identified, in contrast with consistently being < 10 % below 25 m). There also appeared to be a transition of the size of these diatoms from the surface to bottom waters, with larger cells (> 450 µm length) generally making more of a contribution above the SCM (7 : 3 average large to small cell ratio), whereas smaller cells (< 450 µm length) made more of a contribution in and below the SCM (2.5 : 3 average large to small ratio). Curled-chained diatoms, most likely *Chaetoceros spp.* and *Leptocylindrus spp.* (Fig. A2.3), were also identified throughout the water column, although were never > 11 % of phytoplankton identified at any given depth. Curled-chained diatoms did become more significant below 15 m, with a concentration typically > 1 ml^{-1} compared to only 0.0 – 0.4 ml^{-1} above 15 m. The rhizosolenid diatom *P. truncata*, and chained centric diatoms (*Thalassiosira spp.*; Fig. A2.3) were both rare in the surface mixed layer, with concentrations of 0.0 – 0.6 and 0.0 – 0.7 cells ml^{-1} respectively above 15 m, but below the SCM were dominant, generally 10 - 32 % and 10 – 37 % of cells identified respectively, in typical concentrations of 0.4 – 7.9 and 1.4 – 10.4 cells ml^{-1} respectively. Within the SCM chained centric diatoms only appeared near the bottom of the SCM (below 28 m), whereas *P. truncata* was key throughout the SCM (> 9.4 % of cells identified), although made its largest contribution to the community at the lower SCM boundary (generally > 18 % of cells between 29 – 34 m). *Ceratoperidinium* and *Gyrodinium spp.* were present in relatively consistent concentration, typically 1 - 4 cells ml^{-1}, throughout the water column, and were dominant (generally 10 – 30 % of cells identified) in the surface mixed layer alongside ciliates (generally 10 – 58 % of cells identified). Ciliate abundance was changeable throughout the water column, being relatively rare in the bottom mixed layer (generally < 1 cell ml^{-1} and < 5 % of cells identified), but in and above the SCM were in abundances generally of 1 - 6 cells ml^{-1}, although only dominant in the surface layer (above 15 m). *C. lineatum* was absent above 10 m and below this depth was generally identified in concentrations of 0.1 – 2.3 cells ml^{-1}, although was never responsible for > 9 % of cells identified. *C. lineatum* made its largest contribution to the community within the bottom of the SCM, being 6.3 – 8.1 % of cells identified between 30 – 33 m. *C. fusus* was almost absent above the stepped thermocline, but within the SCM was the most dominant taxon, being 41.3 – 80.9 % of cells identified between 25 – 30 m, and having a concentration of 98.6 cells ml^{-1} at maximal chlorophyll concentration. In the bottom mixed layer *C. fusus* remained a dominant part of the community (2.5 – 13.4 cells ml^{-1} and 17.5 – 50.8 % of cells identified) alongside *P. truncata* and chained centric diatoms. Similarly, *Dictyocha spp.* was almost absent above 15 m, but important throughout the rest of the water column (2.1 – 26.9 % of cells identified). However,

Dictyocha spp. became the most dominant taxon just before *C. fusus*, responsible for 18.0 – 26.9 % of cells identified between 23 – 25 m at a concentration of 2.0 - 3.4 cells ml^{-1}, remained in similar abundance in the SCM (1.6 – 4.0 cells ml^{-1}) and then lessened in numbers below 30 m (generally ≤ 1.7 cell ml^{-1}), such that *Dictyocha spp.* were generally less than 10 % of cells identified.

4.4.4. Holographic profiling: Aggregates

What was also evident in the holocam data was the presence of substantial aggregates (Fig. 4.4; examples in Fig. A2.3) below the SCM. The presence of aggregates was investigated in holograms throughout the water column, yet they were only identified below the SCM. These findings suggest the SCM to be a considerable source of carbon flux and the most significant source within the water column, and therefore of great potential significance for carbon storage within sediments of the Western English Channel.

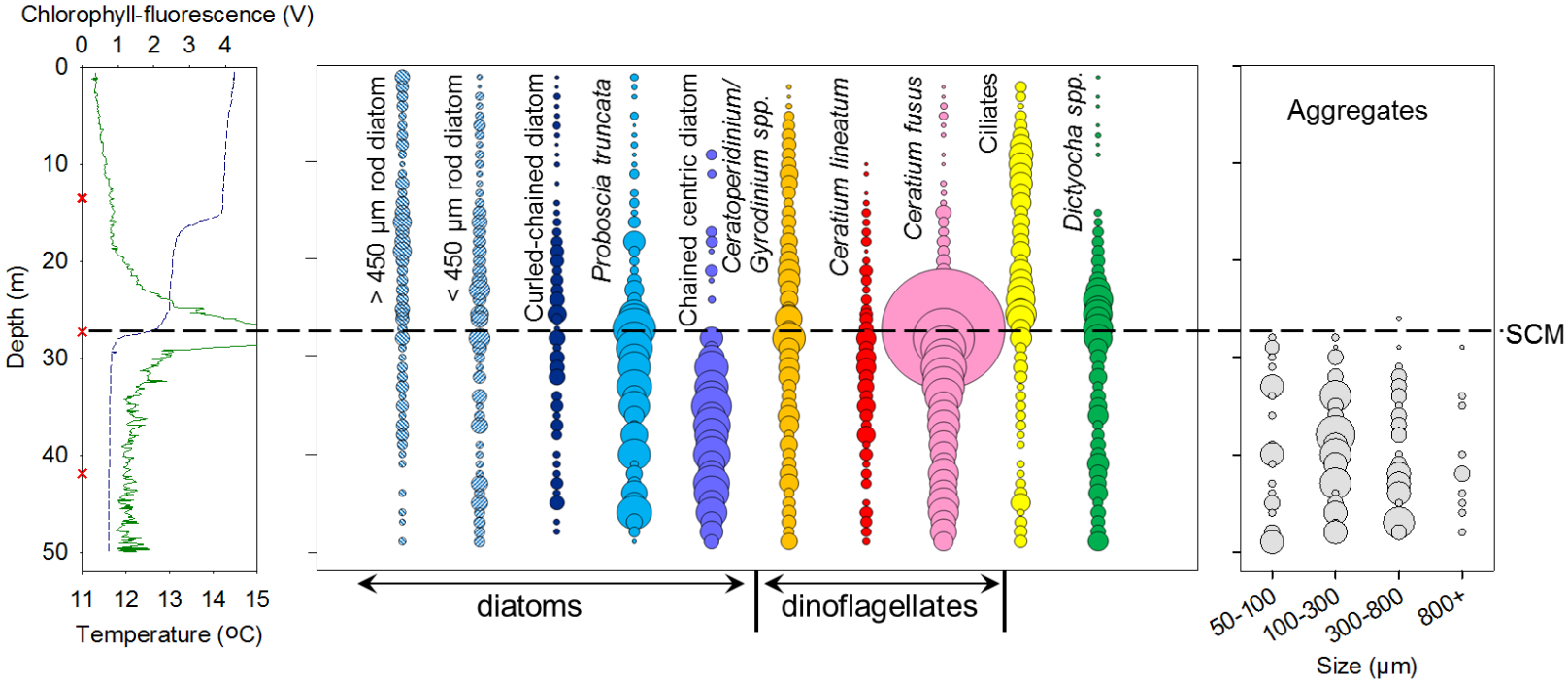

Figure 4.4. Holocam determined abundances of the 10 most numerically dominant large (> 30 µm) phytoplankton at every metre (3 holograms analysed per meter, with exception of SCM where 5 holograms were analysed per meter) through the water column, where circle size is proportional to abundance standardised to maximum abundance. Aggregates counted are shown in the right hand panel of the plot, where circle size is proportional to the number of aggregates counted in the sample volume analysed. The AML CTD Plus V2 probe temperature (dashed blue line) and chlorophyll-fluorescence (green line) depth profile of the holocam profiled site is shown in the left hand panel of the plot, red Xs indicate where discrete water samples were collected.

4.4.5. Holocam results in context of the wider shelf

Sampling the SCM at a further 39 stratified sites (Fig. 4.1 and Fig. A2.1; details in Table A2.2), 10 of which also had samples collected from surface and bottom waters, attested to the significance of the single holographic profile for the wider Western Channel. The phytoplankton community was consistently photosynthetically active (Fv/Fm mean and standard deviation of 0.45 ± 0.06 for deep waters, 0.45 ± 0.03 for the SCM, and 0.48 ± 0.06 for surface waters), of similar size structure (% contribution of micro- and meso-phytoplankton, nano-phytoplankton and pico-phytoplankton to community chlorophyll of 25.1 ± 10.9, 40.4 ± 10.8 and 34.5 ± 13.9 respectively for bottom waters; 25.0 ± 11.2, 54.3 ± 12.0 and 20.7 ± 10.2 respectively for surface waters; and 73.8 ± 15.8, 22.1 ± 14.4 and 4.1 ± 2.7 respectively for the SCM; Table A2.3), and with a taxonomic community structure comparable to that observed at site 1 throughout the survey period (Fig. 4.5 and Table 4.2; data in Table A2.1). A cluster analysis with ANOSIM using biomass data identified the surface, SCM and deep samples to be statistically distinct in terms of taxonomic community structure (p = 0.001), and a global R of 0.82 (R statistic from pairwise tests between 0.75-0.91) indicated these sample clusters were well separated. An nMDS analysis provided a 2D spatial representation of the separation between surface, SCM and deep samples, and a stress level of 0.13 verified the representation to be accurate (Fig. 4.6). Taxa whose cumulative contribution to similarity within a cluster and dissimilarity between clusters was approximately 90 % are given in Table A2.4.

In bottom waters (Fig. 4.5a; data in Table 4.2 and Table A2.1), diatoms, predominantly *P. truncata* and *Chaetoceros spp.*, and dinoflagellates, mainly small naked dinoflagellates and *C. fusus*, were most dominant. The deep sample cluster had an average similarity of 67.5 %, and the top five contributors to this similarity (Table 4.3) were 10 – 20 µm naked dinoflagellates (12.1 %), *P. truncata* (11.7 %), *Chaetoceros spp.* (5.2 %), *Dictyocha spp.* (5.1 %) and large aloricate ciliates (4.8 %). In the surface (Fig. 4.5b; data in Table 4.2 and Table A2.1), dinoflagellates, largely small naked dinoflagellates and *Gyrodinium + Ceratoperidinium spp.*, and ciliates (mostly aloricate) were quite consistently the most dominant. The surface sample cluster had an average similarity of 72.0 %, over 40 % of which was contributed by medium aloricate ciliates (11.9 %), large aloricate ciliates (9.7 %), 10 – 20 µm naked dinoflagellates (8.4 %), *Gyrodinium spp.* (5.8 %) and 20 – 25 µm naked dinoflagellates (5. 4 %) (Table 4.3). Within the SCM (Fig. 4.5c; data in Table 4.2 and Table A2.1) dinoflagellates were generally most dominant, and at over 90 % of sites, *C. fusus* was the most dominant dinoflagellate species. The SCM sample cluster had an average similarity of 67.3 %, the top five contributors being *C. fusus* (16.8 %), large aloricate ciliates (8.8 %), 10 – 20 µm naked dinoflagellates (5.5 %), *P. truncata* (5.1 %) and *Dictyocha spp.* (5.0 %) (Table 4.3).

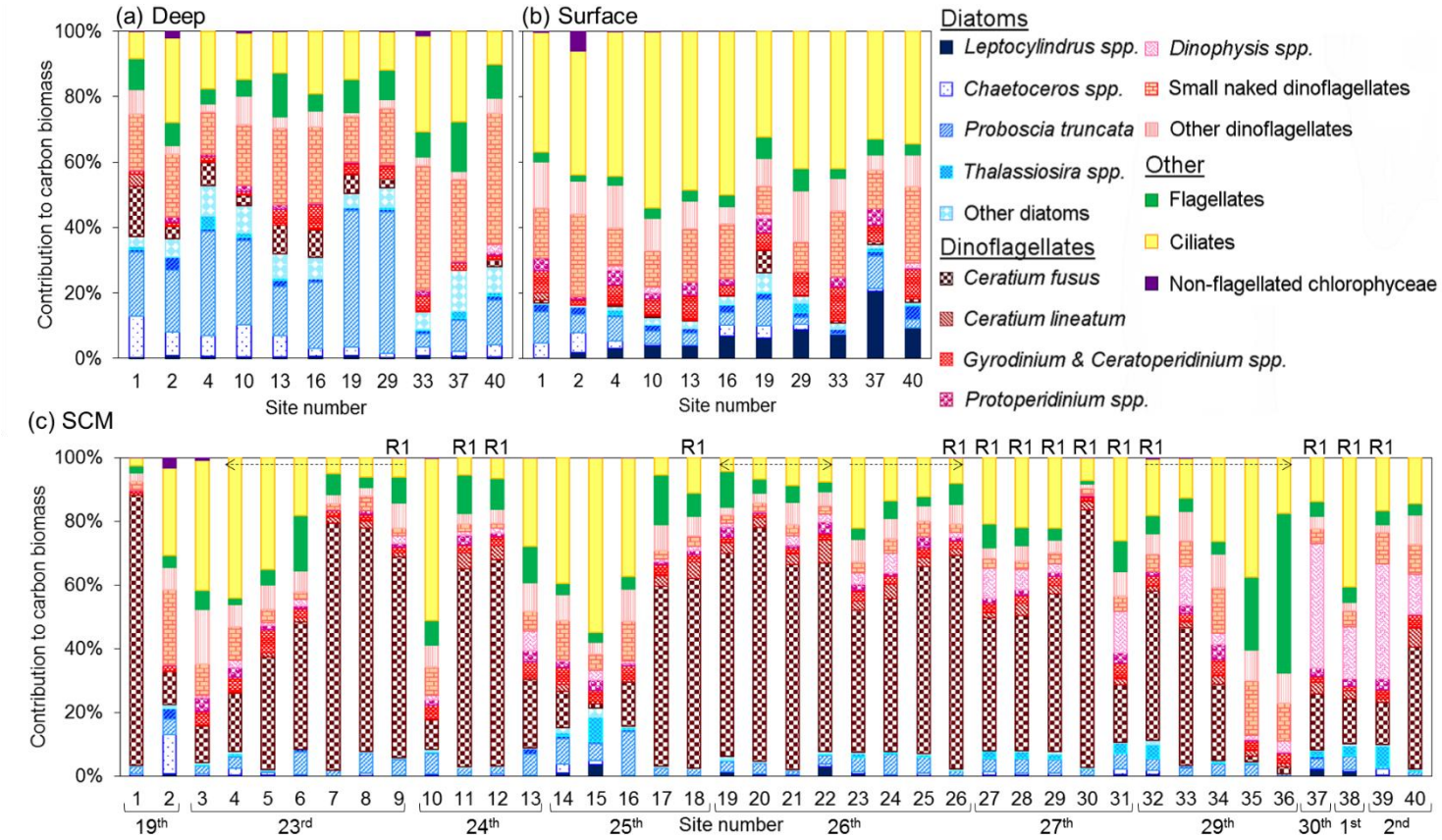

Figure 4.5. Phytoplankton community structure within (a) deep waters (11 sites), (b) surface waters (11 sites) and (c) the SCM (all 40 sites). Percentage contribution of diatom taxa (blue), dinoflagellate taxa (red), flagellates, ciliates and non-flagellated chlorophyceae to community biomass identified by microscopy (NB small naked dinoflagellates refer to 10 – 25 µm naked dinoflagellates not identified to genus/species). On plot (c) dates of sampling are given, samples from repeat station 1 (R1) are indicated, and sites sampled as part of a transect are indicated by an arrow (two arrow head ends indicates an across shore transect and a single arrow head indicates an inshore-offshore transect).

Table 4.2. Contribution of carbon biomass by diatoms, dinoflagellates, flagellates, ciliates, non-flagellated chlorophyceae, and key taxa of these major groups within the surface layer, SCM and bottom mixed layer of the 39 stratified sites sampled within the Western English Channel after the holocam deployment site (site 1). Ranges and mean values given.

	Taxa	Contribution of biomass (%)	
		Range	Mean
Surface	Diatoms	10.8 – 34.9	18.3
	→ *P.truncata*	→ 0.0 – 9.8	4.6
	→ *Chaetoceros spp.*	→ 0.1 – 6.0	1.9
	→ *Leptocylindrus spp.*	→ 1.8 – 20.6	7.1
	→ *P.alata/Rhizosolenia spp.*	→ 0.6 – 4.2	1.9
	→ *Thalassiosira spp.*	→ 0.1 – 3.0	0.7
	Dinoflagellates	27.4 – 45.0	35.3
	→ Small naked dinoflagellates	→ 9.3 – 25.2	15.5
	→ *Gyrodinium + Ceratoperidinium spp.*	→ 1.6 – 10.3	5.9
	Flagellates	1.9 – 6.6	3.9
	Ciliates (mostly aloricate)	32.4 – 53.9	41.9
	Non-flagellated chlorophyceae	0.0 – 6.0	0.6
SCM	Diatoms	0.8 – 22.7	7.2
	→ P.*truncata*	→ 0.0 – 13.7	3.8
	Dinoflagellates	20.5 – 89.0	64.3
	→ *C.fusus*	→ 1.3 – 80.9	39.6
	→ *C.lineatum*	→ 0.0 – 7.3	2.5
	→ *Gyrodinium + Ceratoperidinium spp.*	→ 1.3 – 7.4	3.1
	→ *Protoperidinium spp.*	→ 0.2 – 4.8	1.9
	→ *Dinophysis spp.*	→ 0.0 – 39.1	5.0
	→ Small naked dinoflagellates	→ 1.5 – 23.9	6.3
	Flagellates	1.1 – 50.1	7.8
	→ *Dictyocha spp.*	→ 0.3 – 49.0	5.9
	Ciliates (mostly aloricate)	4.4 – 54.9	20.7
	Non-flagellated chlorophyceae	0.0 – 3.4	0.1
Deep	Diatoms	14.2 – 52.7	37.0
	→ *P.truncata*	→ 4.0 – 43.3	22.4
	→ *Chaetoceros spp.*	→ 1.2 – 9.7	4.4
	Dinoflagellates	24.7 – 51.5	35.4
	→ *C.fusus*	→ 0.0 - 8.7	4.2
	→ Small naked dinoflagellates	→ 12.8 – 40.0	23.2
	Flagellates	4.5 – 15.1	8.8
	→ *Dictyocha spp.*	→ 2.3 – 6.1	3.4
	Ciliates (aloricate and loricate)	8.4 – 29.4	18.3
	Non-flagellated chlorophyceae	0.0 – 2.1	0.4

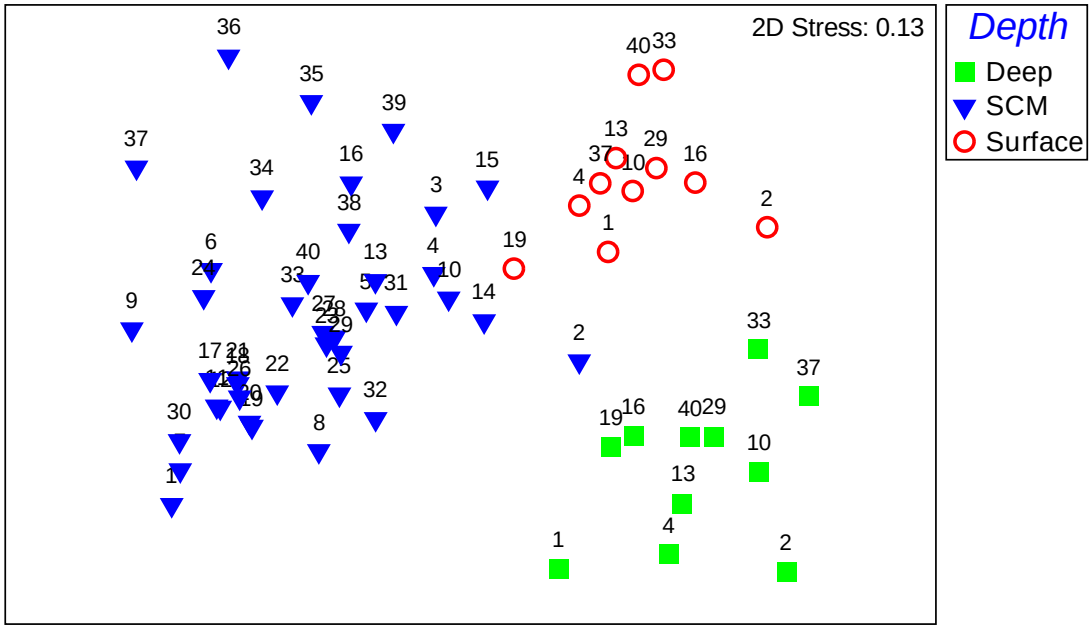

Figure 4.6. nMDS plot representing the similarity in phytoplankton community taxonomic structure within SCM (blue triangles), surface (red circles) and bottom water (green squares) samples, based on carbon biomass values. The 2D stress value is included.

Table 4.3. The five greatest contributors to similarity within each cluster, where cluster 1 (C1) contains deep samples, cluster 2 (C2) contains SCM samples and cluster 3 (C3) contains surface samples. Average similarity within each cluster is also given.

Top five contributors to similarity (with % contributions)	Deep (C1)	SCM (C2)	Surface (C3)
1.	10-20 µm naked dinoflagellates (12.14)	*Ceratium fusus* (16.75)	M aloricate ciliates (11.87)
2.	*Proboscia truncata* (11.65)	L aloricate ciliates (8.82)	L aloricate ciliates (9.72)
3.	*Chaetoceros spp.* (5.22)	10-20 µm naked dinoflagellates (5.46)	10-20 µm naked dinoflagellates (8.39)
4.	*Dictyocha spp.* (5.09)	*Proboscia truncata* (5.14)	*Gyrodinium spp.* (5.81)
5.	L aloricate ciliates (4.82)	*Dictyocha spp.* (4.99)	20-25 µm naked dinoflagellates (5.41)
Cumulative contribution (%)	38.91	41.16	41.21
Average similarity (%)	67.48	67.30	71.96

Sampling at two sites in the Celtic Sea in July 2015 indicated a high abundance and potential biomass dominance of *C. fusus* within the SCM also (Fig. A2.5). This may suggest *C. fusus* to be significant in the SCM not just in the Western Channel, but also further afield over the NW European shelf, further attesting to the relevance of the single holographic profile collected in the Western Channel.

4.5. Discussion

The holocam deployment in the stratified waters of the Western English Channel allowed for identification of the transition of phytoplankton through the water column and how one species was dominant over a small part of the water column. Moreover, further phytoplankton sampling in the Western Channel (and Celtic Sea) put the holocam results in context of the wider shelf.

4.5.1. The dominance of *Ceratium fusus*

The holocam was deployed at a site (site 1) that exhibited a stepped thermocline and an extremely thin (< 10 cm) and intense (28.0 µg l^{-1} maximum chlorophyll concentration) SCM located at the base of the lower (main) thermocline. The SCM was dominated by the mixotrophic dinoflagellate *C. fusus*, whose growth was driven by photoautotrophy (Table 4.1). The dominance of *C. fusus* was so extensive the community was almost monospecific, with C. *fusus* being responsible for 85 % of carbon biomass, as determined by inverted light microscope analysis of a discrete water sample from the SCM, and 81 % of cells identified at maximal chlorophyll using holography (Fig. 4.3 and 4.4). *C. fusus* is characteristic of the NW European shelf, documented as significant in the phytoplankton community for over half a century (Tomczak and Goedecke, 1964, Dodge, 1981, Reid et al., 1987, Beaugrand et al., 2000, Johns and Reid, 2001). This large dinoflagellate is most abundant during summer in areas with a relatively shallow thermocline (Tomczak and Goedecke, 1964, Holligan and Harbour, 1977, Gribble et al., 2007, O'Boyle and Raine, 2007), like that observed in this study (thermocline base at 27 m). Moreover, the *C. fusus* bloom within the thermocline, with the depth of maximum chlorophyll corresponding with the maximum density gradient of 0.13 kg m^{-3} over 0.25 m, agrees with the general observation that a density gradient is a prerequisite for development of a significant dinoflagellate population (Donaghay and Osborn, 1997).

C. fusus possesses many adaptations that could explain the observed dominance of this dinoflagellate within the SCM. Firstly, *C. fusus* can undergo vertical migration, with an average swimming speed reported of 75 µm s^{-1} (Baek et al., 2009). Based on typical turbulent diffusivities

of $10^{-4} – 10^{-6}$ m^2 s^{-1} measured in the thermocline of seasonally stratified NW European shelf seas (Sharples et al., 2001, Palmer et al., 2008, Rippeth et al., 2009) this average swimming speed would allow *C. fusus* to have some control over its location within the thermocline (Péclet number as defined in Ross and Sharples (2008) consistently > 1 using a length scale of 10 m). Therefore, *C. fusus* had the potential means to respond to resource gradients within the thermocline and avoid entrainment into bottom waters from the base of the thermocline. *C. fusus* may also perform luxury consumption of nutrients (Baek et al., 2008a), which is a trait that could enable this dinoflagellate to exploit the episodic nutrient supply from bottom waters into the thermocline characteristic of seasonally stratified shelf seas (Sharples et al., 2001, Williams et al., 2013a, Williams et al., 2013b). Furthermore, *C. fusus* has physiological flexibility, being able to grow in a wide range of light and temperature conditions (Johns and Reid, 2001, Baek et al., 2007, Baek et al., 2008b), which may account for the cosmopolitan nature of the species in the Western English Channel and across the NW European shelf. The optimal growth light level reported for the species in marine conditions is 216 µmol m^{-2} s^{-1} (Baek et al., 2007, Baek et al., 2008b), yet light levels within the SCM at site 1 were roughly only a sixth of that. However, *C. fusus* has a high aspect ratio, being 250 – 350 µm long, but only 12 – 20 µm at maximum diameter, and if these cells were horizontally orientated within the SCM, analogous with the recent observations of Nayak et al. (2016), light absorption may have been greatly enhanced (McFarland et al., 2016). Finally, some *C. fusus* traits may limit predation pressure. For instance, episodes of anoxia have been attributed to *C. fusus* blooms (Onoue, 1990, Spatharis et al., 2009), potentially a means for refuge from predation. Moreover, cells are large and armoured with two elongate apical horns, making ingestion difficult for many predators (Smetacek, 2001, Hamm and Smetacek, 2007), with only the largest copepods documented to graze *Ceratium* (Nielsen, 1991) and declines in the mesozooplankton population reported in association with a *Ceratium* bloom (Smetacek, 1981).

The dominance of *C. fusus* alongside its growth by photoautotrophy is of particular significance as it suggests an important contribution of primary production. This supposition is supported by other observations of *Ceratium* dominating coastal phytoplankton communities where they were reported to contribute substantially to annual primary production (Smetacek, 1984, Nielsen, 1991, Dodge and Marshall, 1994). Distribution and growth of *Ceratium* is dependent upon temperature (Holligan and Harbour, 1977, Dodge and Marshall, 1994, Baek et al., 2007, Baek et al., 2008b), with long term abundance increases on the NW European shelf associated with increasing temperatures (Johns and Reid, 2001). With predicted temperature increases of 1.5 – 4.0 °C by the end of the century (Lowe et al., 2009, Tinker et al., 2016), abundances of *C. fusus* and other *Ceratium spp.* may be enhanced, with increased incidences of *Ceratium* dominated SCM. Such a

change could contradict the commonly held view that climate warming will lead to a reduction in primary production (Steinacher et al., 2010) since *Ceratium spp.* are appreciated to be important contributors to coastal production.

4.5.2. Transition of phytoplankton through the water column

Abundant phytoplankton identified in the water column alongside *C. fusus* using holography (Fig. 4.4 and Fig. A2.4) included rod diatoms (likely rhizosolenids, e.g. *P. alata*), curled-chained diatoms (likely *Chaetoceros spp.* and *Leptocylindrus spp.*), *P. truncata*, chained centric diatoms (*Thalassiosira spp.*), the dinoflagellates *Ceratoperidinium* + *Gyrodinium spp.* and *C. lineatum*, the silicoflagellate *Dictyocha spp.*, and ciliates. These phytoplankton occupied different depths, such that where analysis of discrete samples showed there to be three broad communities present in the water column (surface, SCM and bottom water communities), holography instead showed the situation was much more complex, with a transition of various phytoplankton and community structure through the water column. This transition likely reflected interactions and adaptations of different taxa, and the environmental conditions within the water column, enabling improved understanding of these particular phytoplankton.

C. fusus has a number of adaptations, described above, that may account for its dominance within the SCM, and the almost complete lack of cells above 15 m is consistent with the findings of Baek et al. (2007, 2008b, 2009) who documented an inability of *C. fusus* to grow in strong sunlight and active avoidance of such conditions. Below the thermocline, an Fv/Fm of 0.44 for the > 50 µm fraction in combination with strong tidal flows and associated turbulence in shelf seas (Pingree, 1975, Pingree, 1980, Simpson and Sharples, 2012), suggest these *C. fusus* cells were largely photosynthetically active cells that had been recently mixed out of the SCM. In bottom waters of seasonally stratified temperate shelf seas the strong tidal currents can drive turbulent diffusivities of typically 10^{-1} - 10^{-2} m^2 s^{-1} (Simpson and Sharples, 2012, Tweddle et al., 2013, Williams, 2013), thus for phytoplankton motility to dominate over turbulence (i.e. for the Péclet number to be > 1 (Ross and Sharples, 2008)), sustained swimming speeds in excess of 250 µm s^{-1} and up to approximately 2500 µm s^{-1} would be necessary (based on the bottom layer being 40 m thick). Given that these speeds are beyond the capability of *C. fusus* (Baek et al., 2009) and are in fact generally beyond all documented swimming capabilities of phytoplankton, including ciliates (Kamykowski and McCollum, 1986, Levandowsky and Kaneta, 1987, Sommer, 1988, Ross and Sharples, 2007), indicates that unless turbulence in bottom waters assisted with re-access to the thermocline (Ross and Sharples, 2008), all cells holographically identified below the thermocline had been permanently removed. The fate of such cells was either to be grazed by zooplankton

capable of swimming in tidally energetic bottom waters, or to sink to the sediment (Simpson and Sharples, 2012). Therefore, given cells identified in the water column below the thermocline equated to in excess of 1000 mg C m^{-2} in that instance at site 1 (based on cell count and available biovolume data, and the biovolume – carbon relationships of Menden-Deuer and Lessard (2000)), suggests that these bottom water phytoplankton may have made a significant contribution of carbon transferred to higher trophic levels (either directly or via the mesozooplankton) and carbon export to depth.

C. lineatum and *Dictyocha spp.* had similar distributions to *C. fusus*, but were much less abundant than *C. fusus* within the SCM. The similar distributions of *C. lineatum* and *Dictyocha spp.* to *C. fusus* could reflect similar environmental tolerances. For instance, the general absence of *C. lineatum* above 15 m could indicate it shares the traits of the genus of growth incapacity at, and active avoidance of high light (Baek et al., 2007, Baek et al., 2008b, Baek et al., 2009). The differences in abundance may indicate *C. fusus* had a higher competitive ability relative to *C. lineatum* and *Dictyocha spp.* facilitated by traits better suited to the SCM environment. For example, both *C. lineatum* and *Dictyocha spp.* have smaller aspect ratios than *C.fusus*, which may have limited their growth relative to *C. fusus* by restricting light absorption in the low light conditions of the SCM (McFarland et al., 2016). Also, growth rates of *C. lineatum* have been documented to be slower (~ 0.2 divisions d^{-1}) than those of *C. fusus* (~ 0.3 divisions d^{-1}) at temperatures (~15 °C) approximate to those recorded at the depth of maximum chlorophyll (Nordli, 1957). Following a simple population growth model $P(t) = P_0 \exp [(p - g)t]$ (Geider, 1988), where P(t) is phytoplankton biomass at time t, P_0 is phytoplankton biomass at time 0, p is growth rate and g is grazing mortality, the above growth rates, assuming the grazing mortality term is equal for both species, would result in *C. fusus* population doublings 1.5 times faster than that of *C. lineatum*. Conversely, *C. lineatum* has been observed to grow marginally better than *C. fusus* at temperatures lower than 15 °C (Nordli, 1957) and growth of several *Ceratium* species is strongly temperature dependent (Nordli, 1957, Baek et al., 2007, Baek et al., 2008b). Therefore, lower temperatures (~11.6 °C) on the downslope of the SCM comparative to those on the upslope of the SCM to the depth of maximal fluorescence (12.0 - 13.2 °C) may have been more favourable for *C. lineatum* compared to *C. fusus*, and thus accountable to an extent for its largest contribution observed within the bottom of the SCM. Furthermore, *Dictyocha* has been documented to grow in nitrogen deficient conditions (Wasmund et al., 2015), potentially explaining its dominance at the upper boundary of the main thermocline (23 – 25 m) before the onset of *C. fusus* dominance.

P. truncata and chained centric diatoms (*Thalassiosira*) were not abundant in the surface mixed layer, likely because their growth was not supported in the nutrient deficient waters. High light intensities may also have influenced *P. truncata*, as substantial decreases in growth rates and growth inhibition at light levels exceeding 50 – 155 µmol m^{-2} s^{-1} have been documented for large diameter rhizosolenids (Moore and Villareal, 1996a). At the SCM base these diatoms were dominant with *C. fusus*, likely a result of established diatom traits and mechanisms favourable for growth within the SCM. These include luxury nutrient consumption (Sunda and Huntsman, 1995), vacuole nutrient storage (Dortch, 1982, Raven, 1997, Marchetti et al., 2009), buoyancy regulation (Moore and Villareal, 1996a, Moore and Villareal, 1996b, Woods and Villareal, 2008, Vega and Villareal, 2016), and ability to grow in low light, with *Thalassiosira spp.* and large diameter rhizosolenids documented to grow at light intensities as low as 5 µmol m^{-2} s^{-1}, at rates exceeding 0.2 div. d^{-1} (Goldman, 1993, Moore and Villareal, 1996a, Goldman and McGillicuddy, 2003). Diatom dominance towards the base of the SCM/thermocline is consistent with findings of previous observational and theoretical studies (Huisman et al., 2006, Moore et al., 2006, Hickman et al., 2009), suggested to be due to their immobility preventing them from reaching further upward in the SCM (Ross and Sharples, 2008) and adaptations for growth in the light conditions (intensity and spectral composition) presented at the base of the thermocline (Huisman et al., 2006, Moore et al., 2006, Hickman et al., 2009). However, where chained centric diatoms were only present at the bottom of the SCM, *P.truncata*, while more dominant in the lower reaches of the SCM, was in fact key throughout the SCM. This may be due to rhizosolenid buoyancy regulation, including a capability for positive buoyancy (Moore and Villareal, 1996a, Moore and Villareal, 1996b, Woods and Villareal, 2008, Vega and Villareal, 2016), and at rates sufficient to dominate over turbulent diffusivities typical of the shelf sea thermocline (Péclet number as defined in Ross and Sharples (2008) consistently > 1 based on a length scale of 10 m, turbulent diffusivities of 10^{-4} – 10^{-6} m^2 s^{-1}, and rhizosolenid ascent rates in the order of cm to m hr^{-1} as presented in Moore and Villareal (1996b)).

Ciliates and *Ceratoperidinium* + *Gyrodinium spp.* were present throughout the water column, and since both typically rely on heterotrophic nutrition, it is likely their distribution above the main thermocline largely reflected that of prey items. Rod shaped diatoms and curled-chained diatoms were also present throughout the water column, possibly indicating broader light tolerances. However, their consistently low abundances suggest surface layer conditions did not promote photosynthesis and subsequent growth, supported by a Fv/Fm of 0.07 for the > 50 µm fraction in the surface layer, likely due to low nutrients (Kolber et al., 1988). Instead the < 5 µm fraction, not identified by the holocam, had the highest Fv/Fm (0.41) in the surface and thus was potentially

the most biogeochemically significant. The transition in size of the rod diatoms, thought to be rhizosolenid diatoms such as *Proboscia alata*, through the water column may reflect changes in chain length in response to changing turbulence and/or predator pressure. The greater contribution of longer rods (> 450 µm length) above the SCM may be indicative of lesser wind mixing permitting long chain formation and persistence (Seckbach and Kociolek, 2011), and/or a response to a greater grazer pressure (ciliates dominant above SCM) as for many predators larger prey is difficult to ingest (Smetacek, 2001, Hamm and Smetacek, 2007). In contrast, tidally generated turbulence can disrupt diatom chains (Seckbach and Kociolek, 2011), and therefore could explain the greater contribution of smaller rods (< 450 µm length) below the SCM. The lesser contribution of curled-chained diatoms, most likely *Chaetoceros spp.* and *Leptocylindrus spp.*, above 15 m may be related to grazer abundance (ciliates up to 58 % of cells identified above 15 m), either reflecting cell removal by grazers or reduced chain length of these small diatoms to the extent their size precluded their identification within holograms. The latter is consistent with the findings of Bjærke et al. (2015) who reported chain length of a small diatom to decline in response to grazer cues, which reduced grazing losses.

4.5.3. Phytoplankton community structure across the Western English Channel

SCM taxonomic community structure was on average 67.3 % similar across the 40 sites sampled, and community structure in the surface and bottom waters was broadly similar also, with average similarities of 72.0 % and 67.5 % respectively (Figs. 4.5 and 4.6, and Table 4.3, A2.1 and A2.4). This finding may suggest that community structure throughout the water column as observed using the holocam was typical of and thus relevant across the Western English Channel during the survey (19th June – 2nd July). However, recognition of subtle but distinct changes in phytoplankton community structure is important for our understanding of key species, which could be achieved with multiple holocam deployments.

C. fusus was also identified to be dominant within SCM of the Celtic Sea in July 2015 (Fig. A2.5), indicating wide distributional limits (where conditions are favourable for growth) of these dinoflagellates and perhaps also dispersion of SCM phytoplankton from the Western Channel to the open shelf and vice versa. These findings support that observations made in the Western English Channel are relevant to adjoining open shelf waters.

4.5.4. Methodological considerations and feasibility of future application

Based on data presented in this chapter it is clear *in situ* holography can be a powerful tool when assessing phytoplankton community structure, and it holds many advantages over more traditional techniques. The first advantage is high depth resolution, which allows observation of the transition of phytoplankton taxa through the water column. Therefore, particularly when used in conjunction with physical profiling packages, such as CTD packages and turbulence profilers, holography can help develop our understanding of key taxa, specifically the niches they occupy, which is important for our comprehension of ecological and biogeochemical dynamics in stratified shelf seas, and ultimately our predictions of how shelf sea ecosystems will respond to climate change.

Another advantage is the capture of data *in situ*, which provides a wealth of information not obtained by discrete sampling. *In situ* profiling guarantees full sampling of any SCM, including extremely thin maxima as seen in this study, whose limited vertical extent has often precluded sampling by conventional sampling techniques and strategies in the past. Sampling *in situ* with a non-intrusive instrument can also provide insight into conditions experienced by phytoplankton imaged through analysis of factors including cell orientation and chain length (Malkiel et al., 1999, Talapatra et al., 2013, Nayak et al., 2016). Cell orientation and chain length may have important implications for primary production, community structure and population dynamics, as high aspect ratios due to horizontal cell orientation and/or long chain length have been found to enhance light absorption (McFarland et al., 2016). Finally, *in situ* imaging removes methodological issues associated with collection and preservation of discrete water samples for later analysis, including sample degradation, cell shrinkage and subsampling discrepancies (Uehlinger, 1964, Rott, 1981, Leakey et al., 1994).

A further advantage of *in situ* holography is its capacity to record aggregates in an undisturbed state, thus providing a method for monitoring flux to the seabed. In this study, aggregate data has been presented that suggests the SCM to be a source of considerable carbon export (Fig. 4.4). This method of assessing aggregates could be developed through measurement of the aggregate from perpendicular directions to more accurately estimate its volume and, by extension, particulate organic carbon (POC) content using empirical POC to volume relationships, such as those proposed by Alldredge (1998). Moreover, it is possible to measure *in situ* settling velocity of aggregates using a free-drifting holocam. Therefore, holography could be a viable tool for obtaining quantitative carbon flux data.

Holography does have some limitations at present, but these can be overcome by developing the methodology. Each holographic profile generates an enormous amount of data that requires manual processing, which in this study involved individual reconstruction of each slice of every hologram examined, and manual identification and enumeration of phytoplankton within those hologram slices. Consequently, processing time is currently a limitation, but this issue can be addressed by automating the computational processing procedure, including compression of holograms into 2D composite images (Malkiel et al., 2004, Talapatra et al., 2013, Nayak et al., 2016), and automatic detection, identification and enumeration of phytoplankton using a training dataset of predefined phytoplankton interference patterns. Automation of phytoplankton identification theoretically ensures recognition of phytoplankton cells and prevents identification errors associated with particle overlapping and particle noise, since computers are able to forego preconceived patterns and effectively search for distinguishing characteristics in large amounts of noisy data, something the human eye is not trained to do (Graham and Nimmo Smith, 2010, Loomis, 2011).

A second limitation is pixel size, which prevented phytoplankton below that size (4.65 µm) from being observed, and made it impossible to unambiguously identify some phytoplankton above this threshold to a high, or in many cases, any taxonomic level. To alleviate these issues, pixel size could be reduced, although this would also increase capture of non-plankton particles and therefore only a small reduction in pixel size would be suitable, e.g. 1 µm (Talapatra et al., 2013). Simultaneous deployment of a CTD rosette system for collection of water samples for microscope and/or flow cytometry analysis can also help to overcome issues associated with pixel size. Microscopy and cytometry combined allow identification of phytoplankton of all sizes, and microscopy in particular can act as a sort of 'ground truthing' for the interpretation of phytoplankton holographic diffraction patterns.

In summary, implementation of these methodological developments can minimise processing time, reduce identification errors and improve identification of smaller cells. Therefore, these developments can allow the full potential of holographic technology for assessment of phytoplankton community structure on a large temporal and spatial scale to be reached.

Chapter 5: SCM primary production and the influence of resource availability and the phytoplankton community in the summer stratified waters of the Western English Channel

5.1. Abstract

The Western English Channel is a summer stratified temperate coastal sea where a subsurface chlorophyll maximum (SCM) is commonly observable within the seasonal thermocline. A combination of ^{13}C primary production incubation experiments and Fluorescence Induction and Relaxation (FIRe) measurements of relative electron transport rate (rETR) versus irradiance were used to estimate total water column and SCM layer primary production at 16 sites within the Western English Channel during the summer of 2015 (23rd June – 2nd July). CTD profiles and discrete samples were also collected during this period to allow investigation of variation in SCM layer primary production relative to environmental and biological variables. An SCM was consistently located at the base of the thermocline with a maximum chlorophyll concentration of 2.5 – 15.5 µg l^{-1}. Water column primary production ranged from 36.4 to 112.3 mg C m^{-2} hr^{-1}, 50 % of which, on average, occurred within the SCM layer, which was also an important site of new production (f-ratios of 0.37 – 0.68). Variation in water column primary production between sites was driven by SCM primary production, with half of the variation in SCM primary production accounted for by changes in SCM layer integrated chlorophyll concentration, where changes in SCM chlorophyll were thought to be largely governed by turbulence. Phytoplankton within the SCM were light limited, thus SCM layer primary production was particularly sensitive to changes in irradiance. Furthermore, primary production within the SCM was influenced by phytoplankton community structure. The SCM community was dominated by micro- and meso- phytoplankton (54.1 – 92.4 % of total chlorophyll), but increases in SCM primary production were associated with greater contributions of red fluorescing nano-phytoplankton due to their greater light utilisation efficiency compared to larger cells (> 20 µm). Greater percentages of red nano-phytoplankton generally corresponded to increased stratification during neap tides, which may have implications for our understanding of the relationship between stratification and primary production, and for predictions of how shelf seas could respond to increased stratification caused by climate change in the future.

5.2. Introduction

Primary production by marine phytoplankton forms the foundation of marine food webs and is central in nutrient, oxygen and carbon cycling (Falkowski and Raven, 1997). Variability in primary production is recognised to be governed by complex combinations and interactions of environmental and biological factors (Falkowski and Raven, 1997), most notably light intensity (Cote and Platt, 1984, Platt, 1986), nutrient availability (Platt et al., 1992, Kyewalyanga et al., 1998), temperature (Platt and Jassby, 1976, Harding et al., 1986), turbulence (Lewis et al., 1984), stratification (Gallegos et al., 1983, Holligan et al., 1984c), phytoplankton community composition (Cote and Platt, 1984, Tilstone et al., 1999, Tilstone et al., 2003) and phytoplankton physiological state (Platt and Sathyendranath, 1993, Platt et al., 1993). Therefore, quantification of primary production and understanding the combination of variables governing its magnitude is key for comprehending dynamics and functioning of the marine ecosystem, particularly biogeochemical cycling and trophic dynamics, and for effective environmental management and future climate projections. This is especially the case for the shelf seas, which, despite only accounting for approximately 9 % of the total area of the global ocean (Simpson and Sharples, 2012), are estimated to be responsible for 15 – 30 % of annual oceanic primary production, which in turn supports significant fisheries and particulate carbon export (Pauly et al., 2002, Muller-Karger et al., 2005, Jahnke, 2010).

Within the seasonally stratified waters of temperate and high latitude shelf seas a significant portion of water column photosynthetic biomass is typically found within the subsurface chlorophyll maximum (SCM) associated with the seasonal pycnocline (Holligan and Harbour, 1977, Pingree et al., 1978, Cullen, 1982, Holligan et al., 1984a, Weston et al., 2005, Martin et al., 2010, Hickman et al., 2012, Cullen, 2015). Chlorophyll at the SCM peak can be as much as half an order of magnitude, even up to two orders of magnitude greater than in surface waters (Steele, 1964, Holligan and Harbour, 1977, Holligan et al., 1984a, Sharples et al., 2001, Martin et al., 2010). SCM maximum chlorophyll concentrations observed in the temperate and high latitude shelf sea environment tend to range from values around < 1 – 2 μg l^{-1} in more open shelf waters to greater values, typically > 2 – 15 μg l^{-1} and up to > 50 μg l^{-1}, in more coastal waters/ waters closer to frontal boundaries (Holligan and Harbour, 1977, Holligan et al., 1984a, Holligan et al., 1984b, Richardson et al., 2000, Sharples et al., 2001, Weston et al., 2005, Hickman et al., 2009, Lips et al., 2010, Martin et al., 2010, Hickman et al., 2012, Fishwick, 2017). These high chlorophyll concentrations combined with sufficient light (as high as 10 % of surface irradiance (Holligan et al., 1984a, Simpson and Sharples, 2012)) would suggest that

SCM are hot-spots of primary production. Moreover, given the extended period of time that carbon fixation can occur within these subsurface features as stratification persists, suggests that SCM are major contributors of primary production within the shelf seas, and thus potentially have a key ecological and biogeochemical role within the local and global marine environment. However, quantifying this subsurface production is difficult because it is not detected by satellite remote sensing techniques (Gordon and Clark, 1980, Sathyendranath and Platt, 1993, Joint and Groom, 2000), and alternative techniques of measurement, including ship based measurements and continuous observational measurements by gliders and towed undulators (Weston et al., 2005, Fernand et al., 2013, Hemsley et al., 2015), are spatially and temporally limited. Therefore, the true extent of SCM primary production in the seasonally stratified shelf seas has not been well defined.

Recent large-scale studies on the NW European shelf have demonstrated the importance of the SCM for its contribution of primary production. During investigation of the seasonally stratifying waters of the North Sea, Richardson et al. (1998) showed the SCM accounted for up to 70 % of daily primary production, Weston et al. (2005) estimated the SCM to contribute 58 % of daily primary production and 37 % of annual new production, and Richardson et al. (2000) suggested that SCM new production may exceed that of the spring bloom. In the Celtic Sea, Hickman et al. (2012) estimated 40 – 50 % of daily primary production to be associated with the SCM, equating to approximately half of total annual primary production, and identified the SCM to be an important site of new production. However, a broader scale practical study investigating full water column and SCM primary production (not just at discrete depths) within the summer stratified coastal waters of the Western English Channel, where very high SCM chlorophyll concentrations have often been observed (Holligan and Harbour, 1977, Holligan et al., 1984c, Sharples et al., 2001, Fishwick, 2017), has not been conducted.

The Western English Channel is an area of the NW European continental shelf that becomes stratified in the summer months and is characterised by an SCM associated with the seasonal thermocline (Pingree, 1975, Holligan and Harbour, 1977, Holligan et al., 1984b, Fishwick, 2017). Routine measurements have been made at several locations in the Western English Channel, most notably stations L4 and E1 (Fig. 5.1), for many decades (Harris, 2010, Smyth et al., 2015). However, primary production has seldom been measured and measurements that exist tend to be spatially isolated and/or are not inclusive of the SCM (Holligan et al., 1984c, Garcia and Purdie, 1994, Woods, 2003, Barnes et al., 2014, Barnes et al., 2015b). Consequently, given the high SCM chlorophyll concentrations typical of this region, there is a

need for quantification of SCM primary production and assessment of factors controlling that production over a broader region of the summer stratified Western English Channel.

Here, water column primary production is investigated at a number of sites within the seasonally stratified waters of the Western English Channel during the summer of 2015, with the aim of assessing the importance of SCM primary production and the control of resource availability and the phytoplankton community on that production. Total water column and SCM primary production are estimated in order to determine the contribution of the SCM. f-ratios are presented to evaluate the significance of the SCM for new production within the water column. Furthermore, the influence of chlorophyll concentration, nutrient availability, irradiance levels, phytoplankton photophysiological state and phytoplankton community structure on the magnitude of SCM primary production is investigated.

5.3. Methods

5.3.1. Sampling

The study was conducted in the summer stratified waters of the Western English Channel, offshore Falmouth, UK (Fig. 5.1) between the 23rd June and 2nd July 2015. These stratified waters had characteristic high sea surface temperatures of 13.5 - 18 ^{o}C (data not shown). A SeaBird SBE19plus V2 conductivity, temperature, depth (CTD) probe mounted with a Wet Labs ECO FLNTU fluorometer (sensitivity: 0.025 µg chl/l; fluorescence excitation/emission wavelengths: 470/695 nm) and LI-COR Biospherical PAR sensor was used to collect vertical water column profiles of temperature, salinity, chlorophyll-fluorescence and irradiance at 16 stratified sites that were analysed for primary production (Fig. 5.1). The CTD system was typically deployed at a descent/ascent rate of 0.01 - 0.1 m s^{-1} (rate slowed on approach to SCM), with a data acquisition rate of 2 Hz, which provided vertical resolution of 0.5 – 5 cm.

Water samples were collected at each of the 16 sites using a SBE32 sampling carousel fitted with the CTD (+ additional sensors) and 6 x 5 L Niskin bottles. An SCM water sample was collected (at maximum chlorophyll; see 5.3.2 below) at all 16 sites, and was routinely analysed for chlorophyll concentration, nitrate concentration, the Fluorescence Induction and Relaxation (FIRe) parameter of Fv/Fm, which is a measure of photosynthetic efficiency (Kolber et al., 1988), FIRe measured rETR (relative electron transport rate) vs. irradiance parameters, and for phytoplankton community structure using flow cytometry. Surface water samples were only collected at 7 sites (sites 1, 4, 7, 8, 12, 15 and 16), and were analysed for chlorophyll and

nitrate concentration, and rETR vs. irradiance parameters. At these 7 sites SCM and surface samples were also used in ^{13}C and ^{15}N incubation experiments. Bottom water (hereafter, used interchangeably with the term deep water) samples were also collected at the sites where incubations were conducted, but were only analysed for nitrate and chlorophyll concentration.

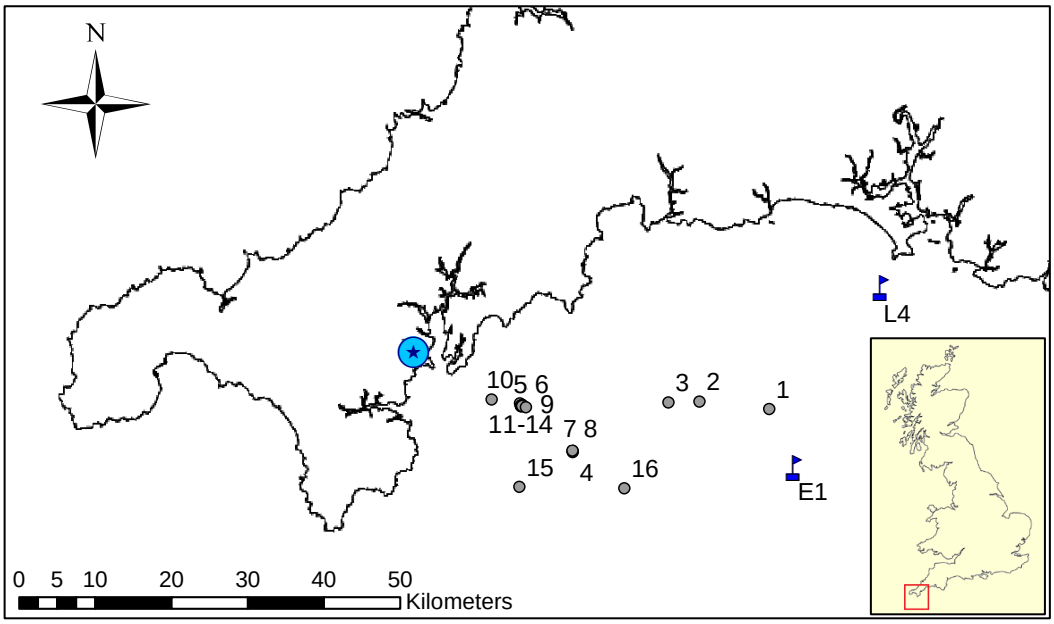

Figure 5.1. Study area in the Western English Channel where sampling occurred between 23rd June and 2nd July 2015. The blue encircled star indicates the location of Falmouth and the observation stations L4 and E1 are marked with blue flags. Circular symbols indicate sampling sites, which are all labelled with their site number (allocated in chronological order; Table A3.1).

5.3.2. Determination of chlorophyll concentration

Samples for chlorophyll analysis were collected by passing 50 ml of water sample through a 25 mm Whatman GF/F filter, which was stored in a -20 °C freezer prior to analysis. Analysis was conducted as soon as possible on return to the lab to avoid error associated with pigment degradation at -20 °C (Graff and Rynearson, 2011). Chlorophyll was extracted in 90 % acetone via sonication and then chlorophyll concentration was fluorometrically determined using a Turner Designs 10AU fluorometer based on the method of Welschmeyer (1994), whereby the fluorometer excited the extracted sample with blue light (436 nm) and the subsequent red fluorescence emission (680 nm) was recorded. Chlorophyll values were used to calibrate the CTD fluorometer. Determining chlorophyll concentrations also allowed identification of where water samples were collected within the SCM, confirming all samples were collected from/very near to the depth of maximum chlorophyll, i.e. relative sampling depth within SCM was consistent (Table A3.1). Thus, confidence could be had that any differences observed in SCM samples of different sampling casts was not a function of the relative depth of sampling within the SCM.

5.3.3. Determination of nitrate concentration

Samples for nitrate analysis were collected by passing water sample through a 25 mm Whatman GF/F filter into a 15 ml polypropylene tube and freezing at -20 °C until analysis following methods of Kremling and Brügmann (1999) and Dore et al. (1996). Nitrate concentrations were determined colorimetrically following standard techniques as described by Grasshoff (1976) and Kirkwood (1996) using a SEAL Analytical QuAAtro segmented flow AutoAnalyser. The nitrate detection limit was 0.03 µmol l^{-1} (NIOZ, 2016, Stinchcombe, 2017).

5.3.4. Flow cytometric analysis of the phytoplankton community

Samples for phytoplankton analysis by flow cytometry were collected by decanting 10 ml of water sample into a polypropylene tube and immediately fixing with glutaraldehyde (0.25 % final concentration) and storing at -80 °C (Marie et al., 2005). Analysis was conducted using a CytoBuoy CytoSense flow cytometer with CytoUSB v5.7.5.7 data acquisition software. Each sample was analysed using two different sets of data acquisition settings, one optimal for larger phytoplankton (meso- and micro phytoplankton: > 20 µm; and nano-phytoplankton: 2 – 20 µm) and the other optimal for small phytoplankton (pico-phytoplankton: < 2 µm). Meso-, micro- and nano-phytoplankton data was acquired using a red fluorescence (RFL) trigger (30 mV) at a flow rate of 10 µl s^{-1} for 150 seconds or 10000 cells. Pico-phytoplankton data was acquired using a sideways scatter (SWS) trigger (25 mV) at a flow rate of 0.1 µl s^{-1} for 10000 cells, and pico-particles with a RFL signal < 10 mV were manually removed from the dataset to ensure exclusion of non-phytoplankton pico-particles/debris/electronic noise. Cell size derived from forwards scatter (FWS) was calibrated using a set of Thermo Fisher Scientific nonfluorescent polystyrene microspheres with a range of diameters (1, 2, 6, 10, 15 µm).

During data acquisition the CytoSense instrument recorded particle pulse shapes of FWS, SWS, RFL and orange fluorescence (OFL). The phytoplankton community could thus be described based on scatter and fluorescence properties by constructing two-dimensional cytograms of these various particle parameters using CytoClus v4.3.1.1 data processing software. For each sample a cytogram of total OFL vs. total RFL (TRFL) was generated to identify cells containing phycoerythrin secondary photopigments (Jeffrey and Vesk, 1997), and a cytogram of total FWS and TRFL was generated to identify cell size. This allowed clusters of orange fluorescing pico-phytoplankton (hereafter orange pico-phytoplankton), red fluorescing pico-phytoplankton (hereafter red pico-phytoplankton), orange fluorescing nano-phytoplankton (hereafter orange nano-phytoplankton), red fluorescing nano-phytoplankton (hereafter red nano-

phytoplankton), and micro- and meso- phytoplankton to be resolved. As TRFL was calculated for each cell, the TRFL of the entire phytoplankton population and of each phytoplankton cluster could be determined, and was used as a proxy for chlorophyll concentration, which in turn is a proxy for biomass. Further analysis was conducted on TRFL data as opposed to abundance data because biomass (TRFL as a proxy) provides a more accurate representation of community structure when the community consists of phytoplankton spanning a great size range, and because biomass is more biogeochemically relevant (Paasche, 1960).

5.3.5. FIRe measurements

Fv/Fm

Fv/Fm values were determined using a Satlantic bench top FIRe instrument. 5 ml of water sample (which was first dark adapted by storing in the dark for at least 25 minutes) was decanted into a cuvette and placed in the FIRe instrument for analysis. The FIRe protocol is given in Bibby et al. (2008); 30 unique iterations from the same sample were averaged, the sample delay was set at 1000 msec and the gain set at between 50 – 70 % of the sensor's saturation. Raw FIRe data was processed to generate the parameters of Fm (maximal fluorescence yield) and Fo (minimal fluorescence yield) based on the biophysical model of Kolber et al. (1988) using MATLAB R2013a. The parameter of Fv/Fm could then be calculated using equation 5.1, which includes blank correction, where the blank was deduced twice daily (beginning and end) by running a water sample in the FIRe instrument that had been filtered through a Whatman GF/F filter:

$$\frac{Fv}{Fm} = \frac{(Fm_{sample} - Fm_{blank}) - (Fo_{sample} - Fo_{blank})}{(Fm_{sample} - Fm_{blank})} \quad (5.1)$$

rETR vs. irradiance parameters

Using the actinic light source and PAR stepping mode on the Satlantic bench top FIRe instrument, rETR as a function of irradiance (E) could be determined. The PAR stepping protocol was set up with 20 PAR increments between 0 – 1000 µmol m^{-2} s^{-1} and a 'PAR on' interval of 90 seconds between data acquisition events, where one data acquisition event comprised of 30 unique iterations. Raw FIRe data was processed to generate the parameters of Fm' (maximum fluorescence yield under actinic light) and F' (steady state fluorescence yield under actinic light) based on the biophysical model of Kolber et al. (1988) using MATLAB R2013a. The parameter of Fq'/Fm' (quantum yield of electron transport through PSII) and ultimately rETR could then be calculated using equations 5.2 and 5.3:

$$Fq'/Fm'(dimensionless) = (Fm' - F')/Fm' \quad (5.2)$$

$$rETR\ (a.u.) = E \times (Fq'/Fm') \quad (5.3)$$

rETR vs. irradiance curves were generated by fitting the E-dependent rETR data to the Jassby and Platt (1976) model using the open source statistical program R v.3.2.3 and the 'phytotools' package (Silsbe and Malkin, 2015). This model was used to derive the parameters of $rETR_{max}$ (maximum relative rate of electron transport), α_{ETE} (electron transport efficiency; given by the initial slope of the light response curve) and Ek (light saturation parameter; µmol m^{-2} s^{-1}).

5.3.6. ^{13}C uptake rates

Standard short (4 hr) ^{13}C uptake incubation experiments were conducted to measure rates of primary production (Hama et al., 1983). Samples collected from two depths (one from surface waters ~10 m and one from the SCM peak) were spiked with $NaH^{13}CO_3$ (0.1 mmol l^{-1} final concentration) and incubated in 1 L polycarbonate bottles at simulated *in situ* water temperature. SCM samples were incubated in a light environment typical at the SCM, specifically at an irradiance level of 15 µmol m^{-2} s^{-1}, based on investigation of irradiance at the SCM from a previous field survey, and in spectral light achieved using spectrally corrected blue (marine blue) light filter by LEE-Filters, UK, following methods of Poulton (2004). Surface samples were incubated in a light environment relatively similar to that experienced at ~10 m, specifically in spectral light that mimicked that *in situ* using spectrally corrected blue (mist blue) light filter by LEE-Filters, UK, following recommendations of Poulton (2004), but at an irradiance level (33 µmol m^{-2} s^{-1}) lower (by at least half) than typical of 10 m depth, as higher irradiance levels could not be achieved without removal of the light filter. Incubations were terminated by filtration through pre-combusted (450 °C, 6 hrs) 25 mm Whatman GF/F filters under low vacuum (< 150 mg Hg) in darkness. Filters were rinsed with pre-filtered seawater from the respective sampling site to remove excess tracer and then stored in petri slides at -20 °C until analysis. Prior to analysis, filters were dried at 40 °C for 24 hours, halved, then packed and pelleted in tin capsules. Analysis was conducted by Iso-Analytical (Crewe, UK) using elemental analysis isotope ratio mass spectrometry (EA-IRMS), the principles of which are described by Fiedler and Proksch (1975). Rates of ^{13}C uptake were determined by applying equations described by Dugdale and Wilkerson (1986) and converted to typical primary production units of mg C m^{-3} hr^{-1}. It is acknowledged that rates determined were somewhere between net and gross primary production, but are assumed representative of net primary production (Dugdale and Wilkerson, 1986, Legendre and Gosselin, 1996, Marra, 2002).

5.3.7. Matching rETRs with ^{13}C fixation

Measurements of rETR vs. irradiance and ^{13}C fixation were made simultaneously on the same sample to allow rETRs to be related to carbon fixation values in order for the parameters of P_{max} (maximum photosynthetic rate) and α_{LHE} (light harvesting efficiency) to be derived from $rETR_{max}$ and α_{ETE} using methods similar to that described by Migné et al. (2007). The relationship between carbon fixation and rETR determined at the same light intensity was modelled and analysed for SCM samples and for surface samples. The relationship was modelled separately for the SCM and surface waters to account for factors of variation between the surface and SCM that could impact any relationship between rETR and carbon fixation, such as phytoplankton community structure, temperature and nutrient availability (Lawrenz et al., 2013). A significant linear correlation was obtained between rETR and carbon fixation for SCM ($R^2 = 0.764$; $p = 0.01$) and surface samples ($R^2 = 0.500$; $p = 0.05$). P_{max} values could then be calculated using the linear equations (Eq. 5.4 and 5.5) derived from regression analysis. Subsequently, values of α_{LHE} could be derived using P_{max}/Ek.

$$SCM: P_{max}(\text{mg C m}^{-3}\ \text{hr}^{-1}) = (0.759 \times rETR_{max}) - 0.148 \quad (5.4)$$

$$Surface: P_{max}(\text{mg C m}^{-3}\ \text{hr}^{-1}) = (0.116 \times rETR_{max}) - 0.337 \quad (5.5)$$

These conversion equations were applied to all SCM and surface rETR vs. irradiance data collected at the 16 sampling sites over the duration of the study. At sites 2, 3, 5, 6, 9, 11, 13 and 14, surface rETR vs. irradiance curve data was not collected, so surface (at 10 m) values of P_{max} and α_{LHE} were assumed to be 4.63 and 0.026 for these sampling sites. This assumption was made as surface values of P_{max} and α_{LHE} were very similar at all sites where rETR vs. irradiance curve data was collected (P_{max} mean of 4.63 and range of 4.02 – 5.05; α_{LHE} mean of 0.026 range of 0.023 – 0.030). SCM and surface photophysiological data was therefore available to apply in estimations of water column primary production at all 16 sampling sites.

To test these relationships for use in estimating primary production, measurements of carbon fixation obtained via ^{13}C incubations were compared to those obtained using FIRe measured rETR vs. irradiance data and conversion equations 5.4 and 5.5 (Fig. 5.2). Agreement between values was good for the SCM, with a mean discrepancy of only 11 %. Agreement between values for surface samples was reasonably good, with the FIRe method overestimating rates of carbon fixation by, on average, 0.3 mg C m^{-3} hr^{-1}.

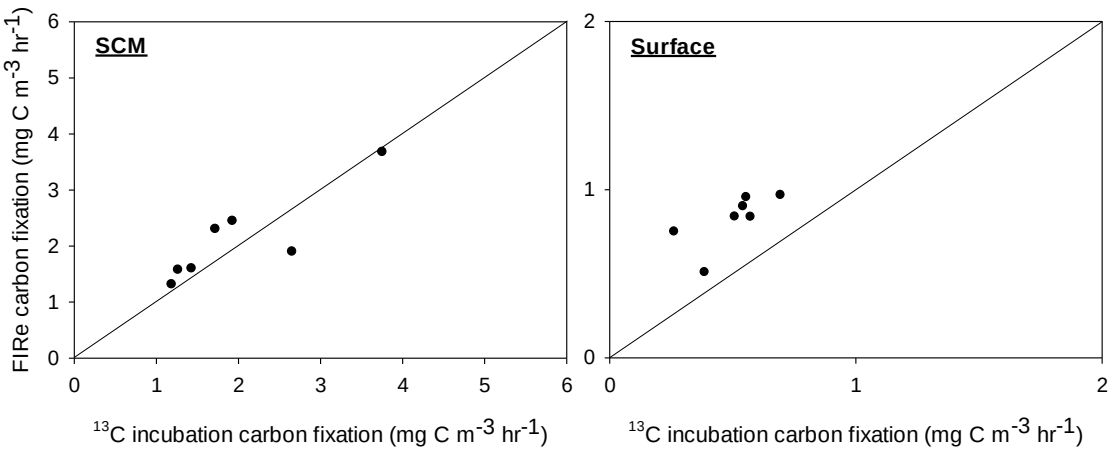

Figure 5.2. Comparison between ^{13}C incubation carbon fixation rates and rates of carbon fixation based on FIRe measured rETR vs. irradiance data. y = x line displayed on both plots.

5.3.8. Integrated primary production

Photophysiological parameters of P_{max} and α_{LHE} were normalised to chlorophyll (P^*_{max} and α_{LHE}*) and profiles of these parameters were determined by linear interpolation through the water column (Hickman et al., 2012). The linear interpolation technique used was based on that of Hickman et al. (2012), except that values were linearly interpolated between sample depths. Values obtained from measurements on the surface discrete sample were assumed representative between 0 m and the depth of the surface sample, and values obtained from measurements on the SCM discrete sample were assumed representative from the depth of the SCM sample to the base of the SCM/thermocline. Along with values of chlorophyll concentration provided by the calibrated CTD fluorometer profile (Chl_{CTD}; mg m^{-3}) and irradiance from the CTD PAR sensor profile (E; µmol m^{-2} s^{-1}), P^*_{max} (mg C mg chl^{-1} hr^{-1}) and α_{LHE}^* (mg C mg chl^{-1} hr^{-1} (µmol m^{-2} s^{-1})$^{-1}$) were used to estimate water column primary production (PP) at 0.25 m depth resolution (z) following equation 5.6 (Hickman et al., 2012):

$$PP(z) = Chl_{CTD}\,(z) \times P^*_{max}(z) \times tanh\left(\frac{E(z)\times\alpha_{LHE}^*(z)}{P^*_{max}(z)}\right) \quad (5.6)$$

When data from the CTD and mounted fluorometer and PAR sensors was not recorded in the top few meters of the water column, chlorophyll concentration was assumed constant between the last value recorded and 0 m, and irradiance was estimated using the light attenuation coefficient (Kd). Knowing the Kd for each sampling site allowed light profiles to be constructed for any sea surface irradiance value, and therefore water column primary production could be modelled for any chosen surface irradiance. As such, primary production

profiles at the 16 sample sites were estimated for the recorded sea surface irradiance at the time of sampling, as well as for the highest (2970 µmol m^{-2} s^{-1}; recorded at site 7 sampled at 14:35 on the 24th June) and lowest (469 µmol m^{-2} s^{-1}; recorded at site 16 sampled at 10:26 on the 2nd July) sea surface irradiances recorded during the study. The potential for significant error in estimates of water column integrated primary production is acknowledged as discussed in section 2.3.7.2, but this error could not be specifically quantified.

5.3.9. ^{15}N uptake and determination of the f-ratio

^{15}N uptake incubation experiments were conducted alongside ^{13}C incubations (Dugdale and Goering, 1967, Slawyk et al., 1977), whereby SCM and surface samples spiked with $NaH^{13}CO_3$ were also spiked with $K^{15}NO_3$ (0.1 µmol l^{-1} final concentration), and a separate sample per depth (one for SCM and one for surface) was spiked with $Cl^{15}NH_4$ (0.1 µmol l^{-1} final concentration). These ^{15}N uptake incubations followed the same experiment protocol as described for ^{13}C uptake incubations, and shared the same sample processing and analysis, and data analysis procedures.

Ambient ammonium concentration, as measured according to the methods of Holmes et al. (1999), was consistently below the instrument detection limit (0.1 µmol l^{-1}) and was therefore assumed to be 0.1 µmol l^{-1} for all samples, guided by ammonium concentrations measured in the stratified waters (at 0, 10 and 20 m) of the Western English Channel from 2007-2014 (Woodward, 2015). It is thus acknowledged that rates of $^{15}NH_4$ uptake and consequently f-ratios may have been underestimated or overestimated as discussed in section 2.3.7.1.

To determine the contribution of new (supported by external sources of N) and regenerated (supported by recycling of N) production to total primary production, the f-ratio was determined using equation 5.7 (Dugdale and Goering, 1967):

$$f\ ratio = \frac{Nitrate\ uptake}{(Nitrate\ uptake + Ammonium\ uptake)} \quad (5.7)$$

5.3.10. Statistical analysis

All relationships presented were investigated by performing linear regression analysis using SigmaPlot 13.0 software. Regressions were model-II, to allow errors on y- and x-axis variables.

5.4. Results

5.4.1. Water column structure and resource distribution

A total of 16 profiles were collected across an approximate area of 1250 km^2 and over a range of tidal conditions from 23rd June to 2nd July 2015 that were assessed for primary production (Fig. 5.1 and 5.3, Table 5.1; details in Table A3.1). Water depth was similar between sample sites, only ranging from 63.1 – 72.5 m, and all profiles exhibited an SCM at a similar depth, between 24.6 – 30.7 m (Fig. 5.3 and Table 5.1). Due to the limited water depth range no relationship was evident between SCM depth and water depth. SCM depth was consistently related to temperature structure, with all maxima being closely associated with the bottom of the thermocline (also the pycnocline as density variability was dominated by temperature; data not shown). The thermocline was typically quite broad, generally with a more gradual change in temperature of 2.0 – 5.0 °C between surface and bottom waters, so that a distinct boundary between the thermocline and the upper mixed layer was generally less than 10 m or could not be identified unambiguously. The difference in temperature between the surface and bottom waters indicated stratification was generally stronger during neap tides (sites 8 – 15), when the difference in temperature was typically > 3 °C compared to a difference commonly < 3 °C during spring tides (sites 1-7, 16) (Fig. 5.3 and Table 5.1; further details in Table A3.1).

SCM were consistently quite limited in their vertical extent, only ranging in thickness (at half maximum intensity of the chlorophyll signal) from less than 1 m to almost 8 m. The span of the SCM layer (the portion of the water column where chlorophyll concentration changed by > 0.3 µg l^{-1} per metre) was far greater (by > 35 %), ranging from 5.8 – 19.8 m, with greater values associated with greater SCM thickness values. The span of the surface layer was generally much broader than that of the SCM layer, such that the SCM layer was typically responsible for less than 40 % of the span of the entire primary productive region of the water column (surface layer + SCM layer only as primary production in bottom waters/below the SCM was assumed to be zero) (Fig. 5.3 and Table 5.1; details in Table A3.1). SCM maximum chlorophyll concentration ranged from 2.5 to 15.5 µg l^{-1}, and higher values typically coincided with higher integrated values of chlorophyll for the SCM layer, which ranged from 10.5 to 95.1 mg m^{-2}. Integrated chlorophyll concentrations in the surface layer were consistently lower than in the SCM layer, specifically between 1.5 and 13.1 mg m^{-2}. Consequently, in spite of generally accounting for a minority of the water column in terms of its span, the SCM layer consistently accounted for a majority (> 60 %) of the chlorophyll within the primary productive portion of the water column (Fig. 5.3 and Table 5.1; further details in Table A3.1).

Irradiance at the sea surface recorded at the time of sampling ranged from 469 – 2970 µmol m^{-2} s^{-1} (Table A3.1 for details) and at the depth of the SCM peak ranged between 12 – 104 µmol m^{-2} s^{-1}, equating to 0.9 – 4.8 % of that at the surface, dependent upon light attenuation (Kd: 0.12 – 0.20 m^{-1}) and SCM depth (24.6 – 30.7 m). Nitrate concentrations at the SCM peak were consistently low, varying only between 0.1 – 0.8 µmol l^{-1}. From the surface layer to bottom waters, concentrations increased from 0.1 – 0.4 µmol l^{-1} to 0.8 – 1.1 µmol l^{-1}. Due to the limited number of data points within the nitrate profiles the exact depth of the nitracline could not be determined. However, nitrate concentrations were very similar/only slightly higher at the SCM peak compared to the surface layer, suggesting that the SCM was located above or at the upper region of the nitracline (Fig. 5.3 and Table 5.1; details provided in Table A3.1).

Table 5.1. Water depth, SCM depth, SCM thickness (at half maximum intensity of the chlorophyll signal), SCM max chlorophyll concentration, percentage of primary productive water column spanned by SCM layer, SCM layer integrated chlorophyll (absolute and as a percentage of the total chlorophyll of the primary productive portion of the water column), difference in temperature between surface (5.5 m) and bottom waters (55 m), irradiance at the SCM peak as a percentage of sea surface irradiance, and SCM discrete nitrate concentration of the 16 stratified sites profiled and assessed for primary production during the survey. The primary productive portion of the water column refers to the surface layer and SCM layer combined, excluding bottom waters where primary production was assumed to be zero.

Site no.	Water depth (m)	SCM depth (m)	SCM thickness (m)	SCM max chl conc. (µg l^{-1})	SCM layer span as % of PP water column	SCM layer integrated chl		Δsurface -bottom temp. (°C)	Irradiance at SCM peak (%)	SCM nitrate conc. (µmol l^{-1})
						mg m^{-2}	% of PP chl			
1	69	26.2	3.7	3.0	28.1	15.7	66.7	2.1	3.9	0.5
2	68	29.8	2.9	10.1	25.0	32.5	84.4	2.5	2.4	0.2
3	67	26.1	3.2	15.5	37.2	60.2	91.1	2.7	2.8	0.4
4	73	28.3	2.8	2.5	24.4	10.5	61.7	3.6	1.6	0.3
5	66	24.8	7.4	12.8	66.2	95.1	98.4	2.0	0.8	0.2
6	66	30.7	7.5	8.7	41.6	72.6	88.5	2.4	0.9	0.1
7	71	27.8	1.2	7.3	19.8	13.9	67.9	3.8	2.3	0.3
8	73	29.6	6.5	3.5	30.0	20.2	79.5	4.1	2.4	0.4
9	66	26.8	2.4	9.2	51.6	41.3	92.3	2.9	2.4	0.2
10	63	24.6	1.1	6.7	28.5	19.3	67.5	3.3	4.8	0.1
11	66	27.7	4.2	4.2	33.9	19.8	74.3	3.4	2.1	0.1
12	66	28.1	2.0	10.2	26.9	27.2	81.7	3.5	2.2	0.5
13	66	27.6	0.1	12.3	31.0	21.5	74.5	3.5	1.4	0.1
14	66	25.7	3.6	5.4	25.9	21.3	62.0	3.2	3.9	0.8
15	72	27.4	4.4	6.2	36.4	35.3	79.8	4.4	3.9	0.2
16	72	27.2	7.6	3.8	38.9	29.2	73.1	5.0	2.5	0.5

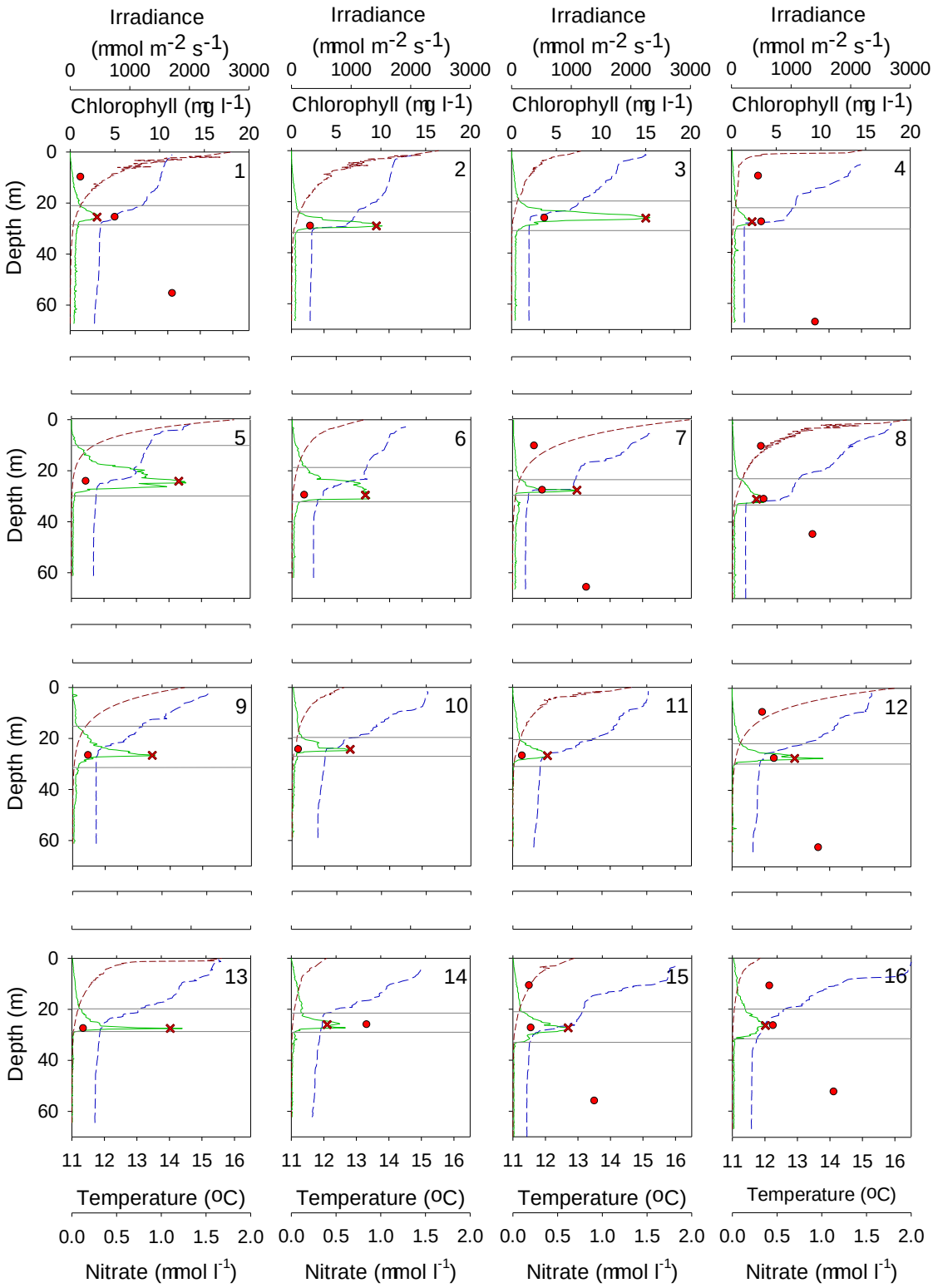

Figure 5.3. Temperature, chlorophyll and irradiance profiles, with discrete nitrate values, for the 16 sites (site numbers in the top right hand corner of each plot) assessed for primary production (details in Table A3.1). The green line represents chlorophyll concentration derived from CTD chlorophyll-fluorescence, the blue long-dashed line represents temperature, the brown short-dashed line represents irradiance, red circles represent nitrate concentration, red Xs where Niskin bottle samples were collected within the SCM (showing all samples were collected from/very near to the depth of maximum chlorophyll; Table A3.1), and the grey horizontal lines indicate upper and lower boundaries of the SCM layer.

5.4.2. Water column primary production

In general, the primary production profile at each site roughly resembled the corresponding chlorophyll profile, with a primary production maximum typically associated with the SCM. Although, despite consistently low chlorophyll above the SCM, levels of primary production were often considerable, with values almost rivalling those at the SCM at some sites (Fig. 5.4).

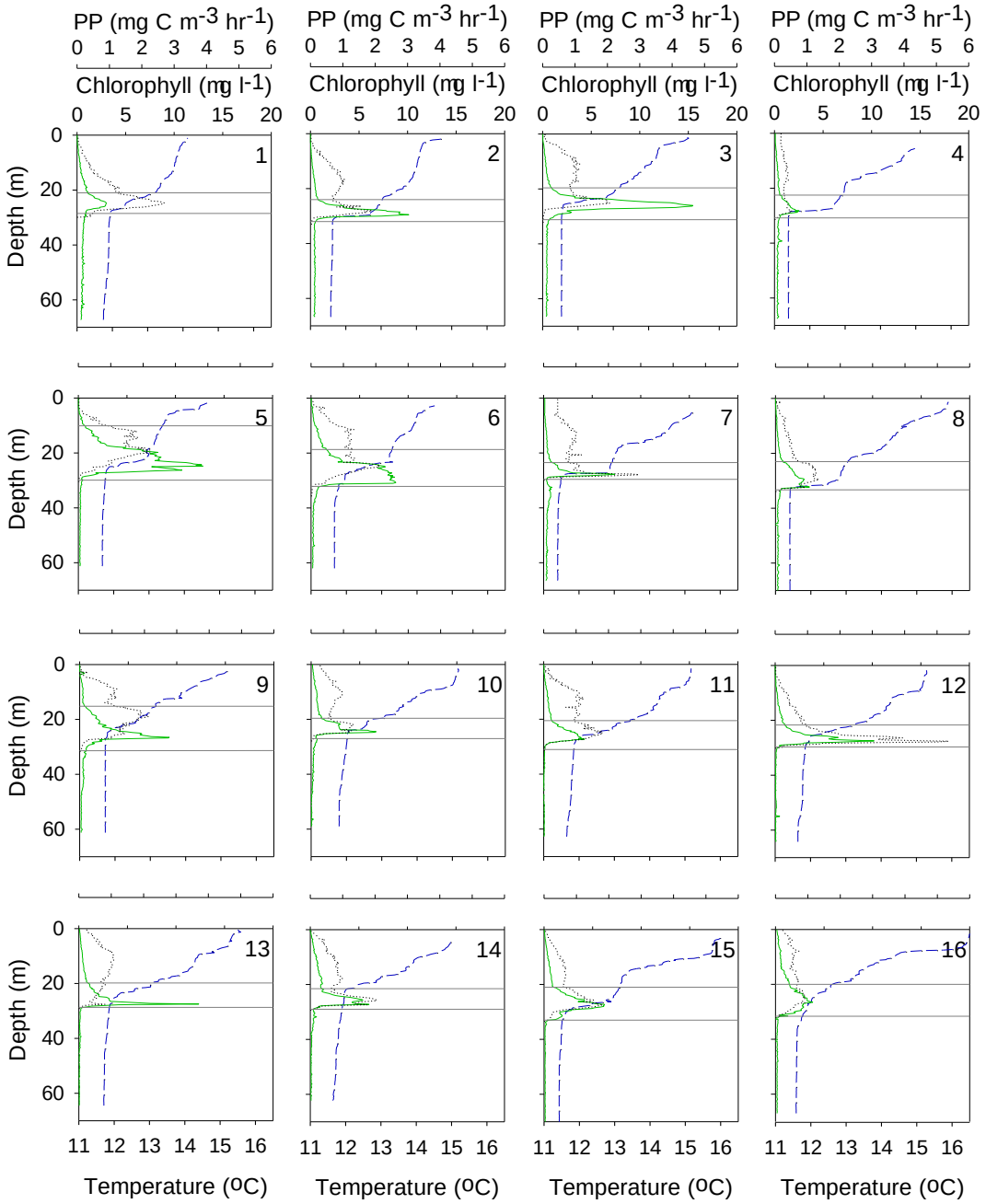

Figure 5.4. Primary production (PP) estimated for the irradiance recorded at the time of sampling, temperature and chlorophyll profiles of the 16 sites (site numbers in the top right hand corner of each plot) assessed for primary production (details in Table A3.1). The dotted black line represents primary production, the green line represents chlorophyll concentration determined from CTD chlorophyll-fluorescence and the blue dashed line represents temperature. The grey horizontal lines indicate the upper and lower boundaries of the SCM layer.

Values of total water column primary production estimated for the irradiance conditions recorded at the time of sampling ranged from 36.4 to 112.3 mg C m^{-2} hr^{-1} (Fig. 5.4 and Table 5.2). The SCM layer was estimated to contribute primary production of 11.0 to 99.0 mg C m^{-2} hr^{-1} and 23.5 to 91.3 % of total water column primary production, which according to available f-ratio data could have constituted significant new production (f-ratio mean 0.49 and range 0.37 – 0.68). Surface layer primary production was estimated at 9.4 to 64.8 mg C m^{-2} hr^{-1}, equating to 8.7 to 76.5 % of total water column production, which f-ratio data suggests was mostly regenerated (f-ratio mean 0.29 and range 0.20 – 0.39) (Fig. 5.4 and Table 5.2).

Table 5.2. Integrated primary production values for the total water column, SCM layer and surface layer at all 16 sampling sites. SCM layer integrated primary production values are also given as a percentage of total water column primary production. f-ratios obtained by conducting ^{15}N uptake incubations using discrete water samples collected from the SCM and surface (~ 10 m) shown on right hand side of table.

Site no.	Integrated primary production (mg C m^{-2} hr^{-1})			SCM layer primary production (%)	f-ratio	
	Total water column	SCM layer	Surface layer		SCM	Surface
1	92.6	53.3	39.3	57.6	0.49	0.29
2	80.8	29.0	51.9	35.9		
3	94.6	38.4	56.1	40.6		
4	36.4	11.0	25.4	30.2	0.40	0.33
5	108.3	99.0	9.4	91.3		
6	112.3	58.9	53.4	52.5		
7	92.6	27.8	64.8	30.1	0.37	0.20
8	70.5	41.1	29.4	58.2	0.42	0.26
9	110.3	72.3	38.0	65.6		
10	72.6	23.8	48.8	32.8		
11	99.3	41.7	57.6	42.0		
12	98.8	67.1	31.7	67.9	0.65	0.39
13	79.3	18.6	60.6	23.5		
14	85.2	33.0	52.2	38.8		
15	77.8	43.1	34.7	55.4	0.42	0.23
16	69.9	31.4	38.5	44.9	0.68	0.35

A general trend was evident where total water column primary production increased with SCM layer primary production (Table 5.2.). Regression analysis identified that 57 % ($R^2 = 0.569$, $p < 0.001$) of the total variation in water column primary production could be explained by the variation in SCM layer primary production (Fig. 5.5a). In contrast, no significant correlation was found between total water column and surface layer primary production (Fig. 5.5b). This result suggests that variation in total water column production was driven by changes in SCM layer primary production and not by the surface layer.

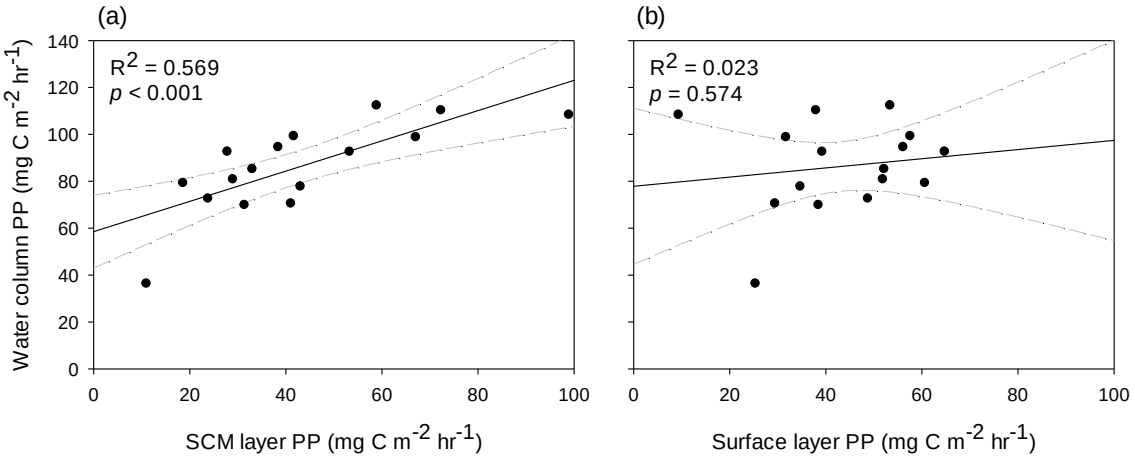

Figure 5.5. Relationship between vertically integrated water column primary production (PP) and (a) vertically integrated SCM layer PP, (b) vertically integrated surface layer PP. All values were estimated for the irradiance recorded at the time of sampling. Regression lines with 95% confidence intervals shown, and p and R^2 values given indicating significance and goodness of fit respectively.

As generally perceptible in the vertical profiles of primary production and chlorophyll (Fig. 5.4), SCM layer primary production was positively correlated with SCM layer integrated chlorophyll (R^2 = 0.513, p = 0.002; Fig.5.6). The greatest SCM layer primary production was estimated at site 5 (99.0 mg C m^{-2} hr^{-1}) where SCM layer chlorophyll was 95.1 mg m^{-2}, and the lowest SCM layer primary production was estimated at site 4 (11.0 mg C m^{-2} hr^{-1}) with SCM layer chlorophyll of 10.5 mg m^{-2} (Fig. 5.4; Tables 5.1 and 5.2). However, variation in SCM layer chlorophyll only accounted for half of the variation in SCM layer primary production, indicating additional key factors influenced SCM primary production. Factors that could have significantly affected SCM primary production in the stratified waters of the Western English Channel include resource (nitrate and light) availability, and phytoplankton community photophysiology and structure.

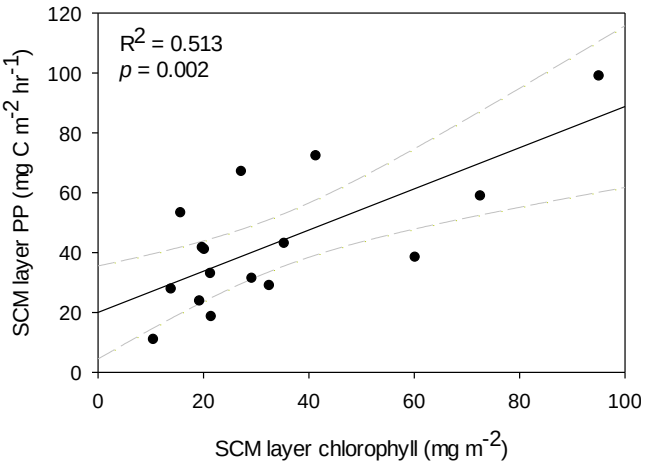

Figure 5.6. Relationship between vertically integrated SCM layer primary production (PP) and vertically integrated SCM layer chlorophyll. PP values were estimated for the irradiance at the time of sampling. Regression line with 95% confidence intervals shown, and p and R^2 values given.

5.4.3. SCM primary production and resources

As a measure of photosynthetic efficiency, Fv/Fm can be used as an indicator of nutrient stress when irradiance is low enough so that non-photochemical quenching is not a factor of influence on photosynthetic efficiency (Kolber et al., 1988, Genty et al., 1989, Falkowski and Raven, 1997). However, SCM Fv/Fm values remained relatively constant across all 16 sampling sites, only ranging from 0.41 to 0.46 (Table 5.3), indicating a consistent photosynthetic efficiency of the SCM phytoplankton community as a whole across sampling sites.

Table 5.3. Fv/Fm values obtained from FIRe measurements on discrete SCM samples.

Site no.	1	2	3	4	5	6	7	8	9	10	11	12	13	14	15	16
Fv/Fm	0.44	0.44	0.45	0.46	0.42	0.45	0.41	0.43	0.44	0.42	0.44	0.46	0.43	0.41	0.45	0.45

On the other hand, SCM layer primary production was positively correlated with irradiance at the SCM peak at the time of sampling ($R^2 = 0.626$, $p < 0.001$; Fig. 5.7). When standardising primary production for sea surface irradiance and modelling for low and high sea surface light conditions, the extent of the effect of changing irradiance could be appreciated. Under low surface light (469 µmol m^{-2} s^{-1}) the SCM layer accounted for 4.7 – 31.6 mg C m^{-2} hr^{-1} and 13.7 – 80.0 % of total water column primary production. Whereas, under high surface light (2970 µmol m^{-2} s^{-1}) the SCM layer was responsible for 27.8 – 138.7 mg C m^{-2} hr^{-1} and 30.1 – 91.3 % of total water column primary production (Fig. 5.8). A change from low to high light conditions thus accounted for a rise in primary production of up to 107.07 mg C m^{-2} hr^{-1}, and an increase in contribution to total water column primary production of, on average, approximately 20 % (Fig. 5.8.). At a third of sites the range in SCM layer primary production from low to high light was similar to (at sites 5, 6 and 9) or greater than (sites 14 and 16) the range in SCM layer primary production estimated for irradiance recorded at the time of sampling between sites.

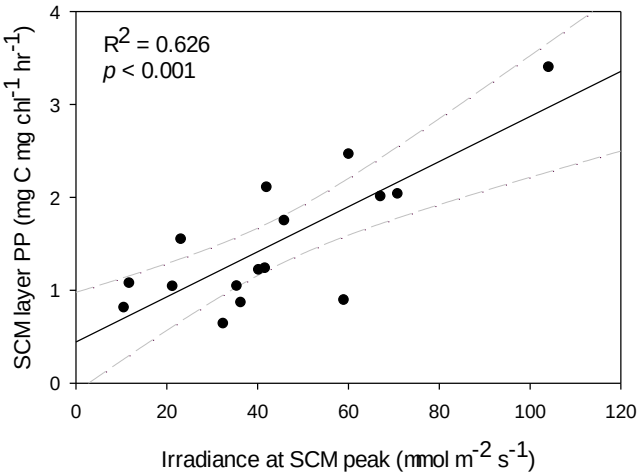

Figure 5.7. Relationship between vertically integrated SCM layer primary production (PP) and irradiance at the SCM peak. All PP values were estimated for the irradiance recorded at the time of sampling and normalised to chlorophyll concentration. Regression line with 95% confidence intervals shown, and *p* and R^2 values given indicating significance and goodness of fit respectively.

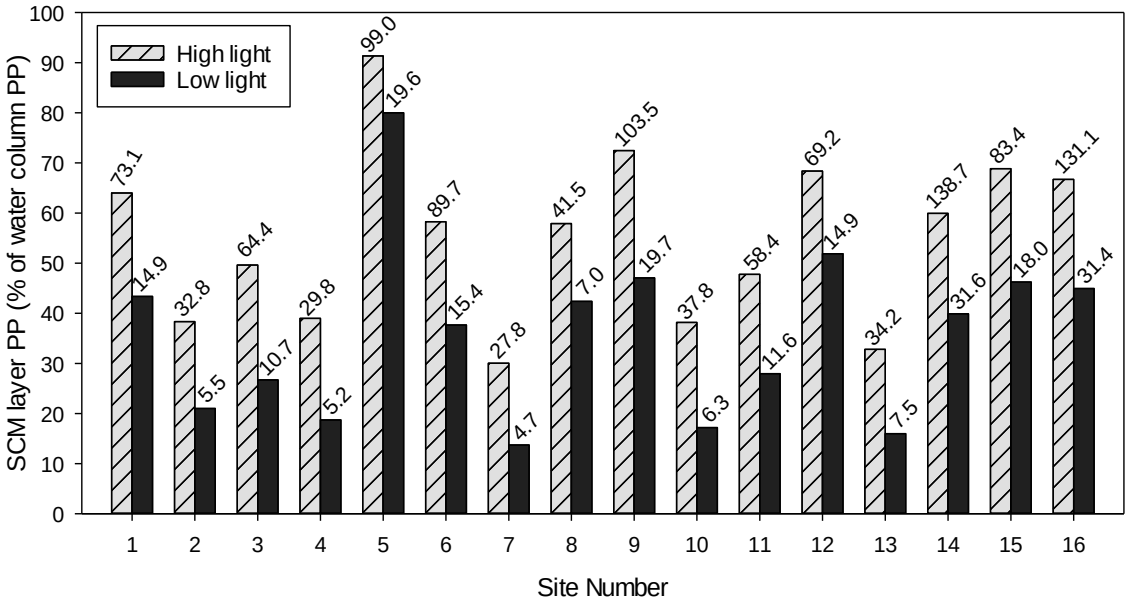

Figure 5.8. Percentage contribution of SCM layer primary production (PP) to total water column production estimated for low (469 µmol m^{-2} s^{-1}) and high (2970 µmol m^{-2} s^{-1}) sea surface light. Corresponding absolute values of primary production (mg C m^{-2} hr^{-1}) are also given above each bar.

5.4.4. SCM primary production and the phytoplankton community

The primary production vs. irradiance parameters of P_{max} and α_{LHE} obtained from FIRe measurements on SCM peak discrete water samples can indicate photophysiological state of the phytoplankton community. A higher P_{max} could suggest a more productive community and greater values of α_{LHE} indicate the community to have a higher efficiency of light utilisation.

SCM peak α_{LHE}^{*} values ranged from 0.003 to 0.068 mg C mg chl^{-1} hr^{-1} (µmol m^{-2} s^{-1})$^{-1}$, and a positive correlation was found between this parameter and SCM peak primary production (R^2 = 0.587, p < 0.001; Fig. 5.9a). Thus, indicating SCM primary production was enhanced when the phytoplankton community was more efficient in its light utilisation. In contrast, no correlation was found between SCM peak primary production and P^{*}_{max} (Fig. 5.9b).

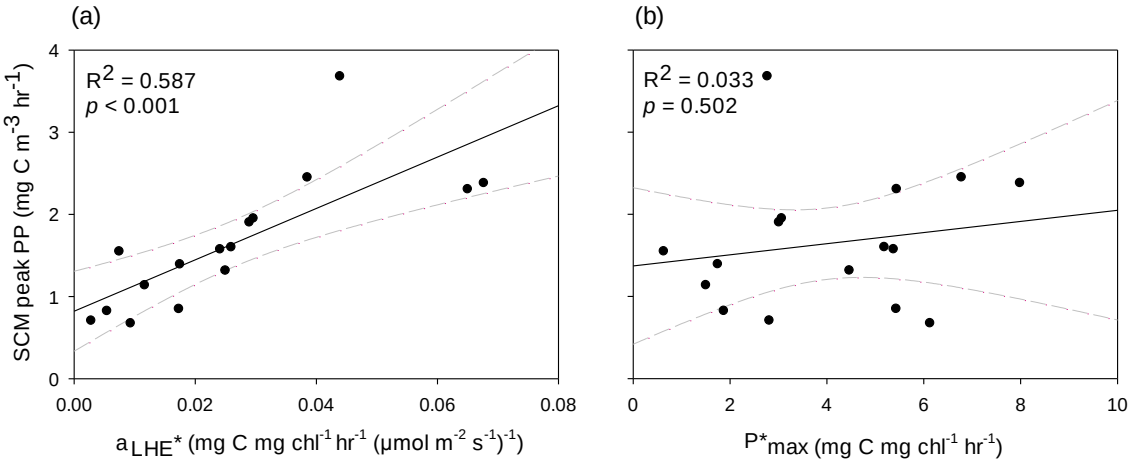

Figure 5.9. Relationship between (a) SCM peak primary production (PP) and α_{LHE}^{*} derived for the SCM peak, and (b) SCM peak PP and P^{*}_{max} derived for the SCM peak. All values were derived from FIRe measurements collected using a discrete water sample from the SCM peak. SCM peak PP values were standardised for irradiance. Regression lines with 95% confidence intervals shown, and p and R^2 values given indicating significance and goodness of fit respectively.

Phytoplankton community structure also had an important role regulating SCM primary production. Micro- and meso-phytoplankton, mainly *Ceratium fusus*, *Ceratium lineatum* and *Proboscia tuncata*, and red fluorescing nano-phytoplankton, including naked dinoflagellates, *Thalassiosira spp.* and prymnesiophytes, contributed most to the SCM community at all 16 sites, with chlorophyll contributions of 54.1 – 92.4 % and 6.1 – 31.8 % respectively (Fig. 5.10; Table A3.2). A positive correlation was found between red nano-phytoplankton contribution to community chlorophyll and SCM peak primary production (R^2 = 0.539, p = 0.001; Fig. 5.10 and 5.11a), and a negative correlation was found between micro- and meso-phytoplankton chlorophyll contribution and SCM peak primary production (R^2 = 0.436, p = 0.005; Fig. 5.10 and 5.11b). Sites where red nano-phytoplankton made a greater contribution were generally more strongly stratified, with contributions > 15 % typically coinciding with a surface to deep water temperature difference > 3 °C (Fig. 5.3, 5.10 and Table 5.1; details in Table A3.1).

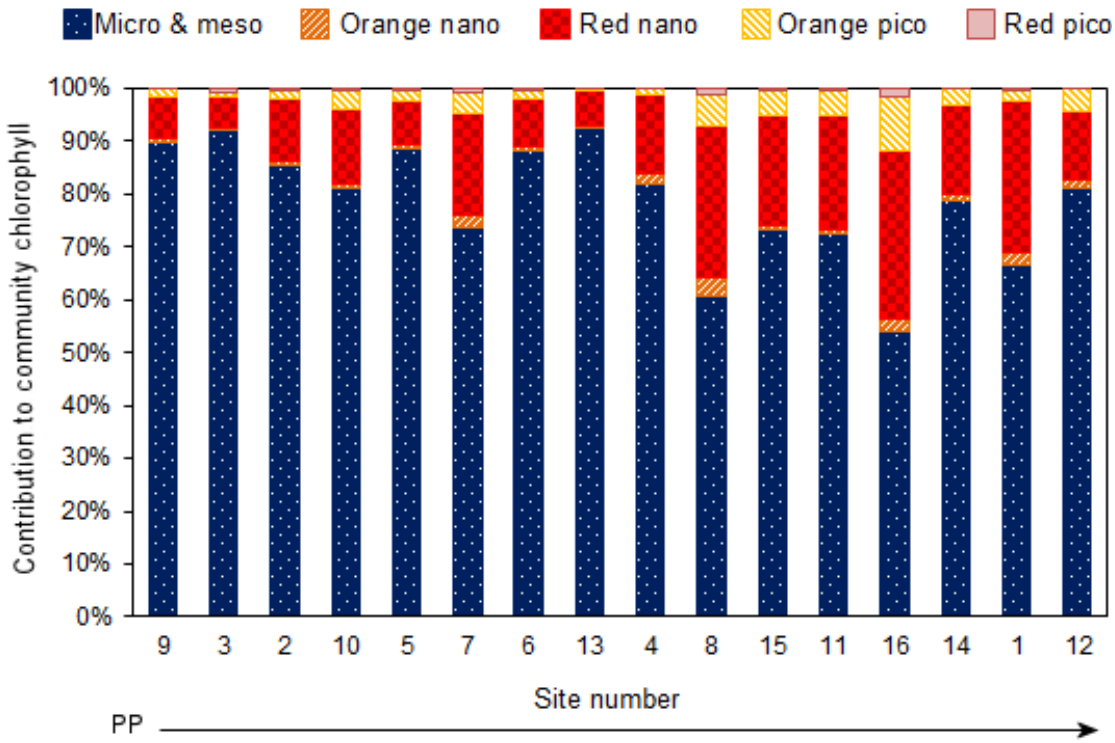

Figure 5.10. Phytoplankton community structure at the SCM peak of all 16 sampling sites: percentage chlorophyll contribution of micro- and meso-phytoplankton, red nano-phytoplankton, orange nano-phytoplankton, red pico-phytoplankton and orange pico-phytoplankton. Sites in order of SCM peak primary production (PP) magnitude (derived from FIRe measurements and standardised for irradiance), from the lowest to highest value as indicated by the arrow. All values obtained from measurements taken using a discrete water sample collected from the SCM peak.

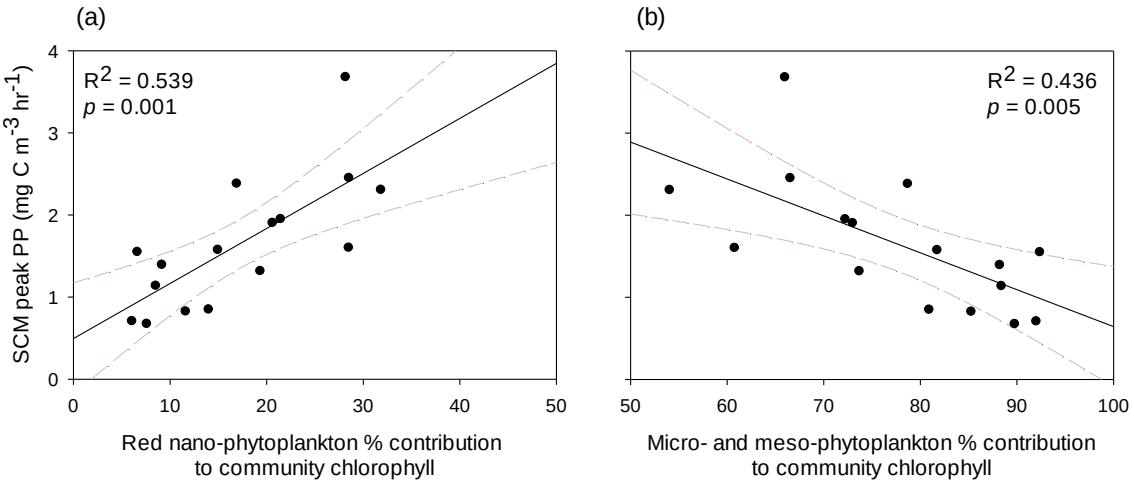

Figure 5.11. Relationship between (a) SCM peak primary production (PP) and red nano-phytoplankton contribution to community chlorophyll within the SCM, and (b) SCM peak PP and micro- and meso-phytoplankton contribution to community chlorophyll within the SCM. All values obtained from measurements collected using a discrete water sample from the SCM peak. SCM peak PP values were derived from FIRe measurements and standardised for irradiance. Regression lines with 95% confidence intervals shown, and *p* and R^2 values given indicating significance and goodness of fit respectively.

A positive correlation was also identified between red nano-phytoplankton chlorophyll contribution to community chlorophyll and α_{LHE}^* ($R^2 = 0.541$, $p = 0.001$; Fig. 5.12a), and a negative correlation between micro- and meso-phytoplankton chlorophyll contribution to community chlorophyll and α_{LHE}^* ($R^2 = 0.534$, $p = 0.001$; Fig. 5.12b). This indicates that the red nano-phytoplankton population had a greater efficiency of light utilisation than the micro- and meso-phytoplankton population, which in turn enhanced SCM peak primary production.

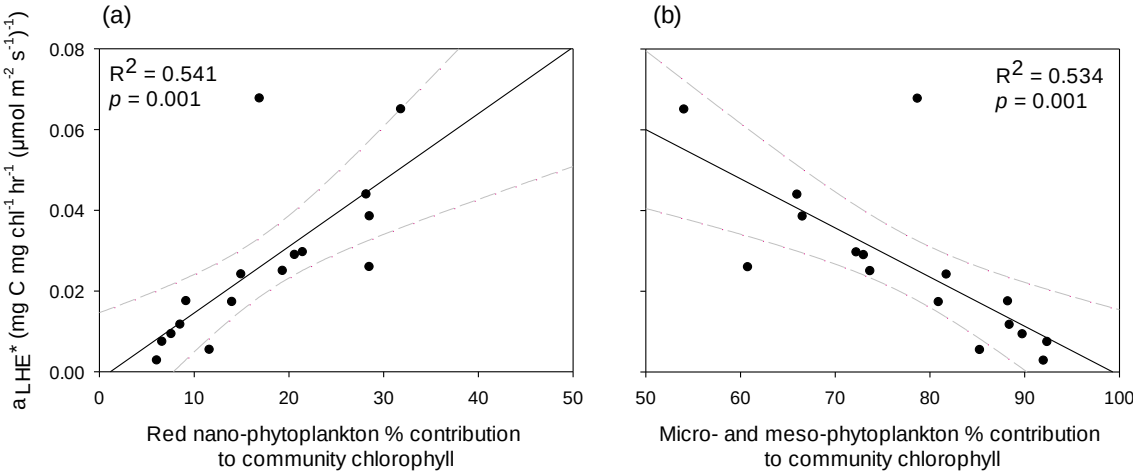

Figure 5.12. Relationship between (a) α_{LHE}^* and red nano-phytoplankton contribution to community chlorophyll, and (b) α_{LHE}^* and micro- and meso-phytoplankton contribution to community chlorophyll. All values obtained from measurements collected using a discrete water sample from the SCM peak. Regression lines with 95% confidence intervals shown, and p and R^2 values given indicating significance and goodness of fit respectively.

5.5. Discussion

5.5.1. Water column structure

During the summer survey period (23rd June – 2nd July) 2015, the stratified waters of the Western English Channel were characterised by nutrient poor surface waters and an SCM located at the base of the thermocline where light levels were < 5 % of that at the sea surface (Fig. 5.3), which is a water column structure typical of seasonally stratified waters of the NW European shelf (Pingree et al., 1978, Holligan et al., 1984b, Richardson et al., 2000, Sharples et al., 2001, Hickman et al., 2012, Simpson and Sharples, 2012), and further afield (Cullen, 1982, Holligan et al., 1984a, Dekshenieks et al., 2001, Rines et al., 2002, Lips et al., 2010, Ryan et al., 2010, Cullen, 2015). Nitrate supply from bottom waters was not apparent (perhaps aside from site 1; Fig 5.4) within SCM, but this may likely be a reflection of insufficient/unsuitable discrete sampling for detection of nitrate enhancement in combination with efficient/full utilisation of any nitrate supply from bottom waters or spread of nitrate from deep water through the SCM

and up into the surface layer (Banse, 1987, Hickman et al., 2012). Chlorophyll concentration within the surface layer was low, typically in the range of 0.1 – 1.3 μg l^{-1} (Fig. 5.3), which is generally consistent with past summer surveys of the area off Falmouth (by the University of Southampton undergraduate Oceanography field course), and past ship-based and satellite observations in the summer stratified Western English Channel (Holligan and Harbour, 1977, Pingree et al., 1978, Holligan et al., 1984c, Fishwick, 2017, NEODAAS, 2018) and wider NW European shelf seas (Richardson et al., 2000, Weston et al., 2005, Hickman et al., 2009, Sharples et al., 2009, Hickman et al., 2012, Williams et al., 2013a, NEODAAS, 2018, PODAAC, 2018). In contrast, SCM maximum chlorophyll concentrations were considerably higher, with an average value and range of 7.6 μg l^{-1} and 2.5 – 15.5 μg l^{-1} respectively (Fig. 5.3 and Table 5.1). These observations are also consistent with those of past June/July surveys conducted by the University of Southampton undergraduate Oceanography field course, as well as with other studies focusing on more coastal waters/ waters closer to frontal boundaries, both on the NW European shelf (Holligan and Harbour, 1977, Holligan et al., 1984b, Joint et al., 1986, Richardson et al., 1998, Sharples et al., 2001, Lips et al., 2010, Fishwick, 2017) and in other temperate to high latitude shelf seas (Holligan et al., 1984a, Sukhanova et al., 2006, Martin et al., 2010, Rines et al., 2010).

As maximum chlorophyll concentrations within the SCM were approximately 1 - 2 orders of magnitude greater than in surface waters, it follows that the SCM layer dominated water column chlorophyll, responsible for 10.5 – 95.1 μg chl l^{-1} and accounting for 61.7 – 98.4 % of the chlorophyll in the water column where primary production could occur. Generally, higher values of SCM layer integrated chlorophyll corresponded with higher SCM maximum chlorophyll concentrations (Fig. 5.3 and Table 5.1). Precisely what controlled the variations in chlorophyll observed between sites is difficult to establish with the available data, but turbulent mixing, largely driven by winds and tides in shelf seas (Pingree, 1975), can have a considerable and multifaceted role in modifying chlorophyll structure. Principally, turbulence may (1) act to disperse/erode a chlorophyll peak and weaken the thermocline such that chlorophyll synthesis can be supported over a broader depth range (Donaghay and Osborn, 1997, Cowles et al., 1998); (2) govern the vertical extent of a SCM, since these subsurface features form in association with turbulent mixing minima within the water column (Sharples et al., 2001, Alldredge et al., 2002, Wang and Goodman, 2009, Macías et al., 2013); (3) enhance the supply of nutrients to the thermocline from the bottom mixed layer, promoting algal growth (Sharples and Tett, 1994, Sharples et al., 2001, Rippeth, 2005, Rippeth et al., 2009, Williams et al., 2013a, Williams et al., 2013b). Nutrients supplied by increased mixing may not be assimilated by

phytoplankton immediately however, especially if the nutrient supply event coincides with low light conditions, such as on cloudy days (Banse, 1987); and (4) promote concentration of cells within the thermocline (low turbulence region) from surface waters as greater turbulence in the surface layer can enhance phytoplankton sedimentation velocity (Ruiz et al., 2004, Macías et al., 2013). The development of broader SCM with higher chlorophyll levels observed during the survey (e.g. sites 5 and 6, both profiled at the end of spring tides; Fig. 5.3 and Table A3.1) may therefore have been facilitated by the potential chlorophyll dispersal, but nutrient enriching effects associated with increased turbulence, such as experienced around spring tides (Sharples et al., 2001, Sharples et al., 2007). On the other hand, the smaller/ broader and less intense SCM detected (e.g. site 1, which was profiled near the end of spring tides, and site 16, which was profiled at the onset of spring tides; Fig. 5.3 and Table A3.1) may have coincided with levels of turbulence where the extent of cell dispersal/losses prevented biomass concentration and proliferation within the SCM. Finally, the formation of the thinnest SCM (< 3 m) observed during the survey (sites 2, 7, 9, 10, 12 and 13, mainly profiled approaching/during neap tides; Fig. 5.3) may have been promoted by low turbulence/a narrow turbulence minimum.

5.5.2. Water column primary production and the importance of the SCM

Values of total water column primary production estimated for the irradiance conditions recorded at the time of sampling ranged from 36.4 to 112.3 mg C m^{-2} hr^{-1} (Table 5.2.). Within the water column a primary production maximum was typically associated with the SCM, with estimates of SCM layer primary production estimated for the irradiance conditions recorded at the time of sampling ranging from 11.0 to 99.0 mg C m^{-2} hr^{-1} (Table 5.2). Thus, the SCM layer consistently accounted for a large proportion of water column primary production despite generally having a smaller vertical extent and minimal light relative to that of the surface layer. Specifically, 23.5 – 91.3 % and on average approximately 50 % of water column primary production occurred within the SCM layer (Fig. 5.4 and Table 5.2). These SCM layer percentage primary production contributions are comparable with results of past observational and theoretical primary production studies conducted for the NW European shelf (Richardson et al., 1998, Richardson et al., 2000, Weston et al., 2005, Hickman et al., 2012, van Leeuwen et al., 2013) that indicate SCM are key contributors to summer and, by extension, annual water column primary production within the seasonally stratifying shelf seas. In contrast, in the open ocean primary production maxima are not seen to be associated with the much deeper chlorophyll maximum (typically around 80 - 130 m), instead maximum rates of primary production occur in and nearer the surface. Primary production measurements taken as part of the time series studies in the North Pacific (Hawaii Ocean Time Series; HOTS) and in the

North Atlantic (Bermuda Atlantic Time Series; BATS) have shown rates of primary production in waters shallower than 50 m to be generally more than twice and even an order of magnitude greater than that at depths coinciding with the chlorophyll maximum, with rates of primary production at the chlorophyll maximum typically reported to be approximately equal to or less than 2.5 mg C m^{-3} d^{-1} (Steinberg et al., 2001, White et al., 2015, Bates, 2018, Lukas, 2018). The finding that the SCM is accountable for significant primary production within seasonally stratified shelf waters reinforces the recognised need for the SCM to be consistently represented in ecosystem models to ensure reliable prediction of biogeochemical and ecological ecosystem dynamics, and ecosystem responses to environmental variation, particularly that which may be presented by future climate change. In addition, given that satellite sensors cannot detect the SCM, this finding is significant as it demonstrates that satellites cannot be relied upon for remotely accurate estimates of primary production in seasonally stratifying shelf waters.

At the SCM peak, f-ratios (Table 5.2) indicated that rates of nitrate uptake (i.e. new production) accounted for 37 – 68 %, and on average 49 %, of the nitrogen requirement of carbon fixation. In contrast, within the surface layer (~ 10 m), f-ratios indicated primary production to be mostly regenerated production as nitrate uptake rates only accounted for 20 – 39 %, and on average 29 %, of the nitrogen requirement of carbon fixation. These findings indicate that the SCM was the most significant site of new production within the summer stratified water column. If an f-ratio of 0.49 was assumed for the entire SCM layer at all sites, and an f-ratio of 0.29 was assumed for the whole surface layer at all sites, new production in the SCM layer would range between 17.8 – 55.0 mg C m^{-2} hr^{-1} compared to only 2.7 – 18.8 mg C m^{-2} hr^{-1} for the surface layer. These estimates of SCM new production, in combination with the long-lived nature of the SCM due to the extended period of time for which stratification persists (approximately 5 months in the Western English Channel) (Pingree, 1975), suggest the SCM may be a particularly substantial contributor of new production within the Western English Channel. These findings of the SCM being a key site of new production within summer stratifying shelf waters is in agreement with direct and indirect findings of many, including Richardson et al. (2000), Sharples et al. (2001), Weston et al. (2005) and Hickman et al. (2012), with Richardson et al. (2000) even arguing that new production associated with the SCM may surpass that associated with the spring bloom. Substantial new production associated with the summer SCM will likely have important consequences for the Western English Channel, including being responsible for a significant contribution of organic carbon exported to depth (Goldman, 1993, Sharples et al., 2001) and providing a vital food source for higher trophic levels,

influencing fisheries and potentially apex predators (Lasker, 1975, Richardson et al., 2000, Heath and Beare, 2008, Scott et al., 2010, Benoit-Bird and McManus, 2012).

Variation in SCM layer primary production was found to drive variation in total water column primary production (Fig. 5.5). Therefore, further emphasising the importance of the SCM for rates of water column carbon fixation in summer stratified shelf waters and highlighting a need to establish how environmental and biological factors govern primary production within such SCM in order to understand how they control production of the entire water column. In agreement with Hickman et al. (2012) changes in the magnitude of photosynthesising biomass within the SCM layer, represented by chlorophyll concentration, only accounted for approximately 50 % of the variation in SCM layer primary production. Consequently, it was clear that additional variables (as discussed in detail below) were responsible for the differences in SCM layer primary production between sampling sites.

5.5.3. Influence of resource availability on SCM primary production

In a stratified water column the opposing vertical gradients of nutrients and light underlie the existence of an SCM (Pingree et al., 1978, Holligan et al., 1984a, Huisman et al., 2006). However, in the Western English Channel during summer 2015, there was no discernible effect of nitrate concentration on primary production within the SCM, with Fv/Fm values (0.41 – 0.46; Table 5.3) indicating that the SCM phytoplankton community as a whole maintained its photosynthetic efficiency across all sampling sites (Suggett et al., 2009b). It is acknowledged that when assessing natural phytoplankton communities, values of Fv/Fm contain a taxonomic 'signature', and as such Fv/Fm data cannot be interpreted solely in terms of physiological variability (Moore et al., 2006, Suggett et al., 2009b). Therefore, any significant variation in photosynthetic efficiency related to the nutrient environment within the SCM in this study may have been masked by the influence of the varying photosynthetic apparatus structure of different taxa on values of Fv/Fm. On the other hand, it may be possible that Fv/Fm values remained relatively constant across sample sites because the key phytoplankton within the SCM community at all sites, namely *Ceratium fusus*, *Ceratium lineatum*, *Proboscia truncata* and red nano-phytoplankton (Fig. 5.10 and Table A3.2), have adaptations that may have enabled them to maintain their photosynthetic efficiency in an environment that had the potential to constrain it, given the intermittent nature of the supply of nutrients that are essential for components of photosynthetic machinery from bottom waters to the thermocline (Sharples et al., 2001, Williams et al., 2013a, Williams et al., 2013b). *Ceratium fusus* and *Ceratium lineatum* are motile, with swimming speeds in excess of 200 µm s^{-1} reported for the genus (Levandowsky

and Kaneta, 1987, Nielsen, 1991, Baek et al., 2009). Based on typical turbulent diffusivities of 10^{-4} – 10^{-6} m^2 s^{-1} measured in the thermocline of seasonally stratified NW European shelf seas (Sharples et al., 2001, Palmer et al., 2008, Rippeth et al., 2009), the swimming capability of these *Ceratium spp.* was more than sufficient to allow some control over their location within the thermocline (Péclet number as defined in Ross and Sharples (2008) consistently > 1 for swimming speeds > 10 µm s^{-1} using a length scale of 10 m). In addition, these dinoflagellates may perform luxury consumption of nutrients (Nielsen, 1991, Baek et al., 2008a, Baek et al., 2009) and are mixotrophs so can gain nutrients through an alternative source (Ward et al., 2011). Therefore, *Ceratium fusus* and *Ceratium lineatum* may have had means to subsist pending nutrient input, and then rapidly respond and capitalise on any episodic supply of nutrients into the thermocline. This may have also been the case for *Proboscia truncata* given that this rhizosolenid diatom has the established diatom traits of luxury nutrient uptake (Sunda and Huntsman, 1995) and nutrient storage within the vacuole (Dortch, 1982, Raven, 1987, Marchetti et al., 2009), in addition to its potential capacity for buoyancy regulation at ascent/descent rates in the order of cm to m hr^{-1} (Moore and Villareal, 1996a, Woods and Villareal, 2008). Finally, nano-phytoplankton have a higher nutrient uptake affinity and assimilation efficiency given their lesser size (Beardall et al., 2009, Finkel et al., 2010), and can have a higher preference for ammonium over nitrate than larger phytoplankton (Dortch, 1990). Therefore, nano-phytoplankton can maintain photosynthesis and subsequently form significant biomass in low nitrogen waters (Chisholm, 1992).

Light intensity was demonstrated to be the most important environmental parameter driving the variation in SCM layer primary production observed between sampling sites, with a change from low to high light conditions, on occasion, accounting for a greater difference in primary production than that between sites (Fig. 5.7 and 5.8). Rates of primary production were estimated to increase by as much as 107.07 mg C m^{-2} hr^{-1} from low light (469 µmol m^{-2} s^{-1} at sea surface) to high light (2970 µmol m^{-2} s^{-1} at sea surface) conditions, and the contribution of the SCM layer to total water column primary production increased, on average, by 20 %. This considerable increase in contribution to water column primary production indicated that SCM phytoplankton were much more sensitive to light variability than surface layer phytoplankton. Consequently, this indicates that primary production within the SCM layer was light limited, which is supported by the correspondence of SCM rates of primary production with the light limited region of the primary production vs. irradiance curves derived from rETR vs. irradiance curves (e.g. Fig. A3.1). Phytoplankton within SCM of stratified water columns photophysiologically acclimatise to the low light conditions in order to optimise their

photosynthetic performance (MacIntyre et al., 2002, Moore et al., 2006), but these results indicate that phytoplankton acclimation was not adequate for maximum rates of primary production to be reached under the light conditions experienced within SCM of the Western English Channel during summer 2015. These findings are consistent with Moore et al. (2006) and Hickman et al. (2012) who identified that the light intensity required to reach maximum photosynthesis (Ek) within the SCM was consistently much higher than that actually experienced by the phytoplankton community within the shelf sea SCM.

5.5.4. Influence of the phytoplankton community on SCM primary production

Primary production of a phytoplankton community is influenced by the photophysiological status and the structure of that community, which is related to water column structure and the resource regime (Geider et al., 1986, Cushing, 1989, Kiørboe, 1993, Platt et al., 1993, Tilstone et al., 1999, Tilstone et al., 2003, Barnes et al., 2015b). In the stratified waters of the Western Channel during summer 2015 it was apparent that P^*_{max} was not key in determining primary production within the SCM, instead, SCM peak primary production was strongly dependent upon α_{LHE}^* (Fig. 5.9). The sensitivity of primary production in the SCM to α_{LHE}^* rather than P^*_{max} can be attributed to the low light conditions and the resulting light limitation of photosynthesis (Falkowski and Raven, 1997, Uitz et al., 2008). In a low light environment, as presented by the SCM, phytoplankton with greater light utilisation efficiency are capable of enhanced rates of primary production relative to phytoplankton with lower light utilisation efficiency. On the other hand, given that the photoacclimation response of the community was insufficient to achieve maximum rates of photosynthesis at the SCM, phytoplankton with a higher photosynthetic potential would be limited in their effect on rates of primary production in low light conditions that prevent achievement of this photosynthetic potential.

Phytoplankton community structure was also an important factor influencing SCM primary production. Larger phytoplankton (> 20 μm) consistently constituted the majority of the community (54.1 – 92.4 %; Fig. 5.10), suggesting they were the key contributors of primary production. However, increases in rates of primary production at the SCM were associated with greater percentage contributions of red fluorescing nano-phytoplankton (Fig. 5.10 and 5.11), due to a higher light utilisation efficiency of the red fluorescing nano-phytoplankton relative to the micro- and meso-phytoplankton (Fig. 5.12). Nano-phytoplankton have often been found to enhance and, by association, control variation in primary production in coastal environments (Tilstone et al., 1999, Barnes et al., 2015b) and in the open ocean (Uitz et al., 2008, Uitz et al., 2010) due to their higher efficiency of light utilisation. This greater light

utilisation efficiency may be attributed to lesser internal light shading of nano-phytoplankton relative to larger phytoplankton (Geider et al., 1986, Beardall et al., 2009, Finkel et al., 2010).

Greater contributions of red nano-phytoplankton were associated with stronger stratification during neap tides. It is possible that nitrate supply to the thermocline was reduced in these conditions given that the magnitude of the vertical nitrate flux from replete bottom waters is reliant upon turbulence driven by a combination of factors inclusive of tides (Sharples and Tett, 1994, Sharples et al., 2001, Rippeth, 2005, Rippeth et al., 2009, Simpson and Sharples, 2012, Williams et al., 2013a, Williams et al., 2013b). If this was the case it is feasible that the SCM phytoplankton community may have consisted of more red nano-phytoplankton when available nitrogen was relatively low. Considerable nano-phytoplankton populations are associated with low nitrogen environments throughout the world's oceans (Uitz et al., 2006), which can be justified by the allometric relationship between phytoplankton size and nutrient uptake (Finkel et al., 2010). Moreover, as the uptake of nitrate and ammonium is light dependent (MacIsaac and Dugdale, 1972), enhanced light absorption efficiency associated with the smaller size of the nano-phytoplankton may have provided an additional advantage for the red nano-phytoplankton within the low light and potentially lower nitrogen conditions of the SCM during periods of increased stratification, which ultimately allowed them to become a bigger part of the community.

Ecologically, a SCM community consistently dominated by micro- and meso- phytoplankton would provide an important source of food for higher trophic levels, either directly or via the mesozooplankton through the traditional food chain (Azam et al., 1983, Cushing, 1989, Fenchel, 2008), and could have a key role in carbon export out of the photic zone (Sournia, 1982a, Kemp et al., 2000, Kemp and Villareal, 2013) and atmospheric carbon dioxide drawdown (Kitidis et al., 2012). On the other hand, the considerable red nano-phytoplankton population within the SCM would contribute organic matter for circulation through the microbial loop, which is important in the rapid recycling of carbon and nutrients above the thermocline (Azam et al., 1983, Cushing, 1989). Given that red nano-phytoplankton biomass was less than that of larger phytoplankton, but caused variation in SCM primary production, generally according to the level of stratification, may suggest that more carbon was circulated in the microbial loop during periods of increased stratification. Moreover, finding nano-phytoplankton responsible for increased primary production apparently in response to enhanced stratification may be important for advancing our understanding of the role of stratification in primary production and for predictions of how the shelf seas could respond to the increased stratification promoted by climate change (Bindoff et al., 2007, Lyman et al., 2010, Steinacher et al., 2010, Capotondi et al., 2012).

5.6. Conclusion

During summer (23rd June – 2nd July) 2015, the stratified waters of the Western English Channel were characterised by nutrient poor surface waters (nitrate ≤ 0.4 µmol l^{-1}), and an SCM located at the base of the thermocline with a maximum chlorophyll concentration of 2.5 – 15.5 µg l^{-1} and light levels < 5 % of that at the sea surface. Water column primary production at 16 sites in these summer stratified waters ranged from 36.4 to 112.3 mg C m^{-2} hr^{-1}. On average, approximately 50 % of this primary production occurred within the SCM layer, which was also identified to be an important site of new production (f-ratios of 0.37 – 0.68). Changes in water column primary production between sites was driven by variation in SCM primary production, further highlighting the importance of the SCM for primary production within seasonally stratified water columns and of representing these subsurface features in ecosystem models. Changes in the amount of photosynthesising biomass (integrated chlorophyll concentration) within the SCM layer only accounted for approximately 50 % of the site to site variability in SCM layer primary production, where chlorophyll structure was thought to be largely governed by turbulence structure and magnitude.

Light intensity was demonstrated to be the most important environmental parameter driving variation in SCM layer primary production due to the SCM community being light limited. Nutrient availability within the SCM layer likely had some influence over the magnitude of primary production, but there was no discernible response of the SCM community to SCM nitrate concentration.

Phytoplankton community photophysiological status and structure were also found to be important factors influencing SCM primary production. Specifically, while micro- and meso-phytoplankton dominated within the SCM (54.1 – 92.4 % of total chlorophyll), increases in SCM primary production were associated with greater contributions of red nano-phytoplankton, attributed to their higher efficiency of light utilisation compared to the larger (> 20 µm) phytoplankton. Sites where the phytoplankton community consisted of a larger percentage of red nano-phytoplankton generally corresponded to increased stratification experienced during neap tides. These findings not only have implications for trophic dynamics and carbon cycling within the Western Channel, but also may be important for improving our understanding of the effect of stratification on primary production and for projections of how the shelf sea ecosystem could respond to increased stratification brought about by future climate change.

Chapter 6: Environmental controls on the interannual variability in chlorophyll and phytoplankton community structure within subsurface chlorophyll maxima in the Western English Channel during summers of 2013 to 2016

6.1. Abstract

The Western English Channel is a summer stratified temperate coastal sea where a subsurface chlorophyll maximum (SCM) is often detectable in association with the seasonal thermocline. In this study, the chlorophyll and phytoplankton community structure of the SCM at a repeat site (50°05.670 N, 004°52.020 W) in the Western Channel sampled in June/July of 2013, 2014, 2015 and 2016 are reported, and interannual variability related to environmental conditions. The highest stability (instantaneous index of stability (IIS) 9.07 on average in 2015), relating to low current velocities, coincided with the highest maximum SCM chlorophyll concentrations (7.3 µg l^{-1} on average). Whereas, low stability (IIS < 0.7 on average), as observed in 2014 and 2016, coincided with greater 50 m to SCM maximum chlorophyll ratios (depth integrated chlorophyll concentration within top 50 m divided by SCM maximum chlorophyll; Chl_{50m}:Chl_{SCM}), indicating dispersal of chlorophyll through the water column. Therefore, stability at the depth interval of the SCM could be considered the most important factor governing SCM chlorophyll structure. Community structure was analysed by flow cytometry and by light microscopy. Both methods of analysis showed community structure within the SCM to be distinct in all years, with stability, temperature and strength of stratification emerging as key governing factors. Greater contributions of red fluorescing nano-phytoplankton (2014 and 2016) were associated with low stability (IIS < 0.7 on average), and larger contributions of orange fluorescing nano-phytoplankton and pico-phytoplankton (2016) were related to enhanced stratification but low stability. Two main relationships were found between community structure identified by microscopy and environmental conditions: (1) change from lower stability (IIS < 3.7 on average in 2013, 2014 and 2016) to very high stability (IIS > 9 on average in 2015) coincided with a shift from a mixed assemblage of diatoms and dinoflagellates to a community dominated by large dinoflagellates (*Ceratium fusus*); and (2) change from cooler (11.6 - 12.1 °C on average in 2013 and 2016) to warmer waters (13.1 °C on average in 2014) corresponded with a shift from smaller (*Chaetoceros spp.* and *Pseudo-nitzschia spp.*) to larger diatoms (large *Rhizosolenia spp.*, *Lauderia annulata* and *Leptocylindrus danicus*). These findings may have implications, in

particular, for the silica cycle, carbon export to depth, and the microbial loop within the Western English Channel. Results also suggest that knowledge of environmental conditions, especially water stability and temperature, may be useful for indication of key SCM taxa.

6.2. Introduction

Phytoplankton are very sensitive to modifications within their environment, with environmental parameters, such as temperature, turbulence, and nutrient concentrations, affecting their physiology at an individual level (Beaugrand et al., 2000, Beaugrand, 2005, Paerl et al., 2007, Simpson and Sharples, 2012). Phytoplankton growth/cell generation is rapid, thus phytoplankton communities respond quickly to environmental changes, enabling them to function as environmental indicators (Beaugrand, 2005, Falkowski and Oliver, 2007). Different communities likely present distinct ecological and biogeochemical functionality due to the great array of taxon-specific properties possessed by these highly diverse microorganisms (Kiørboe et al., 1990, Falkowski et al., 2004, Finkel et al., 2010, Kemp and Villareal, 2013, López-Sandoval et al., 2014). Therefore, given that these microscopic algae form the foundation of marine food webs (Falkowski and Raven, 1997) and are central to biogeochemical and ecological dynamics (Lalli and Parsons, 1997), any impact of environmental change can cascade through the food web, with the potential to have ecosystem level ecological and biogeochemical effects (Beaugrand, 2005, Paerl et al., 2007).

Understanding of the impact of environmental changes on phytoplankton community density and structure is of particular relevance for the shelf seas, since these regions of the marine environment sustain a disproportionately sizeable share (15 – 30 %) of oceanic primary production (Muller-Karger et al., 2005). This primary production supports significant fisheries (Pauly et al., 2002), and is partially responsible for the substantial export of particulate organic carbon (47 % of global annual export) estimated to occur on the shelf (Jahnke, 2010). Moreover, shelf seas are particularly sensitive to climatic variation (Backhaus, 1996, Sharples et al., 2006, Holt et al., 2010, Holt et al., 2016), which given their ecological and biogeochemical significance, makes knowledge of shelf sea phytoplankton and their response to environmental variation especially valuable.

Within seasonally stratified waters of high latitude and temperate shelf seas, considerable phytoplankton biomass is represented by the subsurface chlorophyll maximum (SCM) associated with the seasonal pycnocline (Holligan and Harbour, 1977, Pingree et al., 1978,

Cullen, 1982, Holligan et al., 1984a, Weston et al., 2005, Martin et al., 2010, Hickman et al., 2012, Cullen, 2015). These subsurface features have often been observed with maximum chlorophyll concentrations greater than 4 μg l^{-1} (Holligan et al., 1984a, Holligan et al., 1984b, Richardson et al., 2000, Lips et al., 2010, Martin et al., 2010) and in some cases greater than 40 μg l^{-1} (Sharples et al., 2001, Sullivan et al., 2010a), and can be sustained for periods of months as stratification persists. The SCM is a key site of carbon fixation, estimated to contribute on average, approximately 35 - ≥ 65 % of primary production in a stratified water column (Richardson et al., 1998, Weston et al., 2005, Hickman et al., 2012, Martin et al., 2013). Moreover, the SCM is an important site of new production (Richardson et al., 2000, Weston et al., 2005, Hickman et al., 2012, Williams et al., 2013b), which may even exceed the new production achieved during the spring bloom (Richardson et al., 2000, Hickman et al., 2012). This production has been associated with significant atmospheric carbon dioxide drawdown (Kitidis et al., 2012), a high potential for carbon export to depth (Goldman, 1993, Sharples et al., 2001, Kemp and Villareal, 2013) and vital provision of sustenance for the pelagic food web (Richardson et al., 2000, Heath and Beare, 2008, Scott et al., 2010, Benoit-Bird and McManus, 2012). Thus, there is ample evidence attesting to the biogeochemical and ecological significance of the shelf sea SCM, consequently highlighting a particular need for an improved understanding of the ecology of key SCM phytoplankton.

This study focuses on the Western English Channel, a shallow (45 – 120 m) region of the NW European shelf with relatively weak tides that becomes stratified in the summer months (Pingree, 1980, Dauvin, 2012) and develops a SCM associated with the seasonal thermocline (Pingree, 1975, Holligan and Harbour, 1977, Holligan et al., 1984b, Fishwick, 2017). Hydrography in the Channel is heavily influenced by ambient weather conditions and by the tide (Pingree, 1980), and marked variation in environmental conditions can occur between years (Pingree, 1980, Southward et al., 2005a, Smyth et al., 2010, Barnes et al., 2015b). Furthermore, the Western English Channel is one of the fastest warming regions of the NW European shelf (MCCIP, 2008). The Western Channel is a transition area between the boreal Baltic and North Sea continental systems, and the temperate Atlantic Oceanic system (Southward et al., 2005b, Dauvin, 2012), therefore changes in phytoplankton characteristic of this area brought about by environmental variation may be representative of the wider NW European shelf and possibly the temperate Atlantic.

In general, short-term studies are not sufficient to investigate and better understand the effects of environmental changes on phytoplankton density and community structure, instead long-term study is required. However, long-term phytoplankton studies related to

environmental variation in the Western English Channel (and further afield on the NW European shelf) have primarily dealt with the spring bloom and near surface phytoplankton (Holligan et al., 1983, Irigoien et al., 2000, Beaugrand and Reid, 2003, Wiltshire and Manly, 2004, Sommer and Lengfellner, 2008, Garcia-Soto and Pingree, 2009, Downes-Tettmar et al., 2013, Barnes et al., 2015a). Studies that consider interannual changes in SCM biomass and/or community structure in relation to environmental conditions are scarce (Holligan and Harbour, 1977, Tarran and Bruun, 2015), especially as the depth of the SCM precludes its study by remote sensing (Gordon and Clark, 1980). As such, a sizable portion of our knowledge of the ecology of Western English Channel SCM phytoplankton is based on studies investigating surface waters and associated environmental conditions (Holligan et al., 1983, Beaugrand et al., 2000, Irigoien et al., 2000, Beaugrand and Reid, 2003, Wiltshire and Manly, 2004, Sommer and Lengfellner, 2008, Garcia-Soto and Pingree, 2009, Downes-Tettmar et al., 2013, Barnes et al., 2015a), and laboratory experiments (Hansen, 1992, Moore and Villareal, 1996a, Goldman and McGillicuddy, 2003, Baek et al., 2008b). Therefore, the influence of environmental variables on the concentration and community structure of natural SCM phytoplankton assemblages *in situ* is less well described.

The present study investigated chlorophyll structure, phytoplankton community structure, and associated environmental conditions of the SCM sampled at a coastal site in the Western English Channel during the summers of 2013 to 2016, with the aim of establishing the environmental controls of interannual variability in SCM chlorophyll and phytoplankton community structure. SCM chlorophyll structure is described in terms of thickness, maximum chlorophyll and the 50 m to SCM maximum chlorophyll ratio (depth integrated chlorophyll concentration within top 50 m divided by SCM maximum chlorophyll; hereafter denoted by Chl_{50m}:Chl_{SCM}), and phytoplankton community structure analysed by flow cytometry and by inverted light microscopy is presented. Interannual variation in SCM chlorophyll structure and phytoplankton community composition is assessed, and the influence of environmental factors, including (but not limited to) temperature, buoyancy frequency, stability, nutrient concentrations and ratios, salinity, wind speed and current velocity, is evaluated.

6.3. Methods

6.3.1. Sampling

Samples were collected from the repeat site (50°05.670 N, 004°52.020 W ± 1.5 km; Fig. 6.1) almost on a daily basis and over a range of different states of the semi-diurnal tide (Fig. 6.2) in

the summer stratified waters of the Western English Channel between 24th June – 4th July in 2013, 17th June – 3rd July in 2014, 22nd June – 2nd July in 2015 and 20th – 30th June in 2016. The repeat site had a water depth of approximately 66 m and was chosen based on past data revealing its location to be far enough away from the tidal mixing front to be permanently stratified in June/July, but also within a reasonable travel distance to permit regular sampling.

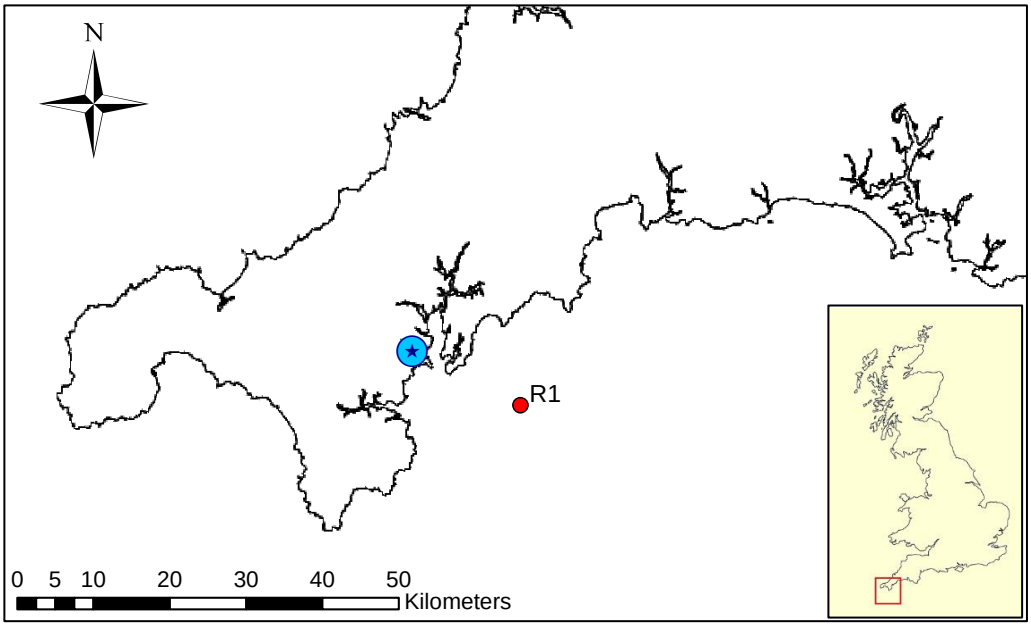

Figure 6.1. Location of the repeat study site (R1) in the Western English Channel where sampling occurred in the summers of 2013 to 2016. The blue encircled star indicates the location of Falmouth.

A SeaBird SBE19plus V2 conductivity, temperature, depth (CTD) probe mounted with a Wet Labs ECO FLNTU fluorometer (sensitivity: 0.025 µg chl/l; fluorescence excitation/emission wavelengths: 470/695 nm) was used to collect water column profiles of temperature, salinity and chlorophyll-fluorescence. The CTD system was typically deployed at a descent/ascent rate of 0.01 - 0.1 m s^{-1} (rate slowed on approach to SCM), with a data acquisition rate of 2 Hz, which provided vertical resolution of 0.5 – 5 cm. Water samples were typically collected from the SCM using a CTD Niskin sampling carousel (6 x 5 L Niskin bottles), but in one case in 2013 using a custom made horizontal sampler mounted on the CTD carousel frame. The horizontal sampler consisted of three 50 ml syringes spaced approximately 20 cm apart, acting as a multiple 'slurp gun' (analysis performed on water sample from the middle syringe), similar in design to the gradient sampler of Bjørnsen and Nielsen (1991). Water samples were analysed for chlorophyll concentration, nutrient (nitrate, phosphate and silicate) concentrations, and phytoplankton community structure by CytoSense flow cytometry and inverted light microscopy. Note that samples for nutrient analysis and flow cytometric analysis were not collected in 2013.

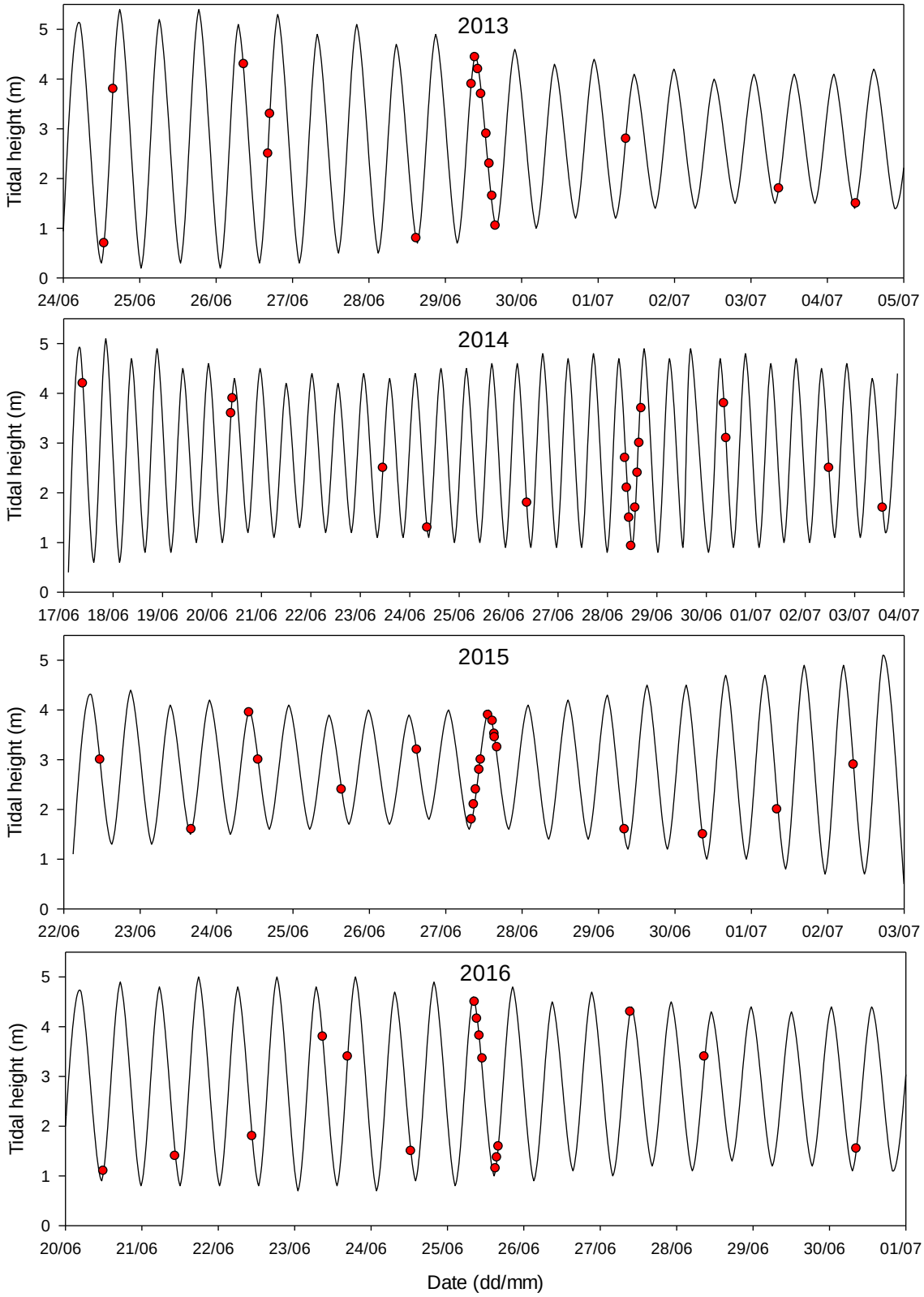

Figure 6.2. Time series plots of tidal height in the Western English Channel during the summer survey periods of 2013, 2014, 2015 and 2016. Red circles indicate when vertical water column profiles were collected at the repeat study site. Labels on the x axis are positioned to correspond with midnight (UTC) on the date detailed. Tidal data was taken from tide tables for Falmouth (Tidetimes.co.uk, no date).

Vertical profiles of buoyancy frequency, a measure of stratification, were computed from CTD data using SBE data processing software, where the buoyancy frequency was calculated using the Fofonoff adiabatic levelling method (Bray and Fofonoff, 1981). Current velocity and velocity shear was measured with a hull mounted RDI Workhorse Mariner 600 kHz ADCP, which combined with CTD density measurements allowed for calculation of the Richardson number (a measure of dynamic stability where a value of 0.25, classically reported by Miles (1961), is typically accepted as the general threshold between a stable and unstable regime) for the depth interval of each SCM, where Ri is defined as:

$$Ri = \frac{-g}{\rho}\frac{\delta\rho\delta z}{\delta U^2} = \frac{N^2}{S^2} \quad (6.1)$$

where N is buoyancy frequency (rad^2 s^{-2}), S is velocity shear (m s^{-1}), g is gravitational acceleration (9.81 m s^{-2}), ρ is *in situ* density (Kg m^{-3}), z is depth (m) and U is horizontal velocity (m s^{-1}).

Shear can greatly vary over the course of a semi-diurnal tidal cycle in a shallow stratified tidal sea, such that temperate shelf sea thermoclines have been shown to be of marginal stability (Rippeth, 2005, Rippeth et al., 2005, Burchard and Rippeth, 2009). Consequently, to establish a careful understanding of the dynamic stability regime associated with a SCM and its influence on that SCM, the Richardson number should ideally be measured over a semi-diurnal tidal cycle. However, it was not logistically possible to calculate Richardson numbers over the course of a tidal cycle during the summer surveys conducted to collect the data presented in this chapter. Instead, velocity shear could only be measured over the duration of the CTD profiling process (~ 15 minutes), which presents the caveat that a Richardson number calculated using velocity shear values measured in this way may not be a strictly accurate representation of the dynamic stability regime associated with the SCM being investigated. Thus, it may not be useful to include such a measurement in an investigation of the environmental controls of SCM chlorophyll and community structure in a shallow stratified tidal sea. However, stability as calculated in this manner, hereafter referred to as the instantaneous index of stability (IIS; a measure of instantaneous stability, a term hereafter used interchangeably with the term stability), was determined at many different states of the semi-diurnal tide during each annual survey (Fig. 6.2). Therefore, there was consideration of tidal cycle variation in shear in the study of the effect of stability on interannual variability in chlorophyll and phytoplankton community structure within the SCM. In addition, interesting relationships were found between the IIS and SCM chlorophyll and phytoplankton community structure, when a relationship with buoyancy frequency was not,

suggesting variation in values of the IIS were not simply dominated by variation in buoyancy frequency. Therefore, it is considered acceptable to include analysis of the IIS in this study.

Wind speed measurements were taken from the WCO L4 autonomous buoy situated at 50° 15.000 N, 004° 13.000 W (PML, 2017) for 2013 and 2014, but in 2015 and 2016 wind speed was logged by an onboard AIRMAR PB150 weather station. Daily rainfall measurements were collected by the PML meteorological station Omni Instruments 6" tipping bucket raingauge (RG200) (Smyth, 2017), and daily solar insolation measurements for the longitude and latitude of the repeat site were taken from NASA's CERES FLASHFlux project (NASA, 2018).

6.3.2. Determination of chlorophyll concentration

Samples for chlorophyll analysis were collected by passing 50 ml of water sample through a 25 mm Whatman GF/F filter and storing at -20 °C prior to analysis. Analysis was conducted as soon as possible after collection to avoid error associated with degradation of pigment at -20 °C (Graff and Rynearson, 2011). Chlorophyll was extracted in 90 % acetone via sonication and its concentration determined using a Turner Designs 10AU fluorometer based on methods of Welschmeyer (1994). The extracted sample was excited with blue light (436 nm) and the subsequent red fluorescence emission (680 nm) was recorded. Chlorophyll values were used for CTD fluorometer calibration, and allowed identification of where water samples were collected within the SCM (Figs. 6.3 – 6.6).

6.3.3. Determination of nutrient concentrations

Samples for nitrate, phosphate and silicate analysis were collected by filtering water sample through a 25 mm Whatman GF/F filter into a 15 ml polypropylene tube, which was stored in a -20 °C freezer until analysis, following methods of Kremling and Brügmann (1999) and Dore et al. (1996). Samples were slowly thawed in a fridge, with regular mixing to allow for depolymerisation of dissolved silicate. Nitrate, phosphate and silicate concentrations were determined following standard colorimetric techniques as described by Grasshoff (1976) and Kirkwood (1996), using a SEAL Analytical QuAAtro segmented flow AutoAnalyser. Detection limits for total nitrate, phosphate and silicate were 0.03 µmol l^{-l} (NIOZ, 2016), 0.01 µmol l^{-l} (NIOZ, 2015a) and 0.02 µmol l^{-l} (NIOZ, 2015b) respectively (Stinchcombe, 2017).

6.3.4. Phytoplankton community structure

Phytoplankton community structure within the SCM was assessed using inverted light microscopy and CytoSense flow cytometry. Flow cytometry allowed for quantification and

description (based on fluorescence signatures) of the pico-phytoplankton and the entire nano-phytoplankton population, not achievable with light microscopy. Microscopy allowed for taxonomic identification of cells ≥ 10 µm, not possible with flow cytometry. Therefore, cells across the entire phytoplankton size range were represented in this study.

6.3.4.1. Inverted light microscopy analysis of the phytoplankton community

Samples for phytoplankton analysis by microscopy were collected by decanting 50 ml of water sample into a darkened glass bottle and preserving in Lugol's iodine (1 % final concentration). Samples were analysed based on the methods of Utermöhl (1958), with 10 ml of preserved sample settled in a sedimentation chamber for 24 hours and cells then identified and counted using a Brunel SP951 inverted trinocular light microscope (individual cells were counted in all cases, whether they be part of a colony/chain or solitary). Numerically dominant taxa (> 50 cells per ml) were counted along a single middle transect under 100x or 250x magnification depending on cell size. Cryptophytes (> 8 µm) and unidentified small naked dinoflagellates (10 – 20 µm and 20 – 25 µm) were also counted along a single middle transect at 250x magnification. All other cells ≥ 10 µm (cells generally unidentifiable below this threshold) were counted at 100x magnification during examination of the entire chamber base plate. A complete list of phytoplankton taxa identified by microscopy is presented in Table A4.1.

Cells were identified to a species level where possible, but were identified to the genus level when species could not be differentiated accurately, e.g. *Chaetoceros spp.*, *Pseudo-nitzschia spp.*, *Rhizosolenia spp.* and *Thalassiosira spp.*. Any remaining unidentified diatoms were grouped as pennate or centric according to size (small: 20 – 40 µm length, medium: 40 – 65 µm length, large: 65 – 110 µm length; and small: 20 – 30 µm diameter, medium: 30 – 50 µm diameter, large: 60 – 150 µm diameter respectively). Unidentified dinoflagellates and ciliates were also grouped according to size and with reference to cell wall structure where appropriate (e.g. 10 – 20 µm and 20 – 25 µm naked dinoflagellates, 10 – 30 µm armoured dinoflagellates, and small (< 20 µm), medium (20 – 40 µm) and large (> 40 µm) aloricate ciliates). Some genera were classified into size categories, including *Pleurosigma* (small, medium and large: ~50 µm, 80 – 170 µm and 170 - 200 µm length), *Thalassiosira* (extra small, small, medium and large: <10 µm, 10 - 25 µm, 25 – 45 µm and > 45 µm height), *Protoperidinium* (small, medium and large: 10 - 30 µm, 30 – 65 µm and 65 - 120 µm diameter) and *Rhizosolenia* (small, medium and large: ≤ 10 µm, 10 – 20 µm and > 20 µm diameter). In the case of *Rhizosolenia*, small diameter cells appeared to be mainly *Rhizosolenia setigera* and *Rhizosolenia imbricata*, and medium and large diameter cells appeared to be mostly *Rhizosolenia imbricata* and *Rhizosolenia styliformis* across the four years.

Cell biovolume was derived for each taxon or taxon size category based on the geometric shapes and formulae of Olenina et al. (2006). Dimensions of at least 30 cells per taxon or taxon size category (only less for rare taxa) were measured with the open source software 'ImageJ'. Cell carbon concentrations were estimated using the carbon - biovolume relationships of Menden-Deuer and Lessard (2000).

6.3.4.2. Flow cytometric analysis of the phytoplankton community

Samples for phytoplankton analysis by flow cytometry were collected by decanting 10 ml of water sample into a polypropylene tube, immediately fixing with glutaraldehyde (0.25 % final concentration) and freezing at -80 °C (Marie et al., 2005). Samples were analysed with a CytoBuoy CytoSense flow cytometer and CytoUSB v5.7.5.7 data acquisition software, using two sets of data acquisition settings; one optimal for small phytoplankton (pico-phytoplankton: < 2 µm) and the other for larger phytoplankton (meso- and micro phytoplankton: 20 - 2000 µm; and nano-phytoplankton: 2 – 20 µm). Pico-phytoplankton data was acquired using a sideways scatter (SWS) trigger (25 mV) at a flow rate of 0.1 µl s^{-1} for 10000 cells, and pico-particles with a red fluorescence (RFL) signal < 10 mV were manually removed from the dataset to ensure exclusion of non-phytoplankton pico-particles/debris/electronic noise. Meso-, micro- and nano-phytoplankton data was acquired using a red fluorescence trigger (30 mV) at a flow rate of 10 µl s^{-1} for 150 seconds or 10000 cells. Cell size derived from forwards scatter (FWS) was calibrated using Thermo Fisher Scientific nonfluorescent polystyrene microspheres of a range of diameters (1, 2, 6, 10, 15 µm).

During data acquisition the CytoSense instrument recorded particle pulse shapes of FWS, SWS, RFL and orange fluorescence (OFL), enabling description of the phytoplankton community based on scatter and fluorescence properties using CytoClus v4.3.1.1 data processing software. For each sample a cytogram of total OFL vs. total RFL (TRFL) was constructed to identify cells containing phycoerythrin secondary photopigments (Jeffrey and Vesk, 1997), and a cytogram of total FWS and TRFL was generated to identify cell size. Clusters of orange fluorescing pico-phytoplankton (hereafter orange pico-phytoplankton), red fluorescing pico-phytoplankton (hereafter red pico-phytoplankton), orange fluorescing nano-phytoplankton (hereafter orange nano-phytoplankton), red fluorescing nano-phytoplankton (hereafter red nano-phytoplankton), and micro- and meso- phytoplankton could thus be resolved. As TRFL was calculated for each cell, the TRFL of the entire phytoplankton population and of each phytoplankton cluster could be determined and was used as a proxy for chlorophyll concentration, which in turn is a proxy for biomass. Note that as samples for flow cytometric analysis were not collected in 2013,

most nano-phytoplankton < 10 µm and all pico-phytoplankton within the SCM community during 2013 are not represented in this study.

6.3.5. Statistical analysis

One way analysis of variance (ANOVA) with post hoc Dunn's pairwise multiple comparison analysis was performed using SigmaPlot 13.0 software to identify significant interannual differences in the SCM chlorophyll structure characteristics of thickness (measured at half maximum intensity of the chlorophyll signal), maximum chlorophyll concentration and Chl_{50m}:Chl_{SCM}. One way ANOVA with post hoc Dunn's pairwise multiple comparison analysis was also performed to detect significant interannual changes in environmental variables that had the potential to significantly influence chlorophyll structure. These variables included SCM depth (as a proxy for mixed layer depth), SCM temperature (measured at maximal chlorophyll concentration), buoyancy frequency (maximum value associated with the thermocline), IIS (determined for the depth interval of the SCM), wind speed (30 – 90 mins before profile), current velocity (water column averaged), solar insolation (day before profile) and SCM nitrate (nutrient status indicator).

Phytoplankton community structure was investigated using PRIMER v6 software (Clarke and Warwick, 2001, Clarke and Gorley, 2006). Statistical analysis was conducted on phytoplankton carbon biomass data derived from microscope analysis of Lugol's preserved phytoplankton samples, and on phytoplankton TRFL (as a proxy for biomass) data collected from CytoSense cytometric analysis. Biomass/biomass proxy data was used instead of abundance data because it provides a more accurate representation of community structure when the community includes taxa of a range of different sizes, and because biomass is of more biogeochemical relevance than abundance (Paasche, 1960). Data was standardised by dividing carbon biomass/TRFL values by the total biomass/TRFL for a given sample, then normalised by square root transformation to moderate the influence of dominant phytoplankton on similarity between samples. To explore similarity of community structure among SCM samples collected at the repeat site over the years of study, cluster analysis with SIMPROF (Similarity Profile Analysis; significance level at 0.05) was performed, using the Bray-Curtis index as the measure of similarity. A threshold of 61 % similarity was applied to group microscope analysed phytoplankton samples by year, and a threshold of 87 % similarity was used to group CytoSense analysed phytoplankton samples by year. Post hoc analysis of similarity (one-way ANOSIM) was applied to determine the level of separation of community structure between years (given by global R value, where values close to 0 indicate no separation and values close to 1 indicate high separation), and a non-metric multi-dimensional scaling (nMDS) plot was used to visually display the separation between samples. Samples with

greater community resemblances were spatially closer than ones that were less similar. The stress level of the nMDS is a measure of how accurate a representation the ordination is, where a value below 0.2 is considered to indicate a good fit (Zuur et al., 2007). SIMPER (Similarity Percentage Analysis) was performed to investigate similarities within year clusters. SIMPER output was also used to identify contributions of each taxon/phytoplankton cell size and fluorescence (red/orange) group to the (average) overall similarity within and dissimilarity between clusters, with a limit of 90 % cumulative contribution.

To analyse the effects of environmental variables on community structure assessed by microscopy (carbon biomass data), and community structure assessed by flow cytometry (TRFL data), Redundancy Analysis (RDA; a constrained form of the linear ordination technique of principle component analysis) was performed using CANOCO 4.5 software (Lepš and Šmilauer, 2003). This multivariate analysis method selects the linear combination of environmental variables that produces the lowest total residual sum of squares in the phytoplankton data (Peterson et al., 2007). RDA was chosen because a Detrending Canonical Correspondence Analysis (DCCA) had identified the largest gradient in the environmental variables to be less than 2 standard deviation units, indicating a unimodal ordination method (Canonical Correspondence Analysis; CCA) would not be appropriate (Lepš and Šmilauer, 2003). For the RDA using carbon biomass phytoplankton data, log transformation was performed, and only taxa that contributed more than 5 % of community biomass were selected for the analysis. For the RDA using TRFL data, values were standardised to the total community TRFL for each given sample, then square root transformed (ter Braak and Šmilauer, 2002). Forward-selection was used to determine environmental variables that significantly influenced phytoplankton distribution and community structure when analysed singly (marginal effects) or together with other forward-selected variables (conditional effects), and Monte Carlo permutation tests provided a measure of statistical significance of each of the forward-selected environmental variables applied in the RDA.

6.4. Results

6.4.1. Environmental conditions and SCM characteristics

In 2013 17 profiles were collected at the repeat site between 24th June and 4th July (Fig. 6.1, 6.2 and 6.3; further details in Table A4.2). All profiles exhibited an SCM located at the base of the thermocline, between 15.5 – 27.8 m depth. Within the top 50 m of the water column 19.4 – 48.1 mg m^{-2} of chlorophyll was present, a considerable portion of which could be attributed to the SCM, which had a maximum chlorophyll concentration of 2.0 – 4.5 µg l^{-1} and thickness of <

1.0 – 11.2 m. At the SCM peak, temperature and salinity were 11.2 to 12.1 °C and 35.2 to 35.3 respectively. Buoyancy frequency reached a maximum within the thermocline (0.0010 – 0.0042 rad^2 s^{-2}), and at the depth interval of the SCM the IIS ranged from 0.25 to 8.19. Wind speed and current velocity were 1.6 – 8.9 m s^{-1} and 0.10 – 0.47 m s^{-1} respectively. Rainfall was fairly minimal (0 – 3 mm d^{-1}) and solar insolation varied between 2.10 – 5.69 kWh m^{-2} d^{-1} (Fig. 6.3; further details in Table A4.2).

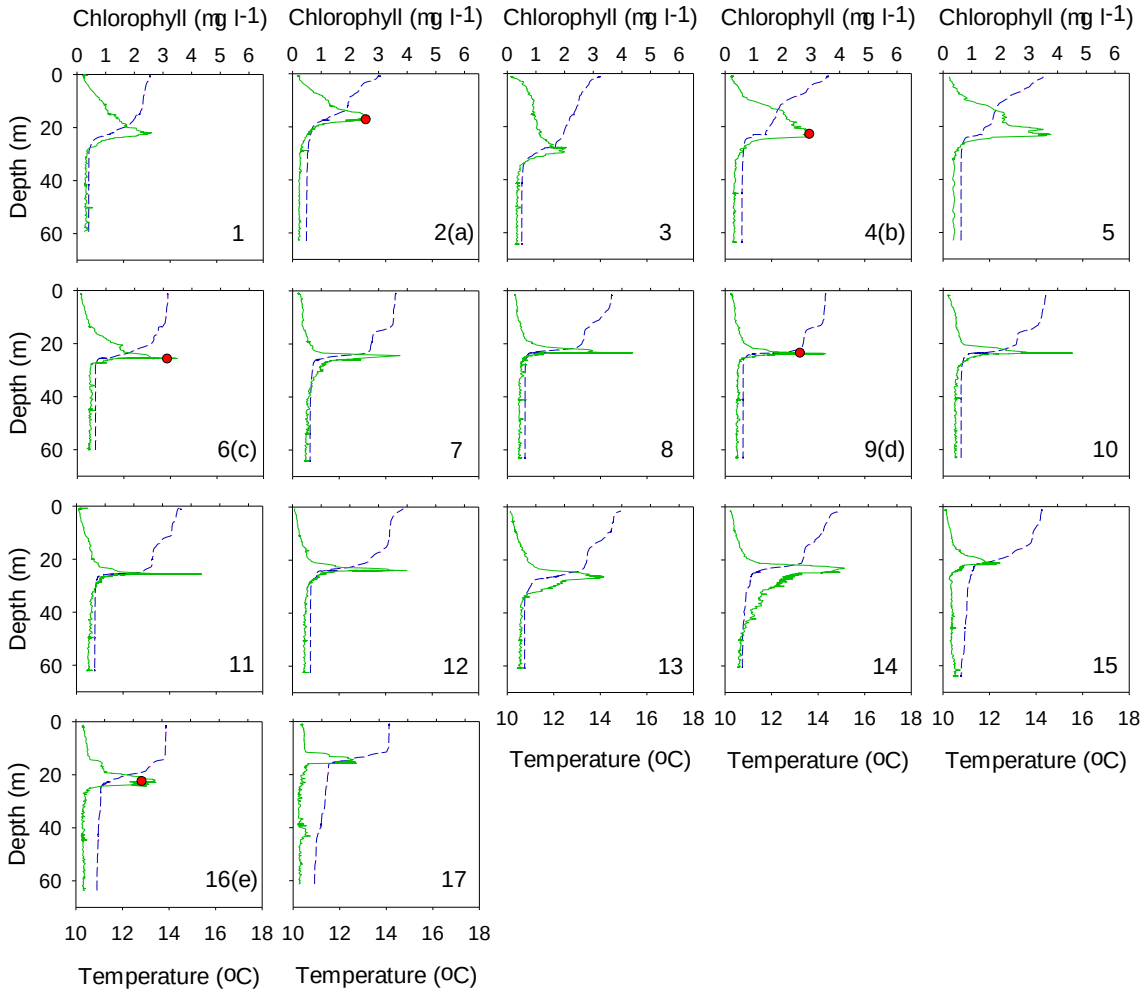

Figure 6.3. Temperature and chlorophyll profiles at the repeat site in the Western English Channel (cast numbers given in the bottom right hand corner of each plot, with phytoplankton sample IDs in brackets) collected during June/July 2013 (further details provided in Table A4.2). The green line represents chlorophyll concentration determined from CTD chlorophyll-fluorescence, the blue dashed line temperature and the red circles where water samples were collected for phytoplankton analysis.

In 2014 18 profiles were collected at the repeat site between 17th June and 3rd July (Fig. 6.1, 6.2 and 6.4; further details provided in Table A4.2). With the exception of 26th June (cast number 6; Fig. 6.4), all profiles exhibited a clear SCM, located between 16.6 - 35.5 m and generally associated with the base of the thermocline. SCM thickness varied between 2.7 – 14.6 m and

maximum chlorophyll concentration was fairly low, typically < 3.5 µg l^{-1}, yet chlorophyll within the top 50 m of the water column consistently exceeded 40 mg m^{-2}. At the depth of the SCM peak temperature ranged from 12.0 to 14.4 ^{o}C, salinity was quite consistent (35.1 to 35.3) and nutrient concentrations were, on average, 0.55, 1.39 and 0.10 µmol l^{-1} for nitrate, silicate and phosphate respectively. The strength of the density gradient was considerable (0.0012 – 0.0058 rad^2 s^{-2}), but at the depth interval of the SCM the IIS was relatively low, ranging from < 0.25 to 1.56. Wind speed and current velocity ranged from 1.1 – 11.7 m s^{-1} and 0.12 – 0.41 m s^{-1} respectively. During the survey there were dry days, but also substantial rainfall (0 – 11 mm d^{-1}) and solar insolation varied between 5.54 – 7.77 kWh m^{-2} d^{-1} (Fig. 6.4; details in Table A4.2).

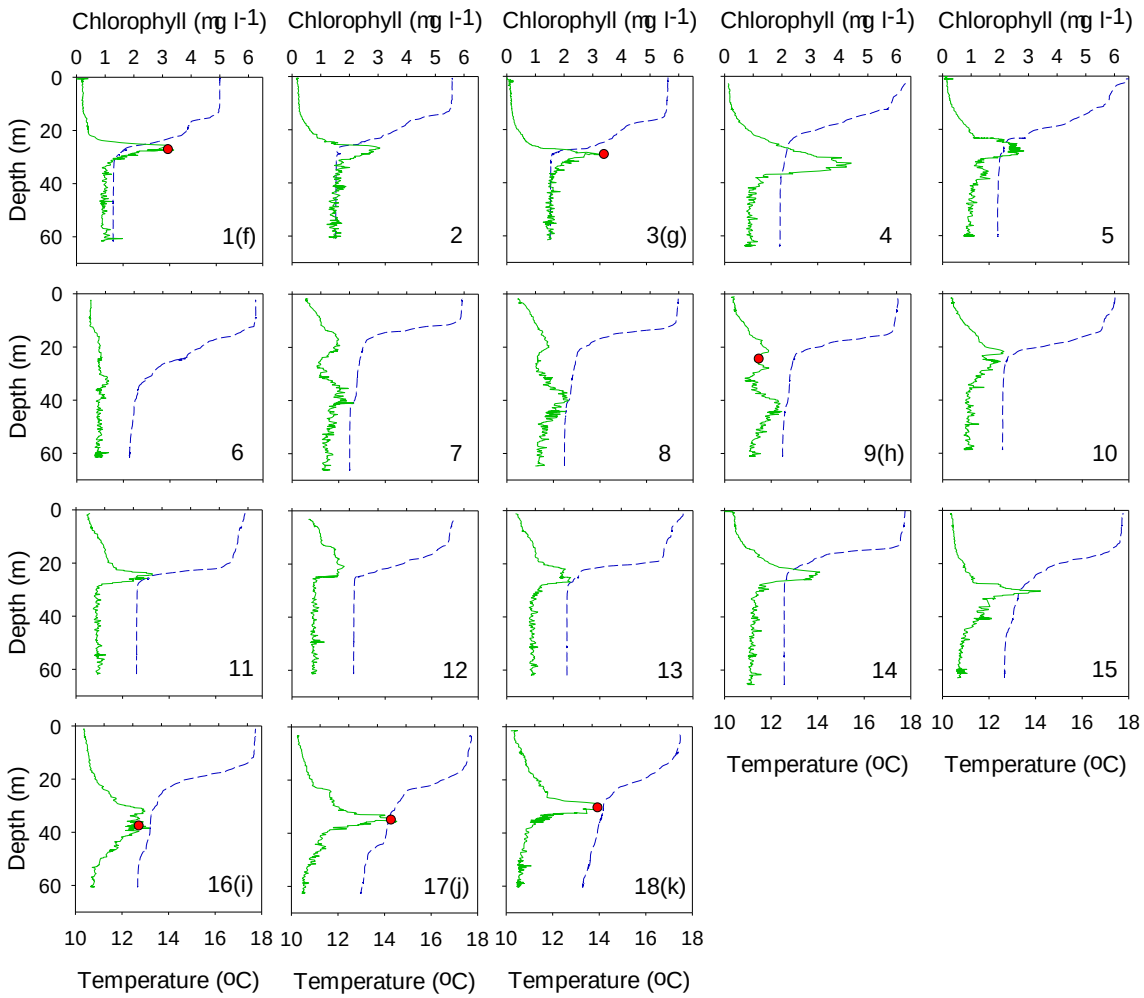

Figure 6.4. Temperature and chlorophyll profiles at the repeat site in the Western English Channel (cast numbers given in the bottom right hand corner of each plot, with phytoplankton sample IDs in brackets) collected during June/July 2014 (further details provided in Table A4.2). The green line represents chlorophyll concentration determined from CTD chlorophyll-fluorescence, the blue dashed line temperature and the red circles where water samples were collected for phytoplankton analysis.

In 2015 20 profiles were collected at the repeat site between 22th June and 2nd July (Fig. 6.1, 6.2 and 6.5; details in Table A4.2). An SCM was present in all profiles, typically corresponding with the base of the thermocline, at a depth of 24.8 – 36.1 m. The top 50 m of the water column was responsible for 18.0 – 99.5 mg m^{-2} of chlorophyll, a majority of which was located within the SCM, which had a maximum chlorophyll concentration of 2.7 – 19.2 µg l^{-1} and a thickness of < 1.0 – 12.0 m. Within the thermocline maximum buoyancy frequency varied from 0.0011 to 0.0032 rad^2 s^{-2} and the IIS was generally high (0.79 – 24.62). Salinity at the SCM peak was constant at 35.3, temperature was 11.7 – 12.5 °C, and average nitrate, silicate and phosphate concentrations were 0.33, 1.14 and 0.15 µmol l^{-1} respectively. Solar insolation, current velocity and wind speed were 3.15 – 7.82 kWh m^{-2} d^{-1}, 0.04 – 0.36 m s^{-1} and 1.5 – 10.0 m s^{-1} respectively, and there was little to no rain (0 – 2 mm d^{-1}) (Fig. 6.5; details in Table A4.2).

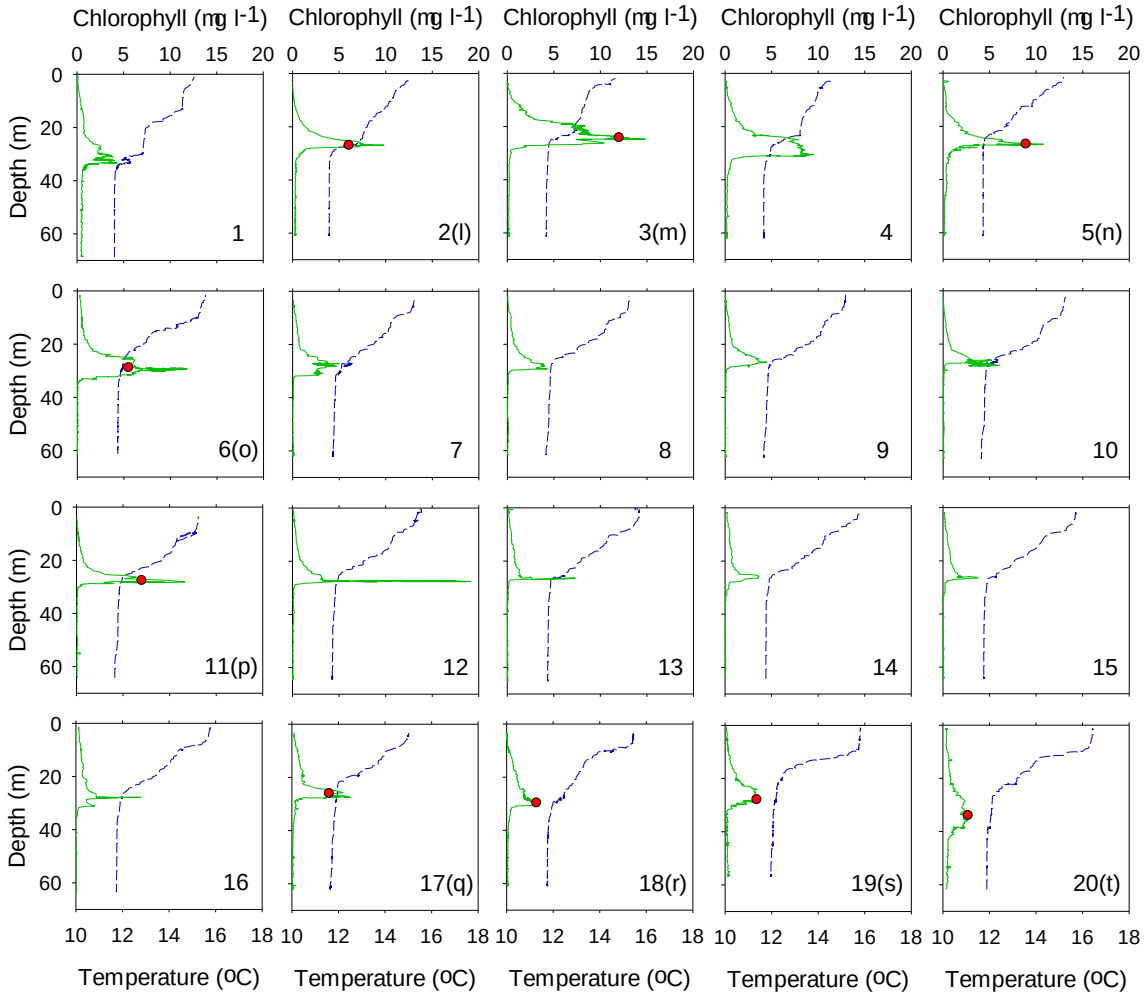

Figure 6.5. Temperature and chlorophyll profiles at the repeat site in the Western English Channel (cast numbers given in the bottom right hand corner of each plot, with phytoplankton sample IDs in brackets) collected during June/July 2015 (further details provided in Table A4.2). The green line represents chlorophyll concentration determined from CTD chlorophyll-fluorescence, the blue dashed line temperature and the red circles where water samples were collected for phytoplankton analysis.

In 2016 16 profiles were taken at the repeat site from the 20th to 30th June (Fig. 6.1, 6.2 and 6.6; details in Table A4.2). The SCM, which varied widely in thickness (< 1.0 – 19.7 m), was typically at the base or just below the thermocline at depths of 12.3 – 34.5 m. Chlorophyll within the top 50 m was consistently high, generally > 40 mg m^{-2}, despite fairly low maximum SCM chlorophyll concentrations (< 2.5 µg l^{-1}) in 63 % of profiles. In the other 37 % of profiles maximum SCM chlorophyll concentration was 3.3 - 6.2 µg l^{-1}. At the SCM peak, temperature varied by over 1 °C (11.8 – 13.1 °C), salinity by 0.2 (35.1 – 35.3), and average nitrate, silicate and phosphate concentrations were 0.39, 0.61 and 0.22 µmol l^{-1} respectively. The density gradient was generally strong, often exceeding 0.0025 rad^2 s^{-2}, yet at the depth interval of the SCM the IIS was low, ranging from < 0.25 to 1.00. Almost no rainfall was recorded over the survey period, the wind reached speeds of 3.2 – 11.9 m s^{-1}, current velocity ranged from 0.16 to 0.35 m s^{-1} and solar insolation varied between 2.29 and 6.90 kWh m^{-2} d^{-1} (Fig. 6.6; details in Table A4.2).

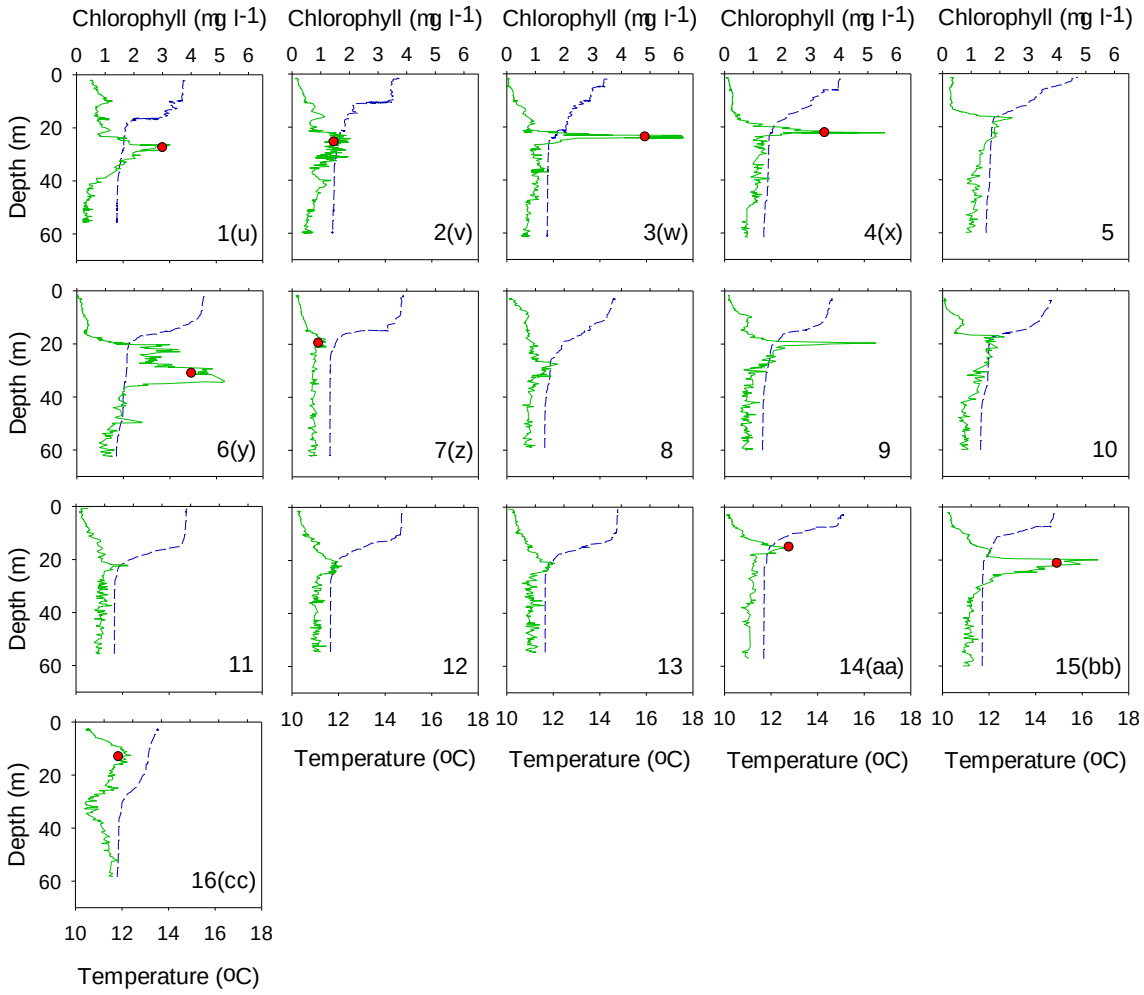

Figure 6.6. Temperature and chlorophyll profiles at the repeat site in the Western English Channel (cast numbers given in the bottom right hand corner of each plot, with phytoplankton sample IDs in brackets) collected during June 2016 (further details provided in Table A4.2). The green line represents chlorophyll concentration determined from CTD chlorophyll-fluorescence, the blue dashed line temperature and the red circles where water samples were collected for phytoplankton analysis.

The interannual variation in SCM characteristics and environmental conditions over the years of 2013 to 2016 is summarised in Table 6.1.

Table 6.1. Mean and standard deviation of SCM characteristics and environmental variables during the summer field surveys of 2013, 2014, 2015 and 2016.

	2013	2014	2015	2016
SCM thickness (m)	4.0 ± 3.2	6.3 ± 3.4	4.1 ± 3.1	7.6 ± 6.5
SCM max chl conc. (µg l^{-1})	3.3 ± 0.8	2.7 ± 0.8	7.3 ± 4.4	3.1 ± 1.8
Top 50 m chl (mg m^{-2})	33.2 ± 9.3	51.9 ± 6.9	42.3 ± 21.5	48.6 ± 12.2
SCM depth (m)	23.0 ± 3.2	26.2 ± 5.0	28.1 ± 2.5	21.7 ± 5.4
SCM temp. (°C)	11.6 ± 0.3	13.1 ± 0.7	12.0 ± 0.2	12.1 ± 0.3
SCM salinity	35.2 ± 0.04	35.2 ± 0.04	35.3 ± 0.01	35.3 ± 0.06
Buoyancy freq. (rad^2 s^{-2})	0.0025±0.0009	0.0029±0.0012	0.0016±0.0005	0.0036±0.0015
IIS	3.64 ± 2.88	0.42 ± 0.41	9.07 ± 7.83	0.62 ± 0.66
Wind speed (m s^{-1})	4.6 ± 1.9	6.4 ± 3.3	5.6 ± 2.2	6.8 ± 2.3
Current velocity (m s^{-1})	0.25 ± 0.12	0.24 ± 0.09	0.14 ± 0.09	0.28 ± 0.06
Solar insolation (kWh m^{-2} d^{-1})	4.34 ± 1.23	6.49 ± 1.34	5.62 ± 1.68	4.40 ± 1.78
Rainfall (mm d^{-1})	0.9 ± 1.3	2.7 ± 3.3	0.3 ± 0.7	0.2 ± 0.6
Nitrate (µmol l^{-1})	-	0.55 ± 0.20	0.33 ± 0.35	0.39 ± 0.12
Silicate (µmol l^{-1})	-	1.39 ± 0.66	1.14 ± 0.63	0.61 ± 0.16
Phosphate (µmol l^{-1})	-	0.10 ± 0.05	0.15 ± 0.09	0.22 ± 0.05

6.4.2. Environmental influence on SCM chlorophyll structure

SCM thickness did not significantly vary over the study years (Fig. 6.7a and Table 6.1), but SCM maximum chlorophyll concentration was significantly higher in 2015 (average of 7.3 µg l^{-1}) compared to 2013 (p = 0.010), 2014 (p < 0.001) and 2016 (p < 0.001), when average values were 3.3, 2.7 and 3.1 µg l^{-1} respectively (Fig. 6.7b and Table 6.1). Chlorophyll within the top 50 m of the water column relative to SCM maximum chlorophyll concentration (Chl_{50m}:Chl_{SCM}) was significantly less in 2013 and 2015 (average ratios of 10.5 and 7.0) compared to 2014 (p = 0.003 and < 0.001 respectively) and 2016 (p = 0.015 and < 0.001 respectively), when Chl_{50m}:Chl_{SCM} averaged 21.7 and 19.3 respectively (Fig. 6.7c and Table 6.1). This indicates chlorophyll was generally more dispersed in the water column in 2014 and 2016 compared to 2013 and 2015.

The higher maximum SCM chlorophyll concentrations and larger contributions of the SCM to water column chlorophyll in 2015 coincided with significantly greater instantaneous stability at the depth interval of the SCM (average IIS of 9.07) than in 2014 (p < 0.001) and 2016 (p < 0.001) (Fig. 6.8a and Table 6.1), despite significantly lower stratification strength in 2015 (p < 0.001; Fig. 6.8b and Table 6.1). The increased IIS values in 2015 coincided with lower current velocities (average current velocity of 0.14 m s^{-1}) than in other years (2013: p = 0.011, 2014: p = 0.014, and 2016: p < 0.001) when current velocity was around 0.10 m s^{-1} faster on average (Fig.

6.8c and Table 6.1). Thus, the lesser maximum SCM chlorophyll concentrations with higher Chl_{50m}:Chl_{SCM} in 2014 and 2016 compared to 2015 may be attributed to significantly reduced stability, with IIS values averaging 0.42 and 0.67 respectively (Fig. 6.8a and Table 6.1). In 2013 the significantly lower Chl_{50m}:Chl_{SCM} relative to 2014 and 2016 may be ascribed to greater stability (average IIS of 3.64) than in 2014 (p = 0.004) and 2016 (p = 0.048) (Fig. 6.8a and Table 6.1). Despite greater instantaneous stability measurements, SCM maximum chlorophyll concentrations were comparatively low, coinciding with significantly lower SCM temperatures than in any other year (p < 0.02) (Fig. 6.8d and Table 6.1).

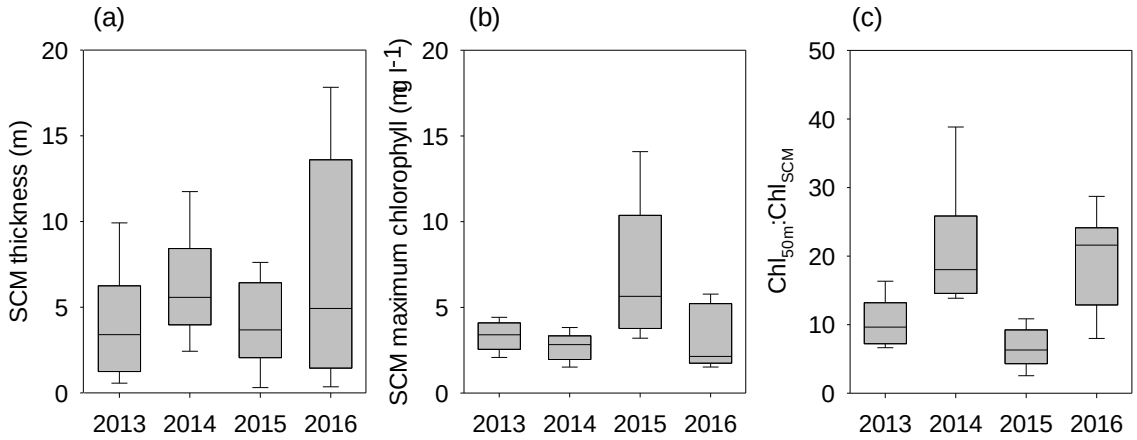

Figure 6.7. Boxplots (median, upper and lower quartile, and minimum and maximum values) of the SCM characteristics of (a) thickness, (b) maximum chlorophyll and (c) Chl_{50m}:Chl_{SCM} for 2013 – 2016.

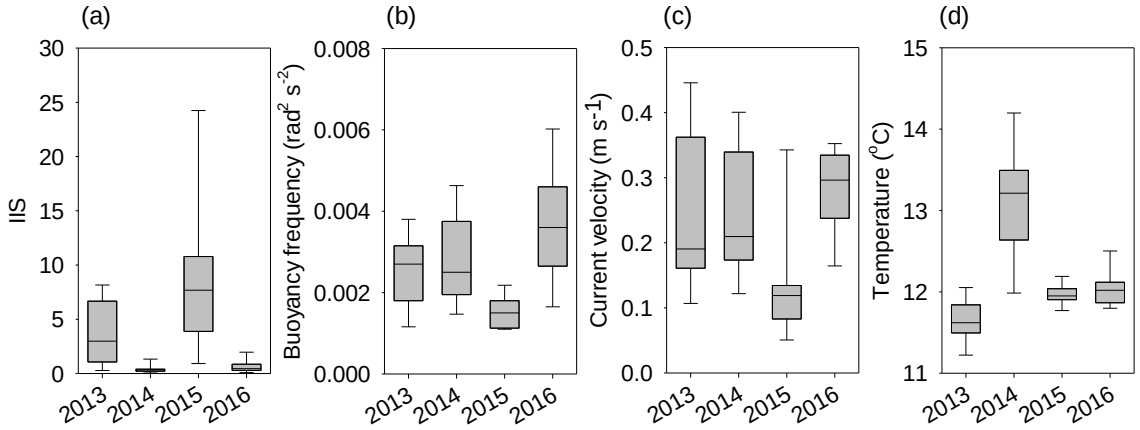

Figure 6.8. Boxplots (median, upper and lower quartile, and minimum and maximum values) for 2013 - 16 of environmental factors (a) IIS, (b) buoyancy frequency, (c) current velocity and (d) SCM temperature.

Other environmental parameters (Table 6.1) that significantly changed during the 4 years of study and had potential to influence SCM chlorophyll structure include nutrient concentration (p = 0.017), solar insolation (p = 0.012), SCM depth as a proxy for mixed layer depth (p < 0.001) and wind speed (p = 0.049). However, a tangible association between these parameters and changing SCM chlorophyll structure over the years of study was not discernible.

6.4.3. SCM phytoplankton community structure

6.4.3.1. Community structure by flow cytometry

In 2014 the community within the SCM was predominantly made up of micro- and meso-phytoplankton, and red nano-phytoplankton, which contributed 30 – 62 % and 32 – 63 % to community TRFL respectively. Orange nano-phytoplankton, orange pico- and red pico-phytoplankton combined consistently contributed less than 8 % to community TRFL (Fig. 6.9). In 2015 larger phytoplankton (micro- and meso-) dominated the SCM community, contributing 67 – 95 % of TRFL. Red nano-phytoplankton also made a notable contribution to the community, contributing 4 – 21 % of TRFL, but orange nano-phytoplankton, orange pico-phytoplankton and red pico-phytoplankton combined, generally never contributed more than 6 % to community TRFL (Fig. 6.9). In 2016 the SCM community was mainly a mix of micro- and meso-phytoplankton, red nano-phytoplankton and orange pico-phytoplankton, contributing 6 – 30 %, 28 – 64 % and 11 – 36 % of TRFL respectively. In contrast, orange nano-phytoplankton and red pico-phytoplankton typically contributed < 7 % to community TRFL (Fig. 6.9).

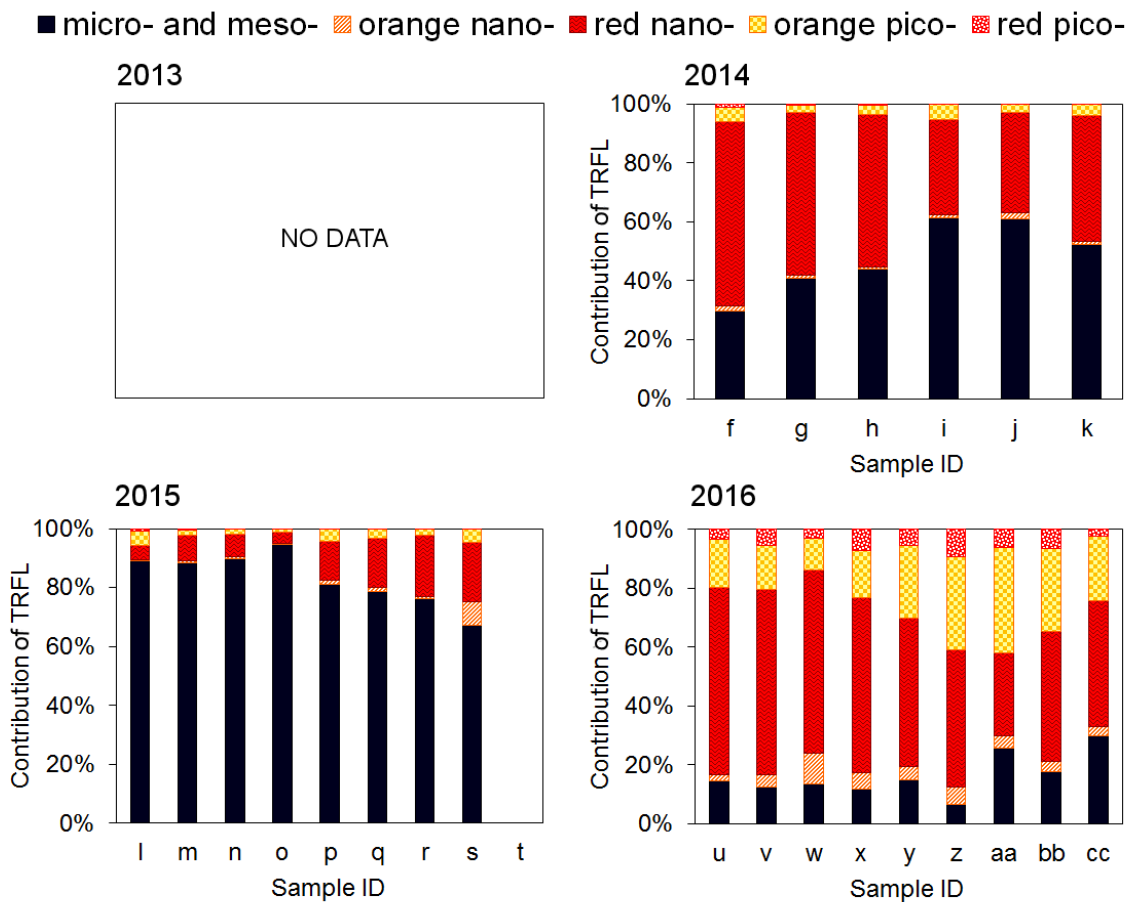

Figure 6.9. Phytoplankton community structure within the SCM at the repeat site in the Western English Channel in summer (June/July) 2014, 2015 and 2016 (details in Table A4.2), based on data compiled using CytoSense flow cytometry (no phytoplankton samples for CytoSense flow cytometry analysis were collected in 2013 or for sample t in 2015).

A cluster analysis with ANOSIM using CytoSense TRFL data identified the SCM phytoplankton community to be statistically distinct between the years of 2014 to 2016 (p = 0.001), and a global R of 0.93 (R statistic from pairwise tests varied from 0.81 to 1) indicated the sample clusters for each year were well separated. nMDS analysis provided a 2D spatial representation of the separation between samples from 2014, 2015 and 2016 based on their phytoplankton TRFL values, and a stress level of 0.03 verified the representation to be accurate (Fig. 6.10).

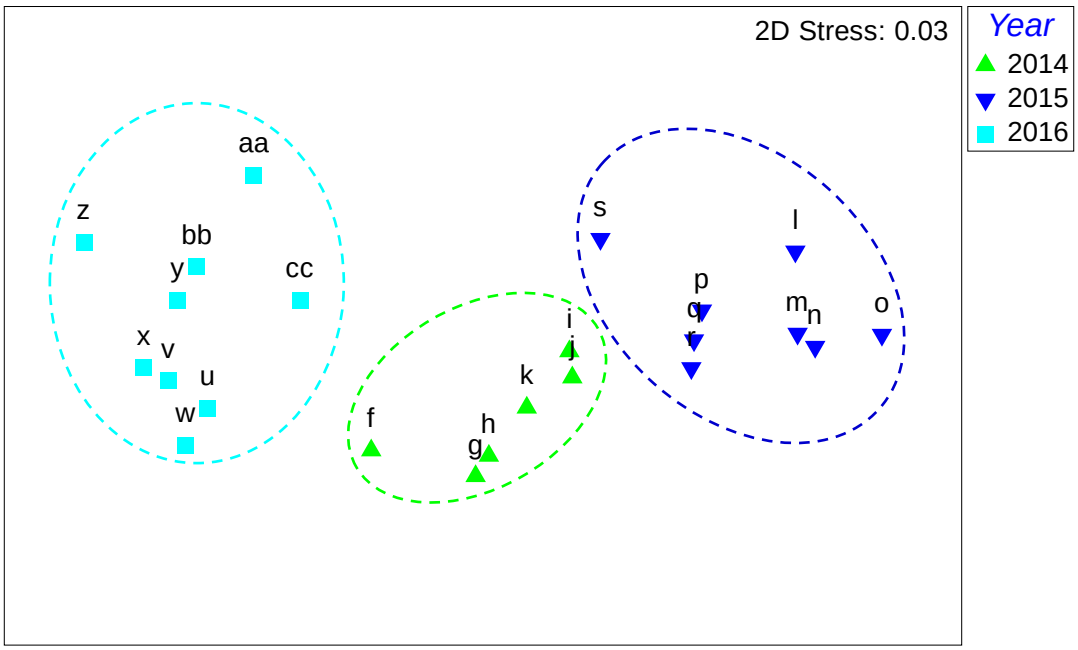

Figure 6.10. nMDS plot representing the similarity in SCM phytoplankton community structure at the repeat site in the Western English Channel between 2014 (green triangles), 2015 (dark blue inverted triangles) and 2016 (light blue squares), based on CytoSense TRFL values. The 2D stress value is included, dotted outlines represent a sample similarity level of 87 % and each sample is labelled with its sample ID.

In 2014 average similarity of samples was 90.9 %, and the top three contributors of this similarity were micro- and meso-phytoplankton (40.5 %), red nano-phytoplankton (39.7 %) and orange pico-phytoplankton (10.8 %). In 2015 average similarity of samples was 89.8 %, and the top three phytoplankton groups responsible for similarity were micro- and meso-phytoplankton (62.5 %), red nano-phytoplankton (19.0 %) and orange pico-phytoplankton (9.6 %). In 2016 average similarity was 89.4 %, and the top three phytoplankton groups accountable for this similarity were red nano-phytoplankton (36.7 %), orange pico-phytoplankton (22.8 %) and micro- and meso- phytoplankton (19.2 %) (Fig. 6.9 and Table 6.2).

Table 6.2. The top three contributors to similarity within each year based on phytoplankton data compiled using CytoSense flow cytometry (no phytoplankton samples for CytoSense flow cytometry analysis were collected in 2013). Average similarity within each year is also given.

	Top three contributors to similarity (with % contributions)			
	2013	2014	2015	2016
1.	-	Micro- and meso-phytoplankton (40.51)	Micro- and meso-phytoplankton (62.50)	Red nano-phytoplankton (36.69)
2.	-	Red nano-phytoplankton (39.65)	Red nano-phytoplankton (18.97)	Orange pico-phytoplankton (22.76)
3.	-	Orange pico-phytoplankton (10.84)	Orange pico-phytoplankton (9.62)	Micro- and meso-phytoplankton (19.19)
Cumulative contribution (%)	-	91.00	91.09	78.63
Average similarity (%)	-	90.88	89.78	89.37

6.4.3.2. Community structure by microscopy

The ≥ 10 µm community within the SCM identified using light microscopy was generally either predominantly a mix of diatoms and dinoflagellates (2013, 2014 and 2016) or strongly dominated by dinoflagellates (2015). The importance of diatoms in the SCM community in 2014 and 2016, and the dominance of dinoflagellates in 2015 is supported by fucoxanthin to chlorophyll a ratios and peridinin to chlorophyll a ratios for 2014 – 2016 (Fig. A4.1).

In 2013 diatoms and dinoflagellates contributed 37 – 63 % and 36 – 62 % of carbon biomass respectively. Ciliates (mostly aloricate) and flagellates (mainly cryptophytes), on the other hand, consistently contributed less than 1.5 % of carbon biomass combined. The diatom population was generally dominated by *Pseudo-nitzschia spp.*, typically responsible for over 30 % of biomass. *Rhizosolenia/Proboscia spp.* and *Chaetoceros spp.* were also noteworthy contributors, accounting for up to 30 % and 6 % of biomass respectively. The dinoflagellate population was dominated by small (10 – 25 µm) naked dinoflagellates (genus/species not identified), *Ceratium lineatum* and *Diplopsalis lenticula*, which accounted for 7 – 26 %, 2 – 22 % and 1 – 18 % of carbon biomass respectively. *Protoperidinium spp.* also made an important contribution to the community, responsible for up to 7 % of carbon biomass (Fig. 6.11; further details provided in Table A4.1).

In 2014 diatoms and dinoflagellates accounted for 3 – 47 % and 41 – 83 % of carbon biomass respectively, and flagellates (largely *Dictyocha spp.*, *Trachelomonas volvocinopsis*, *Chrysochromulina spp.* and *Solenicola setigera*) and ciliates (mix of *Tiarina fusus* and other aloricate ciliates, and tintinnids) only 1 – 4 % and 7 – 13 % respectively. Key diatoms were *Lauderia annulata*, *Leptocylindrus danicus* and *Rhizosolenia/Proboscia spp.*, responsible for up to 13 %, 31 % and 14 % of biomass respectively. The dinoflagellate population was largely dominated by small (10 – 25 µm) naked dinoflagellates (genus/species not identified), *Ceratium lineatum* and *Gyrodinium/Ceratoperidinium spp.*, which contributed 15 – 28 %, 5 – 19 % and 5 – 22 % of carbon biomass respectively. *Dinophysis spp.* and *Polykrikos spp.* also made considerable contributions to the community, accounting for up to 19 % and 11 % of estimated biomass (Fig. 6.11; further details provided in Table A4.1).

In 2015 dinoflagellates typically constituted the majority of the phytoplankton community (generally > 65 %) and the dinoflagellate that was largely responsible for this dominance was *Ceratium fusus*, which accounted for up to 68 % of carbon biomass. Other important dinoflagellates included small (10 – 25 µm) naked dinoflagellates (genus/species not identified), *Ceratium lineatum*, *Dinophysis spp.*, *Gyrodinium/Ceratoperidinium spp.* and *Protoperidinium spp.*, accounting for up to 5 %, 36 %, 3 % and 4 % of the community respectively. Diatoms (chiefly *Chaetoceros spp.*, *Leptocylindrus spp.* and *Proboscia truncata*), flagellates (largely *Chrysochromulina spp.*, cryptophytes*, Dictyocha spp.* and *Solenicola setigera*), ciliates (mainly aloricate, including *Tiarina fusus*) and non-flagellated chlorophyceae contributed 2 – 11 %, 4 – 12 %, 6 – 41 % and 0 – 0.3 % of carbon biomass respectively (Fig. 6.11; details in Table A4.1).

In 2016 diatoms generally contributed 8 – 57 % of community biomass, with *Chaetoceros spp.* being the dominant diatom, accounting for 2 – 36 % of carbon biomass. Other notable diatoms were *Pseudo-nitzschia spp*., *Rhizosolenia/Proboscia spp.* and *Stephanopyxis turris*, which made contributions of up to 16 %, 2 % and 4 % respectively. Dinoflagellates were accountable for 26 – 68 % of the community, primarily due to small (10 – 25 µm) naked dinoflagellates (genus/species not identified), which were responsible for 10 – 37 % of biomass. Other important dinoflagellates included *Ceratium lineatum*, *Gyrodinium/Ceratoperidinium spp.*, *Katodinium glaucum* and *Protoperidinium spp.*, each which made biomass contributions up to 13 %, 9 %, 2 % and 12 % respectively. Ciliates (aloricate and tintinnids), flagellates (mainly *Chrysophaerella longispina*, cryptophytes and *Trachelomonas volvocinopsis*) and non-flagellated chlorophyceae constituted 6 – 56 %, 1 – 7 % and 0 – 0.1 % of the phytoplankton community respectively (Fig. 6.11; further details provided in Table A4.1).

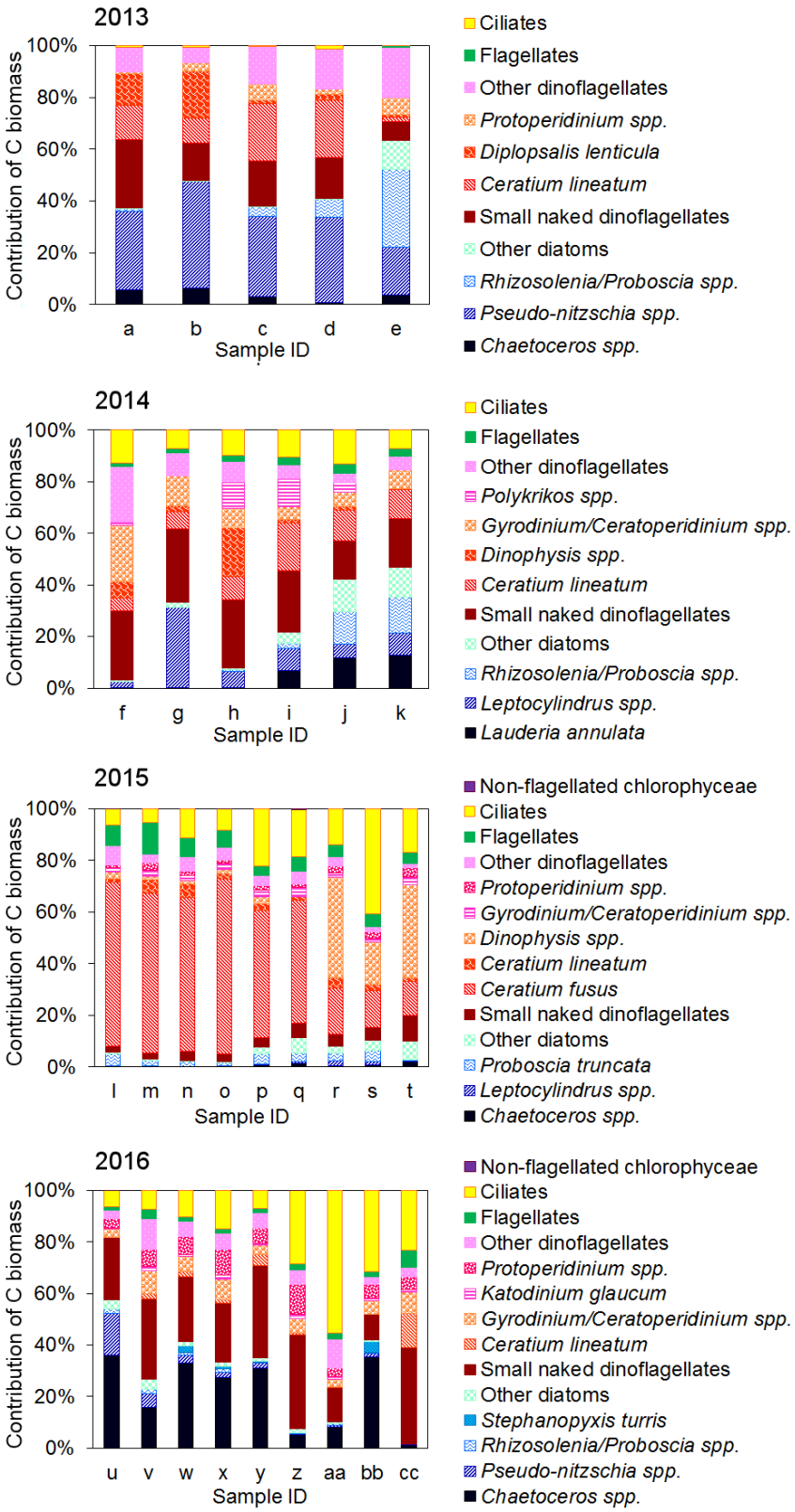

Figure 6.11. Phytoplankton community structure within the SCM at the repeat site in the Western English Channel in summer (June/July) 2013, 2014, 2015 and 2016 (details in Table A4.2), based on data compiled using inverted light microscopy. Diatom taxa carbon biomass is indicated by blue colouration and dinoflagellate taxa carbon biomass by red colouration.

A cluster analysis with ANOSIM using biomass data showed the SCM phytoplankton community to be statistically distinct between the years of 2013 to 2016 (p = 0.001), and a global R of 0.98 (R statistic from pairwise tests varied from 0.94 to 1) indicated the sample clusters for each year were well separated. An nMDS analysis provided a 2D spatial representation of the separation between samples from 2013, 2014, 2015 and 2016 based on their phytoplankton biomass values, and a stress level of 0.1 verified the representation to be accurate (Fig. 6.12). Taxa whose cumulative contribution to similarity within a year was approximately 90 % are given in Table A4.3.

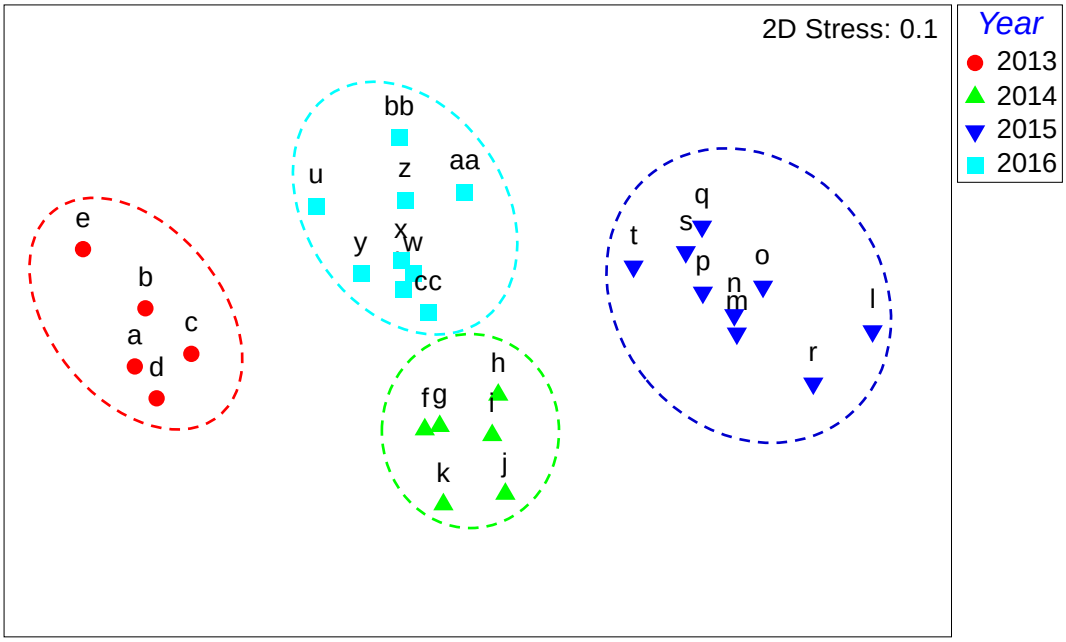

Figure 6.12. nMDS plot representing similarity in SCM phytoplankton community structure at the repeat site in the Western English Channel between 2013 (red circles), 2014 (green triangles), 2015 (dark blue inverted triangles) and 2016 (light blue squares), based on carbon biomass data. The 2D stress value is included, dotted outlines signify a similarity level of 61 % and each sample is labelled with its sample ID.

In 2013 average similarity of samples was 70.4 %, and the top five taxa to account for similarity were small *Pseudo-nitzschia spp.* (20.0 %), 10-20 µm naked dinoflagellates (12.4 %), *Ceratium lineatum* (10.5 %), *Chaetoceros spp.* (6.0 %) and *Diplopsalis lenticula* (5.6 %). In 2014 average similarity of samples was 66.9 %, and the top five contributors of this similarity were 20 - 25 µm naked dinoflagellates (9.3 %), 10 - 20 µm naked dinoflagellates (8.4 %), *Ceratium lineatum* (8.0 %), *Gyrodinium spp.* (6.6 %) and *Leptocylindrus danicus* (6.5 %). In 2015 average similarity of samples was 67.6 %, and the top five taxa responsible for similarity were *Ceratium fusus* (18.5 %), large aloricate ciliates (8.0 %), 10 - 20 µm naked dinoflagellates (5.2 %), *Ceratium lineatum* (4.8 %) and *Proboscia truncata* (4.7 %). In 2016 average similarity was 69.6 %, and the top 5 contributors of this similarity were *Chaetoceros spp.* (10.5 %), 10 - 20 µm naked

dinoflagellates (10.4 %), large aloricate ciliates (8.8 %), 20 - 25 µm naked dinoflagellates (8.8 %) and *Protoperidinium spp.* (5.9 %) (Fig. 6.11 and Table 6.3; full data given in Table A4.3).

Table 6.3. The five greatest contributors to similarity within each year based on phytoplankton data compiled using inverted light microscope analysis. Average similarity within each year is also given.

	Top five contributors to similarity (with % contributions)			
	2013	2014	2015	2016
1.	S *Pseudo-nitzschia spp.* (20.03)	20-25 µm naked dinoflagellates (9.25)	*Ceratium fusus* (18.45)	*Chaetoceros spp.* (10.53)
2.	10-20 µm naked dinoflagellates (12.42)	10-20 µm naked dinoflagellates (8.38)	L aloricate ciliates (8.02)	10-20 µm naked dinoflagellates (10.38)
3.	*Ceratium lineatum* (10.49)	*Ceratium lineatum* (7.97)	10-20 µm naked dinoflagellates (5.24)	L aloricate ciliates (8.79)
4.	*Chaetoceros spp.* (5.97)	*Gyrodinium spp.* (6.60)	*Ceratium lineatum* (4.76)	20-25 µm naked dinoflagellates (8.76)
5.	*Diplopsalis lenticula* (5.57)	*Leptocylindrus danicus* (6.46)	*Proboscia truncata* (4.73)	L *Protoperidinium spp.* (5.90)
Cumulative contribution (%)	54.47	38.66	41.21	44.36
Average similarity (%)	70.38	66.87	67.59	69.59

6.4.4. Environmental influence on SCM phytoplankton community structure

6.4.4.1. Environmental influence on community structure by flow cytometry

Environmental variables that accounted for the variance in TRFL of the five cell size and fluorescence phytoplankton groups (micro-and meso-phytoplankton, red nano-phytoplankton, orange nano-phytoplankton, orange pico-phytoplankton and red pico-phytoplankton) were assessed using RDA (Fig. 6.13 and Table 6.4). In the ordination diagram (Fig. 6.13) the degree of association between the different phytoplankton groups and environmental variables is indicated by their proximity. Close proximity in the same or opposite direction indicates positive or negative correlation and the longer the arrow the stronger the correlation, whereas no proximity suggests a weak or no relationship. All canonical axes explained 99.9 % of the variance (p = 0.003), suggesting the measured environmental variables explained almost all of the variation in the structure of the SCM community as assessed by flow cytometry over the 3 years, when all axes were analysed together (Table 6.4). The eigenvalues (λ, dimensionless; Table 6.4) associated with the environmental variables are shown in the order of the variance

in the data they explained individually (marginal effects – λ_1 in Table 6.4), along with the significance of that variable (according to forward selection and a Monte Carlo permutations test; conditional effects - λ_a in Table 6.4). The variables that were considered to be significant were buoyancy frequency (Buoyancy; $\lambda_a = 0.41$, $p = 0.001$), stability (IIS; $\lambda_a = 0.19$, $p = 0.002$) and silicate concentration (Si; $\lambda_a = 0.15$, $p = 0.002$).

The SCM community was consistently dominated by micro- and meso-phytoplankton when waters had high stability with relatively higher SCM silicate (2015 - mean IIS of 9.07, and mean silicate of 1.14 µmol l^{-1}; Table 6.1). Red nano-phytoplankton accounted for greater proportions of the community in waters with low stability (2014 and 2016 – mean IIS of 0.42 and 0.62 respectively; Table 6.1). Orange nano- and all pico-phytoplankton contributed more to the community when silicate in the SCM was lowest and when stratification was strongest (2016 - mean silicate of 0.61 µmol l^{-1} and buoyancy frequency of 0.0036 rad^2 s^{-2}; Table 6.1) (Fig. 6.13).

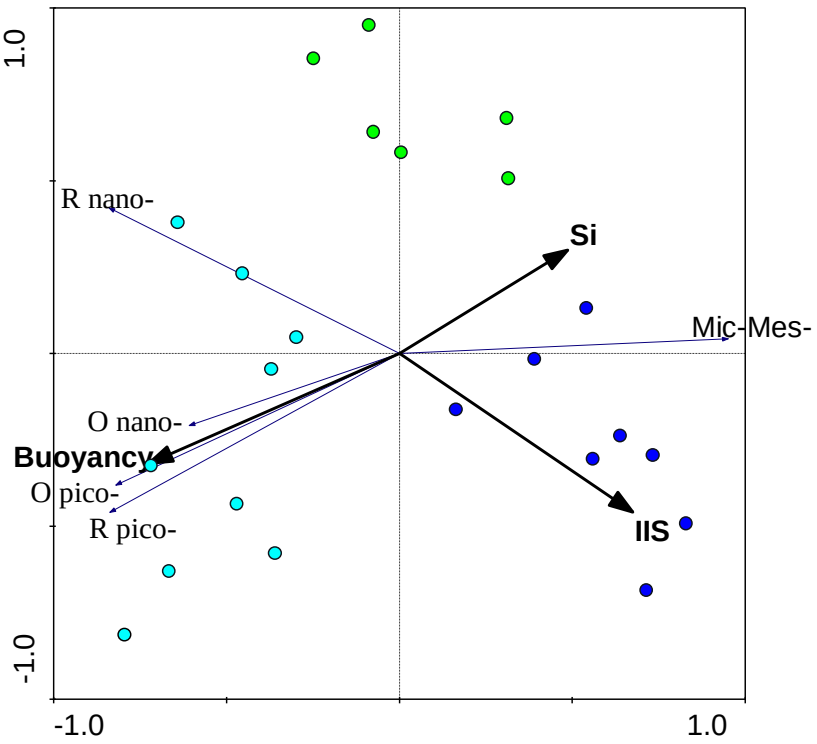

Figure 6.13. Ordination diagram generated from redundancy analysis (RDA). The triplot shows cell size and fluorescence (red/orange) phytoplankton groups (thin blue lines), environmental variables identified to describe a significant portion of the variability in the phytoplankton data by the RDA (thick black lines), and samples (closed circles, where colours refer to year groups: green = 2014, dark blue = 2015, and light blue = 2016). Mic-Mes- refers to micro- and meso-phytoplankton, O nano- is orange nano-phytoplankton, R nano- is red nano-phytoplankton, O pico- is orange pico-phytoplankton, and R pico- is red pico-phytoplankton. The significant environmental variables included buoyancy frequency (buoyancy; rad^2 s^{-2}), instantaneous index of stability (IIS) and silicate concentration (Si; µmol l^{-1}).

Table 6.4. Variance explained by each of the environmental variables included in the redundancy analysis when analysed individually (λ_1, marginal effects) or when analysed together with other forward-selected variables (λ_a, conditional effects). Significant *p* values ($p < 0.05$; in bold) indicate the variables that, combined, significantly explain the variation in the analysis. Buoyancy is buoyancy frequency ($rad^2\ s^{-2}$), IIS is instantaneous index of stability, Si is silicate concentration ($\mu mol\ l^{-1}$), depth is SCM depth (m; as a proxy for mixed layer depth), currents is current velocity ($m\ s^{-1}$), solar is daily solar insolation ($kWh\ m^{-2}\ d^{-1}$), temp is temperature (°C), P is phosphate concentration ($\mu mol\ l^{-1}$), Ni:Si and Ni:P are nitrate to silicate and phosphate ratios, Ni is nitrate concentration ($\mu mol\ l^{-1}$), wind is wind speed ($m\ s^{-1}$) and rain is rainfall ($mm\ d^{-1}$). The RDA summary is also included, where the significance of the first canonical axis is: eigenvalue = 0.770; *F* = 26.759; and *P* = 0.005, and of all canonical axes is: trace = 0.885; *F* = 4.409; and *P* = 0.003.

Marginal Effects		Conditional Effects			
Variable	λ_1	Variable	λ_a	*P*	*F*
Buoyancy	0.41	Buoyancy	0.41	**0.001**	14.84
IIS	0.37	IIS	0.19	**0.002**	9.04
Si	0.19	Si	0.15	**0.002**	11.43
Depth	0.16	Ni:P	0.03	0.086	2.50
Currents	0.11	Rain	0.03	0.103	2.44
Ni:Si	0.11	Salinity	0.02	0.077	2.71
Salinity	0.10	P	0.02	0.134	1.96
Solar	0.09	Depth	0.01	0.535	0.69
Wind	0.07	Wind	0.01	0.700	0.45
Ni:P	0.05	Solar	0.00	0.699	0.42
P	0.05	Ni:Si	0.01	0.597	0.59
Temp	0.04	Ni	0.00	0.780	0.30
Rain	0.02	Currents	0.00	0.863	0.20
Ni	0.01	Temp	0.01	0.891	0.18

Axes	1	2	3	4	Total variance
Eigenvalues	0.770	0.094	0.013	0.008	1
Phyto-environment correlations	0.959	0.860	0.806	0.722	
Cumulative percentage variance					
of phyto data	77.0%	86.4%	87.7%	88.5%	
of phyto-environment relation	87.0%	97.6%	99.1%	99.9%	
Sum of all eigenvalues					1
Sum of all canonical eigenvalues					0.885

6.4.4.2. Environmental influence on community structure by microscopy

Environmental variables that accounted for the variance in the carbon biomass of selected taxa (biomass greater than 5 % of community) were investigated using RDA (Fig. 6.14 and Table 6.5). All canonical axes explained 87.8 % of the variance (p = 0.001), indicating the measured environmental variables explained the majority of the variation in the structure of the SCM community as identified by microscopy over the 4 years samples were collected, when all axes were analysed together (Table 6.5). The eigenvalues (λ, dimensionless; Table 6.5) associated with the environmental variables are shown in the order of the variance in the data they explained individually (marginal effects – λ_1 in Table 6.5), along with the significance of that variable (according to forward selection and a Monte Carlo permutations test; conditional effects - λ_a in Table 6.5). The variables that were considered to be significant were silicate concentration (Si; λ_a = 0.18, p = 0.001) temperature (Temp; λ_a = 0.12, p = 0.002), instantaneous index of stability (IIS; λ_a = 0.10, p = 0.002), nitrate to phosphate ratio (Ni:P; λ_a = 0.05, p = 0.01), nitrate to silicate ratio (Ni:Si; λ_a = 0.06, p = 0.007) and phosphate concentration (P; λ_a = 0.04, p = 0.038).

Dinophysis acuminata and small naked dinoflagellate biomass was present in relatively similar amounts in all years, but increases in biomass were found in association with lower measurements of instantaneous stability (Fig. 6.14). Ciliates were a noteworthy inhabitant of the SCM in all years, but increased biomass was most strongly correlated with greater silicate concentrations (Fig. 6.14). In 2013 and 2016, smaller diatoms (generally < 400 μm^3 in volume: *Chaetoceros spp.* and *Pseudo-nitzschia spp.*) and smaller dinoflagellates (< 15000 μm^3 in volume: *Prorocentrum micans* and *Diplopsalis lentiula*) were common, found in SCM waters that were relatively cooler (mean temperature of 11.6 and 12.1 °C in 2013 and 2016 respectively; Table 6.1), and in the case of 2016, had the lowest silicate concentrations (mean of 0.61 µmol l^{-1}) and Ni:P ratios (mean of 1.77) (Fig. 6.14). Nutrient data is not available for 2013, thus no relationship between taxa and nutrient concentrations or ratios can be derived. In 2014, large *Rhizosolenia spp.*, *Lauderia annulata*, *Leptocylindrus danicus*, *Gyrodinium spp.* and *Polykrikos spp.*, particularly common within the SCM in that year, were strongly correlated with warmer waters and greater silicate concentrations and Ni:P ratios (mean temperature of 13.1 °C, ≥ 1 °C warmer on average than in other years, and mean silicate concentration and Ni:P ratio of 1.39 µmol l^{-1} and 6.48 respectively; Table 6.1) (Fig. 6.14). In 2015 the SCM community was typically dominated by *Ceratium fusus*, strongly correlated with high stability and associated with relatively increased phosphate and silicate concentrations (mean IIS of 9.07, and mean phosphate and silicate of 0.15 and 1.14 µmol l^{-1} respectively; Table 6.1). Extra

small *Thalassiosira spp.*, *Dinophysis acuta* and *Dictyocha spp.*, also common in 2015, were similarly related to these conditions (Fig. 6.14).

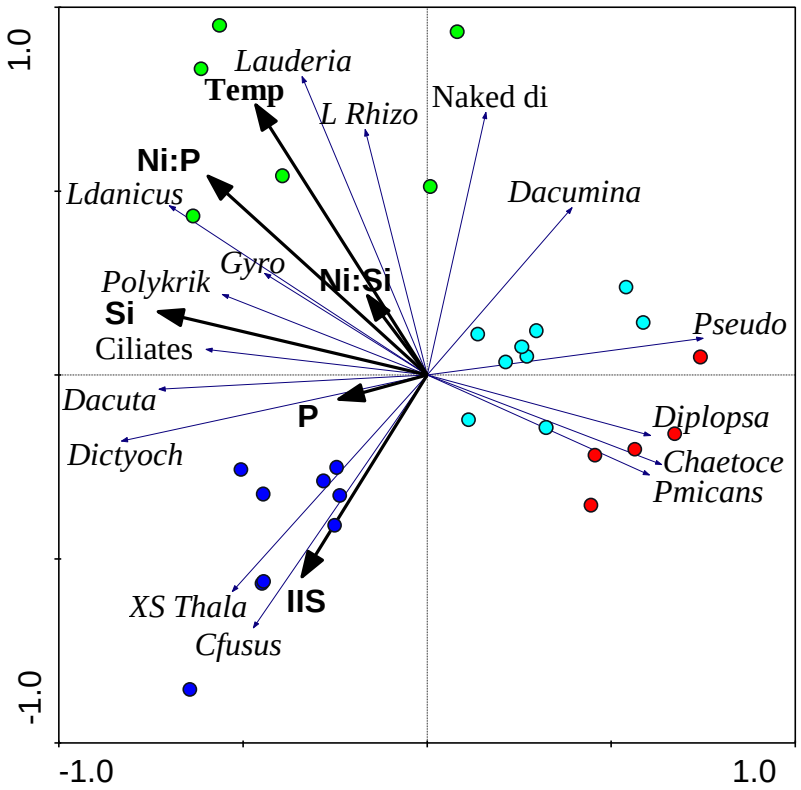

Figure 6.14. Ordination diagram generated from redundancy analysis (RDA). The triplot shows taxa carbon biomass (thin blue lines), environmental variables identified to describe a significant portion of the variability in the phytoplankton taxa data by the RDA (thick black lines), and samples (closed circles, where colours refer to year groups: red = 2013, green = 2014, dark blue = 2015, and light blue = 2016). Only species with ≥ 15 % goodness of fit with the environmental variables are included in the ordination diagram. Naked di refers to small (10 - 25 µm) naked dinoflagellates not identified to genus/species, *Dacumina* is *Dinophysis acuminata*, *Pseudo* is *Pseudo-nitzschia spp.*, *Diplopsa* is *Diplopsalis lenticula*, *Chaetoce* is *Chaetoceros spp.*, *Pmicans* is *Prorocentrum micans*, *Cfusus* is *Ceratium fusus*, *XS Thala* is *Thalassiosira spp.* < 10 µm height, *Dictyoch* is *Dictyocha spp.*, *Dacuta* is *Dinophysis acuta*, *Polykrik* is *Polykrikos spp.*, *Gyro* is *Gyrodinium spp.*, *Ldanicus* is *Leptocylindrus danicus*, *L Rhizo* is *Rhizosolenia spp.* > 20 µm in diameter, and *Lauderia* is *Lauderia annulata*. The significant environmental variables included silicate concentration (Si; µmol l^{-1}), temperature (temp; °C), instantaneous index of stability (IIS), nitrate to phosphate ratio (Ni:P), nitrate to silicate ratio (Ni:Si) and phosphate concentration (P; µmol l^{-1}). Note no nutrient data is available for 2013, thus no relationship between taxa and nutrient concentrations or ratios can be derived based on this ordination.

Table 6.5. Variance explained by each of the environmental variables included in the redundancy analysis when analysed individually (λ_1, marginal effects) or when analysed together with other forward-selected variables (λ_a, conditional effects). Significant *p* values ($p < 0.05$; in bold) indicate the variables that, combined, significantly explain the variation in the analysis. Buoyancy is buoyancy frequency (rad^2 s^{-2}), IIS is instantaneous index of stability, Si is silicate concentration (µmol l^{-1}), depth is SCM depth (m; as a proxy for mixed layer depth), currents is current velocity (m s^{-1}), solar is daily solar insolation (kWh m^{-2} d^{-1}), temp is temperature (° C), P is phosphate concentration (µmol l^{-1}), Ni:Si and Ni:P are nitrate to silicate and phosphate ratios, Ni is nitrate concentration (µmol l^{-1}), wind is wind speed (m s^{-1}) and rain is rainfall (mm d^{-1}). The RDA summary is also included, where the significance of the first canonical axis is: eigenvalue = 0.317; *F* = 6.511; and *P* = 0.005, and of all canonical axes is: trace = 0.723; *F* = 2.609; and *P* = 0.001.

Marginal Effects		Conditional Effects			
Variable	λ_1	Variable	λ_a	*P*	*F*
Si	0.18	Si	0.18	**0.001**	6.09
Temp	0.17	Temp	0.12	**0.002**	4.25
Ni:P	0.17	IIS	0.10	**0.002**	3.99
Salinity	0.11	Ni:P	0.05	**0.010**	2.63
IIS	0.10	Ni:Si	0.06	**0.007**	2.82
Ni	0.10	Buoyancy	0.04	0.111	1.58
Depth	0.09	Salinity	0.03	0.166	1.46
Buoyancy	0.08	Rain	0.02	0.170	1.45
Rain	0.07	Ni	0.02	0.485	0.94
Solar	0.06	P	0.04	**0.038**	2.14
P	0.06	Currents	0.02	0.503	0.90
Ni:Si	0.06	Solar	0.02	0.595	0.82
Currents	0.04	Depth	0.01	0.601	0.78
Wind	0.03	Wind	0.01	0.734	0.61

Axes	1	2	3	4	Total variance
Eigenvalues	0.317	0.187	0.084	0.047	1
Taxa-environment correlations	0.938	0.931	0.850	0.894	
Cumulative percentage variance					
of taxa data	31.7%	50.4%	58.8%	63.4%	
of taxa-environment relation	43.9%	69.8%	81.3%	87.8%	
Sum of all eigenvalues					1
Sum of all canonical eigenvalues					0.723

6.5. Discussion

6.5.1. Influence of environmental variation on SCM chlorophyll structure

During the summer survey periods of 2013 to 2016, the repeat site in the Western English Channel was characterised by an SCM that in most cases was associated with the base of the thermocline, consistent with previous studies on the NW European shelf (Pingree et al., 1978, Holligan et al., 1984b, Richardson et al., 2000, Sharples et al., 2001, Hickman et al., 2012, Fishwick, 2017), and further afield (Cullen, 1982, Holligan et al., 1984a, Dekshenieks et al., 2001, Rines et al., 2002, Lips et al., 2010, Ryan et al., 2010, Cullen, 2015). Chlorophyll structure of the SCM, assessed in terms of thickness, maximum chlorophyll concentration and Chl_{50m}:Chl_{SCM}, varied significantly over the four years of study, specifically with higher maximum SCM chlorophyll concentrations in 2015 (mean and standard deviation of 7.3 ± 4.4 µg l^{-1}; Table 6.1) relative to other years, and higher Chl_{50m}:Chl_{SCM} in 2014 (21.7 ± 9.1) and 2016 (19.3 ± 7.0) compared to 2013 (10.5 ± 3.5) and 2015 (7.0 ± 4.0) (Fig 6.7 and Table 6.1; details provided in Table A4.2). High interannual variability of subsurface chlorophyll of the summer stratified water column is common within the Western English Channel (Fishwick, 2017). This variability may be attributed to a range of environmental variables, including nutrient supply (Sharples and Tett, 1994, Rippeth et al., 2009, Williams et al., 2013a), strength of stratification (Dekshenieks et al., 2001, MacKenzie and Adamson, 2004, McManus et al., 2012), turbulence (Donaghay and Osborn, 1997, Dekshenieks et al., 2001, Sharples et al., 2001, Wang and Goodman, 2009, McManus et al., 2012, Macías et al., 2013, Blauw et al., 2018), mixed layer depth (Pingree et al., 1976, Bissett et al., 1994, Mellard et al., 2011, Gong et al., 2015), temperature (Eppley, 1972, Falkowski and Raven, 1997, Dekshenieks et al., 2001), stability (Pingree et al., 1976, Agustí and Duarte, 1999, Murty et al., 2000, Dekshenieks et al., 2001) and light levels (Fasham et al., 1985, Coon et al., 1987, Falkowski and Raven, 1997, Blauw et al., 2018). However, conditions *in situ* are complex, with multiple variables, which are not independent of each other, acting together at any given time. Therefore, it is common that effects of some variables are not directly discernible (Estrada et al., 1993, Blauw et al., 2018). This is consistent with findings of this study, where only the parameters of IIS, current velocity and temperature had an apparent association with the interannual variability in SCM chlorophyll structure (Fig. 6.7, 6.8 and Table 6.1; further details provided in Table A4.2). It is acknowledged that there are other environmental factors that could not be considered in this study that may have had a role in bringing about the observed interannual variability in SCM chlorophyll structure. For instance, past weather and time since the spring bloom can both impact the chlorophyll

structure of a SCM particularly through their influence on water column density structure (Pingree et al., 1976, Ridderinkhof, 1992, Eslinger and Iverson, 2001, Sharples et al., 2006).

6.5.1.1. Influence of stability (IIS)

In 2013 and 2015 measurements of instantaneous stability at the depth interval of the SCM were significantly greater than in 2014 and 2016 (Fig. 6.8a). Higher stability coincided with lower Chl_{50m}:Chl_{SCM} (Fig. 6.7c), and in 2015 also coincided with particularly high maximum chlorophyll concentrations (Fig. 6.7b). Strength of stratification, given by buoyancy frequency (Table 6.1), was also found to be significantly lower in 2015 compared to the other years. However, unlike with the IIS, no consistent relation of chlorophyll structure to stratification strength was apparent, suggesting it was the balance between stratification strength and velocity shear at the depth interval of the SCM that was key in governing chlorophyll structure, not simply stratification strength. Moreover, the IIS was the only variable that had an apparent association with chlorophyll structure in all four years, potentially suggesting that in any given year, stability is essential in controlling SCM chlorophyll structure in the Western Channel.

Given that increased stability is, by definition, associated with relatively low shear, where turbulent mixing is reduced (Miles, 1961, Galperin et al., 2007), greater stability, as observed in 2013 and 2015, can act to minimise chlorophyll dispersal from the SCM to the surrounding water column (Donaghay and Osborn, 1997, Cowles et al., 1998). This potentially accounts for the lesser Chl_{50m}:Chl_{SCM} in 2013 and 2015 and greater ratios in 2014 and 2016. Furthermore, there are mechanisms associated with greater stability/reduced turbulent mixing that may favour chlorophyll proliferation within the SCM, and could help account for the greater SCM maximum chlorophyll concentrations observed in 2015, including (1) reduced chlorophyll dispersal enabling maintenance and further growth of phytoplankton within the SCM (Donaghay and Osborn, 1997, Cowles et al., 1998); and (2) accumulation of phytoplankton within the SCM relating to changes in phytoplankton sedimentation velocity promoted by the difference in turbulence conditions between the SCM (low turbulence region) and surface waters (high turbulence region) (Ruiz et al., 2004, Macías et al., 2013). One of the main sources of turbulence in the shelf sea environment is tidal generated (Pingree, 1975), and in 2015 current velocity was significantly lower than in the other years (Fig. 6.8c) suggesting low tidal current velocity. The lesser current velocities in 2015 can be related to tidal phase because the majority of profiles were collected during late spring to mid neap tides (Table A4.2) when tidal currents would be weakening/weakest. Reduced tidal generated turbulence may account for the greater stability recorded in 2015.

Lower stability at the depth interval of the SCM could be expected to result in higher concentrations of nutrients within the SCM as a result of an enhanced supply of nutrients from the bottom mixed layer into the thermocline driven by turbulence, with observations of vertical nitrate fluxes in the NW European shelf seas demonstrating rates (mmol m^{-2} d^{-1}) to be enhanced by a factor of 2 to in excess of 10 in correspondence with increased turbulent dissipation (Sharples et al., 2001, Rippeth et al., 2009, Williams et al., 2013b). However, such an inverse relationship was not observed (Table 6.1), which may indicate rapid consumption of nutrients by the phytoplankton community (Zimmerman et al., 1987) and that the nutrient status of the phytoplankton community was dependent on intracellular nutrient concentration and/or organic forms of nitrogen and not solely on extracellular inorganic nutrient availability (Droop, 1977). An increased nutrient supply associated with lower stability can promote phytoplankton growth (Sharples et al., 2001, Williams et al., 2013b), but lower stability can also facilitate cell dispersal from the SCM (Donaghay and Osborn, 1997, Cowles et al., 1998); this in combination with a phytoplankton growth dependence on intracellular and/or organic nutrients, likely accounts, in part, for the absence of a discernible relationship between interannual SCM chlorophyll structure and nutrient concentrations (Table 6.1).

6.5.1.2. Influence of temperature

In 2013, in spite of an increased IIS, maximum chlorophyll concentrations within the SCM were relatively low (Fig. 6.7b) compared to those of the also increased stability SCM of 2015, suggesting another environmental factor may have been limiting growth of the phytoplankton community within the SCM. Temperature within the SCM was found to be significantly lower in 2013, on average by 0.4 – 1.5 °C (Table 6.1), than in 2014, 2015 and 2016 (Fig. 6.8d). Temperature is a fundamental governing factor of phytoplankton growth and processes required for growth, such as resource attainment, and this influence of temperature exists due to the control it exerts over metabolic rates (Eppley, 1972, Raven and Geider, 1988, Moisan et al., 2002). Using the temperature function developed by Bissinger et al. (2008), which derives a Q_{10} temperature coefficient of 1.88, maximum attainable daily growth rates as a function of temperature can be approximated. For 2013 and 2015 rates were estimated to be 1.68 and 1.73 d^{-1} respectively. Entering these growth rates into a simple population growth model $P(t) = P_0 \exp[(p - g)t]$ (Geider, 1988), where P(t) is phytoplankton biomass at time t, P_0 is initial phytoplankton biomass, p is growth rate and g is grazing mortality, and assuming the grazing mortality term is equal for both years, establishes that a doubling of phytoplankton biomass would be 1.03 times slower in the slightly cooler waters of 2013 compared to 2015. These calculations demonstrate that the effect of temperature on growth was not principally

responsible for the relatively low maximum SCM chlorophyll concentrations observed in 2013 compared to 2015. Alternatively, the association between lower temperature and lower maximum chlorophyll concentration may simply have been a reflection of the specific physiology, life history and biological interactions of the phytoplankton that were dominating the SCM at the lower temperatures of 2013.

Temperature within the SCM was significantly higher in 2014, by at least 1 °C on average (Table 6.1), relative to the other three years, but no association between this higher temperature and SCM maximum chlorophyll concentration was observed. Any positive influence of temperature on phytoplankton growth and, by association, SCM chlorophyll concentration was likely too minimal to be observed based on a Q_{10} temperature coefficient of 1.88 (Eppley, 1972, Bissinger et al., 2008). Moreover, a significant positive influence of temperature on phytoplankton growth would likely not have been detected in 2014 anyway because of phytoplankton losses from the SCM associated with the low stability in that year (Fig. 6.8a) offsetting the positive effects of increased temperature, such that significant chlorophyll proliferation within the SCM would have been prevented.

6.5.2. Influence of environmental variation on SCM phytoplankton structure

Between the summer surveys of 2013 to 2016, phytoplankton community structure, as assessed using CytoSense flow cytometry and inverted light microscopy, varied significantly. Environmental variables investigated for their potential influence on phytoplankton community structure included buoyancy frequency, the IIS, temperature, salinity, nutrient concentrations and ratios, SCM depth, current velocity, daily solar insolation, wind speed, and rainfall. However, it is acknowledged that there are other factors not included in this study that have the potential to induce interannual variability in phytoplankton community structure. Three key examples are weather history (Jang et al., 2013, Barnes et al., 2015a, Barnes et al., 2015b), winter nutrient concentrations and ratios (Jang et al., 2013, Barnes et al., 2015b), and the intensity and spectral composition of light at the SCM (Hickman et al., 2009, Latasa et al., 2017).

6.5.2.1. Influence on community structure by flow cytometry

Consistent with the findings of Tarran and Bruun (2015) it was not just larger (> 20 µm) phytoplankton that were important in the SCM community, but also varieties of nano- and pico-phytoplankton. In addition to micro- and meso-phytoplankton, orange and red nano-

phytoplankton, and orange and red pico-phytoplankton consistently contributed to the SCM community at the repeat site in the Western English Channel from 2014 to 2016, only differing in their relative importance (Fig. 6.9). However, SCM phytoplankton community structure as analysed by flow cytometry was statistically distinct in every year of study (Fig. 6.9, 6.10 and Table 6.2) according to environmental characteristics (stratification strength, stability and silicate concentration; Table 6.4) specific to each year (Fig. 6.13). Micro- and meso-phytoplankton were consistently dominant within the SCM when waters were highly stable (IIS mean and standard deviation of 9.07 ± 7.83; Table 6.1) and silicate concentrations were relatively high (1.14 ± 0.63 µmol l^{-1}; Table 6.1) as observed in 2015 (Fig. 6.9 and 6.13). This association between the dominance of larger (> 20 µm) phytoplankton and stability and silicate concentrations largely reflects the taxonomy of the larger cells, which is discussed in detail in section 6.5.2.2.

Red nano-phytoplankton (such as small naked dinoflagellates, chlorophytes and prymnesiophytes as observed by microscopy; details in Table A4.1) accounted for a greater proportion of the community, often being dominant, in waters with lower stability (IIS < 0.7 on average; Table 6.1), as observed in 2014 and 2016 (Fig. 6.9 and 6.13). Two key specific traits that combined may have enabled high contributions and often dominance of nano-phytoplankton within the SCM in low stability conditions, are (1) motility (Kamykowski and McCollum, 1986, Sommer, 1988), facilitating their maintenance and subsequent growth within the SCM, and limiting losses due to turbulent dispersal; and (2) enhanced light utilisation efficiency (Tilstone et al., 1999, Uitz et al., 2008), potentially enabling faster chlorophyll synthesis in the low light conditions of the SCM relative to other phytoplankton, which in turn could act to counterbalance losses to turbulent dispersal. However, low stability conditions were associated with relatively low maximum SCM chlorophyll concentrations (Fig 6.7b and Table 6.1), suggesting that turbulent dispersal may have ultimately prevented significant proliferation of the red nano-phytoplankton community at the depth of the SCM. In addition, as the main grazers of small phytoplankton have growth rates that are comparable to their prey (Kiørboe, 1993), grazing may also have had a key role in restricting proliferation of the red nano-phytoplankton population.

Orange nano-phytoplankton (such as cryptophytes), red pico-phytoplankton (such as prymnesiophytes and chlorophytes) and orange pico-phytoplankton (such as *Synechococcus*) were typically a more minor part of the SCM community from 2014 to 2016 (Fig. 6.9), but their increased contribution was associated with stronger stratification (buoyancy frequency 0.0036

± 0.0015 rad^2 s^{-2}; Table 6.1), as observed in 2016 (Fig. 6.13). Strong stratification can act to greatly reduce the capacity for vertical transfer of nutrients from the bottom mixed layer into the thermocline (Sharples et al., 2001). The subsequent low nutrient availability within the SCM could favour small phytoplankton given the competitive advantage conferred by a higher nutrient uptake affinity (Beardall et al., 2009, Finkel et al., 2010). The increased contribution of orange nano- and pico-phytoplankton, and red pico-phytoplankton also corresponded with low measurements of instantaneous stability at the depth interval of the SCM. However, precisely why increased proportions of these small phytoplankton were associated with low stability in combination with strong stratification is hard to determine. It may be the case that these conditions simply coincided with a nutrient and light (intensity and spectral composition) environment that developed within the SCM before and/or during the 2016 survey that was particularly complementary to the specific nutrient uptake requirements (Marañón, 2015, Farrant et al., 2016) and light absorption capabilities (Kirk, 1994, Hickman et al., 2009, Grébert et al., 2018) of these groups of nano- and pico-phytoplankton, promoting development and/or maintenance of the observed populations.

The increased contributions of orange nano-phytoplankton and pico-phytoplankton were also found in SCM waters with reduced silicate (0.61 ± 0.16 µmol l^{-1} in 2016; Fig. 6.9, 6.13 and Table 6.1). This relationship may reflect silicate accumulation by the orange nano-phytoplankton population (Baines et al., 2012, Ohnemus et al., 2016).

These associations between phytoplankton at the smaller end of the size spectrum and physical water column parameters, while having potential implications for nutrient cycling (Baines et al., 2010) and export to depth (Tang et al., 2014), may be of particular significance for our understanding of trophic dynamics in the Western English Channel and other analogous shelf sea settings, given that smaller phytoplankton are fundamental in the microbial loop (Azam et al., 1983, Cushing, 1989, Fenchel, 2008). Small phytoplankton are key contributors of organic matter for circulation through the microbial loop, which rapidly recirculates nutrients and carbon above the thermocline (Azam et al., 1983). This recycling of organic matter is especially important in stratified waters, as high division rates result in considerable exudate production (Cushing, 1989, Thornton, 2014).

6.5.2.2. Influence of community structure by microscopy

Phytoplankton taxa identified within SCM at the repeat site in the Western English Channel (Table A4.1) are common to the Channel and the wider northern European shelf (Holligan and

Harbour, 1977, Holligan et al., 1980, Reid et al., 1990, Pemberton et al., 2004, Widdicombe et al., 2010), with some also potentially being globally significant. For instance, *Pseudo-nitzschia* was a key contributor to the community during the four years of study, and is observed globally as a ubiquitously dominant component of phytoplankton communities (Trainer et al., 2012). Many taxa were consistently observed within the SCM from 2013 to 2016, only differing in their relative importance. Nonetheless, the structure of the ≥ 10 µm phytoplankton community within the SCM as identified by light microscopy did distinctly vary over the four years of 2013 to 2016 (Fig. 6.11, 6.12 and Table 6.3) according to environmental conditions (silicate concentration, temperature, IIS, nitrate to phosphate and silicate ratios and phosphate concentration; Table 6.5) specific to each year (Fig. 6.14).

In all four years *Dinophysis acuminata* and small naked dinoflagellates made similar contributions of biomass (Fig. 6.11; Table A4.1), suggesting that conditions within the SCM were suitable for some extent of growth every year. However, enhanced biomass of *Dinophysis acuminata* and small naked dinoflagellates was found in SCM waters where measurements of instantaneous stability were lower (Fig. 6.14). Dinoflagellate motility can offer a competitive advantage over non-motile phytoplankton in conditions of reduced stability because it can potentially provide a mechanism to counteract turbulent dispersal from the SCM, facilitating maintenance and subsequent growth within the SCM. Specifically, turbulent diffusivities at the higher end of the typical range measured in the thermocline of seasonally stratified NW European shelf seas fall in the order of 10^{-4} m^2 s^{-1} (Sharples et al., 2001, Palmer et al., 2008, Rippeth et al., 2009), and given typical dinoflagellate swimming speeds of 50 – 1500 µm s^{-1} (Kamykowski and McCollum, 1986, Levandowsky and Kaneta, 1987, Sommer, 1988, Ross and Sharples, 2007), indicates dinoflagellate swimming within the thermocline was viable (Péclet number as defined in Ross and Sharples (2008) consistently > 1 using a length scale of 10 m), providing means for dinoflagellates to maintain a position away from the base of the thermocline, facilitating avoidance of entrainment into bottom waters. However, precisely why biomass of these specific dinoflagellates increased in relation to reduced stability is difficult to establish. Similarly, ciliates were a noteworthy component of the SCM community in all four years (Fig. 6.11; Table A4.1), suggesting they were consistently supported by conditions within the SCM, but increased ciliate biomass was found when silicate concentrations were higher. Ciliates are typically mixotrophic or heterotrophic and therefore their distribution may be strongly dependent on specific prey (Smetacek, 1981, Löder et al., 2011). Their consistent presence in the SCM suggests there was an availability of suitable prey in all years, but their

association with higher silicate concentrations may reflect a predilection for dinoflagellates, flagellates and/or lightly silicified diatoms, such as *Leptocylindrus danicus*.

In 2013, 2014 and 2016 temperature and nutrients (silicate concentration and the Ni:P ratio) emerged as the most important environmental variables governing phytoplankton taxa (Fig. 6.14). In all three years the SCM community was predominantly a mixed assemblage of diatoms and dinoflagellates (Fig. 6.11). However, in 2013 and 2016 smaller diatoms (generally < 400 μm^3 in volume: *Chaetoceros spp.* and *Pseudo-nitzschia spp.*) and smaller dinoflagellates (< 15000 μm^3 in volume: *Prorocentrum micans* and *Diplopsalis lentiula*) were common (Fig. 6.11), identified in SCM waters that were relatively cooler (11.6 ± 0.3 and 12.1 ± 0.3 °C in 2013 and 2016 respectively; Table 6.1), and in the case of 2016, had the lowest silicate concentrations (0.61 ± 0.16 µmol l^{-1}) and Ni:P ratios (1.77 ± 0.32). Whereas in 2014, common diatoms were larger (> 1000 μm^3 in volume: large *Rhizosolenia spp.*, *Lauderia annulata* and *Leptocylindrus danicus*) and so too were the common dinoflagellates (>15000 μm^3 in volume: *Gyrodinium spp.* and *Polykrikos spp.*; Fig. 6.11), found in SCM waters that were relatively warmer (13.1 ± 0.7 °C; Table 6.1), with the highest recorded silicate concentrations (1.39 ± 0.66 µmol l^{-1}) and Ni:P ratios (6.48 ± 3.71) (Fig. 6.14). *Diplopsalis lenticula*, *Gyrodinium spp.* and *Polykrikos spp.* are heterotrophic, thus, their occurrence may simply indicate the presence of suitable prey within the SCM. On the other hand, *Prorocentrum micans* is autotrophic, and its importance in a summer phytoplankton community has previously been linked to temperatures similar to those recorded in this study in 2013 and 2016 (Holligan et al., 1980). *Pseudo-nitzschia spp.* and *Chaetoceros spp.* were ubiquitous in the SCM throughout the four years of study and have often been documented in chlorophyll maxima in previous studies (Holligan and Harbour, 1977, Estrada et al., 1993, Rines et al., 2010, Latasa et al., 2017), suggesting these diatoms are well adapted to life in the pycnocline over a range of different environmental conditions. Yet increased contributions of these smaller diatoms were found in correspondence with cooler SCM waters, which may be related to their growth and temperature effects on this growth. Specifically, small diatoms tend to have higher growth rates (Chisholm, 1992), with *Pseudo-nitzschia spp.* and *Chaetoceros spp.* both characterised by inherently high rates of growth (> 1 division d^{-1}; (Pan et al., 1993, Montagnes and Franklin, 2001)). In addition, changes in temperature can affect the growth rates of different diatoms to differing magnitudes, with the Q_{10} temperature coefficient typically ranging anywhere between 1 and 3 for diatom growth (Raven and Geider, 1988, Montagnes and Franklin, 2001), although this coefficient is not constant for different species because of interactions of other factors, such as light intensity and nutrient availability (Montagnes and Franklin, 2001, Talling,

2012, Sherman et al., 2016). If it was the case that the *Pseudo-nitzschia spp.* and *Chaetoceros spp.* diatoms common in 2013 and 2016 were more minimally affected by the lower SCM temperatures in those years relative to larger diatoms within the SCM, then this in combination with their rapid growth rates may have acted to compensate somewhat for some of their physiological disadvantages compared to larger diatoms (Sicko-Goad et al., 1984, Sommer, 1984, Raven, 1987). Therefore, potentially facilitating enhanced competitive success and thus significant propagation within the SCM in lieu of larger diatoms, as observed in 2013 and 2016. It follows that increased proportions of larger diatoms (large *Rhizosolenia spp.*, *Lauderia annulata* and *Leptocylindrus danicus*) may have occurred within the SCM in 2014 because of the positive effects of temperature on growth, particularly given favourable interaction of other environmental factors (Eppley, 1972, Raven and Geider, 1988, Montagnes and Franklin, 2001, Talling, 2012, Sherman et al., 2016), in combination with the physiological advantages of higher maximum nutrient uptake rates (Sommer, 1984) and disproportionately larger vacuoles for nutrient storage compared to smaller diatoms (Sicko-Goad et al., 1984, Raven, 1987). Given hydrographic conditions are suitable for growth, these nutrient traits provide the potential means for larger diatoms to outcompete smaller diatoms in an environment with a discontinuous nutrient supply, such as presented by the SCM. Furthermore, larger size makes ingestion difficult for many grazers (Smetacek, 2001, Hamm and Smetacek, 2007), which may have helped to reduce cell losses and subsequently enhanced the proportions of large *Rhizosolenia spp.*, *Lauderia annulata* and *Leptocylindrus danicus* in 2014.

As diatoms possess a vacuole that enables nutrient storage (Dortch, 1982, Raven, 1987, Raven, 1997, Marchetti et al., 2009), and can perform luxury nutrient uptake (Sunda and Huntsman, 1995), indicates the nutrient status of the SCM community had a dependency on intracellular nutrient concentrations in 2013, 2014 and 2016. Therefore, significant relationships between key phytoplankton and silicate concentration and the Ni:P ratio in these years (Fig. 6.14) may be more representative of the balance between nutrient uptake and nutrient supply (Anabalón et al., 2016), as opposed to just ambient concentrations and ratios within the SCM.

One key difference between 2013 and 2016 was the magnitude of the IIS at the depth interval of the SCM, with significantly lower stability (IIS of 0.62 ± 0.66; Table 6.1) in 2016 relative to 2013 (IIS of 3.64 ± 2.88; Table 6.1). However, it seems that this difference was not central in affecting community composition (Table 6.5), but it could have affected the relative importance of key phytoplankton taxa so that it was responsible for the distinction in SCM

community structure between 2013 and 2016 (Fig. 6.12). The largest factor causing dissimilarity between the two years was the relative increase of *Chaetoceros spp.* biomass, but decrease in *Pseudo-nitzschia spp.* biomass (accounted for 15.2 % of dissimilarity; data not shown) in 2016 compared to 2013. This may suggest that *Chaetoceros spp.* was better adapted to lesser stability, perhaps because of its possession of spines (Smayda, 1970), which may have facilitated suspension and maintenance within the SCM for longer. On the other hand, higher proportions of *Pseudo-nitzschia spp.* are well documented in relation to increased stratification stability (Rines et al., 2002, Peterson et al., 2007, McManus et al., 2008, Ryan et al., 2010, Du et al., 2016), evidence that *Pseudo-nitzschia spp.* can maintain their health and perform better relative to other diatoms in these higher stability conditions.

In 2015 the SCM community was generally overwhelmingly dominated by *Ceratium fusus* (Fig. 6.11), where measurements of instantaneous stability at the depth interval of the SCM were high (IIS of 9.07 ± 7.83; Table 6.1) (Fig. 6.14). A prevalence of dinoflagellates has often been observed in more stable waters (Pingree et al., 1978, Cushing, 1989, Baek et al., 2007), likely because motility provides means for these phytoplankton to respond to resource gradients within the pycnocline and subsequently exploit the intermittent nutrient supply from bottom waters into the thermocline characteristic of shelf seas (Sharples et al., 2001, Williams et al., 2013a, Williams et al., 2013b). Moreover, it has been suggested that vertical stability is the most important environmental parameter determining the relative abundance of dinoflagellates (Holligan et al., 1980). The results of this study seem to support the supposition of Holligan et al. (1980), as a large dinoflagellate (*Ceratium fusus*: > 15000 μm^3 in volume) was only majorly dominant (2015) in very stable conditions. In all other years, when values of the IIS were typically considerably less, the ≥ 10 µm phytoplankton community was more of a mixed assemblage of diatoms and generally smaller dinoflagellates (Fig. 6.11). Traits that may have enabled the dominance of *Ceratium fusus* over other motile phytoplankton include luxury consumption of nutrients (Baek et al., 2008a), mixotrophy, considerable physiological flexibility (Johns and Reid, 2001, Baek et al., 2007, Baek et al., 2008b), and means of limiting predation pressure, including anoxia (Onoue, 1990, Spatharis et al., 2009) and elongate apical horns (Smetacek, 2001, Hamm and Smetacek, 2007). The dominance of *Ceratium fusus* was also associated with relatively higher/intermediate silicate concentrations (1.14 ± 0.63 µmol l^{-1} in 2015; Table 6.1), and, to a lesser extent, with relatively higher/intermediate phosphate concentrations (0.15 ± 0.09 µmol l^{-1} in 2015; Table 6.1) (Fig. 6.14). This relation to silicate is potentially reflective of the absence of a dominant diatom population at the SCM utilising the

silicate supply, and the relation to phosphate may be indicative of the lesser growth dependence of *Ceratium fusus* on phosphate relative to nitrate (Baek et al., 2008a).

In 2015 extra small *Thalassiosira spp.*, *Dinophysis acuta* and *Dictyocha spp.* were also present with increased biomass relative to other years, thus were associated with the same stability and nutrient conditions as *Ceratium fusus* (Fig. 6.14). The dinoflagellate *Dinophysis acuta* has been previously related to especially high stability (Holligan et al., 1980), suggesting stability conditions within the SCM in 2015 may have been particularly suitable to support the growth of *Dinophysis acuta*. On the other hand, the greater success of *Dinophysis acuta* alongside *Ceratium fusus* may have been more related to the presence of *Tiarina fusus* (Table A4.1), a specific prey item of the predominantly mixotrophic *Dinophysis* genus (Hansen, 1991). *Thalassiosira spp.* and *Dictyocha spp.* both have a siliceous skeleton, and thus require silicate. Therefore, the lack of a dominant population of large diatoms, that otherwise would likely outcompete small diatoms and silicoflagellates, may have facilitated the establishment of a niche for the extra small *Thalassiosira* and *Dictyocha* cells, where silicate was available to support their growth. The competitive advantage conferred by higher nutrient affinity associated with the small size (< 10 µm height) of the *Thalassiosira spp.* (Beardall et al., 2009, Finkel et al., 2010), and the motility of *Dictyocha* may have enabled these taxa to enhance their success alongside the dominant *Ceratium fusus*.

Overall, these associations between different phytoplankton taxa and environmental conditions may have many biogeochemical and ecological implications for the shelf environment given the vast array of taxon specific traits possessed by phytoplankton in this study (Kiørboe et al., 1990, Falkowski et al., 2004, Finkel et al., 2010, Kemp and Villareal, 2013, López-Sandoval et al., 2014). Nonetheless, they may be of particular significance for our understanding of (1) the silica cycle, given that diatoms were almost absent when stability was especially high; (2) carbon export to depth, because of the relationship between larger cells and temperature, and (3) toxic blooms, as some of the key phytoplankton associated with environmental factors are capable of toxicity, e.g. *Pseudo-nitzschia spp.* can produce domoic acid (Mos, 2001) and *Dinophysis acuminata* can produce okadaic acid (Murata et al., 1982).

6.6. Conclusion

During this study, conducted at a repeat site (50°05.670 N, 004°52.020 W) within the summer (late June to early July) stratified waters of the Western English Channel from 2013 to 2016,

interannual variation in environmental conditions was accompanied by significant interannual differences in SCM chlorophyll structure and phytoplankton community structure. Therefore, data on environmental conditions related to the summer SCM in the Western English Channel may be a useful indicator of key SCM phytoplankton and SCM chlorophyll structure.

Significantly higher maximum SCM chlorophyll concentrations were observed in 2015 (7.3 ± 4.4 μg l^{-1}) in association with greater measurements of instantaneous stability at the depth interval of the SCM (IIS of 9.07 ± 7.83), which was related to significantly lower current velocities (0.14 ± 0.09 m s^{-1}). In 2014 and 2016 Chl_{50m}:Chl_{SCM} was significantly greater (> 19 on average compared to < 11 on average in 2013 and 2015), indicating chlorophyll was generally more dispersed in the water column relative to 2013 and 2016, when the SCM accounted for a more substantial proportion of water column chlorophyll. This apparent chlorophyll dispersal corresponded with reduced stability (IIS < 0.7 on average in 2014 and 2015 compared to > 3.5 in 2013 and 2015) in both years. Temperature may have also had some influence on SCM chlorophyll structure, but the IIS was the only variable that had an apparent association with chlorophyll structure in all four years. This potentially suggests that in any given year stability is the most important factor controlling SCM chlorophyll structure in the Western English Channel.

Phytoplankton community structure within the SCM, as identified by CytoSense flow cytometry, was distinct between the years of 2014, 2015 and 2016, mainly relating to interannual variation in stratification strength and stability. Red nano-phytoplankton, such as naked dinoflagellates, chlorophytes and prymnesiophytes, made a greater contribution to the community in low stability conditions (IIS < 0.7 on average), possibly as a result of the advantages that motility and enhanced light utilisation efficiency combined confer within a SCM exposed to greater turbulence. Whereas, orange nano-phytoplankton and pico-phytoplankton, such as cryptophytes, *Synechococcus*, chlorophytes and prymnesiophytes, were more important in the SCM community when stratification was strong, but stability at the depth interval of the SCM was low, reasons for which are difficult to establish. These findings have particular connotations for our understanding of trophic dynamics in these summer stratified waters given the essential role of smaller phytoplankton in the microbial loop.

The structure of the ≥ 10 μm phytoplankton community within the SCM as identified by light microscopy was also distinct in each year of study, predominantly in relation to stability and

temperature. Considerable associations were also found between inorganic nutrients and community structure, but it was likely that nutrient status and subsequent growth of phytoplankton within the SCM had a dependence on intracellular and/or organic nutrient availability and not just the measured ambient concentrations within the SCM. It appeared that the most dominant relationship was the change from lower stability (IIS < 3.7 on average; 2013, 2014 and 2016) to very high stability (IIS > 9 on average; 2015), which was accompanied by a shift from a mixed community of diatoms and dinoflagellates to a community overwhelmingly dominated by large dinoflagellates (*Ceratium fusus*), likely because of the competitive advantage motility confers upon dinoflagellates in highly stable conditions. This finding has implications, in particular, for the silica cycle, given the vital role diatoms have in this cycle, which dinoflagellates do not. The second key relationship was the change from cooler waters (11.6 - 12.1 °C on average; 2013 and 2016) to warmer waters (13.1 °C on average; 2014) within the SCM, largely characterised by a shift from smaller diatoms (*Chaetoceros spp.* and *Pseudo-nitzschia spp.*) to larger diatoms (large *Rhizosolenia spp.*, *Lauderia annulata* and *Leptocylindrus danicus*). This relationship between temperature and size may have particular consequences for carbon export to depth, and the relationship between temperature and certain toxic species (*Pseudo-nitzschia spp*.) may be significant for improving our understanding of toxic blooms. Results from this study may be relevant, not only for the Western English Channel, but also the wider NW European shelf and potentially other analogous shelf sea settings.

Chapter 7: Summary, conclusions and future work

7.1. Synthesis of research

The main aim of this thesis was to investigate SCM in the summer stratified waters of the Western English Channel, specifically their phytoplankton community structure, the primary production and photophysiology of these communities, and environmental parameters influencing the chlorophyll and community structure of SCM. Results presented in chapters 3 – 6 have addressed this aim, and the research questions and objectives specified in chapter 1.

In chapter 3 results from the first detailed study of SCMTL and broader SCM on the NW European shelf were presented, where the study area in the Western English Channel during summer 2013 ranged from being in very close proximity to the tidal mixing front, to a repeat station located far enough away from the front to be permanently stratified, to over 30 km offshore. *Pseudo-nitzschia* was almost exclusively the dominant diatom taxon in SCM and the surrounding water column, with other key taxa including the diatoms *Chaetoceros spp.* and *Proboscia alata/Rhizosolenia spp.*, and the dinoflagellates *Ceratium lineatum, Gyrodinium spp., Protoperidinium spp., Scrippsiella trochoidea*, *Prorocentrum micans*, *Diplopsalis lenticula*, *Dinophysis acuminata* and unidentified small (10 – 25 µm) naked dinoflagellates. However, there were distinctions in community structure between SCMTL and broader SCM. Specifically, greater proportions of *Proboscia alata* and other rhizosolenids, and dinoflagellates *Ceratium lineatum* and *Gyrodinium spp.* were identified in SCMTL, combined with lesser proportions of the diatom *Chaetoceros spp.* and dinoflagellate *Diplopsalis lenticula*. This difference was proposed to occur due to the promotion of different phytoplankton within SCMTL compared to broader SCM, relating to conditions more specific to SCMTL, with *Proboscia alata*, *Ceratium lineatum* and *Gyrodinium spp.* all having documented traits that may have made them better adapted to these SCMTL conditions. SCMTL were a recurrent feature of the summer stratified waters of the Western Channel in 2013 (identified in 18 of 52 water column profiles exhibiting an SCM collected over 11 days). In addition to a reduced vertical extent, these subsurface features were typically characterised by higher maximum chlorophyll concentration, and were apparently governed by thermocline structure (most associated with the sharp lower step of a stepped thermocline) and stronger stratification. Given the intense and prolonged stratification predicted for the NW European shelf with future climate change, it was suggested that SCMTL and associated specialised phytoplankton may become more prevalent, with biogeochemical implications of potentially great significance.

In chapter 4 results from the first high depth resolution taxonomic study of phytoplankton community structure within and throughout an SCM and surrounding water column, measured using *in situ* holography, were presented. The digital in-line holographic camera (holocam) deployment was conducted on one day during a survey in the Western English Channel where 40 stratified sites were sampled over 14 days in the summer of 2015; some sites were in the same general location and others were located further afield (across an approximate area of 2000 km^2). Holography showed there to be transition of phytoplankton through the water column, with different taxa becoming dominant over small depth ranges, suggesting different phytoplankton occupy specific niches within stratified waters. At maximum chlorophyll concentration (28.0 $\mu g\ l^{-1}$) within the SCM the mixotrophic dinoflagellate, *Ceratium fusus*, was overwhelmingly dominant, so that the SCM community was largely monospecific. The growth of *Ceratium fusus* was shown to be driven by photoautotrophy, with important implications for the primary productivity of the SCM. It was suggested that this dinoflagellate was able to dominate to such a degree because of the advantages that its many adaptations confer in a strongly stratified water column. *Ceratium fusus* was almost absent above 15 m, but was still an important part of the community in bottom waters. *Ceratium lineatum* and *Dictyocha spp.*, although much less abundant, had similar distributions to *Ceratium fusus*, but in contrast to *Ceratium fusus*, *Ceratium lineatum* made its largest contributions to the community on the downslope of the SCM and *Dictyocha spp.* was the dominant taxon at the upper boundary of the main thermocline. *Proboscia truncata* and chained centric diatoms (*Thalassiosira*) were dominant alongside *Ceratium fusus* within the base of the SCM and in bottom waters. Taxa that rely on heterotrophic nutrition (ciliates and *Ceratoperidinium* + *Gyrodinium spp.*) were present throughout the water column in varying proportions. Rod shaped diatoms and curled-chained diatoms were also present at all depths, but with low abundances in the surface layer and with a transition in the size of the rod shaped diatoms from above the SCM to below the SCM. These different distributions of the various taxa and the overall transition observed were proposed to reflect interactions and certain traits of each taxon, in combination with environmental conditions within the water column. At depths where discrete water samples were collected, holographic data largely reflected data collected by microscope analysis. Microscope analysis of discrete phytoplankton samples collected from a further 39 sites indicated the community structure to be broadly similar over the wide survey area. Therefore, it was suggested that the holocam data from the one site was representative of other stratified sites across the Western English Channel at the time of the survey, with evidence to suggest that it may have also been relevant for adjoining open shelf waters. However, only by further holocam deployments would subtle, distinct vertical changes in community structure have been recognised at the different sampling sites. Research in chapter 4

illustrated that *in situ* holography can be a powerful tool for assessing phytoplankton community structure, and observations of extensive aggregates below the SCM also showed its potential as a viable tool for obtaining quantitative carbon flux data. However, it was acknowledged that *in situ* holography does currently have limitations, but method developments were suggested that could allow the full potential of holographic technology for assessment of phytoplankton community structure on a large temporal and spatial scale to be reached.

In chapter 5 estimates of water column and SCM layer primary production at 16 sites sampled within the Western English Channel, across an area of 1250 km^2, over 10 days in the summer of 2015 were presented. Estimates of primary production were derived using a combination of ^{13}C incubation experiments and FIRe measurements of relative electron transport rate (rETR) versus irradiance. Primary production profiles roughly resembled corresponding chlorophyll profiles, with a production maximum typically associated with the SCM. On average, roughly 50 % of water column primary production occurred within the SCM layer, which was also identified to be a significant site of new production. Variation in the magnitude of water column primary production between sites was found to be governed by changes in SCM layer primary production, which highlighted the importance of investigating SCM primary production and environmental factors that influence this production. Changes in the amount of photosynthetic biomass within the SCM layer, represented by integrated chlorophyll concentration, accounted for approximately half of the site to site variability in SCM layer primary production. Light intensity was demonstrated to be the most important environmental factor driving variation in SCM layer primary production across the 16 sites, with a change from low to high light, on occasion, accounting for a greater difference in primary production than that between sites. Moreover, phytoplankton community structure and photophysiological status were also shown to be key in influencing SCM primary production, with increased rates of primary production associated with greater proportions of red nano-phytoplankton, which could be attributed to a greater efficiency of light utilisation. As sites where red nano-phytoplankton were more important within the community were related to enhanced stratification, it was suggested that these findings may be important for advancing our understanding of the effect of stratification on primary production and for projections of how the shelf sea ecosystem could respond to increased stratification brought about by future climate change.

In chapter 6 SCM chlorophyll structure and SCM phytoplankton community structure at a repeat site in the Western English Channel from 2013 to 2016 was presented, with their interannual variability related to changes in environmental conditions from year to year.

Chlorophyll structure was assessed in terms of thickness, maximum chlorophyll concentration and the 50 m:SCM maximum chlorophyll ratio (Chl_{50m}:Chl_{SCM}), with interannual variation in the latter two factors detected. The highest stability (IIS 9.07 on average in 2015), relating to low current velocities, coincided with the highest maximum SCM chlorophyll concentrations (7.3 µg l^{-1} on average). Whereas, low stability (IIS < 0.7 on average), as observed in 2014 and 2016, coincided with greater Chl_{50m}:Chl_{SCM}, indicating dispersal of chlorophyll throughout the water column. Temperature may also have had some influence on SCM chlorophyll structure, but stability was the only variable that had an apparent association with chlorophyll structure in all four years. It was therefore proposed that stability at the depth interval of the SCM could be considered the most important factor governing SCM chlorophyll structure. Phytoplankton community structure was assessed by flow cytometry and by inverted light microscopy. Community structure within the SCM as identified by CytoSense flow cytometry was distinct between the years of 2014, 2015 and 2016, mainly relating to interannual variation in stratification strength and stability. In 2015 the community largely comprised of meso- and micro-phytoplankton, but in 2014 and 2016 phytoplankton at the smaller end (< 20 µm) of the size spectrum also made important contributions. In both years, red nano-phytoplankton made substantial contributions, often being dominant, associated with reduced stability (IIS < 0.7 on average), and in 2016 orange nano-phytoplankton and pico-phytoplankton were also important, related to increased strength of stratification, but low stability at the depth interval of the SCM. The structure of the ≥ 10 µm community within the SCM as identified by light microscopy was distinct in each year from 2013 to 2016, predominantly relating to stability and temperature. Two key overarching relationships were found: (1) a shift from a mixed community of diatoms and dinoflagellates (2013, 2014, 2016) to a community overwhelmingly dominated by large dinoflagellates (i.e. *Ceratium fusus*; 2015) was associated with a change from lower stability (IIS < 3.7 on average) to very high stability (IIS > 9 on average); and (2) a shift from smaller diatoms (*Chaetoceros spp.* and *Pseudo-nitzschia spp.*) to larger diatoms (large *Rhizosolenia spp.*, *Lauderia annulata* and *Leptocylindrus danicus*) was related to a change from cooler waters (11.6 - 12.1 °C on average; 2013 and 2016) to warmer waters (13.1 °C on average; 2014) within the SCM. In all cases, reasons were proposed as to why the different relationships between various phytoplankton and environmental parameters may have been observed. It was suggested that the results in chapter 6 may likely have an array of biogeochemical and ecological implications, but in particular, for the microbial loop, the silica cycle, carbon export to depth and toxic phytoplankton blooms. Moreover, it was proposed that environmental conditions, especially stability and temperature, related to the summer SCM in the Western English Channel may be used as indicators of key SCM taxa.

Based on findings presented in the thesis as a whole Tables 7.1 and 7.2, and Figure 7.1 are proposed.

Table 7.1. Typical physical conditions promoting and associated with SCMTL compared to broader SCM within the summer stratified waters of the Western English Channel.

Physical factor	SCMTL	Broader SCM
Thermocline structure (Fig. 3.4)	Stepped	Gradual
Depth (at max. chlorophyll)	> 15 < 40 m	> 5 < 40 m
Stratification	Stronger stratification relative to broader SCM	Weaker stratification relative to SCMTL
Turbulence conditions	Minimal mixing, possibly including a small vertical extent of the turbulence minimum within which the chlorophyll maximum develops	Increased mixing relative to SCMTL, possibly including a larger vertical extent of the turbulence minimum within which the chlorophyll maximum develops

Table 7.2. Phytoplankton traits promoting success within the SCM. All traits are listed with the functions they may facilitate (listed by number as detailed below), and the main phytoplankton groups/taxa they apply to. Functions important for success within the SCM are (1) resource (a. nutrients and b. light) acquisition/efficient utilisation, (2) grazer avoidance, (3) avoidance of removal from the SCM by turbulent mixing, and (4) growth in low light conditions.

Trait	Function	Phytoplankton
Motility	1a, 1b, 2, 3	Dinoflagellates, flagellates and ciliates
High aspect ratio	1a, 1b, 2, 3	Some representatives of all main phytoplankton groups as listed in section 1.1.1., excluding cyanobacteria, e.g. rhizosolenid diatoms, *Ceratium spp.*, *Laboea spp.*, *Eutreptiella spp.*
Vacuole nutrient storage	1a	Diatoms
Luxury nutrient uptake	1a	Diatoms and some dinoflagellates, e.g. *Ceratium spp.*
Small size	1a, 1b, 4	Pico- and nano-phytoplankton
Large size	1a, 2	Micro- and meso-phytoplankton
Higher light utilisation efficiency	1b, 4	Nano-phytoplankton
Colonial	1a, 2	Some diatoms, dinoflagellates and flagellates, e.g. *Chaetoceros spp.*, *Proboscia alata* and *Solenicola setigera*
Mixotrophy/heterotrophy	1a	Some dinoflagellates, flagellates and ciliates, e.g. *Polykrikos schwartzii*, *Ceratium spp.*, *Chrysochromulina spp.*, *Laboea spp.*
Buoyancy control	1a, 1b, 3	Diatoms, with some diatoms capable of positive buoyancy, e.g. rhizosolenids
Armour	2	Diatoms, and some dinoflagellates, flagellates and ciliates
Anoxia induction	2	Some dinoflagellates and ciliates, e.g. *Ceratium fusus* and *Mesodinium rubrum*
Toxin production	2	Some diatoms, dinoflagellates and flagellates e.g. *Pseudo-nitzschia spp.*, *Dinophysis spp.* and *Chrysochromulina spp.*
Long setae/spines	3	Some diatoms, e.g. *Chaetoceros*
Photophysiological flexibility: the photoacclimation response	1b, 4	Cells with photosynthetic apparatus (although the efficiency of the photoacclimation response varies between taxa, e.g. larger cells are more susceptible to the package effect)
Adaptation to grow at low light	4	A variety of phytoplankton species – the so called 'shade flora', e.g. *Ceratium fusus* and large diameter rhizosolenids

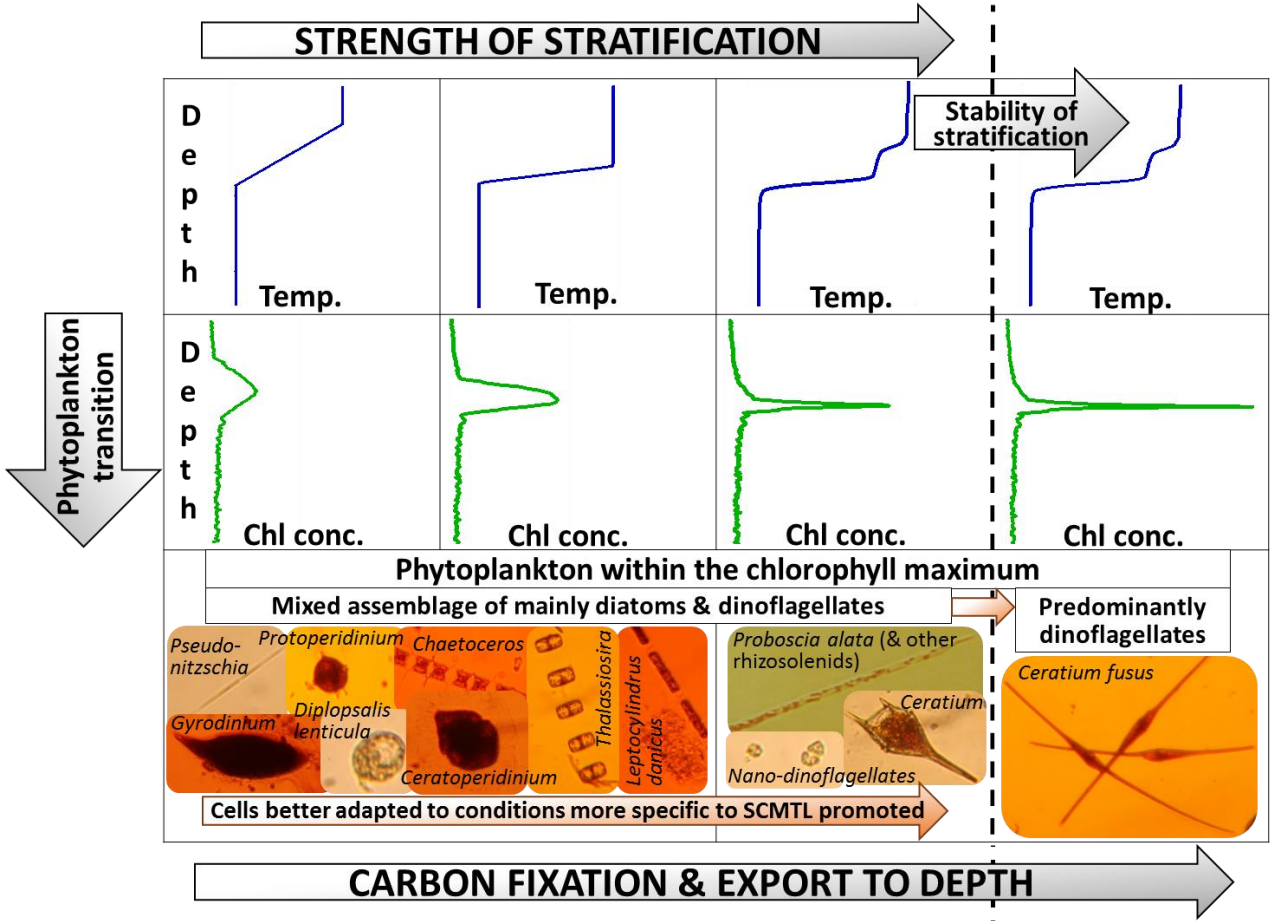

Figure 7.1. Conceptual diagram summarising the main findings of the thesis. In brief, the governing influence of water column structure and stratification on the development of SCMTL over broader SCM and associated phytoplankton community structure, and the key corresponding potential biogeochemical implications. The diagram also includes reference to the transition of phytoplankton through the stratified water column, and the effect of enhanced stability on an SCMTL and its phytoplankton community.

7.2. Main conclusions

From the research presented in this thesis the following four key overarching conclusions can be drawn:-

1. Distinction in phytoplankton community structure between SCMTL and broader SCM may result from promotion of phytoplankton better adapted to SCMTL compared to broader SCM, relating to environmental conditions more specific to SCMTL. As SCMTL were present under conditions of increased stratification compared to broader SCM, the more intense and prolonged stratification projected for the NW European shelf in future due to global warming may be accompanied by an increased prevalence of SCMTL and associated larger-sized SCMTL specialised flora.

2. High depth resolution profiling of phytoplankton community structure in a stratified water column using *in situ* holography can provide identification of the small vertical scale transition of phytoplankton and how one species can be dominant over a small part of the water column. With future developments of the methodology, holography could be used for assessment of the phytoplankton community on a large temporal and spatial scale, and may be a viable tool for obtaining quantitative carbon flux data.

3. Within a coastal summer stratified water column the SCM is a significant contributor of primary production, estimated to account for approximately half of total water column carbon fixation, and is an important site of new production. Variation in total water column primary production was driven by changes in the magnitude of SCM primary production, where variation in SCM primary production was largely governed by chlorophyll concentration, irradiance and the phytoplankton community, particularly red nano-phytoplankton due to their greater light utilisation efficiency.

4. There was significant interannual variation in SCM chlorophyll structure and phytoplankton community structure within the summer stratified waters of the Western English Channel, relating to variability in environmental conditions, in particular, stability at the depth interval of the SCM and water temperature. Therefore, stability and temperature data related to the summer SCM in shelf seas may be a useful indicator of key SCM phytoplankton taxa.

7.3. Key implications of the research

As a whole the research presented in this thesis has demonstrated two key points: (1) natural assemblages of phytoplankton are highly varied and since individual taxa possess an array of taxon-specific properties, study of phytoplankton communities is key for efforts to develop an improved understanding of biogeochemical and ecological dynamics within the marine ecosystem; and (2) the SCM represents a substantial fraction of water column phytoplankton biomass in seasonally stratified shelf seas, thus has a significant role within the shelf environment. These two points have particular implications for the results of model and satellite based investigations and consequently for research practices applied in future studies.

7.3.1. Implications for model based investigations

Models used in the investigation of the ocean system are highly simplified. In addition to not being able to accurately replicate the physics within the marine environment, they do not represent phytoplankton communities in any detail. For example, the IPSL-CM4- LOOP model only distinguishes between small and large phytoplankton, and the Max-Planck Institute for Meteorology (MPIM) Earth System Model only distinguishes between calcite and opal producers and flagellates (Steinacher et al., 2010). Therefore, given the reality that natural phytoplankton assemblages consist of a multitude of different phytoplankton with a variety of traits, these models are unlikely to produce accurate results. This fact has consequences for advances in the design of phytoplankton components of ocean system models in order to enhance confidence in model outputs related to phytoplankton, including primary production and carbon export estimations and projections. Better representation of phytoplankton within models may not only establish an improved understanding of biogeochemical cycling and ecological dynamics, but may also facilitate more accurate predictions of how the marine ecosystem could respond to climate change in the future.

7.3.2. Implications for satellite based investigations

The position of the SCM within the water column renders it invisible to satellites and therefore subsurface primary production cannot be quantified using remote sensing techniques. Yet, the shelf sea SCM is responsible for a considerable proportion of water column photosynthetic biomass, estimated to account for, on average, 50 % of water column primary production, and demonstrated to be a key site of new production and the driver of variation in the magnitude of total water column production in this thesis. Therefore, neglecting to include the production of these shelf sea features in estimations of regional and global primary production has the

potential to result in substantial underestimations. This fact establishes that satellites cannot be relied upon for accurate estimates of primary production and that *in situ* sampling is still important in efforts to further our knowledge of SCM primary production and subsequently the biogeochemical and ecological role of the SCM in shelf seas and globally. Furthermore, the demonstrated significance of the SCM for primary production in seasonally stratifying shelf waters reinforces the recognised need for the SCM to be consistently represented in ocean system models to enable reliable estimation/prediction of biogeochemical and ecological ecosystem dynamics, and ecosystem responses to environmental variation, particularly that which may be presented by future climate change.

7.4. Future work

- In this research SCM were commonly observed to comprise of a mixed phytoplankton assemblage, but intense and largely monospecific blooms within the SCM were also observed, e.g. *Ceratium fusus* dominated the SCM recorded in 2015. It is important to establish the key controls of such subsurface monospecific blooms, especially if they consist of large celled phytoplankton that can contribute disproportionately to primary production, export to depth and carbon transfer through the food web. Further and more focused sampling of such monospecific SCM, including detailed investigation into the physical and biological conditions surrounding these SCM using a combination of discrete sampling and profiling, would help to achieve this.

- Study of primary production within the stratified water column established the SCM to be responsible for substantial production, some of the key species identified within the SCM have been previously associated with extensive carbon export to depth (Sancetta et al., 1991, Kemp et al., 2000), and *in situ* holography imaged numerous aggregates below the SCM. These findings suggest SCM in shelf seas may likely be a considerable source of export, yet, little quantitative data exists on export of carbon from SCM on the NW European shelf. To address this, *in situ* holography (as discussed in chapter 4) and/or marine snow catcher deployments (Riley et al., 2012) could be performed, both of which have the potential to provide quantitative data on carbon flux from the SCM.

- Phytoplankton cell orientation and chain length can influence light absorption (McFarland et al., 2016), which may have important implications for community structure and primary production within a SCM. Therefore, study of chain length and cell

orientation within the SCM relative to stratification and the local shear would be useful for improving our understanding of controls on phytoplankton community structure and the effect of the physical environment on the physiology of key SCM phytoplankton. This can be achieved by deployment of a free fall turbulence profiler with mounted holographic camera.

- The future of SCM under the influences of climate change is uncertain, yet in chapters 3 and 5, in particular, data is presented that could advance our understanding of the role SCM may have in this uncertain future. In chapter 3, a shift in phytoplankton community structure was observed from broader SCM to SCMTL, where SCMTL were associated with increased stratification, perhaps akin to the enhanced stratification predicted for the UK shelf seas with future climate change (Lowe et al., 2009, Sharples et al., 2013, Tinker et al., 2016). However, observations were not sufficient to make a definitive conclusion about whether different phytoplankton were promoted within SCMTL compared to broader SCM. In chapter 5 greater proportions of red nano-phytoplankton within the SCM were also associated with increased stratification. However, environmental conditions relating to these observations were not studied in great detail. Therefore, further investigation of the ecology, physiology and environmental forcing factors relating to key phytoplankton associated with SCMTL and greater stratification is required. This further investigation would need to span a greater temporal and spatial extent, and be inclusive of the entire phytoplankton size spectrum.

Chapter 8: Appendices

Appendix 1

All figures and tables in this appendix are referenced in chapter 3.

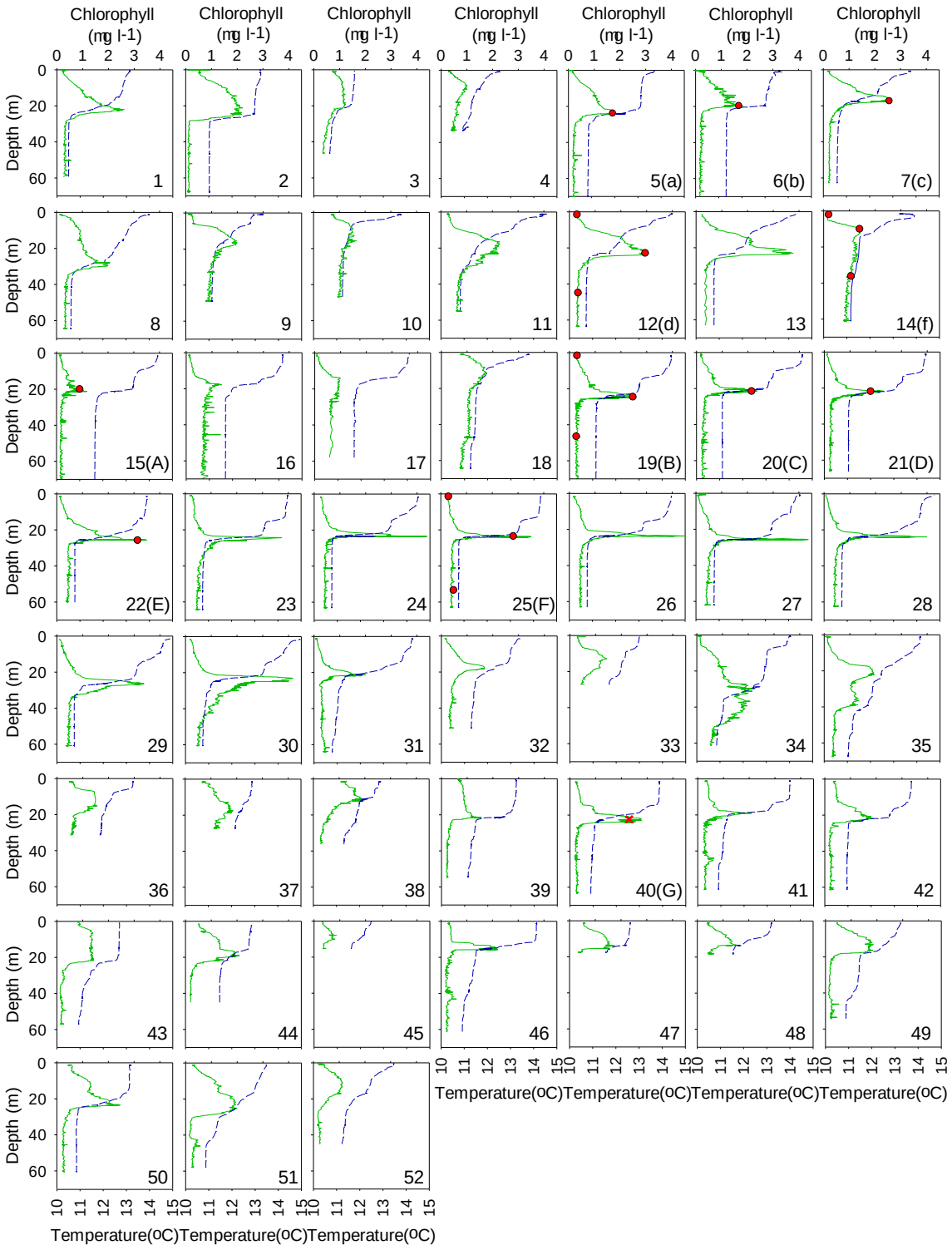

A1.1. Temperature and chlorophyll profiles of the 52 stratified sites (site numbers given in the bottom

right hand corner of each profile plot) profiled in the Western English Channel during June/July 2013 (further details provided in Table A1.1). Sample IDs included in brackets indicate sites from which water samples were collected and analysed for phytoplankton, where an upper case ID indicates a SCMTL and a lower case ID indicates a broader SCM. The green line represents chlorophyll concentration derived from CTD chlorophyll-fluorescence, the blue dashed line represents temperature, the red circles where Niskin water bottle samples were collected and the red X where a slurp gun sample was collected.

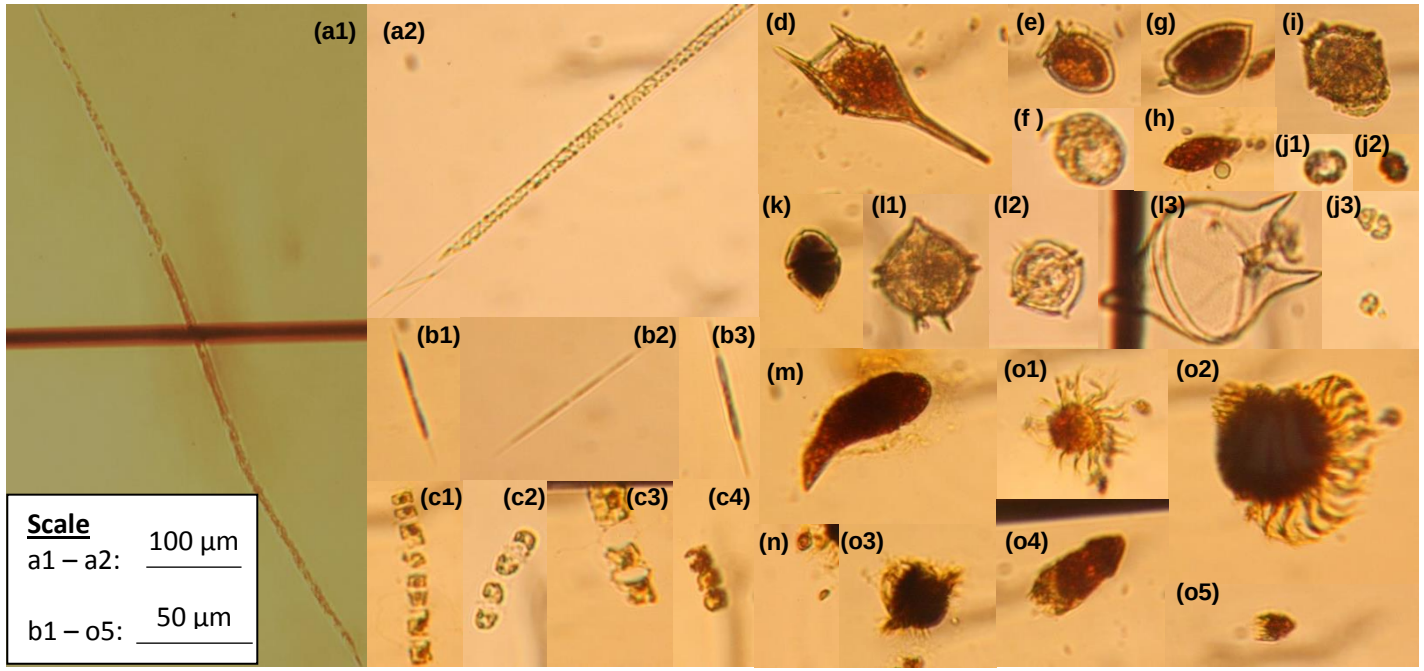

Figure A1.2. Dominant/significant phytoplankton identified in Lugol's iodine preserved samples taken from SCMTL and broader SCM of the Western English Channel in summer 2013. (a1) – (a2) *Proboscia alata/Rhizosolenia spp.*; (b1) – (b3) *Pseudo-nitzschia spp.*; (c1) – (c4) *Chaetoceros spp.*; (d) *Ceratium lineatum*; (e) *Dinophysis acuminata*; (f) *Diplopsalis lenticula*; (g) *Prorocentrum micans*; (h) *Katodinium glaucum*; (i) *Gonyaulax spinifera*; (j1) – (j3) small naked dinoflagellates; (k) *Scrippsiella trochoidea*; (l1) – (l3) *Protoperidinium spp.*; (m) *Gyrodinium spp.*; (n) cryptophytes; (o1) – (o5) ciliates.

Table A1.1. Date, time, location, water depth, SCM maximum chlorophyll concentration, SCM chlorophyll intensity ratio, SCM thickness, SCM depth (at maximal chlorophyll intensity), difference in temperature between surface and bottom waters (where surface temperature was taken at 2 m and bottom water temperature was taken at 45 m, with the exceptions of sites 4, 33, 36, 37, 38, 45, 47 and 48 where the water column was shallower or profiled to less than 45 m and so bottom water temperature was taken at the deepest point in the profile), buoyancy frequency, wind speed, current velocity (unable to calculate for sites 3 and 31 due to missing data) and tidal state details (where spring + 0 coincides with new/full moon phase and neap + 0 coincides with quarter moon phase) of the 52 stratified sites profiled in the Western English Channel during summer 2013. Sites in red are repeat station 1, sites in green are repeat station 2, and sites with a sample ID and SCM sample depth were sampled for phytoplankton analysis, where an upper case ID indicates a SCMTL and a lower case ID indicates a broader SCM. All SCMTL observed are indicated through use of an alternative and bold font for their thickness.

Date	Site no.	Time (UTC)	Latitude	Longitude	Water depth (m)	SCM max chlorophyll concentration (µg L^{-1})	SCM chlorophyll intensity ratio	SCM thickness (m)	SCM depth (m)	Δsurface -bottom temp. (°C)	Buoyancy frequency ($rad^2 s^{-2}$)	Wind speed (m s^{-1})	Current velocity (m s^{-1})	Tidal state	Sample ID	SCM sample depth (m)
24/06	1	12:47	50°05.61N	004°52.28W	66	2.6	8.1	6.2	22.0	2.57	0.0012	8.9	0.47	Spring +0		
	2	14:35	49°59.90N	004°40.41W	74	2.1	19.1	20.1	19.7	2.22	0.0026	9.1	0.24			
	3	16:26	50°07.51N	004°57.82W	50	1.2	2.7	20.3	13.9	1.05	0.0007	10.1	-			
25/06	4	09:28	50°07.52N	004°58.75W	40	1.0	1.9	9.0	9.3	1.21	0.0004	5.4	0.20			
	5	11:29	49°59.98N	004°41.49W	74	1.8	8.5	10.0	23.0	2.55	0.0031	4.3	0.57	Spring +1	**a**	23.2
	6	13:09	49°51.85N	004°43.44W	78	1.6	8.6	10.3	19.6	2.09	0.0029	4.3	0.65		**b**	19.6
	7	15:40	50°05.84N	004°51.96W	66	2.5	9.9	6.3	16.1	2.96	0.0010	3.9	0.11		**c**	16.8
26/06	8	08:40	50°05.83N	004°51.91W	66	2.1	5.9	7.1	27.8	3.06	0.0019	1.6	0.32			
	9	10:36	50°08.00N	004°54.81W	50	1.9	2.1	9.8	17.3	1.74	0.0042	2.2	0.24			
	10	14:36	50°07.04N	004°57.35W	50	1.5	1.4	14.1	13.4	2.23	0.0022	5.4	0.31	Spring +2		
	11	15:25	50°06.68N	004°56.05W	58	2.2	3.3	16.9	18.9	3.54	0.0010	3.7	0.20			
	12	16:20	50°05.71N	004°52.17W	66	3.0	8.7	11.2	22.3	3.59	0.0018	2.9	0.10		**d**	22.4
	13	16:53	50°05.82N	004°51.89W	66	3.6	8.9	9.6	23.0	3.43	0.0020	2.5	0.14			
27	14	09:45	50°05.67N	004°56.77W	63	1.5	2.1	12.8	10.6	2.62	0.0001	1.6	0.21		**e**	10.1

	15	12:58	49°40.95N	005°11.78W	86	1.1	5.3	**2.0**	20.7	2.70	0.0015	1.5	0.71		**A**	20.1
	16	14:23	49°46.53N	005°13.13W	83	1.3	1.9	3.5	17.3	2.46	0.0018	3.6	0.73	Spring		
	17	14:59	49°46.04N	005°13.76W	83	0.9	1.3	12.0	19.2	2.30	0.0015	5.1	0.12	+3		
	18	16:57	50°01.67N	005°01.66W	67	1.7	2.1	14.1	11.1	2.13	0.0015	5.1	0.64			
28/06	19	10:48	50°00.15N	004°40.03W	74	2.5	9.4	**3.9**	24.6	3.25	0.0027	2.9	0.24		**B**	24.7
	20	12:15	50°02.09N	004°44.96W	73	2.2	9.3	**2.1**	21.4	3.45	0.0026	3.6	0.22	Spring	**C**	21.5
	21	13:22	50°03.63N	004°49.41W	69	2.3	9.9	**2.6**	21.7	3.34	0.0028	5.5	0.34	+4	**D**	21.7
	22	14:50	50°05.41N	004°52.13W	66	3.5	7.9	**1.9**	25.6	3.11	0.0033	4.0	0.44		**E**	25.6
29/06	23	08:14	50°05.73N	004°52.29W	66	3.8	8.5	**2.2**	24.4	3.65	0.0037	7.2	0.18			
	24	09:19	50°05.58N	004°52.46W	66	4.4	10.4	**1.5**	23.4	3.72	0.0042	5.4	0.25			
	25	10:15	50°05.69N	004°52.55W	66	3.4	8.8	**0.7**	23.6	3.53	0.0036	3.4	0.19		**F**	23.6
	26	11:15	50°05.63N	004°52.45W	66	4.5	10.2	**1.0**	23.6	3.63	0.0029	3.5	0.16	Spring		
	27	12:53	50°05.72N	004°52.80W	66	4.3	10.1	**0.04**	25.6	3.52	0.0028	4.2	0.19	+5		
	28	13:52	50°05.56N	004°52.74W	66	4.0	9.5	**1.0**	23.9	3.72	0.0027	3.6	0.31			
	29	14:44	50°05.58N	004°52.99W	66	3.3	7.3	**4.5**	26.5	4.00	0.0018	4.3	0.38			
	30	15:45	50°05.56N	004°53.11W	66	4.2	8.9	**4.5**	23.2	3.98	0.0027	5.2	0.43			
01/07	31	08:48	50°05.80N	004°51.86W	66	2.0	6.7	**2.6**	21.2	3.25	0.0016	3.6	-			
	32	10:43	50°07.89N	004°55.42W	65	1.7	4.9	**4.0**	18.3	1.97	0.0009	4.3	0.11	Neap		
	33	11:16	50°08.76N	004°56.97W	32	1.4	2.9	10.2	12.9	1.29	0.0002	5.0	0.18	+0		
	34	13:58	50°03.83N	004°58.94W	60	2.1	3.6	21.3	34.8	2.88	0.0010	4.9	0.10			
	35	15:23	50°00.49N	005°01.69W	72	1.9	4.9	22.5	22.2	2.86	0.0005	7.6	0.29			
02/07	36	09:29	50°05.50N	005°01.49W	56	1.5	2.4	12.4	11.9	1.42	0.0011	5.4	0.10			
	37	11:06	50°07.63N	004°59.06W	40	1.8	1.5	9.0	17.4	0.73	0.0003	5.3	0.17	Neap		
	38	14:17	50°05.30N	005°01.89W	56	1.9	5.5	12.7	11.6	1.50	0.0008	5.5	0.09	+1		
	39	14:50	50°05.34N	004°59.32W	62	1.6	6.5	8.3	21.5	2.09	0.0026	7.5	0.11			
03/07	40	08:49	50°05.72N	004°51.89W	66	2.8	10.7	**4.3**	22.9	2.91	0.0025	7.4	0.17		**G**	22.6
	41	10:12	50°07.41N	004°51.16W	62	2.1	8.0	**2.9**	19.2	2.95	0.0034	7.6	0.13	Neap		
	42	11:19	50°08.97N	004°50.04W	60	1.9	6.7	7.8	21.9	2.78	0.0028	8.2	0.09	+2		
	43	12:23	50°10.71N	004°48.41W	54	1.4	6.6	20.4	14.5	1.62	0.0011	9.0	0.10			
	44	14:00	50°10.47N	004°53.47W	48	2.1	9.4	13.2	18.9	1.36	0.0009	10.6	0.12			

	45	15:15	50°09.37N	004°57.67W	25	0.9	2.3	5.3	7.8	0.81	0.0004	13.9	0.11	
04/07	46	08:59	50°05.64N	004°51.97W	66	2.2	8.7	**3.4**	15.5	3.12	0.0030	6.2	0.19	Neap +3
	47	10:29	50°07.52N	004°59.41W	40	1.8	4.2	9.3	14.0	1.04	0.0015	4.0	0.17	
	48	11:20	50°06.11N	005°02.78W	40	1.5	3.1	6.3	13.3	1.65	0.0013	4.8	0.10	
	49	12:23	50°04.91N	005°00.12W	60	1.8	10.5	12.2	13.3	2.33	0.0014	3.7	0.06	
	50	12:51	50°04.12N	004°58.47W	63	2.5	8.8	6.7	23.6	2.28	0.0020	3.7	0.09	
	51	13:47	50°04.28N	004°59.73W	61	1.9	6.9	18.8	23.2	2.55	0.0005	4.9	0.12	
	52	14:20	50°03.93N	005°02.41W	50	1.1	4.3	13.4	12.9	2.13	0.0007	5.9	0.21	

Table A1.2. Estimated carbon biomass (Pg C ml^{-1}) of phytoplankton taxa identified in samples collected during the 2013 summer field survey in the Western English Channel.

Date	**25/06/13**	**25/06/13**	**25/06/13**	**26/06/13**	**26/06/13**	**26/06/13**	**27/06/13**	**27/06/13**	**27/06/13**
Site number	**5**	**6**	**7**	**12**	**12**	**12**	**14**	**14**	**14**
Sample ID	**a**	**b**	**c**	**d**	**d**	**d**	**e**	**e**	**e**
Sample location	**SCM**	**SCM**	**SCM**	**Bottom**	**SCM**	**Surface**	**Bottom**	**SCM**	**Surface**
Diatoms (Pg C ml^{-1})									
S centric diatom (20-30 µm dia.)	193.5	0.0	0.0	0.0	0.0	0.0	0.0	0.0	0.0
M centric diatom (30-50 µm dia.)	0.0	0.0	149.4	0.0	0.0	0.0	0.0	0.0	0.0
L centric diatom (60-150 µm dia.)	0.0	0.0	0.0	0.0	0.0	0.0	0.0	0.0	0.0
Chaetoceros spp.	8591.8	7732.6	5584.7	710.5	11455.8	2863.9	5155.1	16897.2	3293.5
Cylindrotheca closterium	0.0	0.0	0.0	0.0	0.0	0.0	0.0	0.0	0.0
Dactyliosolen fragilissimus	0.0	604.5	0.0	0.0	0.0	0.0	0.0	0.0	0.0
Detonula confervacea	0.0	0.0	0.0	0.0	0.0	0.0	0.0	0.0	0.0
Diploneis spp.	0.0	0.0	18.1	0.0	18.1	0.0	18.1	0.0	0.0
Eucampia zoodiacus	0.0	0.0	0.0	0.0	0.0	0.0	0.0	0.0	0.0
Guinardia delicatula	0.0	0.0	0.0	0.0	47.3	0.0	0.0	0.0	0.0
Guinardia flaccida	0.0	0.0	0.0	0.0	0.0	0.0	0.0	0.0	0.0
Guinardia striata	0.0	0.0	0.0	0.0	0.0	0.0	0.0	0.0	0.0
Lauderia annulata	0.0	0.0	100.9	0.0	0.0	0.0	0.0	0.0	0.0
Meuniera membranacea	0.0	0.0	0.0	0.0	0.0	0.0	0.0	0.0	0.0
Paralia sulcata	69.9	0.0	0.0	125.9	0.0	0.0	153.9	0.0	0.0
S pennate diatom (20-40 µm length)	0.0	0.0	0.0	0.0	0.0	0.0	0.0	0.0	0.0
M pennate diatom (40-65 µm length)	0.0	119.1	19.9	0.0	19.9	0.0	0.0	0.0	0.0
L pennate diatom (65-110 µm length)	0.0	0.0	0.0	0.0	0.0	0.0	0.0	0.0	0.0

S *Pleurosigma spp.* (~50 µm length)	0.0	0.0	0.0	0.0	0.0	0.0	0.0	0.0	0.0
M *Pleurosigma spp.* (~80-170 µm length)	0.0	0.0	0.0	68.5	0.0	0.0	68.5	68.5	0.0
L *Pleurosigma spp.* (170-200 µm length)	135.9	0.0	0.0	0.0	0.0	0.0	135.9	135.9	0.0
S *Rhizosolenia spp.* (≤ 10 µm dia.)	0.0	133.4	0.0	0.0	0.0	0.0	0.0	0.0	0.0
M *Rhizosolenia spp.* (10-20 µm dia.)	0.0	0.0	366.8	0.0	0.0	366.8	0.0	0.0	0.0
L *Rhizosolenia spp.* (> 20 µm dia.)	0.0	0.0	0.0	0.0	0.0	0.0	0.0	0.0	1897.2
Proboscia alata	1902.5	9951.6	585.4	243.9	390.3	1073.2	487.8	243.9	829.3
Pseudo-nitzschia spp.	41049.0	18651.2	30705.3	3257.9	73546.1	25492.7	7900.3	44143.9	22397.7
Skeletonema costatum	0.0	0.0	0.0	1.8	1.8	0.0	5.4	0.0	0.0
S *Thalassiosira spp.* (10-25 µm height)	83.6	0.0	0.0	0.0	66.9	0.0	0.0	0.0	0.0
M *Thalassiosira spp.* (25-45 µm height)	0.0	0.0	115.7	57.8	404.9	57.8	0.0	0.0	0.0
L *Thalassiosira spp.* (> 45 µm height)	0.0	0.0	71.5	0.0	0.0	0.0	214.4	0.0	0.0
Total diatom carbon (Pg C ml^{-1})	**52026.2**	**37192.5**	**37717.6**	**4466.2**	**85950.9**	**29854.5**	**14139.3**	**61489.4**	**28417.8**
Dinoflagellates (Pg C ml^{-1})									
10-20 µm naked dinoflagellates	12168.6	5726.4	19505.6	3758.0	22905.7	7158.0	3936.9	13600.3	6263.3
20-25 µm naked dinoflagellates	9569.6	638.0	7017.7	0.0	2551.9	4465.8	0.0	1913.9	1913.9
10-30 µm armoured dinoflagellates	757.7	252.6	606.2	50.5	252.6	707.2	353.6	757.7	202.1
Ceratium fusus	200.4	400.8	200.4	0.0	200.4	0.0	0.0	0.0	0.0
Ceratium lineatum	5447.8	0.0	13317.0	807.1	17554.2	0.0	1815.9	605.3	0.0
Ceratium tripos	0.0	0.0	0.0	0.0	0.0	0.0	0.0	0.0	0.0
Dinophysis acuminata	171.8	0.0	1030.8	0.0	687.2	515.4	171.8	3092.4	515.4
Diplopsalis lenticula	0.0	0.0	12545.0	1194.8	32258.5	3385.2	1393.9	6969.4	1593.0
Dissodinium sp.	0.0	0.0	0.0	0.0	0.0	0.0	0.0	0.0	0.0
Gonyaulax spinifera	1702.6	212.8	1277.0	106.4	1383.4	1170.6	425.7	1809.1	425.7
Gyrodinium spp.	2021.3	2627.7	202.1	0.0	202.1	3234.1	606.4	2425.6	606.4
Karenia mikimotoi	3737.5	0.0	1708.6	0.0	533.9	0.0	213.6	1067.9	106.8

Katodinium glaucum	498.0	199.2	2291.0	332.0	5378.8	697.3	298.8	1328.1	265.6
Oblea rotundata	152.1	0.0	76.0	0.0	0.0	0.0	0.0	0.0	0.0
Polykrikos schwartzii	5639.1	0.0	0.0	0.0	0.0	4229.4	0.0	1409.8	0.0
Prorocentrum micans	2199.7	388.2	1035.1	129.4	388.2	4011.2	0.0	2070.3	1164.5
Prorocentrum minimum	579.1	407.5	42.9	21.4	21.4	128.7	21.4	21.4	42.9
S *Protoperidinium spp.* (10-30 µm dia.)	133.5	0.0	66.8	467.4	934.8	400.6	734.5	1135.2	200.3
M *Protoperidinium spp.* (30-65 µm dia.)	0.0	0.0	334.5	669.0	1672.6	1003.5	334.5	2341.6	669.0
L *Protoperidinium spp.* (65-120 µm dia.)	0.0	0.0	0.0	1753.2	3506.5	0.0	0.0	3506.5	0.0
Scrippsiella trochoidea	2309.1	230.9	1154.5	230.9	1154.5	865.9	115.5	2770.9	519.5
Torodinium robustum/teredo	0.0	0.0	32.9	0.0	0.0	0.0	0.0	0.0	0.0
Total dinoflagellate carbon (Pg C ml^{-1})	**47288.2**	**11084.1**	**62444.2**	**9520.2**	**91586.8**	**31972.9**	**10422.5**	**46825.2**	**14488.4**
Flagellates (Pg C ml^{-1})									
Cryptophytes (> 8 µm)	107.1	77.9	58.4	68.2	146.0	38.9	29.2	77.9	29.2
Dictyocha fibula/speculum	0.0	169.0	0.0	0.0	0.0	0.0	0.0	0.0	0.0
Pseudopedinella/Pyramimonas spp.	38.6	0.0	0.0	0.0	0.0	0.0	0.0	0.0	0.0
Total flagellates (Pg C ml^{-1})	**145.7**	**246.9**	**58.4**	**68.2**	**146.0**	**38.9**	**29.2**	**77.9**	**29.2**
Ciliates (Pg C ml^{-1})									
S ciliates (< 20 µm)	509.8	669.2	0.0	95.6	63.7	0.0	0.0	95.6	95.6
M ciliates (20-40 µm)	3265.6	3135.0	783.8	0.0	1045.0	130.6	130.6	783.8	130.6
L ciliates (> 40 µm)	1189.6	3568.7	0.0	0.0	0.0	14877.6	594.8	0.0	0.0
Tintinnids	358.6	0.0	0.0	0.0	179.3	0.0	0.0	0.0	0.0
Total ciliate carbon (Pg C ml^{-1})	**5323.6**	**7372.9**	**783.8**	**95.6**	**1288.0**	**15008.2**	**725.4**	**879.3**	**226.2**

Date	**27/06/13**	**28/06/13**	**28/06/13**	**28/06/13**	**28/06/13**	**28/06/13**	**28/06/13**	**29/06/13**	**29/06/13**	**29/06/13**	**03/07/13**
Site number	**15**	**19**	**19**	**19**	**20**	**21**	**22**	**25**	**25**	**25**	**40**
Sample ID	**A**	**B**	**B**	**B**	**C**	**D**	**E**	**F**	**F**	**F**	**G**
Sample location	**SCM**	**Bottom**	**SCM**	**Surface**	**SCM**	**SCM**	**SCM**	**Bottom**	**SCM**	**Surface**	**SCM (slurp 2)**
Diatoms (Pg C ml^{-1})											
S centric diatom (20-30 µm dia.)	0.0	0.0	386.9	0.0	0.0	0.0	0.0	0.0	0.0	0.0	0.0
M centric diatom (30-50 µm dia.)	0.0	0.0	896.2	298.7	597.5	746.9	448.1	597.5	448.1	896.2	298.7
L centric diatom (60-150 µm dia.)	0.0	0.0	352.8	0.0	352.8	352.8	0.0	0.0	0.0	0.0	352.8
Chaetoceros spp.	0.0	313.9	1404.4	1266.7	2417.8	2092.9	5112.1	567.3	1178.6	1288.8	3595.3
Cylindrotheca closterium	0.0	0.0	0.0	0.0	0.0	2.8	0.0	0.0	0.0	0.0	0.0
Dactyliosolen fragilissimus	120.9	0.0	0.0	0.0	0.0	0.0	0.0	0.0	0.0	0.0	0.0
Detonula confervacea	0.0	0.0	0.0	0.0	0.0	0.0	0.0	0.0	0.0	0.0	0.0
Diploneis spp.	0.0	18.1	0.0	0.0	0.0	54.3	0.0	18.1	18.1	0.0	0.0
Eucampia zoodiacus	0.0	0.0	0.0	0.0	0.0	0.0	0.0	0.0	0.0	0.0	0.0
Guinardia delicatula	47.3	0.0	519.8	0.0	47.3	141.8	141.8	0.0	94.5	0.0	47.3
Guinardia flaccida	0.0	0.0	748.9	0.0	0.0	0.0	0.0	0.0	0.0	0.0	10484.4
Guinardia striata	0.0	0.0	0.0	0.0	0.0	0.0	0.0	0.0	0.0	0.0	0.0
Lauderia annulata	0.0	0.0	0.0	0.0	0.0	0.0	0.0	0.0	0.0	0.0	0.0
Meuniera membranacea	0.0	0.0	0.0	0.0	0.0	0.0	0.0	0.0	0.0	0.0	0.0
Paralia sulcata	0.0	363.7	0.0	0.0	139.9	279.7	83.9	55.9	0.0	0.0	0.0
S pennate diatom (20-40 µm length)	0.0	4.9	0.0	0.0	0.0	0.0	4.9	0.0	0.0	0.0	0.0
M pennate diatom (40-65 µm length)	19.9	19.9	19.9	0.0	0.0	19.9	0.0	0.0	0.0	0.0	0.0
L pennate diatom (65-110 µm length)	0.0	149.3	0.0	0.0	74.6	0.0	0.0	0.0	0.0	0.0	0.0
S *Pleurosigma spp.* (~50 µm length)	0.0	0.0	0.0	0.0	0.0	0.0	0.0	0.0	0.0	0.0	0.0
M *Pleurosigma spp.* (~80-170 µm length)	0.0	0.0	68.5	0.0	0.0	0.0	0.0	0.0	0.0	0.0	0.0

L *Pleurosigma spp.* (170-200 µm length)	0.0	0.0	0.0	0.0	0.0	0.0	0.0	0.0	0.0	0.0	0.0
S *Rhizosolenia spp.* (≤ 10 µm dia.)	66.7	0.0	0.0	0.0	0.0	0.0	0.0	0.0	0.0	0.0	0.0
M *Rhizosolenia spp.* (10-20 µm dia.)	1711.8	0.0	122.3	0.0	0.0	366.8	122.3	122.3	0.0	0.0	0.0
L *Rhizosolenia spp.* (> 20 µm dia.)	3794.4	1264.8	632.4	632.4	3794.4	0.0	0.0	0.0	0.0	0.0	0.0
Proboscia alata	1902.5	1951.3	6195.4	11854.1	4731.9	3805.0	5512.4	146.3	10098.0	1219.6	29357.2
Pseudo-nitzschia spp.	895.9	4886.8	44551.2	10262.2	26958.7	32334.2	49763.7	2606.3	47646.1	10750.9	18406.9
Skeletonema costatum	0.0	0.0	0.0	3.6	0.0	0.0	0.0	0.0	0.0	0.0	0.0
S *Thalassiosira spp.* (10-25 µm height)	0.0	0.0	0.0	0.0	0.0	0.0	0.0	0.0	0.0	0.0	0.0
M *Thalassiosira spp.* (25-45 µm height)	0.0	0.0	0.0	0.0	0.0	115.7	0.0	0.0	0.0	0.0	0.0
L *Thalassiosira spp.* (> 45 µm height)	0.0	0.0	0.0	0.0	0.0	0.0	0.0	0.0	0.0	0.0	0.0
Total diatom carbon (Pg C ml^{-1})	**8559.3**	**8972.6**	**55898.6**	**24317.8**	**39114.9**	**40312.7**	**61189.2**	**4113.7**	**59483.4**	**14155.5**	**62542.6**
Dinoflagellates (Pg C ml^{-1})											
10-20 µm naked dinoflagellates	1968.5	3758.0	11094.9	9842.3	3936.9	6263.3	18431.9	715.8	20221.4	3758.0	6621.2
20-25 µm naked dinoflagellates	0.0	638.0	3827.8	3189.9	0.0	638.0	9569.6	0.0	2551.9	2551.9	638.0
10-30 µm armoured dinoflagellates	0.0	0.0	252.6	101.0	0.0	0.0	202.1	0.0	101.0	101.0	0.0
Ceratium fusus	0.0	0.0	200.4	0.0	0.0	0.0	400.8	0.0	801.6	0.0	0.0
Ceratium lineatum	0.0	201.8	10492.2	0.0	2219.5	605.3	35713.7	0.0	32081.8	605.3	1614.2
Ceratium tripos	0.0	0.0	0.0	0.0	0.0	0.0	0.0	0.0	0.0	0.0	0.0
Dinophysis acuminata	0.0	171.8	1546.2	343.6	859.0	171.8	3264.2	0.0	2233.4	343.6	1889.8
Diplopsalis lenticula	0.0	199.1	2588.6	5774.7	1194.8	995.6	2190.4	0.0	3186.0	1991.3	995.6
Dissodinium sp.	0.0	0.0	0.0	0.0	0.0	559.0	0.0	0.0	0.0	0.0	0.0
Gonyaulax spinifera	0.0	106.4	212.8	106.4	106.4	212.8	1277.0	0.0	1277.0	638.5	851.3
Gyrodinium spp.	0.0	404.3	5255.4	2829.8	2627.7	606.4	7883.1	0.0	8691.7	1212.8	9095.9
Karenia mikimotoi	0.0	0.0	1174.7	0.0	0.0	106.8	2456.1	0.0	1174.7	427.1	427.1
Katodinium glaucum	0.0	33.2	431.6	996.1	199.2	365.2	730.5	0.0	664.1	332.0	365.2

Oblea rotundata	0.0	0.0	0.0	0.0	0.0	0.0	0.0	0.0	0.0	0.0	0.0
Polykrikos schwartzii	0.0	0.0	0.0	2819.6	0.0	0.0	1409.8	0.0	0.0	0.0	0.0
Prorocentrum micans	0.0	388.2	4399.4	1293.9	1293.9	647.0	3623.0	0.0	5952.1	3234.8	5175.7
Prorocentrum minimum	42.9	0.0	0.0	0.0	0.0	0.0	0.0	0.0	0.0	0.0	0.0
S *Protoperidinium spp.* (10-30 µm dia.)	66.8	0.0	667.7	601.0	667.7	66.8	601.0	267.1	1535.8	1268.7	934.8
M *Protoperidinium spp.* (30-65 µm dia.)	0.0	669.0	4014.1	1338.0	3010.6	0.0	669.0	0.0	1338.0	1003.5	2007.1
L *Protoperidinium spp.* (65-120 µm dia.)	0.0	0.0	3506.5	0.0	0.0	0.0	8766.1	0.0	0.0	1753.2	3506.5
Scrippsiella trochoidea	0.0	0.0	1616.3	1096.8	404.1	923.6	2020.4	0.0	1731.8	1385.4	1500.9
Torodinium robustum/teredo	0.0	0.0	0.0	0.0	0.0	32.9	0.0	0.0	0.0	0.0	0.0
Total dinoflagellate carbon (Pg C ml^{-1})	**2078.1**	**6569.7**	**51281.3**	**30333.1**	**16519.9**	**12194.5**	**99208.6**	**982.9**	**83542.2**	**20607.3**	**35623.3**
Flagellates (Pg C ml^{-1})											
Cryptophytes (> 8 µm)	29.2	29.2	38.9	19.5	29.2	38.9	48.7	0.0	68.2	29.2	29.2
Dictyocha fibula/speculum	844.8	0.0	0.0	0.0	0.0	0.0	0.0	0.0	0.0	0.0	337.9
Pseudopedinella/Pyramimonas spp.	0.0	0.0	0.0	0.0	0.0	0.0	0.0	0.0	0.0	15.4	0.0
Total flagellates (Pg C ml^{-1})	**874.0**	**29.2**	**38.9**	**19.5**	**29.2**	**38.9**	**48.7**	**0.0**	**68.2**	**44.7**	**367.1**
Ciliates (Pg C ml^{-1})											
S ciliates (< 20 µm)	95.6	31.9	0.0	0.0	0.0	0.0	0.0	0.0	0.0	63.7	0.0
M ciliates (20-40 µm)	261.3	130.6	391.9	130.6	0.0	522.5	391.9	0.0	130.6	391.9	0.0
L ciliates (> 40 µm)	0.0	0.0	4163.5	2974.0	594.8	594.8	0.0	0.0	1784.4	1189.6	0.0
Tintinnids	0.0	0.0	0.0	0.0	0.0	0.0	0.0	0.0	0.0	0.0	179.3
Total ciliate carbon (Pg C ml^{-1})	**356.8**	**162.5**	**4555.4**	**3104.6**	**594.8**	**1117.3**	**391.9**	**0.0**	**1915.0**	**1645.2**	**179.3**

Table A1.3. Fv/Fm values of sampled SCM, bottom waters and surface waters in the seasonally stratified waters of the Western English Channel during the summer survey in 2013, as determined using a FIRe bench-top instrument.

	Site no.	Fv/Fm		
		SCM	Surface	Bottom
Broader SCM	5	0.41		
	6	0.46		
	7	0.45		
	12	0.42	0.33	0.40
	14	0.49	0.35	0.49
SCMTL	15	0.47		
	19	0.40	0.28	0.37
	20	0.45		
	21	0.46		
	22	0.43		
	25	0.47	0.38	0.50
	40	0.50		

Table A1.4. Percentage contribution of each phytoplankton taxon to the similarity of samples within each cluster (C) and the similarity of SCMTL (C2, 3, 4), with average similarity within each cluster/group given. Also, percentage contribution of each taxon to dissimilarity between clusters (omitted for C1 vs C5, C6; C2 vs C6; C3 vs C6; C4 vs C5, 6 due to limited importance for this particular study), and between SCMTL that were > 68 % similar (cluster 2, 3 and 4) and broader SCM > 68 % similar (cluster 5), with average dissimilarity between each cluster/group given. Numbers in bold and underlined indicate taxa whose cumulative contribution to similarity/dissimilarity were up to approximately 50 %. No similarity data shown for clusters 1, 4 and 6 as these clusters only contained one sample (SCMTL A; SCMTL G; SCM b).

Taxa	Similarity				Dissimilarity									
	C2	C3	C5	SCMTL (C2, 3, 4)	C1 vs C2	C1 vs C3	C1 vs C4	C2 vs C3	C2 vs C4	C2 vs C5	C3 vs C4	C3 vs C5	C5 vs C6	SCMTL (C2, 3, 4) vs broader SCM (C5)
Pseudo-nitzschia spp.	**18.07**	**27.20**	**22.52**	**20.26**	**6.70**	**11.35**	3.46	**7.02**	**6.84**	2.05	**11.80**	**4.49**	1.64	**3.69**
Proboscia alata	**6.49**	**10.46**	1.97	**8.76**	3.70	3.02	3.19	2.35	**14.06**	**6.86**	**10.42**	**7.54**	**11.57**	**8.73**
S *Rhizosolenia spp*. (≤ 10 µm dia.)					1.61	1.85	1.65						1.63	
M R*hizosolenia spp.* (10 - 20 µm dia.)					**7.75**	**8.35**	**8.36**	1.96		1.12	1.62	1.54		1.14
L R*hizosolenia spp.* (> 20 µm dia.)					**11.65**	**10.77**	**12.45**	**6.12**			**5.04**	**4.80**		2.21
Chaetoceros spp.	3.13	**7.76**	**9.51**	5.07	2.73	**5.00**	**4.20**	**3.58**	2.84	**7.38**		**3.31**	3.04	**5.03**
M centric diatom (30 - 50 µm dia.)		4.05		2.35	1.41	2.73		2.13		2.51	2.17	**3.75**		2.73
L centric diatom (60 - 150 µm dia.)		3.11				1.98		2.94	1.85			2.98		1.81
Dactyliosolen fragillissimus					2.17	2.49	2.22						**3.47**	
Paralia sulcata						1.51		2.53			2.38	2.04		
Guinardia delicatula										1.63		1.34		1.30
Guinardia flaccida							**7.17**		**13.30**	1.17	**12.71**			2.61
10 - 20 µm naked dinoflagellates	**10.40**	**10.39**	**13.27**	**10.84**		2.57	3.26	2.34	3.73	1.86	1.73	2.59	1.76	2.48
20 - 25 µm naked dinoflagellates	4.81		5.60	2.72	**4.02**		1.77	**6.24**	**4.72**	**3.50**	2.12	**5.50**	3.20	**4.30**
10 - 30 µm armoured dinoflagellates			2.21					1.71	1.61	1.61		2.62		2.10

Ceratium lineatum	**11.69**	4.17	**6.34**	**6.79**	**9.01**	**3.76**	2.82	**12.59**	**12.88**	**8.19**	1.80	**4.92**	**8.21**	**6.25**
Ceratium fusus								2.65	2.48	1.17		1.13	1.81	1.11
Gyrodinium spp.	**7.03**	4.18	2.06	**6.83**	**4.91**	**3.97**	**6.68**	3.17	3.35	**6.17**	**5.56**	**3.31**	**4.22**	**5.24**
Prorocentrum micans	5.34	4.31	3.01	5.51	**3.95**	3.23	**5.04**	2.53	2.01	3.45	3.84	1.47		2.81
Prorocentrum minimum						1.48				1.32			1.87	1.16
Diplopsalis lenticula	4.09	5.35	5.59	4.57	2.99	**3.48**	2.21		1.71	**8.49**	1.58	**7.01**	**8.73**	**7.55**
Dinophysis acuminata	3.86		2.21	3.77	2.76	2.22	3.05	1.90		2.47	1.89	1.80	3.10	2.11
Scrippsiella trochoidea	3.54	3.33	3.81	3.91	2.45	2.67	2.71			1.35		1.32	1.96	1.26
Karenia mikimotoi	3.02		3.10		2.27		1.45	**3.92**	1.75	1.91	1.69	**3.51**	**3.90**	2.47
S *Protoperidinium spp.* (10 - 30 µm)	2.14			2.38				1.75		1.53		1.46	1.98	1.45
M *Protoperidinium spp.* (30 - 65 µm)	2.41			2.52	2.48	2.84	3.14	**5.47**	2.54	3.02	4.52	**4.29**	2.53	**3.30**
L *Protoperidinium spp.* (65 - 120 µm)	1.84				2.90		**4.15**	**6.38**	3.71	**4.94**	**7.35**	3.01	2.70	**3.92**
Gonyaulax spinifera	1.91		3.90	2.14	1.64		2.04	1.38		1.74		2.25	1.74	1.72
Katodinium glaucum	2.06	2.34	3.70	2.34	1.42	1.75				2.73		2.19	2.24	2.40
Dissodinium sp.								2.43			2.00	1.91		
Polykrikos schwartzii								1.49		**3.81**		3.13	2.81	**3.32**
Dictyocha spp.					**5.74**	**6.59**	**4.59**		2.60		2.28		1.84	
S aloricate ciliates (< 20 µm)					1.93		1.98			1.31			2.68	1.14
M aloricate ciliates (20 - 40 µm)			3.09		2.21	2.44	3.27	2.34	2.03	2.68	1.93	2.53	**4.38**	2.75
L aloricate ciliates (> 40 µm)		4.04			2.15	2.57		3.11	4.43	**4.10**	4.06	2.96	**7.58**	3.01
Tintinnids									1.89		1.66			
Cumulative contribution (%)	91.81	90.69	91.90	90.77	90.54	90.84	90.86	90.05	90.34	90.08	90.16	90.71	90.61	91.09
Average similarity (%)	82.02	73.45	72.19	72.27	-	-	-	-	-	-	-	-	-	-
Average dissimilarity (%)	-	-	-	-	68.49	62.67	67.24	29.13	29.87	30.07	35.49	37.90	42.53	34.87

Appendix 2

All figures and tables in this appendix are referenced in chapter 4.

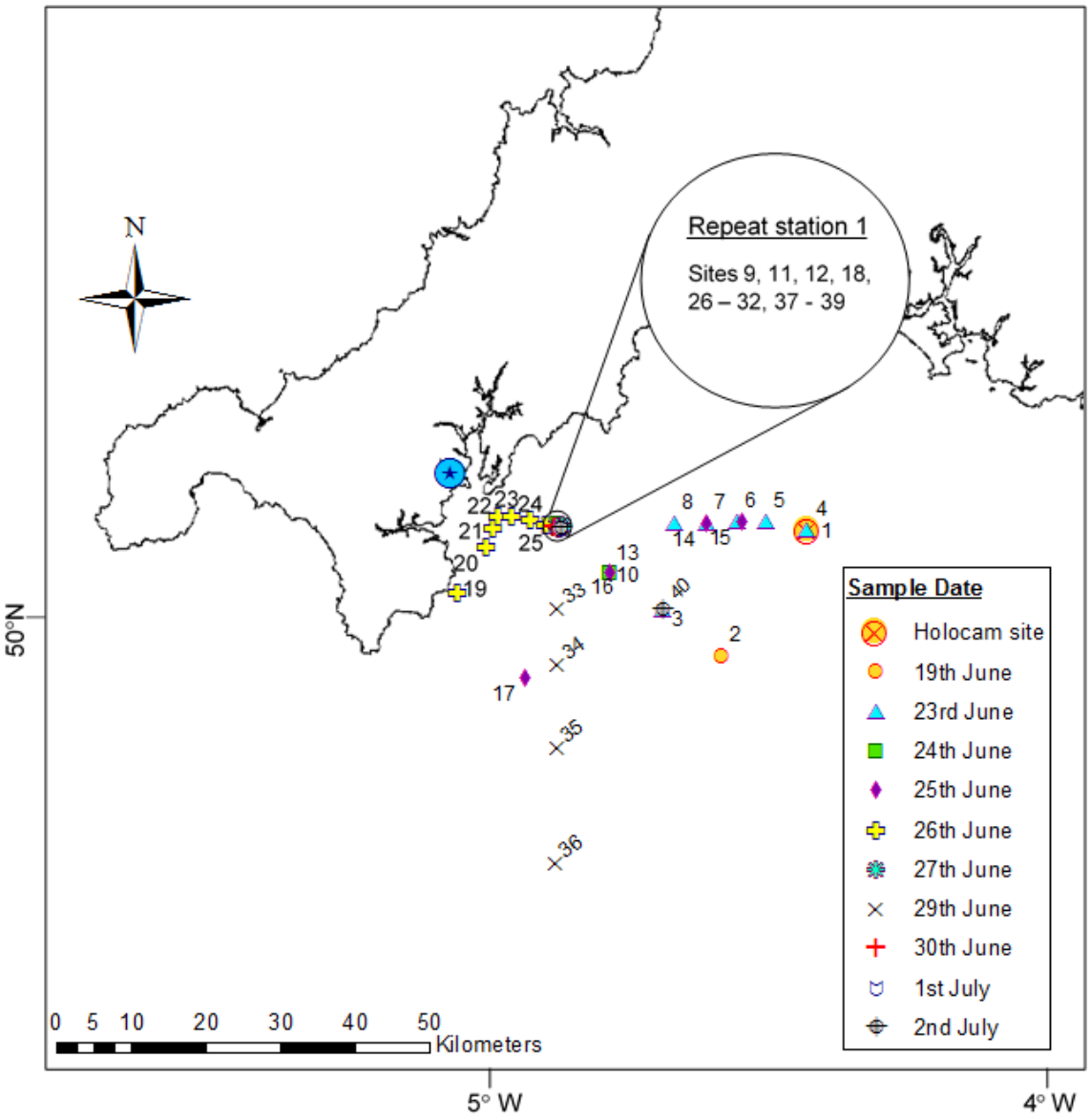

Figure A2.1. Study area in the Western English Channel where sampling occurred between the 19th June and the 2nd July 2015. The encircled blue star indicates the location of Falmouth. Symbols indicate the 40 stratified sites profiled and sampled (symbols labelled with site numbers), and on which date (represented by different symbols). The red/orange encircled cross indicates where the holocam was deployed on the 19th June. Repeat station 1 is indicated, including sites sampled there.

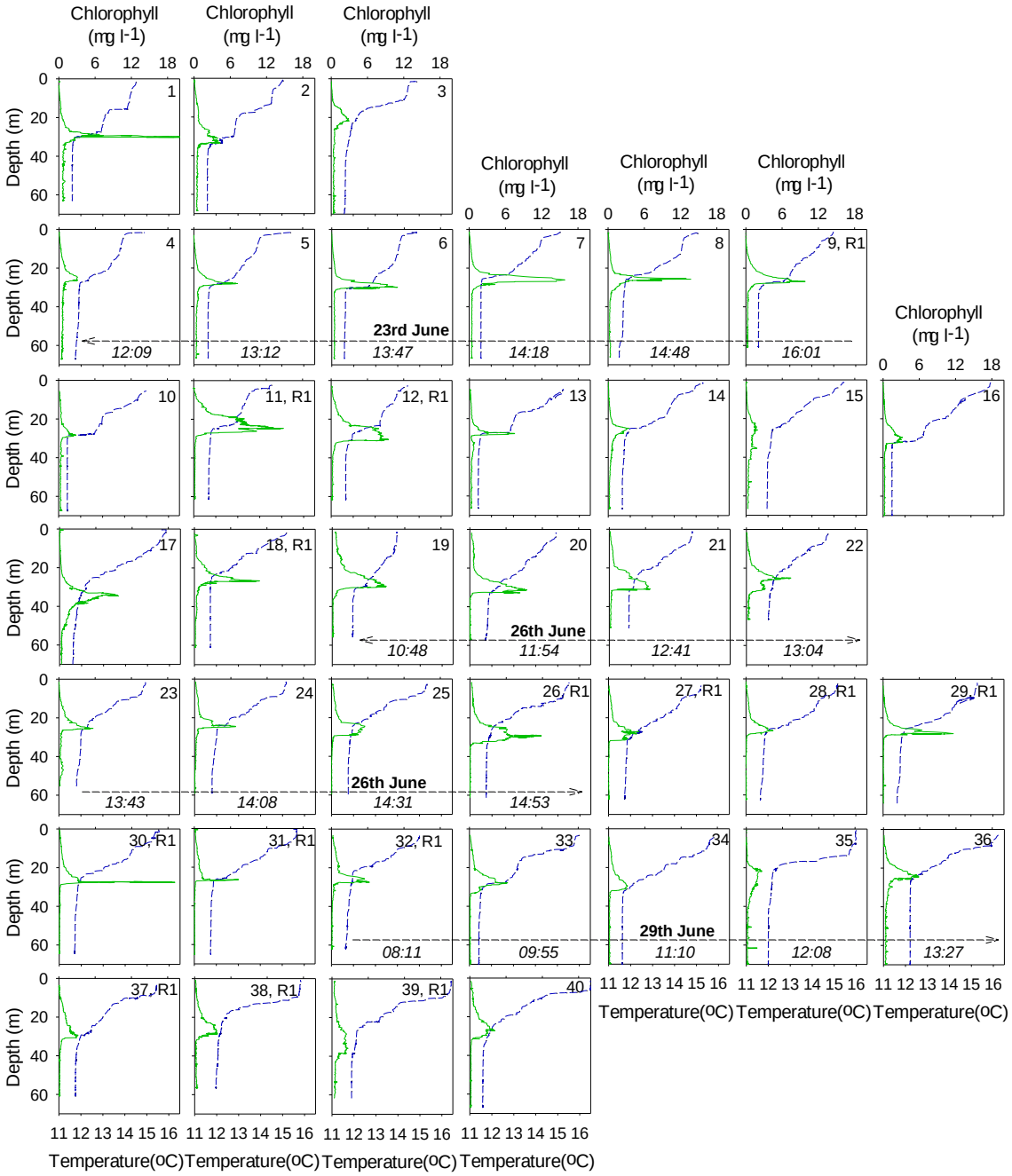

Figure A2.2. Temperature and chlorophyll profiles of the 40 stratified sites (site numbers given in the top right hand corner of each profile plot, and sites profiled at repeat station 1 (R1) are indicated) in the Western English Channel during June/July 2015 (further details provided in Table A2.1). Sites profiled as part of a transect are indicated by an arrow (two arrow head ends indicates an across shore transect and a single arrow head indicates an inshore-offshore transect, where the direction of the arrow indicates movement inshore to offshore), with their profiling date and time given. The green line represents chlorophyll concentration determined from CTD chlorophyll-fluorescence, the blue dashed line represents temperature. Note the chlorophyll peak at site 1 is truncated (max. chlorophyll of 28.0 µg l^{-1}) as the scale has been set to match all other sites.

Phytoplankton	Light microscope image	Holocam image
DIATOMS		
Proboscia truncata		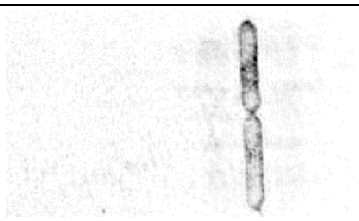
Chained centric diatoms (*Thalassiosira*)	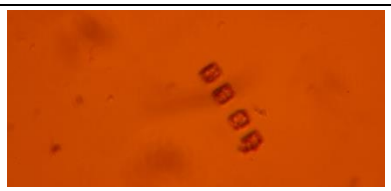	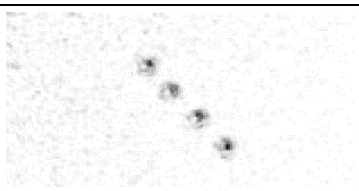
Rod diatoms (likely rhizosolenids e.g. *Proboscia alata*)	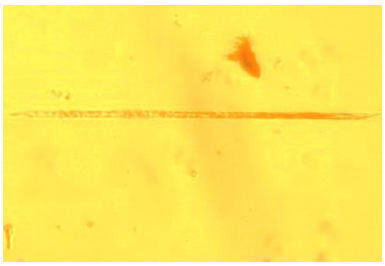	
Curled-chained diatoms (possible mix of *Chaetoceros* and *Leptocylindrus*)	No image	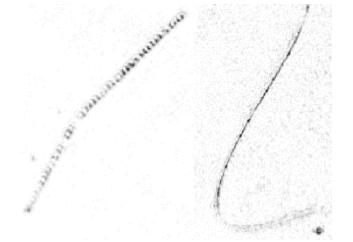
DINOFLAGELLATES		
Ceratium fusus	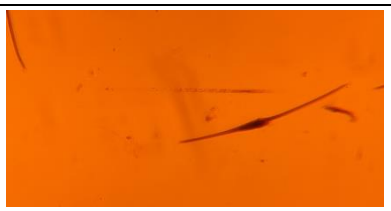	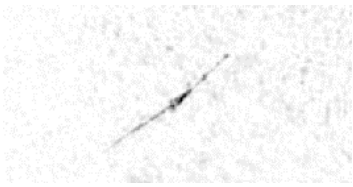
Ceratium lineatum		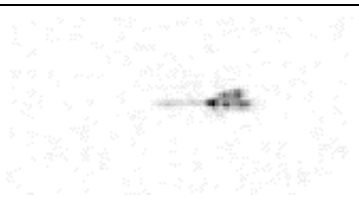
Ceratium macroceros		

Ceratium tripos	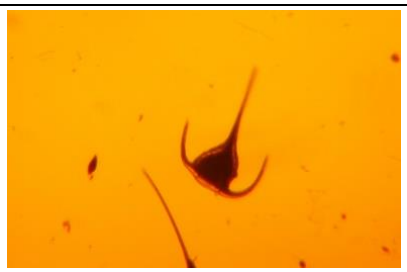	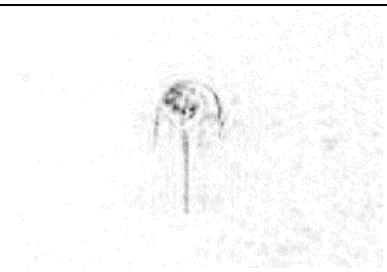
Gyrodinium and *Ceratoperidinium falcatum*	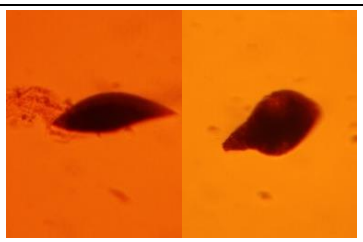	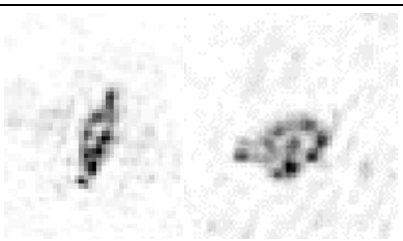
Polykrikos	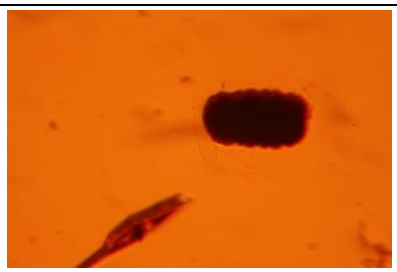	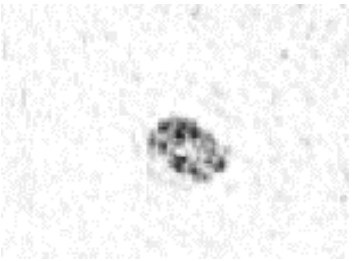
Protoperidinium	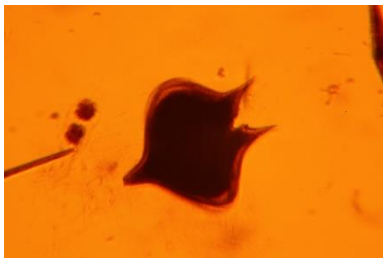	
Noctiluca scintillans		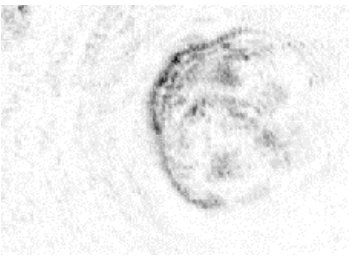
FLAGELLATES		
Dictyocha	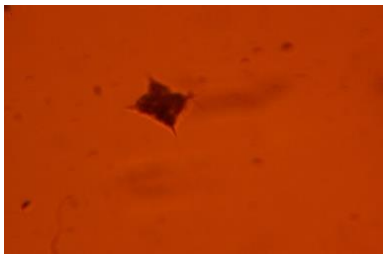	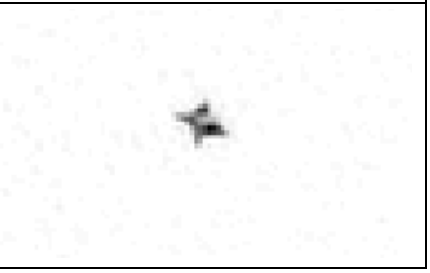

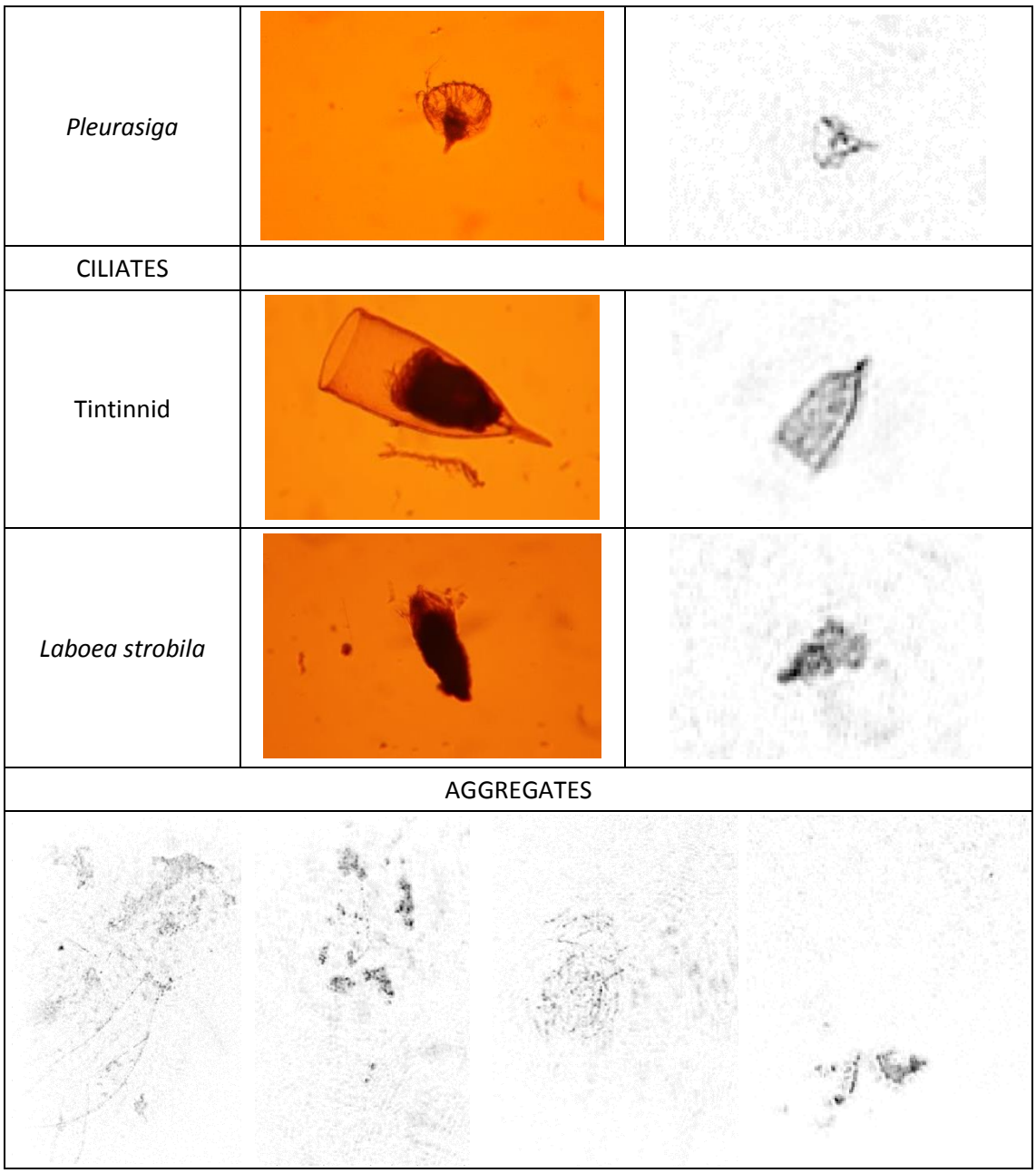

Figure A2.3. A selection of phytoplankton and aggregates distinguished in holograms. Holographic images of phytoplankton are shown next to microscope images of these same phytoplankton preserved in Lugol's iodine for comparison. Holographic images of aggregates are shown in the bottom portion of the figure.

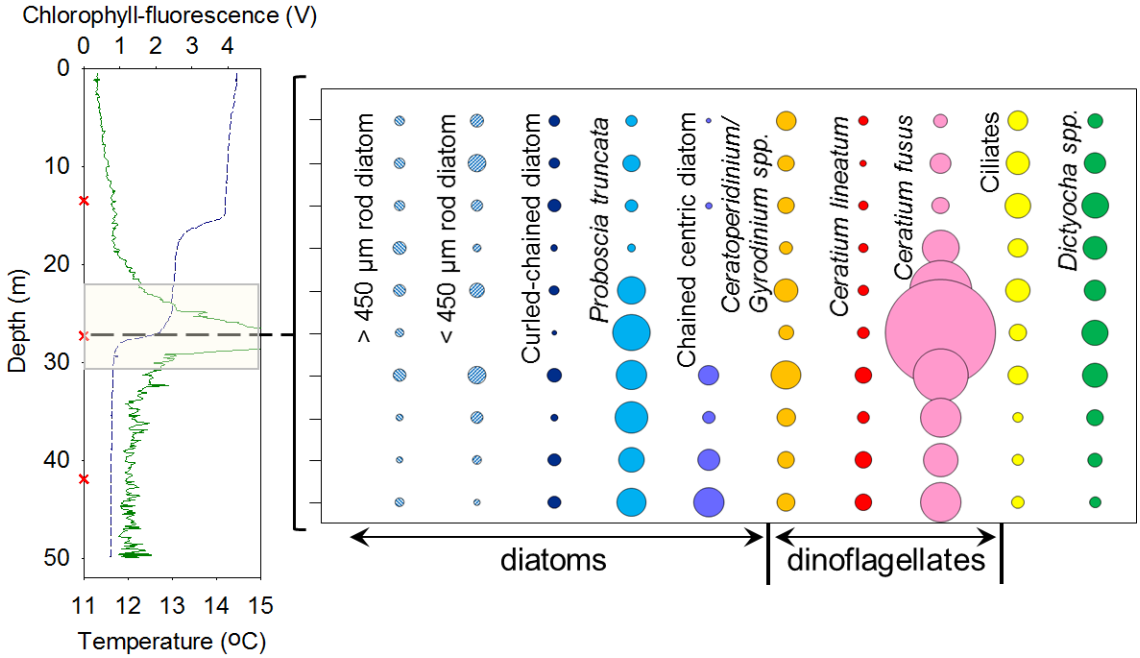

Figure A2.4. Holocam determined abundances of the 10 most numerically dominant large (> 30 µm) phytoplankton at every metre through the SCM only, where circle size is proportional to cell abundance standardised to maximum cell abundance. The corresponding AML CTD Plus V2 probe temperature (dashed blue line) and chlorophyll-fluorescence (green line) depth profile is shown on the left, with the area of the water column (22 – 31 m) represented in the adjacent bubble plot highlighted in grey.

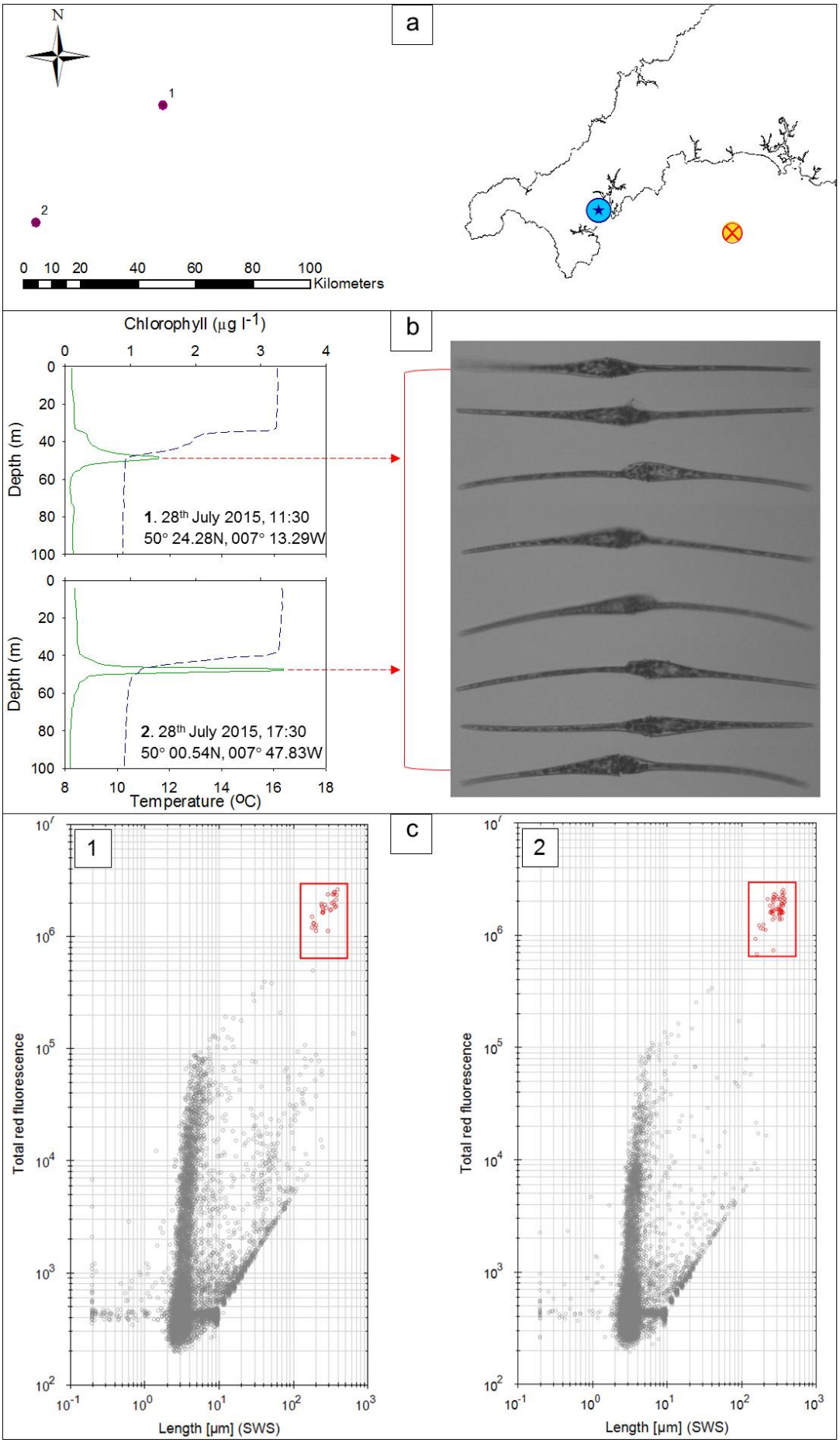
a
N
1
2
0 10 20 40 60 80 100
Kilometers
b
Chlorophyll (µg l-1)
Depth (m)
1. 28th July 2015, 11:30
50° 24.28N, 007° 13.29W
2. 28th July 2015, 17:30
50° 00.54N, 007° 47.83W
Temperature (ºC)
c
1
2
Total red fluorescence
Length [µm] (SWS)

Figure A2.5. Two stratified sites were profiled and sampled in the Celtic Sea in July 2015, approximately 175 km from the study area in the Western English Channel (encircled blue star is Falmouth and red/orange encircled cross is the holocam deployment site), their locations indicated by the numbered purple circles in panel (a) of the figure. Panel (b) shows the temperature and chlorophyll profiles of these two sites exhibiting an SCM. The green line represents chlorophyll concentration determined from CTD chlorophyll-fluorescence and the blue dashed line represents temperature. At both sites samples were collected from the SCM and 10 ml was preserved with 50 % glutaraldehyde solution to a final concentration of 0.25 %. These preserved samples were run in a CytoSense flow cytometer to analyse the phytoplankton community, and 'Image in flow' was enabled to capture photographs (panel (b)) of the most dominant larger (> 30 µm) phytoplankton. Analysis of scan profiles for cells that had been imaged allowed approximate identification and enumeration of cells not imaged. This revealed *Ceratium fusus* (with an approximate size range of 350 - 450 µm) to be abundant (approximately 73 and 249 cells ml^{-1} at site 1 and 2 respectively). The CytoSense sideways scatter (SWS) length vs. red fluorescence plots generated for each sample are shown in panel (c) with *Ceratium fusus* cell clusters in red rectangles, and a selection of CytoSense *Ceratium fusus* images are shown in panel (b).

Table A2.1. Estimated carbon biomass (Pg C ml^{-1}) of phytoplankton taxa identified using inverted light microscopy in Lugol's preserved samples collected during the 2015 summer field survey in the Western English Channel.

Date	**19/06/2015**	**19/06/2015**	**19/06/2015**	**19/06/2015**	**19/06/2015**	**19/06/2015**	**23/06/2015**	**23/06/2015**	**23/06/2015**
Site number	**1**	**1**	**1**	**2**	**2**	**2**	**3**	**4**	**4**
Sample location	**Bottom**	**SCM**	**Surface**	**Bottom**	**SCM**	**Surface**	**SCM**	**Bottom**	**SCM**
Diatoms (Pg C ml^{-1})									
S centric diatom (20-30 µm dia.)	0.0	38.7	0.0	0.0	0.0	0.0	0.0	0.0	0.0
M centric diatom (30-50 µm dia.)	0.0	0.0	0.0	597.5	149.4	0.0	0.0	0.0	149.4
L centric diatom (60-150 µm dia.)	0.0	0.0	0.0	352.8	0.0	0.0	0.0	0.0	0.0
XL centric diatom (> 150 µm dia.)	0.0	0.0	0.0	0.0	0.0	0.0	0.0	0.0	0.0
Cerataulina pelagica	0.0	0.0	0.0	0.0	283.2	94.4	377.6	188.8	94.4
Chaetoceros spp.	10488.7	9770.3	4166.8	3879.4	29167.3	9770.3	2011.5	3879.4	7184.1
Corethron criophylum	0.0	0.0	0.0	0.0	0.0	0.0	0.0	137.8	0.0
Cylindrotheca closterium	244.0	2.8	0.0	14.2	65.2	17.0	19.9	8.5	11.3
Delphineis surirella	0.0	0.0	0.0	0.0	0.0	0.0	0.0	0.0	0.0
Diploneis spp.	325.5	36.2	0.0	54.3	0.0	0.0	0.0	18.1	18.1
Entomoneis spp.	58.2	29.1	0.0	320.3	0.0	0.0	0.0	233.0	0.0
Eucampia zoodiacus	0.0	0.0	0.0	0.0	0.0	0.0	0.0	0.0	0.0
Guinardia delicatula	0.0	0.0	0.0	0.0	0.0	0.0	0.0	0.0	0.0
Guinardia striata	652.9	0.0	0.0	0.0	0.0	0.0	0.0	1741.0	0.0
Lauderia annulata	0.0	201.8	0.0	0.0	0.0	0.0	0.0	336.4	100.9
Leptocylindrus danicus	212.4	96.6	19.3	0.0	289.7	38.6	48.3	144.8	202.8
Leptocylindrus minimus	23.1	100.1	107.8	398.6	1498.1	2901.9	215.7	188.7	402.5
Meuniera membranacea	0.0	0.0	0.0	377.1	0.0	0.0	377.1	1037.1	188.6
Odontella regia/ mobiliensis	316.9	0.0	0.0	0.0	0.0	0.0	0.0	0.0	0.0

Paralia sulcata	195.8	28.0	0.0	167.8	0.0	0.0	0.0	69.9	0.0
S pennate diatom (20-40 µm length)	39.2	0.0	0.0	0.0	0.0	0.0	0.0	0.0	0.0
M pennate diatom (40-65 µm length)	0.0	0.0	0.0	0.0	0.0	0.0	0.0	0.0	0.0
L pennate diatom (65-110 µm length)	0.0	0.0	0.0	74.6	0.0	0.0	0.0	74.6	0.0
S *Pleurosigma spp.* (~50 µm)	10.6	0.0	0.0	0.0	0.0	0.0	0.0	0.0	0.0
M *Pleurosigma spp.* (80-170 µm)	0.0	0.0	0.0	0.0	0.0	0.0	0.0	0.0	0.0
L *Pleurosigma spp.* (170-200 µm)	0.0	0.0	0.0	0.0	0.0	0.0	0.0	0.0	0.0
Proboscia alata	634.2	2439.1	2097.6	2097.6	7317.4	3658.7	926.9	585.4	487.8
Proboscia truncata	16331.0	28893.3	8793.6	10049.8	11306.1	8793.6	7537.4	18843.5	11306.1
S *Pseudo-nitzschia spp.* (< 2.5 µm dia.)	36.1	85.2	113.6	118.8	263.4	20.7	10.3	994.1	821.1
L *Pseudo-nitzschia spp.* (> 2.5 µm dia.)	738.4	896.7	131.9	830.8	2030.7	712.1	131.9	685.7	408.8
S *Rhizosolenia spp.* (≤ 10 µm dia.)	0.0	0.0	0.0	0.0	133.4	0.0	33.3	33.3	33.3
M *Rhizosolenia spp.* (10-20 µm dia.)	0.0	0.0	0.0	0.0	0.0	0.0	0.0	0.0	489.1
L *Rhizosolenia spp.* (> 20 µm dia.)	0.0	0.0	0.0	0.0	0.0	0.0	0.0	0.0	0.0
Thalassionema nitzchioides	31.5	0.0	0.0	0.0	0.0	0.0	0.0	0.0	0.0
XS *Thalassiosira spp.* (< 10 µm height)	313.4	43.5	209.0	47.9	191.5	235.1	1153.6	705.2	1902.4
S *Thalassiosira spp.* (10-25 µm height)	400.9	100.2	0.0	133.6	384.2	16.7	584.6	1419.8	417.6
M *Thalassiosira spp.* (25-45 µm height)	0.0	0.0	0.0	0.0	115.7	0.0	57.8	115.7	0.0
L *Thalassiosira spp.* (> 45 µm height)	0.0	0.0	0.0	0.0	0.0	0.0	0.0	0.0	0.0
Total diatom carbon (Pg C ml^{-1})	**31052.9**	**42761.7**	**15639.6**	**19515.1**	**53195.3**	**26259.1**	**13486.0**	**31440.7**	**24218.1**
Dinoflagellates (Pg C ml^{-1})									
10-20 µm naked dinoflagellates	8589.6	25053.1	10558.1	9663.3	40621.8	31137.4	23621.5	6979.1	24158.3
20-25 µm naked dinoflagellates	5741.8	13397.4	3827.8	638.0	15311.4	9569.6	8293.7	638.0	8931.6
10-30 µm armoured dinoflagellates	1010.3	1717.5	2323.7	404.1	505.1	1717.5	909.3	0.0	151.5
Alexandrium ostenfeldii	0.0	3266.0	1633.0	0.0	408.3	3674.3	2041.3	408.3	3674.3

Amylax triacantha	0.0	0.0	0.0	0.0	0.0	0.0	402.5	0.0	0.0
Ceratium fusus	12825.3	1095601.4	801.6	2004.0	24047.4	200.4	37273.5	4208.3	57513.5
Ceratium lineatum	3026.6	9685.1	2017.7	0.0	0.0	0.0	1210.6	201.8	1210.6
Ceratium macroceros	536.1	1072.3	0.0	0.0	1608.4	0.0	1072.3	0.0	1072.3
Ceratium tripos	0.0	0.0	0.0	0.0	0.0	0.0	1372.5	0.0	0.0
Ceratoperidinium falcatum	534.0	6407.5	1067.9	0.0	1601.9	0.0	4805.6	0.0	7475.4
Dinophysis acuminata	0.0	0.0	0.0	0.0	0.0	0.0	1374.4	0.0	0.0
Dinophysis acuta	0.0	0.0	0.0	0.0	0.0	0.0	706.3	0.0	7062.6
Dinophysis caudata	0.0	0.0	0.0	0.0	0.0	0.0	0.0	0.0	0.0
Dinophysis norvegica	0.0	0.0	0.0	0.0	0.0	0.0	0.0	0.0	0.0
Dinophysis tripos	0.0	0.0	0.0	0.0	0.0	0.0	0.0	0.0	0.0
Dissodinium sp.	1676.9	0.0	0.0	0.0	0.0	0.0	0.0	0.0	0.0
Gonyaulax spinifera	532.1	1277.0	1383.4	212.8	212.8	744.9	1170.6	425.7	851.3
Gyrodinium spp.	202.1	2021.3	5255.4	606.4	2829.8	2627.7	9095.9	1010.7	7074.6
Heterocapsa spp.	0.0	44.5	133.5	0.0	14.8	118.6	8167.3	0.0	14.8
Karenia mikimotoi	0.0	10037.9	0.0	0.0	0.0	0.0	19542.0	0.0	0.0
Katodinium glaucum	265.6	796.9	298.8	232.4	498.0	232.4	1959.0	66.4	597.6
Nematodinium torpedo	86.8	86.8	955.3	86.8	173.7	0.0	0.0	86.8	0.0
Noctiluca scintillans	0.0	0.0	0.0	0.0	0.0	0.0	0.0	0.0	0.0
Oblea rotundata	0.0	0.0	0.0	0.0	0.0	608.3	228.1	152.1	0.0
Phalacroma rotundatum	0.0	0.0	257.6	0.0	0.0	0.0	772.8	0.0	772.8
Polykrikos schwartzii/kofoidii	1676.8	11737.3	3353.5	0.0	8383.8	3353.5	11737.3	0.0	13414.1
Prorocentrum micans	0.0	1035.1	258.8	0.0	905.8	129.4	1293.9	0.0	388.2
Prorocentrum minimum	300.3	729.2	2016.2	214.5	2273.5	5362.1	2166.3	193.0	150.1
Prorocentrum triestinum	0.0	0.0	0.0	0.0	0.0	0.0	0.0	0.0	0.0
S *Protoperidinium spp.* (10-30 µm dia.)	267.1	934.8	1669.3	467.4	400.6	1335.5	467.4	400.6	801.3

M *Protoperidinium spp.* (30-65 µm dia.)	0.0	0.0	0.0	334.5	0.0	0.0	1672.6	0.0	334.5
L *Protoperidinium spp.* (65-120 µm dia.)	0.0	1753.2	1753.2	0.0	0.0	0.0	12272.6	0.0	8766.1
Torodinium robustum/teredo	263.3	230.4	394.9	230.4	98.7	394.9	197.5	164.6	230.4
Total dinoflagellate carbon (Pg C ml^{-1})	**37534.6**	**1186885.0**	**39959.9**	**15094.7**	**99896.0**	**61206.7**	**153826.7**	**14935.3**	**144646.2**
Flagellates (Pg C ml^{-1})									
Chlamydomonas spp.	0.0	0.0	0.0	0.0	0.0	0.0	0.0	0.0	0.0
Chrysochromulina spp.	290.8	2447.8	920.9	145.4	993.7	2229.7	3974.6	290.8	2302.4
Chrysophaerella longispina	5413.3	1041.0	0.0	1457.4	1041.0	0.0	208.2	0.0	208.2
Cryptophytes	125.6	605.2	433.9	285.5	639.4	730.8	536.7	365.4	468.1
Dictyocha fibula/speculum	1351.7	23486.2	844.8	1689.7	6251.7	0.0	14531.0	1351.7	2872.4
Pleurasiga spp.	0.0	488.9	0.0	0.0	0.0	0.0	0.0	0.0	0.0
Solenicola setigera	578.5	374.3	17.0	136.1	136.1	0.0	85.1	629.5	238.2
unidentified spherical flagellate (10-20 µm dia.)	45.4	351.6	493.4	85.1	39.7	164.5	187.2	51.0	136.1
Total flagellate carbon (Pg C ml^{-1})	**7805.3**	**28795.0**	**2710.1**	**3799.1**	**9101.6**	**3124.9**	**19522.7**	**2688.5**	**6225.4**
Non-flagellated chlorophyceae (Pg C ml^{-1})									
Tetraedron spp.	36.3	145.3	327.0	1126.2	7919.9	9627.4	2470.4	0.0	0.0
Oocystaceae sp.	0.0	0.0	0.0	0.0	0.0	0.0	0.0	0.0	0.0
Total non-flagellated chlorophyceae carbon (Pg C ml^{-1})	**36.3**	**145.3**	**327.0**	**1126.2**	**7919.9**	**9627.4**	**2470.4**	**0.0**	**0.0**
Ciliates (Pg C ml^{-1})									
S aloricate ciliates (< 20µm)	502.9	282.9	1383.1	251.5	377.2	1100.2	220.0	408.6	943.0
M aloricate ciliates (20-40 µm)	522.5	1959.4	17765.1	391.9	6270.0	13846.3	4702.5	391.9	41147.1
L aloricate ciliates (> 40 µm)	1189.6	15464.6	10706.2	594.8	38066.6	19628.1	105872.8	1784.4	90408.2
Tiarina fusus	4411.7	4901.8	1960.7	0.0	490.2	3921.5	2450.9	1960.7	1470.6
S bowl shaped tintinnids (20-50 µm length)	0.0	0.0	0.0	179.3	0.0	0.0	0.0	179.3	0.0
L bowl shaped tintinnids (> 60 µm length)	0.0	2144.0	0.0	8576.1	0.0	4288.1	4288.1	4288.1	2144.0

S tapering tintinnids (40-60 µm)	341.0	7161.1	2046.0	3751.0	18243.7	18755.2	15174.7	1534.5	2387.0
L tapering tintinnids (> 60 µm)	0.0	949.9	0.0	0.0	949.9	0.0	475.0	0.0	475.0
Total ciliate carbon (Pg C ml^{-1})	**6967.7**	**32863.7**	**33861.2**	**13744.6**	**64397.7**	**61539.4**	**133184.0**	**10547.5**	**138975.0**

Date	**23/06/2015**	**23/06/2015**	**23/06/2015**	**23/06/2015**	**23/06/2015**	**23/06/2015**	**24/06/2015**	**24/06/2015**	**24/06/2015**
Site number	**4**	**5**	**6**	**7**	**8**	**9**	**10**	**10**	**10**
Sample location	**Surface**	**SCM**	**SCM**	**SCM**	**SCM**	**SCM**	**Bottom**	**SCM**	**Surface**
Diatoms (Pg C ml^{-1})									
S centric diatom (20-30 µm dia.)	0.0	0.0	0.0	0.0	0.0	0.0	0.0	0.0	0.0
M centric diatom (30-50 µm dia.)	0.0	0.0	0.0	149.4	0.0	0.0	0.0	149.4	0.0
L centric diatom (60-150 µm dia.)	352.8	0.0	352.8	0.0	0.0	0.0	0.0	0.0	0.0
XL centric diatom (> 150 µm dia.)	0.0	0.0	0.0	0.0	0.0	0.0	0.0	0.0	0.0
Cerataulina pelagica	283.2	0.0	94.4	94.4	0.0	0.0	188.8	660.9	1227.3
Chaetoceros spp.	3161.0	4454.1	3879.4	1149.4	3161.0	1149.4	4741.5	1293.1	718.4
Corethron criophylum	0.0	137.8	0.0	0.0	0.0	0.0	0.0	0.0	0.0
Cylindrotheca closterium	0.0	2.8	0.0	5.7	11.3	0.0	5.7	19.9	0.0
Delphineis surirella	0.0	0.0	0.0	0.0	0.0	0.0	0.0	0.0	0.0
Diploneis spp.	0.0	18.1	0.0	0.0	36.2	0.0	18.1	36.2	0.0
Entomoneis spp.	0.0	29.1	0.0	29.1	0.0	0.0	116.5	29.1	0.0
Eucampia zoodiacus	0.0	0.0	0.0	0.0	0.0	0.0	168.2	0.0	0.0
Guinardia delicatula	0.0	0.0	0.0	0.0	0.0	0.0	94.5	0.0	0.0
Guinardia striata	435.2	0.0	0.0	0.0	0.0	0.0	0.0	0.0	217.6
Lauderia annulata	0.0	0.0	0.0	0.0	0.0	0.0	0.0	0.0	0.0
Leptocylindrus danicus	3920.1	241.4	77.2	202.8	9.7	183.5	0.0	115.9	3340.8
Leptocylindrus minimus	215.7	980.1	419.8	98.2	161.8	223.4	219.5	441.0	575.8

Meuniera membranacea	0.0	0.0	0.0	0.0	188.6	0.0	0.0	0.0	0.0
Odontella regia/ mobiliensis	0.0	0.0	0.0	0.0	0.0	0.0	0.0	0.0	0.0
Paralia sulcata	0.0	209.8	0.0	0.0	97.9	0.0	461.6	83.9	0.0
S pennate diatom (20-40 µm length)	0.0	0.0	0.0	0.0	0.0	0.0	0.0	0.0	0.0
M pennate diatom (40-65 µm length)	0.0	0.0	0.0	0.0	0.0	0.0	0.0	0.0	0.0
L pennate diatom (65-110 µm length)	0.0	0.0	0.0	0.0	74.6	0.0	74.6	0.0	0.0
S *Pleurosigma spp.* (~50 µm)	0.0	0.0	0.0	0.0	0.0	0.0	0.0	0.0	0.0
M *Pleurosigma spp.* (80-170 µm)	0.0	0.0	0.0	0.0	0.0	0.0	0.0	0.0	0.0
L *Pleurosigma spp.* (170-200 µm)	0.0	0.0	0.0	0.0	0.0	0.0	271.7	0.0	0.0
Proboscia alata	780.5	1463.5	6292.9	1073.2	731.7	1853.7	487.8	1463.5	1902.5
Proboscia truncata	10049.8	0.0	50249.2	16331.0	25124.6	21355.9	12562.3	20099.7	3768.7
S *Pseudo-nitzschia spp.* (< 2.5 µm dia.)	85.2	550.0	10.3	46.5	224.6	20.7	41.3	25.8	85.2
L *Pseudo-nitzschia spp.* (> 2.5 µm dia.)	158.2	725.3	395.6	501.1	501.1	422.0	2571.4	738.4	580.2
S *Rhizosolenia spp.* (≤ 10 µm dia.)	100.0	100.0	33.3	0.0	0.0	0.0	100.0	33.3	0.0
M *Rhizosolenia spp.* (10-20 µm dia.)	0.0	0.0	0.0	0.0	0.0	0.0	0.0	0.0	0.0
L *Rhizosolenia spp.* (> 20 µm dia.)	0.0	0.0	0.0	0.0	0.0	0.0	0.0	0.0	0.0
Thalassionema nitzchioides	0.0	0.0	0.0	0.0	0.0	0.0	0.0	0.0	0.0
XS *Thalassiosira spp.* (< 10 µm height)	1858.8	1223.3	126.2	21.8	178.5	60.9	78.4	522.4	317.8
S *Thalassiosira spp.* (10-25 µm height)	167.0	150.3	0.0	0.0	0.0	0.0	0.0	0.0	0.0
M *Thalassiosira spp.* (25-45 µm height)	0.0	57.8	0.0	0.0	0.0	0.0	520.6	0.0	0.0
L *Thalassiosira spp.* (> 45 µm height)	0.0	0.0	0.0	0.0	71.5	0.0	0.0	0.0	0.0
Total diatom carbon (Pg C ml^{-1})	**21567.7**	**10343.4**	**61931.3**	**19702.5**	**30573.1**	**25269.5**	**22722.5**	**25712.4**	**12734.3**
Dinoflagellates (Pg C ml^{-1})									
10-20 µm naked dinoflagellates	8947.5	14852.9	13242.3	13958.2	12526.5	8589.6	7873.8	22189.9	7694.9
20-25 µm naked dinoflagellates	7017.7	5741.8	5103.8	5103.8	5103.8	1275.9	1275.9	5103.8	3827.8

10-30 µm armoured dinoflagellates	606.2	303.1	454.6	505.1	454.6	151.5	151.5	505.1	353.6
Alexandrium ostenfeldii	816.5	6940.3	7756.8	2449.5	0.0	7756.8	0.0	4082.5	0.0
Amylax triacantha	0.0	0.0	0.0	0.0	0.0	0.0	0.0	0.0	0.0
Ceratium fusus	601.2	170536.4	293980.0	807392.9	272337.3	280954.3	1603.2	28856.9	400.8
Ceratium lineatum	807.1	6053.2	9685.1	19168.4	8676.2	6658.5	0.0	1008.9	403.5
Ceratium macroceros	0.0	1072.3	1608.4	3753.0	2144.6	2680.7	0.0	1608.4	0.0
Ceratium tripos	2745.0	0.0	0.0	0.0	0.0	0.0	0.0	1372.5	0.0
Ceratoperidinium falcatum	534.0	8009.4	4271.7	3737.7	2135.8	2669.8	0.0	2135.8	0.0
Dinophysis acuminata	0.0	171.8	515.4	171.8	0.0	171.8	0.0	1546.2	0.0
Dinophysis acuta	0.0	4237.5	13418.9	0.0	0.0	11300.1	0.0	2825.0	0.0
Dinophysis caudata	0.0	0.0	0.0	0.0	0.0	0.0	0.0	0.0	0.0
Dinophysis norvegica	0.0	0.0	0.0	124.0	0.0	0.0	0.0	0.0	0.0
Dinophysis tripos	1546.1	0.0	773.0	0.0	0.0	0.0	0.0	0.0	1546.1
Dissodinium sp.	0.0	0.0	0.0	0.0	0.0	0.0	0.0	0.0	0.0
Gonyaulax spinifera	1170.6	1702.6	1383.4	1489.8	425.7	319.2	532.1	425.7	1170.6
Gyrodinium spp.	7276.7	27489.9	16776.9	17787.6	6670.3	5053.3	606.4	11117.2	4851.2
Heterocapsa spp.	0.0	0.0	0.0	0.0	0.0	0.0	0.0	29.7	14.8
Karenia mikimotoi	0.0	320.4	1281.4	533.9	0.0	2456.1	0.0	106.8	0.0
Katodinium glaucum	498.0	5478.5	1294.9	6109.3	365.2	996.1	0.0	1195.3	431.6
Nematodinium torpedo	434.2	0.0	0.0	0.0	434.2	86.8	0.0	260.5	173.7
Noctiluca scintillans	0.0	0.0	227081.5	0.0	0.0	227081.5	0.0	0.0	0.0
Oblea rotundata	0.0	0.0	0.0	0.0	0.0	0.0	0.0	0.0	0.0
Phalacroma rotundatum	0.0	515.2	0.0	0.0	257.6	515.2	0.0	0.0	257.6
Polykrikos schwartzii/kofoidii	10060.6	18444.4	31858.5	11737.3	3353.5	16767.6	3353.5	6707.1	5030.3
Prorocentrum micans	129.4	776.4	129.4	776.4	517.6	258.8	0.0	905.8	517.6
Prorocentrum minimum	1029.5	85.8	364.6	214.5	235.9	622.0	21.4	965.2	1758.8

Prorocentrum triestinum	0.0	0.0	0.0	0.0	0.0	0.0	0.0	0.0	0.0
S *Protoperidinium spp.* (10-30 µm dia.)	400.6	1335.5	2203.5	1335.5	601.0	400.6	467.4	801.3	267.1
M *Protoperidinium spp.* (30-65 µm dia.)	669.0	1338.0	0.0	669.0	0.0	334.5	334.5	669.0	0.0
L *Protoperidinium spp.* (65-120 µm dia.)	5259.7	3506.5	3506.5	0.0	3506.5	3506.5	0.0	3506.5	1753.2
Torodinium robustum/teredo	230.4	230.4	0.0	65.8	592.4	131.6	131.6	32.9	197.5
Total dinoflagellate carbon (Pg C ml^{-1})	**50780.1**	**279142.2**	**636690.7**	**897083.4**	**320338.8**	**580739.0**	**16351.5**	**97958.0**	**30650.6**
Flagellates (Pg C ml^{-1})									
Chlamydomonas spp.	0.0	0.0	0.0	0.0	0.0	0.0	0.0	0.0	0.0
Chrysochromulina spp.	1454.1	2641.7	3441.4	2060.0	1308.7	993.7	266.6	1623.8	1163.3
Chrysophaerella longispina	0.0	416.4	208.2	208.2	832.8	0.0	0.0	1041.0	0.0
Cryptophytes	399.6	422.5	319.7	468.1	388.2	422.5	376.8	365.4	296.9
Dictyocha fibula/speculum	1520.7	19093.1	121993.1	63700.0	7941.4	32610.3	1520.7	20275.9	1520.7
Pleurasiga spp.	0.0	488.9	488.9	0.0	488.9	0.0	0.0	0.0	0.0
Solenicola setigera	289.2	544.5	221.2	595.5	1514.3	2126.8	340.3	357.3	170.1
unidentified spherical flagellate (10-20 µm dia.)	198.5	232.5	209.8	175.8	136.1	85.1	17.0	102.1	153.1
Total flagellate carbon (Pg C ml^{-1})	**3862.2**	**23839.5**	**126882.3**	**67207.7**	**12610.4**	**36238.3**	**2521.4**	**23765.4**	**3304.1**
Non-flagellated chlorophyceae (Pg C ml^{-1})									
Tetraedron spp.	109.0	0.0	0.0	0.0	0.0	36.3	290.6	254.3	109.0
Oocystaceae sp.	0.0	0.0	0.0	0.0	0.0	0.0	0.0	0.0	0.0
Total non-flagellated chlorophyceae carbon (Pg C ml^{-1})	**109.0**	**0.0**	**0.0**	**0.0**	**0.0**	**36.3**	**290.6**	**254.3**	**109.0**
Ciliates (Pg C ml^{-1})									
S aloricate ciliates (< 20µm)	5343.8	785.9	974.5	220.0	251.5	220.0	502.9	628.7	1540.3
M aloricate ciliates (20-40 µm)	18026.4	33309.6	23512.6	1698.1	2873.8	10711.3	914.4	18418.2	28476.4
L aloricate ciliates (> 40 µm)	34497.9	122527.0	93382.2	39256.2	13085.4	14869.8	1189.6	124311.3	19033.3
Tiarina fusus	1960.7	3431.3	490.2	2941.1	5882.2	1470.6	1960.7	3921.5	1960.7

S bowl shaped tintinnids (20-50 µm length)	0.0	0.0	0.0	0.0	0.0	0.0	0.0	0.0	0.0
L bowl shaped tintinnids (> 60 µm length)	0.0	0.0	6432.1	0.0	0.0	0.0	0.0	2144.0	2144.0
S tapering tintinnids (40-60 µm)	852.5	9036.6	8525.1	8866.1	1705.0	170.5	1875.5	5967.6	1023.0
L tapering tintinnids (> 60 µm)	0.0	475.0	949.9	0.0	0.0	0.0	475.0	1899.8	475.0
Total ciliate carbon (Pg C ml^{-1})	**60681.3**	**169565.2**	**134266.6**	**52981.6**	**23797.9**	**27442.2**	**6918.1**	**157291.2**	**54652.8**

Date	**24/06/2015**	**24/06/2015**	**24/06/2015**	**24/06/2015**	**24/06/2015**	**25/06/2015**	**25/06/2015**	**25/06/2015**	**25/06/2015**
Site number	**11**	**12**	**13**	**13**	**13**	**14**	**15**	**16**	**16**
Sample location	**SCM**	**SCM**	**Bottom**	**SCM**	**Surface**	**SCM**	**SCM**	**Bottom**	**SCM**
Diatoms (Pg C ml^{-1})									
S centric diatom (20-30 µm dia.)	0.0	0.0	0.0	0.0	0.0	0.0	0.0	0.0	0.0
M centric diatom (30-50 µm dia.)	149.4	149.4	298.7	0.0	298.7	896.2	298.7	0.0	0.0
L centric diatom (60-150 µm dia.)	1763.9	0.0	0.0	0.0	352.8	0.0	0.0	352.8	0.0
XL centric diatom (> 150 µm dia.)	0.0	0.0	0.0	0.0	0.0	0.0	1511.7	0.0	0.0
Cerataulina pelagica	0.0	0.0	0.0	0.0	1227.3	377.6	660.9	0.0	188.8
Chaetoceros spp.	1580.5	2442.6	2729.9	1293.1	431.0	6034.6	2729.9	1005.8	718.4
Corethron criophylum	0.0	0.0	0.0	0.0	0.0	0.0	0.0	0.0	0.0
Cylindrotheca closterium	0.0	0.0	14.2	2.8	0.0	51.1	5.7	2.8	25.5
Delphineis surirella	0.0	0.0	0.0	0.0	0.0	0.0	0.0	0.0	0.0
Diploneis spp.	0.0	0.0	108.5	0.0	0.0	0.0	0.0	108.5	18.1
Entomoneis spp.	0.0	29.1	87.4	0.0	29.1	0.0	0.0	87.4	29.1
Eucampia zoodiacus	0.0	0.0	0.0	0.0	0.0	0.0	0.0	0.0	0.0
Guinardia delicatula	0.0	0.0	94.5	0.0	0.0	0.0	94.5	0.0	0.0
Guinardia striata	0.0	0.0	0.0	0.0	0.0	0.0	652.9	0.0	217.6
Lauderia annulata	0.0	0.0	0.0	0.0	0.0	0.0	0.0	0.0	0.0

Leptocylindrus danicus	19.3	0.0	19.3	0.0	3727.0	212.4	7521.6	231.7	57.9
Leptocylindrus minimus	59.7	63.5	117.5	80.9	448.7	1486.6	140.6	63.5	350.5
Meuniera membranacea	0.0	0.0	0.0	0.0	0.0	0.0	1885.6	0.0	377.1
Odontella regia/ mobiliensis	0.0	0.0	0.0	0.0	0.0	0.0	0.0	0.0	0.0
Paralia sulcata	0.0	0.0	643.4	0.0	83.9	83.9	0.0	797.3	0.0
S pennate diatom (20-40 µm length)	0.0	0.0	0.0	0.0	0.0	0.0	0.0	0.0	0.0
M pennate diatom (40-65 µm length)	0.0	0.0	19.9	0.0	0.0	0.0	0.0	0.0	39.7
L pennate diatom (65-110 µm length)	74.6	0.0	0.0	0.0	0.0	0.0	0.0	149.3	0.0
S *Pleurosigma spp.* (~50 µm)	0.0	0.0	0.0	0.0	0.0	0.0	0.0	0.0	0.0
M *Pleurosigma spp.* (80-170 µm)	0.0	0.0	0.0	0.0	0.0	0.0	0.0	0.0	0.0
L *Pleurosigma spp.* (170-200 µm)	0.0	0.0	135.9	0.0	0.0	0.0	135.9	0.0	0.0
Proboscia alata	195.1	97.6	780.5	5805.1	1756.2	1268.3	536.6	487.8	1951.3
Proboscia truncata	10049.8	8793.6	6281.2	23868.4	3768.7	16331.0	11306.1	8793.6	41455.6
S *Pseudo-nitzschia spp.* (< 2.5 µm dia.)	41.3	28.4	28.4	12.9	100.7	728.1	405.4	80.0	2.6
L *Pseudo-nitzschia spp.* (> 2.5 µm dia.)	342.9	211.0	1687.9	553.8	382.4	725.3	395.6	1265.9	606.6
S *Rhizosolenia spp.* (≤ 10 µm dia.)	0.0	0.0	0.0	0.0	0.0	200.1	300.1	0.0	0.0
M *Rhizosolenia spp.* (10-20 µm dia.)	0.0	0.0	0.0	0.0	0.0	0.0	244.5	0.0	0.0
L *Rhizosolenia spp.* (> 20 µm dia.)	0.0	0.0	0.0	0.0	0.0	0.0	0.0	0.0	0.0
Thalassionema nitzchioides	0.0	0.0	0.0	0.0	0.0	0.0	0.0	0.0	0.0
XS *Thalassiosira spp.* (< 10 µm height)	165.4	130.6	152.4	121.9	87.1	2381.2	16590.1	34.8	1810.9
S *Thalassiosira spp.* (10-25 µm height)	0.0	0.0	0.0	0.0	0.0	0.0	0.0	0.0	0.0
M *Thalassiosira spp.* (25-45 µm height)	0.0	0.0	115.7	0.0	0.0	173.5	0.0	0.0	0.0
L *Thalassiosira spp.* (> 45 µm height)	0.0	0.0	0.0	0.0	0.0	0.0	0.0	0.0	0.0
Total diatom carbon (Pg C ml^{-1})	**14442.0**	**11945.8**	**13315.2**	**31739.0**	**12693.7**	**30950.0**	**45416.3**	**13461.3**	**47849.8**
Dinoflagellates (Pg C ml^{-1})									

10-20 µm naked dinoflagellates	9126.5	5189.6	7873.8	19326.7	10558.1	19326.7	7158.0	8947.5	32569.0
20-25 µm naked dinoflagellates	1913.9	638.0	1913.9	3189.9	7655.7	5741.8	3189.9	1275.9	5741.8
10-30 µm armoured dinoflagellates	252.6	151.5	202.1	252.6	1010.3	1111.3	454.6	101.0	555.7
Alexandrium ostenfeldii	4490.8	6123.8	0.0	8981.6	1224.8	816.5	816.5	0.0	2857.8
Amylax triacantha	0.0	0.0	0.0	0.0	0.0	0.0	0.0	0.0	0.0
Ceratium fusus	299190.3	250895.0	3607.1	78555.0	0.0	23446.3	2805.5	3607.1	42083.0
Ceratium lineatum	25019.8	16343.5	0.0	2421.3	403.5	4439.0	1815.9	201.8	2824.8
Ceratium macroceros	536.1	1608.4	536.1	536.1	0.0	1072.3	536.1	0.0	2680.7
Ceratium tripos	0.0	1372.5	0.0	0.0	0.0	0.0	0.0	0.0	0.0
Ceratoperidinium falcatum	2669.8	5873.6	0.0	4805.6	1067.9	5339.6	2135.8	534.0	1067.9
Dinophysis acuminata	171.8	171.8	0.0	171.8	0.0	171.8	171.8	0.0	171.8
Dinophysis acuta	5650.0	5650.0	0.0	21893.9	0.0	706.3	6356.3	0.0	2118.8
Dinophysis caudata	0.0	0.0	0.0	0.0	0.0	0.0	0.0	0.0	0.0
Dinophysis norvegica	0.0	0.0	0.0	0.0	0.0	0.0	124.0	0.0	0.0
Dinophysis tripos	0.0	0.0	0.0	0.0	0.0	0.0	0.0	0.0	0.0
Dissodinium sp.	0.0	0.0	0.0	0.0	0.0	0.0	0.0	0.0	0.0
Gonyaulax spinifera	532.1	851.3	106.4	1489.8	1064.2	425.7	212.8	0.0	319.2
Gyrodinium spp.	8489.5	5255.4	2021.3	12734.3	7276.7	5457.6	4649.0	2627.7	11521.5
Heterocapsa spp.	14.8	0.0	0.0	14.8	296.6	0.0	0.0	0.0	14.8
Karenia mikimotoi	1708.6	640.7	0.0	3737.5	0.0	0.0	0.0	0.0	213.6
Katodinium glaucum	4814.4	1328.1	265.6	1128.9	298.8	1062.5	531.2	132.8	1128.9
Nematodinium torpedo	434.2	173.7	86.8	0.0	0.0	86.8	173.7	0.0	0.0
Noctiluca scintillans	0.0	0.0	0.0	0.0	0.0	0.0	0.0	0.0	227081.5
Oblea rotundata	0.0	0.0	0.0	0.0	0.0	0.0	0.0	0.0	0.0
Phalacroma rotundatum	515.2	0.0	0.0	0.0	0.0	0.0	515.2	0.0	515.2
Polykrikos schwartzii/kofoidii	1676.8	1676.8	0.0	15090.9	3353.5	10060.6	3353.5	1676.8	18444.4

Prorocentrum micans	0.0	258.8	0.0	517.6	1035.1	517.6	517.6	0.0	517.6
Prorocentrum minimum	772.1	493.3	64.3	235.9	793.6	321.7	493.3	128.7	407.5
Prorocentrum triestinum	0.0	0.0	0.0	0.0	0.0	0.0	0.0	0.0	0.0
S *Protoperidinium spp.* (10-30 µm dia.)	1068.4	734.5	200.3	1736.1	267.1	534.2	133.5	200.3	333.9
M *Protoperidinium spp.* (30-65 µm dia.)	0.0	0.0	334.5	334.5	669.0	0.0	0.0	0.0	334.5
L *Protoperidinium spp.* (65-120 µm dia.)	14025.8	3506.5	0.0	10519.4	3506.5	3506.5	7012.9	0.0	1753.2
Torodinium robustum/teredo	65.8	98.7	164.6	32.9	131.6	0.0	131.6	65.8	65.8
Total dinoflagellate carbon (Pg C ml^{-1})	**383139.4**	**309035.6**	**17377.0**	**187707.1**	**40613.1**	**84144.5**	**43289.1**	**19499.5**	**355322.9**
Flagellates (Pg C ml^{-1})									
Chlamydomonas spp.	0.0	0.0	0.0	0.0	0.0	0.0	0.0	0.0	0.0
Chrysochromulina spp.	1333.0	969.4	145.4	2229.7	2132.7	1066.4	1551.1	72.7	1745.0
Chrysophaerella longispina	0.0	0.0	1665.6	624.6	0.0	0.0	1041.0	0.0	1457.4
Cryptophytes	525.2	639.4	365.4	285.5	696.5	765.0	570.9	605.2	605.2
Dictyocha fibula/speculum	52041.4	30413.8	2534.5	38355.2	506.9	5406.9	1351.7	1351.7	8110.3
Pleurasiga spp.	488.9	488.9	488.9	0.0	0.0	0.0	0.0	0.0	0.0
Solenicola setigera	3402.8	4100.4	374.3	204.2	85.1	187.2	1871.6	204.2	204.2
unidentified spherical flagellate (10-20 µm dia.)	141.8	141.8	5.7	170.1	255.2	147.5	187.2	5.7	124.8
Total flagellate carbon (Pg C ml^{-1})	**57933.1**	**36753.7**	**5579.8**	**41869.2**	**3676.4**	**7572.9**	**6573.4**	**2239.4**	**12246.8**
Non-flagellated chlorophyceae (Pg C ml^{-1})									
Tetraedron spp.	0.0	36.3	72.7	36.3	36.3	0.0	36.3	0.0	36.3
Oocystaceae sp.	0.0	0.0	0.0	0.0	0.0	0.0	0.0	0.0	0.0
Total non-flagellated chlorophyceae carbon (Pg C ml^{-1})	**0.0**	**36.3**	**72.7**	**36.3**	**36.3**	**0.0**	**36.3**	**0.0**	**36.3**
Ciliates (Pg C ml^{-1})									
S aloricate ciliates (< 20µm)	94.3	125.7	251.5	377.2	2923.4	848.7	1508.8	345.8	723.0
M aloricate ciliates (20-40 µm)	8098.8	7576.3	783.8	27953.9	33962.7	9013.2	20377.6	1567.5	22467.6

L aloricate ciliates (> 40 µm)	15464.6	13680.2	594.8	68401.0	15464.6	62453.1	86244.7	1189.6	74348.9
Tiarina fusus	1960.7	3921.5	1960.7	980.4	980.4	1960.7	4411.7	3921.5	1470.6
S bowl shaped tintinnids (20-50 µm length)	0.0	0.0	0.0	0.0	0.0	0.0	0.0	0.0	0.0
L bowl shaped tintinnids (> 60 µm length)	0.0	0.0	0.0	0.0	0.0	0.0	2144.0	0.0	2144.0
S tapering tintinnids (40-60 µm)	852.5	170.5	1705.0	2046.0	682.0	5285.6	1023.0	1364.0	10912.1
L tapering tintinnids (> 60 µm)	0.0	0.0	0.0	949.9	0.0	949.9	475.0	0.0	1424.9
Total ciliate carbon (Pg C ml^{-1})	**26470.9**	**25474.2**	**5295.8**	**100708.4**	**54013.0**	**80511.2**	**116184.8**	**8388.4**	**113491.1**

Date	**25/06/2015**	**25/06/2015**	**25/06/2015**	**26/06/2015**	**26/06/2015**	**26/06/2015**	**26/06/2015**	**26/06/2015**	**26/06/2015**
Site number	**16**	**17**	**18**	**19**	**19**	**19**	**20**	**21**	**22**
Sample location	**Surface**	**SCM**	**SCM**	**Bottom**	**SCM**	**Surface**	**SCM**	**SCM**	**SCM**
Diatoms (Pg C ml^{-1})									
S centric diatom (20-30 µm dia.)	0.0	0.0	0.0	0.0	0.0	0.0	0.0	0.0	0.0
M centric diatom (30-50 µm dia.)	0.0	746.9	149.4	0.0	448.1	0.0	0.0	0.0	0.0
L centric diatom (60-150 µm dia.)	0.0	352.8	0.0	0.0	705.6	0.0	705.6	0.0	352.8
XL centric diatom (> 150 µm dia.)	0.0	0.0	0.0	0.0	0.0	0.0	0.0	0.0	0.0
Cerataulina pelagica	472.0	94.4	0.0	472.0	849.7	1132.9	755.3	188.8	849.7
Chaetoceros spp.	3161.0	718.4	574.7	1005.8	1580.5	6609.3	1149.4	1580.5	3879.4
Corethron criophylum	0.0	0.0	0.0	0.0	0.0	0.0	0.0	0.0	0.0
Cylindrotheca closterium	2.8	11.3	0.0	2.8	2.8	8.5	0.0	0.0	0.0
Delphineis surirella	0.0	0.0	0.0	0.0	0.0	0.0	0.0	0.0	0.0
Diploneis spp.	0.0	0.0	36.2	0.0	0.0	0.0	0.0	0.0	0.0
Entomoneis spp.	0.0	0.0	0.0	145.6	0.0	0.0	0.0	29.1	0.0
Eucampia zoodiacus	0.0	0.0	0.0	0.0	0.0	0.0	0.0	0.0	0.0
Guinardia delicatula	0.0	0.0	0.0	0.0	0.0	378.0	0.0	0.0	0.0

Guinardia striata	1305.7	0.0	0.0	0.0	652.9	0.0	0.0	0.0	217.6
Lauderia annulata	0.0	0.0	0.0	0.0	0.0	235.5	0.0	0.0	0.0
Leptocylindrus danicus	5851.2	357.3	29.0	231.7	6015.4	10601.7	1892.5	289.7	12919.0
Leptocylindrus minimus	637.4	333.1	52.0	107.8	188.7	157.9	40.4	138.6	119.4
Meuniera membranacea	0.0	0.0	0.0	0.0	0.0	0.0	0.0	0.0	0.0
Odontella regia/ mobiliensis	0.0	0.0	0.0	0.0	0.0	0.0	0.0	0.0	0.0
Paralia sulcata	0.0	0.0	0.0	0.0	0.0	0.0	0.0	0.0	0.0
S pennate diatom (20-40 µm length)	0.0	0.0	0.0	0.0	0.0	0.0	0.0	0.0	0.0
M pennate diatom (40-65 µm length)	0.0	0.0	0.0	39.7	19.9	0.0	0.0	19.9	0.0
L pennate diatom (65-110 µm length)	0.0	0.0	0.0	149.3	0.0	0.0	0.0	0.0	0.0
S *Pleurosigma spp.* (~50 µm)	0.0	0.0	0.0	0.0	0.0	0.0	0.0	0.0	0.0
M *Pleurosigma spp.* (80-170 µm)	0.0	0.0	0.0	0.0	0.0	0.0	0.0	0.0	0.0
L *Pleurosigma spp.* (170-200 µm)	0.0	0.0	0.0	0.0	0.0	0.0	0.0	0.0	0.0
Proboscia alata	2146.4	731.7	48.8	341.5	975.6	3073.3	292.7	390.3	634.2
Proboscia truncata	3768.7	11306.1	7537.4	16331.0	17587.2	13818.5	15074.8	5024.9	11306.1
S *Pseudo-nitzschia spp.* (< 2.5 µm dia.)	77.5	5.2	36.1	2.6	95.5	69.7	105.9	93.0	382.1
L *Pseudo-nitzschia spp.* (> 2.5 µm dia.)	527.5	514.3	184.6	817.6	3956.0	8558.1	659.3	474.7	1529.6
S *Rhizosolenia spp.* (≤ 10 µm dia.)	0.0	33.3	0.0	0.0	166.7	166.7	0.0	0.0	100.0
M *Rhizosolenia spp.* (10-20 µm dia.)	0.0	0.0	0.0	0.0	0.0	0.0	0.0	0.0	0.0
L *Rhizosolenia spp.* (> 20 µm dia.)	0.0	0.0	0.0	0.0	0.0	0.0	0.0	0.0	0.0
Thalassionema nitzchioides	0.0	0.0	0.0	0.0	0.0	0.0	0.0	0.0	0.0
XS *Thalassiosira spp.* (< 10 µm height)	195.9	444.0	217.7	87.1	692.2	718.3	343.9	679.1	1750.0
S *Thalassiosira spp.* (10-25 µm height)	0.0	0.0	0.0	0.0	0.0	0.0	0.0	0.0	0.0
M *Thalassiosira spp.* (25-45 µm height)	0.0	57.8	0.0	0.0	0.0	0.0	115.7	0.0	347.1
L *Thalassiosira spp.* (> 45 µm height)	0.0	0.0	0.0	0.0	0.0	0.0	0.0	0.0	0.0

Total diatom carbon (Pg C ml^{-1})	**18146.2**	**15706.7**	**8865.8**	**19734.5**	**33936.8**	**45528.5**	**21135.5**	**8908.6**	**34387.1**
Dinoflagellates (Pg C ml^{-1})									
10-20 µm naked dinoflagellates	11452.8	7873.8	10916.0	5368.5	10021.2	10021.2	10021.2	7873.8	7515.9
20-25 µm naked dinoflagellates	4465.8	5741.8	1913.9	73.6	3189.9	5103.8	1913.9	6379.7	3827.8
10-30 µm armoured dinoflagellates	1212.4	303.1	303.1	50.5	505.1	606.2	50.5	202.1	202.1
Alexandrium ostenfeldii	0.0	17554.9	8573.3	0.0	4899.0	2857.8	4490.8	23678.7	13880.6
Amylax triacantha	0.0	0.0	0.0	0.0	0.0	0.0	0.0	0.0	0.0
Ceratium fusus	200.4	289370.9	221436.9	2204.3	344279.2	11622.9	328047.2	273138.9	259512.0
Ceratium lineatum	0.0	17352.4	19370.1	201.8	17554.2	605.3	13317.0	14527.6	32081.8
Ceratium macroceros	0.0	536.1	1072.3	0.0	536.1	0.0	1072.3	1608.4	0.0
Ceratium tripos	0.0	1372.5	0.0	0.0	1372.5	0.0	1372.5	0.0	0.0
Ceratoperidinium falcatum	0.0	2669.8	1601.9	534.0	1601.9	2135.8	1601.9	1601.9	4805.6
Dinophysis acuminata	0.0	171.8	0.0	0.0	171.8	0.0	171.8	343.6	859.0
Dinophysis acuta	0.0	2825.0	4237.5	0.0	5650.0	2118.8	706.3	12006.4	9887.6
Dinophysis caudata	0.0	0.0	0.0	0.0	0.0	0.0	0.0	0.0	0.0
Dinophysis norvegica	0.0	0.0	0.0	0.0	0.0	0.0	0.0	0.0	0.0
Dinophysis tripos	0.0	1546.1	0.0	0.0	0.0	0.0	0.0	0.0	0.0
Dissodinium sp.	0.0	0.0	0.0	0.0	0.0	0.0	0.0	0.0	0.0
Gonyaulax spinifera	532.1	1489.8	425.7	0.0	744.9	425.7	212.8	319.2	212.8
Gyrodinium spp.	3032.0	14957.7	6468.2	606.4	8287.4	6670.3	4244.8	6266.1	4244.8
Heterocapsa spp.	311.4	44.5	0.0	14.8	0.0	163.1	0.0	0.0	0.0
Karenia mikimotoi	0.0	14629.8	854.3	0.0	533.9	213.6	213.6	533.9	320.4
Katodinium glaucum	464.8	1261.7	9296.8	166.0	597.6	265.6	1560.5	697.3	1726.5
Nematodinium torpedo	0.0	0.0	86.8	0.0	173.7	260.5	86.8	173.7	434.2
Noctiluca scintillans	0.0	0.0	0.0	0.0	0.0	0.0	0.0	0.0	0.0
Oblea rotundata	0.0	0.0	0.0	0.0	0.0	0.0	0.0	0.0	0.0

Phalacroma rotundatum	515.2	0.0	515.2	0.0	0.0	257.6	0.0	515.2	0.0
Polykrikos schwartzii/kofoidii	0.0	1676.8	0.0	0.0	1676.8	8383.8	1676.8	0.0	1676.8
Prorocentrum micans	647.0	258.8	129.4	0.0	258.8	905.8	258.8	0.0	258.8
Prorocentrum minimum	707.8	557.7	536.2	128.7	686.4	300.3	514.8	600.6	278.8
Prorocentrum triestinum	82.5	0.0	0.0	0.0	0.0	41.2	41.2	0.0	0.0
S *Protoperidinium spp.* (10-30 µm dia.)	133.5	801.3	267.1	200.3	267.1	400.6	267.1	534.2	667.7
M *Protoperidinium spp.* (30-65 µm dia.)	0.0	0.0	0.0	0.0	0.0	334.5	334.5	334.5	0.0
L *Protoperidinium spp.* (65-120 µm dia.)	1753.2	3506.5	5259.7	0.0	17532.3	7012.9	1753.2	3506.5	15779.1
Torodinium robustum/teredo	625.3	131.6	32.9	98.7	65.8	98.7	65.8	0.0	98.7
Total dinoflagellate carbon (Pg C ml^{-1})	**26136.2**	**386634.3**	**293297.3**	**9647.7**	**420605.8**	**60806.2**	**373996.1**	**354842.2**	**358271.1**
Flagellates (Pg C ml^{-1})									
Chlamydomonas spp.	0.0	0.0	0.0	0.0	0.0	0.0	0.0	0.0	0.0
Chrysochromulina spp.	1139.1	1478.4	1163.3	145.4	1090.6	1284.5	993.7	969.4	1114.8
Chrysophaerella longispina	208.2	0.0	208.2	0.0	416.4	208.2	208.2	208.2	208.2
Cryptophytes	833.5	730.8	1335.9	890.6	1244.6	765.0	1404.4	765.0	902.0
Dictyocha fibula/speculum	844.8	77217.2	21458.6	1351.7	50520.7	8110.3	9800.0	15713.8	4731.0
Pleurasiga spp.	0.0	0.0	0.0	0.0	0.0	0.0	0.0	0.0	0.0
Solenicola setigera	34.0	578.5	2228.9	1582.3	6839.7	816.7	6448.4	4678.9	6788.7
unidentified spherical flagellate (10-20 µm dia.)	260.9	45.4	124.8	17.0	158.8	68.1	102.1	175.8	204.2
Total flagellate carbon (Pg C ml^{-1})	**3320.5**	**80050.2**	**26519.7**	**3987.1**	**60270.8**	**11252.8**	**18956.8**	**22511.1**	**13948.9**
Non-flagellated chlorophyceae (Pg C ml^{-1})									
Tetraedron spp.	36.3	0.0	0.0	0.0	0.0	0.0	0.0	0.0	0.0
Oocystaceae sp.	0.0	0.0	0.0	0.0	0.0	0.0	0.0	0.0	0.0
Total non-flagellated chlorophyceae carbon (Pg C ml^{-1})	**36.3**	**0.0**	**0.0**	**0.0**	**0.0**	**0.0**	**0.0**	**0.0**	**0.0**
Ciliates (Pg C ml^{-1})									

S aloricate ciliates (< 20µm)	1005.9	408.6	125.7	282.9	31.4	1037.3	220.0	314.3	125.7
M aloricate ciliates (20-40 µm)	32003.3	5747.5	6400.7	2090.0	5486.3	19332.6	7053.8	12017.6	10450.1
L aloricate ciliates (> 40 µm)	11895.8	17248.9	33308.3	2379.2	11895.8	35092.7	21412.5	23196.9	20817.7
Tiarina fusus	1960.7	980.4	1470.6	490.2	3921.5	0.0	1470.6	980.4	1960.7
S bowl shaped tintinnids (20-50 µm length)	0.0	0.0	0.0	0.0	0.0	0.0	0.0	0.0	0.0
L bowl shaped tintinnids (> 60 µm length)	0.0	0.0	0.0	0.0	2144.0	0.0	0.0	0.0	0.0
S tapering tintinnids (40-60 µm)	511.5	3751.0	341.0	511.5	0.0	341.0	511.5	852.5	170.5
L tapering tintinnids (> 60 µm)	475.0	0.0	0.0	0.0	0.0	475.0	0.0	0.0	0.0
Total ciliate carbon (Pg C ml^{-1})	**47852.2**	**28136.5**	**41646.3**	**5753.8**	**23479.0**	**56278.6**	**30668.4**	**37361.6**	**33524.7**

Date	**26/06/2015**	**26/06/2015**	**26/06/2015**	**26/06/2015**	**27/06/2015**	**27/06/2015**	**27/06/2015**	**27/06/2015**	**27/06/2015**
Site number	**23**	**24**	**25**	**26**	**27**	**28**	**29**	**29**	**29**
Sample location	**SCM**	**SCM**	**SCM**	**SCM**	**SCM**	**SCM**	**Bottom**	**SCM**	**Surface**
Diatoms (Pg C ml^{-1})									
S centric diatom (20-30 µm dia.)	0.0	0.0	0.0	0.0	0.0	0.0	0.0	0.0	0.0
M centric diatom (30-50 µm dia.)	0.0	0.0	149.4	0.0	149.4	0.0	149.4	0.0	448.1
L centric diatom (60-150 µm dia.)	352.8	0.0	0.0	0.0	0.0	0.0	352.8	0.0	0.0
XL centric diatom (> 150 µm dia.)	0.0	0.0	0.0	0.0	0.0	0.0	0.0	1511.7	0.0
Cerataulina pelagica	566.5	188.8	283.2	188.8	0.0	0.0	0.0	566.5	566.5
Chaetoceros spp.	2442.6	862.1	2011.5	718.4	2729.9	2155.2	431.0	3304.7	1724.2
Corethron criophylum	0.0	0.0	0.0	0.0	0.0	0.0	0.0	0.0	0.0
Cylindrotheca closterium	0.0	0.0	0.0	0.0	0.0	2.8	2.8	8.5	0.0
Delphineis surirella	0.0	0.0	0.0	0.0	0.0	0.0	0.0	0.0	0.0
Diploneis spp.	0.0	0.0	18.1	36.2	0.0	0.0	18.1	0.0	0.0
Entomoneis spp.	0.0	0.0	0.0	0.0	0.0	0.0	291.2	58.2	0.0

Eucampia zoodiacus	0.0	0.0	0.0	0.0	84.1	0.0	0.0	0.0	0.0
Guinardia delicatula	0.0	0.0	0.0	0.0	0.0	0.0	0.0	0.0	0.0
Guinardia striata	217.6	0.0	217.6	0.0	0.0	0.0	0.0	0.0	0.0
Lauderia annulata	0.0	0.0	0.0	0.0	0.0	0.0	0.0	0.0	67.3
Leptocylindrus danicus	1960.1	666.2	19.3	115.9	888.3	531.1	0.0	337.9	9587.9
Leptocylindrus minimus	90.5	0.0	44.3	77.0	279.2	356.2	59.7	269.6	40.4
Meuniera membranacea	0.0	0.0	0.0	188.6	0.0	0.0	0.0	471.4	0.0
Odontella regia/ mobiliensis	0.0	0.0	0.0	0.0	0.0	0.0	0.0	0.0	0.0
Paralia sulcata	0.0	0.0	0.0	69.9	0.0	0.0	713.4	42.0	0.0
S pennate diatom (20-40 µm length)	0.0	0.0	0.0	0.0	0.0	0.0	0.0	0.0	0.0
M pennate diatom (40-65 µm length)	0.0	0.0	0.0	0.0	0.0	0.0	39.7	19.9	0.0
L pennate diatom (65-110 µm length)	0.0	0.0	0.0	0.0	0.0	0.0	74.6	0.0	0.0
S *Pleurosigma spp.* (~50 µm)	0.0	0.0	0.0	0.0	0.0	0.0	0.0	0.0	0.0
M *Pleurosigma spp.* (80-170 µm)	0.0	0.0	0.0	0.0	0.0	0.0	0.0	0.0	0.0
L *Pleurosigma spp.* (170-200 µm)	0.0	0.0	0.0	0.0	0.0	0.0	0.0	0.0	0.0
Proboscia alata	97.6	390.3	195.1	243.9	487.8	878.1	292.7	243.9	1512.3
Proboscia truncata	15074.8	18843.5	12562.3	5024.9	12562.3	15074.8	15074.8	16331.0	2512.5
S *Pseudo-nitzschia spp.* (< 2.5 µm dia.)	87.8	20.7	139.4	72.3	123.9	142.0	36.1	464.8	235.0
L *Pseudo-nitzschia spp.* (> 2.5 µm dia.)	197.8	224.2	448.3	487.9	79.1	263.7	356.0	316.5	936.2
S *Rhizosolenia spp.* (≤ 10 µm dia.)	0.0	0.0	0.0	0.0	0.0	100.0	0.0	0.0	66.7
M *Rhizosolenia spp.* (10-20 µm dia.)	0.0	0.0	0.0	0.0	0.0	122.3	0.0	244.5	0.0
L *Rhizosolenia spp.* (> 20 µm dia.)	0.0	0.0	0.0	0.0	0.0	0.0	0.0	0.0	0.0
Thalassionema nitzchioides	0.0	0.0	0.0	0.0	0.0	0.0	0.0	0.0	0.0
XS *Thalassiosira spp.* (< 10 µm height)	4222.6	1262.4	1245.0	949.0	7248.1	7378.7	239.4	6355.7	3295.4
S *Thalassiosira spp.* (10-25 µm height)	0.0	0.0	0.0	0.0	0.0	0.0	0.0	0.0	0.0

M *Thalassiosira spp.* (25-45 µm height)	0.0	462.8	0.0	0.0	0.0	0.0	0.0	57.8	0.0
L *Thalassiosira spp.* (> 45 µm height)	0.0	0.0	0.0	0.0	0.0	0.0	0.0	0.0	0.0
Total diatom carbon (Pg C ml^{-1})	**25310.6**	**22920.9**	**17333.7**	**8172.8**	**24632.2**	**27004.9**	**18131.8**	**30604.5**	**20992.4**
Dinoflagellates (Pg C ml^{-1})									
10-20 µm naked dinoflagellates	6979.1	8768.6	7158.0	8410.7	5010.6	5547.5	5368.5	9842.3	8947.5
20-25 µm naked dinoflagellates	5103.8	4465.8	4465.8	1913.9	4465.8	3189.9	638.0	3827.8	1275.9
10-30 µm armoured dinoflagellates	353.6	202.1	303.1	101.0	505.1	505.1	101.0	656.7	353.6
Alexandrium ostenfeldii	14288.9	13472.4	816.5	13064.1	6532.1	6532.1	0.0	6532.1	816.5
Amylax triacantha	0.0	0.0	0.0	0.0	0.0	0.0	0.0	0.0	0.0
Ceratium fusus	149094.1	140677.5	143883.9	249692.6	128453.4	144485.0	1002.0	194183.1	200.4
Ceratium lineatum	10088.6	13720.5	6860.3	7869.1	4640.8	13720.5	0.0	10492.2	0.0
Ceratium macroceros	536.1	0.0	0.0	2144.6	536.1	0.0	0.0	0.0	0.0
Ceratium tripos	1372.5	1372.5	2745.0	1372.5	0.0	0.0	0.0	0.0	0.0
Ceratoperidinium falcatum	5873.6	2669.8	3203.8	4271.7	4805.6	2669.8	0.0	3203.8	534.0
Dinophysis acuminata	687.2	515.4	0.0	0.0	515.4	171.8	0.0	171.8	0.0
Dinophysis acuta	11300.1	16243.9	0.0	5650.0	28250.2	21893.9	0.0	9887.6	0.0
Dinophysis caudata	0.0	0.0	0.0	0.0	662.0	0.0	0.0	0.0	0.0
Dinophysis norvegica	0.0	0.0	0.0	0.0	0.0	0.0	0.0	0.0	0.0
Dinophysis tripos	0.0	1546.1	0.0	0.0	0.0	0.0	0.0	0.0	0.0
Dissodinium sp.	0.0	0.0	0.0	0.0	0.0	0.0	0.0	0.0	0.0
Gonyaulax spinifera	744.9	744.9	319.2	212.8	638.5	532.1	106.4	638.5	957.7
Gyrodinium spp.	5053.3	5053.3	4446.9	5053.3	5053.3	5053.3	1414.9	7681.0	7276.7
Heterocapsa spp.	0.0	0.0	0.0	29.7	29.7	14.8	29.7	14.8	370.7
Karenia mikimotoi	106.8	106.8	213.6	427.1	106.8	106.8	0.0	320.4	0.0
Katodinium glaucum	3021.4	896.5	1427.7	1261.7	564.4	929.7	332.0	3087.9	531.2
Nematodinium torpedo	173.7	173.7	260.5	0.0	0.0	0.0	86.8	173.7	0.0

Noctiluca scintillans	0.0	113540.7	0.0	0.0	0.0	0.0	0.0	0.0	0.0
Oblea rotundata	0.0	0.0	0.0	0.0	0.0	0.0	0.0	0.0	0.0
Phalacroma rotundatum	0.0	0.0	0.0	0.0	0.0	0.0	0.0	0.0	0.0
Polykrikos schwartzii/kofoidii	0.0	0.0	1676.8	0.0	0.0	6707.1	0.0	3353.5	13414.1
Prorocentrum micans	258.8	258.8	776.4	129.4	258.8	388.2	129.4	129.4	129.4
Prorocentrum minimum	343.2	343.2	471.9	450.4	471.9	429.0	128.7	622.0	579.1
Prorocentrum triestinum	0.0	0.0	0.0	0.0	0.0	0.0	0.0	0.0	0.0
S *Protoperidinium spp.* (10-30 µm dia.)	934.8	333.9	200.3	601.0	801.3	734.5	66.8	267.1	0.0
M *Protoperidinium spp.* (30-65 µm dia.)	0.0	334.5	0.0	0.0	0.0	0.0	0.0	334.5	0.0
L *Protoperidinium spp.* (65-120 µm dia.)	5259.7	1753.2	8766.1	3506.5	3506.5	5259.7	0.0	5259.7	0.0
Torodinium robustum/teredo	32.9	0.0	98.7	65.8	65.8	0.0	32.9	32.9	164.6
Total dinoflagellate carbon (Pg C ml^{-1})	**221607.1**	**327194.0**	**188094.5**	**306228.0**	**195874.2**	**218870.7**	**9437.1**	**260712.6**	**35551.5**
Flagellates (Pg C ml^{-1})									
Chlamydomonas spp.	0.0	0.0	0.0	0.0	0.0	0.0	0.0	0.0	712.1
Chrysochromulina spp.	1187.5	1114.8	581.7	872.5	2035.8	2132.7	48.5	1769.2	1308.7
Chrysophaerella longispina	416.4	832.8	208.2	624.6	416.4	416.4	0.0	208.2	416.4
Cryptophytes	593.7	959.1	696.5	1404.4	411.1	491.0	844.9	947.7	1541.4
Dictyocha fibula/speculum	3548.3	8955.2	2196.6	13179.3	14700.0	11658.6	844.8	8279.3	2027.6
Pleurasiga spp.	1466.7	488.9	488.9	977.8	1955.6	977.8	0.0	0.0	0.0
Solenicola setigera	4747.0	3624.0	2824.4	6822.7	2773.3	4083.4	1344.1	3658.1	1191.0
unidentified spherical flagellate (10-20 µm dia.)	136.1	153.1	73.7	136.1	232.5	260.9	56.7	300.6	107.8
Total flagellate carbon (Pg C ml^{-1})	**12095.7**	**16128.0**	**7069.9**	**24017.4**	**22524.7**	**20020.8**	**3139.1**	**15163.0**	**7305.1**
Non-flagellated chlorophyceae (Pg C ml^{-1})									
Tetraedron spp.	0.0	0.0	0.0	36.3	0.0	0.0	36.3	0.0	0.0
Oocystaceae sp.	0.0	0.0	0.0	0.0	0.0	0.0	0.0	0.0	0.0

Total non-flagellated chlorophyceae carbon (Pg C ml^{-1})	**0.0**	**0.0**	**0.0**	**36.3**	**0.0**	**0.0**	**36.3**	**0.0**	**0.0**
Ciliates (Pg C ml^{-1})									
S aloricate ciliates (< 20µm)	471.5	94.3	314.3	62.9	502.9	408.6	377.2	188.6	2766.2
M aloricate ciliates (20-40 µm)	25080.2	22859.5	2873.8	6661.9	23512.6	27823.3	1436.9	13977.0	27431.4
L aloricate ciliates (> 40 µm)	44609.3	15464.6	23196.9	22007.3	36877.0	42230.2	1784.4	65427.0	11895.8
Tiarina fusus	2450.9	980.4	2941.1	980.4	980.4	2450.9	490.2	5882.2	1960.7
S bowl shaped tintinnids (20-50 µm length)	0.0	0.0	0.0	0.0	0.0	0.0	0.0	0.0	0.0
L bowl shaped tintinnids (> 60 µm length)	0.0	0.0	0.0	0.0	0.0	0.0	0.0	0.0	2144.0
S tapering tintinnids (40-60 µm)	1364.0	511.5	682.0	682.0	2557.5	1534.5	0.0	1364.0	170.5
L tapering tintinnids (> 60 µm)	0.0	0.0	0.0	0.0	0.0	0.0	0.0	0.0	0.0
Total ciliate carbon (Pg C ml^{-1})	**73975.9**	**39910.3**	**30008.1**	**30394.4**	**64430.5**	**74447.5**	**4088.7**	**86838.8**	**46368.7**

Date	**27/06/2015**	**27/06/2015**	**29/06/2015**	**29/06/2015**	**29/06/2015**	**29/06/2015**	**29/06/2015**	**29/06/2015**	**29/06/2015**
Site number	**30**	**31**	**32**	**33**	**33**	**33**	**34**	**35**	**36**
Sample location	**SCM**	**SCM**	**SCM**	**Bottom**	**SCM**	**Surface**	**SCM**	**SCM**	**SCM**
Diatoms (Pg C ml^{-1})									
S centric diatom (20-30 µm dia.)	0.0	0.0	0.0	0.0	0.0	77.4	0.0	0.0	0.0
M centric diatom (30-50 µm dia.)	0.0	0.0	298.7	0.0	0.0	0.0	0.0	298.7	0.0
L centric diatom (60-150 µm dia.)	0.0	0.0	0.0	0.0	0.0	0.0	0.0	0.0	0.0
XL centric diatom (> 150 µm dia.)	0.0	0.0	0.0	0.0	0.0	0.0	0.0	0.0	0.0
Cerataulina pelagica	188.8	94.4	188.8	94.4	188.8	755.3	188.8	0.0	0.0
Chaetoceros spp.	1005.8	3592.0	2011.5	862.1	718.4	143.7	574.7	287.4	718.4
Corethron criophylum	0.0	0.0	0.0	0.0	0.0	0.0	0.0	0.0	0.0
Cylindrotheca closterium	2.8	0.0	8.5	8.5	2.8	0.0	0.0	0.0	5.7
Delphineis surirella	0.0	0.0	0.0	0.0	0.0	0.0	0.0	0.0	0.0

Diploneis spp.	36.2	0.0	0.0	54.3	0.0	0.0	0.0	0.0	0.0
Entomoneis spp.	0.0	0.0	0.0	87.4	0.0	0.0	0.0	0.0	0.0
Eucampia zoodiacus	0.0	0.0	0.0	0.0	0.0	0.0	0.0	0.0	0.0
Guinardia delicatula	47.3	0.0	0.0	0.0	0.0	0.0	0.0	0.0	0.0
Guinardia striata	0.0	0.0	0.0	0.0	0.0	870.5	0.0	0.0	0.0
Lauderia annulata	0.0	0.0	0.0	0.0	0.0	0.0	100.9	0.0	0.0
Leptocylindrus danicus	115.9	753.1	589.0	135.2	299.3	7849.9	202.8	0.0	0.0
Leptocylindrus minimus	115.5	460.2	98.2	123.2	82.8	1099.5	75.1	36.6	0.0
Meuniera membranacea	660.0	188.6	94.3	0.0	0.0	0.0	0.0	94.3	0.0
Odontella regia/ mobiliensis	0.0	0.0	0.0	0.0	0.0	0.0	0.0	0.0	0.0
Paralia sulcata	0.0	0.0	209.8	167.8	0.0	0.0	0.0	0.0	0.0
S pennate diatom (20-40 µm length)	0.0	0.0	0.0	0.0	0.0	0.0	0.0	0.0	0.0
M pennate diatom (40-65 µm length)	0.0	0.0	0.0	0.0	0.0	0.0	0.0	19.9	19.9
L pennate diatom (65-110 µm length)	0.0	0.0	74.6	74.6	0.0	0.0	0.0	0.0	0.0
S *Pleurosigma spp.* (~50 µm)	0.0	0.0	0.0	0.0	0.0	0.0	0.0	0.0	0.0
M *Pleurosigma spp.* (80-170 µm)	0.0	0.0	0.0	0.0	0.0	0.0	0.0	0.0	68.5
L *Pleurosigma spp.* (170-200 µm)	0.0	0.0	0.0	0.0	0.0	0.0	0.0	0.0	0.0
Proboscia alata	243.9	146.3	146.3	292.7	2487.9	1707.4	487.8	829.3	195.1
Proboscia truncata	15074.8	10049.8	5024.9	1256.2	7537.4	0.0	8793.6	10049.8	2512.5
S *Pseudo-nitzschia spp.* (< 2.5 µm dia.)	296.9	144.6	720.4	23.2	23.2	90.4	15.5	15.5	25.8
L *Pseudo-nitzschia spp.* (> 2.5 µm dia.)	263.7	92.3	224.2	1160.4	145.1	553.8	52.7	52.7	105.5
S *Rhizosolenia spp.* (≤ 10 µm dia.)	33.3	0.0	166.7	33.3	0.0	33.3	33.3	33.3	0.0
M *Rhizosolenia spp.* (10-20 µm dia.)	0.0	0.0	0.0	0.0	0.0	0.0	0.0	0.0	0.0
L *Rhizosolenia spp.* (> 20 µm dia.)	0.0	0.0	0.0	0.0	0.0	0.0	0.0	0.0	0.0
Thalassionema nitzchioides	0.0	0.0	0.0	0.0	0.0	0.0	0.0	0.0	0.0

XS *Thalassiosira spp.* (< 10 µm height)	1371.3	6917.2	6238.1	126.2	457.1	121.9	1484.4	696.5	478.9
S *Thalassiosira spp.* (10-25 µm height)	0.0	0.0	0.0	0.0	0.0	0.0	0.0	0.0	0.0
M *Thalassiosira spp.* (25-45 µm height)	0.0	0.0	0.0	0.0	57.8	0.0	0.0	0.0	0.0
L *Thalassiosira spp.* (> 45 µm height)	0.0	0.0	0.0	0.0	0.0	0.0	0.0	0.0	0.0
Total diatom carbon (Pg C ml^{-1})	**19456.2**	**22438.7**	**16094.2**	**4499.7**	**12000.7**	**13303.1**	**12009.8**	**12414.1**	**4130.2**
Dinoflagellates (Pg C ml^{-1})									
10-20 µm naked dinoflagellates	8768.6	8231.7	7158.0	11452.8	21653.0	17895.1	25053.1	38653.3	32569.0
20-25 µm naked dinoflagellates	5103.8	1913.9	638.0	638.0	8293.7	7017.7	10845.6	10207.6	28708.8
10-30 µm armoured dinoflagellates	353.6	505.1	252.6	151.5	1060.8	3233.0	353.6	1262.9	11830.6
Alexandrium ostenfeldii	2857.8	7348.6	1633.0	0.0	17963.2	1224.8	13064.1	1224.8	2449.5
Amylax triacantha	0.0	0.0	0.0	0.0	0.0	0.0	0.0	0.0	0.0
Ceratium fusus	591567.1	37674.3	67332.8	0.0	158512.7	801.6	60319.0	5410.7	11021.7
Ceratium lineatum	19168.4	4439.0	2219.5	0.0	7062.0	0.0	6254.9	4842.5	5851.4
Ceratium macroceros	0.0	536.1	2144.6	0.0	0.0	0.0	0.0	5897.5	1072.3
Ceratium tripos	0.0	0.0	0.0	0.0	0.0	0.0	0.0	1372.5	0.0
Ceratoperidinium falcatum	3203.8	3737.7	534.0	0.0	3203.8	534.0	534.0	2135.8	1067.9
Dinophysis acuminata	171.8	515.4	0.0	0.0	171.8	0.0	171.8	1374.4	687.2
Dinophysis acuta	1412.5	26837.7	0.0	0.0	41669.1	0.0	7768.8	2118.8	16950.1
Dinophysis caudata	0.0	0.0	0.0	0.0	662.0	0.0	0.0	0.0	0.0
Dinophysis norvegica	0.0	0.0	0.0	0.0	0.0	0.0	0.0	0.0	0.0
Dinophysis tripos	0.0	0.0	0.0	0.0	2319.1	0.0	773.0	0.0	773.0
Dissodinium sp.	0.0	0.0	0.0	0.0	0.0	0.0	0.0	0.0	0.0
Gonyaulax spinifera	638.5	425.7	106.4	0.0	1064.2	532.1	744.9	425.7	1277.0
Gyrodinium spp.	7478.9	6468.2	4244.8	1617.1	5861.8	12127.9	12330.0	6468.2	14149.2
Heterocapsa spp.	74.1	0.0	0.0	0.0	444.8	2861.8	207.6	207.6	17348.9
Karenia mikimotoi	213.6	0.0	0.0	0.0	8863.3	106.8	8009.0	5766.5	2349.3

Katodinium glaucum	1726.5	1095.7	664.1	398.4	597.6	464.8	2125.0	1527.3	4582.0
Nematodinium torpedo	260.5	173.7	173.7	0.0	0.0	173.7	694.8	434.2	173.7
Noctiluca scintillans	0.0	0.0	0.0	0.0	0.0	0.0	227081.5	113540.7	227081.5
Oblea rotundata	0.0	0.0	0.0	0.0	0.0	0.0	0.0	0.0	2433.3
Phalacroma rotundatum	0.0	0.0	0.0	0.0	257.6	0.0	0.0	0.0	515.2
Polykrikos schwartzii/kofoidii	3353.5	5030.3	1676.8	0.0	1676.8	1676.8	0.0	1676.8	3353.5
Prorocentrum micans	258.8	388.2	129.4	129.4	258.8	1552.7	388.2	129.4	129.4
Prorocentrum minimum	257.4	386.1	150.1	21.4	664.9	214.5	386.1	64.3	0.0
Prorocentrum triestinum	0.0	0.0	0.0	0.0	0.0	0.0	0.0	0.0	0.0
S *Protoperidinium spp.* (10-30 µm dia.)	267.1	467.4	133.5	133.5	801.3	333.9	467.4	1335.5	400.6
M *Protoperidinium spp.* (30-65 µm dia.)	0.0	1003.5	0.0	334.5	0.0	0.0	1003.5	334.5	334.5
L *Protoperidinium spp.* (65-120 µm dia.)	3506.5	5259.7	1753.2	0.0	8766.1	3506.5	10519.4	0.0	1753.2
Torodinium robustum/teredo	164.6	0.0	98.7	98.7	197.5	164.6	98.7	296.2	263.3
Total dinoflagellate carbon (Pg C ml^{-1})	**650807.2**	**112438.1**	**91043.2**	**14975.5**	**292025.9**	**54422.0**	**389194.0**	**206707.7**	**389126.4**
Flagellates (Pg C ml^{-1})									
Chlamydomonas spp.	0.0	0.0	0.0	0.0	0.0	0.0	0.0	712.1	0.0
Chrysochromulina spp.	1526.8	1090.6	218.1	145.4	2108.5	848.2	2399.3	3538.4	3829.2
Chrysophaerella longispina	0.0	208.2	208.2	0.0	416.4	0.0	416.4	208.2	832.8
Cryptophytes	502.4	593.7	479.6	331.1	776.4	1838.3	673.7	1393.0	628.0
Dictyocha fibula/speculum	2365.5	11827.6	2027.6	1013.8	12165.5	337.9	4731.0	58800.0	251758.5
Pleurasiga spp.	0.0	2444.5	1955.6	0.0	0.0	0.0	488.9	0.0	0.0
Solenicola setigera	3794.2	3930.3	3249.7	952.8	204.2	85.1	1361.1	68.1	204.2
unidentified spherical flagellate (10-20 µm dia.)	107.8	124.8	85.1	22.7	147.5	425.3	136.1	187.2	462.8
Total flagellate carbon (Pg C ml^{-1})	**8296.7**	**20219.7**	**8223.8**	**2465.8**	**15818.5**	**3534.9**	**10206.6**	**64906.9**	**257715.5**
Non-flagellated chlorophyceae (Pg C ml^{-1})									

Tetraedron spp.	0.0	0.0	0.0	0.0	0.0	0.0	0.0	72.7	0.0
Oocystaceae sp.	416.6	0.0	416.6	416.6	416.6	0.0	0.0	0.0	0.0
Total non-flagellated chlorophyceae carbon (Pg C ml^{-1})	**416.6**	**0.0**	**416.6**	**416.6**	**416.6**	**0.0**	**0.0**	**72.7**	**0.0**
Ciliates (Pg C ml^{-1})									
S aloricate ciliates (< 20µm)	314.3	377.2	251.5	534.4	660.1	3489.2	754.4	660.1	1131.6
M aloricate ciliates (20-40 µm)	3526.9	20638.9	391.9	522.5	26647.7	33309.6	9927.6	3918.8	14630.1
L aloricate ciliates (> 40 µm)	41040.6	29144.8	23196.9	5947.9	17843.7	14275.0	44014.5	95761.4	67211.4
Tiarina fusus	2941.1	2941.1	1960.7	1960.7	490.2	0.0	980.4	980.4	2941.1
S bowl shaped tintinnids (20-50 µm length)	0.0	0.0	0.0	0.0	0.0	0.0	0.0	0.0	0.0
L bowl shaped tintinnids (> 60 µm length)	2144.0	0.0	0.0	0.0	0.0	0.0	2144.0	0.0	0.0
S tapering tintinnids (40-60 µm)	2216.5	1875.5	0.0	341.0	341.0	341.0	8013.6	5797.1	4433.0
L tapering tintinnids (> 60 µm)	0.0	0.0	0.0	0.0	0.0	475.0	0.0	0.0	0.0
Total ciliate carbon (Pg C ml^{-1})	**52183.5**	**54977.5**	**25800.9**	**9306.5**	**45982.7**	**51889.7**	**65834.5**	**107117.7**	**90347.3**

Date	**30/06/2015**	**30/06/2015**	**30/06/2015**	**01/07/2015**	**02/07/2015**	**02/07/2015**	**02/07/2015**	**02/07/2015**
Site number	**37**	**37**	**37**	**38**	**39**	**40**	**40**	**40**
Sample location	**Bottom**	**SCM**	**Surface**	**SCM**	**SCM**	**Bottom**	**SCM**	**Surface**
Diatoms (Pg C ml^{-1})								
S centric diatom (20-30 µm dia.)	0.0	0.0	0.0	0.0	0.0	0.0	0.0	0.0
M centric diatom (30-50 µm dia.)	448.1	0.0	0.0	298.7	298.7	597.5	298.7	0.0
L centric diatom (60-150 µm dia.)	352.8	0.0	0.0	0.0	352.8	0.0	0.0	0.0
XL centric diatom (> 150 µm dia.)	0.0	0.0	0.0	0.0	0.0	0.0	0.0	0.0
Cerataulina pelagica	94.4	0.0	188.8	188.8	0.0	188.8	0.0	377.6
Chaetoceros spp.	431.0	1149.4	862.1	1580.5	4454.1	1005.8	71.8	143.7
Corethron criophylum	0.0	0.0	0.0	0.0	0.0	0.0	0.0	0.0

Cylindrotheca closterium	5.7	2.8	0.0	5.7	0.0	5.7	2.8	0.0
Delphineis surirella	3.8	0.0	0.0	0.0	0.0	3.8	0.0	0.0
Diploneis spp.	36.2	0.0	0.0	0.0	0.0	72.3	0.0	0.0
Entomoneis spp.	116.5	0.0	0.0	116.5	29.1	145.6	0.0	0.0
Eucampia zoodiacus	336.4	0.0	0.0	0.0	0.0	0.0	0.0	0.0
Guinardia delicatula	0.0	0.0	0.0	0.0	0.0	0.0	0.0	47.3
Guinardia striata	217.6	0.0	217.6	0.0	0.0	0.0	0.0	217.6
Lauderia annulata	0.0	0.0	0.0	0.0	0.0	0.0	0.0	0.0
Leptocylindrus danicus	96.6	5542.3	23636.6	2944.9	482.8	38.6	260.7	9250.0
Leptocylindrus minimus	44.3	250.3	19.3	71.2	279.2	77.0	42.4	61.6
Meuniera membranacea	282.8	0.0	0.0	0.0	0.0	0.0	94.3	0.0
Odontella regia/ mobiliensis	0.0	0.0	0.0	0.0	0.0	0.0	0.0	0.0
Paralia sulcata	223.8	0.0	0.0	181.8	0.0	111.9	0.0	0.0
S pennate diatom (20-40 µm length)	0.0	0.0	0.0	0.0	0.0	4.9	0.0	0.0
M pennate diatom (40-65 µm length)	19.9	0.0	0.0	0.0	0.0	39.7	19.9	0.0
L pennate diatom (65-110 µm length)	74.6	0.0	0.0	0.0	0.0	223.9	0.0	0.0
S *Pleurosigma spp.* (~50 µm)	10.6	0.0	0.0	0.0	0.0	0.0	0.0	0.0
M *Pleurosigma spp.* (80-170 µm)	0.0	0.0	0.0	0.0	0.0	0.0	0.0	0.0
L *Pleurosigma spp.* (170-200 µm)	0.0	0.0	0.0	0.0	0.0	0.0	0.0	0.0
Proboscia alata	146.3	2292.8	1658.6	97.6	97.6	292.7	195.1	4195.3
Proboscia truncata	2512.5	8793.6	11306.1	10049.8	1256.2	3768.7	2512.5	2512.5
S *Pseudo-nitzschia spp.* (< 2.5 µm dia.)	684.2	100.7	69.7	495.8	183.3	204.0	23.2	10.3
L *Pseudo-nitzschia spp.* (> 2.5 µm dia.)	382.4	145.1	804.4	184.6	26.4	540.7	79.1	79.1
S *Rhizosolenia spp.* (≤ 10 µm dia.)	33.3	100.0	66.7	33.3	66.7	66.7	0.0	33.3
M *Rhizosolenia spp.* (10-20 µm dia.)	0.0	0.0	0.0	0.0	122.3	0.0	0.0	0.0

L *Rhizosolenia spp.* (> 20 µm dia.)	0.0	0.0	0.0	0.0	0.0	0.0	0.0	0.0
Thalassionema nitzchioides	0.0	0.0	0.0	0.0	0.0	0.0	0.0	0.0
XS *Thalassiosira spp.* (< 10 µm height)	596.4	5337.0	1275.5	7365.6	15192.7	309.1	1366.9	348.3
S *Thalassiosira spp.* (10-25 µm height)	0.0	0.0	0.0	0.0	0.0	0.0	0.0	0.0
M *Thalassiosira spp.* (25-45 µm height)	0.0	0.0	0.0	0.0	0.0	0.0	0.0	57.8
L *Thalassiosira spp.* (> 45 µm height)	0.0	0.0	0.0	0.0	0.0	0.0	0.0	0.0
Total diatom carbon (Pg C ml^{-1})	**7150.2**	**23714.1**	**40105.4**	**23615.0**	**22841.9**	**7697.3**	**4967.5**	**17334.4**
Dinoflagellates (Pg C ml^{-1})								
10-20 µm naked dinoflagellates	6084.3	8410.7	9663.3	9126.5	15747.7	10379.1	15031.9	12705.5
20-25 µm naked dinoflagellates	638.0	5103.8	3827.8	2551.9	7017.7	638.0	5103.8	10845.6
10-30 µm armoured dinoflagellates	101.0	1212.4	505.1	505.1	606.2	50.5	1010.3	3738.1
Alexandrium ostenfeldii	0.0	5307.3	816.5	2041.3	0.0	408.3	10614.6	1633.0
Amylax triacantha	0.0	0.0	0.0	0.0	0.0	0.0	0.0	0.0
Ceratium fusus	0.0	51702.0	1002.0	32864.8	30059.3	601.2	81560.9	1002.0
Ceratium lineatum	0.0	11299.2	0.0	5851.4	2421.3	0.0	12509.9	0.0
Ceratium macroceros	0.0	0.0	0.0	1072.3	0.0	0.0	0.0	0.0
Ceratium tripos	0.0	1372.5	0.0	0.0	1372.5	0.0	0.0	0.0
Ceratoperidinium falcatum	0.0	1067.9	534.0	534.0	1067.9	0.0	3737.7	1067.9
Dinophysis acuminata	0.0	343.6	0.0	515.4	1374.4	0.0	1202.6	0.0
Dinophysis acuta	0.0	113707.2	0.0	37431.6	80513.2	706.3	24719.0	0.0
Dinophysis caudata	0.0	0.0	0.0	0.0	0.0	0.0	0.0	0.0
Dinophysis norvegica	0.0	0.0	0.0	0.0	0.0	0.0	0.0	0.0
Dinophysis tripos	0.0	0.0	0.0	0.0	773.0	0.0	773.0	1546.1
Dissodinium sp.	0.0	0.0	0.0	0.0	0.0	0.0	0.0	0.0
Gonyaulax spinifera	0.0	1064.2	319.2	0.0	0.0	106.4	319.2	0.0
Gyrodinium spp.	606.4	3840.5	5053.3	2829.8	5659.7	404.3	5255.4	8085.3

Heterocapsa spp.	0.0	59.3	370.7	14.8	252.1	0.0	326.2	430.0
Karenia mikimotoi	0.0	320.4	213.6	106.8	213.6	0.0	3844.3	106.8
Katodinium glaucum	199.2	431.6	464.8	962.9	896.5	332.0	763.7	1361.3
Nematodinium torpedo	0.0	0.0	0.0	86.8	86.8	86.8	260.5	0.0
Noctiluca scintillans	0.0	340622.2	0.0	0.0	0.0	0.0	0.0	0.0
Oblea rotundata	0.0	76.0	0.0	0.0	0.0	0.0	76.0	0.0
Phalacroma rotundatum	0.0	0.0	257.6	0.0	0.0	0.0	515.2	0.0
Polykrikos schwartzii/kofoidii	0.0	0.0	1676.8	0.0	0.0	0.0	1676.8	0.0
Prorocentrum micans	129.4	129.4	258.8	0.0	0.0	129.4	388.2	1811.5
Prorocentrum minimum	85.8	386.1	235.9	150.1	536.2	85.8	128.7	128.7
Prorocentrum triestinum	0.0	0.0	0.0	0.0	41.2	0.0	0.0	0.0
S *Protoperidinium spp.* (10-30 µm dia.)	133.5	267.1	0.0	66.8	0.0	200.3	200.3	0.0
M *Protoperidinium spp.* (30-65 µm dia.)	0.0	669.0	669.0	334.5	1003.5	0.0	334.5	334.5
L *Protoperidinium spp.* (65-120 µm dia.)	0.0	7012.9	5259.7	5259.7	7012.9	0.0	0.0	0.0
Torodinium robustum/teredo	98.7	32.9	296.2	32.9	98.7	65.8	98.7	559.5
Total dinoflagellate carbon (Pg C ml^{-1})	**8076.4**	**554438.3**	**31424.4**	**102339.4**	**156754.4**	**14194.2**	**170451.5**	**45355.7**
Flagellates (Pg C ml^{-1})								
Chlamydomonas spp.	0.0	0.0	0.0	0.0	0.0	0.0	0.0	0.0
Chrysochromulina spp.	121.2	3077.9	1526.8	630.1	2253.9	145.4	1914.6	1066.4
Chrysophaerella longispina	0.0	416.4	0.0	416.4	1249.2	0.0	208.2	0.0
Cryptophytes	570.9	513.8	993.4	890.6	673.7	673.7	924.9	696.5
Dictyocha fibula/speculum	844.8	5575.9	1520.7	675.9	675.9	1182.8	2872.4	675.9
Pleurasiga spp.	977.8	488.9	0.0	2933.4	1466.7	0.0	0.0	0.0
Solenicola setigera	1514.3	3641.0	1293.1	5750.8	3368.8	850.7	1242.0	51.0
unidentified spherical flagellate (10-20 µm dia.)	5.7	62.4	79.4	153.1	215.5	17.0	56.7	952.8

Total flagellate carbon (Pg C ml^{-1})	**4034.6**	**13776.3**	**5413.4**	**11450.3**	**9903.7**	**2869.6**	**7218.8**	**3442.5**
Non-flagellated chlorophyceae (Pg C ml^{-1})								
Tetraedron spp.	0.0	0.0	0.0	0.0	0.0	0.0	0.0	0.0
Oocystaceae sp.	0.0	0.0	0.0	0.0	0.0	0.0	0.0	0.0
Total non-flagellated chlorophyceae carbon (Pg C ml^{-1})	**0.0**	**0.0**	**0.0**	**0.0**	**0.0**	**0.0**	**0.0**	**0.0**
Ciliates (Pg C ml^{-1})								
S aloricate ciliates (< 20µm)	282.9	440.1	943.0	282.9	723.0	691.6	1131.6	691.6
M aloricate ciliates (20-40 µm)	522.5	23512.6	30043.9	3918.8	14499.5	391.9	10972.6	18679.5
L aloricate ciliates (> 40 µm)	2974.0	14275.0	6542.7	79702.0	18438.5	1189.6	16059.4	14275.0
Tiarina fusus	3431.3	490.2	490.2	4901.8	2941.1	0.0	490.2	490.2
S bowl shaped tintinnids (20-50 µm length)	0.0	0.0	0.0	0.0	0.0	0.0	0.0	0.0
L bowl shaped tintinnids (> 60 µm length)	0.0	0.0	0.0	4288.1	0.0	0.0	0.0	0.0
S tapering tintinnids (40-60 µm)	170.5	1023.0	0.0	341.0	1534.5	511.5	1875.5	511.5
L tapering tintinnids (> 60 µm)	0.0	475.0	0.0	949.9	0.0	0.0	475.0	0.0
Total ciliate carbon (Pg C ml^{-1})	**7381.2**	**40215.9**	**38019.8**	**94384.5**	**38136.6**	**2784.5**	**31004.2**	**34647.7**

Table A2.2. Date, time, location, water depth, SCM depth, SCM chlorophyll concentration, SCM thickness (measured at half maximum chlorophyll intensity of the SCM) of the 40 stratified sites profiled and sampled in the Western English Channel during summer 2015. Site numbers in red bold italics are those of sites profiled and sampled at repeat station 1.

Date	Site no.	Time (UTC)	Latitude	Longitude	Water depth (m)	SCM depth (m)	SCM max chl conc. (µg l^{-1})	SCM thickness (m)
19/06	1	09:16	50° 06.07N	4° 24.65W	70	27.0	28.0	0.1
	2	11:30	49° 57.01N	4° 33.68W	75	32.4	3.9	7.8
23/06	3	10:20	50° 00.14N	4° 40.35W	75	21.8	3.0	6.0
	4	12:09	50° 06.10N	4° 24.80W	69	26.2	3.1	3.7
	5	13:12	50° 06.53N	4° 29.35W	68	28.1	7.2	1.5
	6	13:45	50° 06.46N	4° 32.51W	68	29.8	10.8	2.9
	7	14:18	50° 06.31N	4° 35.91W	67	26.1	15.8	3.2
	8	14:48	50° 06.21N	4° 39.47W	68	25.7	13.7	1.5
	9	16:01	50° 05.65N	4° 52.30W	66	26.9	9.2	2.9
24/06	10	08:37	50° 02.54N	4° 46.23W	73	28.3	2.7	2.8
	11	10:12	50° 05.87N	4° 52.23W	66	24.8	14.4	7.4
	12	13:03	50° 05.76N	4° 51.99W	66	30.7	9.0	7.5
	13	14:35	50° 02.60N	4° 46.26W	71	27.8	7.5	1.2
25/06	14	10:04	50° 06.32N	4° 35.96W	69	24.9	3.4	3.7
	15	10:52	50° 06.48N	4° 31.97W	69	25.9	1.7	13.5
	16	12:08	50° 02.65N	4° 46.27W	73	29.6	3.2	6.5
	17	13:36	49° 54.95N	4° 55.13W	82	34.6	9.7	4.4
	18	15:14	50° 05.67N	4° 52.13W	66	26.8	10.8	2.4
26/06	19	10:48	50° 00.73N	5° 02.93W	59	26.6	8.8	6.7
	20	11:54	50° 04.06N	5° 00.06W	60	31.4	9.4	4.9
	21	12:41	50° 05.39N	4° 59.44W	56	29.7	6.3	8.8
	22	13:04	50° 06.29N	4° 58.90W	52	25.4	7.2	2.6
	23	13:43	50° 06.25N	4° 57.40W	60	25.4	5.6	3.0
	24	14:08	50° 06.07N	4° 55.36W	63	24.6	6.8	1.1
	25	14:31	50° 05.83N	4° 53.58W	64	24.9	5.4	6.5
	26	14:53	50° 05.65N	4° 52.05W	66	29.5	11.6	5.0
27/06	***27***	08:05	50° 05.57N	4° 52.01W	66	27.1	4.8	6.5
	28	09:27	50° 05.71N	4° 52.14W	66	27.7	5.4	4.2
	29	11:00	50° 05.65N	4° 52.08W	66	28.1	11.6	2.0
	30	13:17	50° 05.69N	4° 52.00W	66	27.6	19.2	0.1
	31	14:41	50° 05.83N	4° 51.82W	66	26.4	7.3	0.4
29/06	***32***	08:11	50° 05.60N	4° 51.56W	66	25.7	5.5	3.6
	33	09:55	49° 59.94N	4° 51.96W	72	27.4	6.2	4.4

	34	11:10	49° 55.00N	4° 51.79W	81	30.0	3.0	7.7
	35	12:08	49° 50.09N	4° 51.43W	83	21.9	2.5	8.9
	36	13:27	49° 41.99N	4° 51.13W	86	24.5	5.7	4.7
30/06	***37***	08:47	50° 05.73N	4° 52.71W	66	29.3	3.2	6.4
01/07	***38***	08:05	50° 05.53N	4° 51.87W	66	26.9	3.7	7.6
02/07	***39***	08:07	50° 05.57N	4° 51.89W	66	36.1	2.5	12.0
	40	10:26	50° 00.10N	4° 40.43W	72	27.2	4.2	7.6

Table A2.3. Contribution of micro- and meso-phytoplankton (> 20 µm), nano-phytoplankton (2 – 20 µm) and pico-phytoplankton (< 2 µm) to total community red fluorescence (TCRFL; a proxy for chlorophyll and by extension biomass) as identified using CytoSense flow cytometry.

Date	Site no.	Sample location	micro- and meso- (% of TCRFL)	nano- (% of TCRFL)	pico- (% of TCRFL)
19/06/2015	1	Bottom	55.0	33.0	12.0
	1	SCM	95.8	3.7	0.5
	1	Surface	36.1	42.8	21.1
	2	Bottom	27.6	47.1	25.3
	2	SCM	55.2	41.3	3.5
	2	Surface	11.9	70.1	18.1
23/06/2015	3	SCM	42.6	55.2	2.2
	4	Bottom	32.0	50.0	18.0
	4	SCM	66.6	30.9	2.5
	4	Surface	17.0	61.8	21.2
	5	SCM	73.0	23.1	3.8
	6	SCM	85.3	12.6	2.2
	7	SCM	92.0	6.3	1.7
	8	SCM	87.2	10.9	1.9
	9	SCM	89.0	5.3	5.7
24/06/2015	10	Bottom	14.9	50.4	34.7
	10	SCM	81.7	16.9	1.4
	10	Surface	21.3	59.6	19.2
	11	SCM	88.4	9.2	2.4
	12	SCM	88.2	9.7	2.0
	13	Bottom	20.7	55.6	23.7
	13	SCM	73.7	21.5	4.8
	13	Surface	10.7	68.2	21.2
25/06/2015	14	SCM	50.0	41.1	9.0
	15	SCM	54.9	40.7	4.4
	16	Bottom	22.4	35.7	42.0
	16	SCM	60.8	31.9	7.3
	16	Surface	32.2	44.1	23.6
	17	SCM	78.5	19.0	2.6
	18	SCM	89.8	8.4	1.8
26/06/2015	19	Bottom	21.0	45.2	33.8
	19	SCM	91.7	7.1	1.2
	19	Surface	40.2	44.7	15.0
	20	SCM	82.6	8.2	9.2
	21	SCM	88.0	10.7	1.2
	22	SCM	60.9	31.8	7.3
	23	SCM	66.1	28.5	5.4

	24	SCM	80.9	14.8	4.2
	25	SCM	91.9	6.1	2.0
	26	SCM	94.6	4.1	1.2
	27	SCM	79.6	14.4	6.1
	28	SCM	72.2	22.5	5.2
	29	Bottom	21.5	23.3	55.3
27/06/2015	29	SCM	81.0	14.6	4.4
	29	Surface	41.9	43.9	14.2
	30	SCM	92.4	7.0	0.7
	31	SCM	56.5	35.8	7.7
	32	SCM	78.7	18.2	3.1
	33	Bottom	20.1	41.6	38.3
	33	SCM	73.0	21.6	5.4
29/06/2015	33	Surface	14.6	36.7	48.6
	34	SCM	67.2	23.7	9.2
	35	SCM	42.4	50.9	6.6
	36	SCM	59.3	36.4	4.3
	37	Bottom	22.8	23.1	54.1
30/06/2015	37	SCM	76.1	21.7	2.2
	37	Surface	25.8	66.1	8.1
01/07/2015	38	SCM	67.1	28.2	4.7
	39	SCM	42.7	54.5	2.8
	40	Bottom	17.9	39.5	42.6
02/07/2015	40	SCM	54.1	34.1	11.8
	40	Surface	23.0	59.9	17.1

Table A2.4. Percentage contribution of each phytoplankton taxon to the similarity of samples within each cluster and to the dissimilarity between clusters, where cluster 1 (C1) contains deep samples, cluster 2 (C2) contains SCM samples and cluster 3 (C3) contains surface samples. Numbers in bold and underlined indicate taxa whose cumulative contribution to similarity/dissimilarity were up to approximately 50 %. Average similarity within each cluster and dissimilarity between clusters is also given.

Taxa	Similarity			Dissimilarity		
	C1 (Deep)	C2 (SCM)	C3 (Surface)	C1 vs C2	C1 vs C3	C2 vs C3
M centric diatom (30-50 µm dia.)				1.11	1.17	
L centric diatom (60-150 µm dia.)				0.84	0.91	
Cerataulina pelagica			1.27	0.84	1.08	1.20
Chaetoceros spp.	**5.22**	1.91	2.48	**3.23**	**2.62**	1.99
Diploneis spp.				0.75	0.83	
Entomoneis spp.	1.53			1.28	1.39	
Guinardia striata				0.74	1.17	0.88
Leptocylindrus danicus			**4.23**	0.89	**4.48**	**4.59**
Leptocylindrus minimus	1.31			0.75	0.79	0.96
Meuniera membranacea				0.73	0.68	
Paralia sulcata	1.64			1.70	1.84	
L pennate diatom (65-110 µm length)				0.96	1.03	
Proboscia alata	2.89	1.08	3.46	1.54	1.05	2.28
Proboscia truncata	**11.65**	**5.14**	**4.61**	**6.37**	**6.06**	2.16
S *Pseudo-nitzschia spp.* (< 2.5 µm dia.)				0.94	0.84	
L *Pseudo-nitzschia spp.* (> 2.5 µm dia.)	**3.82**		1.51	**2.62**	2.04	1.19
XS *Thalassiosira spp.* (< 10 µm height)	1.54	1.36	1.33	1.27	1.01	1.41
10-20 µm naked dinoflagellates	**12.14**	**5.46**	**8.39**	**5.76**	**3.11**	**3.47**
20-25 µm naked dinoflagellates	3.67	3.24	**5.41**	1.44	2.03	**2.68**
10-30 µm armoured dinoflagellates	1.31	0.98	2.22	0.73	1.28	1.68
Alexandrium ostenfeldii		2.94	1.82	**2.34**	1.95	1.57
Ceratium fusus	**4.02**	**16.75**	1.37	**9.25**	**3.65**	**12.52**
Ceratium lineatum		4.02		**2.64**	1.19	**2.71**
Ceratium macroceros		0.88		1.02		1.04
Ceratoperidinium falcatum		2.48		1.61	1.39	1.12
Dinophysis acuta		2.89		**3.29**		**3.56**
Dinophysis tripos					0.77	0.90
Gonyaulax spinifera		1.08	1.63	0.81	1.11	1.10
Gyrodinium spp.	**3.72**	**4.23**	**5.81**	1.28	**2.11**	**2.40**
Heterocapsa spp.					1.13	1.18
Karenia mikimotoi				1.07		1.05

Katodinium glaucum	1.58	1.75	1.54	0.76	0.73	
Nematodinium torpedo					0.69	
Noctiluca scintillans				**2.72**		**2.95**
Polykrikos schwartzii/kofoidii		1.78	2.98	**2.19**	**3.46**	**2.86**
Prorocentrum micans			1.44		1.31	1.09
Prorocentrum minimum	1.34	0.93	1.73		1.10	1.37
S *Protoperidinium spp.* (10-30 µm dia.)	2.00	1.05		0.84	0.99	0.79
M *Protoperidinium spp.* (30-65 µm dia.)				0.84	0.97	0.78
L *Protoperidinium spp.* (65-120 µm dia.)		2.71	2.24	**2.40**	**2.96**	2.02
Torodinium robustum/teredo	1.45			0.86		0.86
Chrysochromulina spp.	1.66	1.98	2.88		1.12	1.07
Chrysophaerella longispina				1.56	1.47	
Cryptophytes	2.72	1.27	2.01	1.56	1.03	0.99
Dictyocha fibula/speculum	**5.09**	**4.99**	2.00	1.94	**2.10**	**2.82**
Pleurasiga spp.				0.95		
Solenicola setigera	3.04	1.73		1.80	**2.31**	1.23
Tetraedron spp.				0.74	1.17	0.99
S aloricate ciliates (< 20µm)	2.63	0.88	2.93	1.48	1.00	2.24
M aloricate ciliates (20-40 µm)	3.48	**4.65**	**11.87**	1.80	**7.67**	**7.03**
L aloricate ciliates (> 40 µm)	**4.82**	**8.82**	**9.72**	**3.63**	**4.23**	**3.41**
Tiarina fusus	3.52	2.06	1.90	**2.98**	**2.91**	1.40
L bowl shaped tintinnids (> 60 µm length)				1.66	2.06	1.24
S tapering tintinnids (40-60 µm)	2.87	1.74	1.47	2.01	**2.33**	1.70
Cumulative contribution (%)	90.66	90.78	90.24	90.51	90.34	90.43
Average similarity (%)	67.48	67.30	71.96	-	-	-
Average dissimilarity (%)	-	-	-	50.65	44.13	46.64

Appendix 3

All figures and tables in this appendix are referenced in chapter 5.

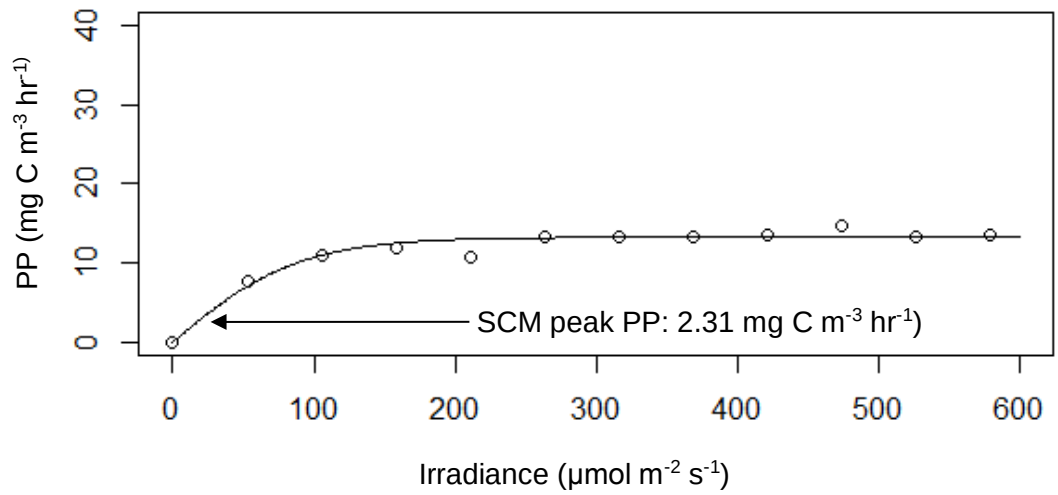

Figure A3.1. Primary production (PP) vs. irradiance curve derived from rETR vs. irradiance curve for the SCM peak at site 16. Primary production at the SCM peak was estimated to be 2.31 mg C m^{-3} hr^{-1}, which lies on the light limited region of the curve (as directed by the arrow).

Table A3.1. Date, time, location, water depth, SCM depth, difference in temperature between surface (at 5.5 m) and bottom waters (at 55 m), SCM thickness, SCM max chlorophyll concentration, metres and percentage of primary productive water column spanned by the SCM layer and the surface layer, SCM layer and surface layer integrated chlorophyll (absolute and as a percentage of the total chlorophyll of the primary productive portion of the water column), irradiance at the sea surface and at the SCM peak (absolute and as a percentage of sea surface irradiance), discrete nitrate concentration at the SCM and for sites 1, 4, 7, 8, 12, 15, 16 also in surface and bottom waters, tidal state details (where spring + 0 coincides with new/full moon phase and neap + 0 coincides with quarter moon phase) and the depth of sampling within the SCM for the 16 stratified sites profiled and assessed for primary production in the Western English Channel during summer 2015. The primary productive portion of the water column refers to the combination of the surface layer and SCM layer, excluding bottom waters as primary production was assumed to be zero below the SCM/in the bottom mixed layer.

Site no.	Date	Time (UTC)	Latitude	Longitude	Water depth (m)	SCM depth (m)	Δsurface-bottom temp. (°C)	SCM thickness (m)	SCM max chl conc. (μg l^{-1})	SCM layer span		Surface layer span	
										m	% of PP water column	m	% of PP water column
1	23/06	12:09	50° 06.10N	4° 24.80W	69	26.2	2.1	3.7	3.0	8.2	28.1	21.0	71.9
2	23/06	13:45	50° 06.46N	4° 32.51W	68	29.8	2.5	2.9	10.1	8.0	25.0	24.0	75.0
3	23/06	14:18	50° 06.31N	4° 35.91W	67	26.1	2.7	3.2	15.5	11.6	37.2	19.6	62.8
4	24/06	08:37	50° 02.54N	4° 46.23W	73	28.3	3.6	2.8	2.5	7.5	24.4	23.3	75.6
5	24/06	10:12	50° 05.87N	4° 52.23W	66	24.8	2.0	7.4	12.8	19.8	66.2	10.1	33.8
6	24/06	13:03	50° 05.76N	4° 51.99W	66	30.7	2.4	7.5	8.7	13.3	41.6	18.7	58.4
7	24/06	14:35	50° 02.60N	4° 46.26W	71	27.8	3.8	1.2	7.3	5.8	19.8	23.5	80.2
8	25/06	12:08	50° 02.65N	4° 46.27W	73	29.6	4.1	6.5	3.5	10.0	30.0	23.3	70.0
9	25/06	15:14	50° 05.67N	4° 52.13W	66	26.8	2.9	2.4	9.2	16.2	51.6	15.2	48.4
10	26/06	14:08	50° 06.07N	4° 55.36W	63	24.6	3.3	1.1	6.7	7.8	28.5	19.6	71.5
11	27/06	09:27	50° 05.71N	4° 52.14W	66	27.7	3.4	4.2	4.2	10.5	33.9	20.5	66.1
12	27/06	11:00	50° 05.65N	4° 52.08W	66	28.1	3.5	2.0	10.2	8.0	26.9	21.7	73.1
13	27/06	13:17	50° 05.69N	4° 52.00W	66	27.6	3.5	0.1	12.3	8.9	31.0	19.8	69.0
14	29/06	08:11	50° 05.60N	4° 51.56W	66	25.7	3.2	3.6	5.4	7.5	25.9	21.5	74.1
15	29/06	09:55	49° 59.94N	4° 51.96W	72	27.4	4.4	4.4	6.2	12.0	36.4	21.0	63.6
16	02/07	10:26	50° 00.10N	4° 40.43W	72	27.2	5.0	7.6	3.8	12.3	38.9	19.3	61.1

Site no.	SCM layer integrated chl		Surface layer integrated chl		Irradiance			Nitrate conc. (µmol l^{-1})			Tidal state	SCM sample depth (m)
	mg m^{-2}	% of PP chl	mg m^{-2}	% of PP chl	Sea surface (µmol m^{-2} s^{-1})	SCM (µmol m^{-2} s^{-1})	SCM % of surface irradiance	Surface waters	Bottom waters	SCM		
1	15.7	66.7	7.8	33.3	2695.7	104.1	3.9	0.1	1.1	0.5	Spring +5	26.2
2	32.5	84.4	6.0	15.6	2468.6	59.0	2.4			0.2	Spring +5	29.6
3	60.2	91.1	5.9	8.9	1162.8	32.5	2.8			0.4	Spring +5	26.3
4	10.5	61.7	6.5	38.3	2189.2	35.5	1.6	0.3	0.9	0.3	Spring +6	28.1
5	95.1	98.4	1.5	1.6	2728.6	21.3	0.8			0.2	Spring +6	24.4
6	72.6	88.5	9.4	11.5	1206.2	10.6	0.9			0.1	Spring +6	30.5
7	13.9	67.9	6.5	32.1	2970.5	67.1	2.3	0.2	0.8	0.3	Spring +6	27.6
8	20.2	79.5	5.2	20.5	2928.9	70.9	2.4	0.3	0.9	0.4	Neap +0	30.0
9	41.3	92.3	3.4	7.7	1880.0	45.9	2.4			0.2	Neap +0	26.6
10	19.3	67.5	9.3	32.5	872.7	41.6	4.8			0.1	Neap +1	24.3
11	19.8	74.3	6.9	25.7	1997.4	42.0	2.1			0.1	Neap +2	27.9
12	27.2	81.7	6.1	18.3	2724.9	60.1	2.2	0.3	1.0	0.5	Neap +2	28.0
13	21.5	74.5	7.4	25.5	2511.7	36.3	1.4			0.1	Neap +2	27.5
14	21.3	62.0	13.1	38.0	592.3	23.2	3.9			0.8	Neap +4	26.0
15	35.3	79.8	9.0	20.2	1033.8	40.3	3.9	0.2	0.9	0.2	Neap +4	27.3
16	29.2	73.1	10.8	26.9	469.0	11.8	2.5	0.4	1.1	0.5	Spring +0	26.8

Table A3.2. Estimated carbon biomass (Pg C ml^{-1}) of phytoplankton taxa identified in SCM samples collected from the 16 sites analysed for primary production during the 2015 summer field survey in the Western English Channel. Samples for phytoplankton analysis were preserved in Lugol's iodine to a final concentration of 1 %, and analysed based on the methods of Utermöhl (1958) using a Brunel SP951 inverted trinocular light microscope. Cell biovolume was calculated for each taxon/taxon size category using geometric shapes and formulae of Olenina et al. (2006), and converted to cell carbon biomass using the carbon - biovolume relationships of Menden-Deuer and Lessard (2000).

Date	**23/06/2015**	**23/06/2015**	**23/06/2015**	**24/06/2015**	**24/06/2015**	**24/06/2015**	**24/06/2015**	**25/06/2015**
Site number	**1**	**2**	**3**	**4**	**5**	**6**	**7**	**8**
Sample location	**SCM**	**SCM**	**SCM**	**SCM**	**SCM**	**SCM**	**SCM**	**SCM**
Diatoms (Pg C ml^{-1})								
S centric diatom (20-30 µm dia.)	0.0	0.0	0.0	0.0	0.0	0.0	0.0	0.0
M centric diatom (30-50 µm dia.)	149.4	0.0	149.4	149.4	149.4	149.4	0.0	0.0
L centric diatom (60-150 µm dia.)	0.0	352.8	0.0	0.0	1763.9	0.0	0.0	0.0
XL centric diatom (> 150 µm dia.)	0.0	0.0	0.0	0.0	0.0	0.0	0.0	0.0
Cerataulina pelagica	94.4	94.4	94.4	660.9	0.0	0.0	0.0	188.8
Chaetoceros spp.	7184.1	3879.4	1149.4	1293.1	1580.5	2442.6	1293.1	718.4
Corethron criophylum	0.0	0.0	0.0	0.0	0.0	0.0	0.0	0.0
Cylindrotheca closterium	11.3	0.0	5.7	19.9	0.0	0.0	2.8	25.5
Delphineis surirella	0.0	0.0	0.0	0.0	0.0	0.0	0.0	0.0
Diploneis spp.	18.1	0.0	0.0	36.2	0.0	0.0	0.0	18.1
Entomoneis spp.	0.0	0.0	29.1	29.1	0.0	29.1	0.0	29.1
Eucampia zoodiacus	0.0	0.0	0.0	0.0	0.0	0.0	0.0	0.0
Guinardia delicatula	0.0	0.0	0.0	0.0	0.0	0.0	0.0	0.0
Guinardia striata	0.0	0.0	0.0	0.0	0.0	0.0	0.0	217.6
Lauderia annulata	100.9	0.0	0.0	0.0	0.0	0.0	0.0	0.0

Leptocylindrus danicus	202.8	77.2	202.8	115.9	19.3	0.0	0.0	57.9
Leptocylindrus minimus	402.5	419.8	98.2	441.0	59.7	63.5	80.9	350.5
Meuniera membranacea	188.6	0.0	0.0	0.0	0.0	0.0	0.0	377.1
Odontella regia/ mobiliensis	0.0	0.0	0.0	0.0	0.0	0.0	0.0	0.0
Paralia sulcata	0.0	0.0	0.0	83.9	0.0	0.0	0.0	0.0
S pennate diatom (20-40 µm length)	0.0	0.0	0.0	0.0	0.0	0.0	0.0	0.0
M pennate diatom (40-65 µm length)	0.0	0.0	0.0	0.0	0.0	0.0	0.0	39.7
L pennate diatom (65-110 µm length)	0.0	0.0	0.0	0.0	74.6	0.0	0.0	0.0
S *Pleurosigma spp.* (~50 µm)	0.0	0.0	0.0	0.0	0.0	0.0	0.0	0.0
M *Pleurosigma spp.* (80-170 µm)	0.0	0.0	0.0	0.0	0.0	0.0	0.0	0.0
L *Pleurosigma spp.* (170-200 µm)	0.0	0.0	0.0	0.0	0.0	0.0	0.0	0.0
Proboscia alata	487.8	6292.9	1073.2	1463.5	195.1	97.6	5805.1	1951.3
Proboscia truncata	11306.1	50249.2	16331.0	20099.7	10049.8	8793.6	23868.4	41455.6
S *Pseudo-nitzschia spp.* (< 2.5 µm dia.)	821.1	10.3	46.5	25.8	41.3	28.4	12.9	2.6
L *Pseudo-nitzschia spp.* (> 2.5 µm dia.)	408.8	395.6	501.1	738.4	342.9	211.0	553.8	606.6
S *Rhizosolenia spp.* (≤ 10 µm dia.)	33.3	33.3	0.0	33.3	0.0	0.0	0.0	0.0
M *Rhizosolenia spp.* (10-20 µm dia.)	489.1	0.0	0.0	0.0	0.0	0.0	0.0	0.0
L *Rhizosolenia spp.* (> 20 µm dia.)	0.0	0.0	0.0	0.0	0.0	0.0	0.0	0.0
Thalassionema nitzchioides	0.0	0.0	0.0	0.0	0.0	0.0	0.0	0.0
XS *Thalassiosira spp.* (< 10 µm height)	1902.4	126.2	21.8	522.4	165.4	130.6	121.9	1810.9
S *Thalassiosira spp.* (10-25 µm height)	417.6	0.0	0.0	0.0	0.0	0.0	0.0	0.0
M *Thalassiosira spp.* (25-45 µm height)	0.0	0.0	0.0	0.0	0.0	0.0	0.0	0.0
L *Thalassiosira spp.* (> 45 µm height)	0.0	0.0	0.0	0.0	0.0	0.0	0.0	0.0
Total diatom carbon (Pg C ml^{-1})	**24218.1**	**61931.3**	**19702.5**	**25712.4**	**14442.0**	**11945.8**	**31739.0**	**47849.8**
Dinoflagellates (Pg C ml^{-1})								

10-20 µm naked dinoflagellates	24158.3	13242.3	13958.2	22189.9	9126.5	5189.6	19326.7	32569.0
20-25 µm naked dinoflagellates	8931.6	5103.8	5103.8	5103.8	1913.9	638.0	3189.9	5741.8
10-30 µm armoured dinoflagellates	151.5	454.6	505.1	505.1	252.6	151.5	252.6	555.7
Alexandrium ostenfeldii	3674.3	7756.8	2449.5	4082.5	4490.8	6123.8	8981.6	2857.8
Amylax triacantha	0.0	0.0	0.0	0.0	0.0	0.0	0.0	0.0
Ceratium fusus	57513.5	293980.0	807392.9	28856.9	299190.3	250895.0	78555.0	42083.0
Ceratium lineatum	1210.6	9685.1	19168.4	1008.9	25019.8	16343.5	2421.3	2824.8
Ceratium macroceros	1072.3	1608.4	3753.0	1608.4	536.1	1608.4	536.1	2680.7
Ceratium tripos	0.0	0.0	0.0	1372.5	0.0	1372.5	0.0	0.0
Ceratoperidinium falcatum	7475.4	4271.7	3737.7	2135.8	2669.8	5873.6	4805.6	1067.9
Dinophysis acuminata	0.0	515.4	171.8	1546.2	171.8	171.8	171.8	171.8
Dinophysis acuta	7062.6	13418.9	0.0	2825.0	5650.0	5650.0	21893.9	2118.8
Dinophysis caudata	0.0	0.0	0.0	0.0	0.0	0.0	0.0	0.0
Dinophysis norvegica	0.0	0.0	124.0	0.0	0.0	0.0	0.0	0.0
Dinophysis tripos	0.0	773.0	0.0	0.0	0.0	0.0	0.0	0.0
Dissodinium sp.	0.0	0.0	0.0	0.0	0.0	0.0	0.0	0.0
Gonyaulax spinifera	851.3	1383.4	1489.8	425.7	532.1	851.3	1489.8	319.2
Gyrodinium spp.	7074.6	16776.9	17787.6	11117.2	8489.5	5255.4	12734.3	11521.5
Heterocapsa spp.	14.8	0.0	0.0	29.7	14.8	0.0	14.8	14.8
Karenia mikimotoi	0.0	1281.4	533.9	106.8	1708.6	640.7	3737.5	213.6
Katodinium glaucum	597.6	1294.9	6109.3	1195.3	4814.4	1328.1	1128.9	1128.9
Nematodinium torpedo	0.0	0.0	0.0	260.5	434.2	173.7	0.0	0.0
Noctiluca scintillans	0.0	227081.5	0.0	0.0	0.0	0.0	0.0	227081.5
Oblea rotundata	0.0	0.0	0.0	0.0	0.0	0.0	0.0	0.0
Phalacroma rotundatum	772.8	0.0	0.0	0.0	515.2	0.0	0.0	515.2

Polykrikos schwartzii/kofoidii	13414.1	31858.5	11737.3	6707.1	1676.8	1676.8	15090.9	18444.4
Prorocentrum micans	388.2	129.4	776.4	905.8	0.0	258.8	517.6	517.6
Prorocentrum minimum	150.1	364.6	214.5	965.2	772.1	493.3	235.9	407.5
Prorocentrum triestinum	0.0	0.0	0.0	0.0	0.0	0.0	0.0	0.0
S *Protoperidinium spp.* (10-30 µm dia.)	801.3	2203.5	1335.5	801.3	1068.4	734.5	1736.1	333.9
M *Protoperidinium spp.* (30-65 µm dia.)	334.5	0.0	669.0	669.0	0.0	0.0	334.5	334.5
L *Protoperidinium spp.* (65-120 µm dia.)	8766.1	3506.5	0.0	3506.5	14025.8	3506.5	10519.4	1753.2
Torodinium robustum/teredo	230.4	0.0	65.8	32.9	65.8	98.7	32.9	65.8
Total dinoflagellate carbon (Pg C ml^{-1})	**144646.2**	**636690.7**	**897083.4**	**97958.0**	**383139.4**	**309035.6**	**187707.1**	**355322.9**
Flagellates (Pg C ml^{-1})								
Chlamydomonas spp.	0.0	0.0	0.0	0.0	0.0	0.0	0.0	0.0
Chrysochromulina spp.	2302.4	3441.4	2060.0	1623.8	1333.0	969.4	2229.7	1745.0
Chrysophaerella longispina	208.2	208.2	208.2	1041.0	0.0	0.0	624.6	1457.4
Cryptophytes	468.1	319.7	468.1	365.4	525.2	639.4	285.5	605.2
Dictyocha fibula/speculum	2872.4	121993.1	63700.0	20275.9	52041.4	30413.8	38355.2	8110.3
Pleurasiga spp.	0.0	488.9	0.0	0.0	488.9	488.9	0.0	0.0
Solenicola setigera	238.2	221.2	595.5	357.3	3402.8	4100.4	204.2	204.2
unidentified spherical flagellate (10-20 µm dia.)	136.1	209.8	175.8	102.1	141.8	141.8	170.1	124.8
Total flagellate carbon (Pg C ml^{-1})	**6225.4**	**126882.3**	**67207.7**	**23765.4**	**57933.1**	**36753.7**	**41869.2**	**12246.8**
Non-flagellated chlorophyceae (Pg C ml^{-1})								
Tetraedron spp.	0.0	0.0	0.0	254.3	0.0	36.3	36.3	36.3
Oocystaceae sp.	0.0	0.0	0.0	0.0	0.0	0.0	0.0	0.0
Total non-flagellated chlorophyceae carbon (Pg C ml^{-1})	**0.0**	**0.0**	**0.0**	**254.3**	**0.0**	**36.3**	**36.3**	**36.3**
Ciliates (Pg C ml^{-1})								
S aloricate ciliates (< 20µm)	943.0	974.5	220.0	628.7	94.3	125.7	377.2	723.0

M aloricate ciliates (20-40 µm)	41147.1	23512.6	1698.1	18418.2	8098.8	7576.3	27953.9	22467.6
L aloricate ciliates (> 40 µm)	90408.2	93382.2	39256.2	124311.3	15464.6	13680.2	68401.0	74348.9
Tiarina fusus	1470.6	490.2	2941.1	3921.5	1960.7	3921.5	980.4	1470.6
S bowl shaped tintinnids (20-50 µm length)	0.0	0.0	0.0	0.0	0.0	0.0	0.0	0.0
L bowl shaped tintinnids (> 60 µm length)	2144.0	6432.1	0.0	2144.0	0.0	0.0	0.0	2144.0
S tapering tintinnids (40-60 µm)	2387.0	8525.1	8866.1	5967.6	852.5	170.5	2046.0	10912.1
L tapering tintinnids (> 60 µm)	475.0	949.9	0.0	1899.8	0.0	0.0	949.9	1424.9
Total ciliate carbon (Pg C ml^{-1})	**138975.0**	**134266.6**	**52981.6**	**157291.2**	**26470.9**	**25474.2**	**100708.4**	**113491.1**

Date	**25/06/2015**	**26/06/2015**	**27/06/2015**	**27/06/2015**	**27/06/2015**	**29/06/2015**	**29/06/2015**	**02/07/2015**
Site number	**9**	**10**	**11**	**12**	**13**	**14**	**15**	**16**
Sample location	**SCM**	**SCM**	**SCM**	**SCM**	**SCM**	**SCM**	**SCM**	**SCM**
Diatoms (Pg C ml^{-1})								
S centric diatom (20-30 µm dia.)	0.0	0.0	0.0	0.0	0.0	0.0	0.0	0.0
M centric diatom (30-50 µm dia.)	149.4	0.0	0.0	0.0	0.0	298.7	0.0	298.7
L centric diatom (60-150 µm dia.)	0.0	0.0	0.0	0.0	0.0	0.0	0.0	0.0
XL centric diatom (> 150 µm dia.)	0.0	0.0	0.0	1511.7	0.0	0.0	0.0	0.0
Cerataulina pelagica	0.0	188.8	0.0	566.5	188.8	188.8	188.8	0.0
Chaetoceros spp.	574.7	862.1	2155.2	3304.7	1005.8	2011.5	718.4	71.8
Corethron criophylum	0.0	0.0	0.0	0.0	0.0	0.0	0.0	0.0
Cylindrotheca closterium	0.0	0.0	2.8	8.5	2.8	8.5	2.8	2.8
Delphineis surirella	0.0	0.0	0.0	0.0	0.0	0.0	0.0	0.0
Diploneis spp.	36.2	0.0	0.0	0.0	36.2	0.0	0.0	0.0
Entomoneis spp.	0.0	0.0	0.0	58.2	0.0	0.0	0.0	0.0

Eucampia zoodiacus	0.0	0.0	0.0	0.0	0.0	0.0	0.0	0.0
Guinardia delicatula	0.0	0.0	0.0	0.0	47.3	0.0	0.0	0.0
Guinardia striata	0.0	0.0	0.0	0.0	0.0	0.0	0.0	0.0
Lauderia annulata	0.0	0.0	0.0	0.0	0.0	0.0	0.0	0.0
Leptocylindrus danicus	29.0	666.2	531.1	337.9	115.9	589.0	299.3	260.7
Leptocylindrus minimus	52.0	0.0	356.2	269.6	115.5	98.2	82.8	42.4
Meuniera membranacea	0.0	0.0	0.0	471.4	660.0	94.3	0.0	94.3
Odontella regia/ mobiliensis	0.0	0.0	0.0	0.0	0.0	0.0	0.0	0.0
Paralia sulcata	0.0	0.0	0.0	42.0	0.0	209.8	0.0	0.0
S pennate diatom (20-40 µm length)	0.0	0.0	0.0	0.0	0.0	0.0	0.0	0.0
M pennate diatom (40-65 µm length)	0.0	0.0	0.0	19.9	0.0	0.0	0.0	19.9
L pennate diatom (65-110 µm length)	0.0	0.0	0.0	0.0	0.0	74.6	0.0	0.0
S *Pleurosigma spp.* (~50 µm)	0.0	0.0	0.0	0.0	0.0	0.0	0.0	0.0
M *Pleurosigma spp.* (80-170 µm)	0.0	0.0	0.0	0.0	0.0	0.0	0.0	0.0
L *Pleurosigma spp.* (170-200 µm)	0.0	0.0	0.0	0.0	0.0	0.0	0.0	0.0
Proboscia alata	48.8	390.3	878.1	243.9	243.9	146.3	2487.9	195.1
Proboscia truncata	7537.4	18843.5	15074.8	16331.0	15074.8	5024.9	7537.4	2512.5
S *Pseudo-nitzschia spp.* (< 2.5 µm dia.)	36.1	20.7	142.0	464.8	296.9	720.4	23.2	23.2
L *Pseudo-nitzschia spp.* (> 2.5 µm dia.)	184.6	224.2	263.7	316.5	263.7	224.2	145.1	79.1
S *Rhizosolenia spp.* (≤ 10 µm dia.)	0.0	0.0	100.0	0.0	33.3	166.7	0.0	0.0
M *Rhizosolenia spp.* (10-20 µm dia.)	0.0	0.0	122.3	244.5	0.0	0.0	0.0	0.0
L *Rhizosolenia spp.* (> 20 µm dia.)	0.0	0.0	0.0	0.0	0.0	0.0	0.0	0.0
Thalassionema nitzchioides	0.0	0.0	0.0	0.0	0.0	0.0	0.0	0.0
XS *Thalassiosira spp.* (< 10 µm height)	217.7	1262.4	7378.7	6355.7	1371.3	6238.1	457.1	1366.9
S *Thalassiosira spp.* (10-25 µm height)	0.0	0.0	0.0	0.0	0.0	0.0	0.0	0.0

M *Thalassiosira spp.* (25-45 µm height)	0.0	462.8	0.0	57.8	0.0	0.0	57.8	0.0
L *Thalassiosira spp.* (> 45 µm height)	0.0	0.0	0.0	0.0	0.0	0.0	0.0	0.0
Total diatom carbon (Pg C ml^{-1})	**8865.8**	**22920.9**	**27004.9**	**30604.5**	**19456.2**	**16094.2**	**12000.7**	**4967.5**
Dinoflagellates (Pg C ml^{-1})								
10-20 µm naked dinoflagellates	10916.0	8768.6	5547.5	9842.3	8768.6	7158.0	21653.0	15031.9
20-25 µm naked dinoflagellates	1913.9	4465.8	3189.9	3827.8	5103.8	638.0	8293.7	5103.8
10-30 µm armoured dinoflagellates	303.1	202.1	505.1	656.7	353.6	252.6	1060.8	1010.3
Alexandrium ostenfeldii	8573.3	13472.4	6532.1	6532.1	2857.8	1633.0	17963.2	10614.6
Amylax triacantha	0.0	0.0	0.0	0.0	0.0	0.0	0.0	0.0
Ceratium fusus	221436.9	140677.5	144485.0	194183.1	591567.1	67332.8	158512.7	81560.9
Ceratium lineatum	19370.1	13720.5	13720.5	10492.2	19168.4	2219.5	7062.0	12509.9
Ceratium macroceros	1072.3	0.0	0.0	0.0	0.0	2144.6	0.0	0.0
Ceratium tripos	0.0	1372.5	0.0	0.0	0.0	0.0	0.0	0.0
Ceratoperidinium falcatum	1601.9	2669.8	2669.8	3203.8	3203.8	534.0	3203.8	3737.7
Dinophysis acuminata	0.0	515.4	171.8	171.8	171.8	0.0	171.8	1202.6
Dinophysis acuta	4237.5	16243.9	21893.9	9887.6	1412.5	0.0	41669.1	24719.0
Dinophysis caudata	0.0	0.0	0.0	0.0	0.0	0.0	662.0	0.0
Dinophysis norvegica	0.0	0.0	0.0	0.0	0.0	0.0	0.0	0.0
Dinophysis tripos	0.0	1546.1	0.0	0.0	0.0	0.0	2319.1	773.0
Dissodinium sp.	0.0	0.0	0.0	0.0	0.0	0.0	0.0	0.0
Gonyaulax spinifera	425.7	744.9	532.1	638.5	638.5	106.4	1064.2	319.2
Gyrodinium spp.	6468.2	5053.3	5053.3	7681.0	7478.9	4244.8	5861.8	5255.4
Heterocapsa spp.	0.0	0.0	14.8	14.8	74.1	0.0	444.8	326.2
Karenia mikimotoi	854.3	106.8	106.8	320.4	213.6	0.0	8863.3	3844.3
Katodinium glaucum	9296.8	896.5	929.7	3087.9	1726.5	664.1	597.6	763.7

Nematodinium torpedo	86.8	173.7	0.0	173.7	260.5	173.7	0.0	260.5
Noctiluca scintillans	0.0	113540.7	0.0	0.0	0.0	0.0	0.0	0.0
Oblea rotundata	0.0	0.0	0.0	0.0	0.0	0.0	0.0	76.0
Phalacroma rotundatum	515.2	0.0	0.0	0.0	0.0	0.0	257.6	515.2
Polykrikos schwartzii/kofoidii	0.0	0.0	6707.1	3353.5	3353.5	1676.8	1676.8	1676.8
Prorocentrum micans	129.4	258.8	388.2	129.4	258.8	129.4	258.8	388.2
Prorocentrum minimum	536.2	343.2	429.0	622.0	257.4	150.1	664.9	128.7
Prorocentrum triestinum	0.0	0.0	0.0	0.0	0.0	0.0	0.0	0.0
S *Protoperidinium spp.* (10-30 µm dia.)	267.1	333.9	734.5	267.1	267.1	133.5	801.3	200.3
M *Protoperidinium spp.* (30-65 µm dia.)	0.0	334.5	0.0	334.5	0.0	0.0	0.0	334.5
L *Protoperidinium spp.* (65-120 µm dia.)	5259.7	1753.2	5259.7	5259.7	3506.5	1753.2	8766.1	0.0
Torodinium robustum/teredo	32.9	0.0	0.0	32.9	164.6	98.7	197.5	98.7
Total dinoflagellate carbon (Pg C ml^{-1})	**293297.3**	**327194.0**	**218870.7**	**260712.6**	**650807.2**	**91043.2**	**292025.9**	**170451.5**
Flagellates (Pg C ml^{-1})								
Chlamydomonas spp.	0.0	0.0	0.0	0.0	0.0	0.0	0.0	0.0
Chrysochromulina spp.	1163.3	1114.8	2132.7	1769.2	1526.8	218.1	2108.5	1914.6
Chrysophaerella longispina	208.2	832.8	416.4	208.2	0.0	208.2	416.4	208.2
Cryptophytes	1335.9	959.1	491.0	947.7	502.4	479.6	776.4	924.9
Dictyocha fibula/speculum	21458.6	8955.2	11658.6	8279.3	2365.5	2027.6	12165.5	2872.4
Pleurasiga spp.	0.0	488.9	977.8	0.0	0.0	1955.6	0.0	0.0
Solenicola setigera	2228.9	3624.0	4083.4	3658.1	3794.2	3249.7	204.2	1242.0
unidentified spherical flagellate (10-20 µm dia.)	124.8	153.1	260.9	300.6	107.8	85.1	147.5	56.7
Total flagellate carbon (Pg C ml^{-1})	**26519.7**	**16128.0**	**20020.8**	**15163.0**	**8296.7**	**8223.8**	**15818.5**	**7218.8**
Non-flagellated chlorophyceae (Pg C ml^{-1})								
Tetraedron spp.	0.0	0.0	0.0	0.0	0.0	0.0	0.0	0.0

Oocystaceae sp.	0.0	0.0	0.0	0.0	416.6	416.6	416.6	0.0
Total non-flagellated chlorophyceae carbon (Pg C ml^{-1})	**0.0**	**0.0**	**0.0**	**0.0**	**416.6**	**416.6**	**416.6**	**0.0**
Ciliates (Pg C ml^{-1})								
S aloricate ciliates (< 20µm)	125.7	94.3	408.6	188.6	314.3	251.5	660.1	1131.6
M aloricate ciliates (20-40 µm)	6400.7	22859.5	27823.3	13977.0	3526.9	391.9	26647.7	10972.6
L aloricate ciliates (> 40 µm)	33308.3	15464.6	42230.2	65427.0	41040.6	23196.9	17843.7	16059.4
Tiarina fusus	1470.6	980.4	2450.9	5882.2	2941.1	1960.7	490.2	490.2
S bowl shaped tintinnids (20-50 µm length)	0.0	0.0	0.0	0.0	0.0	0.0	0.0	0.0
L bowl shaped tintinnids (> 60 µm length)	0.0	0.0	0.0	0.0	2144.0	0.0	0.0	0.0
S tapering tintinnids (40-60 µm)	341.0	511.5	1534.5	1364.0	2216.5	0.0	341.0	1875.5
L tapering tintinnids (> 60 µm)	0.0	0.0	0.0	0.0	0.0	0.0	0.0	475.0
Total ciliate carbon (Pg C ml^{-1})	**41646.3**	**39910.3**	**74447.5**	**86838.8**	**52183.5**	**25800.9**	**45982.7**	**31004.2**

Appendix 4

All figures and tables in this appendix are referenced in chapter 6.

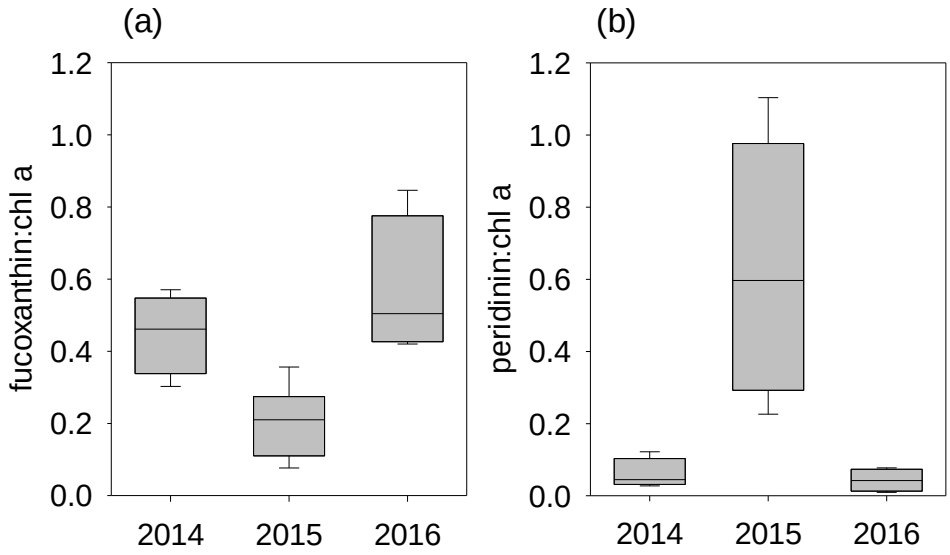

Figure A4.1. Boxplots (median, upper and lower quartile, and minimum and maximum values) of (a) ratio of fucoxanthin to chlorophyll a and (b) ratio of peridinin to chlorophyll a within the SCM at the repeat site in the Western English Channel for the summers (June/July) of 2013 to 2016, as determined by High Performance Liquid Chromatography (HPLC) analysis (Barlow et al., 1997, Gibb et al., 2001). The SCM fucoxanthin to chlorophyll a ratio in 2015 was significantly lower than in 2014 (p = 0.033) and 2016 (p = 0.004), and the SCM peridinin to chlorophyll a ratio in 2015 was significantly greater than in 2014 (p = 0.048) and 2016 (p = 0.016). Therefore, indicating a larger contribution of diatoms to the SCM community in 2014 and 2016 relative to 2015, and a larger contribution of dinoflagellates to the SCM community in 2015. No HPLC samples were collected in 2013.

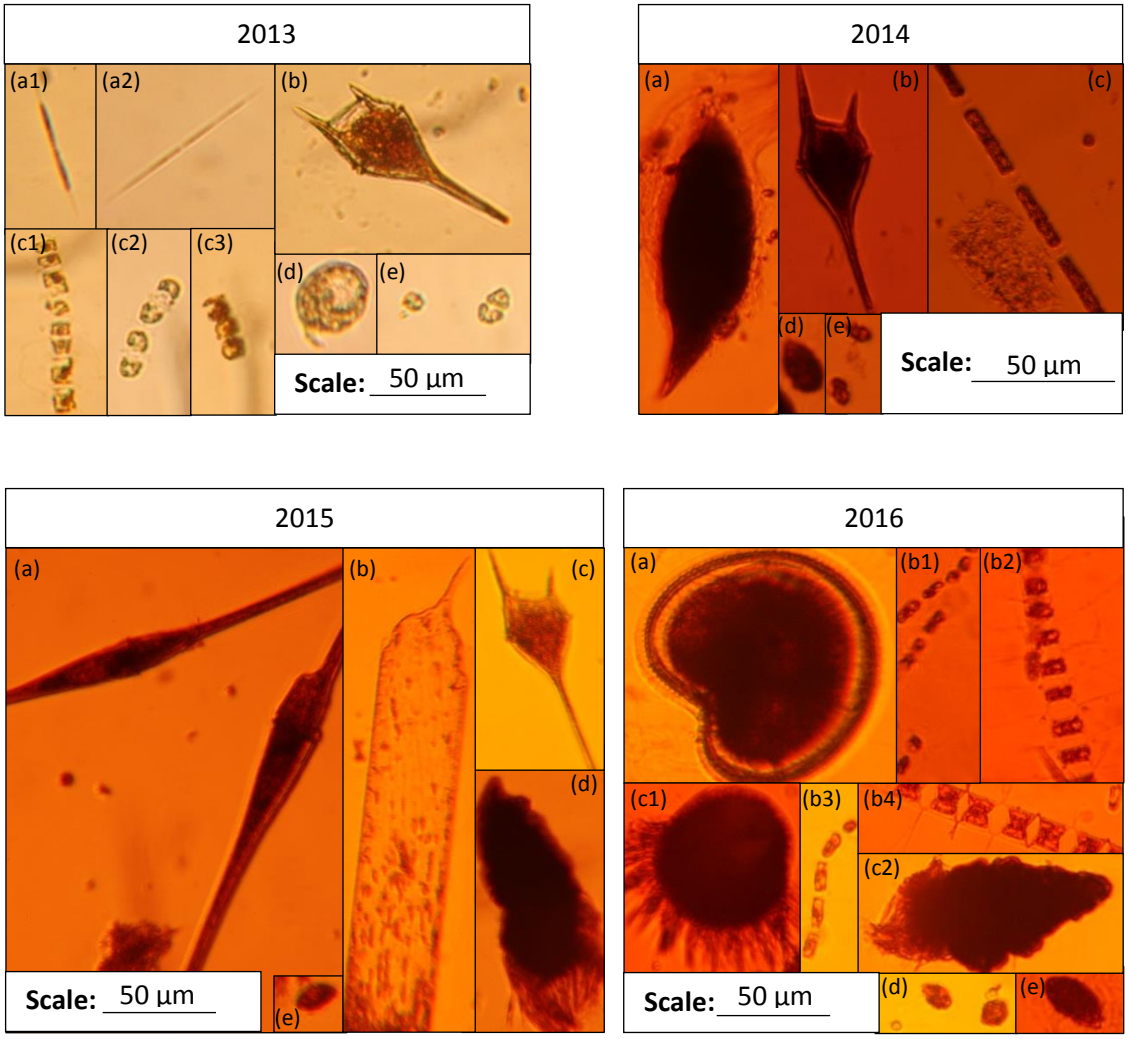

Figure A4.2. The five greatest phytoplankton contributors to SCM phytoplankton community similarity within each year as identified by microscope analysis of Lugol's iodine preserved samples taken from the SCM at the repeat site in the Western English Channel from 2013 to 2016. 2013: (a1) - (a2) S *Pseudo-nitzschia spp*., (b) *Ceratium lineatum*, (c1) – (c3) *Chaetoceros spp*., (d) *Diplopsalis lenticula*, and (e) 10-20 µm naked dinoflagellates. 2014: (a) *Gyrodinium spp.*, (b) *Ceratium lineatum*, (c) *Leptocylindrus danicus*, (d) 20-25 µm naked dinoflagellates, and (e) 10-20 µm naked dinoflagellates. 2015: (a) *Ceratium fusus*, (b) *Proboscia truncata*, (c) *Ceratium lineatum*, (d) L aloricate ciliates, and (e) 10-20 µm naked dinoflagellates. 2016: (a) L *Protoperidinium spp.*, (b1) – (b4) *Chaetoceros spp.*, (c1) – (c2) L aloricate ciliates, (d) 10-20 µm naked dinoflagellates, and (e) 20-25 µm naked dinoflagellates.

Table A4.1. Estimated carbon biomass (Pg C ml^{-1}) of phytoplankton taxa identified in Lugol's iodine preserved phytoplankton samples collected from the repeat site in the Western English Channel during the 2013, 2014, 2015 and 2016 summer field surveys.

Date	**25/06/2013**	**26/06/2013**	**28/06/2013**	**29/06/2013**	**03/07/2013**	**17/06/2014**	**20/06/2014**	**28/06/2014**	**30/06/2014**
Site number	**2**	**4**	**6**	**9**	**16**	**1**	**3**	**9**	**16**
Sample ID	**a**	**b**	**c**	**d**	**e**	**f**	**g**	**h**	**i**
Sample location	**SCM**	**SCM**	**SCM**	**SCM**	**SCM (slurp 2)**	**SCM**	**SCM**	**SCM**	**SCM**
Diatoms (Pg C ml^{-1})									
Asterionellopsis glacialis	0.0	0.0	0.0	0.0	0.0	0.0	0.0	0.0	0.0
S centric diatom (20-30 µm dia.)	0.0	0.0	0.0	0.0	0.0	0.0	0.0	38.7	0.0
M centric diatom (30-50 µm dia.)	149.4	0.0	448.1	448.1	298.7	298.7	149.4	0.0	298.7
L centric diatom (60-150 µm dia.)	0.0	0.0	0.0	0.0	352.8	0.0	1058.3	0.0	705.6
XL centric diatom (> 150 µm dia.)	0.0	0.0	0.0	0.0	0.0	0.0	0.0	0.0	0.0
Cerataulina pelagica	0.0	0.0	0.0	0.0	0.0	188.8	188.8	188.8	0.0
Chaetoceros spp.	5584.7	11455.8	5112.1	1178.6	3595.3	123.5	148.2	185.2	271.7
Cylindrotheca closterium	0.0	0.0	0.0	0.0	0.0	11.3	28.4	28.4	79.4
Diploneis spp.	18.1	18.1	0.0	18.1	0.0	0.0	0.0	0.0	0.0
Entomoneis spp.	0.0	0.0	0.0	0.0	0.0	0.0	29.1	0.0	58.2
Guinardia delicatula	0.0	47.3	141.8	94.5	47.3	472.5	94.5	0.0	94.5
Guinardia flaccida	0.0	0.0	0.0	0.0	10484.4	0.0	0.0	0.0	0.0
Guinardia striata	0.0	0.0	0.0	0.0	0.0	0.0	0.0	0.0	0.0
Lauderia annulata	100.9	0.0	0.0	0.0	0.0	1076.4	201.8	201.8	11167.2
Leptocylindrus danicus	0.0	0.0	0.0	0.0	0.0	7977.0	71792.6	13491.9	14575.2
Leptocylindrus minimus	0.0	0.0	0.0	0.0	0.0	0.0	19.3	0.0	17.3

Meuniera membranacea	0.0	0.0	0.0	0.0	0.0	0.0	0.0	848.5	660.0
Paralia sulcata	0.0	0.0	83.9	0.0	0.0	0.0	167.8	0.0	0.0
S pennate diatom (20-40 µm length)	0.0	0.0	4.9	0.0	0.0	0.0	4.9	0.0	0.0
M pennate diatom (40-65 µm length)	19.9	19.9	0.0	0.0	0.0	0.0	0.0	0.0	39.7
L pennate diatom (65-110 µm length)	0.0	0.0	0.0	0.0	0.0	0.0	0.0	0.0	0.0
XL pennate diatom (110-175 µm length)	0.0	0.0	0.0	0.0	0.0	0.0	0.0	0.0	0.0
S *Pleurosigma spp.* (~50 µm)	0.0	0.0	0.0	0.0	0.0	0.0	0.0	0.0	0.0
M *Pleurosigma spp.* (80-170 µm)	0.0	0.0	0.0	0.0	0.0	0.0	136.9	0.0	273.8
L *Pleurosigma spp.* (170-200 µm)	0.0	0.0	0.0	0.0	0.0	0.0	271.7	0.0	543.4
XL *Pleurosigma spp.* (> 200 µm)	0.0	0.0	0.0	0.0	0.0	0.0	0.0	0.0	196.7
Podosira stelligera	0.0	0.0	0.0	0.0	0.0	0.0	266.3	0.0	0.0
Proboscia alata	585.4	390.3	5512.4	10098.0	29357.2	195.1	48.8	97.6	292.7
Proboscia truncata	0.0	0.0	0.0	0.0	0.0	0.0	0.0	0.0	0.0
S *Pseudo-nitzschia spp.* (< 2.5 µm dia.)	30705.3	73546.1	49763.7	47646.1	18406.9	10.3	18.1	5.2	90.4
L *Pseudo-nitzschia spp.* (> 2.5 µm dia.)	0.0	0.0	0.0	0.0	0.0	1028.6	1622.0	131.9	1081.3
S *Rhizosolenia spp.* (≤ 10 µm dia.)	0.0	0.0	0.0	0.0	0.0	66.7	100.0	166.7	833.7
M *Rhizosolenia spp.* (10-20 µm dia.)	366.8	0.0	122.3	0.0	0.0	0.0	366.8	0.0	0.0
L *Rhizosolenia spp.* (> 20 µm dia.)	0.0	0.0	0.0	0.0	0.0	0.0	0.0	632.4	1897.2
Skeletonema costatum	0.0	1.8	0.0	0.0	0.0	0.0	0.0	0.0	0.0
Stephanopyxis turris	0.0	0.0	0.0	0.0	0.0	0.0	0.0	0.0	797.2
XS *Thalassiosira spp.* (< 10 µm height)	0.0	0.0	0.0	0.0	0.0	0.0	0.0	0.0	0.0
S *Thalassiosira spp.* (10-25 µm height)	0.0	66.9	0.0	0.0	0.0	0.0	0.0	116.9	885.3
M *Thalassiosira spp.* (25-45 µm height)	115.7	404.9	0.0	0.0	0.0	0.0	115.7	0.0	867.7
L *Thalassiosira spp.* (> 45 µm height)	71.5	0.0	0.0	0.0	0.0	0.0	0.0	0.0	0.0
Total diatom carbon (Pg C ml^{-1})	**37717.6**	**85950.9**	**61189.2**	**59483.4**	**62542.6**	**11448.9**	**76829.5**	**16134.0**	**35727.0**

Dinoflagellates (Pg C ml^{-1})									
10-20 µm naked dinoflagellates	19505.6	22905.7	18431.9	20221.4	6621.2	71762.2	39370.8	27917.4	18074.8
20-25 µm naked dinoflagellates	7017.7	2551.9	9569.6	2551.9	638.0	28070.3	26156.4	26794.4	21690.7
10-30 µm armoured dinoflagellates	606.2	252.6	202.1	101.0	0.0	1717.5	505.2	2020.6	50.5
Alexandrium ostenfeldii	0.0	0.0	0.0	0.0	0.0	0.0	0.0	0.0	0.0
Amphidinium carterae	0.0	0.0	0.0	0.0	0.0	333.5	166.8	0.0	166.8
Ceratium fusus	200.4	200.4	400.8	801.6	0.0	801.6	400.8	200.4	0.0
Ceratium lineatum	13317.0	17554.2	35713.7	32081.8	1614.2	18563.0	15738.2	18966.6	30669.3
Ceratium macroceros	0.0	0.0	0.0	0.0	0.0	0.0	0.0	0.0	536.1
Ceratium tripos	0.0	0.0	0.0	0.0	0.0	0.0	0.0	1372.5	0.0
Ceratoperidinium falcatum	0.0	0.0	0.0	0.0	0.0	5339.6	6941.5	3203.8	1067.9
Dinophysis acuminata	1030.8	687.2	3264.2	2233.4	1889.8	10995.1	1889.8	1030.8	687.2
Dinophysis acuta	0.0	0.0	0.0	0.0	0.0	12712.6	2825.0	38137.8	1412.5
Dinophysis norvegica	0.0	0.0	0.0	0.0	0.0	495.9	371.9	124.0	124.0
Dinophysis tripos	0.0	0.0	0.0	0.0	0.0	0.0	0.0	0.0	0.0
Diplopsalis lenticula	12545.0	32258.5	2190.4	3186.0	995.6	0.0	0.0	0.0	0.0
Gonyaulax spinifera	1277.0	1383.4	1277.0	1277.0	851.3	7662.0	3298.9	2979.6	851.3
Gyrodinium spp.	202.1	202.1	7883.1	8691.7	9095.9	75192.7	19606.7	12127.9	7074.6
Heterocapsa spp.	0.0	0.0	0.0	0.0	0.0	3618.0	1749.7	1008.3	59.3
Karenia mikimotoi	1708.6	533.9	2456.1	1174.7	427.1	43569.1	2990.0	533.9	213.6
Katodinium glaucum	2291.0	5378.8	730.5	664.1	365.2	2656.2	2689.4	697.3	996.1
Nematodinium torpedo	0.0	0.0	0.0	0.0	0.0	173.7	260.5	173.7	521.1
Noctiluca scintillans	0.0	0.0	0.0	0.0	0.0	0.0	0.0	0.0	0.0
Oblea rotundata	76.0	0.0	0.0	0.0	0.0	0.0	0.0	0.0	0.0
Phalacroma rotundatum	0.0	0.0	0.0	0.0	0.0	0.0	772.8	257.6	257.6

Polykrikos schwartzii/kofoidii	0.0	0.0	1409.8	0.0	0.0	5639.1	0.0	21146.8	18327.2
Pronoctiluca sp.	0.0	0.0	0.0	0.0	0.0	0.0	0.0	0.0	0.0
Prorocentrum micans	1035.1	388.2	3623.0	5952.1	5175.7	0.0	0.0	129.4	258.8
Prorocentrum minimum	42.9	21.4	0.0	0.0	0.0	42.9	42.9	0.0	42.9
Prorocentrum triestinum	0.0	0.0	0.0	0.0	0.0	0.0	0.0	0.0	0.0
S *Protoperidinium spp.* (10-30 µm dia.)	66.8	934.8	601.0	1535.8	934.8	1201.9	267.1	1268.7	467.4
M *Protoperidinium spp.* (30-65 µm dia.)	334.5	1672.6	669.0	1338.0	2007.1	1338.0	334.5	0.0	0.0
L *Protoperidinium spp.* (65-120 µm dia.)	0.0	3506.5	8766.1	0.0	3506.5	3506.5	5259.7	3506.5	3506.5
Scrippsiella trochoidea	1154.5	1154.5	2020.4	1731.8	1500.9	11525.5	2126.1	2014.2	447.6
Torodinium robustum/teredo	32.9	0.0	0.0	0.0	0.0	263.3	98.7	65.8	164.6
unidentified gymnoid athecate dinoflagellate	0.0	0.0	0.0	0.0	0.0	2007.6	0.0	200.8	0.0
Total dinoflagellate carbon (Pg C ml^{-1})	**62444.2**	**91586.8**	**99208.6**	**83542.2**	**35623.3**	**309187.9**	**133863.5**	**165878.7**	**107668.3**
Flagellates (Pg C ml^{-1})									
Chlamydomonas spp.	0.0	0.0	0.0	0.0	0.0	0.0	0.0	0.0	0.0
Chrysochromulina spp.	0.0	0.0	0.0	0.0	0.0	920.9	727.1	920.9	436.2
Chrysophaerella longispina	0.0	0.0	0.0	0.0	0.0	0.0	0.0	0.0	0.0
Cryptophytes	58.4	146.0	48.7	68.2	29.2	137.0	125.6	91.3	45.7
Cymbomonas tetramitiformis	0.0	0.0	0.0	0.0	0.0	265.5	53.1	283.2	17.7
Dictyocha fibula/speculum	0.0	0.0	0.0	0.0	337.9	337.9	675.9	1689.7	1689.7
Pleurasiga spp.	0.0	0.0	0.0	0.0	0.0	0.0	0.0	0.0	0.0
Pseudopedinella/Pyramimonas spp.	0.0	0.0	0.0	0.0	0.0	0.0	0.0	0.0	0.0
Solenicola setigera	0.0	0.0	0.0	0.0	0.0	0.0	136.1	1497.2	2058.7
Trachelomonas volvocinopsis	0.0	0.0	0.0	0.0	0.0	3299.6	1771.0	652.5	316.9
unidentified spherical flagellate (10-20 µm dia.)	0.0	0.0	0.0	0.0	0.0	34.0	79.4	113.4	124.8
Total flagellate carbon (Pg C ml^{-1})	**58.4**	**146.0**	**48.7**	**68.2**	**367.1**	**4995.0**	**3568.1**	**5248.2**	**4689.6**

Non-flagellated chlorophyceae (Pg C ml^{-1})									
Tetraedron spp.	0.0	0.0	0.0	0.0	0.0	0.0	0.0	0.0	0.0
Oocystaceae sp.	0.0	0.0	0.0	0.0	0.0	0.0	0.0	0.0	0.0
Total non-flagellated chlorophyceae carbon (Pg C ml^{-1})	**0.0**	**0.0**	**0.0**	**0.0**	**0.0**	**0.0**	**0.0**	**0.0**	**0.0**
Ciliates (Pg C ml^{-1})									
S aloricate ciliates (< 20µm)	0.0	63.7	0.0	0.0	0.0	188.6	471.5	1068.8	345.8
M aloricate ciliates (20-40 µm)	783.8	1045.0	391.9	130.6	0.0	2351.3	1306.3	3788.2	3396.3
L aloricate ciliates (> 40 µm)	0.0	0.0	0.0	1784.4	0.0	13085.4	5947.9	11301.0	8327.1
Tiarina fusus	0.0	0.0	0.0	0.0	0.0	6862.6	1470.6	1470.6	3921.5
S bowl shaped tintinnids (20-50 µm length)	0.0	179.3	0.0	0.0	179.3	0.0	717.2	179.3	0.0
L bowl shaped tintinnids (> 60 µm length)	0.0	0.0	0.0	0.0	0.0	0.0	0.0	0.0	0.0
S tapering tintinnids (40-60 µm)	0.0	0.0	0.0	0.0	0.0	24893.3	6990.6	2046.0	1193.5
L tapering tintinnids (> 60 µm)	0.0	0.0	0.0	0.0	0.0	0.0	0.0	475.0	475.0
Total ciliate carbon (Pg C ml^{-1})	**783.8**	**1288.0**	**391.9**	**1915.0**	**179.3**	**47381.1**	**16904.0**	**20328.8**	**17659.1**

Date	**02/07/2014**	**03/07/2014**	**23/06/2015**	**24/06/2015**	**25/06/2015**	**26/06/2015**	**27/06/2015**	**29/06/2015**	**30/06/2015**
Site number	**17**	**18**	**2**	**3**	**5**	**6**	**11**	**17**	**18**
Sample ID	**j**	**k**	**l**	**m**	**n**	**o**	**p**	**q**	**r**
Sample location	**SCM**	**SCM**	**SCM**	**SCM**	**SCM**	**SCM**	**SCM**	**SCM**	**SCM**
Diatoms (Pg C ml^{-1})									
Asterionellopsis glacialis	0.0	0.0	0.0	0.0	0.0	0.0	0.0	0.0	0.0
S centric diatom (20-30 µm dia.)	851.3	541.7	0.0	0.0	0.0	0.0	0.0	0.0	0.0
M centric diatom (30-50 µm dia.)	1195.0	2390.0	0.0	149.4	149.4	0.0	0.0	298.7	0.0
L centric diatom (60-150 µm dia.)	6350.0	352.8	0.0	1763.9	0.0	0.0	0.0	0.0	0.0

XL centric diatom (> 150 µm dia.)	0.0	0.0	0.0	0.0	0.0	0.0	1511.7	0.0	0.0
Cerataulina pelagica	377.6	94.4	0.0	0.0	0.0	188.8	566.5	188.8	0.0
Chaetoceros spp.	913.8	407.5	1149.4	1580.5	574.7	718.4	3304.7	2011.5	1149.4
Cylindrotheca closterium	51.1	68.1	0.0	0.0	0.0	0.0	8.5	8.5	2.8
Diploneis spp.	0.0	0.0	0.0	0.0	36.2	36.2	0.0	0.0	0.0
Entomoneis spp.	116.5	58.2	0.0	0.0	0.0	0.0	58.2	0.0	0.0
Guinardia delicatula	378.0	378.0	0.0	0.0	0.0	0.0	0.0	0.0	0.0
Guinardia flaccida	0.0	0.0	0.0	0.0	0.0	0.0	0.0	0.0	0.0
Guinardia striata	96.4	0.0	0.0	0.0	0.0	0.0	0.0	0.0	0.0
Lauderia annulata	27090.4	27837.2	0.0	0.0	0.0	0.0	0.0	0.0	0.0
Leptocylindrus danicus	12211.6	18908.4	183.5	19.3	29.0	115.9	337.9	589.0	5542.3
Leptocylindrus minimus	42.4	42.4	223.4	59.7	52.0	77.0	269.6	98.2	250.3
Meuniera membranacea	6033.9	7919.4	0.0	0.0	0.0	188.6	471.4	94.3	0.0
Paralia sulcata	55.9	279.7	0.0	0.0	0.0	69.9	42.0	209.8	0.0
S pennate diatom (20-40 µm length)	0.0	0.0	0.0	0.0	0.0	0.0	0.0	0.0	0.0
M pennate diatom (40-65 µm length)	19.9	39.7	0.0	0.0	0.0	0.0	19.9	0.0	0.0
L pennate diatom (65-110 µm length)	74.6	0.0	0.0	74.6	0.0	0.0	0.0	74.6	0.0
XL pennate diatom (110-175 µm length)	0.0	0.0	0.0	0.0	0.0	0.0	0.0	0.0	0.0
S *Pleurosigma spp.* (~50 µm)	0.0	0.0	0.0	0.0	0.0	0.0	0.0	0.0	0.0
M *Pleurosigma spp.* (80-170 µm)	136.9	205.4	0.0	0.0	0.0	0.0	0.0	0.0	0.0
L *Pleurosigma spp.* (170-200 µm)	271.7	815.2	0.0	0.0	0.0	0.0	0.0	0.0	0.0
XL *Pleurosigma spp.* (> 200 µm)	196.7	0.0	0.0	0.0	0.0	0.0	0.0	0.0	0.0
Podosira stelligera	0.0	0.0	0.0	0.0	0.0	0.0	0.0	0.0	0.0
Proboscia alata	2048.8	2926.9	1853.7	195.1	48.8	243.9	243.9	146.3	2292.8
Proboscia truncata	0.0	0.0	21355.9	10049.8	7537.4	5024.9	16331.0	5024.9	8793.6

S *Pseudo-nitzschia spp.* (< 2.5 µm dia.)	56.8	154.9	20.7	41.3	36.1	72.3	464.8	720.4	100.7
L *Pseudo-nitzschia spp.* (> 2.5 µm dia.)	2320.9	4826.4	422.0	342.9	184.6	487.9	316.5	224.2	145.1
S *Rhizosolenia spp.* (≤ 10 µm dia.)	6335.7	6335.7	0.0	0.0	0.0	0.0	0.0	166.7	100.0
M *Rhizosolenia spp.* (10-20 µm dia.)	1956.3	2200.9	0.0	0.0	0.0	0.0	244.5	0.0	0.0
L *Rhizosolenia spp.* (> 20 µm dia.)	18972.2	18972.2	0.0	0.0	0.0	0.0	0.0	0.0	0.0
Skeletonema costatum	0.0	0.0	0.0	0.0	0.0	0.0	0.0	0.0	0.0
Stephanopyxis turris	0.0	0.0	0.0	0.0	0.0	0.0	0.0	0.0	0.0
XS *Thalassiosira spp.* (< 10 µm height)	0.0	0.0	60.9	165.4	217.7	949.0	6355.7	6238.1	5337.0
S *Thalassiosira spp.* (10-25 µm height)	1737.1	451.0	0.0	0.0	0.0	0.0	0.0	0.0	0.0
M *Thalassiosira spp.* (25-45 µm height)	7751.8	6941.9	0.0	0.0	0.0	0.0	57.8	0.0	0.0
L *Thalassiosira spp.* (> 45 µm height)	0.0	0.0	0.0	0.0	0.0	0.0	0.0	0.0	0.0
Total diatom carbon (Pg C ml^{-1})	**97643.5**	**103148.0**	**25269.5**	**14442.0**	**8865.8**	**8172.8**	**30604.5**	**16094.2**	**23714.1**
Dinoflagellates (Pg C ml^{-1})									
10-20 µm naked dinoflagellates	11095.4	13600.8	8589.6	9126.5	10916.0	8410.7	9842.3	7158.0	8410.7
20-25 µm naked dinoflagellates	22966.6	28070.3	1275.9	1913.9	1913.9	1913.9	3827.8	638.0	5103.8
10-30 µm armoured dinoflagellates	202.1	0.0	151.5	252.6	303.1	101.0	656.7	252.6	1212.4
Alexandrium ostenfeldii	0.0	0.0	7756.8	4490.8	8573.3	13064.1	6532.1	1633.0	5307.3
Amphidinium carterae	0.0	0.0	0.0	0.0	0.0	0.0	0.0	0.0	0.0
Ceratium fusus	0.0	0.0	280954.3	299190.3	221436.9	249692.6	194183.1	67332.8	51702.0
Ceratium lineatum	27844.5	24616.2	6658.5	25019.8	19370.1	7869.1	10492.2	2219.5	11299.2
Ceratium macroceros	536.1	0.0	2680.7	536.1	1072.3	2144.6	0.0	2144.6	0.0
Ceratium tripos	0.0	0.0	0.0	0.0	0.0	1372.5	0.0	0.0	1372.5
Ceratoperidinium falcatum	4271.7	1601.9	2669.8	2669.8	1601.9	4271.7	3203.8	534.0	1067.9
Dinophysis acuminata	343.6	343.6	171.8	171.8	0.0	0.0	171.8	0.0	343.6
Dinophysis acuta	2118.8	0.0	11300.1	5650.0	4237.5	5650.0	9887.6	0.0	113707.2

Dinophysis norvegica	0.0	0.0	0.0	0.0	0.0	0.0	0.0	0.0	0.0
Dinophysis tripos	0.0	0.0	0.0	0.0	0.0	0.0	0.0	0.0	0.0
Diplopsalis lenticula	0.0	0.0	0.0	0.0	0.0	0.0	0.0	0.0	0.0
Gonyaulax spinifera	1064.2	2554.0	319.2	532.1	425.7	212.8	638.5	106.4	1064.2
Gyrodinium spp.	8893.8	14755.6	5053.3	8489.5	6468.2	5053.3	7681.0	4244.8	3840.5
Heterocapsa spp.	29.7	29.7	0.0	14.8	0.0	29.7	14.8	0.0	59.3
Karenia mikimotoi	427.1	0.0	2456.1	1708.6	854.3	427.1	320.4	0.0	320.4
Katodinium glaucum	464.8	1128.9	996.1	4814.4	9296.8	1261.7	3087.9	664.1	431.6
Nematodinium torpedo	347.4	173.7	86.8	434.2	86.8	0.0	173.7	173.7	0.0
Noctiluca scintillans	0.0	0.0	227081.5	0.0	0.0	0.0	0.0	0.0	340622.2
Oblea rotundata	0.0	0.0	0.0	0.0	0.0	0.0	0.0	0.0	76.0
Phalacroma rotundatum	0.0	0.0	515.2	515.2	515.2	0.0	0.0	0.0	0.0
Polykrikos schwartzii/kofoidii	8458.7	0.0	16767.6	1676.8	0.0	0.0	3353.5	1676.8	0.0
Pronoctiluca sp.	0.0	0.0	0.0	0.0	0.0	0.0	0.0	0.0	0.0
Prorocentrum micans	0.0	0.0	258.8	0.0	129.4	129.4	129.4	129.4	129.4
Prorocentrum minimum	0.0	0.0	622.0	772.1	536.2	450.4	622.0	150.1	386.1
Prorocentrum triestinum	0.0	0.0	0.0	0.0	0.0	0.0	0.0	0.0	0.0
S *Protoperidinium spp.* (10-30 µm dia.)	534.2	934.8	400.6	1068.4	267.1	601.0	267.1	133.5	267.1
M *Protoperidinium spp.* (30-65 µm dia.)	669.0	669.0	334.5	0.0	0.0	0.0	334.5	0.0	669.0
L *Protoperidinium spp.* (65-120 µm dia.)	3506.5	5259.7	3506.5	14025.8	5259.7	3506.5	5259.7	1753.2	7012.9
Scrippsiella trochoidea	111.9	223.8	0.0	0.0	0.0	0.0	0.0	0.0	0.0
Torodinium robustum/teredo	263.3	263.3	131.6	65.8	32.9	65.8	32.9	98.7	32.9
unidentified gymnoid athecate dinoflagellate	200.8	200.8	0.0	0.0	0.0	0.0	0.0	0.0	0.0
Total dinoflagellate carbon (Pg C ml^{-1})	**94350.1**	**94426.0**	**580739.0**	**383139.4**	**293297.3**	**306228.0**	**260712.6**	**91043.2**	**554438.3**
Flagellates (Pg C ml^{-1})									

Chlamydomonas spp.	0.0	0.0	0.0	0.0	0.0	0.0	0.0	0.0	0.0
Chrysochromulina spp.	96.9	145.4	993.7	1333.0	1163.3	872.5	1769.2	218.1	3077.9
Chrysophaerella longispina	1873.8	832.8	0.0	0.0	208.2	624.6	208.2	208.2	416.4
Cryptophytes	34.2	102.7	422.5	525.2	1335.9	1404.4	947.7	479.6	513.8
Cymbomonas tetramitiformis	35.4	0.0	0.0	0.0	0.0	0.0	0.0	0.0	0.0
Dictyocha fibula/speculum	337.9	675.9	32610.3	52041.4	21458.6	13179.3	8279.3	2027.6	5575.9
Pleurasiga spp.	0.0	0.0	0.0	488.9	0.0	977.8	0.0	1955.6	488.9
Pseudopedinella/Pyramimonas spp.	0.0	0.0	0.0	0.0	0.0	0.0	0.0	0.0	0.0
Solenicola setigera	5444.5	4015.3	2126.8	3402.8	2228.9	6822.7	3658.1	3249.7	3641.0
Trachelomonas volvocinopsis	205.1	223.7	0.0	0.0	0.0	0.0	0.0	0.0	0.0
unidentified spherical flagellate (10-20 µm dia.)	124.8	215.5	85.1	141.8	124.8	136.1	300.6	85.1	62.4
Total flagellate carbon (Pg C ml^{-1})	**8152.7**	**6211.3**	**36238.3**	**57933.1**	**26519.7**	**24017.4**	**15163.0**	**8223.8**	**13776.3**
Non-flagellated chlorophyceae (Pg C ml^{-1})									
Tetraedron spp.	0.0	0.0	36.3	0.0	0.0	36.3	0.0	0.0	0.0
Oocystaceae sp.	0.0	0.0	0.0	0.0	0.0	0.0	0.0	416.6	0.0
Total non-flagellated chlorophyceae carbon (Pg C ml^{-1})	**0.0**	**0.0**	**36.3**	**0.0**	**0.0**	**36.3**	**0.0**	**416.6**	**0.0**
Ciliates (Pg C ml^{-1})									
S aloricate ciliates (< 20µm)	754.4	691.5	220.0	94.3	125.7	62.9	188.6	251.5	440.1
M aloricate ciliates (20-40 µm)	8621.3	2612.5	10711.3	8098.8	6400.7	6661.9	13977.0	391.9	23512.6
L aloricate ciliates (> 40 µm)	10706.2	5947.9	14869.8	15464.6	33308.3	22007.3	65427.0	23196.9	14275.0
Tiarina fusus	1960.7	3431.3	1470.6	1960.7	1470.6	980.4	5882.2	1960.7	490.2
S bowl shaped tintinnids (20-50 µm length)	0.0	0.0	0.0	0.0	0.0	0.0	0.0	0.0	0.0
L bowl shaped tintinnids (> 60 µm length)	2144.0	2144.0	0.0	0.0	0.0	0.0	0.0	0.0	0.0
S tapering tintinnids (40-60 µm)	6479.1	1364.0	170.5	852.5	341.0	682.0	1364.0	0.0	1023.0
L tapering tintinnids (> 60 µm)	0.0	0.0	0.0	0.0	0.0	0.0	0.0	0.0	475.0

Total ciliate carbon (Pg C ml^{-1})	**30665.8**	**16191.3**	**27442.2**	**26470.9**	**41646.3**	**30394.4**	**86838.8**	**25800.9**	**40215.9**

Date	**01/07/2015**	**02/07/2015**	**20/06/2016**	**21/06/2016**	**22/06/2016**	**23/06/2016**	**24/06/2016**	**25/06/2016**	**27/06/2016**
Site number	**19**	**20**	**1**	**2**	**3**	**4**	**6**	**7**	**14**
Sample ID	**s**	**t**	**u**	**v**	**w**	**x**	**y**	**z**	**aa**
Sample location	**SCM**	**SCM**	**SCM**	**SCM**	**SCM**	**SCM**	**SCM**	**SCM**	**SCM**
Diatoms (Pg C ml^{-1})									
Asterionellopsis glacialis	0.0	0.0	10.0	0.0	0.0	0.0	0.0	3.3	0.0
S centric diatom (20-30 µm dia.)	0.0	0.0	0.0	0.0	0.0	0.0	0.0	0.0	0.0
M centric diatom (30-50 µm dia.)	298.7	298.7	298.7	0.0	298.7	149.4	1195.0	0.0	0.0
L centric diatom (60-150 µm dia.)	0.0	352.8	352.8	0.0	352.8	352.8	0.0	0.0	0.0
XL centric diatom (> 150 µm dia.)	0.0	0.0	0.0	0.0	0.0	0.0	0.0	0.0	0.0
Cerataulina pelagica	188.8	0.0	0.0	377.6	94.4	0.0	0.0	0.0	0.0
Chaetoceros spp.	1580.5	4454.1	41183.6	13633.7	72348.8	46156.0	55570.9	6815.4	19595.3
Cylindrotheca closterium	5.7	0.0	368.8	147.5	227.0	885.1	136.2	59.6	25.5
Diploneis spp.	0.0	0.0	0.0	0.0	36.2	0.0	0.0	0.0	0.0
Entomoneis spp.	116.5	29.1	58.2	29.1	0.0	29.1	29.1	0.0	58.2
Guinardia delicatula	0.0	0.0	141.8	0.0	0.0	0.0	0.0	0.0	0.0
Guinardia flaccida	0.0	0.0	0.0	0.0	0.0	0.0	0.0	0.0	0.0
Guinardia striata	0.0	0.0	0.0	0.0	0.0	0.0	0.0	0.0	0.0
Lauderia annulata	0.0	0.0	0.0	0.0	0.0	0.0	0.0	0.0	0.0
Leptocylindrus danicus	2944.9	482.8	38.6	260.7	19.3	77.2	29.0	0.0	0.0
Leptocylindrus minimus	71.2	279.2	25.0	287.0	79.0	256.2	42.4	46.2	23.1
Meuniera membranacea	0.0	0.0	2262.7	1791.3	1791.3	188.6	0.0	565.7	188.6

Paralia sulcata	181.8	0.0	0.0	167.8	195.8	97.9	28.0	125.9	0.0
S pennate diatom (20-40 µm length)	0.0	0.0	194.7	0.0	17.7	44.2	17.7	0.0	0.0
M pennate diatom (40-65 µm length)	0.0	0.0	0.0	36.9	86.0	36.9	61.4	0.0	36.9
L pennate diatom (65-110 µm length)	0.0	0.0	0.0	0.0	223.9	0.0	0.0	0.0	0.0
XL pennate diatom (110-175 µm length)	0.0	0.0	0.0	0.0	0.0	0.0	29.8	0.0	0.0
S *Pleurosigma spp.* (~50 µm)	0.0	0.0	0.0	0.0	0.0	0.0	0.0	0.0	0.0
M *Pleurosigma spp.* (80-170 µm)	0.0	0.0	136.9	68.5	68.5	410.8	68.5	0.0	68.5
L *Pleurosigma spp.* (170-200 µm)	0.0	0.0	135.9	0.0	271.7	0.0	135.9	135.9	0.0
XL *Pleurosigma spp.* (> 200 µm)	0.0	0.0	0.0	196.7	0.0	0.0	196.7	0.0	0.0
Podosira stelligera	0.0	0.0	0.0	0.0	0.0	0.0	0.0	0.0	0.0
Proboscia alata	97.6	97.6	341.5	243.9	390.3	439.0	48.8	146.3	195.1
Proboscia truncata	10049.8	1256.2	0.0	0.0	0.0	0.0	0.0	0.0	0.0
S *Pseudo-nitzschia spp.* (< 2.5 µm dia.)	495.8	183.3	18515.6	4344.1	6551.7	3560.7	3631.9	640.9	1709.1
L *Pseudo-nitzschia spp.* (> 2.5 µm dia.)	184.6	26.4	163.7	95.5	163.7	68.2	95.5	0.0	27.3
S *Rhizosolenia spp.* (≤ 10 µm dia.)	33.3	66.7	1529.3	611.7	841.1	382.3	458.8	152.9	76.5
M *Rhizosolenia spp.* (10-20 µm dia.)	0.0	122.3	0.0	489.1	0.0	0.0	0.0	0.0	0.0
L *Rhizosolenia spp.* (> 20 µm dia.)	0.0	0.0	0.0	0.0	978.1	978.1	0.0	0.0	978.1
Skeletonema costatum	0.0	0.0	0.0	0.0	0.0	0.0	0.0	0.0	0.0
Stephanopyxis turris	0.0	0.0	0.0	0.0	5979.2	1993.1	398.6	0.0	0.0
XS *Thalassiosira spp.* (< 10 µm height)	7365.6	15192.7	0.0	0.0	0.0	0.0	0.0	0.0	0.0
S *Thalassiosira spp.* (10-25 µm height)	0.0	0.0	50.1	16.7	66.8	33.4	83.5	1453.2	1419.8
M *Thalassiosira spp.* (25-45 µm height)	0.0	0.0	0.0	0.0	0.0	0.0	115.7	0.0	0.0
L *Thalassiosira spp.* (> 45 µm height)	0.0	0.0	0.0	0.0	0.0	0.0	0.0	0.0	0.0
Total diatom carbon (Pg C ml^{-1})	**23615.0**	**22841.9**	**65807.9**	**22797.7**	**91081.9**	**56139.0**	**62373.3**	**10145.3**	**24401.9**
Dinoflagellates (Pg C ml^{-1})									

10-20 µm naked dinoflagellates	9126.5	15747.7	21287.0	18921.8	30102.8	23437.2	29027.7	15266.4	15051.4
20-25 µm naked dinoflagellates	2551.9	7017.7	6632.3	7579.7	24634.1	15159.5	35056.2	33161.3	16106.9
10-30 µm armoured dinoflagellates	505.1	606.2	1215.6	1539.7	1215.6	810.4	2350.1	81.0	405.2
Alexandrium ostenfeldii	2041.3	0.0	0.0	408.3	0.0	0.0	0.0	0.0	0.0
Amphidinium carterae	0.0	0.0	500.3	500.3	583.7	416.9	750.5	0.0	83.4
Ceratium fusus	32864.8	30059.3	0.0	200.4	400.8	200.4	200.4	0.0	400.8
Ceratium lineatum	5851.4	2421.3	0.0	1815.9	4439.0	2219.5	7667.3	605.3	605.3
Ceratium macroceros	1072.3	0.0	0.0	0.0	536.1	536.1	0.0	536.1	0.0
Ceratium tripos	0.0	1372.5	0.0	0.0	0.0	0.0	0.0	0.0	0.0
Ceratoperidinium falcatum	534.0	1067.9	1067.9	3737.7	3203.8	4805.6	534.0	1067.9	4805.6
Dinophysis acuminata	515.4	1374.4	146.2	731.0	2924.0	2193.0	3801.2	1462.0	13011.7
Dinophysis acuta	37431.6	80513.2	0.0	3531.3	3531.3	0.0	0.0	0.0	8475.1
Dinophysis norvegica	0.0	0.0	0.0	0.0	0.0	0.0	0.0	0.0	0.0
Dinophysis tripos	0.0	773.0	0.0	0.0	0.0	0.0	0.0	0.0	0.0
Diplopsalis lenticula	0.0	0.0	0.0	0.0	0.0	0.0	0.0	0.0	0.0
Gonyaulax spinifera	0.0	0.0	494.3	865.0	988.6	1730.1	1730.1	1606.5	247.2
Gyrodinium spp.	2829.8	5659.7	2425.6	3840.5	10106.6	8691.6	6063.9	6468.2	2425.6
Heterocapsa spp.	14.8	252.1	281.7	163.1	163.1	148.3	652.4	44.5	89.0
Karenia mikimotoi	106.8	213.6	0.0	106.8	213.6	106.8	106.8	0.0	0.0
Katodinium glaucum	962.9	896.5	664.1	1294.9	1195.3	2722.6	1261.7	2291.0	2457.0
Nematodinium torpedo	86.8	86.8	0.0	0.0	173.7	0.0	0.0	0.0	86.8
Noctiluca scintillans	0.0	0.0	0.0	0.0	0.0	0.0	0.0	0.0	0.0
Oblea rotundata	0.0	0.0	0.0	0.0	0.0	0.0	0.0	0.0	0.0
Phalacroma rotundatum	0.0	0.0	0.0	515.2	257.6	0.0	0.0	0.0	0.0
Polykrikos schwartzii/kofoidii	0.0	0.0	0.0	0.0	0.0	1676.8	0.0	0.0	0.0

Pronoctiluca sp.	0.0	0.0	0.0	0.0	37.0	0.0	0.0	0.0	37.0
Prorocentrum micans	0.0	0.0	455.1	303.4	606.7	1213.5	303.4	910.1	1668.5
Prorocentrum minimum	150.1	536.2	0.0	0.0	21.4	21.4	0.0	42.9	0.0
Prorocentrum triestinum	0.0	41.2	0.0	0.0	0.0	0.0	0.0	0.0	0.0
S *Protoperidinium spp.* (10-30 µm dia.)	66.8	0.0	520.3	594.7	446.0	520.3	1858.3	74.3	371.7
M *Protoperidinium spp.* (30-65 µm dia.)	334.5	1003.5	1500.7	250.1	1250.6	1500.7	1750.9	750.4	750.4
L *Protoperidinium spp.* (65-120 µm dia.)	5259.7	7012.9	1933.4	4833.4	13533.5	14500.2	6766.7	14500.2	6766.7
Scrippsiella trochoidea	0.0	0.0	111.9	111.9	391.6	279.7	167.8	167.8	111.9
Torodinium robustum/teredo	32.9	98.7	131.6	131.6	131.6	164.6	98.7	296.2	427.8
unidentified gymnoid athecate dinoflagellate	0.0	0.0	401.5	1204.5	1204.5	1405.3	401.5	2409.1	1003.8
Total dinoflagellate carbon (Pg C ml^{-1})	**102339.4**	**156754.4**	**39769.4**	**53181.3**	**102292.7**	**84460.5**	**100549.7**	**81741.3**	**75388.8**
Flagellates (Pg C ml^{-1})									
Chlamydomonas spp.	0.0	0.0	0.0	0.0	0.0	0.0	0.0	0.0	0.0
Chrysochromulina spp.	630.1	2253.9	24.2	0.0	24.2	24.2	0.0	48.5	24.2
Chrysophaerella longispina	416.4	1249.2	0.0	1249.2	1873.8	624.6	416.4	416.4	3331.3
Cryptophytes	890.6	673.7	1221.3	1198.5	1426.8	1152.8	1438.2	1438.2	913.1
Cymbomonas tetramitiformis	0.0	0.0	0.0	0.0	0.0	8.9	0.0	0.0	0.0
Dictyocha fibula/speculum	675.9	675.9	0.0	169.0	0.0	169.0	0.0	0.0	337.9
Pleurasiga spp.	2933.4	1466.7	0.0	0.0	0.0	0.0	0.0	0.0	0.0
Pseudopedinella/Pyramimonas spp.	0.0	0.0	0.0	0.0	0.0	0.0	0.0	0.0	0.0
Solenicola setigera	5750.8	3368.8	0.0	0.0	34.0	51.0	51.0	0.0	34.0
Trachelomonas volvocinopsis	0.0	0.0	482.4	425.6	496.5	283.7	1106.6	368.9	496.5
unidentified spherical flagellate (10-20 µm dia.)	153.1	215.5	22.7	17.0	90.7	147.4	221.2	584.1	175.8
Total flagellate carbon (Pg C ml^{-1})	**11450.3**	**9903.7**	**1750.6**	**3059.3**	**3946.1**	**2461.7**	**3233.4**	**2856.0**	**5312.9**
Non-flagellated chlorophyceae (Pg C ml^{-1})									

Tetraedron spp.	0.0	0.0	0.0	0.0	0.0	0.0	0.0	0.0	0.0
Oocystaceae sp.	0.0	0.0	36.3	0.0	0.0	0.0	0.0	72.7	0.0
Total non-flagellated chlorophyceae carbon (Pg C ml^{-1})	**0.0**	**0.0**	**36.3**	**0.0**	**0.0**	**0.0**	**0.0**	**72.7**	**0.0**
Ciliates (Pg C ml^{-1})									
S aloricate ciliates (< 20µm)	282.9	723.0	314.3	220.0	282.9	660.1	1225.9	1288.8	1131.6
M aloricate ciliates (20-40 µm)	3918.8	14499.5	1748.3	643.9	2023.4	3035.5	2759.1	4141.1	12769.7
L aloricate ciliates (> 40 µm)	79702.0	18438.5	3034.1	5056.8	15757.8	17193.2	8384.6	29916.9	116763.8
Tiarina fusus	4901.8	2941.1	0.0	0.0	0.0	0.0	0.0	0.0	490.2
S bowl shaped tintinnids (20-50 µm length)	0.0	0.0	0.0	179.3	0.0	0.0	0.0	0.0	0.0
L bowl shaped tintinnids (> 60 µm length)	4288.1	0.0	2144.0	0.0	4288.1	4288.1	0.0	2144.0	0.0
S tapering tintinnids (40-60 µm)	341.0	1534.5	0.0	170.5	170.5	170.5	0.0	511.5	0.0
L tapering tintinnids (> 60 µm)	949.9	0.0	0.0	0.0	0.0	0.0	0.0	0.0	0.0
Total ciliate carbon (Pg C ml^{-1})	**94384.5**	**38136.6**	**7240.7**	**6270.6**	**22522.7**	**25347.4**	**12369.6**	**38002.3**	**131155.3**

Date	**28/06/2016**	**30/06/2016**
Site number	**15**	**16**
Sample ID	**bb**	**cc**
Sample location	**SCM**	**SCM**
Diatoms (Pg C ml^{-1})		
Asterionellopsis glacialis	0.0	0.0
S centric diatom (20-30 µm dia.)	38.7	0.0
M centric diatom (30-50 µm dia.)	0.0	0.0
L centric diatom (60-150 µm dia.)	0.0	0.0
XL centric diatom (> 150 µm dia.)	0.0	0.0

Cerataulina pelagica	0.0	0.0
Chaetoceros spp.	45637.9	2679.0
Cylindrotheca closterium	70.9	51.1
Diploneis spp.	36.2	0.0
Entomoneis spp.	145.6	29.1
Guinardia delicatula	0.0	0.0
Guinardia flaccida	0.0	0.0
Guinardia striata	0.0	0.0
Lauderia annulata	0.0	0.0
Leptocylindrus danicus	0.0	0.0
Leptocylindrus minimus	163.7	0.0
Meuniera membranacea	188.6	0.0
Paralia sulcata	0.0	0.0
S pennate diatom (20-40 µm length)	8.8	8.8
M pennate diatom (40-65 µm length)	73.7	12.3
L pennate diatom (65-110 µm length)	0.0	0.0
XL pennate diatom (110-175 µm length)	0.0	0.0
S *Pleurosigma spp.* (~50 µm)	0.0	0.0
M *Pleurosigma spp.* (80-170 µm)	0.0	136.9
L *Pleurosigma spp.* (170-200 µm)	0.0	0.0
XL *Pleurosigma spp.* (> 200 µm)	0.0	0.0
Podosira stelligera	0.0	0.0
Proboscia alata	146.3	48.8
Proboscia truncata	0.0	0.0
S *Pseudo-nitzschia spp.* (< 2.5 µm dia.)	1922.8	164.3

L *Pseudo-nitzschia spp.* (> 2.5 µm dia.)	40.9	0.0
S *Rhizosolenia spp.* (≤ 10 µm dia.)	0.0	0.0
M *Rhizosolenia spp.* (10-20 µm dia.)	0.0	0.0
L *Rhizosolenia spp.* (> 20 µm dia.)	0.0	0.0
Skeletonema costatum	0.0	0.0
Stephanopyxis turris	5580.6	0.0
XS *Thalassiosira spp.* (< 10 µm height)	0.0	0.0
S *Thalassiosira spp.* (10-25 µm height)	150.3	50.1
M *Thalassiosira spp.* (25-45 µm height)	0.0	0.0
L *Thalassiosira spp.* (> 45 µm height)	0.0	0.0
Total diatom carbon (Pg C ml^{-1})	**54205.1**	**3180.5**
Dinoflagellates (Pg C ml^{-1})		
10-20 µm naked dinoflagellates	8170.8	32898.1
20-25 µm naked dinoflagellates	4737.3	36003.7
10-30 µm armoured dinoflagellates	243.1	810.4
Alexandrium ostenfeldii	0.0	0.0
Amphidinium carterae	416.9	333.5
Ceratium fusus	0.0	1202.4
Ceratium lineatum	0.0	24212.6
Ceratium macroceros	0.0	0.0
Ceratium tripos	1372.5	0.0
Ceratoperidinium falcatum	3203.8	2135.8
Dinophysis acuminata	146.2	292.4
Dinophysis acuta	0.0	706.3
Dinophysis norvegica	0.0	0.0

Dinophysis tripos	0.0	0.0
Diplopsalis lenticula	0.0	0.0
Gonyaulax spinifera	494.3	1235.8
Gyrodinium spp.	3436.2	12734.3
Heterocapsa spp.	133.5	252.1
Karenia mikimotoi	0.0	320.4
Katodinium glaucum	1228.5	2357.4
Nematodinium torpedo	86.8	0.0
Noctiluca scintillans	0.0	0.0
Oblea rotundata	0.0	0.0
Phalacroma rotundatum	0.0	0.0
Polykrikos schwartzii/kofoidii	0.0	0.0
Pronoctiluca sp.	0.0	0.0
Prorocentrum micans	151.7	758.4
Prorocentrum minimum	0.0	128.7
Prorocentrum triestinum	0.0	0.0
S *Protoperidinium spp.* (10-30 µm dia.)	594.7	1115.0
M *Protoperidinium spp.* (30-65 µm dia.)	750.4	1750.9
L *Protoperidinium spp.* (65-120 µm dia.)	5800.1	5800.1
Scrippsiella trochoidea	55.9	55.9
Torodinium robustum/teredo	131.6	230.4
unidentified gymnoid athecate dinoflagellate	602.3	602.3
Total dinoflagellate carbon (Pg C ml^{-1})	**31756.6**	**125936.7**
Flagellates (Pg C ml^{-1})		
Chlamydomonas spp.	0.0	0.0

Chrysochromulina spp.	24.2	169.6
Chrysophaerella longispina	208.2	7911.8
Cryptophytes	1540.9	1723.5
Cymbomonas tetramitiformis	0.0	62.0
Dictyocha fibula/speculum	0.0	337.9
Pleurasiga spp.	0.0	0.0
Pseudopedinella/Pyramimonas spp.	24.7	0.0
Solenicola setigera	51.0	0.0
Trachelomonas volvocinopsis	539.1	1972.0
unidentified spherical flagellate (10-20 µm dia.)	62.4	170.1
Total flagellate carbon (Pg C ml^{-1})	**2450.6**	**12346.9**
Non-flagellated chlorophyceae (Pg C ml^{-1})		
Tetraedron spp.	0.0	0.0
Oocystaceae sp.	0.0	0.0
Total non-flagellated chlorophyceae carbon (Pg C ml^{-1})	**0.0**	**0.0**
Ciliates (Pg C ml^{-1})		
S aloricate ciliates (< 20µm)	534.4	2577.6
M aloricate ciliates (20-40 µm)	1470.0	2389.7
L aloricate ciliates (> 40 µm)	38725.5	35397.8
Tiarina fusus	0.0	0.0
S bowl shaped tintinnids (20-50 µm length)	0.0	0.0
L bowl shaped tintinnids (> 60 µm length)	0.0	2144.0
S tapering tintinnids (40-60 µm)	0.0	170.5
L tapering tintinnids (> 60 µm)	0.0	0.0
Total ciliate carbon (Pg C ml^{-1})	**40729.9**	**42679.6**

Table A4.2. Date, cast number, time, SCM depth (at maximum chlorophyll), SCM thickness (at half maximum chlorophyll), SCM maximum chlorophyll concentration, chlorophyll concentration within the top 50 m of the water column, SCM temperature (at the peak), SCM salinity (at the peak), buoyancy frequency (maximum value associated with thermocline), instantaneous index of stability (IIS; for depth interval of SCM), wind speed (30 – 90 mins before profile), current velocity (water column averaged), tidal state (where spring + 0 coincides with new/full moon phase and neap + 0 coincides with quarter moon phase), solar insolation (day before profile), rainfall, SCM nitrate, SCM silicate, SCM phosphate, SCM nitrate to phosphate ratio, and SCM nitrate to silicate ratio at the repeat site in the Western English Channel during the summer field surveys of 2013, 2014, 2015 and 2016. Casts with a phytoplankton sample ID were sampled for phytoplankton analysis (only by inverted light microscopy in 2013). Missing/unavailable data is indicated by – and (D) within the 'SCM max chl conc.' column indicates the presence of a double chlorophyll peak, but details only provided on the upper peak, which corresponded with the thermocline.

Year	Cast no.	Date	Time (UTC)	SCM depth (m)	SCM thickness (m)	SCM max chl conc. (µg l^{-1})	Top 50 m integrated chl (mg m^{-2})	SCM temp. (°C)	SCM salinity	Buoyancy frequency (rad^2 s^{-2})	IIS	Wind speed (m s^{-1})	Current velocity (m s^{-1})	Tidal state	Solar insolation (kWh m^{-2} d^{-1})	Rainfall (mm d^{-1})	SCM nutrients (µmol l^{-1})					Phyto-sample ID
																	Ni	Si	P	Ni:P	Ni:Si	
2013	1	24/06	12:47	22.0	6.2	2.6	35.8	11.5	35.2	0.0012	3.35	8.9	0.47	Spring +0	5.45	0.0	-	-	-	-	-	
	2	25/06	15:40	16.1	6.3	2.5	32.6	11.6	35.2	0.0010	6.67	3.9	0.11	Spring +1	5.69	2.3	-	-	-	-	-	a
	3		08:40	27.8	7.1	2.1	39.2	12.1	35.2	0.0019	2.98	1.6	0.32				-	-	-	-	-	
	4	26/06	16:20	22.3	11.2	3.0	47.3	11.8	35.2	0.0018	0.29	2.9	0.10	Spring +2	5.35	0.0	-	-	-	-	-	b
	5		16:53	23.0	9.6	3.6	48.1	11.6	35.2	0.0020	1.06	2.5	0.14				-	-	-	-	-	
	6	28/06	14:50	25.6	1.9	3.5	31.2	11.2	35.3	0.0033	0.74	4.0	0.44	Spring +4	4.62	2.8	-	-	-	-	-	c
	7		08:14	24.4	2.2	3.8	32.8	11.9	35.2	0.0037	1.75	7.2	0.18				-	-	-	-	-	
	8		09:19	23.4	1.5	4.4	28.3	11.8	35.2	0.0042	7.00	5.4	0.25				-	-	-	-	-	
	9		10:15	23.6	0.7	3.4	25.9	11.2	35.3	0.0036	-	3.4	0.19				-	-	-	-	-	d
	10	29/06	11:15	23.6	1.0	4.5	30.1	11.5	35.2	0.0029	2.57	3.5	0.16	Spring +5	3.46	0.0	-	-	-	-	-	
	11		12:53	25.6	0.04	4.3	29.4	11.5	35.3	0.0028	8.13	4.2	0.19				-	-	-	-	-	
	12		13:52	23.9	1.0	4.0	26.9	11.5	35.3	0.0027	4.81	3.6	0.31				-	-	-	-	-	
	13		14:44	26.5	4.5	3.3	37.1	11.9	35.2	0.0018	1.17	4.3	0.38				-	-	-	-	-	
	14		15:45	23.2	4.5	4.2	52.4	11.8	35.2	0.0027	5.67	5.2	0.43				-	-	-	-	-	

	15	01/07	08:48	21.2	2.6	2.0	19.4	11.7	35.2	0.0016	-	3.6	-	Neap +0	3.60	0.0	-	-	-	-	-	
	16	03/07	08:49	22.9	4.3	2.8	27.0	11.4	35.3	0.0025	8.19	7.4	0.17	Neap +2	2.10	0.0	-	-	-	-	-	e
	17	04/07	08:59	15.5	3.4	2.2	20.9	12.1	35.3	0.0030	0.25	6.2	0.19	Neap +3	4.47	3.0	-	-	-	-	-	
2014	1	17/06	09:14	25.9	3.5	3.3	41.8	12.4	35.3	0.0018	-	9.1	-	Spring +4	5.54	11.0	0.40	1.14	0.06	6.8	0.3	f
	2	20/06	09:15	27.0	4.5	3.1	55.4	12.0	35.2	0.0028	-	9.1	-	Neap +0	7.77	6.8	-	-	-	-	-	
	3		09:58	29.3	2.7	3.4	50.1	12.0	35.2	0.0037	-	9.7	-				0.50	1.57	0.11	4.4	0.3	g
	4	23/06	11:01	32.8	7.5	4.4	62.6	12.6	35.2	0.0018	0.58	3.2	0.17	Neap +3	7.26	4.3	-	-	-	-	-	
	5	24/06	08:28	28.1	6.3	2.8	51.0	12.6	35.2	0.0020	0.05	1.2	0.35	Neap +4	7.69	0.0	-	-	-	-	-	
	6	26/06	08:57	NO SCM	NO SCM	NO SCM	36.0	12.6	35.2	0.0020	0.21	11.7	0.39	Neap +6	5.80	5.3	-	-	-	-	-	
	7	28/06	08:32	16.6	4.7	1.6 (D)	61.3	13.5	35.2	0.0036	0.37	4.2	0.20	Spring +1	6.52	0.0	-	-	-	-	-	
	8		09:26	20.1	9.1	1.5 (D)	62.9	13.3	35.2	0.0039	1.17	6.9	0.18				-	-	-	-	-	
	9		10:32	21.6	13.5	1.5 (D)	53.9	13.4	35.2	0.0034	0.33	11.5	0.34				0.48	0.97	0.06	8.7	0.5	h
	10		11:32	22.4	9.8	2.1	52.4	13.1	35.2	0.0022	0.23	5.4	0.41				-	-	-	-	-	
	11		13:31	24.2	4.0	2.7	45.2	13.6	35.2	0.0045	0.36	7.9	0.21				-	-	-	-	-	
	12		14:34	20.9	11.4	1.8	48.7	14.4	35.2	0.0024	1.56	6.9	0.12				-	-	-	-	-	
	13		15:27	26.8	6.7	2.2	50.6	12.8	35.2	0.0040	0.35	-	0.12				-	-	-	-	-	
	14		16:28	23.1	4.9	3.3	56.4	12.8	35.2	0.0058	0.25	1.1	0.24				-	-	-	-	-	
	15	30/06	08:32	30.3	7.0	3.4	48.5	13.3	35.2	0.0026	0.14	3.4	0.16	Spring +3	7.27	0.0	-	-	-	-	-	
	16		09:40	32.2	14.6	2.4	55.7	13.3	35.2	0.0021	0.40	3.7	0.18				0.94	1.02	0.08	12.6	0.9	i
	17	02/07	11:34	35.5	3.9	3.7	52.0	14.2	35.1	0.0015	0.04	7.0	0.26	Spring +5	5.90	4.3	0.45	2.66	0.17	2.7	0.2	j
	18	03/07	13:35	30.4	4.9	3.3	49.8	14.2	35.1	0.0012	0.32	7.2	0.27	Spring +6	7.56	0.0	0.53	0.99	0.14	3.7	0.5	k
2015	1	22/06	11:22	31.3	3.8	4.3	44.9	11.7	35.3	0.0020	10.45	8.1	0.05	Spring +4	6.02	0.0	-	-	-	-	-	
	2	23/06	16:02	26.9	2.9	9.2	49.5	12.5	35.3	0.0020	20.86	5.3	0.35	Spring +5	3.15	2.0	0.23	0.55	0.07	3.2	0.4	l
	3	24/06	10:12	24.8	7.4	14.4	99.5	12.1	35.3	0.0011	5.69	1.5	0.12	Spring +6	6.69	0.8	0.16	1.17	0.13	1.3	0.1	m
	4		13:03	30.7	7.5	9.0	88.0	11.9	35.3	0.0016	1.42	5.5	0.09				0.14	1.44	0.14	1.0	0.1	
	5	25/06	15:14	26.8	2.4	10.8	52.8	11.8	35.3	0.0015	11.34	4.9	0.13	Neap +0	5.02	0.0	0.18	1.50	0.16	1.1	0.1	n
	6	26/06	14:53	29.5	5.0	11.6	65.7	11.9	35.3	0.0022	8.32	5.2	0.11	Neap +1	7.52	0.0	0.12	1.54	0.11	1.1	0.1	o
	7	27/06	08:05	27.1	6.5	4.8	35.9	12.1	35.3	0.0011	7.51	4.3	0.12	Neap +2	5.13	0.0	0.46	1.32	0.23	2.0	0.4	
	8		08:48	28.2	4.5	4.0	28.3	11.9	35.3	0.0018	7.85	6.2	0.12				-	-	-	-	-	
	9		09:27	27.7	4.2	5.4	27.4	12.0	35.3	0.0011	4.72	8.3	0.08				0.11	0.49	0.08	1.4	0.2	
	10		10:33	28.1	2.4	5.8	23.9	11.9	35.3	0.0018	6.77	7.6	0.05				-	-	-	-	-	

	11		11:00	28.1	2.0	11.6	40.1	11.9	35.3	0.0013	8.73	7.6	0.04				0.47	0.77	0.11	4.4	0.6	p
	12		13:17	27.6	0.1	19.2	31.9	11.9	35.3	0.0017	3.60	6.9	0.14				0.13	1.72	0.19	0.7	0.1	
	13		14:41	26.4	0.4	7.3	18.0	11.9	35.3	0.0011	4.91	5.2	0.13				0.09	0.54	0.10	0.9	0.2	
	14		15:15	26.4	2.5	3.6	24.3	12.0	35.3	0.0014	10.89	5.5	0.10				-	-	-	-	-	
	15		15:23	26.5	0.7	3.6	21.2	12.0	35.3	0.0016	30.25	5.8	0.10				-	-	-	-	-	
	16		16:08	27.8	0.3	7.0	28.4	11.9	35.3	0.0012	24.62	6.7	0.05				-	-	-	-	-	
	17	29/06	08:11	25.7	3.6	5.5	40.3	12.0	35.3	0.0015	0.79	2.0	0.23	Neap +4	4.43	0.0	0.84	1.13	0.30	2.8	0.7	q
	18	30/06	08:47	29.3	6.4	3.2	32.5	12.0	35.3	0.0011	9.29	10.0	0.36	Neap +5	7.09	0.0	0.25	0.30	0.07	3.6	0.8	r
	19	01/07	08:05	26.9	7.6	3.7	40.2	12.2	35.3	0.0032	0.86	1.5	0.24	Neap +6	7.82	0.0	1.29	2.67	0.38	3.4	0.5	s
	20	02/07	08:07	36.1	12.0	2.7	52.4	12.0	35.3	0.0015	2.44	4.1	0.13	Spring +0	3.28	0.0	0.11	0.86	0.09	1.2	0.1	t
	1	20/06	11:52	27.4	12.6	3.3	50.3	12.0	35.2	0.0026	0.33	6.2	0.33	Spring +0	2.29	0.0	-	-	-	-	-	u
	2	21/06	10:23	24.3	12.7	2.0	44.2	12.0	35.3	0.0056	0.12	4.9	0.33	Spring +1	4.46	0.0	0.61	0.89	0.31	2.0	0.7	v
	3	22/06	10:37	24.1	1.2	6.2	46.3	12.1	35.2	0.0030	0.78	3.1	0.35	Spring +2	5.92	0.0	0.25	0.41	0.15	1.6	0.6	w
	4	23/06	08:49	22.2	0.4	5.6	46.0	12.0	35.3	0.0036	0.73	4.8	0.22	Spring +3	3.30	0.0	0.49	0.71	0.28	1.7	0.7	x
	5		16:38	16.5	13.9	2.1	54.1	12.2	35.2	0.0018	0.28	6.3	0.16				0.33	0.72	0.20	1.6	0.5	
	6	24/06	12:28	34.5	15.0	5.1	85.1	12.1	35.2	0.0036	0.40	10.3	0.34	Spring +4	6.58	0.0	0.31	0.42	0.21	1.4	0.7	y
	7		08:31	19.1	4.2	1.2	33.5	11.9	35.3	0.0070	0.01	5.5	0.33				0.36	0.48	0.18	2.0	0.8	z
2016	8		09:16	28.5	7.4	1.7	40.5	11.9	35.3	0.0020	0.41	5.5	0.34				-	-	-	-	-	
	9		10:03	19.6	1.1	5.3	47.9	12.1	35.3	0.0038	0.42	6.4	0.27				0.46	0.81	0.24	1.9	0.6	
	10	25/06	11:00	17.4	19.7	2.2	47.7	12.1	35.3	0.0028	0.42	6.7	0.24	Spring +5	5.89	0.0	-	-	-	-	-	
	11		15:05	22.4	0.2	1.8	39.2	11.9	35.3	0.0028	-	8.1	-				-	-	-	-	-	
	12		15:32	22.1	5.7	1.7	41.2	11.8	35.3	0.0040	-	8.8	-				-	-	-	-	-	
	13		16:02	21.2	3.9	1.7	39.5	11.8	35.3	0.0048	1.00	8.8	0.24				0.41	0.58	0.20	2.0	0.7	
	14	27/06	09:27	15.4	2.3	2.2	45.4	11.9	35.3	0.0048	0.23	4.9	0.29	Neap +0	2.38	2.0	0.36	0.61	0.19	1.9	0.6	aa
	15	28/06	08:43	19.9	3.9	5.4	65.4	11.8	35.3	0.0038	2.69	11.9	0.17	Neap +1	6.90	0.0	0.49	0.45	0.23	2.2	1.1	bb
	16	30/06	08:28	12.3	17.1	1.8	51.4	13.1	35.1	0.0013	0.93	7.0	0.30	Neap +3	3.21	0.0	0.20	0.62	0.18	1.1	0.3	cc

Table A4.3. Percentage contribution of each phytoplankton taxon to the similarity of Lugol's iodine preserved phytoplankton samples collected in each year. Numbers in bold and underlined indicate taxa whose cumulative contribution to similarity were up to approximately 50 %.

Taxa	2013	2014	2015	2016
Chaetoceros spp.	**5.97**	0.79	1.91	**10.53**
Lauderia annulata		2.44		
Leptocylindrus danicus		**6.46**	0.79	
Meuniera membranacea		0.89		0.88
Proboscia alata	4.10	0.78	0.79	0.89
Proboscia truncata			**4.73**	
S *Pseudo-nitzschia spp.* (< 2.5 µm dia.)	**20.03**			3.03
L *Pseudo-nitzschia spp.* (> 2.5 µm dia.)		1.64		
S *Rhizosolenia spp.* (≤ 10 µm dia.)		1.03		
L *Rhizosolenia spp.* (> 20 µm dia.)		1.23		
XS *Thalassiosira spp.* (< 10 µm height)			1.91	
M *Thalassiosira spp.* (25-45 µm height)		0.72		
10-20 µm naked dinoflagellates	**12.42**	**8.38**	**5.24**	**10.38**
20-25 µm naked dinoflagellates	4.69	**9.25**	2.50	**8.76**
10-30 µm armoured dinoflagellates			0.96	1.69
Alexandrium ostenfeldii			3.03	
Amphidinium carterae				1.07
Ceratium fusus			**18.45**	
Ceratium lineatum	**10.49**	**7.97**	**4.76**	1.76
Ceratium macroceros			0.83	
Ceratoperidinium falcatum		2.93	2.15	3.20
Dinophysis acuminata	3.68	1.54		2.09
Dinophysis acuta		2.12	**4.39**	
Diplopsalis lenticula	**5.57**			
Gonyaulax spinifera	3.55	2.59		2.09
Gyrodinium spp.	3.72	**6.60**	3.99	**5.24**
Heterocapsa spp.		0.79		0.87
Karenia mikimotoi	2.83	0.98	0.86	
Katodinium glaucum	2.90	1.80	1.95	2.90
Nematodinium torpedo		0.81		
Polykrikos schwartzii/kofoidii		2.07		
Prorocentrum micans	3.88			1.67
Prorocentrum minimum			1.14	
S *Protoperidinium spp.* (10-30 µm dia.)		1.37		1.55
M *Protoperidinium spp.* (30-65 µm dia.)	2.82			2.28
L *Protoperidinium spp.* (65-120 µm dia.)		**3.55**	3.88	**5.90**

Scrippsiella trochoidea	3.83	1.38		
Torodinium robustum/teredo		0.68		0.96
unidentified gymnoid athecate dinoflagellate				2.02
Chrysochromulina spp.		1.02	1.79	
Chrysophaerella longispina				1.53
Cryptophytes			1.46	2.71
Dictyocha fibula/speculum		1.31	4.07	
Solenicola setigera		1.34	3.14	
Trachelomonas volvocinopsis		1.21		1.68
S aloricate ciliates (< 20 µm)		1.17		1.81
M aloricate ciliates (20-40 µm)		2.79	**4.43**	3.51
L aloricate ciliates (> 40 µm)		**5.25**	**8.02**	**8.79**
Tiarina fusus		2.74	2.18	
L bowl shaped tintinnids (> 60 µm length)				1.08
S tapering tintinnids (40-60 µm)		**3.04**	0.96	
Cumulative contribution (%)	90.45	90.67	90.31	90.86
Average similarity (%)	70.38	66.87	67.59	69.59

Appendix 5

This appendix is a data report for 2014 and 2016, and is presented on the enclosed CD. All sites sampled in 2013 and 2015 are represented in the previous data chapters (chapters 3 – 6), but only repeat station 1 data collected during the 2014 and 2016 field surveys is presented. Therefore, all CTD and phytoplankton biomass data collected in the seasonally stratified waters of the Western English Channel during the summers of 2014 and 2016 is displayed in this data report.

Chapter 9: References

AGAWIN, N. S. R., DUARTE, C. M. & AGUSTÍ, S. 2000. Nutrient and temperature control of the contribution of picoplankton to phytoplankton biomass and production. *Limnology and Oceanography,* 45**,** 591-600.

AGUSTÍ, S. 1991. Allometric scaling of light absorption and scattering by phytoplankton cells. *Canadian Journal of Fisheries and Aquatic Sciences,* 48**,** 763-767.

AGUSTÍ, S. & DUARTE, C. M. 1999. Phytoplankton chlorophyll *a* distribution and water column stability in the central Atlantic Ocean. *Oceanologica Acta,* 22**,** 193-203.

ALLDREDGE, A. 1998. The carbon, nitrogen and mass content of marine snow as a function of aggregate size. *Deep-Sea Research I,* 45**,** 529-541.

ALLDREDGE, A. L., COWLES, T. J., MACINTYRE, S., RINES, J. E. B., DONAGHAY, P. L., GREENLAW, C. F., HOLLIDAY, D. V., DEKSHENIEKS, M. M., SULLIVAN, J. M. & ZANEVELD, J. R. V. 2002. Occurrence and mechanisms of formation of a dramatic thin layer of marine snow in a shallow Pacific fjord. *Marine Ecology Progress Series,* 233**,** 1-12.

ALLDREDGE, A. L., PASSOW, U. & HADDOCK, S. H. D. 1998. The characteristics and transparent exopolymer particle (TEP) content of marine snow formed from thecate dinoflagellates. *Journal of Plankton Research,* 20**,** 393-406.

ALSHATTI, A. 2016. *RE: Photograph of the CytoSense in operation.*

ANABALÓN, V., MORALES, C. E., GONZÁLEZ, H. E., MENSCHEL, E., SCHNEIDER, W., HORMAZABAL, S., VALENCIA, L. & ESCRIBANO, R. 2016. Micro-phytoplankton community structure in the coastal upwelling zone off Concepción (central Chile): annual and inter-annual fluctuations in a highly dynamic environment. *Progress in Oceanography,* 149**,** 174-188.

ARBONES, B., FIGUEIRAS, F. G. & VARELA, R. 2000. Action spectrum and maximum quantum yield of carbon fixation in natural phytoplankton populations: implications for primary production estimates in the ocean. *Journal of Marine Systems,* 26**,** 97-114.

AYERS, G. P. & GILLETT, R. W. 2000. DMS and its oxidation products in the remote marine atmosphere: implications for climate and atmospheric chemistry. *Journal of Sea Research,* 43**,** 275-286.

AZAM, F., FENCHEL, T., FIELD, J. G., GRAY, J. S., MEYER-REIL, L. A. & THINGSTAD, F. 1983. The ecological role of water-column microbes in the sea. *Marine Ecology Progress Series,* 10**,** 257-263.

BACKHAUS, J. O. 1996. Climate-sensitivity of European marginal seas, derived from the interpretation of modelling studies. *Journal of Marine Systems,* 7**,** 361-382.

BADGER, M. R., VON CAEMMERER, S., RUUSKA, S. & NAKANO, H. 2000. Electron flow to oxygen in higher plants and algae: rates and control of direct photoreduction (Mehler reaction) and rubisco oxygenase. *Philosophical Transactions of the Royal Society London D,* 355**,** 1433-1446.

BAEK, S. H., SHIMODE, S., HAN, M. S. & KIKUCHI, T. 2008a. Growth of dinoflagellates, *Ceratium furca* and *Ceratium fusus* in Sagami Bay, Japan: The role of nutrients. *Harmful Algae,* 7**,** 729-739.

BAEK, S. H., SHIMODE, S. & KIKUCHI, T. 2007. Reproductive ecology of the dominant dinoflagellate, *Ceratium fusus*, in coastal area of Sagami Bay, Japan. *Journal of Oceanography,* 63**,** 35-45.

BAEK, S. H., SHIMODE, S. & KIKUCHI, T. 2008b. Growth of dinoflagellates, *Ceratium furca* and *Ceratium fusus* in Sagami Bay, Japan: The role of temperature, light intensity and photoperiod. *Harmful Algae,* 7**,** 163-173.

BAEK, S. H., SHIMODE, S., SHIN, K., HAN, M.-S. & KIKUCHI, T. 2009. Growth of dinoflagellates, *Ceratium furca* and *Ceratium fusus* in Sagami Bay, Japan: The role of vertical migration and cell division. *Harmful Algae,* 8**,** 843-856.

BAINES, S. B., TWINING, B. S., BRZEZINSKI, M. A., KRAUSE, J. W., VOGT, S., ASSAEL, D. & MCDANIEL, H. 2012. Significant silicon accumulation by marine picocyanobacteria. *Nature Geoscience Letters,* 5**,** 886-891.

BAINES, S. B., TWINING, B. S., BRZEZINSKI, M. A., NELSON, D. M. & FISHER, N. S. 2010. Causes and biogeochemical implications of regional differences in silicification of marine diatoms. *Global Biogeochemical Cycles,* 24**,** doi:10.1029/2010GB003856.

BAKER, N. R. 2008. Chlorophyll fluorescence: A probe of photosynthesis *in vivo*. *Annual Review of Plant Biology,* 59**,** 89-113.

BANSE, K. 1982. Cell volumes, maximal growth rates of unicellular algae and ciliates, and the role of ciliates in the marine pelagial. *Limnology and Oceanography,* 27**,** 1059-1071.

BANSE, K. 1987. Clouds, deep chlorophyll maxima and the nutrient supply to the mixed layer of stratified water bodies. *Journal of Plankton Research,* 9**,** 1031-1036.

BARLOW, R. G., CUMMINGS, D. G. & GIBB, S. W. 1997. Improved resolution of mono- and divinyl chlorophylls a and b and zeaxanthin and lutein in phytoplankton extracts using reverse phase C-8 HPLC. *Marine Ecology Progress Series,* 161**,** 303-307.

BARNES, M. K., TILSTONE, G. H., SMYTH, T. J., SUGGETT, D. J., ASTORECA, R., LANCELOT, C. & KROMKAMP, J. C. 2014. Absorption-based algorithm of primary production for total and size-fractionated phytoplankton in coastal waters. *Marine Ecology Progress Series,* 504**,** 73-89.

BARNES, M. K., TILSTONE, G. H., SMYTH, T. J., WIDDICOMBE, C. E., GLOËL, J., ROBINSON, C., KAISER, J. & SUGGETT, D. J. 2015a. Drivers and effects of *Karenia mikimotoi* blooms in the western English Channel. *Progress in Oceanography,* 137**,** 456-469.

BARNES, M. K., TILSTONE, G. H., SUGGETT, D. J., WIDDICOMBE, C. E., BRUUN, J., MARTINEZ-VICENTE, V. & SMYTH, T. J. 2015b. Temporal variability in total, micro- and nano-phytoplankton primary production at a coastal site in the Western English Channel. *Progress in Oceanography,* 137**,** 470-483.

BATES, N. 2018. Bermuda Atlantic Time-series observations 1988-2016: primary production. Bermuda Institute of Ocean Sciences.

BEARDALL, J., ALLEN, D., BRAGG, J., FINKEL, Z. V., FLYNN, K. J., QUIGG, A., REES, T. A. V., RICHARDSON, A. & RAVEN, J. A. 2009. Allometry and stoichiometry of unicellular, colonial and multicellular phytoplankton. *New Phytologist,* 181**,** 295-309.

BEAUGRAND, G. 2005. Monitoring pelagic ecosystems using plankton indicators. *ICES Journal of Marine Science,* 62**,** 333-338.

BEAUGRAND, G., IBANEZ, F. & REID, P. C. 2000. Spatial, seasonal and long-term fluctuations of plankton in relation to hydroclimatic features in the English Channel, Celtic Sea and Bay of Biscay. *Marine Ecology Progress Series,* 200**,** 93-102.

BEAUGRAND, G. & REID, P. C. 2003. Long-term changes in phytoplankton, zooplankton and salmon related to climate. *Global Change Biology,* 9**,** 801-817.

BEER, T. 1983. *Environmental Oceanography: An Introduction to the Behaviour of Coastal Waters*, Pergamon Press.

BEGLEY, I. 2016. *RE: DIC in the Western English Channel June/July 2008-2014.*

BENOIT-BIRD, K. J., COWLES, T. J. & WINGARD, C. E. 2009. Edge gradients provide evidence of ecological interactions in planktonic thin layers. *Limnology and Oceanography,* 54**,** 1382-1392.

BENOIT-BIRD, K. J. & MCMANUS, M. A. 2012. Bottom-up regulation of a pelagic community through spatial aggregations. *Biology Letters,* 8**,** 813-816.

BENOIT-BIRD, K. J., MOLINE, M. A., WALUK, C. M. & ROBBINS, I. C. 2010. Integrated measurements of acoustical and optical thin layers I: vertical scales of association. *Continental Shelf Research,* 30**,** 17-28.

BERNER, T., DUBINSKY, Z., WYMAN, K. & FALKOWSKI, P. G. 1989. Photoadaptation and the package effect in *Dunaliella-Tertiolecta* (Chlorophyceae). *Journal of Phycology,* 25**,** 70-78.

BHAT, S. R., DEVI, P., D'SOUZA, L., VERLECAR, X. N. & NAIK, C. G. 2006. Harmful algal blooms. *In:* SONAK, S. (ed.) *Multiple Dimensions of Global Environmental Change.* India: TERI Press.

BIBBY, T. S., GORBUNOV, M. Y., WYMAN, K. W. & FALKOWSKI, P. G. 2008. Photosynthetic community responses to upwelling in mesoscale eddies in the subtropical North Atlantic and Pacific Oceans. *Deep-Sea Research II,* 55**,** 1310-1320.

BILLET, D. S. M., LAMPITT, R. S., RICE, A. L. & MANTOURA, R. F. C. 1983. Seasonal sedimentation of phytoplankton to the deep sea benthos. *Nature,* 302**,** 520-522.

BINDOFF, N. L., WILLEBRAND, J., ARTALE, V., CAZENAVE, A., GREGORY, J., GULEV, S., HANAWA, K., LE QUERE, C., LEVITUS, S., NOJIRI, Y., SHUM, C. K., TALLEY, L. D. & UNNIKRISHNAN, A. 2007. Observations: Ocean climate change and sea level. *In:* SOLOMON, S., QIN, D., MANNING, M., CHEN, Z., MARQUIS, M., AVERYT, K. B., TIGNOR, M. & MILLER, H. L. (eds.) *Climate Change 2007: The Physical Science Basis.* Cambridge: Cambridge University Press.

BIRCH, D. A., YOUNG, W. R. & FRANKS, P. J. S. 2008. Thin layers of plankton: Formation by shear and death by diffusion. *Deep-Sea Research Part I-Oceanographic Research Papers,* 55**,** 277-295.

BISSETT, W. P., MEYERS, M. B., WALSH, J. J. & MÜLLER-KARGER, F. E. 1994. The effects of temporal variability of mixed layer depth in primary productivity around Bermuda. *Journal of Geophysical Research,* 99**,** 7539-7553.

BISSINGER, J. E., MONTAGNES, D. J. S., SHARPLES, J. & ATKINSON, D. 2008. Predicting marine phytoplankton maximum growth rates from temperature: improving on the Eppley curve using quantile regression. *Limnology and Oceanography,* 53**,** 487-493.

BJÆRKE, O., JONSSON, P. R., ALAM, A. & SELANDER, E. 2015. Is chain length in phytoplankton regulated to evade predation? *Journal of Plankton Research,* 37**,** 1110-1119.

BJØRNSEN, P. K. & NIELSEN, T. G. 1991. Decimeter scale heterogeneity in the plankton during a pycnocline bloom of *Gyrodinium aureolum*. *Marine Ecology Progress Series,* 73**,** 263-267.

BLASCO, D., PACKARD, T. T. & GARFIELD, P. C. 1982. Size dependence of growth rate, respiratory electron transport system activity, and chemical composition in marine diatoms in the laboratory. *Journal of Phycology,* 18**,** 58-63.

BLAUW, A. N., BENINCÀ, E., LAANE, R. W. P. M., GREENWOOD, N. & HUISMAN, J. 2018. Predictability and environmental drivers of chlorophyll fluctuations vary across different time scales and regions of the North Sea. *Progress in Oceanography,* 161**,** 1-18.

BRAY, N. A. & FOFONOFF, N. P. 1981. Available potential energy for MODE eddies. *Journal of Physical Oceanography,* 11**,** 30-46.

BRZEZINSKI, M. A. 1985. The Si:C:N ratio of marine diatoms: interspecific variability and the effect of some environmental variables. *Journal of Phycology,* 21**,** 347-357.

BUCHAN, A., LECLEIR, G. R., GULVIK, C. A. & GONZÁLEZ, J. M. 2014. Master recyclers: features and functions of bacteria associated with phytoplankton blooms. *Nature Reviews Microbiology,* 12**,** 686-698.

BURCHARD, H. & RIPPETH, T. P. 2009. Generation of bulk shear spikes in shallow stratified tidal seas. *Journal of Physical Oceanography,* 39**,** 969-985.

BURY, S. J., OWEN, N. J. P. & PRESTON, T. 1995. ^{13}C and ^{15}N uptake by phytoplankton in the marginal ice zone of the Bellingshausen Sea. *Deep Sea Research Part II: Topical Studies in Oceanography,* 42**,** 1225-1252.

BUSKEY, E. J. 1997. Behavioral components of feeding selectivity of the heterotrophic dinoflagellate *Protoperdinium pellucidum*. *Marine Ecology Progress Series,* 153**,** 77-89.

BUSKEY, E. J., COOULTER, C. & STROM, S. 1993. Locomotory patterns of microzooplankton: potential effects on food selectivity of larval fish. *Bulletin of Marine Science,* 53**,** 29-43.

CABIOCH, L. 1968. Contribution à la connaissance des peuplements benthiques de la Manche occidentale. *Cahiers de Biologie Marine,* 9**,** 493-720.

CALBET, A. 2001. Mesozooplankton grazing impact on primary production: a global comparative analysis in marine ecosystems. *Limnology and Oceanography,* 46**,** 1824-1830.

CALVO-DÍAZ, A., MORAN, X., NOGUEIRA, E., BODE, A. & VARELA, M. 2004. Picoplankton community structure along the northern Iberian continental margin in late winter-early spring. *Journal of Plankton Research,* 26**,** 1069-1081.

CAPOTONDI, A. 2010. ENSO ocean dynamics: Simulation by coupled general circulation models. Climate dynamics: Why does climate vary? *Geophysical Monograph Series,* 189**,** 53-64.

CAPOTONDI, A., ALEXANDER, M. A., BOND, N. A., CURCHITSER, E. N. & SCOTT, J. D. 2012. Enhanced upper ocean stratification with climate change in the CMIP3 models. *Journal of Geophysical Research: Oceans,* 117**,** doi: 10.1029/2011JC007409.

CARTER, R. A., MCMURRAY, H. F. & LARGIER, J. L. 1987. Thermocline characteristics and phytoplankton dynamics in Agulhas Bank waters. *South African Journal of Marine Science,* 5**,** 327-336.

CEMBELLA, A. D. 2003. Chemical ecology of eukaryotic microalgae in marine ecosystems. *Phycologia,* 42**,** 420-447.

CERMEÑO, P., DE VARGAS, C., ABRANTES, F. & FALKOWSKI, P. G. 2010. Phytoplankton biogeography and community stability in the ocean. *PLoS ONE,* 5**,** e10037, doi: 10.1371/journal.pone.0010037.

CHAN, A. T. 1980. Relationship between photosynthesis, growth and carbon/chlorophyll a ratio. *Journal of Phycology,* 16**,** 428-432.

CHERITON, O. M., MCMANUS, M. A., STACEY, M. T. & STEINBUCK, J. V. 2009. Physical and biological controls on the maintenance and dissipation of a thin phytoplankton layer. *Marine Ecology Progress Series,* 378**,** 55-69.

CHESSON, P. 1994. Multispecies competition in variable environments. *Theoretical Population Biology,* 45**,** 227-276.

CHESSON, P. 2008. Quantifying and testing species co-existence mechanisms. *In:* VALLADARES, F., CAMACHO, A., ELOSEGUI, A., ESTRADA, M., GRACIA, C., SENAR, J. C. & GILI, J. M. (eds.) *Unity in Diversity: Reflections on Ecology after the Legacy of Ramon Margalef.* Madrid, Spain: Fundación Banco Bilbao Vizcaya Argentaria.

CHESSON, P., GEBAUER, R. L. E., SCHWINNING, S., HUNTLY, N., WIEGAND, K., ERNEST, S. K. M., SHER, A., NOVOPINSKY, A. & WETZIN, J. F. 2004. Resource pulses, species interactions, and diversity maintenance in arid and semi-arid environments. *Oecologia,* 141**,** 236-253.

CHISHOLM, S. W. 1992. Phytoplankton size. *In:* FALKOWSKI, P. G. & WOODHEAF, A. D. (eds.) *Primary Productivity and Biogeochemical Cycles in the Sea. Plenum.* USA: Springer.

CHISHOLM, S. W., OLSON, R. J., ZETTLER, E. R., GOERICKE, R., WATERBURY, J. & WELSCHMEYER, N. 1988. A novel free-living prochlorophyte abundant in the oceanic euphotic zone. *Letters to Nature,* 334**,** 340-343.

CHURNSIDE, J. H. & DONAGHAY, P. L. 2009. Thin scattering layers observed by airborne lidar. *ICES Journal of Marine Science,* 66**,** 778-789.

CHURNSIDE, J. H. & MARCHBANKS, R. D. 2015. Subsurface plankton layers in the Arctic Ocean. *Geophysical Research Letters,* 42**,** 4896-4902.

CLARKE, K. R. & GORLEY, R. N. 2006. *PRIMER v6: User Manual/ Tutorial,* Plymouth, PRIMER-E.

CLARKE, K. R. & WARWICK, R. M. 2001. *Change in Marine Communities: An approach to statistical analysis and interpretation,* Plymouth, PRIMER-E.

COLLIER, B. D., COX, G. W., JOHNSON, A. W. & MILLER, P. C. 1972. *Dynamic Ecology,* New Jersey, Prentice-Hall.

COLLOS, Y. 1983. Transient situations in nitrate assimilation by marine diatoms. 4. Non-linear phenomena and the estimation of the maximum uptake rate. *Journal of Plankton Research,* 5**,** 677-691.

COLLOS, Y. 2002. Determination of particulate carbon and nitrogen in coastal waters. *In:* SUBBA RAO, D. V. (ed.) *Pelagic Ecology Methodology.* Lisse: Balkema.

CONNELL, J. H. 1978. Diversity in tropical rain forests and coral reefs. *Science,* 199**,** 1302-1310.

CONNELL, J. H. 1979. Tropical rain forests and coral reefs as open non-equilibrium systems. *In:* ANDERSON, R. M., TURNER, B. D. & TAYLOR, L. R. (eds.) *Population Dynamics.* Oxford, UK: Blackwell Scientific.

COON, T. G., LOPEZ, M., RICHERSON, P. J., POWELL, T. M. & GOLDMAN, C. R. 1987. Summer dynamics of the deep chlorophyll maximum in Lake Tahoe. *Journal of Plankton Research,* 9**,** 327-344.

COSGROVE, J. & BOROWITZKA, M. A. 2010. Chlorophyll fluorescence terminology: An introduction. *In:* SUGGETT, D. J., PRÁŠIL, O. & BOROWITZKA, M. A. (eds.) *Chlorophyll a Fluorescence in Aquatic Sciences: Methods and Applications.* Dordrecht, The Netherlands: Springer.

COTE, B. & PLATT, T. 1984. Utility of the light-saturation curve as an operational model for quantifying effects of environmental conditions on phytoplankton photosynthesis. *Marine Ecology Progress Series,* 18**,** 57-66.

COWLES, T. J., DESIDERIO, R. A. & CARR, M. E. 1998. Small-scale planktonic structure: persistence and trophic consequences. *Oceanography,* 111**,** 4-9.

CRAWFORD, D. W. & PURDIE, D. A. 1992. Evidence for avoidance of flushing from an estuary by a planktonic phototrophic ciliate. *Marine Ecology Progress Series,* 79**,** 259-265.

CRUMP, B. C., CORNWELL, J. C. & HEWSON, I. 2011. *Life in the Dead Zone: Microbial respiration, production, diversity and gene expression in seasonally anoxic estuarine waters (NSF-OCE 0961920)* [Online]. http://www.people.vcu.edu/~dylee/projects_LDZ.html. [Accessed 19 May 2017].

CULLEN, J. J. 1982. The deep chlorophyll maximum - comparing vertical profiles of chlorophyll-a. *Canadian Journal of Fisheries and Aquatic Sciences,* 39**,** 791-803.

CULLEN, J. J. 2001. Plankton: Primary production methods. *In:* STEELE, J., THORPE, S. & TUREKIAN, K. (eds.) *Encyclopedia of Ocean Sciences.* San Diego, USA: Academic Press.

CULLEN, J. J. 2015. Subsurface chlorophyll maximum layers: enduring enigma or mystery solved? *Annual Review of Marine Science,* 7**,** 207-239.

CULLEN, J. J. & EPPLEY, R. W. 1981. Chlorophyll maximum layers of the Southern California Bight and possible mechanisms of their formation and maintenance. *Oceanologica Acta,* 4**,** 23-32.

CULLEN, J. J. & HORRIGAN, S. G. 1981. Effects of nitrate on the diurnal vertical migration, carbon to nitrogen ratio, and the photosynthetic capacity of the dinoflagellate *Gymnodinium splendens*. *Marine Biology,* 62**,** 81-89.

CUSHING, D. H. 1989. A difference in structure between ecosystems in strongly stratified waters and in those that are only weakly stratified. *Journal of Plankton Research,* 11**,** 1-13.

CYTOBUOY 2014. CytoSense Manual: Installation, operation and maintenance. The Netherlands: CytoBuoy.

DALE, A. C., LEVINE, M. D., BARTH, J. A. & AUSTIN, J. A. 2006. A dye tracer reveals cross-shelf dispersion and interleaving on the Oregon shelf. *Geophysical Research Letters,* 33**,** L03604, doi:10.1029/2005GL024959.

DAUVIN, J.-C. 2012. Are the eastern and western basins of the English Channel two separate ecosystems? *Marine Pollution Bulletin,* 64**,** 463-471.

DAVY, R., GNATIUK, N., PETTERSSON, L. & BOBYLEV, L. 2017. Climate change impacts on wind energy potential in the European domain with a focus on the Black Sea. *Renewable and Sustainable Energy Reviews***,** doi.org/10.1016/j.rser.2017.05.253.

DE VOOYS, C. G. N. 1979. Primary production in aquatic environments. *In:* BOLIN, B., DEGENS, E. T., KEMPE, S. & KETNER, P. (eds.) *SCOPE 13: The Global Carbon Cycle.* London, UK: Wiley.

DEKSHENIEKS, M. M., DONAGHAY, P. L., SULLIVAN, J. M., RINES, J. E. B., OSBORN, T. R. & TWARDOWSKI, M. S. 2001. Temporal and spatial occurrence of thin phytoplankton layers in relation to physical processes. *Marine Ecology Progress Series,* 223**,** 61-71.

DENNY, M. W. 1993. *Air and Water: The Biology and Physics of Life's Media,* Princeton, Princeton University Press.

DODGE, J. D. 1981. *Provisional Atlas of the Marine Dinoflagellates of the British Isles,* Institute of Terrestrial Ecology, Monks Wood Experimental Station, Huntingdon, Biological Records Centre.

DODGE, J. D. & MARSHALL, H. G. 1994. Biogeographic analysis of the armored planktonic dinoflagellate *Ceratium* in the North Atlantic and adjacent seas. *Journal of Phycology,* 30**,** 905-922.

DONAGHAY, P. L. & OSBORN, T. R. 1997. Toward a theory of biological-physical control of harmful algal bloom dynamics and impacts. *Limnology and Oceanography,* 42**,** 1283-1296.

DONAGHAY, P. L., RINES, H. M. & SIEBURTH, J. M. 1992. Simultaneous sampling of fine scale biological, chemical, and physical structure in stratified waters. *Archiv für Hydrobiologie Beiheft, Ergebnisse der Limnologie,* 36**,** 97-108.

DONAGHAY, P. L. & RYAN, J. 2012. Case study: thin layers. California, USA: MBARI.

DORE, J. E., HOULIHAN, T., HEBEL, D. V., TIEN, G., TUPAS, L. & KARL, D. M. 1996. Freezing as a method of sample preservation for the analysis of dissolved inorganic nutrients in seawater. *Marine Chemistry,* 53**,** 173-185.

DORTCH, Q. 1982. Effect of growth-conditions on accumulation of internal nitrate, ammonium, amino-acids, and protein in three marine diatoms. *Journal of Experimental Marine Biology and Ecology,* 61**,** 243-264.

DORTCH, Q. 1990. The interaction between ammonium and nitrate uptake in phytoplankton. *Marine Ecology Progress Series,* 61**,** 183-201.

DOWNES-TETTMAR, N., ROWLAND, S., WIDDICOMBE, C., WOODWARD, M. & LLEWELLYN, C. 2013. Seasonal variation in *Pseudo-nitzschia spp.* and domoic acid in the Western English Channel. *Continental Shelf Research,* 53**,** 40-49.

DROOP, M. R. 1977. An approach to quantitative nutrition of phytoplankton. *Journal of Eukaryotic Microbiology,* 24**,** 528-532.

DU, X., PETERSON, W., FISHER, J., HUNTER, M. & PETERSON, J. 2016. Initiation and development of a toxic and persistent *Pseudo-nitzschia* bloom off the Oregon coast in spring/summer 2015. *PLoS One,* 11**,** doi:10.1371/journal.pone.0163977.

DUBINSKY, Z., FALKOWSKI, P. G. & WYMAN, K. 1986. Light harvesting and utilisation by phytoplankton. *Plant Cell Physiology,* 27**,** 1335-1349.

DUGDALE, R. C. & GOERING, J. J. 1967. Uptake of new and regenerated forms of nitrogen in primary productivity. *Limnology and Oceanography,* 12**,** 196-206.

DUGDALE, R. C. & WILKERSON, F. P. 1986. The use of ^{15}N to measure nitrogen uptake in eutrophic oceans; experimental considerations. *Limnology and Oceanography,* 31**,** 673-690.

DUGDALE, R. C. & WILKERSON, F. P. 1998. Silicate regulation of new production in the equatorial Pacific upwelling. *Nature,* 391**,** 270-273.

DURHAM, W. M., KESSLER, J. O. & STOCKER, R. 2009. Disruption of vertical motility by shear triggers formation of thin phytoplankton layers. *Science,* 323**,** 1067-1070.

DURHAM, W. M. & STOCKER, R. 2012. Thin phytoplankton layers: Characteristics, mechanisms, and consequences. *Annual Review of Marine Science,* 4**,** 177-207.

EPPLEY, R. W. 1972. Temperature and phytoplankton growth in the sea. *Fishery Bulletin,* 70**,** 1063-1085.

EPPLEY, R. W., HOLM-HARISEN, O. & STRICKLAND, J. D. H. 1968. Some observations of the vertical migration of dinoflagellates. *Journal of Phycology,* 4**,** 333-340.

ERGA, S. R., LIE, G. C., AARO, L. H., FRETTE, O. & HAMRE, B. 2015. Migratory behaviour of *Skeletonema grethae* (Bacillariophyceae) in stratified waters. *Diatom Research,* 30**,** 13-25.

ESLINGER, D. L. & IVERSON, R. L. 2001. The effects of convective and wind-driven mixing on spring phytoplankton dynamics in the Southeastern Bering Sea middle shelf domain. *Continental Shelf Research,* 21**,** 627-650.

ESTRADA, M. 1996. Primary production in the northwestern Mediterranean. *Scientia Marina,* 60**,** 55-64.

ESTRADA, M., MARRASÉ , C., LATASA, M., BERDALET, E., DELGADO, M. & RIERA, T. 1993. Variability of deep chlorophyll maximum characteristics in the Northwestern Mediterranean. *Marine Ecology Progress Series,* 92**,** 289-300.

FALKOWSKI, P. G. 2000. Rationalizing elemental ratios in unicellular algae. *Journal of Phycology,* 36**,** 3-6.

FALKOWSKI, P. G. 2012. Ocean science: the power of plankton. *Nature,* 483**,** S17-S20.

FALKOWSKI, P. G., BARBER, R. T. & SMETACEK, V. 1998. Biogeochemical controls and feedbacks on ocean primary production. *Science,* 281**,** 200-206.

FALKOWSKI, P. G., KATZ, M. E., KNOLL, A. H., QUIGG, A., RAVEN, J. A., SCHOFIELD, O. & TAYLOR, F. J. R. 2004. The evolution of modern eukaryotic phytoplankton. *Science,* 305**,** 354-360.

FALKOWSKI, P. G. & OLIVER, M. J. 2007. Mix and match: how climate selects phytoplankton. *Nature Reviews Microbiology,* 5**,** 813-819.

FALKOWSKI, P. G. & OWENS, T. G. 1980. Light shade adaptation: two strategies in marine phytoplankton. *Plant Physiology,* 66**,** 632-635.

FALKOWSKI, P. G. & RAVEN, J. A. 1997. *Aquatic Photosynthesis,* UK, Blackwell Science.

FARRANT, G. K., DORÉ, H., CORNEJO-CASTILLO, F. M., PARTENSKY, F., RATIN, M., OSTROWSKI, M., PITT, F. D., WINCKER, P., SCANLAN, D. J., IUDICONE, D., ACINAS, S. G. & GARCZAREK, L. 2016. Delineating ecologically significant taxonomic units from global patters of marine picocyanobacteria. *PNAS,* 113**,** E3365-E3374.

FASHAM, M. J. R., PLATT, T., IRWIN, B. & JONES, K. 1985. Factors affecting the spatial pattern of the deep chlorophyll maximum in the region of the Azores Front. 14**,** 129-165.

FENCHEL, T. 2008. The microbial loop - 25 years later. *Journal of Experimental Marine Biology and Ecology,* 366**,** 99-103.

FENNEL, K. & BOSS, E. 2003. Subsurface maxima of phytoplankton and chlorophyll: steady-state solutions from a simple model. *Limnology and Oceanography,* 48**,** 1521-34.

FERNAND, L., WESTON, K., MORRIS, T., GREENWOOD, N., BROWN, J. & JICKELLS, T. 2013. The contribution of the deep chlorophyll maximum to primary production in a seasonally stratified shelf sea, the North Sea. *Biogeochemistry,* 113**,** 153-166.

FERNANDO, H. J. S. 1991. Turbulent mixing in stratified fluids. *Annual Review of Fluid Mechanics,* 23**,** 455-493.

FIEDLER, R. & PROKSCH, G. 1975. The determination of nitrogen-15 by emission and mass spectrometry in biochemical analysis: a review. *Analytica chimica acta,* 78**,** 1-62.

FIELD, C., BEHRENFELD, M., RANDERSON, J. & FALKOWSKI, P. 1998. Primary production of the biosphere: integrating terrestrial and oceanic components. *Science,* 281**,** 237-240.

FINKEL, Z. V., BEARDALL, J., FLYNN, K. J., QUIGG, A., REES, T. A. V. & RAVEN, J. A. 2010. Phytoplankton in a changing world: cell size and elemental stoichiometry. *Journal of Plankton Research,* 32**,** 119-137.

FINKEL, Z. V., IRWIN, A. J. & SCHOFIELD, O. 2004. Resource limitation alters the 3/4 size scaling of metabolic rates in phytoplankton. *Marine Ecology Progress Series,* 273**,** 269-279.

FISHER, G. 2018. *RE: RV Callista ADCP maximum profiling range.* Type to BARNETT, M. L.

FISHER, T. R., CARLSON, P. R. & BARBER, R. T. 1981. Some problems in the interpretation of ammonium uptake kinetics. *Marine Biology Letters,* 2**,** 33-44.

FISHWICK, J. R. 2017. CTD profiles (depth, pressure, temperature, salinity, potential temperature, density, fluorescence, transmissance, downwelling PAR, dissolved oxygen concentration) binned to 0.5 m and 0.25 m at sites L4 and E1 in the Western English Channel between January 2002 and December 2016. British Oceanographic Data Centre - Natural Environment Research Council UK.

FLOMBAUM, P., GALLEGOS, J. L., GORDILLO, R. A., RINCÓN, J., ZABALA, L. L., JIAO, N., KARL, D. M., LI, W. K. W., LOMAS, M. W., VENEZIANO, D., VERA, C.S., VRUGT, J. A. & MARTINY, A. C. 2013. Present and future global distributions of the marine Cyanobacteria *Prochlorococcus* and *Synechococcus*. *PNAS,* 110**,** 9824-9829.

FOLLOWS, M. J., DUTKIEWICZ, S., GRANT, S. & CHISHOLM, S. W. 2007. Emergent biogeography of microbial communities in a model ocean. *Science,* 315**,** 1843-1846.

FRAGOSO, G. M., POULTON, A. J., YASHAYAEV, I. M., HEAD, E. J. H. & PURDIE, D. A. 2017. Spring phytoplankton communities of the Labrador Sea (2005-2014): pigment signatures, photophysiology and elemental ratios. *Biogeosciences,* 14**,** 1235-1259.

FUJIKI, T. & SATOTU, T. 2002. Variability in chlorophyll a specific absorption coefficient in marine phytoplankton as a function of cell size and irradiance. *Journal of Plankton Research,* 24**,** 859-874.

FURNAS, M. J. 1982. An evaluation of two diffusion culture techniques for estimating phytoplankton growth rates *in situ*. *Marine Biology,* 70**,** 63-72.

FURNAS, M. J. 1990. *In situ* growth rates of marine phytoplankton: approaches to measurement, community and species growth rates. *Journal of Plankton Research,* 12**,** 1117-1151.

GALLEGOS, C. L., PLATT, T., HARRISON, W. G. & IRWIN, B. 1983. Photosynthetic parameters of arctic marine phytoplankton: vertical variations and time scales of adaptation. *Limnology and Oceanography,* 28**,** 698-708.

GALPERIN, B., SUKORIANSKY, S. & ANDERSON, P. S. 2007. On the critical Richardson number in stably stratified turbulence. *Atmospheric Science Letters,* 8**,** 65-69.

GARCIA, V. M. T. & PURDIE, D. A. 1994. Primary production studies during a *Gyrodinium cf. aureolum* (Dinophyceae) bloom in the western English Channel. *Marine Biology,* 119**,** 297-305.

GARCIA-SOTO, C. & PINGREE, R. D. 2009. Spring and summer blooms of phytoplankton (SeaWiFS/MODIS) along a ferry line in the Bay of Biscay and western English Channel. *Continental Shelf Research,* 29**,** 1111-1122.

GEIDER, R. J. 1988. Estimating the growth and loss rates of phytoplankton from time-series observations of ^{14}-C-bicarbonate uptake. *Marine Ecology Progress Series,* 43**,** 125-138.

GEIDER, R. J., PLATT, T. & RAVEN, J. A. 1986. Size dependence of growth and photosynthesis in diatoms: a synthesis. *Marine Ecology Progress Series,* 30**,** 93-104.

GENTY, B., BRIANTAIS, J. M. & BAKER, N. R. 1989. The relationship between the quantum yield of photosynthesis electron transport and quenching of chlorophyll fluorescence. *Biochimica et Biophysica Acta,* 990**,** 87-92.

GHOSAL, S., ROGERS, M. & WRAY, A. 2000. The turbulent life of phytoplankton. *Center for Turbulence Research, proceedings of the summer program 2000: 31-45.*

GIBB, S. W., CUMMINGS, D. G., IRIGOIEN, X., BARLOW, R. G., FAUZI, R. & MANTOURA, R. F. C. 2001. Phytoplankton pigment chemotaxonomy of the northeastern Atlantic. *Deep Sea Research Part II: Topical Studies in Oceanography,* 48**,** 795-823.

GIBBS, C. F. 1979. Chlorophyll b interference in the fluorometric determination of chlorophyll a and 'phaeopigments'. *Australian Journal of Marine and Freshwater Research,* 30**,** 597-606.

GIESKES, W. W. C., KRAAY, G. W. & BAARS, M. A. 1979. Current ^{14}C methods for measuring primary production: Gross underestimates in oceanic waters. *Netherlands Journal of Sea Research,* 13**,** 58-78.

GOLDMAN, J. C. 1993. Potential role of large oceanic diatoms in new primary production. *Deep-Sea Research,* 40**,** 159-168.

GOLDMAN, J. C. & MCGILLICUDDY, D. J. 2003. Effect of large marine diatoms growing at low light on episodic new production. *Limnology and Oceanography,* 48**,** 1176-1182.

GOMI, Y., FUKUCHI, M. & TANIGUCHI, A. 2010. Diatom assemblages at subsurface chlorophyll maximum layer in the eastern Indian sector of the Southern Ocean in summer. *Journal of Plankton Research,* 32**,** 1039-1050.

GONG, X., SHI, J., GAO, H. W. & YAO, X. H. 2015. Steady-state solutions for subsurface chlorophyll maximum in stratified water columns with a bell-shaped vertical profile of chlorophyll. *Biogeosciences,* 12**,** 905-919.

GORDON, H. R. & CLARK, K. 1980. Remote sensing optical properties of a stratified ocean: An improved intepretation. *Applied Optics,* 19**,** 3428-3430.

GRAFF, J. R. & RYNEARSON, T. A. 2011. Extraction method influences the recovery of phytoplankton pigments from natural assemblages. *Limnology and Oceanography: Methods,* 9**,** 129-139.

GRAHAM, G. W., DAVIES, E. J., NIMMO SMITH, W. A. M., BOWERS, D. G. & BRAITHWAITE, K. M. 2012. Interpreting LISST-100X measurements of particles with complex shape using digital in-line holography. *Journal of Geophysical Research: Oceans,* 117**,** C05034, doi:10.1029/2011JC007613.

GRAHAM, G. W. & NIMMO SMITH, W. A. M. 2010. The application of holography to the analysis of size and settling velocity of suspended cohesive sediments. *Limnology and Oceanography: Methods,* 8**,** 1-15.

GRAHAM, L. & WILCOX, L. 2000. Introduction to the algae - occurrence, relationships, nutrition, definition, general features. *In:* GRAHAM, L. & WILCOX, L. (eds.) *Alage.* New Jersey: Prentice-Hall.

GRASSHOFF, K. 1976. *Methods of Seawater Analysis,* Weinheim, Germany, Verlag Chemie.

GREER, A. T., COWEN, R. K., GUIGAND, C. M., MCMANUS, M. A., SEVADJIAN, J. C. & TIMMERMAN, A. H. V. 2013. Relationships between phytoplankton thin layers and the fine-scale vertical distributions of two trophic levels of zooplankton. *Journal of Plankton Research,* 35**,** 939-956.

GRIBBLE, K. E., NOLAN, G. & ANDERSON, D. M. 2007. Biodiversity, biogeography, and potential trophic impact of *Protoperidinium spp.* (Dinophyceae) off the southwestern coast of Ireland. *Journal of Plankton Research,* 29**,** 931-947.

GRÉBERT, T., DORÉ, H., PARTENSKY, F., FARRANT, G. K., BOSS, E. S., PICHERAL, M., GUIDI, L., PESANT, S., SCANLAN, D. J., WINCKER, P., ACINAS, S. G., KEHOE, D. M. & GARCZAREK, L. 2018. Light color acclimation is a key process in the global ocean distribution of *Synechococcus* cyanobacteria. *PNAS,* 115**,** E2010-E2019.

GÓMEZ, F. 2012. A quantitative review of the lifestyle, habitat and trophic diversity of dinoflagellates (Dinoflagellata, Alveolata). *Systematics and Biodiversity,* 10**,** 267-275.

HALL, J. A. 1991. Long-term preservation of picophytoplankton for counting by fluorescence microscopy. *British Phycological Journal,* 26**,** 169-174.

HAMA, T., MIYAZAKI, T., OGAWA, Y., IWAKUMA, T., TUKAHASHI, M., OTSUKI, A. & ICHIMURA, S. 1983. Measurement of photosynthetic production of a marine phytoplankton population using a stable ^{13}C isotope. *Marine Biology,* 73**,** 31-36.

HAMM, C. & SMETACEK, V. 2007. Armor: Why, when, how. *In:* FALKOWSKI, P. G. & KNOLL, A. H. (eds.) *Evolution of Primary Producers in the Sea.* Burlington, USA: Elsevier.

HAMM, C. E., MERKEL, R., SPRINGER, O., JURKOJC, P., MAIER, C., PRECHTEL, K. & SMETACEK, V. 2003. Architecture and material properties of diatom shells provide effective mechanical protection. *Nature,* 421**,** 841-843.

HANSEN, P. J. 1991. *Dinophysis* - a planktonic dinoflagellate genus which can act both as a prey and predator of ciliate. *Marine Ecology Progress Series,* 69**,** 201-204.

HANSEN, P. J. 1992. Prey size selection, feeding rates and growth dynamics of heterotrophic dinoflagellates with special emphasis on *Gyrodinium spirale*. *Marine Biology,* 114**,** 327-334.

HARDING, L. W. J., MEESON, B. W. & FISHER, T. R. J. 1986. Phytoplankton production in two east coast estuaries: photosynthesis-light functions and patterns of carbon assimilation in Chesapeake and Delware Bays. *Estuarine, Coastal and Shelf Science,* 23**,** 773-806.

HARRIS, R. 2010. The L4 time-series: The first 20 years. *Journal of Plankton Research,* 32**,** 577-583.

HEALEY, F. P. 1978. Physiological indicators of nutrient deficiency in algae. *Mitteilungen der Internationale Vereinigung für Theoretische und Angewandte Limnologie,* 21**,** 34-41.

HEATH, M. R. & BEARE, D. J. 2008. New primary production in northwest European shelf seas, 1960-2003. *Marine Ecology Progress Series,* 363**,** 183-203.

HEINRICH, A. K. 1962. The life histories of plankton animals and seasonal cycles of plankton communities in the ocean. *Journal du Conseil Permanent International pour l'Exploration de la mer,* 27**,** 15-24.

HEMMINGSEN, A. M. 1960. Energy metabolism as related to body size and respiratory surfaces, and its evolution. *Reports of the Steno Memorial Hospital,* 9**,** 15-22.

HEMSLEY, V. S., SMYTH, T. J., MARTIN, A. P., FRAJKA-WILLIAMS, E., THOMPSON, A. F., DAMERELL, G. & PAINTER, S. 2015. Estimating oceanic primary production using vertical irradiance and chlorophyll profiles from ocean gliders in the North Atlantic. *Environmental Science and Technology,* 49**,** 11612-11621.

HERBERT, D., ELSWORTH, R. & TELLING, R. C. 1956. The continuous culture of bacteria: a theoretical and experimental study. *Journal of General Microbiology,* 14**,** 601-622.

HICKMAN, A. E., HOLLIGAN, P. M., MOORE, C. M., SHARPLES, J., KRIVTSOV, V. & PALMER, M. R. 2009. Distribution and chromatic adaptation of phytoplankton within a shelf sea thermocline. *Limnology and Oceanography,* 54**,** 525-536.

HICKMAN, A. E., MOORE, C. M., SHARPLES, J., LUCAS, M. I., TILSTONE, G. H., KRIVTSOV, V. & HOLLIGAN, P. M. 2012. Primary production and nitrate uptake within the seasonal thermocline of a stratified shelf sea. *Marine Ecology Progress Series,* 463**,** 39-57.

HOLLIDAY, D. V., PIEPER, R. E., GREENLAW, C. F. & DAWSON, J. K. 1998. Acoustical sensing of small scale vertical structures in zooplankton assemblages. *Oceanography,* 11**,** 18-23.

HOLLIGAN, P. M., BALCH, W. M. & YENTSCH, C. M. 1984a. The significance of subsurface chlorophyll, nitrite and ammonium maxima in relation to nitrogen for phytoplankton growth in stratified waters of the Gulf of Maine. *Journal of Marine Research,* 42**,** 1051-1073.

HOLLIGAN, P. M. & HARBOUR, D. S. 1977. The vertical distribution and succession of phytoplankton in the western English channel in 1975 and 1976. *Journal of the Marine Biological Association of the UK,* 57**,** 1075-1093.

HOLLIGAN, P. M., HARRIS, R. P., NEWELL, R. C., HARBOUR, D. S., HEAD, R. N., LINLEY, E. A. S., LUCAS, M. I., TRANTER, P. R. G. & WEEKLEY, C. M. 1984b. Vertical distribution and partitioning of organic carbon in mixed, frontal and stratified waters of the English Channel. *Marine Ecology Progress Series,* 14**,** 111-127.

HOLLIGAN, P. M., MADDOCK, L. & DODGE, J. D. 1980. The distribution of dinoflagellates around the British Isles in July 1977: a multivariate analysis. *Journal of the Marine Biological Association, UK,* 60**,** 851-867.

HOLLIGAN, P. M., VIOLLIER, M., DUPOUY, C. & AIKEN, J. 1983. Satellite studies on the distributions of chlorophyll and dinoflagellate blooms in the western English Channel. *Continental Shelf Research,* 2**,** 81-96.

HOLLIGAN, P. M., WILLIAMS, P. J. L., PURDIE, D. & HARRIS, R. P. 1984c. Photosynthesis, respiration and nitrogen supply of plankton populations in stratified, frontal and tidally mixed shelf waters. *Marine Ecology Progress Series,* 17**,** 201-213.

HOLM-HANSEN, O. & HEWES, C. D. 2004. Deep chlorophyll-a maxima (DCMs) in Antarctic waters - I. Relationships between DCMs and the physical, chemical, and optical conditions in the upper water column. *Polar Biology,* 27**,** 699-710.

HOLMES, J. J., WEGER, H. G. & TURPIN, D. H. 1989. Chlorophyll a florescence predicts total photosynthetic electron flow to CO_2 or NO_3^-/NO_2^- under transient conditions. *Plant Physiology,* 91**,** 3311-337.

HOLMES, R. M., AMINOT, A., KÉROUEL, R., HOOKER, B. A. & PETERSON, B. J. 1999. A simple and precise method for measuring ammonium in marine and freshwater ecosystems. *Canadian Journal of Fisheries and Aquatic Sciences,* 56**,** 1801-1808.

HOLT, J., BUTENSCHÖN, M., WAKELIN, S. L., ARTIOLI, Y. & ALLEN, J. I. 2012. Oceanic controls on the primary production of the northwest European continental shelf: Model experiments under recent past conditions and a potential future scenario. *Biogeosciences,* 9**,** 97-117.

HOLT, J., SCHRUM, C., CANNABY, H., DAEWEL, U., ALLEN, I., ARTIOLI, Y., BOPP, L., BUTENSCHON, M., FACH, B. A., HARLE, J., PUSHPADAS, D., SALIHOGLU, B. & WAKELIN, S. 2016. Potential impacts of climate change on the primary production of regional seas: A comparative analysis of five European seas. *Progress in Oceanography,* 140**,** 91-115.

HOLT, J., WAKELIN, S., LOWE, J. & TINKER, J. 2010. The potential impacts of climate change on the hydrography of the northwest European continental shelf. *Progress in Oceanography,* 86**,** 361-379.

HONJO, S., MANGANINI, S. J., KRISHFIELD, R. A. & FRANCOIS, R. 2008. Particulate organic carbon fluxes to the ocean interior and factors controlling the biological pump: A synthesis of global sediment trap programs since 1983. *Progress in Oceanography,* 76**,** 217-285.

HOPPENRATH, M., ELBRÄCHTER, M. & DREBES, G. 2009. *Marine Phytoplankton,* Stuttgart, Kleine Senckenberg-Reihe.

HOWARD, J., BABIJ, E., GRIFFIS, R., HELMUTH, B., HIMES-CORNELL, A., NIEMIER, P., ORBACH, M., PETES, L., ALLEN, S., AUAD, G., AUER, C., BEARD, R., BOATMAN, M., BOND, N., BOYER, T., BROWN, D., CLAY, P., CRANE, K., CROSS, S., DALTON, M., DIAMOND, J., DIAZ, R., DORTCH, Q., DUFFY, E., FRAUQUIER, D., FISHER, W., GRAHAM, M., HALPERN, B., HANSEN, L., HAYUM, B., HERRICK, S., HOLLOWED, A., HUTCHINS, D., JEWETT, E., JIN, D., KNOWLTON, N., KOTOWICZ, D., KRISTIANSEN, T., LITTLE, P., LOPEZ, C., LORING, P., LUMPKIN, R., MACE, A., MENGERINK, K., MORRISON, J. R., MURRAY, J., NORMAN, K., O'DONNELL, J., OVERLAND, J., PARSONS, R., PETTIGREW, N., PFEIFFER, L., PIDGEON, E., PLUMMER, M., POLOVINA, J., QUINTRELL, J., ROWLES, T., RUNGE, J., RUST, M., SANFORD, E., SEND, U., SINGER, M., SPEIR, C., STANITSKI, D., THORNBER, C., WILSON, C. & XUE, Y. 2013. Oceans and marine resources in a changing climate. *In:* HUGHES, R. N., HUGHES, D. J. & SMITH, I. P. (eds.) *Oceanography and Marine Biology: An Annual Review.* Boca Raton, USA: CRC Press.

HUISMAN, J., THI, N. N. P., KARL, D. M. & SOMMEIJER, B. 2006. Reduced mixing generates oscillations and chaos in the oceanic deep chlorophyll maximum. *Nature,* 439**,** 322-325.

HUTCHINSON, G. E. 1961. The paradox of the plankton. *The American Naturalist,* 95**,** 137-145.

IRIGOIEN, X., HARRIS, R. P., HEAD, R. N. & HARBOUR, D. 2000. North Atlantic Oscillation and spring bloom phytoplankton composition in the English Channel. *Journal of Plankton Research,* 22**,** 2367-2371.

IRIGOIEN, X., HUISMAN, J. & HARRIS, R. P. 2004. Global biodiversity patterns of marine phytoplankton and zooplankton. *Letters to Nature,* 429**,** 863-867.

JAHNKE, R. A. 2010. Global synthesis. *In:* LIU, K. K., ATKINSON, L., QUINONES, R. A. & TALAUE-MCMANUS, L. (eds.) *Carbon and Nutrient Fluxes in Continental Margins: A Global Synthesis.* Berlin: Springer-Verlag.

JANG, P.-G., SHIN, H. H., BAEK, S. H., JANG, M. C., LEE, T. S. & SHIN, K. 2013. Nutrient distribution and effects on phytoplankton assemblages in the western Korea/Tsushima Strait. *New Zealand Journal of Marine and Freshwater Research,* 47**,** 21-37.

JANZEN, C. 2012. *SBE data processing software, manual,* Washington, USA, SeaBird Electronics.

JASSBY, A. D. & PLATT, T. 1976. Mathematical formulation of the relationship between photosynthesis and light for phytoplankton. *Limnology and Oceanography,* 21**,** 540-547.

JEFFREY, S. W. & HUMPHREY, G. F. 1975. New spectrophotometric equations for determining chlorophylls a, b, c1 and c2 in higher plants, algae and natural phytoplankton. *Biochemie und Physiologie der Pflanzen BPP,* 167**,** 191-194.

JEFFREY, S. W. & VESK, M. 1997. Introduction to marine phytoplankton and their pigment signatures. *In:* JEFFREY, S. W., MANTOURA, R. F. & WRIGHT, S. W. (eds.) *Phytoplankton pigments in oceanography: guidelines to modern methods.* Paris: UNESCO Publishing.

JIAO, N., HERNDL, G. J., HANSELL, D. A., BENNER, R., KATTNER, G., WILHELM, S. W., KITCHMAN, D. L., WEINBAUER, M. G., LUO, T., CHEN, F. & AZAM, F. 2010. Microbial production of recalcitrant dissolved organic matter: long-term carbon storage in the global ocean. *Nature Reviews Microbiology,* 8**,** 593-599.

JIN, X., GRUBER, N., DUNNE, J. P., SARMIENTO, J. L. & ARMSTRONG, R. A. 2006. Diagnosing the contribution of phytoplankton functional groups to the production and export of particulate organic carbon, $CaCO_3$, and opal from global nutrient and alkalinity distributions. *Global Biogeochemical Cycles,* 20**,** GB2015, doi:10.1029/2005GB002532.

JOHNS, D. G. & REID, P. C. 2001. Technical report TR_005: An overview of plankton ecology in the North Sea. *Strategic Environmental Assessment - SEA2.* Plymouth, UK: SAHFOS.

JOINT, I. & GROOM, I. 2000. Estimation of phytoplankton production from space: current status and future potential of satellite remote sensing. *Journal of Experimental Marine Biology and Ecology,* 250**,** 233-255.

JOINT, I. R., OWENS, N. J. P. & POMROY, A. J. 1986. Seasonal production of photosynthetic picoplankton and nanoplankton in the Celtic Sea. *Marine Ecology Progress Series,* 28**,** 251-258.

JONES, A. R., HOSEGOOD, P., WYNN, R. B., DE BOER, M. N., BUTLER-COWDRY, S. & EMBLING, C. B. 2014. Fine-scale hydrodynamics influence the spatio-temporal distribution of harbour porpoises at a coastal hotspot. *Progress in Oceanography,* 128**,** 30-48.

KAMENIR, Y., DUBINSKY, Z. & HARRIS, R. 2010. Taxonomic size structure consistency of the English Channel phytoplankton. *Journal of Experimental Marine Biology and Ecology,* 383**,** 105-110.

KAMYKOWSKI, D. & MCCOLLUM, S. A. 1986. The temperature acclimatised swimming speed of selected marine dinoflagellates. *Journal of Plankton Research,* 8**,** 275-287.

KAMYKOWSKI, D., MCCOLLUM, S. A. & KIRKPATRICK, G. J. 1989. A comparison of the environmentally modulated swimming behaviour of several photosynthetic marine dinoflagellates. *In:* OKAICHI, T., ANDERSON, D. M. & NEMOTO, T. (eds.) *Red Tides: Environmental Science and Toxicology.* Amsterdam: Elsevier.

KAMYKOWSKI, D., REED, R. E. & KIRKPATRICK, G. J. 1992. Comparison of sinking velocity, swimming velocity, rotation and path characteristics among six marine dinoflagellate species. *Marine Biology,* 113**,** 319-328.

KATANO, T., YOSHIDA, M., LEE, J., HAN, M.-S. & HAYAMI, Y. 2009. Fixation of *Chattonella antiqua* and *C. marina* (Raphidophyceae) using Hepes-buffered paraformaldehyde and glutaraldehyde for flow cytometry and light microscopy. *Phycologia,* 48**,** 473-479.

KATZ, J., DONAGHAY, P. L., ZHANG, J., KING, S. & RUSSELL, K. 1999. Submersible holocamera for detection of particle characteristics and motions in the ocean. *Deep-Sea Research I,* 46**,** 1455-1481.

KEMP, A. E. S., PEARCE, R. B., GRIGOROV, I., RANCE, J., LANGE, C. B., QUILTY, P. & SALTER, I. 2006. Production of giant marine diatoms and their export at oceanic frontal zones: Implications for Si and C flux from stratified oceans. *Global Biogeochemical Cycles,* 20**,** GB4S04 doi:10.1029/2006GB002698.

KEMP, A. E. S., PIKE, J., PEARCE, R. B. & LANGE, C. B. 2000. The "Fall dump" - a new perspective on the role of a "shade flora" in the annual cycle of diatom production and export flux. *Deep-Sea Research Part II: Topical Studies in Oceanography,* 47**,** 2129-2154.

KEMP, A. E. S. & VILLAREAL, T. A. 2013. High diatom production and export in stratified waters – A potential negative feedback to global warming. *Progress in Oceanography,* 119**,** 4-23.

KIRK, J. T. O. 1994. *Light and Photosynthesis in Aquatic Ecosystems,* Cambridge, Cambridge University Press.

KIRKWOOD, D. 1996. Nutrients: Practical notes on their determination in seawater. *ICES Techniques in Marine Environmental Sciences No.17.* Copenhagen, Denmark: ICES.

KITIDIS, V., HARDMAN-MOUNTFORD, N. J., LITT, E., BROWN, I., CUMMINGS, D., HARTMAN, S., HYDES, D., FISHWICK, J. R., HARRIS, C., MARTINEZ-VICENTE, V., WOODWARD, E. M. S. & SMYTH, T. J. 2012. Seasonal dynamics of the carbonate system in the Western English Channel. *Continental Shelf Research,* 42**,** 30-40.

KIØRBOE, T. 1993. Turbulence, phytoplankton cell size and the structure of pelagic food webs. *Advances in Marine Biology,* 29**,** 1-61.

KIØRBOE, T., KAAS, H., KRUSE, B., MØHLENBERG, F., TISELIUS, P. & ÆRTEBJERG, G. 1990. The structure of the pelagic food web in relation to water column structure in the Skagerrak. *Marine Ecology Progress Series,* 59**,** 19-32.

KLAUSMEIER, C. A., LITCHMAN, E., DAUFRESNE, T. & LEVIN, S. A. 2008. Phytoplankton stoichometry. *Ecological Research,* 23**,** 479-485.

KLEIBER, M. 1932. Body size and metabolism. *Hilgardia,* 6**,** 315-353.

KOBLÍŽEK, M., KAFTAN, D. & NEDBAL, L. 2001. On the relationship between non-photochemical quenching of chlorophyll fluorescence and the photosystem II harvesting efficiency. A repetitive flash fluorescence induction study. *Photosynthesis Research,* 68**,** 141-152.

KOLBER, Z., ZEHR, J. & FALKOWSKI, P. 1988. Effects of growth irradiance and nitrogen limitation on photosynthetic energy conversion in photosystem II. *Plant Physiology,* 88**,** 923-929.

KONONEN, K., HALLFORS, S., KOKKONEN, M., KUOSA, H., LAANEMETS, J., PAVELSON, J. & AUTIO, R. 1998. Development of a subsurface chlorophyll maximum at the entrance to the Gulf of Finland, Baltic Sea. *Limnology and Oceanography,* 43**,** 1089-1106.

KREMLING, K. & BRÜGMANN, L. 1999. Filtration and storage. *In:* GRASSHOFF, K., KREMLING, K. & EHRHARDT, M. (eds.) *Methods of Seawater Analysis.* Weinheim, Germany: Wiley-VCH.

KROMKAMP, J., BARRANGUET, C. & PEENE, J. 1998. Determination of microphytobenthos PSII quantum efficiency and photosynthetic activity by means of variable chlorophyll fluorescence. *Marine Ecology Progress Series,* 162**,** 45-55.

KROMKAMP, J. C., DIJKMAN, N. A., PEENE, J., SIMIS, S. G. H. & GONS, H. J. 2008. Estimating phytoplankton primary production in Lake Ijsselmeer (The Netherlands) using variable fluorescence (PAM-FRRF) and C-uptake techniques. *European Journal of Phycology,* 43**,** 327-344.

KROMKAMP, J. C. & FORSTER, R. M. 2003. The use of variable fluorescence measurements in aquatic ecosystems: Differences between multiple and single turnover measuring protocols and suggested terminology. *European Journal of Phycology,* 38**,** 103-112.

KWAK, J. H., LEE, S. H., HWANG, J., SUH, Y.-S., PARK, H. J., CHANGE, K.-I., KIM, K.-R. & KANG, C.-K. 2014. Summer primary productivity and phytoplankton community composition driven by different hydrographic structures in the East/Japan Sea and the Western Subarctic Pacific. *Journal of Geophysical Research: Oceans,* 119**,** 4505-4519.

KYEWALYANGA, M. N., PLATT, T., SATHYENDRANATH, S., LUTZ, V. A. & STUART, V. 1998. Seasonal variations in physiological parameters of phytoplankton across the North Atlantic. *Journal of Plankton Research,* 20**,** 17-42.

LALLI, C. M. & PARSONS, T. R. 1997. *Biological Oceanography: An Introduction,* London, Butterworth-Heinemann.

LANDRY, M. R. & CALBET, A. 2004. Microzooplankton production in the oceans. *ICES Journal of Marine Science,* 61**,** 501-507.

LASKER, R. 1975. Field criteria for survival of anchovy larvae: relation between inshore chlorophyll maximum layers and successful first feeding. *Fish Bulletin,* 73**,** 453-462.

LATASA, M., CABELLO, A. M., MORÁN, X. A. G., MASSANA, R. & SCHAREK, R. 2017. Distribution of phytoplankton groups within the deep chlorophyll maximum. *Limnology and Oceanography,* 62**,** 665-685.

LAVAL-PEUTO, M. & RASSOULZADEGAN, F. 1988. Autofluorescence of marine planktonic Oligotrichina and other ciliates. *Hydrobiologia,* 159**,** 99-110.

LAVIN, A., VALDES, L., SANCHEZ, F., ABAUNZA, P., FOREST, A., BOUCHER, J., LAZURE, P. & JEGOU, A.-M. 2006. Chapter 24. The Bay of Biscay: The encountering of the ocean and the shelf. *In:* ROBINSON, A. R. & BRINK, K. H. (eds.) *The Sea.* Cambridge, MA, USA: Harvard University Press.

LAWRENZ, E., SILSBE, G., CAPUZZO, E., YLÖSTALO, P., FORSTER, R. M., SIMIS, S. G. H., PRÁŠIL, O., KROMKAMP, J. C., HICKMAN, A. E., MOORE, C. M., FORGET, M.-H., GEIDER, R. J. & SUGGETT, D. J. 2013. Predicting the electron requirement for carbon fixation in seas and oceans. *PLoS ONE,* 8**,** e58137, doi: 10.1371/journal.pone.0058137.

LAWS, E. A., FALKOWSKI, P. G., SMITH JR, W. O., DUCKLOW, H. & MCCARTHY, J. J. 2000. Temperature effects on export production in the open ocean. *Global Biogeochemical cycles,* 14**,** 1231-1246.

LEAKEY, R. J. G., BURKILL, P. H. & SLEIGH, M. A. 1994. A comparison of fixatives for the estimation of abundance and biovolume of marine planktonic ciliate populations. *Journal of Plankton Research,* 16**,** 375-389.

LEE-FILTERS. no date-a. *LEE-Filters colour filters 061 Mist Blue* [Online]. http://www.leefilters.com/lighting/colour-list.html. [Accessed 16 March 2017].

LEE-FILTERS. no date-b. *LEE-Filters colour filters 131 Marine Blue* [Online]. http://www.leefilters.com/lighting/colour-list.html. [Accessed 16 March 2017].

LEGENDRE, L. & GOSSELIN, M. 1996. Estimation of N or C uptake rates by phytoplankton using ^{15}N or ^{13}C: revisiting the usual computation formulae. *Journal of Plankton Research,* 19**,** 263-271.

LEHANE, L. & LEWIS, R. J. 2000. Ciguatera: recent advances, but the risk remains. *International Journal of Food Microbiology,* 61**,** 91-125.

LEPŠ , J. & ŠMILAUER, P. 2003. *Multivariate Analysis of Ecological Data using CANOCO,* USA, Cambridge University Press.

LEVANDOWSKY, M. & KANETA, P. J. 1987. Behaviour in dinoflagellates. *In:* TAYLOR, F. J. R. (ed.) *The Biology of Dinoflagellates.* Oxford: Blackwell Scientific.

LEWIS, M. R., HARRISON, W. G., OAKEY, N. S., HERBERT, D. & PLATT, T. 1986. Vertical nitrate fluxes in the oligotrophic ocean. *Science,* 234**,** 870-873.

LEWIS, M. R., HORNE, E. P. W., CULLEN, J. J., OAKEY, N. S. & PLATT, T. 1984. Turbulent motions may control phytoplankton photosynthesis in the upper ocean. *Nature,* 311**,** 49-50.

LINDHOLM, T. 1985. *Mesodinium rubrum* - a unique photosynthetic ciliate. *Advances in Aquatic Microbiology,* 3**,** 1-48.

LIPS, U., LIPS, I., LIBLIK, T. & KUVALDINA, N. 2010. Processes responsible for the formation and maintenance of sub-surface chlorophyll maxima in the Gulf of Finland. *Estuarine, Coastal and Shelf Science,* 88**,** 339-349.

LITCHMAN, E. & KLAUSMEIER, C. A. 2008. Trait-Based Community Ecology of Phytoplankton. *Annual Review of Ecology Evolution and Systematics,* 39**,** 615-639.

LITCHMAN, E., KLAUSMEIER, C. A., SCHOFIELD, O. M. & FALKOWSKI, P. G. 2007. The role of functional traits and trade-offs in structuring phytoplankton communities: scaling from cellular to ecosystem level. *Ecology Letters,* 10**,** 1170-1181.

LLEWELLYN, C. A., FISHWICK, J. R. & BLACKFORD, J. C. 2005. Phytoplankton community assemblage in the English Channel: a comparsion using chlorophyll a derived from HPLC-CHEMTAX and carbon derived from microscopy cell counts. *Journal of Plankton Research,* 27**,** 103-119.

LOMAS, M. W., GILBERT, P. M., BERG, G. M. & BURFORD, M. 1996. Characterisation of nitrogen uptake by natural populations of *Aureococcus anophagefferens* (Chrysophyceae) as a function of incubation duration, substrate concentration, light, and temperature. *Journal of Phycology,* 32**,** 907-916.

LONGHURST, A. R. 1998. *Ecological Geography of the Sea,* San Diego, USA, Academic Press.

LOOMIS, N. C. 2011. *Computational imaging and automated identification for aqueous environments.* PhD, Massachusetts Institute of Technology and Wood Hole Oceanographic Institution.

LORENZEN, C. J. 1966. A method for the continuous measurement of *in vivo* chlorophyll concentration. *Deep-Sea Research,* 13**,** 223-227.

LOWE, J. A., HOWARD, T. P., PARDAENS, A., TINKER, J., HOLT, J., WAKELIN, S., MILNE, G., LEAKE, J., WOLF, J., HORSBURGH, K., REEDER, T., JENKINS, G., RIDLEY, J., DYE, S. & BRADLEY, S. 2009. *UK Climate Projections Science Report: Marine and coastal projections,* Exeter, UK, Met Office Hadley Centre.

LUKAS, R. 2018. Hawaii Ocean Time-series observations 1988-2016: primary production. University of Hawaii at Manoa, supported by the U.S. National Science Foundation.

LYMAN, J. M., GOOD, S. A., GOURETSKI, V. V., ISHII, M., JOHNSON, G. C., PALMER, M. D., SMITH, D. M. & WILLIS, J. K. 2010. Robust warming of the global upper ocean. *Nature,* 465**,** 334-337.

LÓPEZ-SANDOVAL, D. C., RODRÍGUEZ-RAMOS, T., CERMEÑO, P., SOBRINO, C. & MARAÑÓN, E. 2014. Photosynthesis and respiration in marine phytoplankton: Relationship with cell size, taxonomic affiliation, and growth phase. *Journal of Experimental Marine Biology and Ecology,* 457**,** 151-159.

LÓPEZ-URRUTIA, A., SAN MARTIN, E., HARRIS, R. P. & IRIGOIEN, X. 2006. Scaling the metabolic balance of the oceans. *Proceedings of the National Academy of Science of the United States of America,* 103**,** 8739-8744.

LÖDER, M. G. J., MEUNIER, C., WILTSHIRE, K. & ABERLE, N. 2011. The role of ciliates, heterotrophic dinoflagellates and copepods in structuring spring plankton communities at Helgoland Roads, North Sea. *Marine Biology,* 158**,** 1551-1580.

MACINTYRE, H. L., KANA, T. M., ANNING, T. & GEIDER, R. J. 2002. Photoacclimation of photosynthesis irradiance response curves and photosynthetic pigments in microalgae and cyanobacteria. *Journal of Phycology,* 38**,** 17-38.

MACINTYRE, J. G., CULLEN, J. J. & CEMBELLA, A. D. 1997. Vertical migration, nutrition and toxicity in the dinoflagellate *Alexandrium tamarense*. *Marine Ecology Progress Series,* 148**,** 201-216.

MACISAAC, J. J. & DUGDALE, R. C. 1972. Interactions of light and inorganic nitrogen in controlling nitrogen uptake in the sea. *Deep Sea Research and Oceanographic Abstracts,* 19**,** 209-232.

MACKENZIE, L. & ADAMSON, J. 2004. Water column stratification and the spatial and temporal distribution of phytoplankton biomass in Tasman Bay, New Zealand: implications for aquaculture. *New Zealand Journal of Marine and Freshwater Research,* 38**,** 705-728.

MACÍAS, D., RODRÍGUEZ-SANTANA, Á., RAMÍREZ-ROMERO, E., BRUNO, M., PELEGRÍ, J. L., SANGRÁ, P., AGUIAR-GONZÁLEZ, B. & GARCÍA, C. M. 2013. Turbulence as a driver for vertical plankton distribution in the subsurface upper ocean. *Scientia Marina,* 74**,** 541-549.

MALKIEL, E., ABRAS, J. N. & KATZ, J. 2004. Automated scanning and measurement of particle distributions within a holographic reconstructed volume. *Measurement Science and Technology,* 15**,** 601-612.

MALKIEL, E., ALQUADDOOMI, O. & KATZ, J. 1999. Measurements of plankton distribution in the ocean using submersible holography. *Measurement Science and Technology,* 10**,** 1142-1152.

MANN, D. G. 1999. The species concept in diatoms. *Phycologia,* 38**,** 437-495.

MANTOURA, R. F. C. & REPETA, D. J. 1997. Calibration methods for HPLC. *In:* JEFFREY, S. W., MANTOURA, R. F. C. & WRIGHT, S. W. (eds.) *Phytoplankton Pigments in Oceanography: Guidelines to Modern Methods.* Paris, France: UNESCO Publishing.

MARAÑÓN, E. 2009. Phytoplankton size structure. *In:* STEELE, J. H. (ed.) *Encyclopedia of Ocean Sciences: Marine Biology.* London: Academic Press.

MARAÑÓN, E. 2015. Cell size as a key determinant of phytoplankton metabolism and community structure. *Annual Review of Marine Science,* 7**,** 241-264.

MARAÑÓN, E., CERMEÑO, P., LÓPEZ-SANDOVAL, D. C., RODRÍGUEZ-RAMOS, T., SOBRINO, C., HUETE-ORTEGA, M., BLANCO, J. M. & RODRÍGUEZ, J. 2013. Unimodal size scaling of phytoplankton growth and the size dependence of nutrient uptake and use. *Ecology Letters,* 16**,** 371-379.

MARAÑÓN, E., LORENZO, M. P., CERMEÑO, P. & MOURIÑO-CARBALLIDO, B. 2018. Nutrient limitation suppresses the temperature dependence of phytoplankton metabolic rates. *The ISME Journal,* 12**,** 1836-1845.

MARCHETTI, A., MALDONADO, M. T., LANE, E. S. & HARRISON, P. J. 2006. Iron requirements of the pennate diatom *Pseudo-nitzschia*: Comparison of oceanic (high-nitrate, low-chlorophyll waters) and coastal species. *Limnology and Oceanography,* 41**,** 2092-2101.

MARCHETTI, A., PARKER, M. S., MOCCIA, L. P., LIN, E. O., ARRIETA, A. L., RIBALET, F., MURPHY, M. E. P., MALDONADO, M. T. & ARMBRUST, E. V. 2009. Ferritin is used for iron storage in bloom-forming marine pennate diatoms. *Nature,* 457**,** 467-470.

MARIE, D., SIMON, N. & VAULOT, D. 2005. Phytoplankton cell counting by flow cytometry. *In:* ANDERSEN, R. A. (ed.) *Algal Culturing Techniques.* USA: Academic Press.

MARRA, J. 2002. Approaches to the measurement of plankton production. *In:* WILLIAMS, P. J. L. B., THOMAS, D. N. & REYNOLDS, C. S. (eds.) *Phytoplankton Productivity: Carbon Assimilation in Marine and Freshwater Ecosystems.* Cambridge: Blackwells.

MARTIN, J., DUMONT, D. & TREMBLAY, J.-E. 2013. Contribution of subsurface chlorophyll maxima to primary production in the coastal Beaufort Sea (Canadian Arctic: A model assessment. *Journal of Geophysical Research: Oceans,* 118**,** 5873-5886.

MARTIN, J., TREMBLAY, J. E., GAGNON, J., TREMBLAY, G., LAPOUSSIERE, A., JOSE, C., POULIN, M., GOSSELIN, M., GRATTON, Y. & MICHEL, C. 2010. Prevalence, structure and properties of subsurface chlorophyll maxima in Canadian Arctic waters. *Marine Ecology Progress Series,* 412**,** 69-84.

MCCIP 2008. Marine climate changes impacts annual report card 2007 - 2008. *In:* BAXTER, J. M., BUCKLEY, P. J. & WALLACE, C. J. (eds.). Lowestoft: MCCIP.

MCFARLAND, M., SULLIVAN, J. M., TWARDOWSKI, M. S. & NAYAK, A. R. Effect of orientation on light absorption by colonial diatoms (poster). AGU Ocean Sciences Meeting, 2016 New Orleans.

MCMANUS, G. B. & FUHRMAN, J. A. 1986. Photosynthetic pigments in the ciliate *Laboea strobila* from Long Island Sound, USA. *Journal of Plankton Research,* 8**,** 317-327.

MCMANUS, M. A., ALLDREDGE, A. L., BARNARD, A. H., BOSS, E., CASE, J. F., COWLES, T. J., DONAGHAY, P. L., EISNER, L. B., GIFFORD, D. J., GREENLAW, C. F., HERREN, C. M., HOLLIDAY, D. V., JOHNSON, D., MACINTYRE, S., MCGEHEE, D. M., OSBORN, T. R., PERRY, M. J., PIEPER, R. E., RINES, J. E. B., SMITH, D. C., SULLIVAN, J. M., TALBOT, M. K., TWARDOWSKI, M. S., WEIDEMANN, A. & ZANEVELD, J. R. 2003. Characteristics, distribution and persistence of thin layers over a 48 hour period. *Marine Ecology Progress Series,* 261**,** 1-19.

MCMANUS, M. A., KUDELA, R. M., SILVER, M. W., STEWARD, G. F., DONAGHAY, P. L. & SULLIVAN, J. M. 2008. Cryptic blooms: are thin layers the missing connection? *Estuaries and Coasts,* 31**,** 396-401.

MCMANUS, M. A., SEVADJIAN, J. C., BENOIT-BIRD, K. J., CHERITON, O. M., TIMMERMAN, A. H. V. & WALUK, C. M. 2012. Observations of thin layers in coastal Hawaiian waters. *Estuaries and Coasts,* 35**,** 1119-1127.

MELLARD, J. P., YOSHIYAMA, K., LITCHMAN, E. & KLAUSMEIER, C. A. 2011. The vertical distribution of phytoplankton in stratified water columns. *Journal of Theoretical Biology,* 269**,** 16-30.

MENDEN-DEUER, S. 2008. Spatial and temporal characteristics of plankton-rich layers in a shalllow, temperate fjord. *Marine Ecology Progress Series,* 355**,** 21-30.

MENDEN-DEUER, S., LESSARD, E. & SATTERBERG, J. 2001. Effect of preservation on dinoflagellate and diatom cell volume, and consequences for carbon biomass predictions. *Marine Ecology Progress Series,* 222**,** 41-50.

MENDEN-DEUER, S. & LESSARD, E. J. 2000. Carbon to volume relationships for dinoflagellates, diatoms, and other protist plankton. *Limnology and Oceanography,* 45**,** 569-579.

MENDEN-DEUER, S., LESSARD, E. J., SATTERBERG, J. & GRÜNBAUM, D. 2005. Growth rates and starvation survival of three species of the pallium-feeding, thecate dinoflagellate genus *Protoperidinium Aquatic Microbial Ecology,* 41**,** 145-152.

MIGNÉ, A., GÉVAERT, F., CRÉACH, A., SPILMONT, N., CHEVALIER, E. & DAVOULT, D. 2007. Photosynthetic activity of intertidal microphytobenthic communities during emersion: *in situ* measurements of chlorophyll fluorescence (PAM) and CO_2 flux (IRGA). *Journal of Phycology,* 43**,** 864-873.

MILES, J. 1961. On the stability of heterogeneous shear flows. *Journal of Fluid Mechanics,* 10**,** 496-508.

MILLIMAN, J. 1993. Production and accumulation of calcium carbonate in the ocean: budget of a nonsteady state. *Global Biogeochemical Cycles,* 7**,** 927-957.

MOISAN, J. R., MOISAN, T. A. & ABBOT, M. R. 2002. Modelling the effect of temperature on the maximum growth rates of phytoplankton populations. *Ecological Modelling,* 153**,** 197-215.

MONTAGNES, D. J. S. 1996. Growth responses of planktonic ciliates in the genera *Strobilidium* and *Strombidium*. *Marine Ecology Progress Series,* 130**,** 241-254.

MONTAGNES, D. J. S., BERGES, J. A., HARRISON, P. J. & TAYLOR, F. J. R. 1994. Estimating carbon, nitrogen, protein and chlorophyll a from volume in marine phytoplankton. *Limnology and Oceanography,* 39**,** 1044-1060.

MONTAGNES, D. J. S. & FRANKLIN, D. J. 2001. Effect of temperature on diatom volume, growth rate, and carbon and nitrogen content: reconsidering some paradigms. *Limnology and Oceanography,* 46**,** 2008-2018.

MOORE, C. M. 2016. *RE: FIRe data at high actinic light.* Type to BARNETT, M. L.

MOORE, C. M. 2017. *RE: Spectral correction.* Type to BARNETT, M. L.

MOORE, C. M., SUGGETT, D. J., HICKMAN, A. E., KIM, Y. N., TWEDDLE, J. F., SHARPLES, J., GEIDER, R. J. & HOLLIGAN, P. M. 2006. Phytoplankton photoacclimation and

photoadaptation in response to environmental gradients in a shelf sea. *Limnology and Oceanography,* 51**,** 936-949.

MOORE, J. K. & VILLAREAL, T. A. 1996a. Buoyancy and growth characteristics of three positively buoyant marine diatoms. *Marine Ecology-Progress Series,* 132**,** 203-213.

MOORE, J. K. & VILLAREAL, T. A. 1996b. Size-ascent rate relationships in positively buoyant marine diatoms. *Limnology and Oceanography,* 41**,** 1514-1520.

MOREL, A., ANTOINE, D., BABIN, M. & DANDONNEAU, Y. 1996. Measuring and modeled primary production in the northeast Atlantic (EUMELI JGOFS program): the impact of natural variations in photosynthetic parameters on model predictive skill. *Deep-Sea Research I,* 43**,** 1273-1304.

MOREL, A. & BRICAUD, A. 1981. Theoretical results concerning light-absorption in a discrete medium, and application to specific absorption of phytoplankton. *Deep-Sea Research Part I: Oceanographic Research Papers,* 28**,** 1375-1393.

MORK, M. 1981. Circulation phenomena and frontal dynamics of the Norwegian coastal current. *Philosophical Transactions of the Royal Society A,* 302**,** 635-647.

MOS, L. 2001. Domoic acid: A fascinating marine toxin. *Environmental Toxicology and Pharmacology,* 9**,** 79-85.

MULLER-KARGER, F. E., VARELA, R., THUNELL, R., LUERSSEN, R., HU, C. & WALSH, J. J. 2005. The importance of continental margins in the global carbon cycle. *Geophysical Research Letters,* 32**,** L01602, doi:10.1029/2004GL021346.

MURATA, M., SHIMATANI, M., SUGITANI, H., OSHIMA, Y. & YASUMOTO, T. 1982. Isolation and structural elucidation of the causative toxin of the diarrhetic shellfish poisoning. *Bulletin of the Japanese Society for the Science of Fish,* 48**,** 549-552.

MURCHIE, E. H. & LAWSON, T. 2013. Chlorophyll fluorescence analysis: a guide to good practice and understanding some new applications. *Journal of Experimental Botany,* 64**,** 3983-3998.

MURTY, V. S. N., GUPTA, G. V. M., SARMA, V. V., RAO, B. P., JYOTHI, D., SHASTRI, P. N. M. & SUPRAVENNA, Y. 2000. Effect of vertical stability and circulation on the depth of the chlorophyll maximum in the Bay of Bengal during May-June, 1996. *Deep-Sea Research Part I: Oceanographic Research Papers,* 47**,** 859-873.

NASA 2018. Daily solar insolation at 50^{o} 05.670 N, 004^{o} 52.020 W for June/July 2013 - 2016 taken from CERES Fast Longwave And SHortwave Radiative Fluxes (FLASHFlux) project. NASA.

NAUSTVOLL, L.-J. 1998. Growth and grazing by the thecate heterotrophic dinoflagellate *Diplopsalis lenticula* (Diplopsalidaceae, Dinophyceae). *Phycologia,* 37**,** 1-9.

NAYAK, A. R., TWARDOWSKI, M. S., SULLIVAN, J. M., MCFARLAND, M., STOCKLEY, N. & NARDELLI, S. A field study of particle orientation in shear flow (poster). AGU Ocean Sciences Meeting, 2016 New Orleans.

NEODAAS 2018. Chlorophyll (OC5) data generated by PML from data obtained by the MODIS on the Aqua satellite produced by NEODAAS. NERC.

NIELSEN, T. G. 1991. Contribution of zooplankton grazing to the decline of a *Ceratium* bloom. *Limnology and Oceanography,* 36**,** 1091-1106.

NIOZ 2015a. QuAAtro Applications Method No. Q-064-05 Rev. 8: Phosphate in Water and Seawater. Den Hoorn (Texel), The Netherlands: Nederlands Instituut for Onderzoek der Zee (Royal Netherlands Institute for Sea Research).

NIOZ 2015b. QuAAtro Applications Method No. Q-066-05 Rev.5: Silicate in Water and Seawater. Den Hoorn (Texel), The Netherlands: Nederlands Instituut for Onderzoek der Zee (Royal Netherlands Institute for Sea Research).

NIOZ 2015c. QuAAtro Applications Method No. Q-070-05 Rev. 6: Nitrite in Water and Seawater. Den Hoorn (Texel), The Netherlands: Nederlands Instituut for Onderzoek der Zee (Royal Netherlands Institute for Sea Research).

NIOZ 2016. QuAAtro Applications Method No. Q-068-05 Rev. 11: Nitrate and Nitrite in Water and Seawater. Den Hoorn (Texel), The Netherlands: Nederlands Instituut for Onderzoek der Zee (Royal Netherlands Institute for Sea Research).

NORDLI, E. 1957. Experimental studies on the ecology of ceratia. *Oikos,* 8**,** 200-265.

O'BOYLE, S. & RAINE, R. 2007. The influence of local and regional oceanographic processes in phytoplankton distribution in continental shelf waters off north-western Ireland. *Biology and Environment Proceedings of the Royal Irish Academy,* 107**,** 95-109.

OHNEMUS, D. C., RAUSCHENBERG, S., KRAUSE, J. W., BRZEZINSKI, M. A., COLLIER, J. L., GERACI-YEE, S., BAINES, S. B. & TWINING, B. S. 2016. Silicon content of individual cells of *Synechococcus* from the North Atlantic Ocean. *Marine Chemistry,* 187**,** 16-24.

OLENINA, I., HAJDU, S., EDLER, L., ANDERSSON, A., WASMUND, N., BUSCH, S., GÖBEL, J., GROMISZ, S., HUSEBY, S., HUTTUNEN, M., JAANUS, A., KOKKONEN, P., LEDAINE, I. & NIEMKIEWICZ, E. Biovolumes and size-classes of phytoplankton in the Baltic Sea. HELCOM Baltic Sea Environment Proceedings No.106, 2006. 1-144.

ONOUE, Y. 1990. Massive fish kills by a *Ceratium fusus* red tide in Kagoshima Bay, Japan. *Red Tide Newsletter,* 3**,** 2.

ORLANSKI, I. & BRYAN, K. 1969. Formation of the thermocline step structure by large-amplitude internal gravity waves. *Journal of Geophysical Research,* 74**,** 6975-6983.

OWEN, K. R. 2014. *Flow cytometric investigation of the size spectrum of North Sea phytoplankton communities.* PhD, University of East Anglia.

PAASCHE, E. 1960. On the relationship between primary production and standing stock of phytoplankton. *Journal of the International Council for the Exploration of the Sea,* 26**,** 33-48.

PAERL, H. W., VALDES-WEAVER, L. M., JOYNER, A. R. & WINKLEMANN, V. 2007. Phytoplankton indicators of ecological change in the eutrophying Pamlico Sound system, North Carolina. *Ecological Applications,* 17**,** s88-s101.

PALMER, M. R., RIPPETH, T. & SIMPSON, J. H. 2008. An investigation of internal mixing in a seasonally stratified shelf sea. *Journal of Geophysical Research,* 113**,** C12005, doi:10.1029/2007JC004531.

PAN, Y., SUBBA RAO, D. V., MANN, K. H., LI, W. K. W. & WARNOCK, R. E. 1993. Temperature dependence of growth and carbon assimilation in *Nitzschia pungens f. multiseries*, the causative diatom of domoic acid poisoning. *In:* SMAYDA, T. J. & SHIMIZU, Y. (eds.) *Toxic Phytoplankton Blooms in the Sea.* New York: Elsevier.

PARSLOW, J. S., BOYD, P. W., RINTOUL, S. R. & GRIFFITHS, F. B. 2001. A persistent subsurface chlorophyll maximum in the Interpolar Frontal Zone south of Australia: Seasonal progression and implications for phytoplankton-light-nutrient interactions. *Journal of Geophysical Research-Oceans,* 106**,** 31543-31557.

PARSONS, T. R. & BLACKBOURN, D. J. 1968. Pigments of the ciliate, *Mesodinium rubrum* (Lohmann). *Netherlands Journal of Sea Research,* 4**,** 27-31.

PARTENSKY, F., HESS, W. R. & VAULOT, D. 1999. *Prochlorococcus*, a marine photosynthetic prokaryote of global significance. *Microbiology and Molecular Biology Reviews,* 63**,** 106-127.

PASSOW, U. & CARLSON, C. A. 2012. The biological pump in a high CO2 world. *Marine Ecology Progress Series,* 470**,** 249-271.

PAULY, D., CHRISTENSEN, V., GUÉ NETTE, S., PITCHER, T. J., SUMAILA, U. R., WALTERS, C. J., WATSON, R. & ZELLER, D. 2002. Towards sustainability in world fisheries. *Nature,* 418**,** 689-695.

PEDERSEN, F. B. 1994. The oceanographic and biological tidal cycle succession in shallow sea fronts in the North Sea and the English Channel. *Estuarine, Coastal and Shelf Science,* 38**,** 249-269.

PEMBERTON, K., REES, A. P., MILLER, P. I., RAINE, R. & JOINT, I. 2004. The influence of water body characteristics on phytoplankton diversity and production in the Celtic Sea. *Continental Shelf Research,* 24**,** 2011-2028.

PEPERZAK, L., VRIELING, E. G., SANDEE, B. & RUTTEN, T. 2000. Immuno flow cytometry in marine phytoplankton research. *Marine Science,* 64**,** 165-181.

PERRY, M. J., TALBOT, M. C. & ALBERETE, R. S. 1981. Photoadaptation in marine phytoplankton: response of the photosynthetic unit. *Marine Biology,* 62**,** 91-101.

PETERSON, T. D., TOEWS, H. N. J., ROBINSON, C. L. K. & HARRISON, P. J. 2007. Nutrient and phytoplankton dynamics in the Queen Charlotte Islands (Canada) during the summer upwelling seasons of 2001 - 2002. *Journal of Plankton Research,* 29**,** 219-239.

PINGREE, R. D. 1975. The advance and retreat of the thermocline on the continental shelf. *Journal of the Marine Biological Association of the UK,* 55**,** 965-974.

PINGREE, R. D. 1978. Cyclonic eddies and cross-frontal mixing. *Journal of the Marine Biological Association of the UK,* 58**,** 955-963.

PINGREE, R. D. 1980. Chapter 13: Physical Oceanography of the Celtic Sea and English Channel. *Elsevier Oceanography Series,* 24**,** 415-465.

PINGREE, R. D. & GRIFFITHS, D. K. 1978. Tidal fronts on the shelf seas around the British Isles. *Journal of Geophysical Research, Oceans and Atmospheres,* 83**,** 4615-4622.

PINGREE, R. D., HOLLIGAN, P. M. & MARDELL, G. T. 1978. The effects of vertical stability on phytoplankton distribution in the summer on the northwest European shelf. *Deep-Sea Research,* 25**,** 1011-1028.

PINGREE, R. D., HOLLIGAN, P. M. & MARDELL, G. T. 1979. Phytoplankton growth and cyclonic eddies. *Nature,* 278**,** 245-247.

PINGREE, R. D., HOLLIGAN, P. M., MARDELL, G. T. & HEAD, R. N. 1976. Influence of physical stability on spring, summer and autumn phytoplankton blooms in Celtic Sea. *Journal of the Marine Biological Association of the UK,* 56**,** 845-873.

PLANAS, D., AGUSTI, S., DUARTE, C. M., GRANATA, T. C. & MERINO, M. 1999. Nitrate uptake and diffusive nitrate supply in the Central Atlantic. *Limnology and Oceanography,* 44**,** 116-126.

PLATT, T. 1986. Primary production of the ocean water column as a function of surface light intensity: algorithms for remote sensing. *Deep-Sea Research,* 33**,** 149-163.

PLATT, T. & JASSBY, A. D. 1976. The relationship between photosynthesis and light for natural assemblage of coastal marine phytoplankton. *Journal of Phycology,* 12**,** 421-430.

PLATT, T. & SATHYENDRANATH, S. 1993. Estimators of primary production for interpretation of remotely sensed data on ocean colour. *Journal of Geophysical Research,* 98**,** 14561-14576.

PLATT, T., SATHYENDRANATH, S., JOINT, I. & FASHAM, M. J. R. 1993. Photosynthetic characteristics of the phytoplankton in the Celtic Sea during late spring. *Fisheries Oceanography,* 2**,** 191-201.

PLATT, T., SATHYENDRANATH, S., ULLOA, O., HARRISON, W. G., HOEPFFNER, N. & GOES, J. 1992. Nutrient control of phytoplankton photosynthesis in the western North Atlantic. *Nature,* 356**,** 229-331.

PML 2013. L4 autonomous buoy data (AirMar wind speed) collected once per hour at site L4 in the Western English Channel between June and July 2013. NERC.

PML 2017. L4 autonomous buoy AirMar data for the Western English Channel during June/July 2013-2016. NERC.

PODAAC 2018. Chlorophyll data generated by SOTO from data obtained by the MODIS on the Aqua satellite produced by PODAAC. NASA.

POULTON, A. J. 2004. AMT Phase II primary production (14C) methodology. Southampton: National Oceanography Centre, Southampton.

POULTON, A. J., SANDERS, R., HOLLIGAN, P. M., STINCHCOMBE, M. C., ADEY, T. R., BROWN, L. & CHAMBERLAIN, K. 2006. Phytoplankton mineralization in the tropical and subtropical

Atlantic Ocean. *Global Biogeochemical Cycles,* 20**,** GB4002, doi:10.1029/2006GB002712.

PRAIRIE, J. C., FRANKS, P. J. S. & JAFFE, J. S. 2010. Cryptic peaks: invisible vertical structure in fluorescent particles revealed using a planar laser imaging fluorometer. *Limnology and Oceanography,* 55**,** 1943-1958.

PÉREZ, M. T., DOLAN, J. R. & FUKAI, E. 1997. Planktonic oligotrich ciliates in the NW Mediterranean: growth rates and consumption by copepods. *Marine Ecology Progress Series,* 155**,** 89-101.

RALSTON, D. K., MCGILLICUDDY, D. J. & TOWNSEND, D. W. 2007. Asynchronous vertical migration and bimodal distribution of motile phytoplankton. *Journal of Plankton Research,* 29**,** 803-821.

RAVEN, J. A. 1983. The Transport and Function of Silicon in Plants. *Biological Reviews of the Cambridge Philosophical Society,* 58**,** 179-207.

RAVEN, J. A. 1986. Photosynthetic picoplankton. *Canadian Journal of Fisheries and Aquatic Sciences,* 214**,** 1-70.

RAVEN, J. A. 1987. The role of vacuoles. *New Phytologist,* 106**,** 357-422.

RAVEN, J. A. 1997. The vacuole: a cost-benefit analysis. *Advances in Botanical Research Incorporating Advances in Plant Pathology,* 25**,** 59-86.

RAVEN, J. A. 2000. The flagellate condition. *In:* LEADBEATER, B. S. C. & GREEN, J. C. (eds.) *The Flagellates: Unity, Diversity and Evolution.* London: Taylor and Francis Limited.

RAVEN, J. A. & GEIDER, R. J. 1988. Temperature and algal growth. *New Phytologist,* 110**,** 441-461.

REDFIELD, A. C. 1958. The biological control of chemical factors in the environment. *American Scientist,* 46**,** 205-221.

REID, P. C., FISCHER, A. C., LEWIS-BROWN, E., MEREDITH, M. P., SPARROW, M., ANDERSSON, A. J., ANTIA, A., BATES, N. R., BATHMANN, U., BEAUGRAND, G., BRIX, H., DYE, S., EDWARDS, M., FUREVIK, T., GANGSTØ, R., HÁTÚN, H., HOPCROFT, R. R., KENDALL, M., KASTEN, S., KEELING, R., LE QUÉRÉ, C., MACKENZIE, F. T., MALIN, G., MAURITZEN, C., OLAFSSON, J., PAULL, C., RIGNOT, E., SHIMADA, K., VOGT, M., WALLACE, C., WANG, Z. & WASHINGTON, R. 2009. Impacts of the oceans on climate change. *In:* SIMS, D. W. (ed.) *Advances in Marine Biology.* Burlington: Academic Press.

REID, P. C., LANCELOT, C., GIESKES, W. W. C., HAGMEIER, E. & WEICHART, G. 1990. Phytoplankton of the North Sea and its dynamics: a review. *Netherlands Journal of Sea Research,* 26**,** 295-331.

REID, P. C., ROBINSON, G. A. & HUNT, H. G. 1987. Spatial and temporal patterns of marine blooms in the Northeastern Atlantic and North Sea from the Continuous Plankton Recorder survey. *Rapports et Proces-verbaux des Réunions. Conseil International pour l'Éxploration de la Mer,* 187**,** 27-37.

REVELANTE, N. & GILMARTIN, M. 1973. Some observations of the chlorophyll maximum and primary production in the eastern North Pacific. *Internationale Revue der Gesamten Hydrobiologie,* 58**,** 819-834.

RICHARDSON, K., NIELSEN, T. G., PEDERSEN, F. B., HEILMANN, J. P., LOKKEGAARD, B. & KAAS, H. 1998. Spatial heterogeneity in the structure of the planktonic food web in the North Sea. *Marine Ecology Progress Series,* 168**,** 197-211.

RICHARDSON, K., RASMUSSEN, B., BUNK, T. & MOURITSEN, L. T. 2003. Multiple subsurface phytoplankton blooms occurring simultaneously in the Skagerrak. *Journal of Plankton Research,* 25**,** 799-813.

RICHARDSON, K., VISSER, A. W. & PEDERSEN, F. B. 2000. Subsurface phytoplankton blooms fuel pelagic production in the North Sea. *Journal of Plankton Research,* 22**,** 1663-1671.

RICHARDSON, T. L. & CULLEN, J. J. 1995. Changes in buoyancy and chemical composition during growth of a coastal marine diatom. *Marine Ecology Progress Series,* 128**,** 77-90.

RIDDERINKHOF, H. 1992. On the effects of variability in meteorological forcing on the vertical structure of a stratified water column. *Continental Shelf Research,* 12**,** 25-36.

RILEY, J. S., SANDERS, R., MARSAY, C., LE MOIGNE, F. A. C., ACHTERBERG, E. P. & POULTON, A. J. 2012. The relative contribution of fast and slow sinking particles to ocean carbon export. *Global Biogeochemical Cycles,* 26.

RINES, J. E. B., DONAGHAY, P. L., DEKSHENIEKS, M. M., SULLIVAN, J. M. & TWARDOWSKI, M. S. 2002. Thin layers and camouflage: Hidden *Pseudo-nitzschia* populations in a fjord in the San Juan Islands, Washington, USA. *Marine Ecology Progress Series,* 225**,** 123-137.

RINES, J. E. B., MCFARLAND, M. N., DONAGHAY, P. L. & SULLIVAN, J. M. 2010. Thin layers and species-specific characterization of the phytoplankton community in Monterey Bay, California, USA. *Continental Shelf Research,* 30**,** 66-80.

RIPPETH, T. 2005. Mixing in seasonally stratified shelf seas: a shifting paradigm. *Philosophical Transactions of the Royal Society A,* 363**,** 2837-2854.

RIPPETH, T., PALMER, M. R., SIMPSON, J. H., FISHER, N. R. & SHARPLES, J. 2005. Thermocline mixing in summer stratified continental shelf seas. *Geophysical Research Letters,* 32**,** L05602, doi:10.1029/2004GL02214.

RIPPETH, T., WILES, P. J., PALMER, M. R., SHARPLES, J. & TWEDDLE, J. 2009. The diapycnal nutrient flux and shear-induced diapycnal mixing in the seasonally stratified western Irish Sea. *Continental Shelf Research,* 29**,** 1580-1587.

ROBINSON, C., TILSTONE, G. H., REES, A. P., SMYTHE, T. J., FISHWICK, J. R., TARRAN, G. A., LUZ, B., BARKAN, E. & DAVID, E. 2009. Comparison of *in vitro* and *in situ* plankton production determinations. *Aquatic Microbial Ecology,* 54**,** 13-34.

RODHE, J., TETT, P. & WULFF, F. 2006. Chapter 26. The Baltic and North Seas: a regional review of some important physical-chemical-biological interaction processess. *In:* ROBINSON, A. R. & BRINK, K. (eds.) *The Sea.* Cambridge, MA, USA: Harvard University Press.

ROSS, O. N. & SHARPLES, J. 2007. Phytoplankton motility and the competition for nutrients in the thermocline. *Marine Ecology Progress Series,* 347**,** 21-38.

ROSS, O. N. & SHARPLES, J. 2008. Swimming for survival: A role of phytoplankton motility in a stratified turbulent environment. *Journal of Marine Systems,* 70**,** 248-262.

ROTT, E. 1981. Some results from phytoplankton counting intercalibrations. *Swiss Journal of Hydrology,* 43**,** 34-62.

ROUND, F. E., CRAWFORD, R. M. & MANN, D. G. 1990. *The Diatoms: Biology and Morphology of the Genera,* Cambridge, Cambridge University Press.

ROUSSEAUX, C. S. & GREGG, W. W. 2014. Interannual variation in phytoplankton primary production at a global scale. *Remote Sensing,* 6**,** 1-19.

RUIZ, J., MACÍAS, D. & PETERS, F. 2004. Turbulence increases the average settling velocity of phytoplankton cells. *PNAS,* 101**,** 17720-17724.

RYAN, J. P., MCMANUS, M. A., PADUAN, J. D. & CHAVEZ, F. P. 2008. Phytoplankton thin layers caused by shear in frontal zones of a coastal upwelling system. *Marine Ecology Progress Series,* 354**,** 21-34.

RYAN, J. P., MCMANUS, M. A. & SULLIVAN, J. M. 2010. Interacting physical, chemical and biological forcing of phytoplankton thin-layer variability in Monterey Bay, California. *Continental Shelf Research,* 30**,** 7-16.

RYTHER, J. H. & MENZEL, D. W. 1959. Light adaptation by marine phytoplankton. *Limnology and Oceanography,* 4**,** 492-497.

RÍOS, F., KILIAN, R. & MUTSCHKE, E. 2016. Chlorophyll-a thin layers in the Magellan fjord system: the role of the water column stratification. *Continental Shelf Research,* 124**,** 1-12.

SAFRAN, P. 2009. *Fisheries and Aquaculture,* Oxford, UK, Eolss Publishers/UNESCO.

SANCETTA, C. 1994. Mediterranean sapropels: seasonal stratification yields high production and carbon flux. *Paleoceanography,* 9**,** 195-196.

SANCETTA, C., VILLAREAL, T. A. & FALKOWSKI, P. 1991. Massive fluxes of rhizosolenid diatoms: a common occurrence? *Limnology and Oceanography,* 36**,** 1452-1457.

SATHYENDRANATH, S. & PLATT, T. 1993. Remote sensing of water-column primary production. *ICES Marine Science Symposia,* 197**,** 236-243.

SATO, M., TAKEDA, S. & FURUYA, K. 2006. Effects of long-term sample preservation on flow cytometric analysis of natural populations of pico- and nanophytoplankton. *Journal of Oceanography,* 62**,** 903-908.

SCOTT, B. E., SHARPLES, J., ROSS, O. N., WANG, J., PIERCE, G. J. & CAMPHUYSEN, C. J. 2010. Sub-surface hotspots in shallow seas: fine-scale limited locations of top predator foraging habitat indicated by tidal mixing and sub-surface chlorophyll. *Marine Ecology Progress Series,* 408**,** 207-226.

SECKBACH, J. & KOCIOLEK, J. P. 2011. *The Diatom World,* The Netherlands, Spinger.

SEEYAVE, S., PROBYN, T., ÁLVAREZ-SALGADO, X. A., FIGUEIRAS, F. G., PURDIE, D. A., BARTON, E. D. & LUCAS, M. 2013. Nitrogen uptake of phytoplankton assemblages under contrasting upwelling and downwelling conditions: the Ría de Vigo, NW Iberia. *Estuarine, Coastal and Shelf Science,* 124**,** 1-12.

SHARPLES, J. 2008. Potential impacts of the spring-neap tidal cycle on shelf sea primary production. *Journal of Plankton Research,* 30**,** 183-197.

SHARPLES, J., HOLT, J. & DYE, S. R. 2013. Impacts of climate change on shelf sea stratification. *MCCIP Science Review***,** 67-70.

SHARPLES, J., MOORE, C. M., HICKMAN, A. E., HOLLIGAN, P. M., TWEDDLE, J. F., PALMER, M. R. & SIMPSON, J. H. 2009. Internal tidal mixing as a control on continental margin ecosystems. *Geophysical Research Letters,* 36**,** L23603, doi: 10.1029/2009GL040683.

SHARPLES, J., MOORE, C. M., RIPPETH, T. P., HOLLIGAN, P. M., HYDES, D. J., FISHER, N. R. & SIMPSON, J. H. 2001. Phytoplankton distribution and survival in the thermocline. *Limnology and Oceanography,* 46**,** 486-496.

SHARPLES, J., ROSS, O. N., SCOTT, B. E., GREENSTREET, S. P. R. & FRASER, H. 2006. Inter-annual variability in the timing of stratification and the spring bloom in the North-western North Sea. *Continental Shelf Research,* 26**,** 733-751.

SHARPLES, J. & TETT, P. 1994. Modelling the effect of physical variability on the midwater chlorophyll maximum. *Journal of Marine Research,* 52**,** 219-238.

SHARPLES, J., TWEDDLE, J. F., GREEN, J. A. M., PALMER, M. R., KIM, Y. N., HICKMAN, A. E., HOLLIGAN, P. M., MOORE, C. M., RIPPETH, T. P., SIMPSON, J. H. & KRIVTSOV, V. 2007. Spring-neap modulation of internal tide mixing and vertical nitrate fluxes at a shelf edge in summer. *Limnology and Oceanography,* 52**,** 1735-1747.

SHERMAN, E., MOORE, J. K., PRIMEAU, F. & TANOUYE, D. 2016. Temperature influence on phytoplankton community growth rates. *Global Biogeochemical Cycles,* 30**,** 550-559.

SHIGESADA, N. & OKUBO, A. 1981. Analysis of the self-shading effect on algal vertical distribution in natural water. *Journal of Mathematical Biology,* 12**,** 311-326.

SICKO-GOAD, L. M., SCHELSKE, C. L. & STOERMER, E. F. 1984. Estimation of intracellular carbon and silica content of diatoms from natural assemblages using morphometric techniques. *Limnology and Oceanography,* 29**,** 1170-1178.

SIEBURTH, J. M., SMETACEK, V. & LENZ, J. 1978. Pelagic ecosystem structure: heterotrophic compartments of the plankton and their relationship to plankton size fractions. *Limnology and Oceanography,* 23**,** 1256-1263.

SILSBE, G. M. & KROMKAMP, J. C. 2012. Modelling the irradiance dependency of the quantum efficiency of photosynthesis. *Limnology and Oceanography: Methods,* 10**,** 645-652.

SILSBE, G. M. & MALKIN, S. Y. 2015. Package 'phytotools': Fit PE or RLC data to Jassby and Platt 1976. The Comprehensive R Archive Network (CRAN).

SIMON, N., CRAS, A., FOULON, E. & LEMÉE, R. 2009. Diversity and evolution of marine phytoplankton. *Comptes Rendus Biologies,* 332**,** 159-170.

SIMPSON, J. H. & HUNTER, J. R. 1974. Fronts in the Irish Sea. *Nature,* 250**,** 404-406.

SIMPSON, J. H. & SHARPLES, J. 2012. *Introduction to the physical and biological oceanography of shelf seas,* Cambridge, Cambridge University Press.

SLAWYK, G., COLLOS, Y. & AUCLAIR, J. C. 1977. The use of the ^{13}C and ^{15}N isotopes for the simultaneous measurements of carbon and nitrogen turnover rates in marine phytoplankton. *Limnology and Oceanography,* 22**,** 925-932.

SLEIGH, M. A. 2000. Trophic strategies. *In:* LEADBEATER, B. S. C. & GREEN, J. C. (eds.) *The Flagellates: Unity, Diversity and Evolution.* London: Taylor and Francis Limited.

SMALLEY, G. W., COATS, D. W. & STOECKER, D. K. 2003. Feeding in the mixotrophic dinoflagellate *Ceratium furca* is influenced by intracellular nutrient concentrations. *Marine Ecology Progress Series,* 262**,** 137-151.

SMAYDA, T. J. 1970. The suspension and sinking of phytoplankton in the sea. *Oceanography and Marine Biology: An Annual Review,* 8**,** 353-414.

SMAYDA, T. J. 1997. What is a bloom? A commentary. *Limnology and Oceanography,* 42**,** 1132-1136.

SMETACEK, V. 1981. The annual cycle of protozooplankton in Kiel Bight. *Marine Biology,* 63**,** 1-11.

SMETACEK, V. 1984. The food supply to the benthos. In Flows of energy and materials in marine ecosystems: Theory and practice. NATO Conference Series 4. *Marine Science,* 13. Plenum.

SMETACEK, V. 1985. Role of sinking in diatom life-history cycles: ecological, evolutionary and geological significance. *Marine Biology,* 84**,** 239-251.

SMETACEK, V. 2001. A watery arms race. *Nature,* 411**,** 745-745.

SMITH, W. O. & BARBER, R. T. 1979. A carbon budget for the autotrophic ciliate *Mesodinium rubrum Journal of Phycology,* 15**,** 27-33.

SMYTH, T. 2017. Rainfall data logged by the Omni Instruments 6" tipping bucket raingauge (RG200) of the PML meteorological station between 2013 and 2016. NERC.

SMYTH, T., ATKINSON, A., WIDDICOMBE, S., FROST, M., ALLEN, I., FISHWICK, J., QUEIRÓS, A., SIMS, D. & BARANGE, M. 2015. The Western Channel Observatory. *Progress in Oceanography,* 137**,** 335-341.

SMYTH, T. J., FISHWICK, J. R., AL-MOOSAWI, L., CUMMINGS, D. G., HARRIS, C., KITIDIS, V., REES, A., MARTINEZ-VICENTE, V. & WOODWARD, E. M. S. 2010. A broad spatio-temporal view of the Western English Channel observatory. *Journal of Plankton Research,* 32**,** 585-601.

SOMMER, U. 1984. The paradox of the plankton: fluctuations of phosphorus availability maintain diversity of phytoplankton in flow-through cultures. *Limnology and Oceanography,* 29**,** 633-636.

SOMMER, U. 1988. Some size relationships in phytoflagellate motility. *Hydrobiologia,* 161**,** 125-131.

SOMMER, U. & LENGFELLNER, K. 2008. Climate change and the timing, magnitude, and composition of the phytoplankton spring bloom. *Global Change Biology,* 14**,** 1199-1208.

SORENSEN, G. 2009. The role of the virus-phytoplankton system in marine biogeochemical cycling: possible impacts of climate change. *The Plymouth Student Scientist,* 2**,** 289-302.

SOURNIA, A. 1982a. Form and function in marine phytoplankton. *Biological Reviews,* 57**,** 347-394.

SOURNIA, A. 1982b. Is there a shade flora in the marine plankton? *Journal of Plankton Research,* 4**,** 391-399.

SOURNIA, A., CHRETIENNOT-DINET, M. J. & RICARD, M. 1991. Marine-phytoplankton - how many species in the world ocean. *Journal of Plankton Research,* 13**,** 1093-1099.

SOUTHWARD, A. J., LANGMEAD, O., HARDMAN-MOUNTFORD, N. J., AIKEN, J., BOALCH, G. T., DANDO, P. R., GENNER, M. J., JOINT, I., KENDALL, M. A., HALLIDAY, N. C., HARRIS, R. P.,

LEAPER, R., MIESZKOWSKA, N., PINGREE, R. D., RICHARDSON, A. J., SIMS, D. W., SMITH, T., WALNE, A. W. & HAWKINS, S. J. 2005a. A review of long-term research in the western English Channel. *In:* SOUTHWARD, A. J., TYLER, P. A., YOUNG, C. M. & FUIMAN, L. A. (eds.) *Advances in Marine Biology.* San Diego, USA: Elsevier Academic Press.

SOUTHWARD, A. J., LANGMEAD, O., HARDMAN-MOUNTFORD, N. J., AIKEN, J., BOALCH, G. T., DANDO, P. R., GENNER, M. J., JOINT, I., KENDALL, M. A., HALLIDAY, N. C., HARRIS, R. P., LEAPER, R., MIESZKOWSKA, N., PINGREE, R. D., RICHARDSON, A. J., SIMS, D. W., SMITH, T., WALNE, A. W. & HAWKINS, S. J. 2005b. Long-term oceanographic and ecological research in the Western English Channel. *In:* SOUTHWARD, A. J., TYLER, P. A., YOUNG, C. M. & FUIMAN, L. A. (eds.) *Advance in Marine Biology.* San Diego, USA: Elsevier Academic Press.

SPATHARIS, S., DOLAPSAKIS, N. P., ECONOMOU-AMILLI, A., TSIRTSIS, G. & DANIELIDIS, D. B. 2009. Dynamics of potentially harmful microalgae in a confined Mediterranean Gulf—Assessing the risk of bloom formation. *Harmful Algae,* 8**,** 736-743.

STACEY, M. T., MCMANUS, M. A. & STEINBUCK, J. V. 2007. Convergences and divergences and thin layer formation and maintenance. *Limnology and Oceanography,* 52**,** 1523-1532.

STEELE, J. H. 1964. A study of production in the Gulf of Mexico. *Journal of Marine Research,* 22**,** 211-221.

STEELE, J. H. & YENTSCH, C. S. 1960. The vertical distribution of chlorophyll. *Journal of the Marine Biological Association of the UK,* 39**,** 217-226.

STEFELS, J. & VAN BOEKEL, W. H. M. 1993. Production of DMS from dissolved DMSP in axenic cultures of the marine phytoplankton species *Phaeocystis sp.* . *Marine Ecology Progress Series,* 97**,** 11-18.

STEINACHER, M., JOOS, F., FRÖLICHER, T. L., BOPP, L., CADULE, P., COCCO, V., DONEY, S. C., GEHLEN, M., LINDSAY, K., MOORE, J. K., SCHNEIDER, B. & SEGSCHNEIDER, J. 2010. Projected 21st century decrease in marine productivity: A multi-model analysis. *Biogeosciences,* 7**,** 979-1005.

STEINBERG, D. K., CARLSON, C. A., BATES, N. R., JOHNSON, R. J., MICHAELS, A. F. & KNAP, A. H. 2001. Overview of the US JGOFS Bermuda Atlantic Time-series Study (BATS): a decade-scale look at ocean biology and biogeochemistry. *Deep-Sea Research II,* 48**,** 1405-1447.

STEINBUCK, J. V., GENIN, A., MONISMITH, S. G., KOSEFF, J. R., HOLZMAN, R. & LABIOSA, R. G. 2010. Turbulent mixing in fine-scale phytoplankton layers: Observations and inferences of layer dynamics. *Continental Shelf Research,* 30**,** 442-455.

STEINBUCK, J. V., STACEY, M., MCMANUS, M. A., CHERITON, O. M. & RYAN, J. 2009. Observations of turbulent mixing in a phytoplankton thin layer. *Marine Ecology Progress Series,* 378**,** 55-69.

STINCHCOMBE, M. 2017. *RE: Nitrate, phosphate and silicate detection limits of a SEAL Analytical QuAAtro segmented flow AutoAnalyser.* Type to BARNETT, M.

STOECKER, D. K., MICHAELS, A. E. & DAVIS, L. H. 1987. Large proportion of marine planktonic ciliates found to contain functional chloroplasts. *Nature,* 326**,** 790-792.

STOECKER, D. K., PUTT, M., DAVIS, L. H. & MICHAELS, A. E. 1991. Photosynthesis in *Mesodinium rubrum*: species-specific measurements and comparison to community rates. *Marine Ecology Progress Series,* 73**,** 245-252.

STOECKER, D. K., TANIGUCHI, A. & MICHAELS, A. E. 1989. Abundance of autotrophic, mixotrophic and heterotrophic planktonic ciliates in shelf and slope waters. *Marine Ecology Progress Series,* 50**,** 241-254.

STOKES, G. G. 1851. On the effect of the internal friction of fluids on the motion of pendulums. *Cambridge Philosophical Transactions,* 9**,** 8-106.

STRICKLAND, J. D. H. & PARSONS, T. R. 1972. *A Practical Handbook of Seawater Analysis,* Ottawa, Fisheries research board of Canada.

SUGGETT, D. J., MACINTYRE, H. L., KANA, T. M. & GEIDER, R. J. 2009a. Comparing electron transport with gas exchange: parameterising exchange rates between alternative photosynthetic currencies for eukaryotic phytoplankton. *Aquatic Microbial Ecology,* 56**,** 147-162.

SUGGETT, D. J., MOORE, C. M. & GEIDER, R. J. 2010. Estimating aquatic productivity from active fluorescence measurements. *In:* SUGGETT, D. J., PRÁŠIL, O. & BOROWITZKA, M. A. (eds.) *Chlorophyll a Fluorescence in Aquatic Sciences: Methods and Applications.* Dordrecht, The Netherlands: Springer.

SUGGETT, D. J., MOORE, M. C., HICKMAN, A. E. & GEIDER, R. J. 2009b. Interpretation of fast repetition rate (FRR) fluorescence: signatures of phytoplankton community structure versus physiological state. *Marine Ecology Progress Series,* 376**,** 1-19.

SUKHANOVA, I. N., FLINT, M. V., WHITLEDGE, T. E., STOCKWELL, D. A. & RHO, T. K. 2006. Mass development of the planktonic diatom *Proboscia alata* over the Bering Sea shelf in the summer season. *Oceanology,* 46**,** 200-216.

SULLIVAN, J. M., DONAGHAY, P. L. & RINES, J. E. B. 2010a. Coastal thin layer dynamics: Consequences to biology and optics. *Continental Shelf Research,* 30**,** 50-65.

SULLIVAN, J. M., TWARDOWSKI, M. S., DONAGHAY, P. L. & FREEMAN, S. A. 2005. Use of optical scattering to discriminate particle types in coastal waters. *Applied Optics,* 44**,** 1667-1680.

SULLIVAN, J. M., VAN HOLLIDAY, D., MCFARLAND, M., MCMANUS, M. A., CHERITON, O. M., BENOIT-BIRD, K. J., GOODMAN, L., WANG, Z. K., RYAN, J. P., STACEY, M., GREENLAW, C. & MOLINE, M. A. 2010b. Layered organization in the coastal ocean: An introduction to planktonic thin layers and the LOCO project. *Continental Shelf Research,* 30**,** 1-6.

SUN, H., HENDRY, D. C., PLAYER, M. & WATSON, J. 2007. *In situ* underwater electronic holographic camera for studies of plankton. *IEEE Journal of Oceanic Engineering,* 32**,** 373-382.

SUNDA, W. G. & HUNTSMAN, S. A. 1995. Iron uptake and growth limitation in oceanic and coastal phytoplankton. *Marine Chemistry,* 50**,** 189-206.

SUTTLE, C. 2005. Viruses in the sea. *Nature,* 437**,** 356-361.

SVERDRUP, H. U. 1953. On conditions for the vernal blooming of phytoplankton. *Journal du Conseil,* 18**,** 287-95.

TALAPATRA, S., HONG, J. R., MCFARLAND, M., NAYAK, A. R., ZHANG, C., KATZ, J., SULLIVAN, J., TWARDOWSKI, M., RINES, J. & DONAGHAY, P. 2013. Characterization of biophysical interactions in the water column using *in situ* digital holography. *Marine Ecology Progress Series,* 473**,** 29-51.

TALLING, J. F. 2012. Temperature increase – an uncertain stimulant of algal growth and primary production in fresh waters. *Freshwater Reviews,* 5**,** 73-84.

TANG, E. P. Y. 1995. The allometry of algal growth rates. *Journal of Plankton Research,* 17**,** 1325-1335.

TANG, E. P. Y. 1996. Why do dinoflagellates have lower growth rates? *Journal of Phycology,* 32**,** 80-84.

TANG, T., KISSLINGER, K. & LEE, C. 2014. Silicate deposition during decomposition of cyanobacteria may promote export of picophytoplankton to the deep ocean. *Nature Communications,* 5**,** doi:10.1038/ncomms5143.

TARRAN, G. A. & BRUUN, J. T. 2015. Nanoplankton and picoplankton in the Western English Channel: Abundance and seasonality from 2007–2013. *Progress in Oceanography,* 137**,** 446-455.

TELEDYNE 2011. *Acoustic Doppler Current Profiler: Principles of operation a practical primer, user manual,* California, USA, Teledyne RD Instruments.

TER BRAAK, C. J. F. & ŠMILAUER, P. 2002. *CANOCO Reference Manual and CanoDraw for Windows User's Guide: Software for Canonical Community Ordination (version 4.5),* Ithaca, New York, Microcomputer Power.

THINGSTAD, T. F., OVREAS, L., EGGE, J. K., LOVDAL, T. & HELDAL, M. 2005. Use of non-limiting substrates to increase size; a generic strategy to simultaneously optimize uptake and minimize predation in pelagic osmotrophs? *Ecology Letters,* 8**,** 675-682.

THORNTON, D. C. O. 2002. Diatom aggregation in the sea: mechanisms and ecological implications. *European Journal of Phycology,* 37**,** 149-161.

THORNTON, D. C. O. 2012. Primary production in the ocean. *In:* NAJAFPOUR, M. M. (ed.) *Advances in Photosynthesis - Fundamental Aspects.* Croatia: InTech.

THORNTON, D. C. O. 2014. Dissolved organic matter (DOM) release by phytoplankton in the contemporary and future ocean. *European Journal of Phycology,* 49**,** 20-46.

THURMAN, H. V. 1997. *Introductory Oceanography,* USA, Prentice Hall.

THYSSEN, M., ALVAIN, S., LEFÈBVRE, A., DESSAILLY, D., RIJKEBOER, M., GUISELIN, N., CREACH, V. & ARTIGAS, L.-F. 2015. High-resolution analysis of a North Sea phytoplankton community structure based on *in situ* flow cytometry observations and potential implication for remote sensing. *Biogeosciences,* 12**,** 4051-4066.

TIDETIMES.CO.UK. no date. *Falmouth Tide Times* [Online]. https://www.tidetimes.co.uk/falmouth-tide-times. [Accessed 20 September 2018].

TILSTONE, G. H., FIGUEIRAS, F. G., FERMIN, E. G. & ARBONES, B. 1999. Significance of nanophytoplankton photosynthesis and primary production in a coastal upwelling system (Ria de Vigo, NW Spain). *Marine Ecology Progress Series,* 183**,** 13-27.

TILSTONE, G. H., FIGUEIRAS, F. G., LORENZO, L. M. & ARBONES, B. 2003. Phytoplankton composition, photosynthesis and primary production during different hydrographic conditions at the Northwest Iberian upwelling system. *Marine Ecology Progress Series,* 252**,** 89-104.

TINKER, J., LOWE, J., PARDAENS, A., HOLT, J. & BARCIELA, R. 2016. Uncertainty in climate projections for the 21st century northwest European shelf seas. *Progress in Oceanography,* 148**,** 56-73.

TITMAN, D. 1976. Ecological competition between algae: experimental confirmation of resource-based competition theory. *Science,* 192**,** 463-465.

TOMAS, C. R. 1997. *Identifying Marine Phytoplankton,* San Diego, Academic Press.

TOMCZAK, G. & GOEDECKE, E. 1964. Die thermische schichtung der Nordsee auf Grund des mittleren Jahrganges der Temperatur in 1/2° - und 1° Feldern. *Deutsche Hydrographische Zeitschrift (Erganzheft Reihe B),* 8**,** 1-182.

TRAINER, V. L., BATES, S. S., LUNDHOLM, N., THESSEN, A. E., COCHLAN, W. P., ADAMS, N. G. & TRICK, C. G. 2012. *Pseudo-nitzschia* physiological ecology, phylogeny, toxicity, monitoring and impacts on ecosystem health. *Harmful Algae,* 14**,** 271-300.

TRAINER, V. L., HICKEY, B. M. & BATES, S. S. 2008. Toxic diatoms. *In:* WALSH, P. J., SMITH, S. L., FLEMING, L. E., SOLO-GEBRIELE, H. & GERWICK, W. H. (eds.) *Oceans and Human Health: Risks and Remedies from the Sea.* New York: Elsevier Science Publishers.

TRAINER, V. L., PITCHER, G. C., REGUERA, B. & SMAYDA, T. J. 2010. The distribution and impacts of harmful algal bloom species in eastern boundary upwelling systems. *Progress in Oceanography,* 85**,** 33-52.

TURNER, J. T. & TESTER, P. A. 1997. Toxic marine phytoplankton, zooplankton grazers, and pelagic food webs. *Limnology and Oceanography,* 42**,** 1203-1214.

TWEDDLE, J. F., SHARPLES, J., PALMER, M. R., DAVIDSON, K. & MCNEILL, S. 2013. Enhanced nutrient fluxes at the shelf sea seasonal thermocline caused by stratified flow over a bank. *Progress in Oceanography,* 117**,** 37-47.

UEHLINGER, V. 1964. Etude statistique des méthodes de dénombrement planctonique. *Archives des Sciences,* 17**,** 11-223.

UITZ, J., CLAUSTRE, H., GENTILI, B. & STRAMSKI, D. 2010. Phytoplankton class-specific primary production in the world's oceans: seasonal and interannual variability from satellite observations. *Global Biogeochemical Cycles,* 24**,** doi:10.1029/2009GB003680.

UITZ, J., CLAUSTRE, H., MOREL, A. & HOOKER, S. B. 2006. Vertical distribution of phytoplankton communities in open ocean: An assessment based on surface chlorophyll. *Journal of Geophysical Research: Oceans,* 111**,** doi:10.1029/2005JC003207.

UITZ, J., HUOT, Y., BRUYANT, F., BABIN, M. & CLAUSTRE, H. 2008. Relating phytoplankton photophysiological properties to community structure on large scales. *Limnology and Oceanography,* 53**,** 614-630.

UTERMÖHL, H. 1958. Improvement of the quantitative methods for phytoplankton. *International Association of Theoretical and Applied Limnology,* 9**,** 1-38.

VAN LEEUWEN, S. M., VAN DER MOLEN, J., RUARDIJ, P., FERNAND, L. & JICKELLS, T. 2013. Modelling the contribution of deep chlorophyll maxima to annual primary production in the North Sea. *Biogeochemistry,* 113**,** 137-152.

VEGA, E. P. & VILLAREAL, T. A. 2016. Are small diatoms capable of positive buoyancy? (poster). *AGU Ocean Sciences Meeting.* New Orleans.

VELDHUIS, M. J. W. & KRAAY, G. W. 2004. Phytoplankton in the subtropical Atlantic Ocean: towards a better assessment of biomass and composition. *Deep-Sea Research Part I - Oceanographic Research Papers,* 51**,** 507-530.

VELO-SUÁREZ, L., GONZÁLEZ-GIL, S., GENTIEN, P., LUNVEN, M., BECHEMIN, C., FERNAND, L., RAINE, R. & REGUERA, B. 2008. Thin layers of *Pseudo-nitzschia spp.* and the fate of *Dinophysis acuminata* during an upwelling–downwelling cycle in a Galician Ria. *Limnology and Oceanography,* 53**,** 1816-1834.

VERITY, P. G. & PAFFENHOFER, G. A. 1996. On assessment of prey ingestion by copepods. *Journal of Plankton Research,* 18**,** 1767-1779.

VILLAREAL, T. A. 1988. Positive buoyancy in the oceanic diatom *Rhizosolenia debyana* H. Peragallo. *Deep-Sea Research,* 35**,** 1037-1045.

WAITE, A., FISHER, A., THOMPSON, P. A. & HARRISON, P. J. 1997. Sinking rate versus cell volume relationships illuminate sinking rate control mechanisms in marine diatoms. *Marine Ecology Progress Series,* 157**,** 97-108.

WAITE, A. & HARRISON, P. J. 1992. Role of sinking and ascent during sexual reproduction in the marine diatom *Ditylum brightwellii*. *Marine Ecology Progress Series,* 87**,** 113-122.

WANG, Z. & GOODMAN, L. 2009. Evolution of the spatial structure of a thin phytoplankton layer into a turbulent field. *Marine Ecology Progress Series,* 374**,** 57-74.

WANGPRASEURT, D., TAMBURIC, B., SZABÓ, M., SUGGETT, D., RALPH, P. J. & KHÜL, M. 2014. Spectral effects on *Symbiodinium* photobiology studied with a programmable light engine. *PLoS ONE,* 9**,** e112809, doi: 10.1371/journal.pone.0112809.

WARD, B. A., DUTKIEWICZ, S., BARTON, A. D. & FOLLOWS, M. J. 2011. Biophyiscal aspects of resource acquisition and competition in algal mixotrophs. *The American Naturalist,* 178**,** 98-112.

WASMUND, N., DUTZ, J., POLLEHNE, F., SIEGEL, H. & ZETTLER, M. L. 2015. Marine Science Report No. 98: Biological assessment of the Baltic Sea 2014. *Marine Science***,** doi: 10.12754/msr-2015-0098.

WATERBURY, J. B., WILLEY, J. M., FRANKS, D. G., VALOIS, F. W. & WATSON, S. W. 1985. A cyanobacterium capable of swimming motility. *Science,* 230**,** 74-76.

WEBSTER, D. R., TRUE, A. C., WEISSBURG, M. J. & YEN, J. Copepod behaviour in thin layers of toxic algae (poster). AGU Ocean Sciences Meeting, 2016 New Orleans.

WELSCHMEYER, N. A. 1994. Fluorometric analysis of chlorophyll a in the presence of chlorophyll b and pheopigments. *Limnology and Oceanography,* 39**,** 1985-1992.

WESTON, K., FERNAND, L., MILLS, D. K., DELAHUNTY, R. & BROWN, J. 2005. Primary production in the deep chlorophyll maximum of the central North Sea. *Journal of Plankton Research,* 27**,** 909-922.

WHITE, A. E., LETELIER, R. M., WHITMIRE, A. L., BARONE, B., BIDIGARE, R. R., CHURCH, M. J. & KARL, D. M. 2015. Phenology of particle size distributions and primary productivity in

the North Pacific subtropical gyre (Station ALOHA). *Journal of Geophysical Research: Oceans,* 120**,** 7381-7399.

WIDDICOMBE, C. E., ELOIRE, D., HARBOUR, D., HARRIS, R. P. & SOMERFIELD, P. J. 2010. Long-term phytoplankton community dynamics in the Western English Channel. *Journal of Plankton Research,* 32**,** 643-655.

WILLEY, J. M. & WATERBURY, J. B. 1989. Chemotaxis toward nitrogenous compounds by swimming strains of marine *Synechococcus spp. . Applied and Environmental Microbiology,* 55**,** 1888-1894.

WILLIAMS, C. 2013. *The supply of nutrients to the subsurface chlorophyll maximum in temperate shelf seas.* PhD, University of Liverpool.

WILLIAMS, C., SHARPLES, J., GREEN, M., MAHAFFEY, C. & RIPPETH, T. 2013a. The maintenance of the subsurface chlorophyll maximum in the stratified western Irish Sea. *Limnology and Oceanography: Fluids and Environments,* 3**,** 61-73.

WILLIAMS, C., SHARPLES, J., MAHAFFEY, C. & RIPPETH, T. 2013b. Wind-driven nutrient pulses to the subsurface chlorophyll maximum in seasonally stratified shelf seas. *Geophysical Research Letters,* 40**,** 5467-5472.

WILSON, J. B. 2011. The twelve theories of co-existence in plant communities: the doubtful, the important and the unexplored. *Journal of Vegetation Science,* 22**,** 184-195.

WILTSHIRE, K. H. & MANLY, B. F. J. 2004. The warming trend at Helgoland Roads, North Sea: phytoplankton response. *Helgoland Marine Research,* 58**,** 269-273.

WOOD, A. M. 1985. Adaptation of the photosynthetic apparatus of marine ultraphytoplankton to natural light fields. *Nature,* 316**,** 253-255.

WOODS, K. 2003. *Development and assessment of novel techniques to measure primary production in the Celtic Sea and English Channel.* PhD, University of Southampton.

WOODS, S. & VILLAREAL, T. A. 2008. Intracellular ion concentrations and cell sap density in positively buoyant oceanic phytoplankton. *Nova Hedwigia Beihefte,* 133**,** 131-145.

WOODWARD, M. 2015. Nutrient concentrations (nitrate, nitrite, ammonium, phosphate, silicate) at sites L4 and E1 in the Western English Channel during the summers (June/July) of 2007-2014. British Oceanographic Data Centre - Natural Environment Research Council UK.

YIH, W., KIM, H. S., JEONG, H. J., MYUNG, G. & KIM, Y. G. 2004. Ingestion of cryptophyte cells by the marine photosynthetic ciliate *Mesodinium rubrum*. *Aquatic Microbial Ecology,* 36**,** 165-170.

YOOL, A. & TYRRELL, T. 2003. Role of diatoms in regulating the ocean's silicon cycle. *Global Biogeochemical Cycles,* 17**,** 1103, doi:10.1029/2002GB002018.

ZEHR, J., BENCH, S. R., MONDRAGON, E. A., MCCARREN, J. & DE-LONG, E. F. 2007. Low genomic diversity in tropical oceanic N_2-fixing cyanobacteria. *PNAS,* 104**,** 17907-17812.

ZHANG, J.-Z. & BERBERIAN, G. A. 1997. Method 366.0: Determination of dissolved silicate in estuarine and coastal waters by gas segmented continuous flow colorimetric analysis. Cincinnati, Ohio: U.S. Environmental Protection Agency.

ZHANG, J.-Z., ORTNER, P. B. & FISCHER, C. 1997. Method 353.4: Determination of nitrate and nitrite in estuarine and coastal waters by gas segmented continuous flow colorimetric analysis. Cincinnati, Ohio: U.S. Environmental Protection Agency.

ZHANG, Y., RYAN, J. P., BELLINGHAM, J. G., HARVEY, J. B. J. & MCEWEN, R. S. 2012. Autonomous detection and sampling of water types and fronts in a coastal upwelling system by an autonomous underwater vehicle. *Limnology and Oceanography: Methods,* 10**,** 934-951.

ZIMMERMAN, R. C., KREMER, J. N. & DUGDALE, R. C. 1987. Acceleration of nutrient uptake by phytoplankton in a coastal upwelling ecosystem: a modelling analysis. *Limnology and Oceanography,* 32**,** 359-367.

ZIMMERMANN, C. F. & KEEFE, C. 1997. Method 365.5: Determination of orthophosphate in estuarine and coastal waters by automated colorimetric analysis. Cincinnati, Ohio: U.S. Environmental Protection Agency.

ZIMMERMANN, C. F., KEEFE, C. W. & BASHE, J. 1997. Method 440.0: Determination of carbon and nitrogen in sediments and particulates of estuarine/coastal waters using elemental analysis. Cincinnati, Ohio: U.S. Environmental Protection Agency.

ZUBKOV, M., SLEIGH, M. & BURKHILL, P. 2000. Assaying picoplankton distribution by flow cytometry of underway samples collected along a meridional transect across the Atlantic Ocean. *Aquatic Microbial Ecology,* 21**,** 13-20.

ZUUR, A. F., IENO, E. N. & SMITH, G. M. 2007. *Analysing Ecological Data,* New York, Springer.